STUDIA UNIVERSITATIS
BABEŞ-BOLYAI

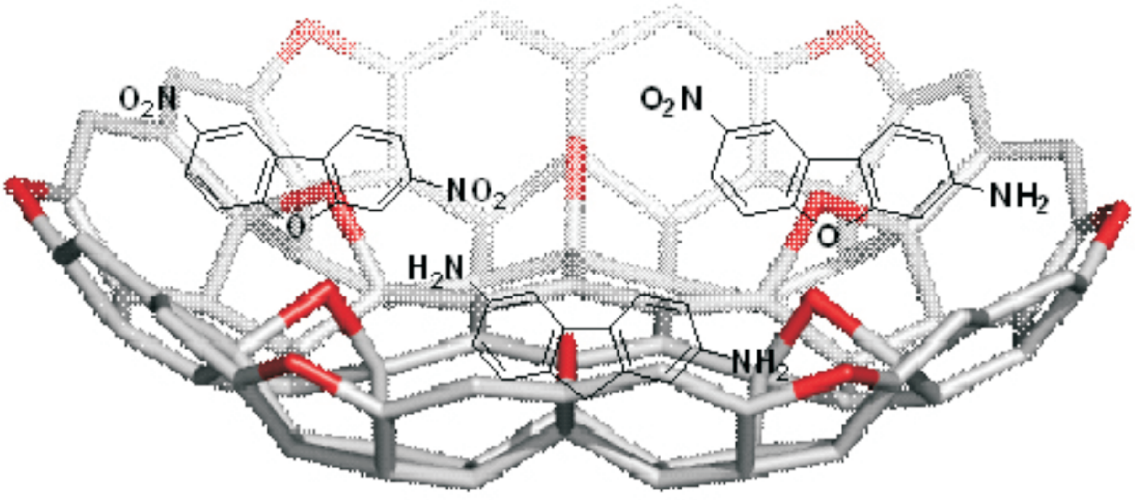

CHEMIA

4/2009
tom I

ANUL LIV **2009**

S T U D I A

UNIVERSITATIS BABEŞ-BOLYAI

CHEMIA

4

tom I

Desktop Editing Office: 51ST B.P. Hasdeu Street, Cluj-Napoca, Romania, Phone + 40 264-405352

CUPRINS – CONTENT – SOMMAIRE – INHALT

Studia Universitatis Babes-Bolyai Chemia has been selected for coverage in Thomson Reuters products and custom information services. Beginning with V. 53 (1) 2008, this publication is indexed and abstracted in the following:

- Science Citation Index Expanded (also known as SciSearch®)
- Chemistry Citation Index®
- Journal Citation Reports/Science Edition

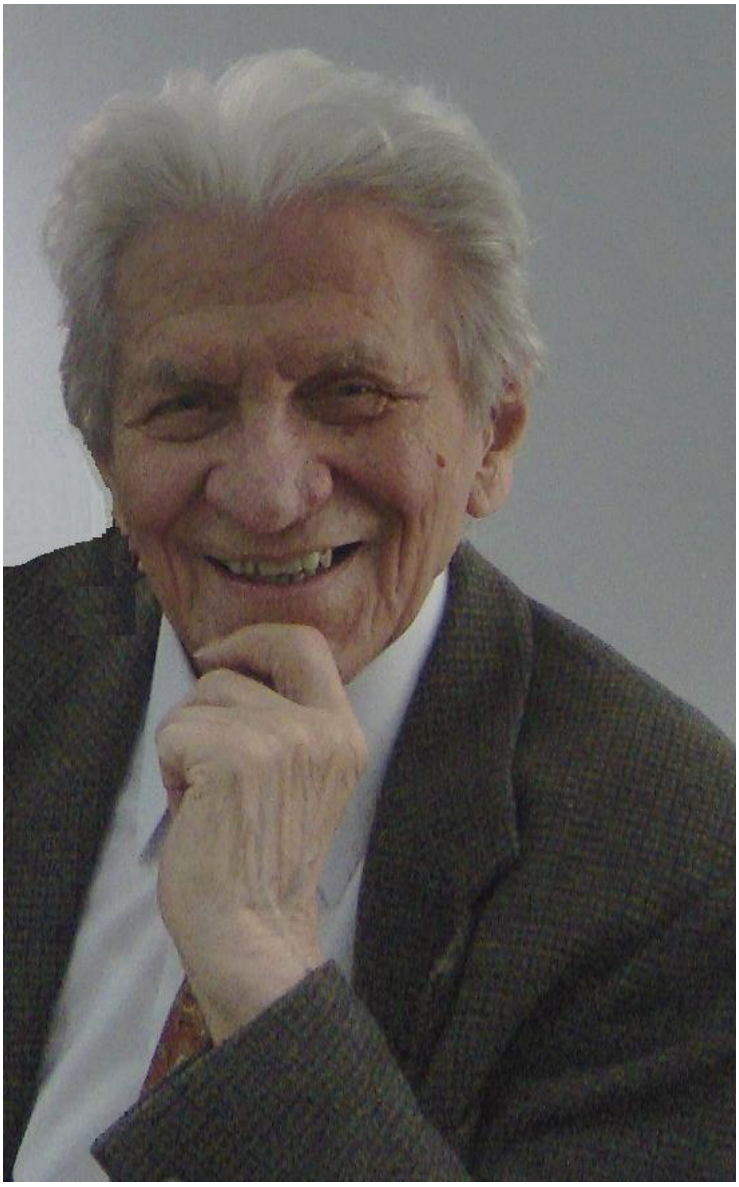

Professor Valer Fărcăşan at his 90th anniversary
October the 3rd 2009

STUDIA UNIVERSITATIS BABEŞ-BOLYAI, CHEMIA, LIV, 4, 2009

NEW WAYS FOR OLD STRUCTURES

FLORIN DAN IRIMIE[a], CSABA PAIZS[a], MONICA TOSA[a], PAULA PODEA[a]

ABSTRACT. Classical heterocyclic structures of furan, benzofuran, dibenzofuran, phenothiazine and benzothiazole type, previously synthesized and studied by Professor Fărcăşan, were derivatized using cell- or enzyme-assisted regio-, chemo- and stereoselective techniques, providing compounds extremely difficult or even impossible to produce by traditional chemical methods. The present report underlines the high potential of biocatalysis to perform selective enantiomer- and enantiotope-transformations with remarkable conversion rates and purities.

Keywords: heterocycles, bezofuran, (furyl)benzothiazole, regioselectivity, chemoselectivity, enantiomer-selectivity, enantiotop-selectivity

INTRODUCTION

Heterocyclic systems of type benzofuran, benzothiazole, (furyl)benzothiazole, dibenzofuran are found as building-blocks for compounds with specific biological activities, as antimicrobial and antifungal agents [1 - 2] cytotoxic compounds [3], antidiabetics [4 - 5] etc.

These basic five membered heterocycles were prepared and functionalised thanks to the pioneering works of Professor Farcasanu research group in the period of 1950 – 1980' [6-14]. Thus, during the initial heterosynthesis state of art, really nice achievements had been accomplished using traditional means of synthesis and analysis.

Over the years, the above heterocyclic structures were much developed, as a need for diversifying their applicability area, for example by increasing the selectivity of biological impact of the products.

Nowadays, the insertion of the initial heterocyclic systems in new compounds with high structural complexity became possible, by means of highly selective techniques, with increased efficiency and compatibility with the environment. Among these techniques, enzymatic and cellular biocatalysis detaches through their advantages concerning activity and selectivity, which impose biocatalysis as a powerful tool with a reliable future.

[a] *"Babes-Bolyai" University, Department of Biochemistry and Biochemical Engineering, 11 Arany Jànos st., 400 028 Cluj-Napoca, ROMANIA, irimie@chem.ubbcluj.ro*

The present dedicated mini-review is intended to highlight these recent advances in highly functionalised five membered heterocyclic chemistry, in a biochemical approach.

1. Regioselective processes

Regioselectivity is an undeniable advantage of enzymatic activity, making possible the discrimination and modification of chemically identical structures, located in different environments. For example, hydrolases express most evidently this property, being used for manipulation of polyfunctional bio compounds as carbohydrates [15], nucleosides [16], steroids [17]. Thus, Michael additions [18], hydroxylations [19 - 20] and several reduction reactions [21 - 22] are good examples of enzymatic regioselective processes.

In context, dibenzofuran was used as a substrate in the research group of Professor Fărcăşan. Thus, by nitration, 3-nitro-, and 3,8-dinitrobenzofuran were obtained. Reduction of 3-nitrodibenzofuran to 3-aminodibenzofuran and that of 3,8-dinitrobenzofuran to 3-amino-8-nitrodibenzofuran, in the presence of baker's yeast was accomplished by our group in 1997 (Scheme 1) [23].

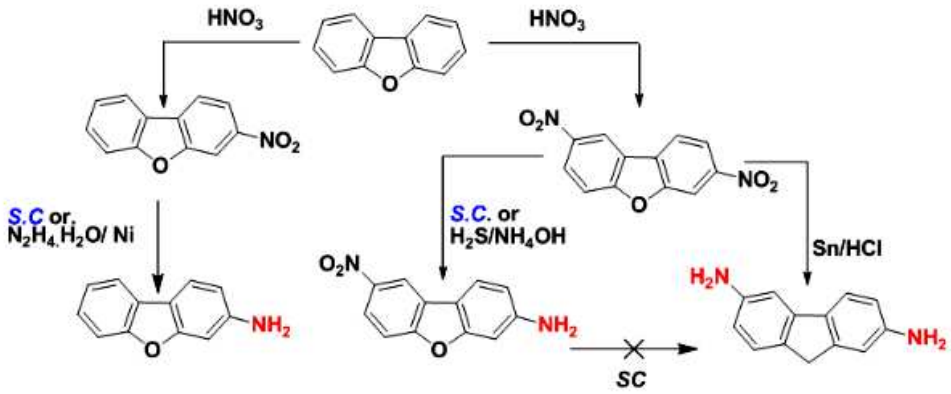

Scheme 1

The chemoselective processes involve the selective transformation of just one functional group from two or more functionally related groups which may be present i) on different substrates (substrate chemoselectivity - chemospecificity) or ii) on the same substrate (product chemoselectivity or merely chemoselectivity) [24].

For example, Baker's yeast can selectively reduce the aldehyde group attached to a heterocyclic skeleton, such as (phenyl)furan, which has functional groups potentially vulnerable to the enzymatic equipment of yeast, nitro for reduction and ethoxycarbonyl for hydrolysis [23, 24] (Scheme 2).

2. Stereoselective processes

Stereoselectivity may be one of the major advantages of biocatalysis.

Through processes assisted by stereoselective biocatalysts, compounds with high enantiopurity can be produced. Enantiopurity is a necessary condition for bioactive compouds, because their two stereoisomers have different biological properties. At the same time, the impure nature of the unwanted enantiomer affects the economy of the synthesis. The preference of biocatalyst for a certain surface or enantiotope group in the substrate's structure conducts to the preferential forming of a certain enantiomeric product. This kind of preference defines *an enantiotope-selective process* and creates, from a symmetrical structure, a chiral one [24]. Through the preference of the biocatalyst for one of the two enantiomers of a racemic mixture, a converted enantiomer is obtained, while the other one, the unmodified enantiomer, remains in the medium. This process we entitled as *enantiomer-selective*.

Several illustrative examples of us will be discusssed hereafter.

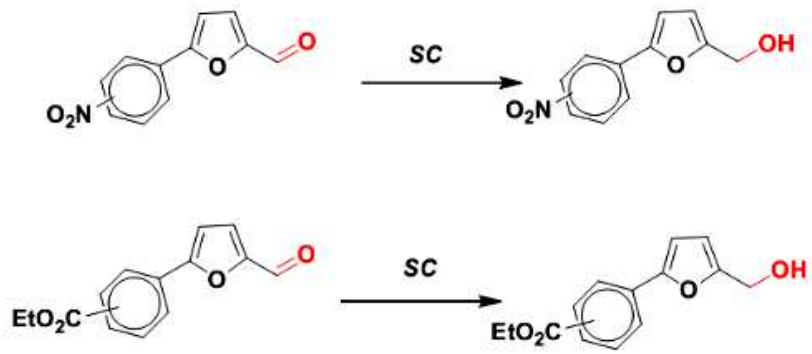

Scheme 2

2.1. Enantiotope selective-processes

These processes allow desymmetrization of prochiral substrates, which posess either enantiotope faces or enantiotope groups, resulting in enantiopure compounds according to the selectivity of the biocatalyst.

Our group transformed 2-substituted (methyl, acetoxymethyl) benzothiazole keto-derivatives into the corresponding secondary alcohols by enantiotope-selective reduction of their prochiral carbonyl group. The biocatalyst used was Baker's yeast (*Saccharomyces Cerevisiae, SC*) which contains a complex dehydrogenase equipment, able to catalyze redox processes. Due to the presence of several dehydrogenases, some of them with opposite selectivity, the latter can be modulated by using certain additives, or by modifying the operating conditions, fermentative or non-fermentative, in order to optimise the working system.

There is a general rule, known as that of Prelog, which states that in the reduction of a prochiral ketone with a biocatalyst, a secondary alcohol with (*S*) configuration is formed. This rule can be explained by mean of the topology of the catalytic site of a dehydrogenase present in the yeast (Figure 1).

For example, reduction of (2-oxo-2-hetaryl)ethyl acetates **3a-d** and (2-hydroxy-1-hetaryl)ethanones **4a-d** (Scheme 3) was performed with opposite enantiotope preference affording, after optimization, excellent yields (92-94%) and good enantiomeric excesses (89-99%), for each enantiomer of the hetarylethane-1,2-diols **5a-d** [25]. One can note the fast hydrolysis of the intermediates (*R*)-(2-hydroxy-2-hetaryl)ethyl acetates, post slow reduction step, by the enzymatic equipment of Baker's yeast. Similar results we obtained in the case of 1-(benzofuran-2-yl)ethanols and ethane-1,2-diols [26]

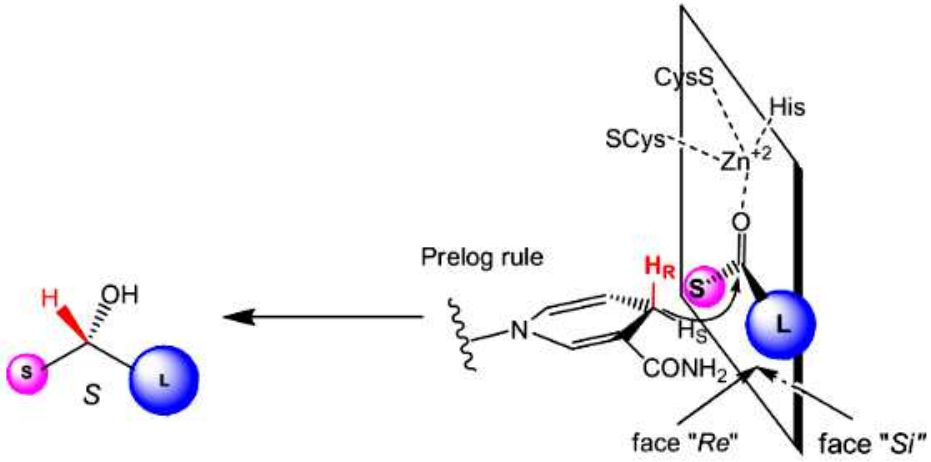

Figure 1. Topology of catalytic site of alcohol dehydrogenase from Baker`s yeast

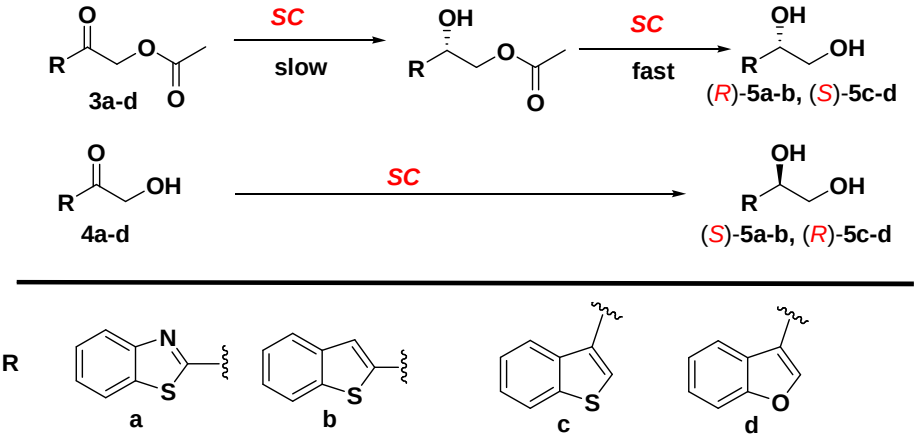

Scheme 3

2.2. Enantiomer selective processes

If biocatalysis assisted *enantiotope-selective processes* can be applied to prochiral substrates, *enantiomer-selective processes* are used to transform enantiomeric mixtures, most frequently racemic, in their nature. *Enantiomer-selectivity* implies that one enantiomer is converted faster than the other one. The reaction products will have different values of a certain separation property (solubility, melting point, etc.). So, the untransformed enantiomer can be easier separated from the reacted one. This system defines a kinetic resolution.

2.2.1. Kinetic resolution

An illustrative example of kinetic resolution is that of substituted 1-(benzofuran-2-yl)ethanols racemates (*rac*-**1a-d**, Scheme 4). They were synthesized upon unselective reduction of certain substituted 1-(benzofuran-2-yl)ethanones [27].

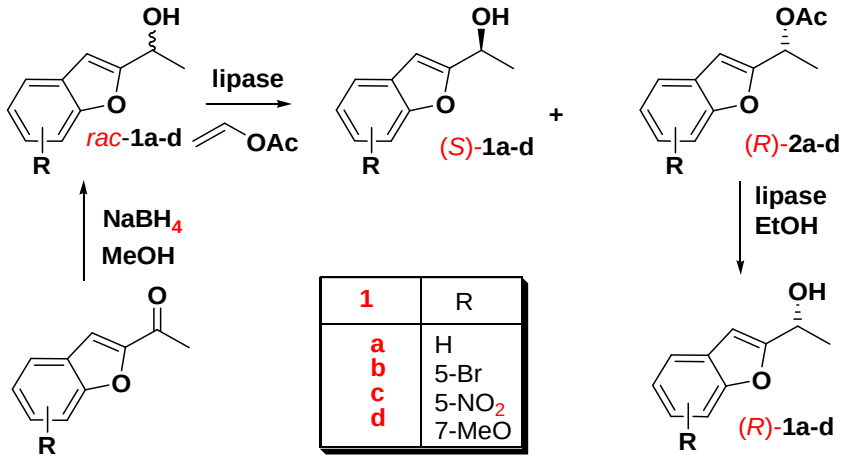

Scheme 4

The enantiopreference of enzyme for certain configuration can also be exploited for synthetic purposes [28].

Thus, starting from a racemic mixture, if enzyme is (*S*) selective, it will mediate only the acylation of a the (*S*) hetarylethanol, leaving the (*R*) alcohol unaffected (Scheme 5, the nature of heterocycles is the same as in Scheme 3). If the same enzyme will catalyze the hydrolysis of a racemic mixture of *O*-acylated hetarylethanols, such as *rac*-**2a-d**, the product will be the (*S*) alcohol, and the (*R*) ester remains untransformed. So, using racemates, *via* *O*-acylation, one can isolate the (*R*) alcohol, and by hydrolysis the (*S*) enantiomer becomes accessible. To conclude, by exploiting the conservation of enantiopreference of a lipase, one can obtain any of the two enantiomers, up to desire, from their racemic mixture, by mean a selective acylation or unselective acylation followed by a selective hydrolysis

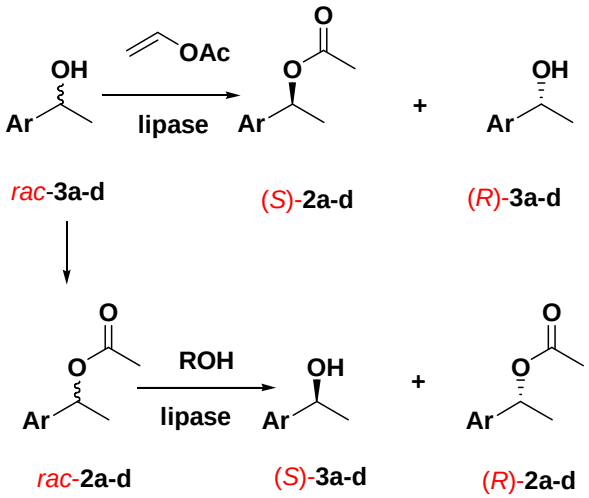

Scheme 5

However, the main drawback of kinetic resolution remains the maximum conversion as 50% calculated with respect to the racemic mixture.

2.2.2. Dynamic kinetic resolutions (DKR)

DKR are alternatives to kinetic resolutions, which eliminate the main disadvantage of kinetic resolutions: the limitation of conversion to 50%. Indeed the enatiopreference for one enantiomer leaves the other one unmodified, hence creating problems of i) separation (even if they are not as important as in the case of separation of enantiomers) and ii) in finding an applicability for the "non-preferred" enantiomer.

The DKR mechanism is simple and useful in systems for which one can find a reaction of racemization involving the starting enantiomers **A** and **B** (Scheme 6), [29 - 30].

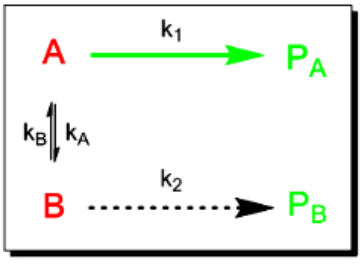

Scheme 6

If **A** is the preferred enantiomer by the biocatalyst, its concentration will be decreasing faster than that of **B**. Similarly, the concentration of product $\mathbf{P_A}$ will be increasing faster than the concentration of $\mathbf{P_B}$, these being the conditions for a successful kinetic resolution.

In contrast, if the system allows racemization of mixture of **A** and **B**, as **A** is consumed, a part of **B** is converted into **A**, to reestablish the equilibrium.

To setup an efficient DKR system as good selectivity, it is necessary that direct reaction(s), **A → P_A** and **B → P_B**, be irreversible. That is, the racemization rate should be greater than direct transformation rate, $k_{rac} > max(k_1,k_2)$. Side reactions and product racemization should be avoided and generally, the **DKR** methodology is limited, so far, to compounds having a single stereocenter.

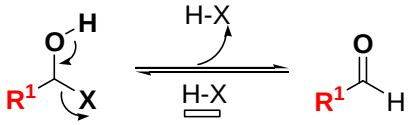

X = CN, OR^2, SR^2, NHR^2

Scheme 7

The key feature of a DKR system is the racemization system. One of the most valuable systems are those in which, by sequence elimination – addition, such the one described in Scheme 7, the stereogenic center is firstly suppressed then recreated in a totally unselective manner. Another strategy can be used when, at the stereogenic center, one can find a "mobile proton" activated by an electron withdrawing group.

For instance, by applying the DKR mthodology, we were able to obtain α-(hetaryl)cyanomethyl acylates from the corresponding cyanohydrins (Scheme 8) in high enatiopure forms [31-33] with good conversions.

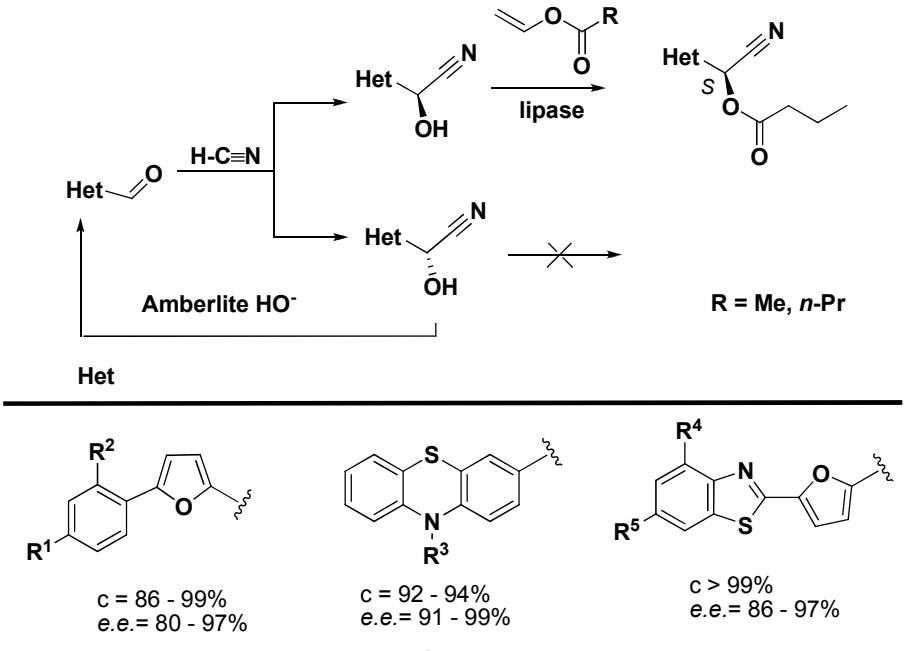

Scheme 8

The racemization step consisted of elimination – addition of hydrogen cyanide in the presence of a basic resin, Amberlite IRA-904.

The DKR we also used for the preparation of some hetaryl L-alanines of high enantiopurity [34] in a chemical and enzymatic sequence (Scheme 9). The racemization step in this DKR system had 4-(hetaryl)methyl-2-methyloxazol-5(4*H*)-ones, *rac*-**11a-d**, as a substrates [34]. We demonstrated that, due to the low pKa of their C-4 proton combined with a high reactivity against different nucleophiles, 2-substituted oxazol-5(4*H*)-ones are excellent substrates to undergo enzymatic dynamic kinetic resolution [35].

The oxazolone ring opening was performed through lipase-mediated alcoholysis. The L-hetaryl aminoacid was released after the basic hydrolysis of the ester bond (**III**, Scheme 9) followed by the enzymatic hydrolysis of the amidic bond. Consequently, this last enzymatic *N*-deprotection made a second chiral selection, promoting a final enantiopurity almost absolute. The global conversion of chemoenzymatic synthesis of enantiopure L-benzofuranyl- and L-benzo[*b*]thiophenyl alanines ranged between 76-85%. It was by far greater than the maximal theoretical conversion of enzymatic kinetic resolution assisted by Acylase I (50%).

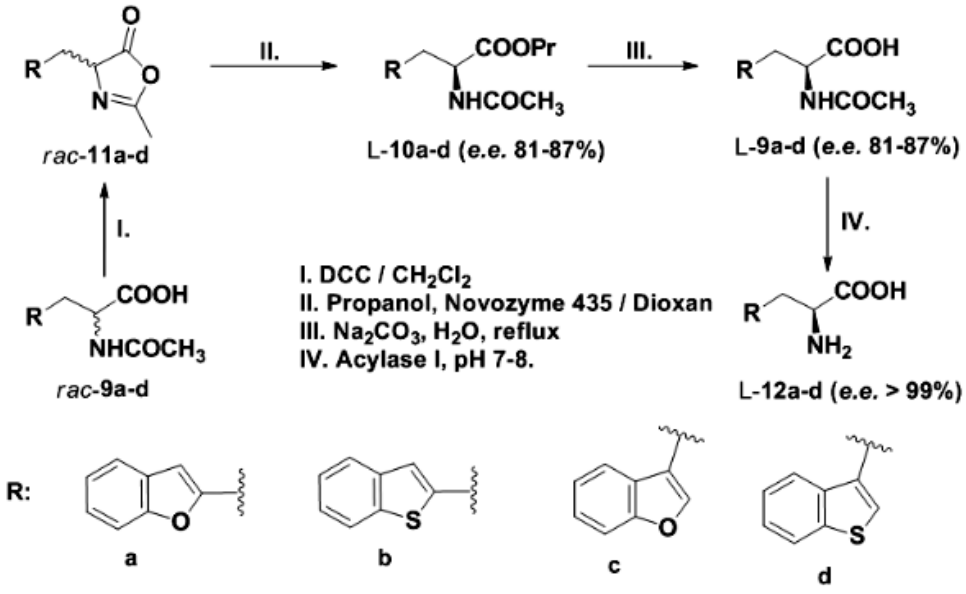

Scheme 9

3. Green processes

One of the most important features of a biocatalyst is its compatibility with the environment, face to the aggressivity of certain chemocatalysts and substrates. An illustrative example is provided by the cyclization of thiofuranilides assisted by *Saccharomyces Cerevisiae* (Scheme 10) [36].

The mechanism of cyclization involves the hydride ion transfer from thioenolic form to the NAD^+ cofactor. The chemical oxidant conventionally used is potassium dichromate. The conversions of the chemical *vs.* biochemical protocol are comparable [36].

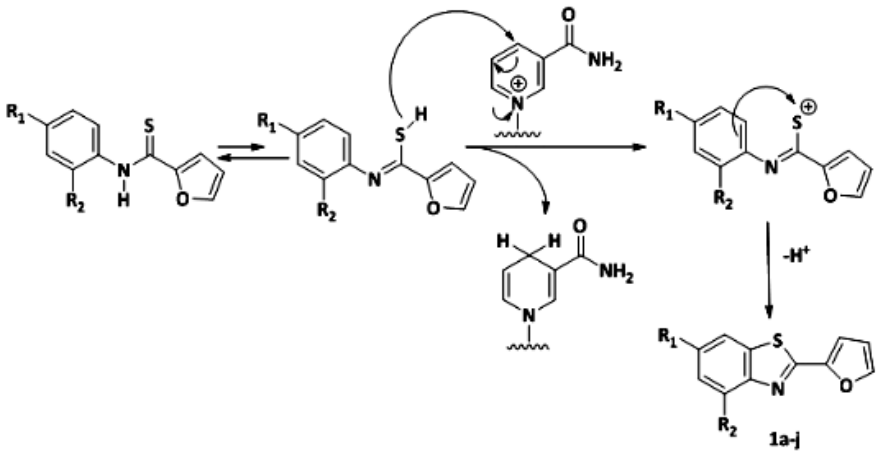

Scheme 10

CONCLUSIONS

Biotransformations are versatile, environmentally friendly, selective ways for synthesis of organic compounds, particularly chiral ones with high enantiopurity, being able to replace toxic and environmental aggressive catalysts or reagents.

ACKNOWLEDGMENTS

We kindly wish to express here our gratitude to Professor Valer Fărcăşan, for his helpful advices and discussions along the years.

REFERENCES

1. F. Messina, M. Botta, F. Corelli, A. Paladino. *Tetrahedron: Asymmetry,* **2000**, *11*: 4895.
2. B.F. Abdel-Wahab, H.A. Abdel-Aziz, E.M. Ahmed. *European Journal of Medicinal Chemistry,* **2009**, *44*: 2632.
3. K. Kaniwa, T. Ohtsuki, Y. Yamamoto, M. Ishibashi. *Tetrahedron Letters,* **2006**, *47*: 1505.
4. L. Di Nunno, C. Franchini, A. Scilimati, M.S. Sinicropi, P. Tortorella. *Tetrahedron: Asymmetry,* **2000**, *11*: 1571.
5. H. Moreno-Díaz, R. Villalobos-Molina, R. Ortiz-Andrade, D. Díaz-Coutiño, J.L. Medina-Franco, S.P. Webster, M. Binnie, S. Estrada-Soto, M. Ibarra-Barajas, I. León-Rivera, G. Navarrete-Vázquez. *Bioorganic & Medicinal Chemistry Letters,* **2008**, *18*: 2871.

6. C. Bodea, V. Farcasan, I. Oprean. *Studii si Cercetari de Chimie,* **1965**, *13*: 1157.
7. C. Bodea, V. Farcasan, I. Oprean. *Revue Roumaine de Chimie,* **1966**, *11*: 1117.
8. C. Bodea, V. Farcasan, T. Panea. *Revue Roumaine de Chimie,* **1966**, *11*: 239.
9. V. Farcasan, F. Paiu. *Studia Universitatis Babes-Bolyai, Chemia,* **1966**: 107.
10. V. Farcasan, I. Mester. *Studia Universitatis Babes-Bolyai, Chemia,* **1967**, *12*: 69.
11. C. Bodea, V. Farcasan, T. Panea. *Revue Roumaine de Chimie,* **1968**, *13*: 971.
12. V. Farcasan, I. Balazs. *Studia Universitatis Babes-Bolyai, Chemia,* **1968**, *13*: 123.
13. V. Farcasan, F. Paiu. *Studia Universitatis Babes-Bolyai, Chemia,* **1968**, *13*: 103.
14. V. Farcasan, S. Florea. *Journal fuer Praktische Chemie (Leipzig),* **1970**, *312*: 1007.
15. A. Xia, Q. Wu, B. Liu, X. Lin. *Enzyme and Microbial Technology,* **2008**, *42*: 414.
16. N. Li, M.-H. Zong, D. Ma. *Tetrahedron,* **2009**, *65*: 1063.
17. M.M. Cruz Silva, S. Riva, M.L. Sá e Melo. *Tetrahedron,* **2005**, *61*: 3065.
18. J.-L. Wang, J.-M. Xu, Q. Wu, D.-S. Lv, X.-F. Lin. *Tetrahedron,* **2009**, *65*: 2531.
19. M. Rahman, C. Hayes Sutter, G.L. Emmert, T.R. Sutter. *Toxicology and Applied Pharmacology,* **2006**, *216*: 469.
20. C. Roh, S.-H. Seo, K.-Y. Choi, M. Cha, B.P. Pandey, J.-H. Kim, J.-S. Park, D.H. Kim, I.S. Chang, B.-G. Kim. *Journal of Bioscience and Bioengineering,* **2009**, *108*: 41.
21. C.L. Davey, L.W. Powell, N.J. Turner, A. Wells. *Tetrahedron Letters,* **1994**, *35*: 7867.
22. K. Nakamura, S.-i. Kondo, Y. Kawai, K. Hida, K. Kitano, A. Ohno. *Tetrahedron: Asymmetry,* **1996**, *7*: 409.
23. F.-D. Irimie, C. Paizs, M.-I. Tosa, C. Afloroaei, V. Miclaus. *Heterocyclic Communications,* **1997**, *3*: 549.
24. F.D. Irimie, C. Paisz, M. Tosa. "Biotransformari in sinteza organica, aspecte fundamentale". Napoca Star, **2006**
25. P.V. Podea, C. Paizs, M.I. Tosa, F.D. Irimie. *Tetrahedron Asymmetry,* **2008**, *19*: 1959.
26. C. Paizs, M. Tosa, C. Majdik, P. Moldovan, L. Novak, P. Kolonits, A. Marcovici, F.-D. Irimie, L. Poppe. *Tetrahedron Asymmetry,* **2003**, *14*: 1495.
27. C. Paizs, M. Tosa, V. Bodai, G. Szakacs, I. Kmecz, B. Simandi, C. Majdik, L. Novak, F.-D. Irimie, L. Poppe. *Tetrahedron Asymmetry,* **2003**, *14*: 1943.
28. M. Tosa, S. Pilbak, P. Moldovan, C. Paizs, G. Szatzker, G. Szakacs, L. Novak, F.-D. Irimie, L. Poppe. *Tetrahedron Asymmetry,* **2008**, *19*: 1844.
29. H. Pellissier. *Tetrahedron,* **2008**, *64*: 1563.
30. A. Kamal, M.A. Azhar, T. Krishnaji, M.S. Malik, S. Azeeza. *Coordination Chemistry Reviews,* **2008**, *252*: 569.
31. C. Paizs, P. Taehtinen, M. Tosa, C. Majdik, F.-D. Irimie, L.T. Kanerva. *Tetrahedron,* **2004**, *60*: 10533.
32. C. Paizs, M. Tosa, C. Majdik, P. Tahtinen, F.D. Irimie, L.T. Kanerva. *Tetrahedron Asymmetry,* **2003**, *14*: 619.
33. C. Paizs, P. Tahtinen, K. Lundell, L. Poppe, F.-D. Irimie, L.T. Kanerva. *Tetrahedron Asymmetry,* **2003**, *14*: 1895.
34. P.V. Podea, M.I. Tosa, C. Paizs, F.D. Irimie. *Tetrahedron Asymmetry,* **2008**, *19*: 500.
35. S.A. Brown, M.-C. Parker, N.J. Turner. *Tetrahedron: Asymmetry,* **2000**, *11*: 1687.
36. C. Paisz, C. Majdik, M. Tosa, R. Misca, F.D. Irimie. *Romanian Biotechnological Letters,* **2001**, *6*: 325.

STUDIA UNIVERSITATIS BABEŞ-BOLYAI, CHEMIA, LIV, 4, 2009

SYNTHESIS AND FLUORESCENCE PROPERTIES OF NEW SCHIFF BASES CONTAINING PHENOTHIAZINE UNITS

EMESE GÁL[a], LUIZA GĂINĂ[a], TAMÁS LOVÁSZ[a], CASTELIA CRISTEA[a] AND LUMINIȚA SILAGHI-DUMITRESCU[a]

ABSTRACT. New heterocyclic Schiff bases exhibiting fluorescent properties were obtained in good yields by thermal condensation of (10-alkyl)-3-formyl-10*H*phenothiazine derivatives with aromatic amines. Structural characterization was based on high resolution NMR, UV-Vis and fluorescence spectroscopy. Emission maxima were situated in the range 524-588 nm showing large Stokes shifts.

Keywords: Schiff bases, formylphenothiazine, fluorescence spectroscopy.

INTRODUCTION

Schiff bases characterized by diverse structural properties can be obtained by relatively simple preparation procedures based on condensation reaction of aromatic amines and carbonyl derivatives [1] This synthetic flexibility enabled the design of molecular structures with tuneable properties and numerous representative derivatives found a wide variety of applications in many fields such as biology (due to similarities with natural biological compounds [2] analytical chemistry (optical, electrochemical, and chromatographic sensors) [3,4] and materials chemistry (*e.g.* due to electroluminescent properties required in *light emitting diodes* OLED, PLED)

Successful application of Schiff bases requires a careful study of their characteristics because many of these azomethines are chemically unstable and show a pronounced tendency to be involved in tautomeric equilibria, hydrolysis, or formation of ionized species [5]

Schiff bases containing phenothiazine units were obtained either by condensation of N-alkyl-3-aminophenothiazine derivatives with benzaldehyde derivatives [6,7], or by condensation of N-alkyl-3-formylphenothiazine derivatives with aromatic primary amines such as aniline [8], aminobenzoic acid derivatives [9] and 5-amino-1-phenyl-pyrazol derivatives [10]. Previous studies regarding the preparation of *bis*-Schiff bases containing phenothiazine units indicate also two alternative synthetic routes, the condensation of N-alkyl-3-formylphenothiazine derivatives with aliphatic or aromatic diamines [10,11] as well as condensation

[a] *Universitatea Babeş-Bolyai, Facultatea de Chimie şi Inginerie Chimică, Str. Kogălniceanu, Nr. 1, RO-400084 Cluj-Napoca, Romania, castelia@chem.ubbcluj.ro*

of N-alkyl-3,7-diformylphenothiazine with amines [12]. Polyazomethine-type conjugated polymers with alternating phenothiazine (PZ) and azomethine units (-C=N-), were synthesized and their electroluminescent properties were studied from the viewpoint of polymer structure vs. emission color and efficiency. Single- and double-layer ***p**olymer **l**ight-**e**mitting **d**iode* PLEDs were fabricated [13]. The conjugated copolymer, poly[N-(2-ethylhexyl)phenothiazine-alt-6-Ph phenanthridine] [poly(PZ-PTI)], with azomethine linkages, was also synthesized by a Schiff-base reaction. Single-layered and double-layered PLED made with poly(PZ-PTI) as an emitting layer were fabricated and exhibited EL (emission) at 572 nm [14].

The aim of this work is to add new data to our previous reports, by describing the synthesis and structural characterization of new Schiff bases containing phenothiazine units and to emphasize their electroluminescent properties by fluorescence spectroscopy.

RESULTS AND DISCUSSION

A series of new Schiff bases **3-4** were obtained by the condensation of 10-alkyl-3-formylphenothiazine **1** with aniline*/p*-aminobenzoic acid derivatives **2** as shown in scheme 1.

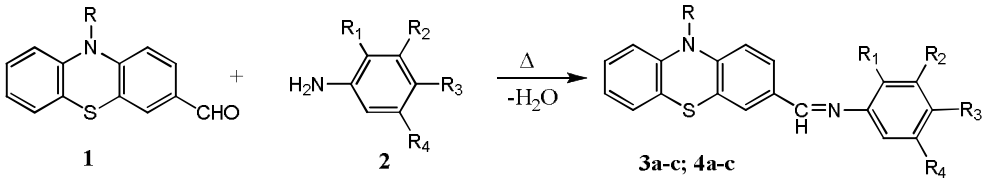

3.a.: R= -CH_2-CH_3; R_1= R_2=R_4= H; R_3 = -COOH
3.b.: R = -CH_2-CH_3; R_1 = Cl, R_2,=R_3= H; R_4 = -COOH
3.c.: R = -CH_2-CH_3; R_1=R_2=R_4= H; R_3 = -OCH_3
4.a.: R = -CH_3; R_1=R_2=R_4= H; R_3 = -COOH
4.b.: R= -CH_3; R_1 = Cl, R_2=R_3= H; R_4 = -COOH
4.c.: R = -CH_3; R_1=R_2=R_4 = H; R_3 = -Cl

Scheme 1

Similar conditions consisting of heating the reaction mixture to reflux in ethanol solution, were applied for the condensation of 10-alkyl-3,7-diformylphenothiazine with aniline*/p*-aminobenzoic acid derivatives leading to *bis*-Schiff bases **5a-c** (scheme 2).

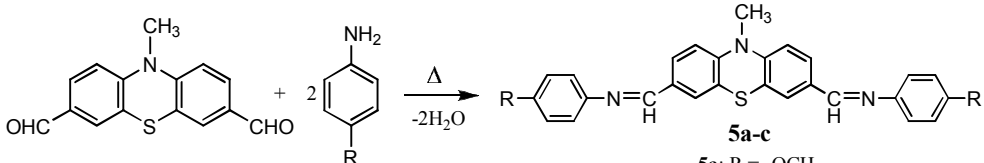

5a: R = -OCH_3
5b: R = -Br
5c: R = -COOH

Scheme 2

Bis-Schiff base **6** was obtained in good yields by the condensation of 3-formyl-10*H*-phenothiazine [15] with *p,p'*-diamino diphenylmethane (scheme 3). Due to unsubstituted NH group in the heterocycle unit, oxidation occurs easily in the presence of air.

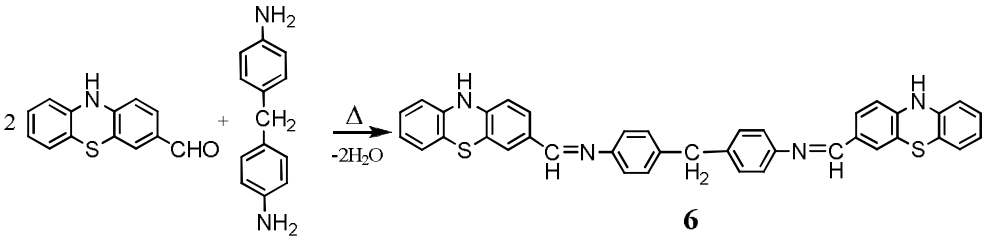

6

Scheme 3

The structure assignment of new Schiff bases **3-6** is supported by spectroscopic data. EI mass spectra revealed the corresponding molecular peaks. In particular, azomethine group can be clearly identified by the appearance of the characteristic proton and carbon resonances in NMR spectra, as a deshielded singlet signal situated at 8.3-8.5 ppm in the ^{1}H-NMR spectra and a signal situated at 153-160 ppm in the ^{13}C-NMR spectra.

The absorption of the *e.m*. radiation in the UV-Vis domain generated electronic spectra with characteristic maxima presented in table 1 for both starting materials (3-formyl-phenothiazine derivatives) and new Schiff bases. All Schiff bases **3-6** contain the same cromophor unit consisting of an extended π conjugated system containing phenothiazinyl and phenyl aromatic units linked by an azomethine group and thus, very similar absorption maxima were recorded in the UV spectra. However, a small bathochromic shift can be noticed for lowest energy absorption maxima of *bis*-Schiff bases **5** as compared to mono Schiff bases **3**-**4**.

As expected, substitution of the heterocyclic nitrogen atom does not exert great influence upon the position of the absorption maxima. Small shifts can be correlated with the nature of auxochrome groups attached in position *meta* or *para* of the phenyl units.

The emission spectra of Schiff bases **3-6** contain broad bands in the range 525-588 nm with large Stokes shifts (6000-8600 cm^{-1}) as shown in Table 1.

The Schiff bases **3a** and **4a** are characterized by lower energy emission maxima ($\lambda_{max,\ em}$ 588 nm and 583 nm respectively) as compared to *bis*-Schiff base **5c** ($\lambda_{max,\ em}$ 535 nm). Meanwhile, the smallest Stokes shifts were observed for *bis*-Schiff bases **5** (5800-6100 cm^{-1}), a fact in agreement with literature data stating that great Stokes shifts can be assigned to large geometrical changes upon excitation from nonplanar ground state to a essentially planarized excited state [16].

Table 1. Electronic properties of Schiff base determined by UV-Vis and LE spectroscopy in THF

Compound	Absorption $\lambda_{max, abs}$ [nm]	Emission $\lambda_{max, em}$ [nm]	Stokes shift (cm^{-1})
3.a.	243, 278, **392**	**588**	8500
3.b.	245, 279, **389**	572	8200
3.c.	236, 273, **379**	528	7400
4.a.	243, 275, **388**	**583**	8600
4.b.	244, 285, **381**	554	8200
4.c.	239, 275, **380**	545	8000
5.a.	234, 290, **401**	524	5800
5.b.	241, 298, **411**[a]	546	5900
5.c.	287, **404**	**535**	6100
6.	244, 294, **399**[a]	525	6000
10-Me-3-formyl-phenothiazine	286, **377**[a]	525	7500
10-Et-3-formyl-phenothiazine	294, **381**[a]	528	7300
10*H*-3-formyl-phenothiazine	292, **393**[a]	523	6300
10-Me-3,7-diformyl-phenothiazine	284, **394**[a]	521	6200

[a]-the UV-Vis, and Fluorescence spectra were recorded in ACN

CONCLUSIONS

Thermal condensation of (10-alkyl)-3-formyl-10*H*phenothiazine derivatives with aromatic amines generate heterocyclic Schiff bases characterized by green-yellow fluorescence. The exhibited emission maxima were situated in the range 524-588 nm showing large Stokes shifts (6000-8500 cm^{-1}), thus recommending these compounds for possible applications in nonlinear optical materials.

EXPERIMENTAL SECTION

FT-IR spectrometer Bruker Vector 22; 300 MHz NMR spectrometer Bruker; UV-Vis spectrometer Perkin Elmer Lambda 35; Luminescence Spectrometer Perkin Elmer LS 55; EI MS Shimadzu QP 2010; Merck reagents.

4-((10-ethyl-10*H*phenothiazin-3yl)-methylenamino)benzoic acid 3.a.
3-Formyl-10-ethyl-phenothiazine 0.5g (1.9mmol) and p-amino-benzoic acid 0.268g (1.9mmol) were refluxed in ethanol for 24 hours. After solvent evaporation an orange powder product with melting point 249℃ w as obtained in 80% yield.
MS (EI) m/z= 374 (63%) $M^{+\cdot}$
^{1}H NMR, 400 MHz, DMSO-d_6: -CH_2 δ= 3.98 ppm (q, ^3J=6.80 Hz, 2H) -CH_2; δ= 1.34 ppm (t, ^3J=6.8 Hz, 3H) -CH_3; δ= 7.13 ppm, (d, ^3J= 8.8 Hz, 1H) H_1; δ= 7.75 ppm, (d, ^3J= 8.8 Hz, 1H) H_2, δ=8.50 ppm, (s, 1H) CH=N; δ=7.67 ppm, (s, 1H) H_4; δ=7.07 ppm, (d, ^3J= 8 Hz, 1H) H_6; δ=6.98 ppm, (t, ^3J= 8 Hz, 1H) H_7; δ= 7.22 ppm, (t, ^3J= 7.6 Hz, 1H) H_8; δ=7.16 ppm, (d, ^3J= 7.6 Hz, 1H) H_9; δ= 7.97 ppm, (d, ^3J=8.4 Hz, 2H) $H_{2',6'}$; δ= 7.29 ppm, (d, ^3J=8.4 Hz, 2H) $H_{3'5'}$; δ= 12.85 ppm, (s, 1H) -COOH.

^{13}C NMR, DMSO-d_6: δ ppm 12.5 (-CH_2), 41.5 (-CH_3), 127.1 (C_1), 129.3 (C_2), 130.1 (C_3), 126.8 (C_4), 124.6 (C_{4a}), 122.8 (C_{5a}), 115.8 (C_6), 123.1 (C_7), 127.9 (C_8), 115.2 (C_9), 143.1 (C_{9a}), 160.6 (CH=N), 155.5 ($C_{1'}$), 130.5 ($C_{2',6'}$) 121 ($C_{3'5'}$), 121.9 ($C_{4'}$), 167.2 (COOH).

4-Chloro-3-((10-ethyl-10H-phenothiazin-3-yl)methyleneamino)benzoic acid 3.b.

3-formyl-10-ethyl-phenothiazine 0.5g (1.9mmol) and 3-amino-4-chloro-benzoic acid 0.266g (1.9mmol) were were stirred at 78℃ for 24 hours in isoamyl-alcohol. The product was purified by recrystallization from ethyl acetate. A light green coloured solid precipitate, with melting point 209℃, was co llected by filtration. Yield 50%.

MS: m/z= 408/410(73%) $M^{+\cdot}$

^{1}H NMR, 400 MHz, DMSO-d_6: δ= 3.97 ppm (q, ^3J=7 Hz, 2H) CH_2; δ= 1.33 ppm (t, ^3J=7 Hz, 3H) CH_3; δ= 7.14 ppm, (d, ^3J=8.4 Hz, 1H) H_1; δ= 7.79 ppm, (d, ^3J=8.4 Hz, 1H) H_2, δ=8.51 ppm, (s, 1H) CH=N; δ=7.69 ppm, (s, 1H) H_4; δ=7.05 ppm, (d, ^3J=8.4 Hz, 1H) H_6; δ=6.98 ppm, (dd, ^3J=8.4 Hz, ^3J=8 Hz, 1H) H_7; δ= 7.21 ppm, (dd, ^3J= 9.2 Hz, ^3J=8 Hz, 1H) H_8; δ=7.12 ppm, (d, ^3J= 9.2 Hz, 1H) H_9, δ= 7.71 ppm (s, 1H) $H_{2'}$; δ= 7.76 ppm, (d, ^3J= 8.4 Hz, 1H) $H_{6'}$; δ= 7.63 ppm, (d, ^3J= 8.4 Hz, 1H) $H_{5'}$.

^{13}C NMR, DMSO-d_6: δ ppm: 12.2 (-CH_2), 41.5 (-CH_3), 126.7 (C_1), 129.2 (C_2), 130.6 (C_3), 161.5 (C=N), 129.9 (C_4), 127.3 (C_{4a}), 122.6 (C_{5a}), 115.8 (C_6), 122.9 (C_7), 126.8 (C_8), 115.6 (C_9), 142.8 (C_{9a}), 144.8 (C_{10a}), 148.6 ($C_{3'}$), 127.3 ($C_{4'}$), 120.4 ($C_{5'}$), 121.7 ($C_{6'}$), 131.8 ($C_{1'}$), 147.2 ($C_{2'}$), 166.2 (COOH).

4-methoxy-N-((10-ethyl-10*H*-phenothiazin-3-yl)methylene)aniline 3.c.

3-formyl-10-ethyl-phenothiazine 0.5g (1.9mmol) and p-metoxy-aniline 0.246g (2.1mmol) were refluxed in ethyl alcohol for 24 hours. The product was purified by recrystallization from ethanol. A lemon-yellow coloured solid precipitate was collected by filtration, with melting point 108℃. Yield 76%.

MS: m/z= 360 (76%) $M^{+\cdot}$

^{1}H NMR, 400 MHz, DMSO-d_6: δ= 3.93 ppm (q, ^3J=7 Hz 2H) -CH_2; δ= 1.41 ppm (t, ^3J=7 Hz 3H) CH_3; δ= 6.86 ppm, (d, ^3J= 8.40 Hz, 1H), H_1; δ= 7.58 ppm, (d, ^3J= 8.40 Hz, 1H) H_2: δ=8.30 ppm, (s, 1H) CH=N; δ=7.63 ppm, (s, 1H) H_4; δ=7.09 ppm, (d, ^3J= 8 Hz 1H) H_6; δ=6.91 ppm, (t, ^3J= 8 Hz, 1H) H_7; δ= 7.58 ppm, (t, ^3J= 8 Hz, 1H) H_8; δ= 6.84 ppm, (d, ^3J= 8.4 Hz 1H) H_9, δ= 6.90 ppm (d, ^3J= 8.8 Hz, 2H) $H_{2',6'}$; δ= 7.18 ppm, (d, ^3J= 8.8 Hz, 2H) $H_{3',5'}$.

^{13}C NMR, DMSO-d_6 δ ppm: 12.9 (CH_2), 42.1 (CH_3), 55.4 (OCH_3)114.6 (C_1), 128.3 (C_2), 130.9 (C_3), 153.8 (C=N), 126.9 (C_4), 124.4 (C_{4a}) 123.6 (C_{5a}), 127.3 (C_6), 122.8 (C_7), 127.3 (C_8), 115.2 (C_9), 143.8 (C_{9a}), 147.2 (C_{10a}), 144.9 ($C_{1'}$), δ= 114.3 ($C_{2',6'}$), 122.1 ($C_{3',5'}$), 158.0 (C_4).

4-((10-methyl-10Hphenothiazin-3yl)-methylenamino)benzoic acid 4.a.

3-formyl-10-methyl-phenothiazine 0.5g (2.0mmol) and p-amino-benzoic acid 0.28g (2.0mmol) were refluxed in ethyl alcohol for 24 hours. The product was purified by recrystallization from toluene. After filtration an orange yellow coloured solid precipitate was collected by filtration, with melting point 256℃. Yield 70%.

MS: m/z= 360 (68%) $M^{+\cdot}$

^{1}H NMR, 400 MHz, DMSO-d_6: δ= 3.5 ppm (s, 3H) CH_3; δ= 6.99 ppm, (d, ^3J= 5.2 Hz, 1H) H_1; δ= 7.71 ppm, (d, ^3J= 5.2 Hz, 1H) H_2, δ=8.51 ppm, (s, 1H) CH=N; δ=7.70 ppm (s, 1H) H_4; δ=7.19 ppm, (d, ^3J= 6.4 Hz, 1H) H_6; δ=7.03 ppm, (dd, ^3J= 6.4 Hz,

^3J= 8.2 Hz 1H) H_7; δ= 7.24 ppm, (t, ^3J= 8.2 Hz, ^3J= 7.6 Hz, 1H) H_8; δ=7.02 ppm, (d, ^3J= 7.6 Hz, 1H) H_9; δ= 7.26 ppm, (d, ^3J= 8.4 Hz, 2H), $H_{3',5'}$; δ= 7.98 ppm, (d, ^3J= 8.4 Hz, 2H) $H_{2',6}$; δ= 9.80 ppm, (s, 1H) -COOH.

^{13}C NMR, DMSO-d_6 δ ppm**:** 35.5 (-CH_3), 114.6 (**C_1**), 159.5 (C=N), 126.8 (C_4), 126.5 (C_{4a}), 126.9 (C_6), 129.5 (C_7), 121.2 (C_8), 142.5 (C_{9a}), 144.8 (C_{10a}), 118,4 (C_{5a}), 155.5 ($C_{1'}$), 130.5 ($C_{2',6'}$), 121 ($C_{3'5'}$), 121.9 ($C_{4'}$), 167 (COOH).

4-chloro-3-((10-methyl-10H-phenothiazin-3-yl)methyleneamino)benzoic acid 4.b.

3-formyl-10-methyl-phenothiazine 0.5g (2.0mmol) and 3-amino-4-chloro-benzoic acid 0.53g (2.0mmol) were heated at 78℃ in isoamyl -alcohol under stirring for 24 hours. The product was purified by recrystallization from ethyl acetate. After filtration an orange yellow coloured solid precipitate was collected by filtration, with melting point 243-244℃. Yield 80%.

MS: m/z= 394/396 (72%) $M^{+\cdot}$

^{1}H NMR, 300 MHz, DMSO-d_6: δ= 3.38 ppm (s, 3H) **-**CH_3; δ= 7.02 ppm, (d, ^3J= 7.8 Hz, 1H) H_1; δ= 7.81 ppm, (d, ^3J= 7.8 Hz, 1H) H_2; δ=8.51 ppm, (s, 1H) CH=N; δ=7.70 ppm, (s, 1H) H_4; δ=7.19 ppm, (d, ^3J= 8.1 Hz, 1H) H_6; δ=6.99 ppm, (t, ^3J= 8 Hz,1H) H_7; δ= 7.24 ppm, (t, ^3J= 8 Hz, 1H) H_8; δ=7.08 ppm, (d, ^3J= 8.4 Hz, 1H) H_9, δ= 7.60 ppm, (d, ^3J= 8.1 Hz, 1H) $H_{5'}$; δ= 7.76 ppm, (d, ^3J= 8.1 Hz, 1H) $H_{6'}$; δ= 7.73 ppm, (s, 1H) $H_{2'}$.

4-Chloro-N-((10-methyl-10H-phenothiazin-3-yl)methylene)aniline 4.c.

3-formyl-10-methyl-phenothiazine 1g (4.14mmol) and 4-chloroaniline 0.53g (4.14mmol) were refluxed in ethanol for 6 hours. After filtration an orange yellow coloured solid precipitate with melting point 125℃ was collected. Yield 98%.

MS m/z= 349/401 (100%) $M^{+\cdot}$

^{1}H NMR, 300 MHz, $CDCl_3$: δ= 3.42 ppm (s, 3H) CH_3; δ= 6.82 ppm (d, ^3J= 8.4 Hz, 1H) H_1; δ= 7.63 ppm (d, ^3J= 8.4 Hz, 1H) H_2; δ=8.29 ppm (s, 1H) CH=N; δ=7.70 ppm, (s, 1H) H_4; δ=7.22 ppm (d, ^3J= 7.0 Hz, 1H) H_6; δ=6.98 ppm, (t, ^3J= 7.2 Hz, 1H) H_7; δ= 7.23 ppm (t, ^3J= 7.2 Hz, 1H) H_8; δ=6.85 ppm (d, ^3J= 8.4 Hz, 1H) H_9; δ= 7.35 ppm (d, ^3J= 8.6 Hz, 2H) $H_{2',6'}$; δ= 7.14 ppm, (d, ^3J= 8.6 Hz, 2H) $H_{3',5'}$.

^{13}C NMR, $CDCl_3$ δ ppm**:** 35.6 (-CH_3), 126.9 (C_1), 129.1 (C_2), 130.5 (C_3), 159.2 (C=N), δ= 129.2 (C_4), 122.7 (C_{5a}), 114.5 (C_6), 123.1 (C_7), 123.9 (C_8), 114.5 (C_9), 144.7 (C_{9a}), 144.8 (C_{10a}), 118,5 (C_{4a}) 148.6 (C_1), 127.2 ($C_{2',6'}$), 122.2 ($C_{3'5'}$), 150.6 ($C_{4'}$).

***N,N'*-(10-methyl-10*H*-phenothiazine-3,7-diyl)bis(methan-1yl-1-ylidene)bis (4-methoxyaniline) 5.a.**

3,7-diformyl-10-methyl-phenothiazine 0.5g (1.86mmol) and 4-methoxy-aniline 0.45g (3.7mmol) were refluxed in ethanol under stirring for 16 hours. After filtration an orange yellow coloured solid was obtained, melting point 234℃. Yield 68%.

MS m/z= 479 (100%) $M^{+\cdot}$

^{1}H NMR, 300 MHz, $CDCl_3$: δ= 3.47 ppm (s, 3H) CH_3; OCH_3 δ= 3.85 ppm, (s, 6H); δ= 6.86 ppm, (d, ^3J= 8.4 Hz, 2H) $H_{1,9}$; δ= 7.64 ppm, (d, ^3J= 8.4 Hz, 2H) $H_{2,8}$; δ=8.36 ppm, (s, 2H) CH=N; δ=7.71 ppm, (s, 2H) $H_{4,6}$; δ= 6.94 ppm, (d, ^3J= 8.8 Hz, 4H) $H_{2'2'',6'6''}$; δ= 7.23 ppm, (d, ^3J= 8.8 Hz, 4H) $H_{3'3''5'5''}$.

^{13}C NMR, $CDCl_3$ δ (ppm)**:** 35.9 (-CH_3), 55.5 (-OCH_3); 126.7 ($C_{1,9}$), 128.7 ($C_{2,8}$), 131.6 ($C_{3,7}$), 158.1 (C=N), 122.2 ($C_{4,6}$), 124.4 ($C_{4a,5a}$) 147.2($C_{9a,10a}$) 114.8 ($C_{2'2'',6'6''}$), 148.1 ($C_{1'1''}$), 124.8 ($C_{3'3''5'5''}$), 156.7 ($C_{4'4''}$).

***N,N'*-(10-methyl-10*H*-phenothiazine-3,7-diyl)bis(methan-1yl-1-ylidene)bis (4-bromoaniline) 5.b.**

3,7-diformyl-10-methyl-phenothiazine 0.5g (1.86mmol) and 4-bromoaniline 0.64g (3.72mmol) were refluxed in ethanol was stirred for 10 hours at 78℃.. After filtration an orange yellow coloured solid precipitate was obtained, with melting point 222-224℃. Yield 58%.

MS m/z= 575/577/579 (100%) $M^{+\cdot}$

^{1}H NMR, 300 MHz, $CDCl_3$: δ= 3.49 ppm (s, 3H) CH_3; δ= 6.88 ppm, (d, ^{3}J= 8.4 Hz, 2H) $H_{1,9}$; δ= 7.65 ppm, (d, ^{3}J= 8.4 Hz, 2H) $H_{2,8}$; δ=8.31 ppm, (s, 2H) CH=N; δ=7.72 ppm, (s, 2H) $H_{4,6}$; δ= 7.51 ppm, (d, ^{3}J= 8.6 Hz, 4H) $H_{2',2''6'6''}$,; δ= 7.09 ppm, (d, ^{3}J= 8.6 Hz, 4H) $H_{3'3''5'5''}$.

^{13}C NMR, $CDCl_3$ δ (ppm)**:** 30.9 (-CH_3); 126.9 ($C_{1,9}$), 129,2 ($C_{2,8}$), 131.2 ($C_{3,7}$), 158.9 (C=N), 122.6 ($C_{4,6}$), 118.2 ($C_{4a,5a}$) 144.8 ($C_{9a,10a}$) 114.8 ($C_{2'2'',6'6''}$),147,5 ($C_{1'1''}$), 124.8 ($C_{3'3''5'5''}$), 122.3 ($C_{4'4''}$).

***4,4'*-(10-methyl-10*H*-phenothiazine-3,7-diyl)bis(methan-1yl-1-ylidene)bis(aza-1-yl-1-ylidene)dibenzoic acid 5.c.**

3,7-diformyl-10-methyl-phenothiazine 0.39g (1.4mmol) and p-amino-benzoic acid 0.39g (2.8mmol) in ethyl alcohol was refluxed for 24 hours at 78℃. The product was purified by recrystallization from ethanol. An orange coloured solid precipitate was collected by filtration, with melting point 308℃ (decomp.). Yield 75%.

^{1}H NMR, 400 MHz, DMSO-d6: δ= 3.38 ppm (s, 3H) CH_3; δ= 6.66 ppm, (d, ^{3}J= 8.4 Hz, 2H) $H_{1,9}$; δ= 7.61 ppm, (d, ^{3}J= 8.4 Hz, 2H) $H_{2,8}$; δ=8.30 ppm, (s, 2H) CH=N; δ=7.65 ppm, (s, 2H) $H_{4,6}$; δ= 7.981 ppm, (d, ^{3}J= 7.6 Hz, 4H) $H_{2',2''6'6''}$,; δ= 7.29 ppm, (d, ^{3}J= 7.6 Hz, 4H) $H_{3'3''5'5''}$.

^{13}C NMR, DMSO-d6: δ (ppm)**:** 35.6 (-CH_3); 115.3 ($C_{1,9}$), 120,9 ($C_{2,8}$), 131.2 ($C_{3,7}$), 159 (C=N), 125.8 ($C_{4,6}$), 124.6 ($C_{4a,5a}$), 147.8, 143.1 ($C_{9a,10a}$), 130.6 ($C_{2'2'',6'6''}$), 138.8 ($C_{1'1''}$), 121.0 ($C_{3'3''5'5''}$), 128.5 ($C_{4'4''}$).

4,4'-methylene*bis*(N-(10*H*-phenothiazin-3-yl)methylene)aniline)-4,4'-methylenedianiline 6

3-formil-10*H*-phenothiazine 0.6g (2.6mmol) and *p,p'*-diamino-diphenyl-methane 0.26g (1.3mmol) in ethyl alcohol was refluxed for 6 hours. The product was filtered and then purified by recrystallization from toluene. A lemon yellow coloured solid precipitate was collected by filtration, with melting point 310℃. Yield 65%. m/z= 616 ($M^{+\cdot}$, rel. int. 100%)

^{1}H NMR, 400 MHz, DMSO-d_6: δ= 3.95 ppm, (s, 2H) –CH_2-; δ= 6.73 ppm, (d, ^{3}J= 8.4 Hz, 2H) H_1; δ= 6.93 ppm, (d, ^{3}J= 8.4 Hz, 2H) H_2; δ=8.36 ppm, (s, 2H) CH=N; δ=7.43 ppm, (s, 2H) H_4; δ=7.51 ppm, (d, ^{3}J= 8.4 Hz, 2H) H_6; δ=6.79 ppm, (t, ^{3}J= 8.4 Hz, 2H) H_7; δ= 7.10 ppm, (t, ^{3}J= 8.4 Hz, 2H) H_8; δ=6.70 ppm, (d, ^{3}J= 8 Hz, 2H), H_9; δ= 7.14 ppm, (d, ^{3}J= 8.4 Hz, 4H), $H_{2'2'',6'6''}$; δ= 7.25 ppm, (d, ^{3}J= 8.4 Hz, 4H) $H_{3'3'',5'5''}$; δ= 9.01 ppm, (s, 2H) NH.

^{13}C NMR, DMSO-d_6: δ ppm: 114.1 (C_1), 125.2 (C_2), 158.4 (C=N), 126.1 (C_4), δ128.9 (C_6), 122.5 (C_7), 127.7 (C_8), 114.7 (C_9), 144.5 (C_{9a}), 148.3 (C_{10a}), 122.9 (C_{5a}) 123.9 (C_{4a}) 138.7 ($C_{1',1''}$), 121.0 ($C_{2'2'',6'6''}$), 130.6 ($C_{3'3'',5'5''}$), 138.7 ($C_{4',4''}$), 40,9 (CH_2).

ACKNOWLEDGMENTS

Financial support from Roumanian Ministery of Education, Research and Inovation, for Coop. Bil. 40/10.06.08 Ro-Ua is greatly acknowledged.

REFERENCES

1. S. Patai Ed., "The Chemistry of the Carbon-Nitrogen Double Bond", J. Wiley & Sons, London, **1970**.
2. U. Spichiger-Keller, "Chemical Sesors and Biosensors for Medical and Biological Applications", Wiley-VCH, Weinheim, **1998**.
3. E. Jungreis, S. Thabet, "Analytical Applications of Schiff bases", Marcell Dekker, New York, **1969**.
4. N. I. Mohamed, E. Salah, A. Sharif, *E-Journal of Chemistry http://www.e-journals.net,* **2007**, *4* (4), 531.
5. a) Z. Cimerman, Z. Stefanac, *Polyhedron*, **1985**, *4,* 1755; b) N. Galic, Z. Cimerman, V. Tomisic, *Anal*. *Chim*. *Acta*, **1997**, *343*, 135.
6. V.A. Skorodumov, S.V. Zhuravlev, *Russian J. Org. Chem.,* **1965,** *2* (1), 363.
7. D. Simov, Ek.M. Simova, *Doklady Bolgarskoi Akademii Nauk,* **1958**, *11*, 407.
8. M. Jitaru, G. Petrica, L.I. Gaina, C. Cristea, T. Lovasz, I.A. Silberg, *Rev. Roum. Chim.,* **2002**, *47* (3-4), 249.
9. D.S. Belei, I. Ciocoiu, C. Ciocoiu, E. Bacu, *Anal. St. Univ. "Al. I. Cuza" Iasi, Chimie*, **2001**, *9*, 155.
10. L. Gaina, T. Lovasz, I.A. Silberg, C. Cristea, S. Udrea, *Heterocycl. Commun.*, **2001**, *7* (6), 549.
11. W. Kremers, J.W. Steele, *Can. J. Chem.,* **1967**, *45*, 745
12. K. Rehse, T. Siedel, *Arch. Pharm*., **1992**, *325*, 235.
13. W. Jeon, Y. Kwon, J.J. Baek, L.S. Park, E.W. Lee, Y.S. Han, H.T. Kim., *J. Nonlinear Opt. Phys. Mater.*, **2005**, *14* (4), 545.
14. Y.S. Han, S.D. Kim, Y. Kwon, K.H. Choi, L.S. Park, *Mol. Cryst. Liq. Cryst.,* **2006**, *459*, 119.
15. L. Gaina, C. Cristea, C. Moldovan, D. Porumb, E. Surducan, C. Deleanu, A. Mahamoud, J. Barbe and I.A. Silberg, *Int. J. Mol. Sci*., **2007**, *8*, 70.
16. L. Yang, J.K. Feng, A.M. Ren, *J. Org. Chem*., **2005**, *70*, 5987.

STUDIA UNIVERSITATIS BABEŞ-BOLYAI, CHEMIA, LIV, 4, 2009

ON OMEGA POLYNOMIALS OF C_{40n+6} FULLERENES

MARYAM JALALI[a] AND MODJTABA GHORBANI[a]

ABSTRACT. The Omega polynomial is defined as $\Omega(G,x)=\sum_s m\cdot x^s$ where m(G,s) is the number of ops strips of length s. Also, the Sadhana polynomial is defined as $Sd(G,x)=\sum_s m(G,s)\cdot x^{|E|-s}$. This last polynomial has been defined to evaluate the Sadhana index of a molecular graph. In this paper, the Omega and Sadhana polynomials of an infinite family of fullerenes is computed for the first time.

Keywords: Fullerene, Omega and Sadhana Polynomials, Sadhana Index.

INTRODUCTION

Fullerenes are polyhedral molecules, consisting solely of carbon atoms. Fullerenes C_n can be drawn for n = 20 and for all even $n \geq 24$. They have n carbon atoms, 3n/2 bonds, 12 pentagonal and n/2-10 hexagonal faces. The most important member of the family of fullerenes is C_{60} [1, 2].

Let G = (V, E) be a connected bipartite graph with the vertex set V = V(G) and the edge set E = E(G), without loops and multiple edges. Two edges e = (u,v) and f = (x,y) of a graph G are called equidistant if the two ends of one edge show the same distance to the other edge. However, the distance between edges can be defined in several modes, as presented below. The distance from a vertex z to an edge e = (u,v) is taken as the minimum distance between the given point and the two endpoints of that edge [3]:

$$d(z,e)=\min\{d(z,u),d(z,v)\} \quad (1)$$

Then, the edge $e=(u,v)$ is equidistant to $f=(x,y)$ if:

$$d(x,e)=d(y,e) \quad (2)$$

Or the edges e = (u, v) and f = (x, y) are equidistant if:

$$d(x,e)=d(y,e) \text{ and } d(u,f)=d(v,f) \quad (3)$$

[a] *Department of Mathematics, Faculty of Science, Shahid Rajaei Teacher Training University, Tehran, 16785–136, I R. Iran; Ghorbani30@gmail.com; Institute of Nanoscience and Nanotechnology, University of Kashan, Kashan 87317-51167, I. R. Iran*

A second definition for equidistant edges joins the conditions for (topologically) parallel and perpendicular edges [4]:

$$d(v,x) = d(v,y) + 1 = d(u,x) + 1 = d(u,y), \text{ for } \square \text{ edges} \quad (4)$$

$$d(u,x) = d(u,y) = d(v,x) = d(v,y), \text{ for } \perp \text{ edges} \quad (5)$$

Omega Polynomial

Two edges e = (u, v) and f = (x, y) of G are called codistant (briefly: e co f) if they obey the topologically parallel edges relation (4).

For some edges of a connected graph G there are the following relations satisfied [5, 6]:

$$e \text{ co } e \quad (6)$$

$$e \text{ co } f \Leftrightarrow f \text{ co } e \quad (7)$$

$$e \text{ co } f \;\&\; f \text{ co } h \Rightarrow e \text{ co } h \quad (8)$$

though the relation (8) is not always valid.

Let $C(e) := \{f \in E(G); f \text{ co } e\}$ denote the set of edges in G, codistant to the edge $e \in E(G)$. If relation co is an equivalence relation (i.e., all the elements of C(e) satisfy the relations (6) to (8), then G is called a co-graph. Consequently, C(e) is called an orthogonal cut oc of G and E(G) is the union of disjoint orthogonal cuts: $E(G) = C_1 \cup C_2 \cup ... \cup C_k$ and $Ci \cap Cj = Ø$ for $i \neq j$, and $i, j = 1, 2, .., k$. Observe co is a Θ relation, (Djoković-Winkler [7,8], relations (6) to (8)), and G is a co-graph if and only if it is a partial cube [9], as Klavžar correctly stated in a recent paper [10].

If any two consecutive edges of an edge-cut sequence are topologically parallel within the same face of the covering, such a sequence is called an opposite edge strip ops, which is a quasi-orthogonal cut qoc strip. This means the transitivity relation (8) of the co relation is not necessarily obeyed. Any oc strip is an ops but the reverse is not always true.

Let m(G,s) be the number of ops of length s (i.e., the number of cut-off edges) in the graph G; for the sake of simplicity, m(G,s) will hereafter be written as m. The counting polynomials, defined on the ground of ops strips, [3, 5, 11-14] are as follows:

$$\Omega(G,x) = \sum_s m \cdot x^s \quad (9)$$

$$Sd(G,x) = \sum_s m x^{(|E(G)| - s)} \quad (10)$$

In a counting polynomial, the first derivative (in x=1) defines the type of property which is counted:

$$\Omega'(G,1) = \sum_s m \cdot s = e = |E(G)| \quad (11)$$

$$Sd'(G,1) = \sum_s m(|E(G)| - s) = Sd(G) \quad (12)$$

The Sadhana index Sd(G) of a graph G was defined by Khadikar *et al*. [12, 13] while the Sadhana polynomial by Ashrafi *et al*. [14]. From the definition of Omega polynomial, one can obtain the Sadhana polynomial by replacing x^s with $x^{|E(G)|-s}$ in Omega polynomial. Then the Sadhana index will be the first derivative of Sd(G,x) evaluated in x=1 [14]. Our notations are standard as taken from the textbooks and articles on Graph Theory [15-24].

Example 1. Suppose K_n denotes the complete graph on n vertices (see Figure 1). Then we have:

$$\Omega(K_n, x) = \binom{n}{2} x = (1/2)n(n-1)x\,; \quad Sd(K_n, x) = (1/2)n(n-1)x^{(1/2)(n^2-n-2)}$$

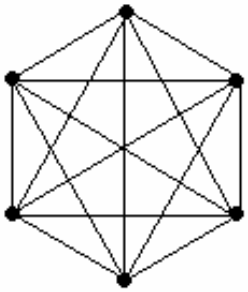

Figure1. Complete graph K_6.

Example 2. Let C_n denotes the cycle of length n. Then we have:

$$\Omega(C_n, x) = \begin{cases} \frac{n}{2}x^2 & 2 \mid n \\ nx & 2 \nmid n \end{cases}; \quad Sd(C_n, x) = \begin{cases} \frac{n}{2}x^{n-2} & 2 \mid n \\ nx^{n-1} & 2 \nmid n \end{cases}.$$

Example 3. Let T_n be a tree on n vertices. We know that $|E(T_n)| = n-1$. Thus, $\Omega(T_n, x) = (n-1)x;\ Sd(T_n, x) = (n-1)x^{n-2}$.

RESULTS AND DISCUSSION

The aim of this section is to compute the counting polynomials of equidistant edges (Omega and Sadhana polynomials) of an infinite family C_{40n+6} of fullerenes with 40n+6 carbon atoms and 60n+9 bonds (the graph in Figure 2 is n = 2).

Theorem. The omega polynomial of fullerene graph C_{40n+6} is as follows:

$$\Omega(G,x)=\begin{cases} a(x)+4x^{2n}+4x^{2n+1}+4x^{4n-1}+2x^{4n} & 5\mid n \\ a(x)+2x^{4n+3}+8x^{2n-2}+2x^{4n+4}+2x^{4n+1} & 5\mid n-1 \\ a(x)+8x^{2n}+4x^{2n-1}+2x^{4n}+2x^{4n+2} & 5\mid n-2 \\ a(x)+4x^{2n-2}+4x^{2n+2}+4x^{4n-1}+2x^{4n+2} & 5\mid n-3 \\ a(x)+4x^{2n-2}+4x^{2n-1}+4x^{2n}+2x^{4n+3}+x^{8n+6} & 5\mid n-4 \end{cases}$$

in which $a(x)=x+9x^2+4x^3+2x^4+(2n-3)x^{10}$.

Proof. By Figure 2, there are ten distinct cases of ops strips. We denote the corresponding edges by e_1, e_2, …, e_{10}. By using Table 1 and Figure 3 the proof is completed.

Corollary. The Sadhana polynomial of the fullerene graph C_{40n+6} is as follows:

$$Sd(G,x)=\begin{cases} b(x)+4x^{|E|-2n}+4x^{|E|-2n-1}+4x^{|E|-4n+1}+2x^{|E|-4n} & 5\mid n \\ b(x)+2x^{|E|-4n-3}+8x^{|E|-2n+2}+2x^{|E|-4n-4}+2x^{|E|-4n-1} & 5\mid n-1 \\ b(x)+8x^{|E|-2n}+4x^{|E|-2n+1}+2x^{|E|-4n}+2x^{|E|-4n-2} & 5\mid n-2 \\ b(x)+4x^{|E|-2n+2}+4x^{|E|-2n-2}+4x^{|E|-4n+1}+2x^{|E|-4n-2} & 5\mid n-3 \\ b(x)+4x^{|E|-2n+2}+4x^{|E|-2n+1}+4x^{|E|-2n}+2x^{|E|-4n-3}+x^{|E|-8n-6} & 5\mid n-4 \end{cases}$$

in which $b(x)=x^{|E|-1}+9x^{|E|-2}+4x^{|E|-3}+2x^{|E|-4}+(2n-3)x^{|E|-10}$

and $|E|=60n+9$.

Table 1. The number of opposite edges of e_i, $1\le i\le 10$.

No.	Number of opposite edges	Type of Edges
1	1	e_1
9	2	e_2
4	3	e_3
2	4	e_4
2n-3	10	e_5

2	$\begin{cases} 2n+1 & 5 \mid n \\ 4n+3 & 5 \mid n-1 \\ 2n & 5 \mid n-4, n-2 \\ 2n+2 & 5 \mid n-3 \end{cases}$	e_6
$\begin{cases} 2 \\ 4 \\ 4 \end{cases}$	$\begin{cases} 4n-1 & 5 \mid n-3 \\ 2n & 5 \mid n, n-2 \\ 2n-2 & 5 \mid n-1, n-4 \end{cases}$	e_7
$\begin{cases} 4 \\ 4 \\ 2 \end{cases}$	$\begin{cases} 2n-2 & 5 \mid n-1, n-3 \\ 2n-1 & 5 \mid n-2, n-4 \\ 4n-1 & 5 \mid n \end{cases}$	e_8
$\begin{cases} 1 \\ 2 \\ 2 \\ 2 \end{cases}$	$\begin{cases} 8n+6 & 5 \mid n-4 \\ 4n+2 & 5 \mid n-3 \\ 4n+4 & 5 \mid n-1 \\ 4n & 5 \mid n, n-2 \end{cases}$	e_9
2	$\begin{cases} 4n-1 & 5 \mid n, n-3 \\ 4n+1 & 5 \mid n-1 \\ 4n+2 & 5 \mid n-2 \\ 4n+3 & 5 \mid n-4 \end{cases}$	e_{10}
2	$\begin{cases} 2n+1 & 5 \mid n \\ 2n & 5 \mid n-2, n-4 \\ 2n+2 & 5 \mid n-3 \end{cases}$	e_{11}

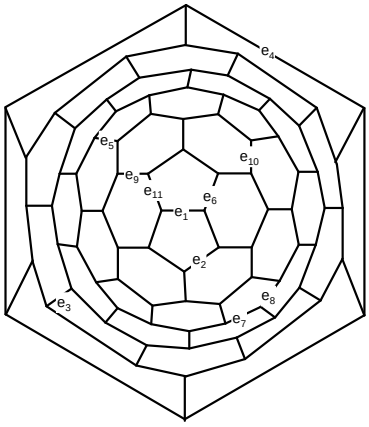

Figure 2. The graph of fullerene C_{40n+6} for n=2.

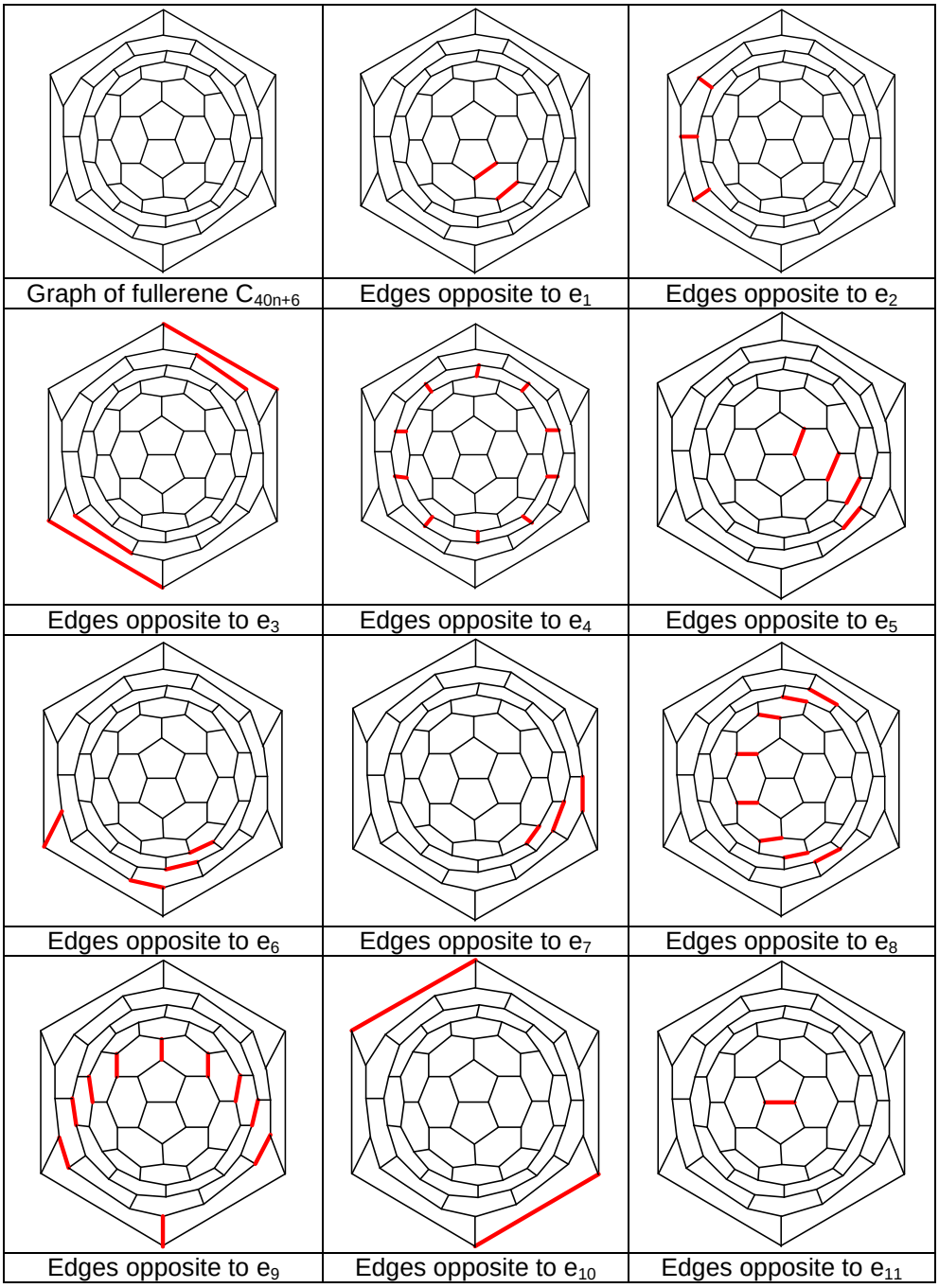

Figure 3. The main cases of opposite edge strips ops in fullerenes C_{40n+6}

CONCLUSIONS

The Omega polynomial was defined by M. V. Diudea in view of counting the opposite edge strips of any length in the graph. He also computed this polynomial for some nanostructures. In this paper, the Omega and the related Sadhana polynomials of an infinite class of fullerenes of formula C_{40n+6} was computed for the first time.

REFERENCES

1. H.W. Kroto, J.R. Heath, S.C. O'Brien, R.F. Curl, R.E. Smalley, *Nature*, **1985**, *318,* 162.
2. H.W. Kroto, J.E. Fichier, D.E. Cox, The Fullerene, Pergamon Press, New York **1993**.
3. M.V. Diudea, S. Cigher, P.E. John, *MATCH Commun. Math. Comput.*, **2008**, *60,* 237.
4. P.E. John, A.E. Vizitiu, S. Cigher, M.V. Diudea, *MATCH Commun. Math. Comput. Chem.*, **2007**, *57,* 479.
5. M.V. Diudea, *Carpath. J. Math.,* **2006**, *22,* 43.
6. M.V. Diudea, S. Cigher, A.E. Vizitiu, O. Ursu, P.E. John, *Croat. Chem. Acta*, **2006**, *79,* 445.
7. D.Ž. Djoković, *J. Combin. Theory Ser. B*, **1973**, *14,* 263.
8. P.M. Winkler, *Discrete Appl. Math.*, **1984**, *8*, 209.
9. S. Ovchinikov, arXiv: 0704.0010v1 math CO. 31 Mar, **2007**.
10. S. Klavžar, *MATCH Commun. Math. Comput. Chem.*, **2008**, *59,* 217.
11. M.V. Diudea, S. Cigher, A.E. Vizitiu, M.S. Florescu and P.E. John, *J. Math. Chem*., **2009**, *45*, 316.
12. P.V. Khadikar, *Nat. Acad. Sci. Letters*, **2000**, *23,* 113.
13. P.E. John, P.V. Khadikar, J. Singh, *J. Math. Chem.*, **2007**, *42,* 37.
14. A.R. Ashrafi, M. Ghorbani and M. Jalali, *Ind. J. Chem.*, **2008**, *47A,* 535.
15. N. Trinajstic, "Chemical Graph Theory", CRC Press, *Boca Raton, FL*, **1992**.
16. A.R. Ashrafi, M. Jalali, M. Ghorbani, M.V. Diudea, *MATCH Commun. Math. Comput. Chem.*, **2008**, *60,* 905.
17. M. Ghorbani, A.R. Ashrafi, *J. Comput. Theor. Nanosci.*, **2006**, *3, 1*.
18. A.R. Ashrafi, M. Ghorbani and M. Jalali, *J. Theor. Comput. Chem.*, **2008**, *7,* 221.
19. A.R. Ashrafi, M. Ghorbani, *MATCH Commun. Math. Comput. Chem.*, **2008**, *60,* 359.
20. M. Ghorbani, and M. Jalali, *Digest Journal of Nanomaterials and Biostructures*, **2008**, *3* (4), 269.
21. M. Ghorbani and M. Jalali, *MATCH Commun. Math. Comput. Chem.*, **2009**, *62*, 353.

22. A.R. Ashrafi, M. Jalali, M. Ghorbani and M.V. Diudea, *MATCH Commun. Math. Comput. Chem.,* 2008, *60* (3), 905.

23. A.R. Ashrafi, M. Ghorbani and M. Jalali, *Digest Journal of Nanomaterials and Biostructures*, **2008**, *3* (4), 245.

24. M. Jalali and M. Ghorbani*, Studia Universitatis Babes-Bolyai, Chemia*, **2009**, *2,* 145.

STUDIA UNIVERSITATIS BABEŞ-BOLYAI, CHEMIA, LIV, 4, 2009

PHENOL REMOVAL FROM WATER USING CARBON AEROGEL AS ADSORBENT

ANDRADA MĂICĂNEANU[a], COSMIN COTEȚ[a], VIRGINIA DANCIU[a], MARIA STANCA[a]

ABSTRACT. This paper presents experimental results obtained in the process of phenol adsorption from synthetic wastewaters in batch conditions using a carbon aerogel (CA) as adsorbent. Influence of the phenol initial concentration and contact type over the process efficiency was studied. The carbon aerogel adsorbent was prepared by polycondensation of resorcinol and formaldehyde followed by drying in supercritical condition with liquid CO_2 and a pyrolysis step. Morpho-structural characteristics of carbon aerogel were investigated using transmission electron microscopy (TEM), scanning electron microscopy (SEM), X-ray diffraction (XRD) and specific surface area determination using nitrogen adsorption (BET method). Obtained carbon aerogel proved to be an efficient adsorbent for phenol from wastewaters. Adsorption efficiencies up to 94.32% were reached.

Keywords: carbon aerogel, phenol, adsorption

INTRODUCTION

The presence of phenol and phenolic compounds in wastewaters can result in the contamination of both surface and ground waters with important negative consequences over the environment. The choice of treatment, in case of wastewaters polluted with phenol and phenolic compounds, depends on the concentration, which can varies from 0.1 to 6800 mg/dm^3 depending on the wastewater source (pulp and paper industry, refineries, coking operations, coal processing) [1], economics, efficiency, easy control and reliability [2].

Adsorption technology is a widely used technique, efficient for the removal of organic pollutants from wastewaters. The most usual adsorbents for organic pollutants removal from wastewaters are activated carbons, which proved to have excellent adsorption capacities [1,3,4]. Due to their high initial cost and the need for an expensive regeneration [3,4] alternative adsorbents or low-cost sources for the preparation of activated carbons were considered. As non-conventional low-cost adsorbents of phenol and phenolic compounds from wastewaters, were tested: (a) natural materials such as clay minerals (raw or modified), siliceous materials (e.g. perlite, dolomite, glasses), zeolites,

[a] *Universitatea Babeş-Bolyai, Facultatea de Chimie şi Inginerie Chimică, Str. Kogălniceanu, Nr.1, RO-400084 Cluj-Napoca, România, andrada@chem.ubbcluj.ro*

apatite, rectorite, attapulgite [3-13]; (b) bioadsorbents such as chitin, chitosan, peat, coal, plants and dead or living microorganisms (bacteria, fungi, yeast, algae) [3,4,14-17]; (c) agricultural and industrial by-product or waste materials (sawdust, rice husk, bark, fly ash, sludge, red mud), [3,4,18-20]. Synthetic zeolites and different type of polymeric resins were also considered as an alternative to activated carbons for phenol adsorption [1,4,21-28]. Activated carbons used as adsorbents for phenol removal can be prepared from solid wastes and coal based materials. Because there are renewable, abundant, inexpensive and require little processing, agricultural wastes are considered to be very important materials in the obtaining of activated carbons. Corn cob, nut shells, apricot stone shell, coffee grounds, coconut shell, olive stones or oil-palm shells are just a few examples of materials that can be transformed in activated carbons [3,4,29-35]. Novel adsorbents such as carbon nanotubes, hybrid xerogels, Mg Al layered double hydroxides, or macromolecule grafted on SiO_2 can be also used to remove phenol form aqueous solutions [36-39].

Due to their high surface area, high open porosity and controllable morpho-structural characteristics, carbon aerogels, could be considered as attractive materials for adsorption of organic pollutants (*e.g.* phenol) from wastewaters [40,41]. These materials can be obtained by carbonization of organic aerogels, which are prepared from the sol–gel polycondensation of certain organic monomers, such as resorcinol and formaldehyde in Na_2CO_3 catalysis [41-43]. The skeletal structure of resulted wet gels is maintained by a supercritical drying with CO_2. Before the pyrolysis process, monolithic solids with high porosity and specific surface areas are obtained.

This paper presents experimental results obtained in the process of phenol adsorption from synthetic wastewaters in batch conditions using a carbon aerogel (CA) as adsorbent. Influence of the phenol initial concentration and contact type over the process efficiency was studied. The morpho-structural characteristics of the carbon aerogel were investigated using transmission electron microscopy (TEM), scanning electron microscopy (SEM), X-ray diffraction (XRD), specific surface area and porosity determinations using nitrogen adsorption-desorption isotherms (BET method).

RESULTS AND DISCUSSION

Carbon aerogel morpho-structural characterization

By TEM (figure 1) and SEM (figure 2) images, the nanostructure and mesoporosity of the carbon aerogel framework are evidenced.

The analysis of XRD patterns shows an amorphous structure for carbon aerogel sample, with two large peaks at about $2\theta = 24^o$ and 44^o (figure 3).

Specific surface area and pore size distribution of the prepared carbon aerogel, were 850 m^2/g and 20-50 nm, respectively.

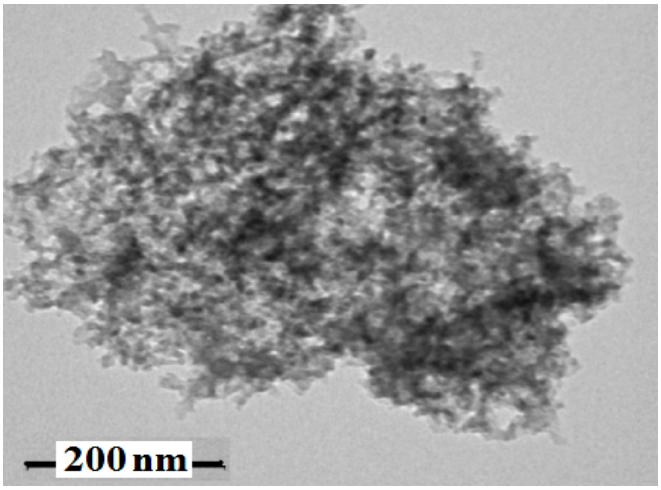

Figure 1. TEM image of the carbon aerogel sample.

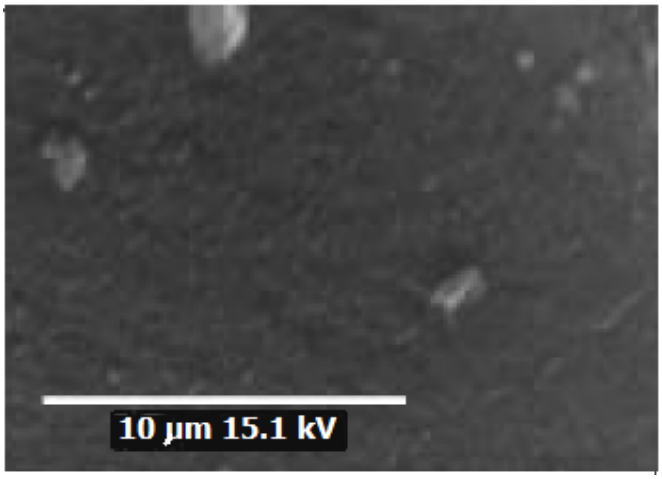

Figure 2. SEM image of the carbon aerogel sample.

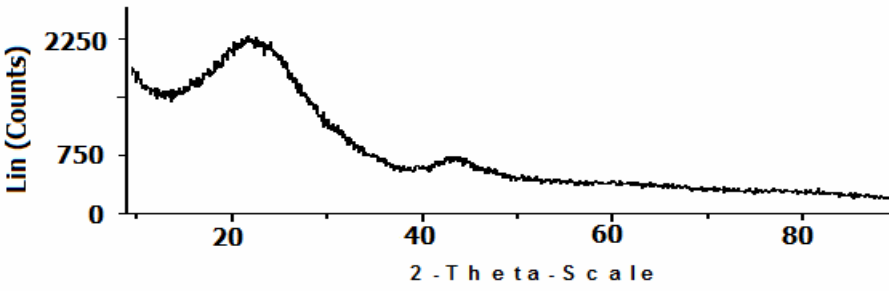

Figure 3. XRD patterns of the carbon aerogel sample.

Phenol adsorption results

Results obtained in case of carbon aerogel (CA) adsorbent and phenolic wastewater as ***immobile phases*** in a batch reactor (static conditions) are presented in figures 4 and 5.

Adsorption efficiency evolutions in time for the three more diluted phenolic wastewaters (5, 10 and 25 mg phenol/L) are presented in figure 4. A slowly increase of the adsorption efficiency is observed in the first 30 minutes reaching to equilibrium. Equilibrium was reached after 30 minutes for all three solutions, while the maximum adsorption efficiency was calculated to be 72.46% for 25 mg/L solution. In case of the two more concentrated phenolic wastewaters, 50 and 100 mg/L, equilibrium was reached in 8 hours, while the adsorption capacity increased with 15% for 100 mg/L solution.

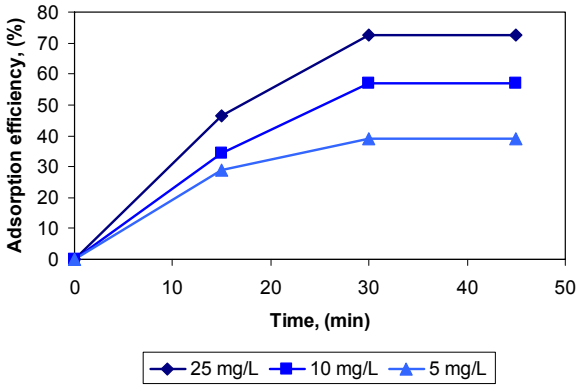

Figure 4. Adsorption efficiency evolution in time during phenol removal process on CA adsorbent (0.1 g), in static conditions, for C_i = 5, 10 and 25 mg phenol/L (100 cm^3).

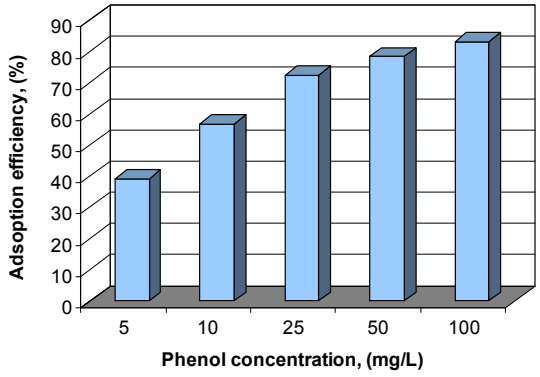

Figure 5. Influence of the initial phenol concentration over the maximum adsorption efficiency, during phenol removal process on 0.1 grams CA adsorbent in static conditions.

Influence of the initial phenol concentration over the maximum adsorption efficiency, during phenol removal process on 0.1 grams CA adsorbent in static conditions is presented in figure 5. It can be observed that with an increase of the initial concentration of phenol, adsorption efficiency increases up to 83.28% which is the maximum value calculated for 100 mg/L solution.

Results obtained in case of carbon aerogel (CA) adsorbent and phenolic wastewater as ***mobile phases*** under magnetic stirring in a batch reactor (dynamic conditions) are presented in figures 6, 7 and 8.

Adsorption efficiencies evolution in time for the two sets of solutions is presented in figures 6 and 7. In case of the more diluted phenolic wastewaters, maximum adsorption efficiency was reached after 10 minutes (equilibrium), with values very close to those obtained after 5 minutes (figure 6). Maximum adsorption efficiency was calculated to be 88.30% for 25 mg/L solution. In case of 50 and 100 mg/L solutions, figure 7, equilibrium was reached slower, after 60 minutes, while adsorption efficiency increased with around 7% for 100 mg/L solution.

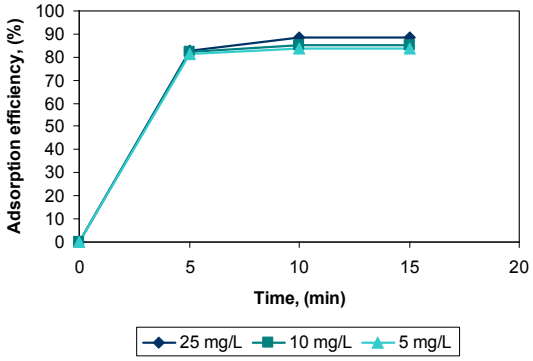

Figure 6. Adsorption efficiency evolution in time during phenol removal process on CA adsorbent (0.1 g), in dynamic conditions, for C_i = 5, 10 and 25 mg phenol/L (100 cm^3).

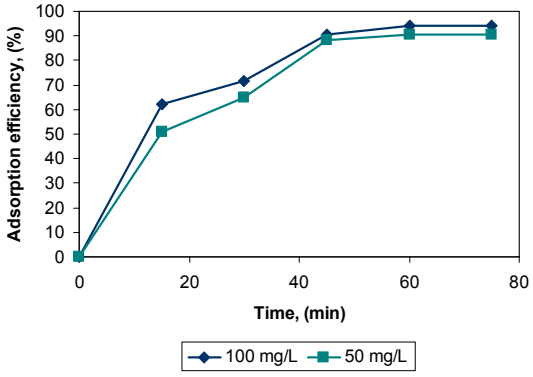

Figure 7. Adsorption efficiency evolution in time during phenol removal process on CA adsorbent (0.1 g), in dynamic conditions, for C_i = 50 and 100 mg phenol/L.

If we compare the maximum adsorption efficiencies calculated for all five initial concentrations, same evolution as in case of static conditions was observed, figure 8. A closer inspection of the adsorption efficiency values lead us to the conclusion that dynamic conditions are more efficient for the adsorption of phenol from synthetic wastewaters, figures 5 and 8, due to the elimination of diffusion limitations.

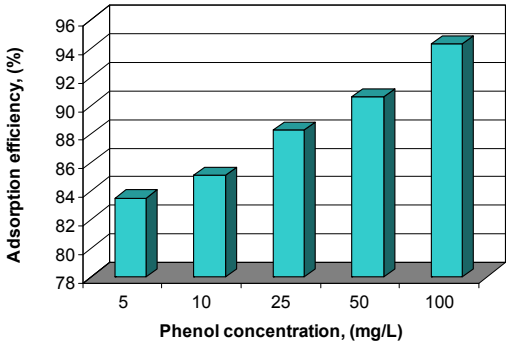

Figure 8. Influence of the initial phenol concentration over the maximum adsorption efficiency, during phenol removal process on 0.1 grams CA adsorbent in dynamic conditions.

EXPERIMENTAL SECTION

Carbon aerogel preparation

Using resorcinol (98% purity), formaldehyde (37% solution), Na_2CO_3 (99.9% purity), all from Aldrich, and deionised water, a resorcinol-formaldehyde wet gel was prepared. Resorcinol (0.29 moles) was dissolved in deionised water at a certain ratio (R/W = 0.2 g/cm^3). Solution of formaldehyde was added to the resorcinol solution (R/F = 0.5) in vigorous stirring. After that, Na_2CO_3 in 0.1 M aqueous solution was added as catalyst (C) to the previous mixture (R/C = 50). The solution was placed into tightly closed glass moulds (7 cm – length $\times$ 1 cm – internal diameter) and cured: 1 day at room temperature, 1 day at 50^{o}C and 3 days at 70^{o}C. The resorcinol-formaldehyde gel obtained in this way was washed with acetone and dried with CO_2 in supercritical conditions, when a resorcinol-formaldehyde aerogel was formed. This organic aerogel was then pyrolysed in N_2 atmosphere for 2 h at 850^{o}C with the formation of the carbon aerogel (CA) [41].

Carbon aerogel morpho-structural investigations

Transmission electron microscopy (TEM) of the metal doped carbon aerogels was performed with a Hitachi H-7000 microscope operating at 125 keV.

Scanning electron microscopy investigation was performed with a JSM-6400 (Scanning Microscope).

X-ray diffraction patterns were recorded in a θ–2θ Bragg–Bretano geometry with a Siemens D5000 powder diffractometer with Cu-K_α incident radiation (λ = 1.5406 Å) and a graphite monochromator.

Specific surface area determinations were performed using Brunauer-Emmett-Teller (BET) method using an ASAP 2000 surface area analyzer (Micrometrics Instruments Corp.). Prior to determination, samples of approximately 0.03 g were heated to 130°C under vacuum (10^{-5} Torr) for at least 18 h to remove all adsorbed species.

Phenol adsorption – working conditions

Phenol adsorption was realised in a batch reactor with adsorbent and phenolic wastewater as immobile phases (static conditions) and with adsorbent and phenolic wastewater under magnetic stirring (dynamic conditions) at room temperature. 0.1 g carbon aerogel, brought at a grain size of d < 250 μm using an appropriate sieve, were contacted with 100 cm^3 synthetic wastewater containing phenol – 5, 10, 25, 50 and 100 mg phenol/L. During the experiment, determination of the organic compounds in solution was carried out every 15 minutes (5, 10, 25 mg phenol/L) and 1 or 3 hours (50, 100 mg phenol/L) in static conditions, and every 5 minutes (5, 10, 25 mg phenol/L) and 15 minutes (50, 100 mg phenol/L) in dynamic conditions until equilibrium was reached. Taking in account the fact that in this stage of the research we were interested to see how this type of material acts as adsorbent for phenol, we used $KMnO_4$ chemical oxygen demand, CCO-Mn, method in order to establish the final concentration of the organics in solution. This determination is currently used in environmental laboratories for wastewaters characterization (STAS 3002/85, SR ISO 6060/96) according to Romanian legislation [44].

The evolution of phenol removal process was followed by means of adsorption efficiency (calculated using chemical oxygen demand values as CCO-Mn at a moment *t* and the initial CCO-Mn value), eq. (1).

$$\mathbf{E_{ads} = \frac{C_i - C_t}{C_i} \cdot 100} \quad (1)$$

where,

C_i is the CCO-Mn initial value, in mg $KMnO_4/dm^3$

C_t is the CCO-Mn value at moment *t*, in mg $KMnO_4/dm^3$.

CONCLUSIONS

A carbon aerogel sample was prepared by polycondensation of resorcinol and formaldehyde followed by drying in supercritical condition with CO_2 and a pyrolysys step. Morpho-structural characterization (TEM, SEM, XRD, BET method) of the prepared carbon aerogel proved that this is a amorphous mesoporous nanomaterial with a high specific surface area.

The influence of the working conditions (static and dynamic) and phenol concentration in wastewater were studied in order to establish their influence over the phenol adsorption process on carbon aerogel. An increase in the concentration and the utilization of the magnetic stirring led to an increase of the adsorption efficiency. Prepared carbon aerogel proved to be an efficient adsorbent for phenol from wastewaters. Adsorption efficiencies up to 94.32% were reached.

Further studies will be performed in order to establish the optimum working conditions for adsorption of phenol using carbon aerogel and also to establish kinetic and adsorption equilibrium models.

ACKNOWLEDGMENTS

Authors would like to thank EU Marie Curie Training Site Grant HPMT-CT-2000-0006, Romanian National University Research Council Grant CNCSIS Td 402/2006-2007, and also to research group of Prof. Elies Molins and Dr. Anna Roig from Institut de Ciencia de Materials de Barcelona (Spain).

REFERENCES

1. G. Busca, S. Berardinelli, C. Resini, L. Arrighi, *Journal of Hazardous Materials*, **2008**, *160*, 265.
2. A. Alejandre, F. Medina, A. Fortuny, P. Salagre, J.E. Sueiras, *Applied Catalysis B: Environmental*, **1998**, *16*, 53.
3. Md. Ahmarizzaman, *Advances in Colloid and Interface Science*, **2008**, *143*, 48.
4. S-H. Lin, R-S. Juang, *Journal of Environmental Management*, **2009**, *90*, 1336.
5. U.F. Alkaram, A.A. Mukhlis, A.H. AlDujaili, *Journal of Hazardous Materials*, **2009**, *169*, 324.
6. A. Bahdoda, S. El Asria, A. Saoiabia, T. Coradinb, A. Laghzizila, *Water Research*, **2009**, *43*, 313.
7. Y. Huang, X. Ma, G. Liang, H. Yan, *Chemical Engineering Journal*, **2008**, *141*, 1.
8. J. Huang, X. Wanga, Q. Jina, Y. Liua, Y. Wangb, *Journal of Environmental Management*, **2007**, *84*, 229.
9. L. Xu, L. Zhu, *Colloids and Surfaces A*, **2007**, *307*, 1.
10. M. Sprynskyy, T. Ligor, M. Lebedynets, B. Buszewski, *Journal of Hazardous Materials*, **2009**, *169*, 847.
11. S. Richards, A. Bouazza, *Applied Clay Science*, **2007**, *37*, 133.
12. Z. Rawajfih, N. Nsour, *Journal of Colloid and Interface Science*, **2006**, *298*, 39.
13. R. Liu, R.L. Frost, W.N. Martens, Y. Yuan, *Journal of Colloid and Interface Science*, **2008**, *327*, 287.

14. H. Polat, M. Molva, M. Polat, *International Journal for Mineral Processing*, **2006**, *79*, 264.
15. H. Cherifia, S. Haninia, F. Bentaharb, *Desalination*, 2009, *244*, 177.
16. A.Y. Dursun, C. Seda Kalayci, *Journal of Hazardous Materials*, **2005**, *B123*, 151.
17. A.E. Navarro, R.F. Portales, M.R. Sun-Kou, B.P. Llanos, *Journal of Hazardous Materials*, **2008**, *156*, 405.
18. A.T. Mohd Din, B.H. Hameed, A.L. Ahmad, *Journal of Hazardous Materials*, **2009**, *161*, 1522.
19. G. Dursun, H. Cicek, A.Y. Dursun, *Journal of Hazardous Materials*, **2005**, *B125*, 175.
20. S.P. Kamble, P.A. Mangrulkar, A.K. Bansiwal, S.S. Rayalu, *Chemical Engineering Journal*, **2008**, *138*, 73.
21. M. Carmona, A. De Lucas, J.L. Valverde, B. Velasco, J.F. Rodrıguez, *Chemical Engineering Journal*, **2006**, *117*, 155.
22. J-H. Huang, K-L. Huang, A-T. Wang, Q. Yang, *Journal of Colloid and Interface Science*, **2008**, *327*, 302.
23. W. Zhang, Q. Dua, B. Pan, L. Lv, C. Honga, Z. Jianga, D. Konga, *Colloids and Surfaces A*, **2009**, *346*, 34.
24. X. Zeng, Y. Fan, G. Wu, C. Wang, R. Shi, *Journal of Hazardous Materials*, **2009**, *169*, 1022.
25. M-C. Xu, Y. Zhou, J-H. Huang, *Journal of Colloid and Interface Science*, **2008**, *327*, 9.
26. B. Pan, B. Pan, W. Zhang, Q. Zhang, Q. Zhang, S. Zheng, *Journal of Hazardous Materials*, **2008**, *157*, 293.
27. P.A. Mangrulkar, S.P. Kamblea, J. Meshramb, S.S. Rayalua, *Journal of Hazardous Materials*, **2008**, *160*, 414.
28. F-Q. Liu, M-F. Xia, S-L. Yao, A-M. Li a, H-S. Wu, J-L. Chen, *Journal of Hazardous Materials*, **2008**, *152*, 715.
29. N. El Hannafi, M.A. Boumakhla, T. Berrama, Z. Bendjama, *Desalination*, **2008**, *223,* 264.
30. B.H. Hameed, A.A. Rahman, *Journal of Hazardous Materials*, **2008**, *160*, 576.
31. Z. Ioannou, J. Simitzis, *Journal of Hazardous Materials*, **2009**, in press, corrected proof, on-line
32. V. Srihari, A. Das, *Desalination*, **2008**, *225*, 220.
33. K.P. Singh, A. Malik, S. Sinha, P. Ojha, *Journal of Hazardous Materials*, **2008**, *150*, 626.
34. D. Richard, M. de Lourdes Delgado Nunez, D. Schweich, *Chemical Engineering Journal*, **2009**, *148*, 1.
35. A.C. Lua, Q. Jia, *Chemical Engineering Journal*, **2009**, *150*, 455.
36. K. Haghbeen, R.L. Legge, *Chemical Engineering Journal*, **2009**, *150*, 1.
37. P.E. Diaz-Flores, F. Lopez-Urıas, M. Terrones, J. R. Rangel-Mendez, *Journal of Colloid and Interface Science*, **2009**, *334*, 124.

38. S. Chena, Z.P. Xub, Q. Zhangc, G.Q. Max Lub, Z.P. Haod, S. Liub, *Separation and Purification Technology*, **2009**, *67*, 194.

39. F. An, B. Gao, *Journal of Hazardous Materials*, **2008**, *152*, 1186.

40. S.A. Al-Muhtaseb, J.A. Ritter, *Advanced Materials,* **2003**, *15*, 101.

41. L.C. Cotet, A. Roig, I.C. Popescu, V. Cosoveanu, E. Molins, V. Danciu, *Revue Roumaine de Chimie*, **200**7, *52*, 1077.

42. R.W. Pekala, US patent 4873218, **1989**.

43. R.W. Pekala, C.T. Alviso, F.M. Kong, S.S. Hulsey, *Journal of Non-Crystalline Solids*, **1992**, *145*, 90.

44. Law 458/2002, 311/2004, 107/1996, 311/2004, 112/2006, HG 188/2002, HG 352/2005.

STUDIA UNIVERSITATIS BABEŞ-BOLYAI, CHEMIA, LIV, 4, 2009

THE DEVELOPMENT OF A MPC CONTROLLER FOR A HEAT INTEGRATED FLUID CATALYTIC CRACKING PLANT

MIHAELA-HILDA MORAR[a] AND PAUL ŞERBAN AGACHI[a]

ABSTRACT. The use of the advanced control techniques is necessary because, now, the PID control is no more competitive in the 20% of the industrial applications when special dynamics are involved. By implementing an advanced control system one can push the process unit to a more profitable region without affecting the operation constraints. In previous works an industrial FCC plant from a Romanian refinery was studied from the point of view of heat integration and steady state performance of the new heat exchanger network (HEN) design. In this study the improvement of the same FCC plant was done by implementing an advanced control scheme capable to maintain stabilized the heat transfer through the plant. Model Predictive Control (MPC) is one of the most used advanced control techniques in process control. A MPC controller was developed for an industrial fluid catalytic cracking (FCC) plant using Aspen HYSYS. The developed MPC controller results enable to establish that the strategy of the advance control imposed is a very efficient one in case of a FCC heat integrated plant.

Keywords: fluid catalytic cracking, heat integration, model predictive control, dynamic state.

INTRODUCTION

Due to its complexity the interest of solving problems related to the FCC process is worldwide spread. There has been a continuous effort to improve the efficiency and yield of the FCC unit during the time. There are many articles that present the problem of the FCC process modeling, simulation and control the most significant being [1] - [12] and just a few articles in which the study is related to the problem of energy integration [15].

The FCC process description is very difficult due to several reasons: the complexity of the chemical reactions mechanism, complex hydrodynamics, strong interaction between the operation of the main reactor and of the regenerator and due to the operation constrains imposed by the new HEN.

The aim of our research was to develop a MPC control scheme capable to control the FCC plant with the new HEN design obtained in a previous

[a] *Universitatea Babeş-Bolyai, Facultatea de Chimie şi Inginerie Chimică, Str. Kogălniceanu, Nr. 1, RO-400084 Cluj-Napoca,Romania, mmorar@chem.ubbcluj.ro*

work [13], [14]. The implementation of a MPC control scheme can provide a high stability of the plant knowing that the heat integration induces more instability in the process.

For reaching the purpose of this research, a FCC plant dynamic simulator was build in Aspen HYSYS using real industrial data related to material fluxes, temperatures, pressures, equipments size and geometry, etc. The data have been provided by a Romanian refinery.

MODEL PREDICTIVE CONTROL

The Model Predictive Control (MPC) is one of the most used advanced control technique in process control. In 1980s it was developed to meet the specialized control needs of power plants and petroleum refineries (ex. [15], [16]). Nowadays, can also be found in a wide variety of application areas like: chemicals, food processing, automotive, aerospace, metallurgy, pulp and paper, etc.

As it can be seen in Figure 1, the main idea of MPC is to choose the control action by repeatedly solving an optimal control problem. Therefore, MPC is based on iterative, finite horizon optimization of a plant model. At time "t", the current plant state is analyzed and a "cost minimizing" control strategy is computed, using a numerical minimization algorithm (Euler-Lagrange numerical method), for a very short time horizon in the future.

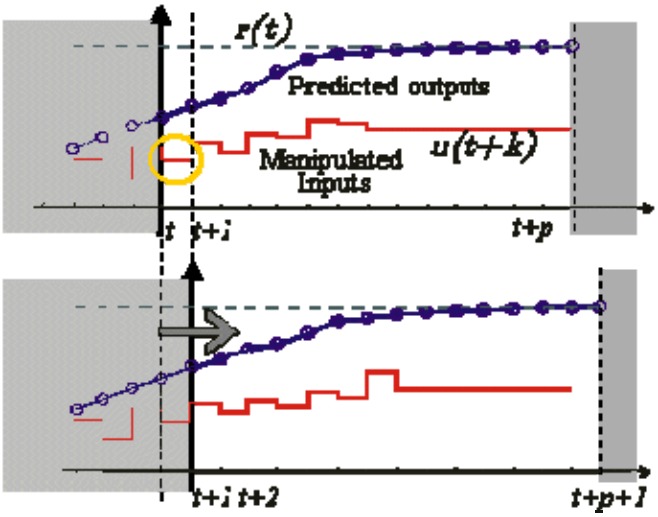

Figure 1. The MPC finite horizon

The MPC is also called receding horizon control because the prediction horizon keeps changing forward.

In Figure 2 the basic structure of MPC is presented. The model predictive control algorithm uses the models and current plant measurements in every moment in time to calculate the future moves for the safety.

Consequently, the process model plays an important role in the controller. The chosen model must be able to catch the process dynamics in order to predict the future outputs with high precision. Also, the model must be simple to be implemented and understood.

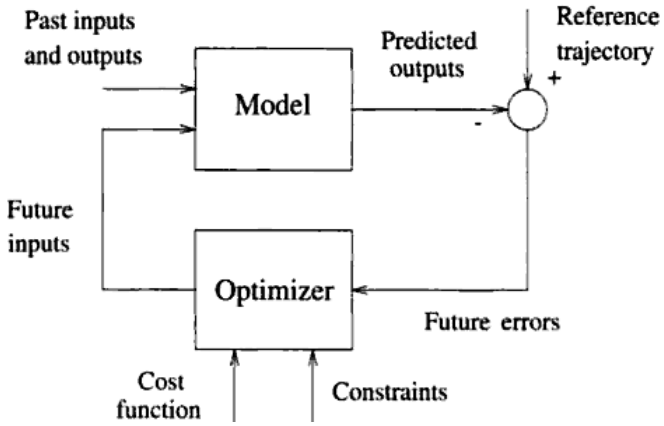

Figure 2. The basic MPC structure [16]

There are many types of models used in different formulations such as truncated impulse response model, step response model, state space model, transfer function model, etc. A typical MPC contains the behavior of multiple Single Input Single Output (SISO) controllers and de-couplers and uses a process model like first order model or step response model.

Comparing with the PID controller, the MPC controller main difference is represented by the necessity to build the process model that has to be implemented in the MPC controller structure.

THE DEVELOPMENT OF THE MPC CONTROLLER

The dynamic simulations performed revealed that only 5 controllers of PID type are necessary in order to obtain a proper stability of the FCC column. The stability of the column is reflected in the quality of heat transfer through the HEN. The development of the MPC controller for controlling the FCC column is based on the data provided by those 5 controllers that were able to settle the FCC column behavior at normal functioning conditions. The PID control scheme of the FCC column is presented in Figure 3.

MPC controller from the Aspen HYSYS object palette allows implementing up to a maximum 12 pairs of controlled variables (CV) and manipulated variables (MV). At the moment, the only MPC Control Algorithm that is implemented in the Aspen HYSYS software is the unconstrained MPC. This algorithm does not consider constraints on either controlled or manipulated variables.

In this case, 5 inputs (process /controlled variable – PV/CV) and 5 outputs (output target objects/manipulated variable – OP/MV) MPC is developed.

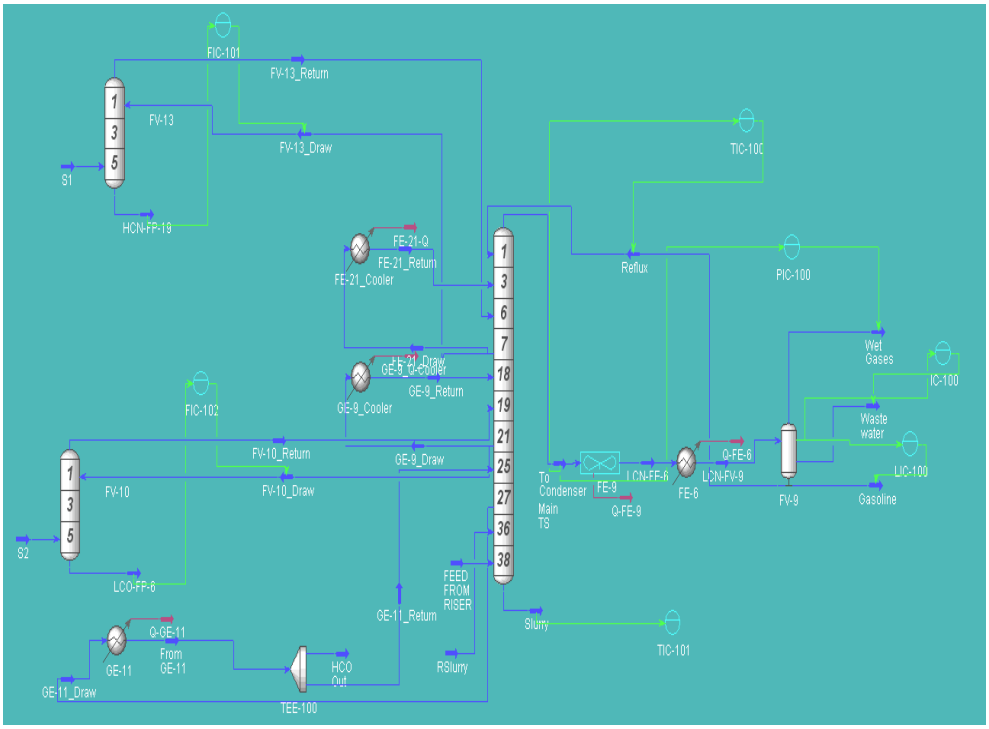

Figure 3. The PID control scheme of the FCC column

The controlled and the manipulated variables are summarized in Table 1.

Table 1. MPC control scheme selected variables

Controlled Variable		Manipulated Variable	
CV1	To Condenser stream temperature	**MV1**	Reflux flow rate
CV2	Condenser Liquid % Level	**MV2**	Gasoline flow rate
CV3	FV-13 bottom HCN flow rate	**MV3**	FV-13 HCN feed flow rate
CV4	FV-10 bottom LCO flow rate	**MV4**	FV-10 LCO feed flow rate
CV5	Slurry temperature	**MV5**	Column recycle slurry flow rate

"To Condenser" stream represents the top column output stream that passes two heat exchangers and enters in the condenser. The FV-10 and FV-13 (see Figure 3) are the side strippers of the FCC column. The stream which represents the bottom product of FV-13 (HCN stripper) is named HCN-FP-19. The stream which represents the bottom product of FV-10 (LCO stripper) is named LCO-FP-6. The Slurry stream is the bottom product of the FCC column.

Having all these specified the way of the MPC strategy implementation is presented as follows.

The Aspen HYSYS has implemented two options to specify the MPC controller model: the Step response model and the First order model. The model used in this case, for the MPC is the First Order model.

The first order model implementation is possible if the process gain (Kp), the process time constant (Tp) and the delay are known. With these process parameters it is possible to obtain the step response matrix necessary to build the internal MPC model.

The identification of those parameters could be realized by developing step response tests for each manipulated variable using the implemented PID control scheme from the dynamic state model. Consequently, a +10% step was used for each manipulated variable and the effect on the controlled variable was registered.

The step response tests provided the process gains, the time constants and the delays necessary for building the MPC controller. These parameters are presented in Table 2.

Table 2. First order model process parameters

MV / CV	MV1	MV2	MV3	MV4	MV5
CV1	Kp = -2.35 T = 2.56 τ = 0	Kp = 0.567 T = 15.66 τ = 0	Kp = -1.5182 T = 45.83 τ = 6.66	Kp = -1.5526 T = 77.083 τ = 0	Kp = -0.9611 T = 16.183 τ = 0
CV2	Kp = -0.15685 T = 3.033 τ = 0	Kp = -0.312 T = 8.33 τ = 0	Kp = -0.068 T = 58.75 τ = 0	Kp = -0.0775 T = 58.583 τ = 0	Kp = -0.0738 T = 20.016 τ = 0
CV3	Kp = -0.2043 T = 29.03 τ = 0	Kp = 0.1147 T = 32.16 τ = 0	Kp = 1.41 T = 0.01 τ = 0	Kp = -0.061 T = 113.5 τ = 7.33	Kp = -0.00456 T = 42.316 τ = 0
CV4	Kp = -0.66 T = 34.783 τ = 0	Kp = 0.39 T = 24.08 τ = 0	Kp = 0.437 T = 21.75 τ = 1.583	Kp = 7.436 T = 0.01 τ = 0	Kp = -0.1452 T = 26.85 τ = 0
CV5	Kp = -0.3741 T = 14.06 τ = 0	Kp = 0.32 T = 12.33 τ = 0	Kp = 0.28 T = 8.916 τ = 0	Kp = 1.156 T = 6.5 τ = 0	Kp = -1.151 T = 4.28 τ = 0

The process parameters were used to determine the 5x5 MPC step response matrix necessary for implementation of the MPC controller internal model. The dimensions of the generated step response matrix are 50x25.

After establishing the MPC controlled and manipulated variables and after determining the internal MPC model, the MPC controller was implemented in the FCC heat integrated plant dynamic model.

RESULTS AND DISCUSSIONS

The MPC control performances were analyzed in order to verify if the MPC controller was properly developed.

In order to perform the MPC performance analysis, several diagrams were developed in which the colors established for the variables are: red – the setpoint, green – the controlled variable, blue – the manipulated variable.

During the performance analysis it was observed that the MPC controller can not entirely stabilize the LCO-FP-6 flow rate, but the control action is good enough in order to have a proper operation of the HEN. The Figure 4 shows the behavior of the LCO-FP-6 flow over the time.

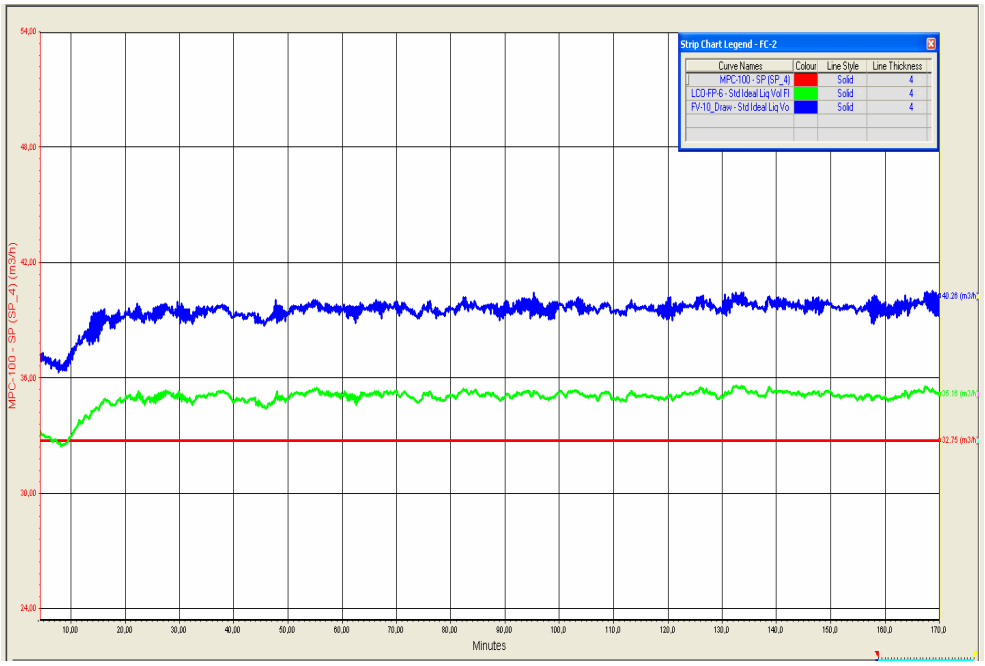

Figure 4. The performance of the LCO FP-6 flow control

As it can be seen in Figure 5, despite the LCO-FP-6 flow variation after stopping the noise amplification, the HCN-FP-19 flow control, which was the most affected by the noise, presents a good behavior and time stability. The HCN-FP-19 stream represents the bottom product stream of the FV-13 side-stripper which enters in the FE-24 heat exchanger.

The MPC control could reach the setpoint from industry for the Slurry temperature meaning that the controller model was successfully developed.

Further analysis regarding the HEN operation suggested that working at the set point value for the slurry temperature destabilizes the heat transfer of the HEN. This because working at the setpoint the quantity of the slurry entering in the HEN is not sufficient enough to sustain an efficient heat transfer as it was imposed in order to have a successfully heat integrated plant. This problem appears, as has been explained before, due to the geometrical data implemented in the FCC column model. Those data are not entirely the one that the real FCC column has. In order to solve the problem with the optimum heat transfer in the HEN, the system was operated near the value of the setpoint which assure the quantity of the slurry needed for an optimum operation of the heat exchangers. In these conditions the slurry temperature is approaching the setpoint and is stabilized at the value of 352^0C as can be seen in Figure 6.

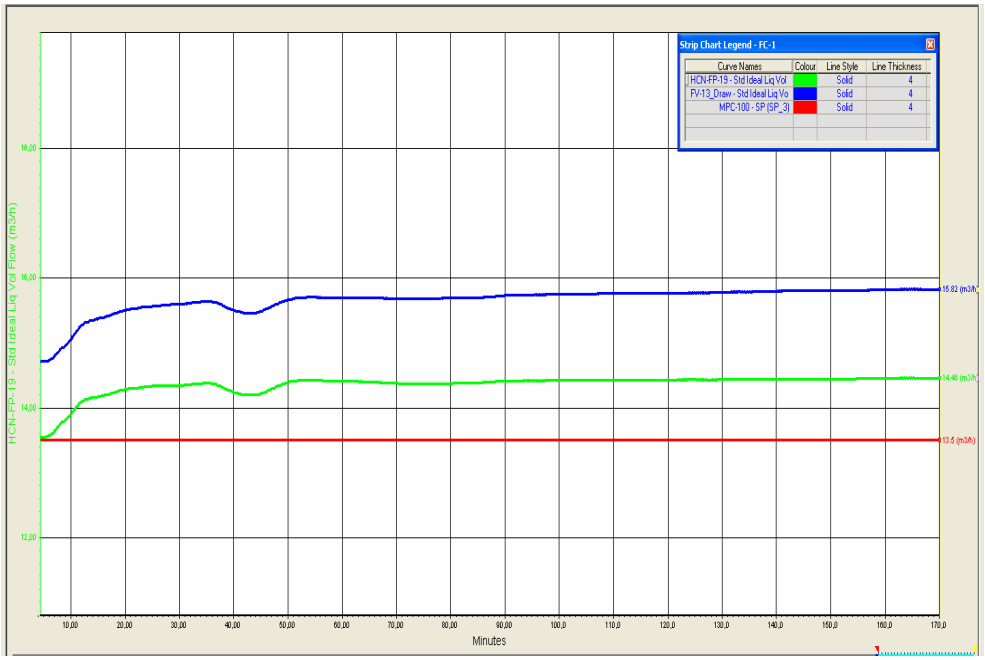

Figure 5. The performance of the HCN-FP-19 flow control

Beside the negative impact on the heat exchangers, the decreasing of the RSlurry flow rate presents another inconvenience. The role of the RSlurry stream in the column is to cool the effluent vapor stream from the riser that enters at the bottom of the column. If the cooling is not sufficient the column fractionation efficiency decreases considerably. The quality of the column products is compromised. Therefore, it is vital to have sufficient RSlurry quantity to handle the vapors proper cooling.

Consequently, the RSlurry flow control valve was set to the following values: 0% opening – 200.1 m^3/h and 100% opening – 346.8 m^3/h.

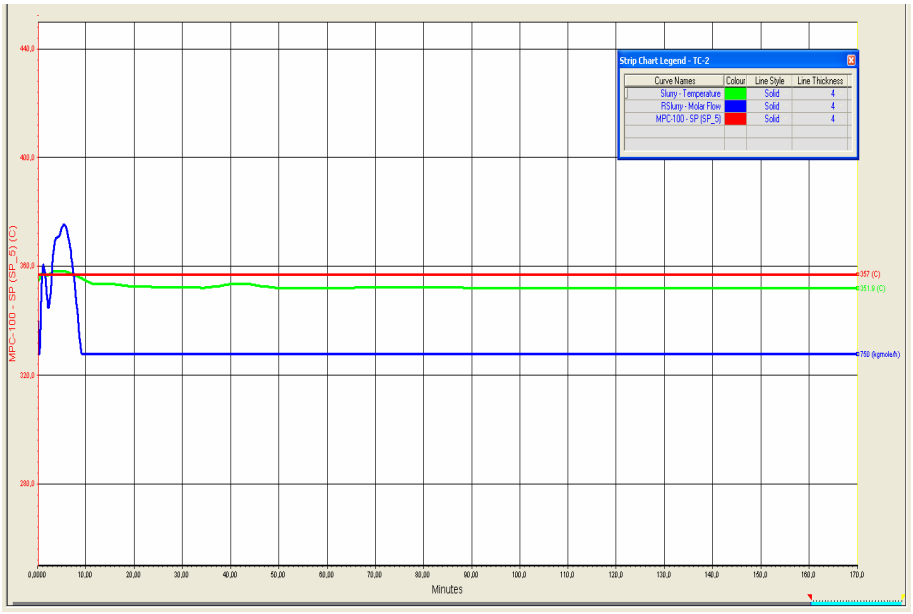

Figure 6. The performance of the Slurry temperature control

However, it is known from the real plant that the range of temperature for the slurry stream, in order to have a proper operation, is 345 – 360^{0}C. This means that the obtained value of the slurry temperature (352^{0}C) is an appropriate one. In these conditions the approach adopted is correct. The goal of maintaining an optimum heat transfer in the HEN has been realized. Another observation is that even if a lower temperature than the setpoint of the slurry stream is used this doesn't affect the heat transfer in the HEN.

Comparing with the PID control, the MPC provides better results in controlling the temperature of the top output stream of the column (To Condenser). The PID temperature controller – TIC-100 achieves the set point after 30 minutes from starting the simulation. Meanwhile, as it can be seen in Figure 7, the MPC controller needs only 10 minutes from the simulation start to attain the setpoint.

Also, better control performance can be observed in controlling the liquid percent level of the FV-9 condenser. The MPC control has faster response than the PID level controller LIC-100 which follows the set point line after 40 minutes. The MPC controller needs only 25 minutes to bring the level at the setpoint. The MPC liquid level control performance is presented in Figure 8.

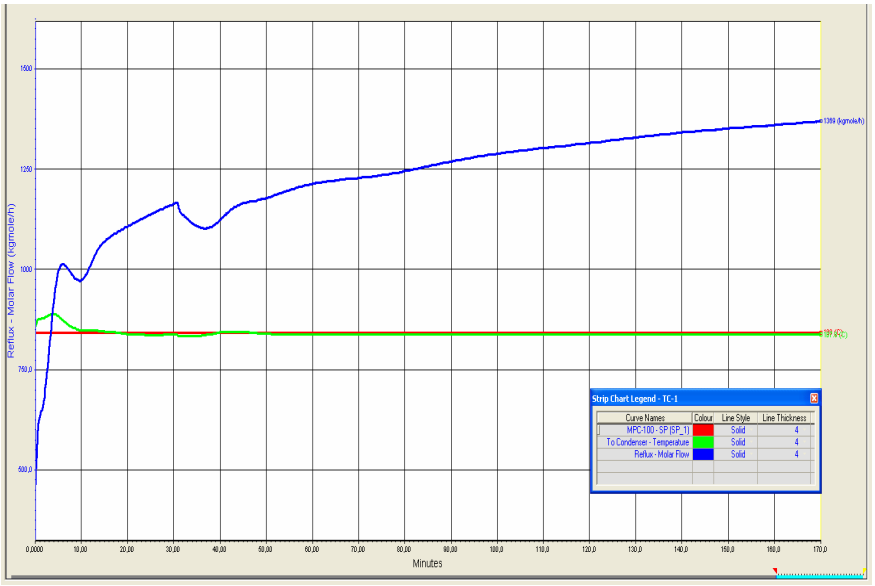

Figure 7. The performance of the temperature control of the column top product

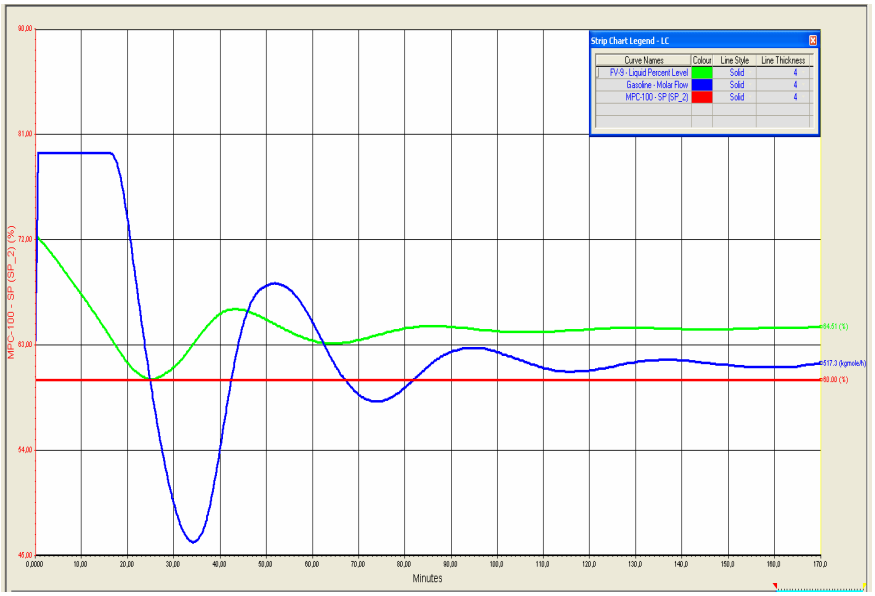

Figure 8. The performance of the condenser liquid percent level control

The liquid level from the condenser can be exactly maintained at 60% neither by PID controller nor by MPC controller because it is dependent on the column calculation of the output streams composition. The level reaches the steady state at around 65%.

The performance analysis of the MPC controller revealed that this controller is very efficient in case of the FCC heat integrated plant model proposed in this research.

CONCLUSIONS

In the last years, the model predictive control (MPC) has become a preferred control strategy for a large number of processes. This advanced control method was developed to meet the specialized control needs especially of the petroleum refineries.

The MPC can decrease the operating costs with approximately 2% - 6% [17] of the existing operating cost related to the real PID control scheme of a real plant because a MPC controller is capable to maintain the variation of the controlled variables much closer to the setpoint than PID controllers. Therefore, the plant is exploited at its maximum capacity.

Comparing with the PID controller, the MPC controller presents the necessity to build a process model. Many types of models such as truncated impulse response model, step response model, state space model, transfer function model, etc. can be used.

Based on the control demands of the heat integrated FCC plant and on the results obtained with PID control strategy, 5x5 MPC controller was developed using the First Order model.

In this case the estimation of model states and parameters is critical. The successful implementation of the MPC controller depends on them.

The identification of the process parameters that are needed for the first order model development (the process gain - Kp, the process time constant - Tp and the delay) was realized by developing step response tests for each manipulated variable.

After the parameter were calculated they were used to build the 5x5 MPC step response matrix necessary for determining the MPC controller internal model. In this way arise a new MPC controller capable to handle the control of the FCC column. The developed MPC controller results enable to establish that the strategy of the advanced control imposed is a very efficient one in case of a FCC heat integrated plant.

Regarding the MPC controller development, the novelty is using an easy method for the internal MPC model development. This method is fast and very useful in implementing an advanced control scheme at industrial scale. The step response tests in the real plant are insecure and costly especially in a continuous process. Any kind of these step control tests are able to compromise the quality of the products and to destabilize the industrial plant followed by undesirable incidents and costs.

LIST OF ABREVIATIONS

CV	controlled variable
FCC	fluid catalytic cracking
HCN	heavy cat naphta
HEN	heat exchanger network
LCO	light cycle oil
MPC	model predictive control
MV	manipulated variable
OP	output target object
PID	proportional-integral-derivative
PV	process variable
SISO	single input single output

REFERENCES

1. A. Arbel, I.H. Rinard, R. Shinnar, *Industrial & Engineering Chemistry Research*, **1996**, *35*, 2215.
2. P. Grosdidier, A. Mason, A. Aitolahti, P. Heinonen, V. Vanhamäki, *Computer and Chemical Engineering*, **1993**, *17*, 165.
3. I.S. Han, C.B. Chung, *Chemical Engineering Science*, **2001**, *56*, 1951.
4. I.S. Han, J.B. Riggs, C.B. Chung, *Chemical Engineering and Processing*, **2004**, *43*, 1063.
5. S.M. Jacob, B. Gross, S.E. Voltz, V.M. Weekman, *AIChE Journal*, **1976**, *22*, 701.
6. H. Kurihara, "Optimal Control of Fluid Catalytic Cracking Processes", PhD. Thesis, MIT, **1967**.
7. E. Lee, F.R. Jr. Groves*, Transactions SOC. Comput. Simulation*, **1985**, *2*, 219.
8. W. Lee, A.M. Kugelman, *Industrial and Engineering Chemistry Process Design and Development*, **1973**, *12*, 197.
9. M. Hovd, S. Skogestad, *AIChE Journal*, **1993**, *39*, 1938.
10. R.C. McFarlane, R.C. Reineman, "Multivariable optimizing control of a model IV fluid catalytic cracking unit", AIChE Spring National Meeting, Orlando, FL., **1990**.
11. R.C. McFarlane, R.C. Reineman, J.F. Bartee, C. Georgakis, *Computer and Chemical Engineering,* **1993**, *17*, 275.

12. V.W. Weekman, D. M. Nace, *AIChE Journal*, **1970**, *16*, 397.
13. E. Jara-Morante, M. Morar, P.Ş. Agachi, Heat integration of an industrial fluid catalytic cracking plant, *Studia Universitatis Babes-Bolyai Chemia*, **2009**, *LIV(1),* 69.
14. M. Morar, P.S. Agachi, *Computer Aided Chemical Engineering*, **2009**, *26*, 465.
15. R.A. Abou-Jeyab, Y.P. Gupta, *Industrial & Engineering Chemistry Research* **1996**, *35*, 3581.
16. A.K. Jana, A.N. Samanta, S. Ganguly, *Computers & Chemical Engineering*, **2009**, *33*, 1484.
17. J.S. Anderson, Process control opportunities and benefits analysis, *Proc. Advanced Control for the Process Industries*, Cambridge, 9-11th Sept., **1992**.
18. A.B. Al-Riyami, J. Klemes, S. Perry, *Applied Thermal Engineering*, **2001**, *21*, 1449.
19. E.F. Camacho, C. Bordons, "Model Predictive Control", Springer-Verlag London, **2004**.
20. P.S. Agachi, Z.K. Nagy, M.V. Cristea, A. Imre-Lucaci, "Model Based Control. Case Studies in Process Engineering", Wiley – VCH, **2008**.
21. N. Alsop, J.M. Ferrer, "Step-test free APC implementation using dynamic simulation", Process Control Spring National Meeting, Orlando, FL, April 24-27, **2006**.
22. A. Kalafatis, K. Patel, M. Harmse, Q. Zheng, M. Craik, *Hydrocarbon Processing*, **2006**, February issue, 93.
23. G.A. Kautzman, W. Korchinski, M. Brown, *Hydrocarbon Processing*, **2006**, October issue.
24. R. Lien, J. Deshmukh, Y. Zhu, "How much can we increase the efficiency of MPC identification?", NPRA Decision Support and Automation Conference, September, San Antonio, **2003**.

STUDIA UNIVERSITATIS BABEŞ-BOLYAI, CHEMIA, LIV, 4, 2009

THE CONSTRUCTION AND CALIBRATION OF A ROTATING VISCOMETER

NICU BORŞ[a], ANDRA TĂMAŞ[b], ZENO GROPŞIAN[b]

ABSTRACT. The paper describes the construction and calibration of a modified Couette rotating rheometer for the study of the hydraulic effects that are specific to the motion in ring-shaped spaces limited by two glass concentric cylinders; the inner cylinder is mechanically driven, the outer one is positioned by the balance which is established between the viscous friction force and the torsion force developed in the elastic muff used for its fixation.The measurement and adjustment of the rotation speed by modulating the frequency of the electric current are presented, as well as the measurement of the torsion moment on the outer cylinder, at different elongation forces and elastic muff thicknesses, in correlation with constructive-functional characteristics.

Keywords: coaxial cylinders, rotational rheometer, sheear rate, shear stress, torsion, viscosity

INTRODUCTION

The liquids rotational motion is especially encountered to the devices working from chemical industry: centrifugal pumps, vessels with stirring, centrifugal separators, some types of evaporators, rotating columns (for absorption, rectification, extraction). The hydrodynamic regime of the flow process is expressed by Reynolds criteria (Re), defined as the ratio of inertia forces to viscous forces, or by Taylor number (Ta), which represents the ratio of centrifugal and viscous forces. The flow characterization in ring-shaped spaces is expressed by the Reynolds-Taylor criteria [1,2] which depends on the cylinders geometry, the liquid nature and the intensity of rotational motion (revolution n, angular velocity Ω):

$$\mathrm{Re}=\frac{n\cdot d^2\cdot\rho}{\eta};\ Ta=\frac{\pi\cdot n\cdot\left(r_o^2-r_i^2\right)\cdot\rho}{\eta};\ Ta_{\mathrm{Re}}=\frac{\Omega\cdot r_i\cdot(r_o-r_i)\cdot\rho}{\eta} \qquad (1\text{-a,b,c})$$

The effect of deformation forces of concentric liquid layers, moving at different velocities, leads to the friction forces appearance that are in direct correlation with the nature of the substance (its viscosity). Determination of

[a] *Dinkelberg Analitics GmbH Germany, nicu.bors@online.de*
[b] *Universitatea "Politehnica"din Timişoara, Facultatea de Chimie Industriala si Ingineria Mediului, P-ta Victoriei Nr.2, RO-300006 Timisoara, andra.tamas@chim.upt.ro*

flow regime, particularly the transient one, has special importance on these forces; their reduction (Toms effect) through the addition of small quantities (ppm) of specific substances (surfactants [3], linear polymers [4-6], fibers), leads to energy consumption decreasing.

The liquids rotational motion is specific to rotational viscometers (Couette, Rheotest and modified Couette) that, alongside rheological characterization, assure the detailed study of the transient regime and the turbulence, defining the Taylor-Couette flow.

The rheometer that was made and tested (modified Couette type) contains two concentric glass cylinders; the inner cylinder is rotated around its axis by an asyncronous electric motor with adjustable rotation speed using a transmission; the outer cylinder is elastically fixed with a rubber tube which allows a partially rotation with a central angle $\Delta\theta$; this angle is the measure of the torsion moment M_t [4]. The rubber tube provides the hydraulic closure of the ring-shaped space where the liquid is introduced to study its rheological behavior. This cylinder is suspended to the upper side through a torsionable thread which assures the centering and controlled straining of the elastic tube-cylinder-thread system [3, 4]. The viscometer's Duran glass cylinders have the following characteristics: height H= 290mm; inner radius r_i= 40mm, outer radius r_o= 42mm, ring-shaped thickness $\Delta r= r_o-r_i$= 2mm; r_o/r_i=1.05.

The driving shaft is provided with a sealing system and a disk for measuring the rotation speed; the entire cylinder system is placed in a controlled temperature environment.

RESULTS AND DISCUSSION

The measurement of the inner cylinder rotation speed

The rotor rotation speed n_r is calculated using equations (2a, b, c) as a function of its slide s as compared with the synchronism rotation n_s determined by the triphasic currents system (p- the number of winding pole pairs):

$$n_r = n_s \cdot (1-s); \qquad s = \frac{n_s - n_r}{n_r}; \qquad n_s = 60 \cdot \frac{\nu}{p}; \tag{2-a,b,c}$$

At synchronism, the shaft will have the rotation speed n_{Ax-s} (eq.3a):

$$n_{Ax-s} = n_s \cdot R_t = 60 \cdot \frac{\nu}{2} \cdot \frac{1}{3} = 10 \cdot \nu; \tag{3a}$$

The real rotation speed of the device shaft n_{Ax} (eq. 3b):

$$n_{Ax} = (1-s) \cdot n_{Ax-s} = 10 \cdot (1-s) \cdot \nu; \tag{3b}$$

The factor f represents the ratio between these two rotation speeds (eq. 4):

$$f = \frac{n_{Ax}}{n_{Ax-s}} = \frac{(1-s)\cdot n_{Ax}}{n_{Ax-s}} = (1-s); \tag{4}$$

By modifying the electric current frequency, the values of the f factor (the ratio between the real and the synchronism rotations) have been experimentally determined, which is shown in Figure 1, both for the no-load situation (without friction to the sealing system) and for the loaded situation. This factor tends to 0.97 (in no-load situation) and 0.9, respectively. The rotation speeds actually used are between 30 and 200 rpm and can be reached for frequencies between 5 and 20Hz (0.65 < f < 0.9).

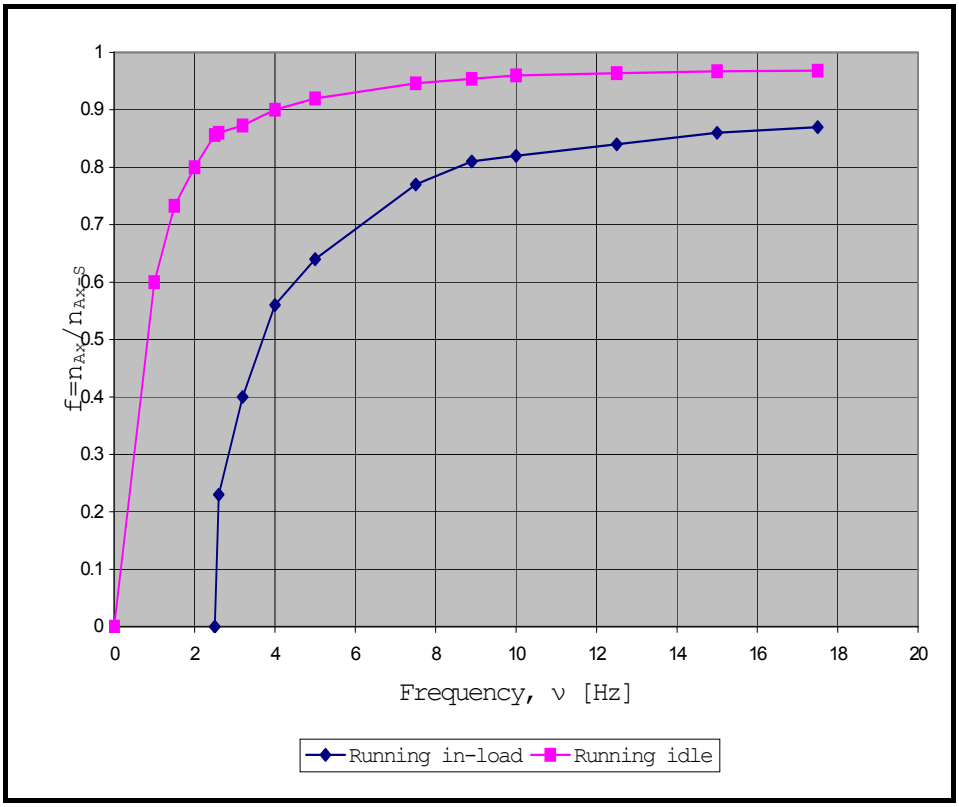

Figure 1. The influence of feed current frequency on the rotation ratio.

Depending on the inner cylinder rotation speed and the geometrical dimensions of the two cylinders, the functional sizes which define the rheological behavior can be calculated (Table 1).

Table 1. Rheometer functional sizes.

Size	General relation	Characteristic relation**
Shear rate, γ [s^{-1}]	$\gamma = \frac{2 \cdot \pi \cdot r_o^2}{r_o^2 - r_i^2} \cdot n$	$\gamma = 67.5 \cdot n$
Shear stress*, τ [Pa]	$\tau = \eta \cdot \gamma$	$\tau = 67.5 \cdot \eta \cdot n$
Friction force, F_f [N]	$F_f = 2 \cdot \pi \cdot H \cdot r_o \cdot \tau$	$F_f = 5.17 \cdot \eta \cdot n$
Torsion moment, M_t [N.m]	$M_t = F_f \cdot r_o$	$M_t = 0.22 \cdot \eta \cdot n$

* For Newtonian fluids: η - dynamic viscosity, $Pa \cdot s$; n - rotation speed, s^{-1}.

** For rheometer dimensions, m : $r_i = 0.04$, $r_o = 0.042$, $H = 0.29$.

The measurement of muff elongation force

The outer glass cylinder is attached to the gasket body by means of a rubber muff with the following characteristics: material – natural rubber/ butadiene-styrene; hardness 40±5 Shore A; inner diameter 90mm; wall thickness 0.5, 1.0 and 1.5mm, muff length 180mm, Figure 2.

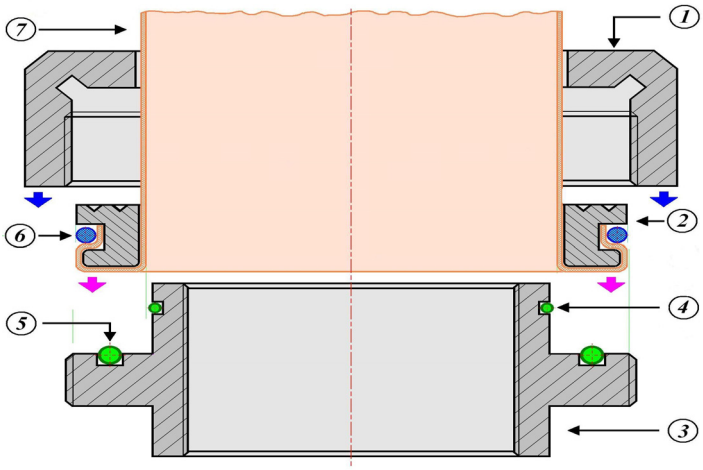

Figure 2. The fitting of rubber elastic muff
1- nut; **2**- aluminium ring; **3**- fixing socket; **4**, **5, 6**- fittings O-Ring; **7**- rubber muff.

The cylinder is suspended to the upper side by means of a torsionable thread which assures the cylinders centering and the control of system straining. The elongation is achieved either using an electric system (stepper motor) or through a screw system.

The measurement of the elongation force is assured by a bimetal force sensor (KD24S type); the obtained results can be locally displayed (digital size) or transmitted to a computer.

The torsion measurement of the outer cylinder

The torsion measurement of the outer cylinder is achieved by using a linear measure magnetic system, without contact, composed of a magnetic belt fixed on the outer surface of an aluminium disk, solidary fitted with the outer cylinder and a magnetic sensor fixed on the viscometer body to a distance between 0.1 and 2mm in comparison with the magnetic tape.

The magnetic belt moving in front of the sensor generates impulses that can be counted (experimentally was obtained 224.4 impulses/rotation or 0.028 radian/impulse). The correlation between the torsion angle of the outer cylinder $\Delta\theta$ and the torsion moment M_t was achieved using two torsion balances (Figure 3a, b) for different elongation forces and thicknesses of the elastic muff. The results are shown in Figure 4a, b, c.

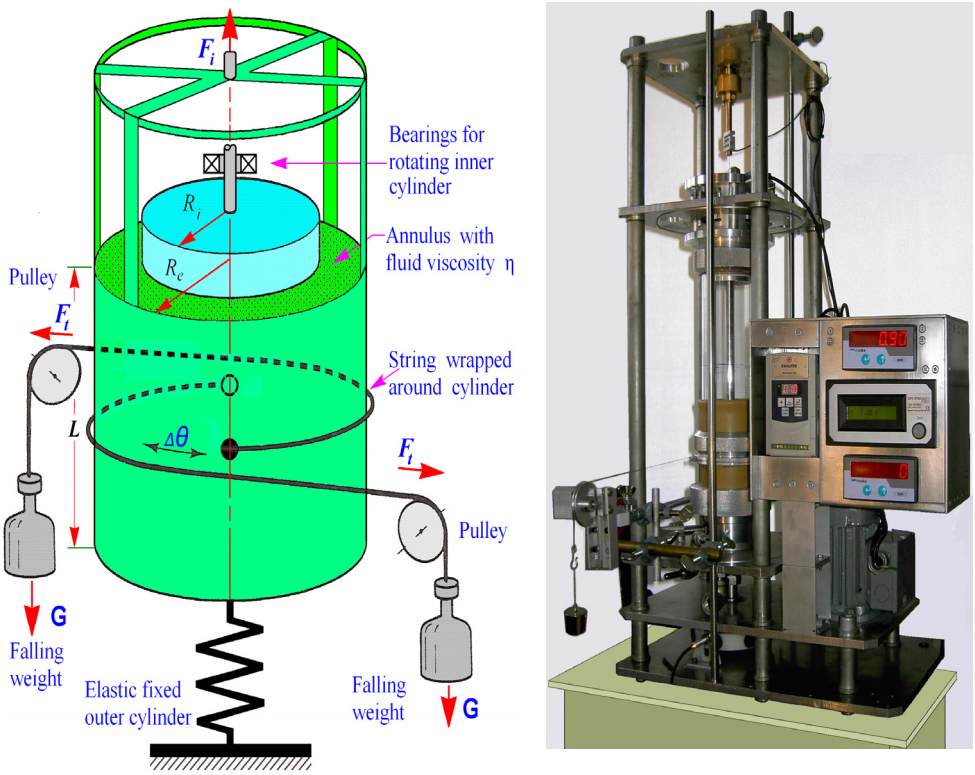

Figure 3a, b. The torsion measurement of the outer cylinder.

From these pictures presented it is found that an increase of muff thickness assures a better stability against the elongation force modification (Figure 4a and 4b), as well as a good linearity (Figure 4c).

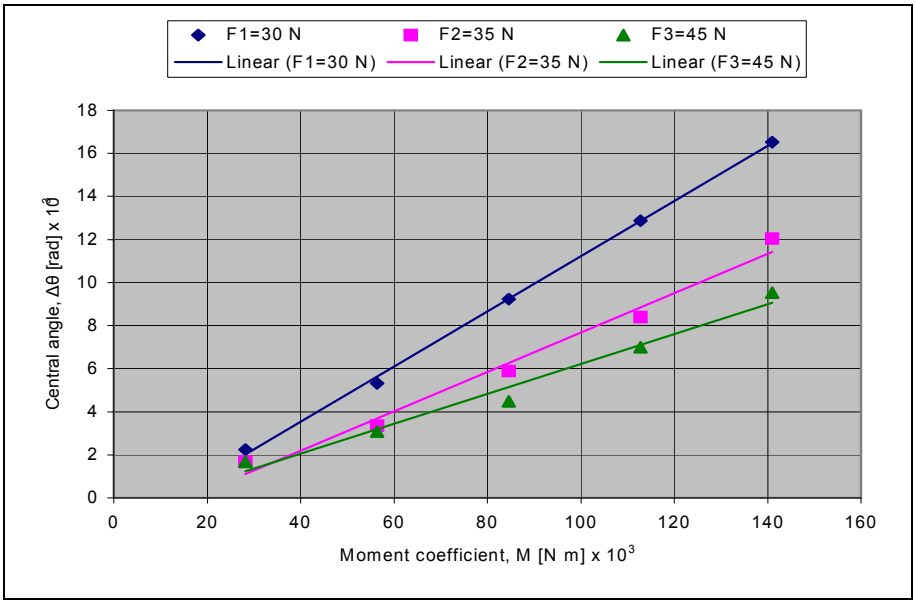

Figure 4a. $\Delta\theta = f(M_t)$ dependence, at different elongation forces, for δ_m= 1mm.

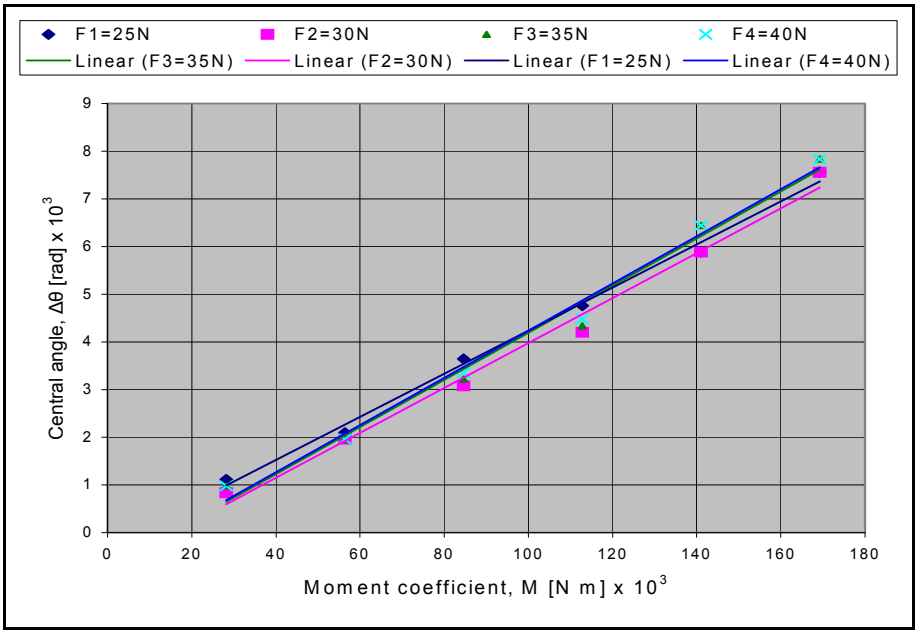

Figure 4b. $\Delta\theta = f(M_t)$ dependence, at different elongation forces, for δ_m= 1.5mm.

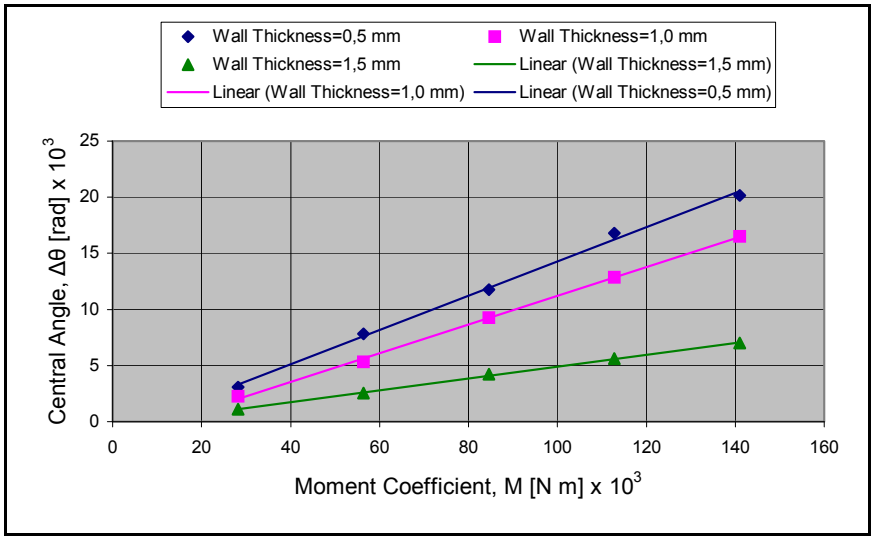

Figure 4c. $\Delta\theta = f(M_t)$ dependence, at different elastic muff thicknesses, for elongation force F= 30N.

CONCLUSIONS

A modified Couette type rotational viscometer with two glass concentric cylinders has been designed and realised.

The rotation speed adjustment is obtained through the electric current frequency modulation; the standardization curve frequency-revolution was experimentally traced;

It was experimentally established the effect of the torsion moment caused by the viscous friction force on the rotation angle of the outer cylinder assembled using an elastic muff.

The correlation between the torsion moment and the rotation angle was determined for different elongation force values and elastic muff thicknesses so as to determine the domain which is nearest to linearity.

EXPERIMENTAL

The rheometer constructive-functional scheme is presented in Figure 5.

The shaft is driven by using an asincron motor with power P= 180W and rotation speed n= 1360 rpm (at 50Hz); the transmission ratio $R_t = 1/3$, frequency domain $1 < \nu < 120Hz$, frequency step $\Delta\nu = 0.1Hz$. It is thus possible to achieve rotation speeds of the inner cylinder $6 < n_{Ax} < 1080$ rpm.

The inner cylinder revolution is measured using an inductive proximity detector; the data are digitally indicated and it is possible to transfer them to a computer.

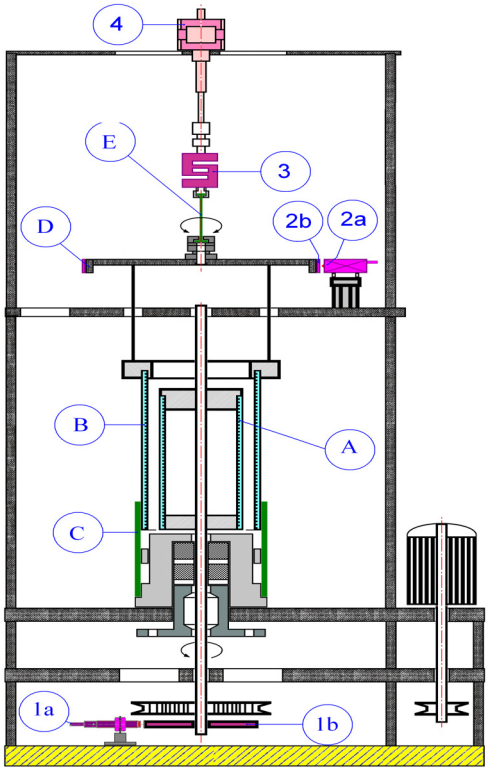

Figure 5. The scheme of experimental device
A- inner cylinder; **B**- outer cylinder; **C**- elastic tube; **D**- device for the free height regulation of the elastic tube; **E**- elongation thread; **1a**- inductive proximity detector IE 5260 (rotation sensor); **1b**- camp late E89010 (accessory to 1a); **2a**- magnetic measurement system for cylinder torsion; **2b**- magnetic tape; **3**- force detector KD24S; **4**- elongation system driven by a stepper motor.

REFERENCES

1. M.A. Couette, *Annales de Chimie et de Physique,* **1890***, 21*, 433.
2. N. Latrache, A. Ezersky, I. Mutabazi, 13th International Couette-Taylor Workshop, Barcelona, July 3-5, **2003**.
3. A. Tamas, N. Bors, R. Minea, *Buletinul Universitatii Petrol-Gaze din Ploiesti,* Seria Tehnica*,* **2008***, LX,* 4B*,* 105.
4. N. Bors, A. Tamas, Z. Gropsian, *Buletinul Stiintific al Universitatii Politehnica Timisoara,* Seria Chimie si Ingineria Mediului, **2008**, *53*, 1-2, 16.
5. J.L. Lumley, *J. Polymer Science, Macromol. Reviews,* **1973**, *7*, 263.
6. A. Gyrand, H.-W. Bewersdorff, “Drag Reduction of Turbulent Flows by Additives”, Kluwer Academic Publishier, Dordrecht, The Nederlands, **1995**.

STUDIA UNIVERSITATIS BABEŞ-BOLYAI, CHEMIA, LIV, 4, 2009

CHEMICAL CONTENTS IDENTIFICATION ON GC-MS FROM SELECTED SPECIES OF MACROMYCETES

DUMITRU RISTOIU[a], EMOKE-DALMA KOVACS[b], MARCEL PÂRVU[b], LUMINIȚA SILAGHI-DUMITRESCU[c]

ABSTRACT. Edible (Xerula radicata), inedible (Russula foetens), semi-edible (Lactarius piperatus) and poisonous mushrooms (Amanita phalloides) were analyzed on gas chromatography-mass spectrometry for its chemical contents. Analysis performed on GC-MS shown a high content of phenolic compounds in these basidiomycete species. Differences between chemical contents with 45 % were observed between young and mature species. Content of selected phallotoxins was determined in Amanita phalloides species.

Keywords: volatile compounds, organic fractions, basidiomycetes, GC-MS

INTRODUCTION

Mushrooms in the division of basidiomycota are worldwide distributed. Four species such as Xerula radicata, Russula foetens, Lactarius piperatus and Amanita phalloides, found in Faget forest, were studied for chemical compounds content.

Edible basidiomycetes such as Xerula radicata, commonly known as the rooting shaker or beech rooter is an edible basidiomycete fungus of the genus Xerula. As many researches shown, *Xerula radicata* is appreciated due to its medicinal properties as antihypertensive effects due to contain oudenone ((S)-2-[4,5-dyhydro-5-propyl-2-(3H)-furylidene]), an antihypertensive molecule. This molecule is a fungal metabolite and was reported as a strong inhibitor of catecholamine biosynthesis, inhibiting the enzymes phenylalanine and tyrosine hydroxylase (1). Different study has shown that the physiological effect of this enzyme inhibition is the reduction of blood pressure (2). Also Xerula radicata has been shown to contain an antibiotic named oudemansin X (E-β-methoxyacrylate oudemansin X, antifungal metametabolite), which lacked antibacterial activity against various organisms tested, but showed a good antifungal activity (3). *Lactarius piperatus* also known as the peppery milk cap is a semi-edible

[a] *Universitatea Babeş-Bolyai, Facultatea de Ştiința Mediului, Str. Fântânele, Nr. 30, RO-400294 Cluj-Napoca,Romania*
[b] *Universitatea Babeş-Bolyai, Facultatea de Biologie si Geologie, Str. Gh. Bilascu, Nr. 44, RO-400015 Cluj-Napoca, Romania*
[c] *Universitatea Babeş-Bolyai, Facultatea de Chimie şi Inginerie Chimică, Str. Kogălniceanu, Nr. 1, RO-400084 Cluj-Napoca, Romania*

(depending on regions from world, for example in Romania this mushroom is consumed by many people) basidiomycete fungus of the genus Lactarius. It's known also to have some antioxidant activity, based on its chemical content (4). *Russula foetens* named also as Fetid russula is an inedible fungus of genus Russula, but recent medical studies shown that due to its polysaccharides content present antitumoral effects (5, 6, 7). As poisonous mushroom, Amanita Phalloides was studied, known also with Death cap name. These species of Amanita genus is a seriously poisonous basodiomycetes fungus, its toxicities is thanks to presence of two main group of toxins such as amatoxins and the phallotoxins, both multicyclic peptides, spread throughout the mushroom tissue (8).

RESULTS AND DISCUSSION

The volatile fractions were obtained from the fresh mushrooms fruiting bodies and analyzed as described in experimental section. The results obtained for the four species studied are presented in table 1.

Table 1. Volatile compounds present in the four basidiomycetes studied (Percent of the total ion current, GC-MS*,**)

Compounds	Xerula r. (%)	Lactarius p. (%)	Russula f. (%)	Amanita ph. (%)
Phenol	0.8	0.9	1.1	2.9
Hexanal	0.5	-	0.4	0.8
2.4-decadienal	-	-	0.2	0.5
2-undecanone	0.1	0.1	0.2	0.2
Acetic acid	1.2	1.1	1.2	2.1
Hydroxy acetic acid	-	-	-	0.1
Hexadecanoic acid	1.1	0.8	0.7	1.3
Hydroxyquinone monopryl ether	0.5	0.4	1.2	2.8
Acetic acid phenyl ether	0.1	0.1	0.5	0.3
Hexadecanoic acid ethyl ester	1.5	1.8	0.9	2.2

*) The ion current generated depends on the characteristics of the compound concerned and is not a true quantification.

**) All matching (as percentages) of mass spectrometry data with literature data were in the range of 83 – 98 %.

The most founded compounds in all mushroom samples were the phenolic compounds. These results in quietly normal, based on the several researches reported in the last decades. They also suggested that the production of phenolic compounds originates from an evolutionary ancestral biochemical shift. Some research sustain that these phenolic compounds may be involved in a chemical mechanism against insects and microorganisms (9).

After the comparison of chemical contents results in each parts of the analyzed mushroom it was observed that in the cap and flesh higher value with 20 – 30 % were determined than in the stem of the same basidiomycete's species. Also for volatile compounds the levels were higher in the young mushrooms species with 15 % than in the mature mushrooms (for the same species), but the content of some organic compounds (such as urea, tyrosine, proline, glycine, resorcinol and catechol) were lower with almost 45 % than in the mature mushrooms as shown in table 2.

Table 2. The main organic fraction constituents in xerula radicata and Lactarius piperatus basidiomycetes as a comparation between young and mature mushrooms (Percent of the total ion current, GC-MS*,**)

Compounds	Xerula r.		Lactarius p	
	Young sp.	***Mature sp.***	***Young sp.***	***Mature sp.***
Urea	3.5	4.9	3.3	5.0
Tyrosine	-	-	-	0.1
Proline	0.3	0.7	0.2	0.5
Glycine	-	0.2	-	-
Resorcinol	0.2	0.3	-	0.2
Catechol	0.3	1.2	0.1	0.4
Valine	-	0.3	-	0.2
Leucine	0.1	0.4	-	-

*) The ion current generated depends on the characteristics of the compound concerned and is not a true quantification.

**) All matching (as percentages) of mass spectrometry data with literature data were in the range of 83 – 98 %.

In Amanita phalloides were also identified α-amanitin, β-amanitin, amanin and amanullin in an average of 0.5 % in mature species. Also compounds such as phalloidin, phalloicin and prophalloin belonging to phallotoxin class, characteristic for these species was determinate in an average of 0.8 % in mature mushrooms.

CONCLUSIONS

The results obtained add new stocks to the knowledge on the chemical composition of the selected species mushrooms belonging basodiomycetes division studied in this work. These dates help to provide further explanation for their reported toxicity or positive medical effects in some health anomaly.

EXPERIMENTAL SECTION

Collection of samples: The four basidiomycetes were collected from Faget forest, near Cluj-Napoca, Romania in June 2009.

Extraction: The fresh fruiting bodies of basidiomycetes were separated as: cap, gills, flesh and stem. All of these parts were cut again in very small species as possible, and from them 10 g from every group was put to leach with trichloromethane for 1 hour in order to establish volatile compounds content for each species of basidiomycetes. Also the same think was done but with ethanol and for 24 hour in order to establish the organic compounds content in each mushroom species. After soak they were extracted with headspace heated ultrasound apparatus (Elmasonic S 10 H) for 1 hour for separate the volatile compounds. The solid phase microextractiom technique was performed on each sample in order to analyze the organic compounds contents from mushroom samples.

Analysis of volatile organic compounds: They were analyzed by gas chromatography with electron capture detector (ECD) and flame ionization detector (FID) with Trace GC Ultra apparatus and DSQ II quadupole mass spectrometry. TR-V1 cyanopropylphenyl polysiloxane based phase capillary column (30 m $\times$ 0.53 mm ID $\times$ 3.0 μm) was used to perform all analysis. The FID detector temperature was set at 300 °C and the ECD detector at 250 °C. The mixture was heated at 80 °C for 30 minutes. The temperature program was programmed from 40 – 220 °C at a rate of 7 °C min^{-1}, and nitrogen was used as carrier gas.

Analysis of organic compounds: They were analyzed on gas chromatography coupled to an guadrupole mass spectrometer (DSQ II – FOCUS GC) with columns Thermo TR-WaxMS (30 m $\times$ 0.25 mm ID $\times$ 0.25 μm). The ion source was set at 270 °C and the ionization voltage at 70 eV. The column temperature program was set from 40 °C with 5 °C min^{-1} to 100 °C, with 3 minutes hold time and after that continued with 10 °C min^{-1} to 280 °C and maintained at this temperature for 7 minutes. Helium was used as carrier gas.

REFERENCES

1. M. Ohno, M. Okamoto, N. Kawabe, H. Umezawa, T. Takeuchi, H. Iinuma, S. Takahash, *Journal of American Chemical Society*, **1971**, *93*(5), 1285.
2. T. Nagatsu, I. Nagatsu, H. Umezawa, T. Takeuchi, *Biochem Pharmacol*, **1971**, *20*(9), 2505.
3. T. Anke, A. Werle, M. Bross, W. Steglich, *Journal of Antibiotics (Tokyo)*, **1990**, *43*(8), 1010.
4. L. Barros, P. Baptista, ICFR Ferreira, *Journal of Food Chem Toxicology*, **2007**, *45*, 1731.
5. S. Ohtsuka, S. Ueno, C. Yoshikumi, F. Hirose, Y. Ohmura, T. Wada, T. Fujii, E. Takahashi, *UK Patent 1331513*, **1973**.
6. XN, Wang, JH. Shen, JC. Du, JK. Liu, *Journal of Antibiotics (Tokyo)*, **2006**, *59*(10), 669.
7. XN. Wang, F. Wang, JC. Du, HM. Ge, RX. Tan, JK. Liu, *Journal of Chemical Science*, **2005**, *60*(10), 1065.
8. J. Vetter, *Journal of Toxicon*, **1998**, *36*(1), 13.
9. A. Del signore, F. Romeo, M. Giaccio, *Mycol Res*, **1997**, *101*, 552.

STUDIA UNIVERSITATIS BABEŞ-BOLYAI, CHEMIA, LIV, 4, 2009

CO-CRYSTALLIZATION OF MERCAPTO-1,3,4-THIADIAZOLE DERIVATIVES WITH *ORTHO*-FUNCTIONALIZED PYRIDINES AND SPECTRAL CHARACTERIZATION IN SOLID STATE

ANDREA E. PASCUI[a], MONICA M. VENTER[a]*, VASILE N. BERCEAN[b]

ABSTRACT. Co-crystallization of 2,5-dimercapto-1,3,4-thiadiazole (DMTD) and (3*H*-2-thioxo-1,3,4-thiadiazol-2-yl)thioacetic acid (H_2L) with *ortho*-functionalized pyridines in 1:1 molar ratio produced three molecular complexes: DMTD·2,2'-bipy (1), H_2L·2,2'-bipy (2) and H_2L·2-H_2NPy (3), respectively. The structure of compounds 1–3 was characterized in solid state by microanalysis and FT-IR, FT-Raman and electronic spectroscopy. The spectral data suggest the formation of proton transfer molecular complexes (1) or association products (2, 3). Acid-base C=O···HN and C=O···HO intermolecular interactions are enphasized for compounds 2 and 3.

Keywords: mercapto-1,3,4-thiadiazole derivatives, co-crystallization, spectroscopy

INTRODUCTION

The co-crystallization products have been also named co-crystals and this term has been extensively used as well as criticized in recent years. There were published different interpretations of its meaning, from common multi-component crystals to multiple crystal systems.[1] The latest interpretation was given by Desiraju[2] who also pointed out the term's ambiguity and recalled that "*(…) it would do one good to remember that we had (and still have) a perfectly good word to describe multi-component crystals, which have specific noncovalent interactions between the distinct molecules, and this is molecular complex".* It is the molecular complex formation and characterization that concerns our present work.

Initially, molecular complexes have been constructed mainly through heteromeric N–H···O, O–H···O and N–H···N hydrogen bonds. Recently, high order systems have been generated through combination of these strong and directional non-covalent connectivities and other interactions, such as halogen-bonding.[3]

[a] *"Babeş-Bolyai" University, Faculty of Chemistry and Chemical Engineering, RO-400028 Cluj-Napoca, Romania. monica@chem.ubbcluj.ro*

[b] *"Politehnica" University, Faculty of Industrial Chemistry and Environment Engineering, RO-300006 Timişoara, Romania.*

Our studies in the field of supramolecular chemistry have focused on heterocyclic thione donors containing at least one thioamide group. Compounds such as 2,4,6-trimercaptotriazine (TMT) or mercapto-1,3,4-thiadiazole derivatives (MTD) proved valuable candidates for building supramolecular structures through hydrogen bonding and S···S interactions.[4,5] In addition, Rao et al. successfully co-crystallized TMT with melamine, tricyanuric acid or 4,4'-bipyridine, engineering channel-type nanostructured crystals. Some of these compounds have proved excellent zeolitic properties.[6-9] In spite of the plethora of publications discussing co-crystallization of organic acids and bases, there are very few reports on molecular complexes containing MTD moieties. For example, there is one crystallographic evidence concerning the co-crystallization ability of MTD compounds and refers to (4,4'-bipyridine)·(5-amino-1,3,4-thiadiazole-2(3*H*)-thione) in 1:2 ratio.[10]

In several of our recent works we reported synthetic procedures and spectral studies on (3*H*-2-thioxo-1,3,4-thiadiazol-2-yl)thioacetic acid, $C_2HN_2S_3CH_2COOH$ (H_2L) and related metal complexes. The neutral H_2L consists of a 2,5-dimercapto-1,3,4-thiadiazole, $C_2H_2N_2S_3$ (DMTD) skeleton extended with one pendant acetic fragment (Fig. 1).

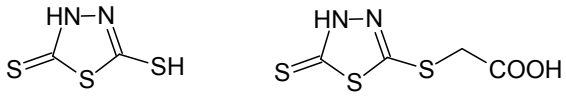

DMTD **H_2L**

Figure 1. Schematic drawing of 2,5-dimercapto-1,3,4-thiadiazole (DMTD) and (3*H*-2-thioxo-1,3,4-thiadiazol-2-yl)thioacetic acid (H_2L).

Both compounds reveal acidic behaviour. Thus, first step deprotonation of DMTD and H_2L leads to monoanions, which have been identified in metal salts and complexes. The remaining proton is located on the nitrogen[11-13] or sulphur atom[14] in the case of DMTD and on the nitrogen atom in the case of H_2L.[15-17] Further deprotonation of the title acids leads to dianions, also present in several metallic derivatives.

The aim of this work is to study the co-crystallization versatility of H_2L by comparison with that of DMTD using 2-aminopyridine (2-H_2NPy) and 2,2'-bipyridyl (2,2'-bipy) as acceptors. Thus, here we report the preparation of three molecular complexes DMTD·2,2'-bipy (**1**), H_2L·2,2'-bipy (**2**) and H_2L·2-H_2NPy (**3**). The co-crystallization ratio was elucidated by microanalysis. Due to the lack of suitable crystals for single-crystal X-ray diffraction, the structure of the molecular complexes (**1**–**3**) and the acid-base association was investigated in solid state by FT-IR, FT-Raman, and electronic spectroscopy. Similar studies on molecular complexes containing acceptors of higher symmetry (i.e. *para*-functionalized pyridines), as well as structural studies in solution are in progress.

RESULTS AND DISCUSSION

Co-crystallization of DMTD and H_2L with 2,2'-bipy and 2-H_2NPy in 1:1 molar ratio, produced three molecular complexes: DMTD·2,2'-bipy (**1**), H_2L·2,2'-bipy (**2**) and H_2L·2-H_2NPy (**3**). All the reactions worked in methanol solution, at room temperature or gentle heating. The products are stable during recrystallization from methanol, except compound **1** which shows traces of decomposition products during purification. All complexes are air and light stable in solid state.

The co-crystallization ability of the acids can be roughly estimated from the difference in pK_a between the conjugate acid of the base and the acid. According to literature, the proton transfer should occur for $\Delta pK_a > 3.75$.[18] Taking into account the pK_a values of DMTD (-1.36 and 7.5)[19] and the pK_b values of 2,2'-bipy (9.5 and 14.1) we can predict a single proton transfer from DMTD to 2,2'-bipy ($\Delta pK_a = 5.8$). Unfortunately, no acidity data could be found for H_2L in order to do similar calculations.

The FT-IR and Raman spectra of DMTD, H_2L and the corresponding molecular complexes **1**–**3** were recorded in solid state, in the 4000–400 and 3500–200 cm^{-1} spectral ranges, respectively. The spectra of the products are presented in Fig. 2. The most relevant spectral data are listed in Table 1 and 2. Assignments of the starting material vibrational modes were made according to literature data.[20-24] The vibrational behaviour of DMTD and related compounds was extensively investigated by F. Hipler et al.[20,21] as both matrix isolated species (IR) and bulk material (Raman). Their assignments support our IR and Raman data recorded for DMTD in solid state. As it concerns the H_2L derivative, we have already reported a brief vibrational characterization[23] and we will use our assignments in further discussions.

DMTD as free and co-crystallized acid: One of the main structural characteristics of DMTD is the co-existence of the thione (HNC=S) and thiol (NC-SH) tautomeric forms in the same molecule, as proved by spectral and crystallographic evidences.[20,21,25] The thione tautomer of DMTD is characterized in the IR and Raman spectra by the assignment of the ν(NH) and δ(NH) vibrational modes. Thus, the IR spectrum of pure DMTD shows a complicated broad feature in the 3200–2700 cm^{-1} spectral range, characteristic for the ν(NH) fundamental of poliazolic heterocycles.[22] However, the assignment of the ν(NH) stretching vibration at 3051 cm^{-1} is in good agreement with literature data.[20,21] The NH group deformation is well represented by the first two thioamide bands: ν(C=N)/δ(NH) (1502 cm^{-1}) and δ(NH) (1450 cm^{-1}). It is worth mentioning that the position and relative intensity of these bands change significantly in the absence of the thione tautomer.

For example, the spectra of the symmetrically S-substituted derivative 2,5-bis(*tert*-butyldithio)-1,3,4-thiadiazole, reveal only the ν(C=N) fundamentals in the 1471–1442 cm^{-1} region.[21]

The IR and Raman spectra of the co-crystallized product (**1**) exhibit the expected ν(NH) modes in the 3075–3042 cm^{-1} spectral range. However, the assignment of these bands to the thiadiazole and/or – in case of proton transfer – to the pyridinium NH groups is ambiguous.

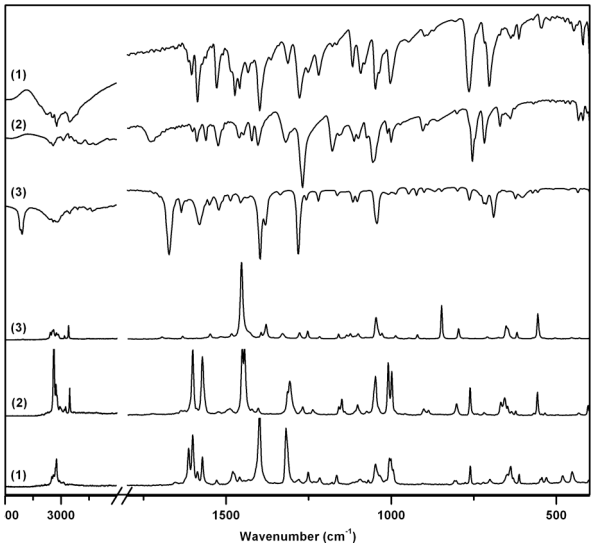

Figure 2. The IR and Raman spectra of DMTD·2,2'-bipy (**1**), H_2L·2,2'-bipy (**2**) and H_2L·2-H_2NPy (**3**).

Table 1. Selected vibrational data (cm^{-1}) for **DMTD** and DMTD·2,2'-bipy (**1**)

DMTD		DMTD·2,2'-Bipy (1)		Vibrational Assignment
IR	**Raman**	**IR**	**Raman**	
3051 s,br	3056 w	3042 s	3040 ms	ν(NH)
2471 m,br	2489 m,br			ν(SH)
		1587 s	1585 m	$\nu(ring)_{Py}$
1502 vs	1512 mw	1528 s	1530 w	ν(CN) / δ(NH)
1450 m	1453 vs	1472 s	1479 m	δ(NH) + $\nu(ring)_{Py}$
		1457 s	1458 w	
1260 vs	1283 mw	1281 s	1281 mw	ν(CN)
1075 mw	1080 m			ν(CS) / δ(SH)
1048 s	1042 m	1047 s	1048 m	ν_{as}(S=C-S)
		1002 s	1006 ms	$\nu(ring)_{Py}$
939 mw	942 w			δ(SH)
		763 s	761 ms	$\delta(CH)_{Py}$
712 s	716 w	703 s	701 w	ν_{as}(CSC)
658 mw	659 vs	640 w	638 ms	ν_s(CSC)

Abbreviations: w – weak, mw – medium weak, m – medium, ms – medium strong, s – strong, vs – very strong, ν - stretching, δ - bending, br – broad, Py – pyridyl ring.

Table 2. Selected vibrational data (cm^{-1}) for **H_2L**, $H_2L{\cdot}2,2'$-bipy (**2**) and $H_2L{\cdot}2\text{-}H_2NPy$ (**3**).

H_2L[23]		$H_2L{\cdot}2,2'$-Bipy (2)		$H_2L{\cdot}2\text{-}H_2NPy$ (3)		Vibrational Assignment
IR	**Raman**	**IR**	**Raman**	**IR**	**Raman**	
				3346 s		$\nu(NH_2)$
3093 ms,br	3103 w	3071 m,br	3070 vs	3070 m	3073 m	$\nu(NH)$
2950 ms	2953 m	2984 mw	2965 w		2975 w	$\nu_{as}(CH_2)$
2903s	2915 s	2926 w	2928 m	2939 mw	2939 m	$\nu_s(CH_2)$
1693 vs	1693 m	1725 m,br	1724 vw	1672 vs	1697 w	$\nu(C=O)$
				1635 m	1634 w	$\delta(NH_2)$
		1587 m	1574 vs	1579 s		$\nu(ring)_{Py}$
		1561 m		1549 mw	1549 mw	
1494 vs	1497 w	1521 m	1522 w	1522 m	1519 vw	$\nu(CN) / \delta(NH)$
		1460 m	1491 w	1487w	1485 w	$\nu(ring)_{Py}$
1448 mw	1453 vs	1449 m	1446 vs	1454 mw	1456 vs	$\delta(NH)$
		1423 m	1443 vs	1434 w		$\nu(ring)_{Py}$
1293 s	1303 w	1269 vs	1270 mw	1281 vs	1279 mw	$\nu(CN)$
1051 vs	1051 s	1057 s	1050 s	10413 s	1048 s	$\nu_{as}(S=C\text{-}S)$
		1002 ms	1001 s	1005 w		$\nu(ring)_{Py}$
		754 s	764 ms	764 m	798 m	$\delta(CH)_{Py}$
724 s	726 w	715 m	719 w	719 m	710 w	$\nu_{as}(CSC)_{endo}$
670 m	678 s	666 mw	670 m	690 s	654 m	$\nu_s(CSC)_{endo}$

Abbreviations: w – weak, mw – medium weak, m – medium, ms – medium strong, s – strong, vs – very strong, br – broad, ν - stretching, δ - bending, endo – endocyclic, Py – pyridyl ring.

The same ambiguity may arise from the assignment of the second thioamide band of the acid in the 1479–1457 cm^{-1} region, due to the closeness of the ν(C=N)/ν(C=C) stretching vibration of the pyridyl ring. On the other hand, the first thioamide band of the co-crystallized DMTD can be clearly located (1528 cm^{-1}) and reveals a positive shift by 26 cm^{-1} when compared to the homologue value of the free acid. This vibrational behaviour may suggest an additional and/or stronger involvement of the NH groups into hydrogen bonding during co-crystallization.[24]

The thiol tautomer of DMTD is characterized in the IR and Raman spectra by the assignment of the ν(SH) and δ(SH) fundamentals. Thus, the spectra of pure DMTD show medium, broad bands assigned to ν(SH) mode at 2489–2471 cm^{-1}. In addition, the SH group deformation can be found in the 1080–1075 and 942–939 cm^{-1} narrow ranges. The IR and Raman spectra of the co-crystallized product (**1**) do not exhibit any of the previously mentioned bands. As a consequence, the acid may be present in the molecular complex either as thione-thione or thione-thiolate tautomer.

H_2L as free and co-crystallized acid: The donor ability of H_2L is governed by the presence of the thiadiazole heterocycle and the carboxylic group of the pendant arm. Similarly to DMTD, the heterocyclic fragment could exist as thione or thiol tautomer but in this case we have proved that the thione tautomeric form settles in solid state.[23] Thus, it was possible to assign the ν(NH) fundamental despite the complicate structure of the broad band (3100–2500 cm^{-1}) produced by the carboxylic OH group vibrations. The same ν(NH) mode was located in the IR and Raman spectra of **2** and **3** around 3070 cm^{-1}, suggesting that the H_2L molecule saves its thione tautomeric form during co-crystallization. In addition, none of the Raman spectra reveals characteristic ν(SH) bands for the free and co-crystallized acid. This structural feature is even more obvious when we analyse the pattern of the first two thioamide bands. The IR spectrum of the pure H_2L shows a very strong ν(C=N)/δ(NH) band (1494 cm^{-1}) and a medium-to-weak δ(NH) band (1448 cm^{-1}). In the corresponding Raman spectrum, the two bands switch relative intensities. This spectral feature is very well reproduced by the IR and Raman spectra of **2** and **3** confirming that the heterocycle remains protonated. In addition, the positive shift of the ν(C=N)/δ(NH) mode in the spectra of **2** and **3** by up to 28 cm^{-1} suggests an additional and/or stronger involvement of the NH groups into intermolecular interactions.[24]

The carboxylic fragment of the pendant chain is best characterized by the ν(C=O) vibrational mode assignment at 1693 cm^{-1} as a very strong IR band. The position of this band is significantly shifted in the spectra of the molecular complexes towards higher wavenumbers by 32 cm^{-1} (**2**) or lower wavenumbers by 21 cm^{-1} (**3**). The negative shift of the ν(C=O) band does not reach the values reported for the related ν_{as}(COO) fundamental (1641–1577 cm^{-1}) in the IR spectra of metallic derivatives containing the acid as carboxylato monanion.[15-17] As a

consequence, the carboxyl group of H_2L saves its protonated form during co-crystallization. According to literature data, the location of the ν(C=O) mode in the approx. 1730–1700 cm^{-1} region may suggest C=O···H-N interactions, while the location in the approx. 1700–1660 cm^{-1} region could be the result of C=O···H-O interactions.[26] However, the IR spectrum of **3** lacks the medium-to-strong, broad band in the 955–915 cm^{-1} range, assigned to the δ_{op}(OH···O) mode in carboxylic acid dimmers.[24]

Ortho-functionalized pyridine acceptors: The IR and Raman spectra of the molecular complexes **1**–**3** show characteristic frequencies for the 2,2'-bipy and 2-H_2NPy acceptors. Among the most important vibrational modes, the ν(ring) and δ(CH) were located in the 1600–1400 and 800 – 750 cm^{-1}, respectively. In addition, the $\nu(NH_2)$ and $\delta(NH_2)$ fundamentals of 2-H_2NPy were found in the expected spectral regions. The positive shift of the $\delta(NH_2)$ modes in the IR spectrum of **3** by 7 cm^{-1} suggests a strengthen of the hydrogen bonds involving this group.[24]

The electronic spectra of the molecular complexes **1**–**3** along with those of the corresponding starting materials were recorded in solid state, in the 200–800 nm spectral range (Fig. 3). The spectra reveal different patterns depending on the nature of the donor acid. Thus, the spectrum of compound **1** consists of a large band which broadens towards visible domain by approx. 100 and 200 nm when compared to the spectra of DMTD and 2,2'-bipy, respectively. Several electronic studies on solutions of molecular complexes and salts containing functionalized pyridinium moieties (i.e. 2- and 4-H_2NPyH^+, 4,4'-bipyH_2^{2+}) have revealed bathochromic shifts of the UV-bands when compared with those of the neutral pyridine derivatives and donor acids.[27-30] Moreover, in the case of pyridine-2,6-bis(monothiocarboxylic) acid · 2-aminopyridine proton transfer complex the electronic spectrum shows the formation of a new peak in the longer wavelength domain besides the red-shift of the expected bands.[27] In this respect, we can afford to suggest that the electronic behaviour of **1** is a result of the proton transfer from DMTD to 2,2'-bipy and the consequent interaction between the resulting charged species.

On the opposite, the spectra of **2** and **3** show no such significant changes in the shape and position of the initial bands. More specific, the spectrum of **2** consists of a large band (200-400 nm) which reveals four peaks at 216, 262, 304 and 355 nm. These peaks meet their correspondence in the spectra of starting materials, except the 304 nm maximum which seams to mediate the 293 nm transition of H_2L and the 319 nm transition of 2,2'-bipy. Similarly, the spectrum of **3** shows a UV band with four broad maximums at 216, 239, 297, 338-357 nm. These values are also comparable with those found for the starting materials, except the 297 nm maximum which is slightly red-shifted by 4 nm.

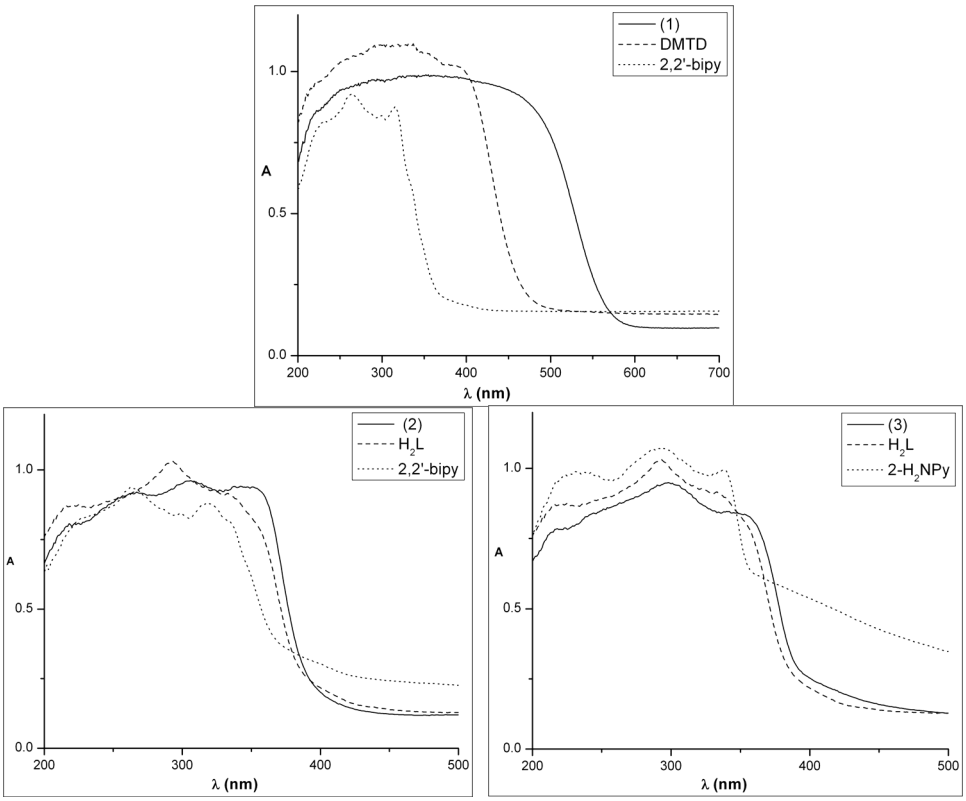

Figure 3. The electronic spectra of DMTD·2,2'-bipy (**1**), H_2L·2,2'-bipy (**2**), H_2L·2-H_2NPy (**3**) and the corresponding starting materials.

CONCLUSIONS

The co-crystallization of DMTD and H_2L with *ortho*-functionalized pyridines in 1:1 molar ratio allows the formation of molecular complexes **1**–**3**.

The vibrational behaviour of DMTD·2,2'-bipy (**1**) is consistent with the thione-thione or thione-thiolato tautomeric form of the DMTD moiety. Taking into account the major bathochromic shift in the electronic spectrum of **1**, as well as the prediction of the ΔpK_a rule, we suggest an ionic structure containing the thione-thiolato DMTD anion and the monoprotonated 2,2'-bipy cation.

The spectral investigation of H_2L·2,2'-bipy (**2**) and H_2L·2-H_2NPy (**3**) clearly shows that these molecular complexes cannot be the result of a proton transfer, but a simple association process. According to the vibrational data, we may predict different acid-base association scenarios for the two compounds (Fig. 4). Thus, for compound **2** N-H···O hydrogen bonding is suggested between the carbonyl and the NH groups of H_2L. This interaction leaves the possibility

of N_{Py}···H-O connections between the base and the acid. The vibrational data of **3** suggests intermolecular O-H···O hydrogen bonding between the carboxyl groups of neighboring acids. Consequently, the most probable acid-base connection could be the N-H··· N_{Py} interaction.

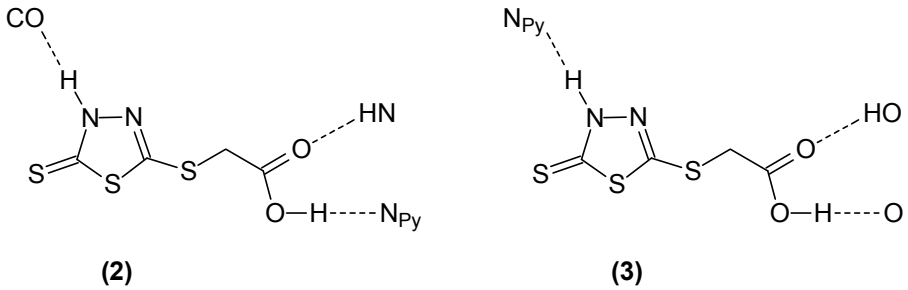

(2) **(3)**

Figure 4. Proposed acid-base association patterns for compounds H_2L·2,2'-bipy (**2**) and H_2L·2-H_2NPy (**3**)

EXPERIMENTAL SECTION

Methods and materials: Elemental analyses were obtained on a VarioEL apparatus from Elementar Analysensysteme GmbH. Melting points (uncorrected) were measured in the 30-360°C range using a KRUSS KSPI digital apparatus. FT-IR and FT-Raman spectra on solid samples were recorded using a Bruker FT-IR Equinox 55 spectrometer with an integrated FRA 106 S Raman module. The excitation of the Raman spectra was performed using the 1064 nm line from a Nd:YAG laser with an output power of 250 mW. An InGaAs detector operating at room temperature was used. FT-IR spectra were also recorded on KBr pellets using a FT-IR JASCO 600 Spectrometer. The spectral resolution was 2 cm^{-1}. Electronic spectra were recorded on solid samples at room temperature, in the 200-800 nm spectral range, using a Jasco V-670 UV/VIS/NIR spectrophotometer.

The starting materials and solvents were purchased from commercial sources (Merck and Reagents Com.) as analytical pure substances and were used with no further purification or drying. The preparation of (3*H*-2-thioxo-1,3,4-thiadiazol-5-yl)thioacetic acid (**H_2L**) was reported elsewhere.[23]

Synthesis: Methanol solutions of donors and acceptors in 1:1 molar ratio were mixed for 30 min. at room temperature (**2** and **3**) or gentle heating (**1**). Compounds **1** and **2** were crystallized from the reaction mixture at low temperature (approx. 5°C). Compound **3** precipitated from the reaction mixture as white powder. Reaction and purification details as well as brief characterization of the products are given bellow:

2,5-Dimercapto-1,3,4-thiadiazole·2,2'-bipyridyl·CH_3OH (1). The product crystallized from the reaction mixture as orange microcrystalline solid of analytical purity. Recrystallization from methanol shows traces of decomposition products. Yield: 0.57 g, 93%; mp: 120-2°C. Microanalysis: found (calc. for $C_{12}H_{10}N_4S_3 \cdot CH_4O$, MW 338.48) C 46.21 (46.13), H 3.91 (4.17), N 16.96 (16.55).

(3*H*-2-thioxo-1,3,4-thiadiazol-2-yl)thioacetic acid·2,2'-bipyridyl·0.25H_2O (2). The product recrystallized from MeOH as colorless fine needles. Yield: 0.57 g, 78%; mp: 118-20°C. Microanalysis: found (calc. for $C_{14}H_{12}N_4O_2S_3 \cdot 0.25H_2O$, MW 368.978) C 45.46 (45.57), H 3.07 (3.41), N 15.20 (15.18).

(3*H*-2-thioxo-1,3,4-thiadiazol-2-yl)thioacetic acid·2-aminopyridine (3). The product recrystallized from hot MeOH as colorless fine needles. Yield: 0.57 g, 93%; mp: 226-30°C (dec.). Microanalysis: found (calc. for $C_9H_{10}N_4O_2S_3$, MW 302.403) C 35.82 (35.75), H 2.87 (3.33), N 18.02 (18.53).

ACKNOWLEDGMENTS

The authors thank The National University Research Council Romania for financial support during the course of this work (Grant CNCSIS-A/2007-2008, 14-25/1449) and the "Babes-Bolyai" University Cluj-Napoca for a Performance Research Fellowship (A.E. Pascui). M.M. Venter thanks Prof.Dr. Mircea Darabantu for useful discussions.

REFERENCES

1. A.D. Bond, *CrystEngComm*, **2007**, *9*, 833.
2. G.R. Desiraju, *CrystEngComm*, **2003**, *5*, 466.
3. C.B. Aakeroy, J. Desper, M Fasulo, I. Hussain, B. Levina, N. Schultheiss, *CrystEngComm*, **2008**, *10*, 1816.
4. V. Bercean, C. Crainic, I. Haiduc, M.F. Mahon, K.C. Molloy, M.M. Venter, P.J. Wilson, *J. Chem. Soc., Dalton Trans*., **2002**, 1036.
5. M.F. Mahon, K.C. Molloy, M.M. Venter, I. Haiduc, *Inorg. Chim. Acta*, **2003**, *348*, 75.
6. A. Ranganathan, V.R. Pedireddi, S. Chatterjee, C.N.R. Rao, *J. Mater. Chem.*, **1999**, *9*, 2407.
7. S. Ahn, J.P. Reddy, B.M. Kariuki, S. Chatterjee, A. Ranganathan, V.R. Pedireddi, C.N.R. Rao, K.D.M. Harris, *Chem.-Eur.J.,* **2005**, *11*, 2433.
8. V.R. Pedireddi, S. Chatterjee, A. Ranganathan, C.N.R. Rao, *J. Am. Chem. Soc.,* **1997**, *119*, 10867.
9. A. Ranganathan, V.R. Pedireddi, C.N.R. Rao, *J. Am. Chem. Soc.,* **1999***, 121*, 1752.
10. Q.-J. Deng, M.-X. Yao, M.-H. Zeng, *Acta Crystallogr.,* **2005***, E61*, o2239.

11. P. Mura, B.G. Olby, S.D. Robinson, *Inorg. Chim. Acta,* **1985***, 97*, 45.
12. H. Tannai, K. Tsuge, Y. Sasaki, O. Hatozaki, N. Oyama *Dalton Trans.,* **2003***,* 2353.
13. V. Wee L. Ng, S.L. Kuan, Z. Weng, W.K. Leong, J.J.Vittal, L.L. Koh, G.K. Tan, L.Y. Goh, *J. Organomet. Chem.,* **2005***, 690*, 2323.
14. P. Mura, S.D. Robinson, *Eur. Cryst. Meeting,* **1982***, 7*, 208.
15. M.M. Venter, V. Chis, S. Cinta Pinzaru, V.N. Bercean, M. Ilici, I. Haiduc, *Studia Univ. Babes-Bolyai, Ser. Chem*., **2006**, *LI(2),* 65.
16. M.M. Venter, A. Pascui, V.N. Bercean, S. Cinta Pinzaru, *Studia Univ. Babes-Bolyai, Ser. Chem.*, **2007**, *LII(1),* 55.
17. M.M. Venter, V.N. Bercean, M. Ilici, S. Cinta Pinzaru, *Rev. Roum. Chim*., **2007**, *52(1-2)*, 75.
18. B.R. Bhogala, S. Basavoju, A. Nangia, *CrystEngComm*, **2005**, *7*, 551.
19. L. Huang, F. Tang, B. Hu, J. Shen, T. Yu, Q. Meng, *J. Phys. Chem. B,* **2001**, *105,* 7984.
20. F. Hipler, R.A. Fischer, J. Müller, *J. Chem. Soc*., *Perkin Trans.,* **2002**, *2*, 1620.
21. F. Hipler, M. Winter, R.A. Fischer, *J. Molec. Struct*., **2003**, *658*, 179.
22. H.G.M. Edwards, A.F. Johnson, E.E. Lawson, *J. Molec. Struct*., **1995**, *351*, 51.
23. M.M. Venter, S. Cinta Pinzaru, I. Haiduc, V. Bercean, *Studia Univ. Babes-Bolyai, Physica*, **2004**, *XLIX(3),* 285.
24. G. Socrates, “Infrared and Raman Characteristic Group Frequencies. Tables and Charts”, 3rd ed., Wiley, Chichester, 2001, chapter 9,10 and 12.
25. J.W. Bats, *Acta Cristallogr.*, **1976**, *B32*, 2866.
26. Z. Gu, R. Zambrano, A. McDermott, *J. Am. Chem. Soc*., **1994**, *116*, 6368.
27. A. Moghimi, S.M. Moosavi, D. Kordestani, B. Maddah, M. Shamsipur, H. Aghabozorg, F. Ramezanipour, G. Kickelbick, *J. Molec. Struct*. **2007**, *828*, 38.
28. B.B. Ivanova, M.G. Arnaudov, H. Mayer-Figge, *Polyhedron*, **2005**, *24*, 1624.
29. B.B. Koleva, T. Kolev, T. Tsanev, S. Kotov, H. Mayer-Figge, R.W. Seidel, W.S. Sheldrick, *J. Molec. Struct*., **2008**, *881*, 146.
30. T. Dorn, C. Janiak, K. Abu-Shandi, *CrystEngComm*, **2005**, *7*, 633.

STUDIA UNIVERSITATIS BABEŞ-BOLYAI, CHEMIA, LIV, 4, 2009

MECHANISTIC STUDY OF SE AND GE SEMICONDUCTORS ELECTRODEPOSITION

BOGDAN TUTUNARU[a], ADRIANA SAMIDE[a], MIRCEA PREDA[a]

ABSTRACT. The electrodeposition and mechanism of nucleation of Se and Se-Ge films was studied in this work. The employed experimental techniques were potentiostatic polarization and chronoamperometry. The initial deposition of Se film by potentiostatic polarization shows that the crystallization potential of -0,40 V and corresponding densities linearly depends on the H_2SeO_3 concentration and potential scan rate. The simultaneous presence of both species in the bath composition produced a new peak at -0,50 V. The chronoamperometric study indicate a 3D complex mechanism for Se and Se-Ge electrodeposition. The morphological changes in surface of working electrode was analysed with an Euromex microscope.

Keywords: Semiconductors, Se and Se_2Ge electrodeposition, nucleation mechanism

INTRODUCTION

Selenium is essential for life when consumption of foods contain 0,1 mg kg^{-1} of this element, and is toxic when dietary levels are above 1 mg kg^{-1} [1]. In the human body, selenium is bond by covalent carbon-selenium bonds and some inorganic selenium salts have powerful cancer chemopreventive effects.

Semiconductors were found that they can replace or compete with monocrystalline materials in photoelectrochemical cells [2]. The photo-induced changes observed in semiconductor compounds are attributed to the amorphous state [3]. Selenium has played an important role in the production of metal selenides (ZnSe, MgSe, FeSe, PbSe, SnSe, CdSe etc.) [4-8]. This kind of compounds presents interesting applications such as optical filters, solar cells, laser materials [9,10].

One of the most adequate method to obtain a thin film of semiconductor or metal-selenide compound is electrodeposition [11]. Selenium electrodeposition is a side reaction in the cathodic synthesis of metal selenides [12].

To our knowledge, electrodeposition of Se-Ge has not been reported in the literature. Hence, we have attempted in the present study to deposit a Se-Ge thin film by electrodeposition.

[a] *Faculty of Chemistry, University of Craiova, Calea Bucureşti, no. 107i, Craiova, Romania*

RESULTS AND DISCUSSION

In the electrochemical deposition of Se the electrodeposition potential and the corresponding densities were found to depend on sweep rate and concentration of the electrolyte. Figure 1 shows the cathodic curves obtained in solutions containing H_2SeO_3 at three different concentrations.

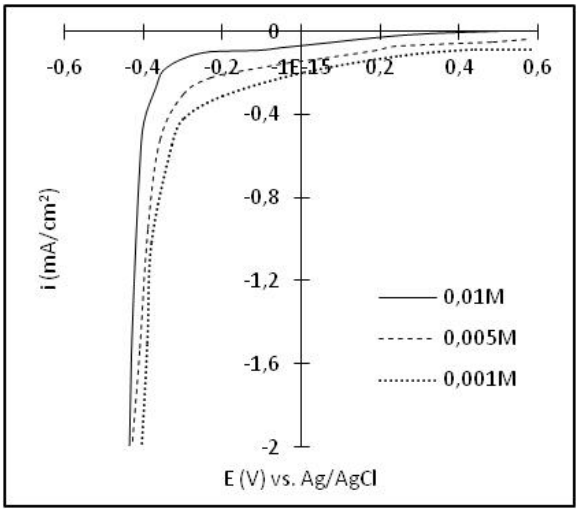

Figure 1. Cathodic curves obtained during selenium deposition onto Pt electrode from 0,01; 0,005 and 0,001 M H_2SeO_3 aqueous solutions, pH=2.

The potential scan was initiated in the negative direction from open circuit potential vs. Ag/AgCl. The reduction wave starts at -0.40 V vs. Ag/AgCl when selenous acid is present in the electrolyte with 0.01 M concentration.

In the case of selenium the crystallization potential and the corresponding current densities linearly depends on the concentration of H_2SeO_3 in solution.

Further analysis at various scan rates (fig. 2) showed clearly a linear variation of the crystallization potential with different scan rate (insert of figure 2).

The current densities are proportional to the scan rate and the crystallization potential is moving to the more positive direction, these features are characteristic for an irreversible system [13,14].

Reduction of the selenium species without the germanium precursor in the electrolyte, starts at -0,4 V vs. Ag/AgCl according to reaction:

$$SeO_3^{2-} + 3H_2O + 4e \rightarrow Se + 6HO^- \quad (E^0 = -0{,}366\ V) \qquad (1)$$

Metallic selenium electrodeposition is also indicated by the purplish colour of the deposit.

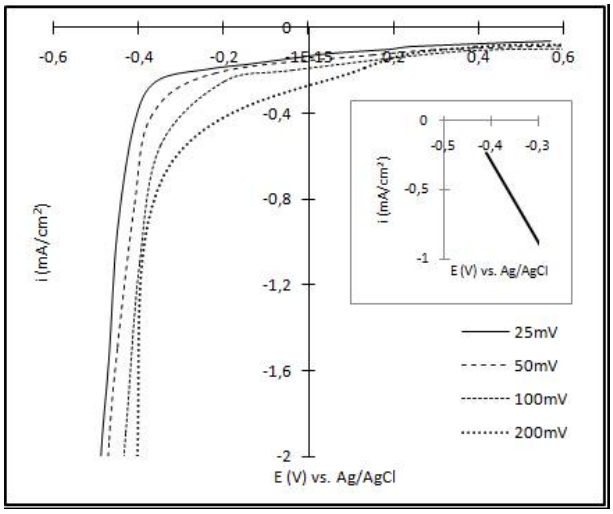

Figure 2. Cathodic polarization curves for Pt electrode at different scan rates in plating bath, H_2SeO_3 0,005 M, pH=2.

We performed a chronoamperometric study in order to examine the nucleation of selenium and selenium-germanium electrodeposition. Figure 3 shows a set of potentiostatic current transients for 0, 10, 30 and 50 mV overcharges obtained during the electrochemical deposition of selenium onto platinum electrode from a 0,005 M H_2SeO_3 solution.

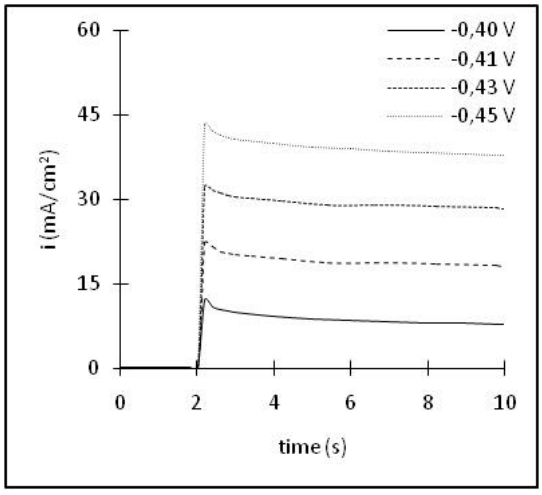

Figure 3. Potentiostatic current transients for the electrodeposition of selenium onto Pt electrode from 0,005 M H_2SeO_3, pH=2.

Experimental current transients are presented in a nondimensional form by ploting i/i_{max} vs. t/t_{max} (2D) and $(i/i_{max})^2$ vs. t/t_{max} (3D) and compared with theoretical values for instantaneous and progressive nucleation, respectively (fig. 4).

As can observe from figure 4, one can affirm that the selenium electrodeposition on the platinum electrode, in the given experimental conditions, take place after a combinatorial kinetic of 3D nucleation.

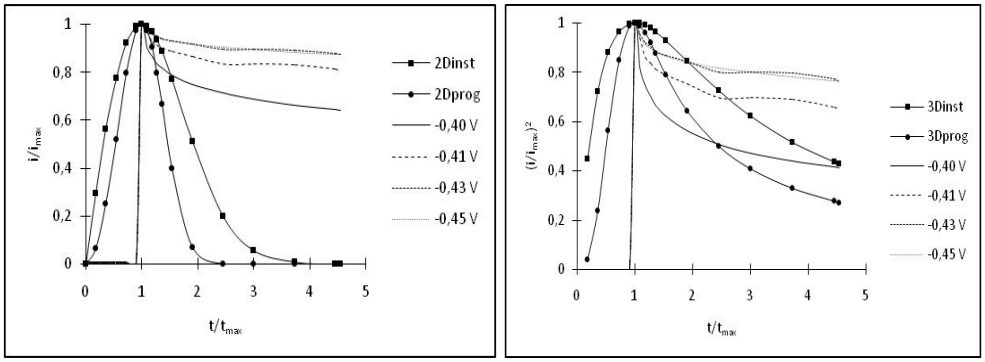

Figure 4. Comparison of the theoretical nondimensional plots for 2D (fig. 4a) and 3D (fig. 4b) for instantaneous and progressive Se nucleation to the experimental current transients in fig. 3.

The simultaneous presence of both species in the bath composition produced noticeable changes in the cathodic response. It can be seen in fig. 5 that a new peak appears during the scan in the negative direction at -0,50 V vs. Ag/AgCl.

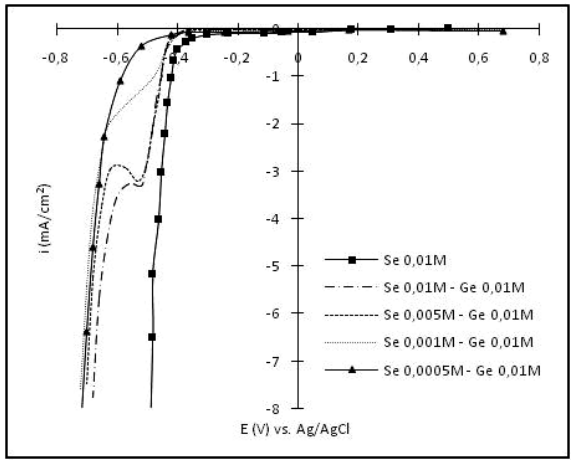

Figure 5. Cathodic curves for Pt electrode obtained during Se and Se-Ge electrodeposition.

We note that the cathodic current densities of this peak are decreasing with the Se concentration decrease. This peak may be ascribed to the formation of Se-Ge on the substrate. The $GeCl_4$ is hydrolyzed with distilled water to produce GeO_2; in this conditions we have to consider the possibility that this peak can be atributed to the GeO_2 reduction to GeO (E^0 = -0.370 V). At more negative potentials further reductions of the deposited selenium to H_2Se and/or germanium species to H_4Ge are possible. Selenium being nobler, it is expected to be deposited first. At selenium concentrations of $5 \cdot 10^{-4}$ M or smaller this peak is not more evident.

The nucleation mechanism of selenium-germanium electrodeposition was study by the chronoamperommetry methode. The corresponding potentiostatic current transients for 0, 10, 30 and 50 mV overpotentials obtained during the electrochemical deposition of selenium-germanium onto platinum electrode from a 0,005 M H_2SeO_3, 0,01 M $GeCl_4$ solution are presented in figure 6.

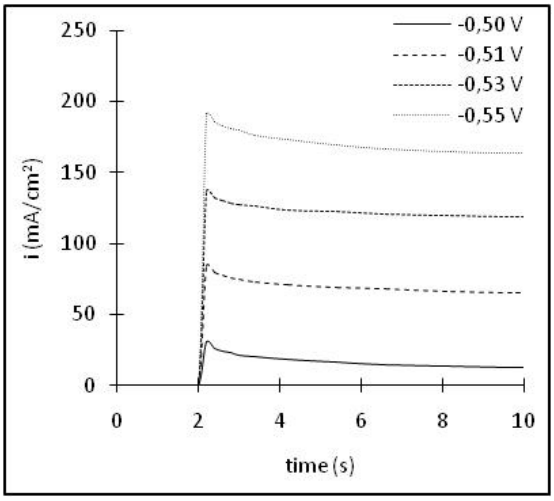

Figure 6. Potentiostatic current transients for the electrodeposition of selenium-germanium onto Pt electrode from 0,005 M H_2SeO_3, 0,01 M $GeCl_4$, pH=2.

From fig. 6 it may be observed that at shorter times there is a maximum current transient that, in this case, can be associated with a process where diffusion-controlled nucleation of selenium and germanium occurs simultaneously at the platinum electrode surface. After this maximum current, in each case the i-t plot passes through a falling current and then approaches to the limiting diffusion current to a planar electrode.

Experimental current transients compared with theoretical one for selenium-germanium instantaneous and progressive nucleation are presented in fig. 7.

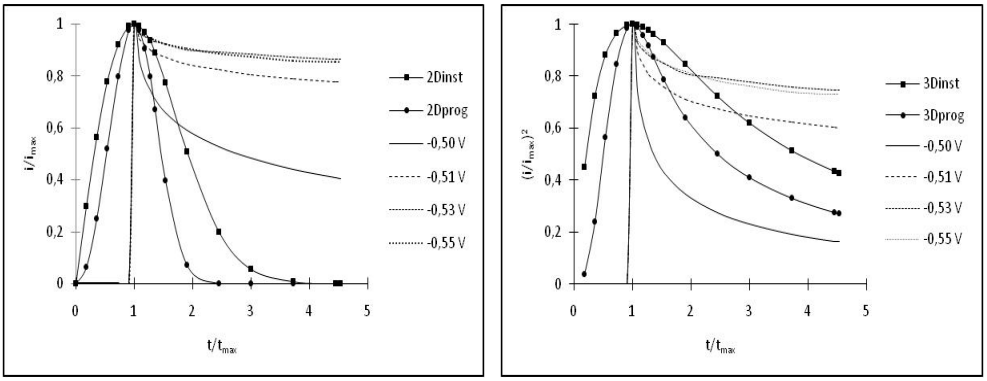

Figure 7. Comparison of the theoretical nondimensional plots for 2D (fig. 7a) and 3D (fig. 7b) for instantaneous and progressive Se-Ge nucleation to the experimental current transients in fig. 6.

Similar to selenium electrodeposition, when the both species are present in the electrolyte composition, at nucleation potential the mechanism fallow the progressive one and at higher overpotentials is changing to instantaneous.

The morphological changes in surface electrode were observed with an Euromex microscope. Figure 8a presents the surface morphology of Pt electrode before electrodeposition; figure 8b presents the surface morphology of deposited selenium and figure 8c presents the selenium-germanium deposit morphology.

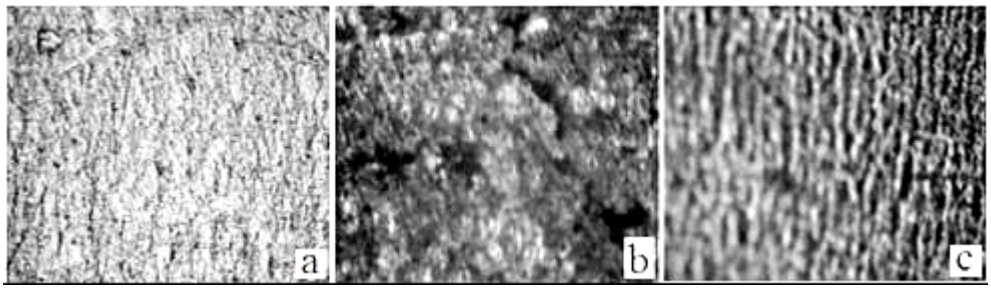

Figure 8. Surface morphology of: Pt electrode before electrodeposition (a), Se (b) and Se-Ge (c) deposited layer.

CONCLUSIONS

The Se and Se-Ge films were deposited onto Pt surface by potentiostatic polarization.

In the electrochemical deposition of Se, the electrodeposition potential and corresponding densities were found to depend on sweep rate and concentration of the electrolyte.

Selenium and selenium-germanium electrodeposition on the platinum electrode, in the given experimental conditions, take place after a combinatorial kinetic of instantaneous and progressive 3D nucleation.

EXPERIMENTAL SECTION

All electrochemical measurements were performed with the Keithley 2420 3A SourceMeter potentiostat/galvanostat. Experimental data recording was carried out in a standard electrochemical cell with three electrodes. The Ag/AgCl, KCl (saturated) was used as the reference electrode to which all potentials are quoted. The working and auxiliary electrodes were made from platinum foils with 1,0 cm^2 geometric area. The Se and Se-Ge films were deposited onto Pt surface by potentiostatic polarization.

All the chemicals used in this work were of analytical grade (99,5%) excepting H_2SeO_3 which was of standard purity (99,99%).

The electrolyte bath for Se deposition comprised of H_2SeO_3 solution, pH = 2 ± 0,05 (by adding HNO_3) and the working temperature was of 20 ± 2 ˚C. The pH of the electrolytic bath was measured using digital pH-meter (HANNA instruments). In order to analyse the influence of H_2SeO_3 concentration, three values of electrolyte concentration were used 0,01; 0,005 and 0,001M.

In the electrolyte bath for Se-Ge electrodeposition, the concentration of H_2SeO_3 was varied from 0,01M to 0,005; 0,001 and 0,0005M while the concentration of $GeCl_4$ was kept constant at 0,01M.

The chronoamperometry methode was used to analyse the nucleation mechanism of Se and Se-Ge electrodeposition.

After the deposition, the films were washed, dried and their morphology were analysed by an Euromex microscope.

REFERENCES

1. O. Wada, N. Kurihara, N. Yamazaki, *Jap. J. Nutr. Assesss.*,**1993**, *10*, 199.
2. V. Plaskov, Solar Energy Conversion, Springer, Berlin, **1990**.
3. P. Nagels, E. Sleeckx, R. Callaerts, L. Tichy, *Solid Stade Commun.*, **1995**, *94*, 49.
4. R. Kowalik, P. Zabinski, K. Fitzner, *Electrochim. Acta*, **2008**, *53*, 6148.
5. T. Mahaligam, A. Kathalingam, C. Sanjeeviraja, R. Chandramohan, J.P. Chu, Y.D. Kim, S. Velumani, *Materials Characterization*, **2007**, *58*, 735.
6. S. Thanikaikarasan, T. Mahalingam, S. Sundaram, A. Kathalingam, Y.D. Kim, T. Kim, *Vacuum*, **2009**, *83*, 1066.
7. M.F. Cabral, H.B. Suffredini, V.A. Perosa, S.T. Tanimoto, S.A.S. Machado, *Appl. Surf. Sci.*, **2008**, *254*, 5612.

8. Z. Zainal, A.J. Ali, A. Kasim, M.Z. Hussein, *Solar Energy & Solar Cells*, **2003**, *79*, 125.
9. W.Z. Wang, Y. Geng, P. Yan, F.Y. Liu, Y. Xie, Y.T. Qian, *J. Am. Chem. Soc.*, **1999**, *121*, 4062.
10. W.B. Zhao, J.J. Zhu, H.Y. Chen, *J. Cryst. Growth*, **2003**, *252*, 587.
11. K. Rajeshwar, *Adv. Mater.*, **1992**, *4*, 1.
12. M.S. Kazacos, B. Miller, *J. Electrochem. Soc.*, **1980**, *127*, 869.
13. Southampton Electrochemitry Group, Instrumental Methods in Electrochemistry, Ellis Horwood, Chichester, UK, **1985**.
14. R.H. Wopschall, I. Shain, *Anal. Chem.*, **1976**, *39*, 1514.

STUDIA UNIVERSITATIS BABEŞ-BOLYAI, CHEMIA, LIV, 4, 2009

ARTIFICIAL NEURAL NETWORKS USED FOR THE SIMULATION OF THE BATCH FERMENTATION BIOREACTOR

VASILE MIRCEA CRISTEA[a], IMRE LUCACI ARPAD[a], ŞIPOŞ ANCA[b], BRĂTFĂLEAN DORINA[a], PAUL ŞERBAN AGACHI[a]

ABSTRACT. The paper presents the modelling results of the batch alcoholic fermentation bioreactor using both the first principle and the Artificial Neural Networks (ANN) approach. For the nonlinear fermentation process the first principle model validated with experimental data considers for the biomass the Monod and for substrate the Bovée and Strehaiano models, including the temperature influence. It has been used for the ANN model development. A design and training methodology is proposed for statistical modelling based on artificial neural networks. Comparison between the two models is performed revealing the incentives of the ANN modelling method for reducing the computational time and sparing the computer resources.

Keywords: alcoholic fermentation, Artificial Neural Networks, modelling

INTRODUCTION

Winemaking technology is a complex process implying a succession of operations affected by the large variety of must and microbiota. The grape juice transformation into wine is substantially influenced by the wine makers' tradition and processing techniques are usually emerged from their experience [1]. Investigation of the mechanisms and phenomena lying behind the alcoholic fermentation is difficult as the stoichiometry and kinetics of the biochemical processes are only possible by lumping the numerous involved components and due to the need for simplifying the biomass characterization [2]. The oenologists claim that organoleptic properties of the wine are also dependent on the alcoholic fermentation in a very complex relationship [3, 4].

The alcoholic fermentation of wine is a biochemical process of transforming the sugar into alcohol and CO_2. Metabolites are the result of enzymatic reactions for the different metabolic paths [5]. Kinetics of the enzymatic reactions, as well as of the chemical reactions, is influenced by a set of factors. The most important of them are: composition of the culture medium, concentration of the limiting substrate, temperature, pH, concentration of the dissolved oxygen and stirring intensity. Setting optimal conditions for the

[a] *Babeş-Bolyai University of Cluj-Napoca, Faculty of Chemistry and Chemical Engineering, 11 Arany Ianos Street, 400028, Cluj-Napoca, Romania, mcristea@chem.ubbcluj.ro*

[b] *Lucian Blaga University of Sibiu, Faculty of Food Industry, 7-9 Dr. Ion Rațiu Street, 550024 Sibiu, Romania*

development of the fermentative process is directly related to the knowledge of the way of influencing the enzymatic reactions. Interaction between variables is strong as the change of a single parameter may affect the all the others [6].

Due to all these aspects the need for building reliable models is obvious and is highly appreciated as they may serve for better understanding the intrinsic processes and consequently, for optimizing the wine production according to the desired criteria [7, 8]. The first principle modelling allows logical description and interpretation of the involved phenomena, on the expense of a substantial modelling effort and with possible errors. Development of the analytical models is complex and time consuming as they imply a good knowledge of the phenomena and processes taking place inside the modelled system. Statistical mathematical models (such as the Artificial Neural Networks models) are based on observation data and measurements originating from the process. The statistical models require less effort and may reduce the modelling errors if an appropriate set of data is available [9-11].

In this paper a new statistical model based on Artificial Neural Networks (ANN) is proposed as an alternative to the first principle modelling of the alcoholic fermentation process performed in a batch bioreactor. Comparison between the first principle and ANN modelling results is performed, showing the benefits of the proposed ANN approach.

RESULTS AND DISCUSSION

A previously developed first principle model was available and used to generate the sets of input-target data further employed for training the ANN. The detailed analytical model used in the present work is described in [12]. This model has been validated with experimental data. Each of the biomass latent, exponential growing and decline phase has been described. Consequently, specific kinetic models of the biomass, substrate and alcohol have been considered. For substrate consumption the Bovée and Strehaiano model has been used [13]. Heat balances for the bioreactor vessel and jacket have been also accounted for.

This ANN based modelling approach has been considered as the first step for investigating the capability of designing and training an ANN model of the fermentation bioreactor. The developed ANN model design and training procedure may be considered as a prerequisite for the future step consisting in building the ANN dynamic simulator based on pure experimental data.

As the aim of the study bas been the development of a dynamic simulator of the alcoholic fermentation process, the following main process variables have been selected to demonstrate the time evolution of the process: substrate (glucose) concentration, biomass (Saccharomyces cerevisiae) concentration, alcohol concentration, reactor temperature and jacketed reactor cooling agent temperature. The ANNs based models have been designed and trained for revealing the dynamics of the five previously mentioned process variables, as a result of starting from different initial conditions of the batch fermentation

process. These initial conditions are specified by the subsequent variables: reactor inventory initial temperature, substrate initial concentration and biomass initial concentration. A sampling time of 3 hours has been considered for all process variables. One distinct ANN has been developed for each of the five process variables. Each of these ANNs has 3 inputs (the initial conditions) and 68 outputs. The outputs are the values of the respective process variable at the 68 moments of time multiples of the sampling time (starting with moment 0 h and finishing with moment 201 h). Two hidden layers with 3 and 4 neurons were used.

The set of training and testing data consists in 546 *input-desired output* pairs of data. The main part (75%) of the available set of data has been used for the training and validation step of the ANN model building. A quarter (25%) of the set of data has been used for testing the already trained ANN. Training and validation subset of data has been further divided: 75% of data was used for training and the rest for validation [14].

Following the training and validation step, the first testing step has been performed in order to assess the quality of the trained ANN. This testing step has been carried out on the set of input-desired output pairs of testing data not involved in the first training and validation step. Results obtained by the trained ANN on the set of testing data show a good quality of the training phase, as the correlation coefficients (R-value) for the set of ANN simulated and desired output (targets) sets of data are close to unity. They are not presented in the paper due to space saving reasons and to the next more comprehensive test.

The second testing step and more ample assessment of the prediction ability of the trained ANN have been performed for a new set of input data not yet used during the previous training-validation-testing steps and comparison with the analytical simulation results has been accomplished. These comparative first principle and ANN model simulations used random chosen initial conditions consisting in the following particular values: reactor inventory initial temperature $T_0=299\ K$, substrate initial concentration $S_0=190\ g/l$ and biomass initial concentration $X_0=0.75\ g/l$.

The comparative results between the analytical simulation and ANN simulation results, obtained for the five investigated process variables, are presented in Figures 1 to 5.

The simulation results reveal a good training procedure of the ANN, demonstrated by very close values of the bioreactor main process variables obtained with the first principle and the ANN models. For the substrate concentration, alcohol concentration and reactor inventory temperature the simulated evolutions of the variables are almost identical. For the biomass concentration and cooling agent temperature variables almost identical values have been also obtained for the periods of time when the change of these variables is reduced. For the time interval when the two previously mentioned variables have large changes in time, such as the time interval between 30h and 45 h, some differences may be noticed. But these differences, featuring in fact reduced relative errors, are mainly caused by the use of a relative large

sampling time compared to the time interval when the involved variables show large changes in time. It is expected that by reducing the sampling time these not essential differences to become smaller. According to the obtained results it may be appreciated the good fit between the ANN model and first principle model behaviour.

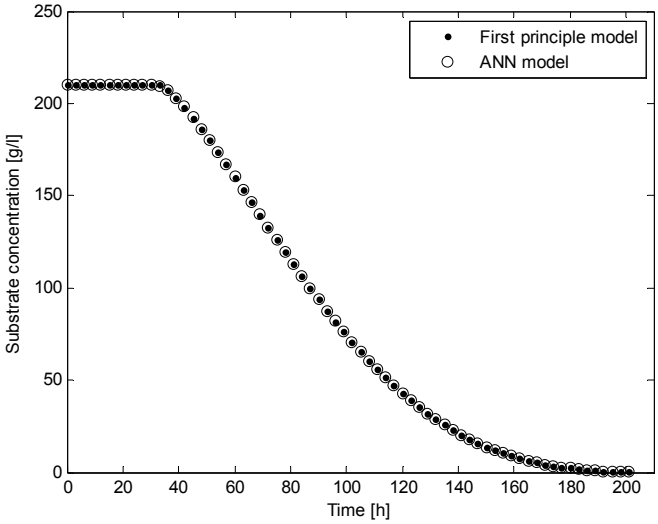

Figure 1. Comparative simulation results obtained by the first principle model and the ANN model, for the substrate concentration variable

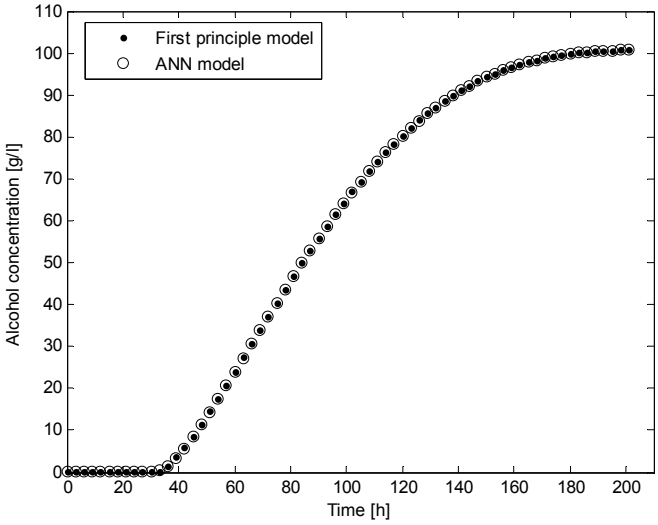

Figure 2. Comparative simulation results obtained by the first principle model and the ANN model, for the alcohol concentration variable

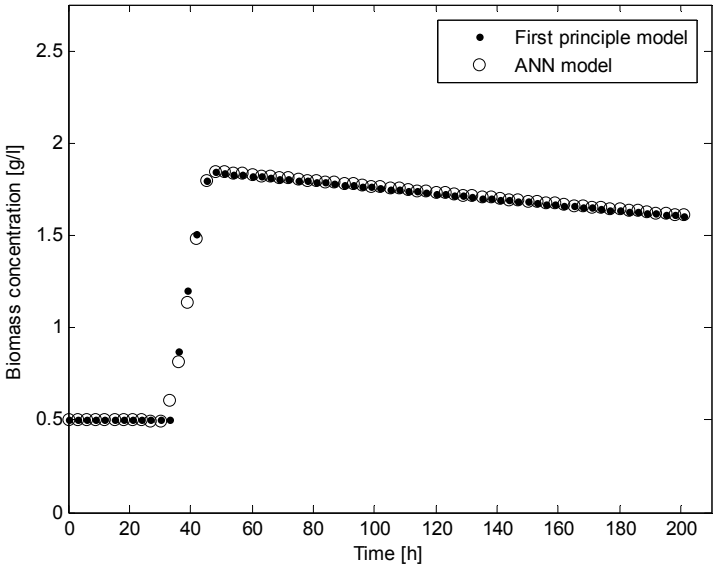

Figure 3. Comparative simulation results obtained by the first principle model and the ANN model, for the biomass concentration variable

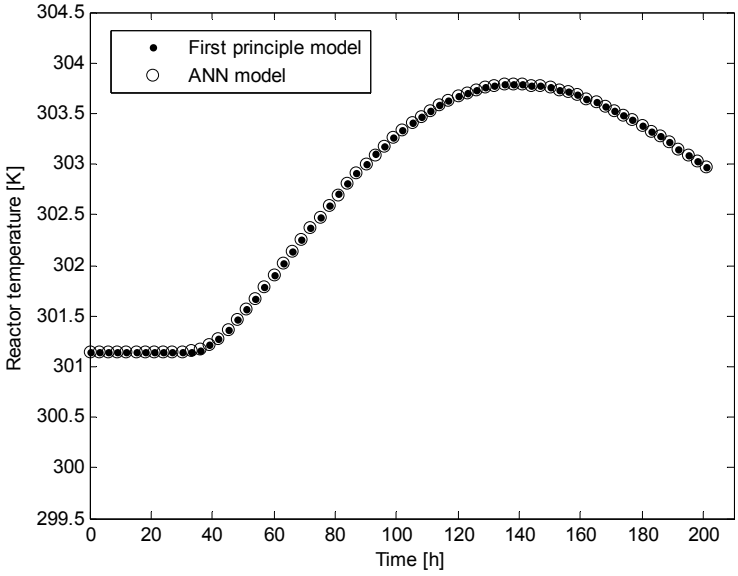

Figure 4. Comparative simulation results obtained by the first principle model and the ANN model, for the reactor temperature variable

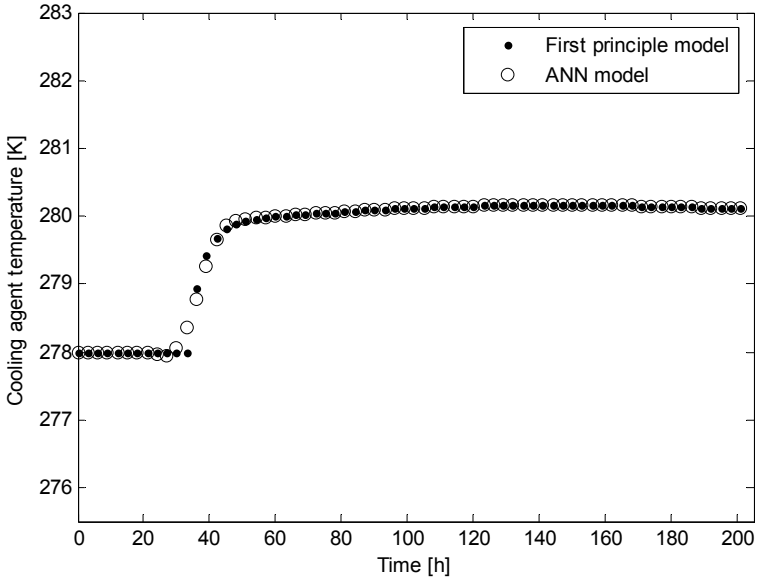

Figure 5. Comparative simulation results obtained by the first principle model and the ANN model, for the reactor cooling agent temperature variable

CONCLUSIONS

The paper presents the simulation results of successfully using Artificial Neural Networks for modelling the dynamic behaviour of the alcoholic fermentation bioreactor main process variables. The way the ANN has been designed and subsequently trained proved to be efficient for obtaining a useful dynamic simulator. The reduced relative errors proved by the good fit between the desired process outputs and the ANN simulated outputs are proofs of the ANN performance. Incentives of the ANN based model consist in the development of an efficient methodology of building the ANN model of the complex alcoholic fermentation bioreactor associated to the reduced modelling effort. The ANN model may exclusively rely on experimental data and implicitly does not imply comprehensive knowledge of the detailed physical, chemical and biological first principle description.

Another main advantage of the ANN based modelling consists in the important reduction of the simulation time (exceeding one order of magnitude), hence resulting in an efficient management of the computing resources. This incentive may become much appreciated for its potential use in bioreactor real time control applications based on mathematical models where implementation feasibility is very challenging.

EXPERIMENTAL SECTION

The ANN architecture for the batch alcoholic fermentation process consists in a feedforward ANN having four layers (one input, two hidden and one output layers), for which the weights and biases have been trained according to the backpropagation training algorithm [15]. The number of neurons in the hidden layers (4 and 3) has been set on the basis of a heuristic procedure, as a consequence of the errors analysis performed during the repeated training steps. The neurons transfer function in the hidden layers has been selected to be *tansig* (hyperbolic tangent sigmoid) and for the output layer *purelin* (linear). The quasi-Newton type Levenberg-Marquardt algorithm has been used for training the ANN. Overfitting has been avoided by early stopping, improving the generalization capability of the ANN.

During the repeated training sequences, random initial values have been used for the ANN weights and biases in order to prevent convergence to local minima. The input and desired output sets of data have been scaled (based on minimum and maximum values) and principal component analysis has been used for improving the computation precision and training performance.

ACKNOWLEDGMENTS

Funding from the grant PNCDI II 100CP/I, CAPACITATI 142 and 71-006 is gratefully acknowledged by the authors.

REFERENCES

1. J. Blouin, E. Peynaud, Connaissance et travail du vin, Dunod, Paris, **2001**, 87.
2. M. A. J. Torija, N. Rozès, M. Poblet, J.M. Guillamón, A. Mas, *International Journal of Food and Microbiology*, **2003**, *80*, 47.
3. C. Flanzy, Œnologie - Fondements scientifiques et techniques, **1999**, Techniques & Documentation, Paris.
4. P. Ribéreau-Gayon, D. Dubourdieu, B. Donèche, A. Lonvaud, Handbook enology. The microbiology of wine and vinifications, Vol. I, **2000**, Wiley, West Sussex, 49.
5. H. Fariha, A. A. Shah, A. Hameed, *Enzyme and Microbial Technology*, **2006**, *39*, 235.
6. A. Houde, A. Kademi, D. Leblanc, *Applied Biochemistry and Biotechnology*, **2004**, *118*, 155.
7. W. Wiechert, *Journal of Biotechnology*, **2002**, *94*, 37.
8. B. Srinivasan, S. Palanki, D. Bonvin, *Computers and Chemical Engineering*, **2003**, *27*, 1.

9. M.T Hagan, M.H. Menhaj, T, *IEEE Transaction on Neural Networks*, **1994**, *5*, 989.
10. V. M. Cristea, S. P. Agachi, *Studia Universitatis Babes-Bolyai*, **2005**, *L, 2*, 65.
11. S. Haykin, Neural Networks: A Comprehensive Foundation, **1994**, MacMillan College Publshing Co., New-York, Chapter 6.
12. A. Sipos, X.M. Meyer, P. Strehaiano, *Acta Alimentaria*, **2007**, *36*, 429.
13. J. P. Boveé, P. Strehaiano, G. Goma, Y. Sevely, *Biotechnology and Bioengineering*, **1984**, *26*, 328.
14. V. M. Cristea, R. Roman, P. S. Agachi, **2009**, *Studia Universitatis Seria Chemia*, *1*, 125.
15. Neural Networks Toolbox 6.0.1.User Guide, **2008**, Matlab 7.7, MathWorks Inc.

STUDIA UNIVERSITATIS BABEŞ-BOLYAI, CHEMIA, LIV, 4, 2009

SYNTHESIS, SPECTROSCOPIC AND ELECTROCHEMICAL CHARACTERIZATION OF A NEW CHROMIUM (III) SUBSTITUTED DAWSON POLYOXOMETALATE

ADRIAN-RAUL TOMŞA[a], DANIELA CIOLOBOC[a], ANA MARIA TODEA[a,b], RADU SILAGHI-DUMITRESCU[b], GRIGORE DAMIAN[c] AND MARIANA RUSU[b]

ABSTRACT. A new chromium (III) substituted Dawson 2-molybdo-15-tungsto-2-phosphate $K_7[Cr(H_2O)P_2Mo_2W_{15}O_{61}]\cdot 17H_2O$ was synthesized by reaction of Cr(III) chloride with monolacunary Dawson molybdo-tungsto-diphosphates $[P_2Mo_2W_{15}O_{61}]^{10-}$ in aqueous solution. The complex has been characterized using spectroscopic and electrochemical techniques. The FT-IR spectroscopic data indicate that the polyanion overall symmetry is restored after the coordination of Cr(III). Coordination of chromium (III) is further supported by the ^{31}P-NMR, EPR and UV-Vis electronic absorption spectroscopy results. Cyclic voltammograms of the chromium (III) complex exhibit three pairs of oxidation/reduction waves with negative $\varepsilon^{0`}$values. These waves were assigned to two molybdenum-centered single electron redox processes and one tungsten-centered two electrons process. A positive shift of these waves when going from Dawson monolacunary complex to its Cr(III) complex. A modified Dawson structure was inferred from the results for the new chromium (III) complex, in which the chromium and molybdenum atoms are located to the same cap of the anion.

Keywords: polyoxometalate, Dawson structure, chromium, FT-IR spectroscopy, UV-Vis spectroscopy, NMR-spectroscopy, EPR-spectroscopy

INTRODUCTION

Polyoxometalates (POMs) comprise a rich and diverse family of metal-oxygen clusters of the early transition metals in high oxidation states, most commonly V(V), Mo(VI) and W(VI), with unique versatility in terms of shape, polarity, redox potentials, surface charge distribution, acidity, and solubility [1-4].

These compounds have promising applications in various domains, including catalysis [5,6], electrocatalysis [7], medicine [8,9], molecular conduction [10-12], magnetism [13], photochemistry [14,15], luminescence [16], analytical chemistry [17] and materials science [18].

[a] *"Babeş-Bolyai" University, "Raluca Ripan" Institute for Research in Chemistry, 30 Fântânele St., Cluj-Napoca, Romania, rtomsa@yahoo.com*

[b] *"Babeş-Bolyai" University, Faculty of Chemistry and Chemical Engineering, 11 Arany Janos St., RO-400028, Cluj-Napoca, Romania, mrusu@chem.ubbcluj.ro*

[c] *"Babeş-Bolyai" University, Faculty of Physics, 1 Mihail Kogălniceanu St., RO-400084, Cluj-Napoca, Romania*

The synthesis of polyoxometalates is mostly rather simple and straightforward, once the proper reactions conditions have been identified. However, the mechanism of formation of polyoxometalates is not yet well understood and is commonly described as self-assembly. Therefore, the design of novel polyoxometalates remains a challenge for synthetic chemists.

The most rational synthesis of new polyoxometalates uses the lacunary precursors prepared from the corresponding complete polyoxometalate species, by loss of one or more **MO_6** octahedra. Reaction of a stable lacunary polyoxometalate with transition metal ions mostly leads to a product in which the polyoxometalate framework remains unchanged.

For instance, under hydrolytic conditions, in the presence of Na_2CO_3, the α-$[P_2W_{18}O_{62}]^{6-}$ Dawson polyoxometalate loses three capping WO_6 octahedra, yielding a Dawson trilacunary polyoxotungstate derivative [α-$P_2W_{15}O_{56}]^{12-}$ [19]. Furthermore, the reaction of the trilacunary derivative [α-$P_2W_{15}O_{56}]^{12-}$ with molybdate, carried out in mild conditions, allows the selective addition of two molybdenum atoms in an apical site of [α-$P_2W_{15}O_{56}]^{12-}$ [20]. Complexes of the resulting monolacunary Dawson polyanion, [α_2-$P_2Mo_2W_{15}O_{61}]^{10-}$, with a first row transition metal cation are of particular interest for their electrocatalytic properties [21-23].

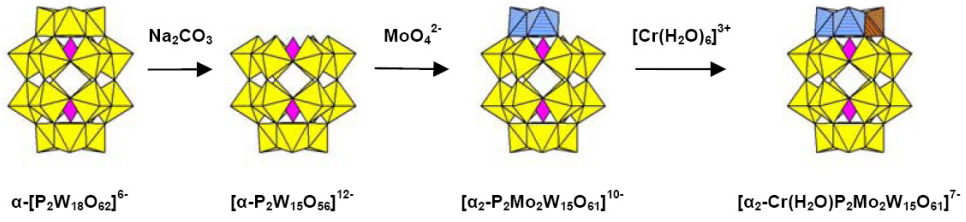

Figure 1. The preparation scheme of **α_2-$CrP_2Mo_2W_{15}$**.

Herein we report the synthesis, spectroscopic and electrochemical characterization of a new chromium (III) complex of Dawson monolacunary polyoxometalate [α_2-$P_2Mo_2W_{15}O_{61}]^{10-}$, as aqueous soluble potassium salt. The K_4Li_3[α_2-$Cr(H_2O)P_2Mo_2W_{15}O_{61}]\cdot 17H_2O$ complex (**α_2-$CrP_2Mo_2W_{15}$**) has been characterized by elemental and TG-DSC analysis, UV-Vis, FT-IR and ^{31}P-NMR spectroscopy, EPR, as well as by electrochemical measurements.

RESULTS AND DISCUSSION

The new chromium (III) polyoxometalate complex was synthesized in aqueous solution by reacting the potassium salt of the monolacunary Dawson polyoxometalate K_{10}[α_2-$P_2Mo_2W_{15}O_{61}]\cdot 18H_2O$ (**α_2-$P_2Mo_2W_{15}$**) with chromium (III) chloride. In order to avoid the migration of molybdenum atoms, which may

give numerous isomers, the synthesis must be performed in acidic solution heated to 40°C. Isolation of the products as potassium salts resulted in relatively good yields of the polyoxometalate complex.

The thermal stability of **α_2-$CrP_2Mo_2W_{15}$** was investigated by TG-DSC. The differential scanning calorimetry curve for **α_2-$CrP_2Mo_2W_{15}$** shows four endothermic and one exothermic processes in the region from 20°C to 650°C (Figure 2).

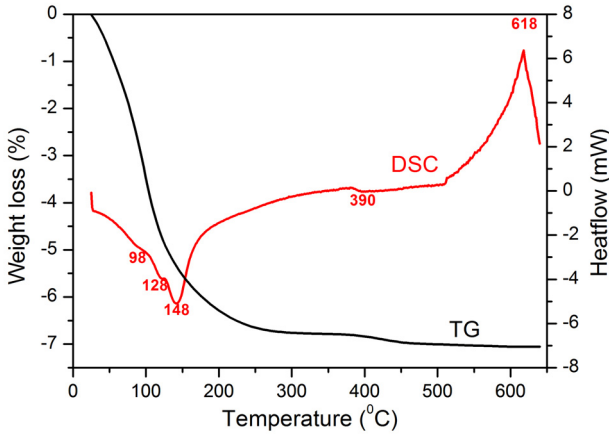

Figure 2. TG and DSC curves of **α_2-$CrP_2Mo_2W_{15}$**.

The three endothermic processes from ~25°C to 200°C are attributed to the desorption of 17 water molecules from the lattice structure. The endothermic process from ~380°C to 450°C is assigned to the loss of the coordination water molecule attached to Cr(III). The exothermic process observed from 500°C to 650°C coresponds to the collapse of the polyoxometalate framework. This assignement is also supported by FT-IR spectra, which show significant changes in the P-O and M-O (M= Mo, W) stretching modes after heating to 650°C (Figure 3).

The FT-IR spectrum of chromium (III) complex **α_2-$CrP_2Mo_2W_{15}$** in the P-O and M-O stretching region is shown in Figure 3, along with those of the monolacunary ligand **α_2-$P_2Mo_2W_{15}$** and complete Dawson polyoxometalate, $K_6[P_2W_{18}O_{62}]\cdot 14H_2O$ (**α-P_2W_{18}**).

As expected, in the FT-IR spectrum of the ligand **α_2-$P_2Mo_2W_{15}$**, the P-O vibration band, recorded between 1200 and 1000 cm^{-1}, is split, due to the decrease of the local symmetry. When Cr (III) fills the vacancy, the symmetry is restored. As a consequence, the FT-IR spectra of **α_2-$CrP_2Mo_2W_{15}$** and **α-P_2W_{18}** are similar. However, the spectrum of **α_2-$CrP_2Mo_2W_{15}$** exhibits an additional vibration band, recorded at 686 cm^{-1}, which was assigned to the stretching vibration $\nu_{(Cr\text{-}O)}$ [24,25].

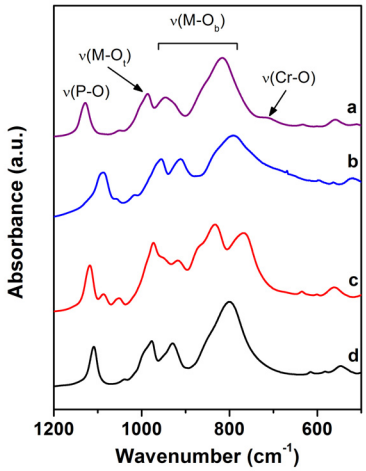

Figure 3. FT-IR spectra of **α_2-$CrP_2Mo_2W_{15}$** (a), **α_2-$CrP_2Mo_2W_{15}$** heated to 650ºC (b) **α_2-$P_2Mo_2W_{15}$** (c) and **α-P_2W_{18}** (d).

The vibrations in the 1000-700 cm^{-1} range were assigned to the asymmetric stretching of the bridges (M-O$_b$-M) and of the terminal bonds (M-O$_t$) [26]. Mention should be made of the fact that the stretching vibrations are shifted towards higher wavelengths, after the coordination of Cr(III), thus suggesting an increase of the polyoxoanion cohesion [26].

In the UV spectrum of **α_2-$CrP_2Mo_2W_{15}$,** the two characteristic bands, assigned to the dπ-pπ charge transfer transitions M←O$_t$ and M←O$_b$ (M is Mo or W; O$_t$ is a terminal oxygen and O$_b$ is a bridging oxygen), were recorded at ~50000 cm^{-1} and ~35273 cm^{-1} [27, 28] (Figure 4a).

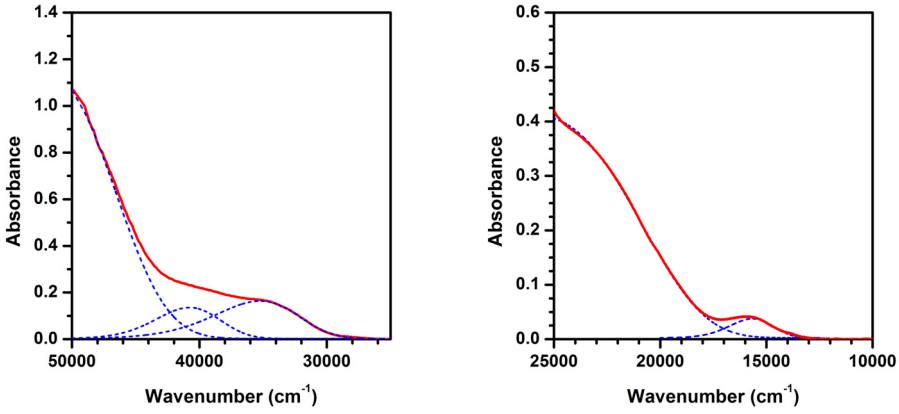

Figure 4. The UV (a) and visible (b) electronic spectra of **α_2-$CrP_2Mo_2W_{15}$** recorded in aqueous solution. The Gaussian components are represented with dashed lines.

The visible spectrum provides information about the local environment of Cr(III) (Figure 4b). Two bands characteristic of the chromium complexes, registered at 15650 cm^{-1} and 23446 cm^{-1} were assigned to $^4T_{2g}(F) \leftarrow {}^4A_{2g}(F)$ (v_1) and $^4T_{1g}(F) \leftarrow {}^4A_{2g}(F)$ (v_2) transitions, respectively. The v_3 band, assigned to $^4T_{1g}(P) \leftarrow {}^4A_{2g}(F)$ transition [29], overlaps the dπ-pπ charge transfer transitions $M \leftarrow O_t$ and $M \leftarrow O_b$ specific to the polyoxometalate structure, and appear as a shoulder at 40703 cm^{-1}. This assignment is supported by the calculation of the spectral parameters according to the method proposed by Lever (Dq= 1565 cm^{-1}, Dq/B=1.25, v_3/B=32.51, B=1252 cm^{-1}) [30].

While the ^{31}P-NMR of the ligand **α_2-$P_2Mo_2W_{15}$** shows a clean two-line spectrum with signals at -3.15 and -11.97 ppm, the spectrum of the Cr(III) complex **α_2-$CrP_2Mo_2W_{15}$** shows only a broadened peak at -11.58 ppm (Figure 5), which was assigned to P(2), the farthest phosphorus atom from the Cr(III) coordination site [31,32]. The phosphorus atom which is closest to the site of Cr(III) incorporation, P(1), was not observed probably because of the strong interaction with the paramagnetic ion.

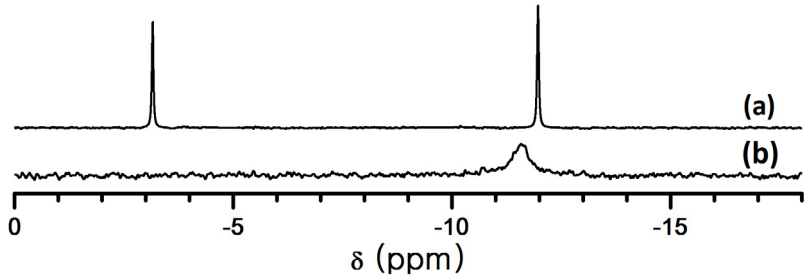

Figure 5. ^{31}P NMR spectra of **α_2-$P_2Mo_2W_{15}$** (a) and **α_2-$CrP_2Mo_2W_{15}$** (b), recorded in D_2O.

The EPR spectrum of **α_2-$CrP_2Mo_2W_{15}$** is shown in Figure 6. Low-temperature EPR spectra of other Cr(III)-substituted polyoxometalates reported before at 77K [24] show rhombic signals with features centered at 1500, 2000 and 3500 G, which are suggestive of a rhombohedrally distorted CrO_6 octahedron. Similarly, in our case, the low-field resonances in a range of g=3-6 indicate the presence of isolated Cr(III) species in orthorhombically distorted octahedral environments with S=3/2. The best fit of the simulated experimental spectrum at low field (1000-2000 G) was obtained assuming a Lorenzian line shape and two magnetic non- equivalent sites of chromium ions in a 0.55 to 0.45 ratio. The parameters for the first species were g_x= 5.11, g_y= 5.09, g_z= 5.0, and A_x= 251, A_y= 442, A_z= 494, which are characteristic of orthorhombically distorted symmetry. The parameters of the second species, g_x=4.1, g_y=3.53, g_z=3.22, and A_x=195, A_y=124, A_z=127, are characteristic of octahedral local symmetry [33]. These two magnetically- non-enequivalent species of Cr(III) are assigned to two different crystalline form of the polyoxometalate complex.

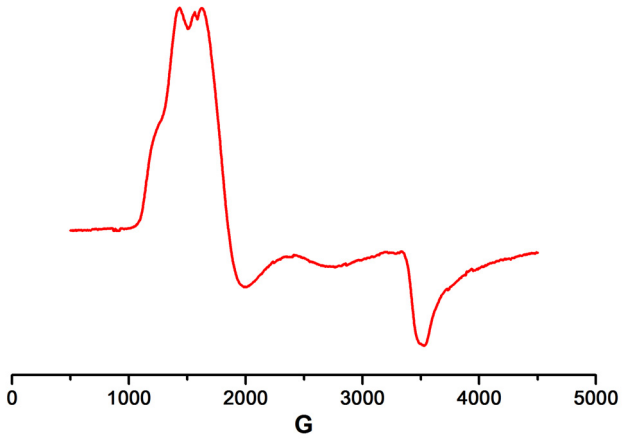

Figure 6. Low-temperature X-band EPR spectrum of **α_2-$CrP_2Mo_2W_{15}$**.

The electrochemical response of **α_2-$CrP_2Mo_2W_{15}$** in aqueous solution consists of three successive redox peak pairs in the negative potential range (Figure 7).

Peaks I and II were assigned to two molybdenum-centered single electron redox processes, while peak III corresponds to a two electrons tungsten-centered process [34]. The recorded cyclic voltammogram for the chromium (III) complex is very similar to those of **α_2-$P_2Mo_2W_{15}$**. Only a slight negative shift in the peak potentials was observed for **α_2-$CrP_2Mo_2W_{15}$** relative to the monolacunary ligand.

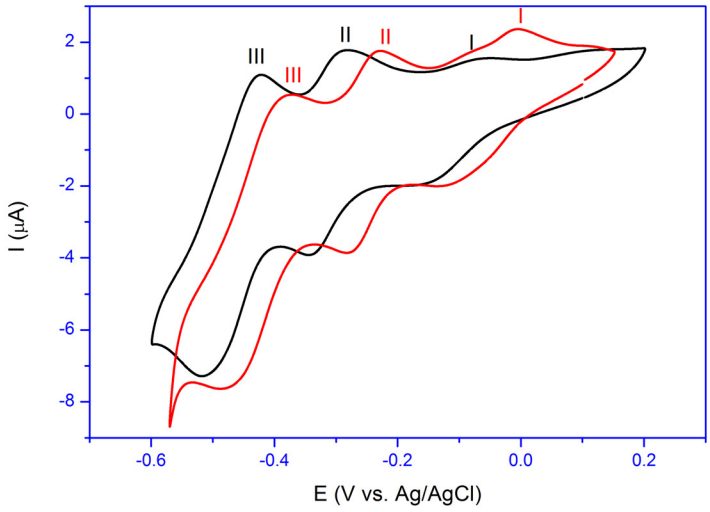

Figure 7. Cyclic voltammograms of **α_2-$CrP_2Mo_2W_{15}$** (black) and **α_2-$P_2Mo_2W_{15}$** ligand (red), recorded in 0.5 M HSO_4^- buffer solutions (pH= 3.0), sweep rate 10 mV s^{-1}.

Table 1. CV data for the chromium (III) complex and the parent Dawson monolacunary polyoxometalate.

Process	E_{pa} (V)	E_{pc} (V)	$\varepsilon^{0'}$ (V)	ΔE_p (V)
α_2-$P_2Mo_2W_{15}$				
I	-0.003	-0.102	-0.0525	0.099
II	-0.234	-0.279	-0.2565	0.045
III	-0.374	-0.485	-0.4295	0.111
α_2-$CrP_2Mo_2W_{15}$				
I	-0.052	-0.114	-0.0830	0.062
II	-0.287	-0.329	-0.3080	0.042
III	-0.419	-0.514	-0.4665	0.095

E_{pa}, oxidation potential; E_{pc}, reduction potential; $\varepsilon^{0'}$, formal standard potential estimated as the average of anodic and cathodic peak potentials; ΔE_p the difference between the redox peak potentials. Experimental conditions: 0.5 M HSO_4^- buffer solution; pH= 3.0, 25°C; glassy carbon working electrode; scan rate 10 mV s^{-1}; c=10^{-3} M, potentials recorded vs Ag/AgCl.

The formal standard potential $\varepsilon^{0`}$ (estimated as the average value of anodic and cathodic peak potentials) shows a negative shift with increasing values of pH (Figure 8a). For all three peaks, the $\varepsilon^{0`}$ versus pH dependences are linear, with slopes of 102.01 (I), 75.06 (II) and 73.96 (III) mV/ΔpH. The anodic to cathodic peak separation values (Δ*E*) and the described pH dependence are probably consistent with the fact that a single electron as well as one proton are involved in each redox process I and II, while two electrons and two protons are involved in the redox process III [32, 35-38].

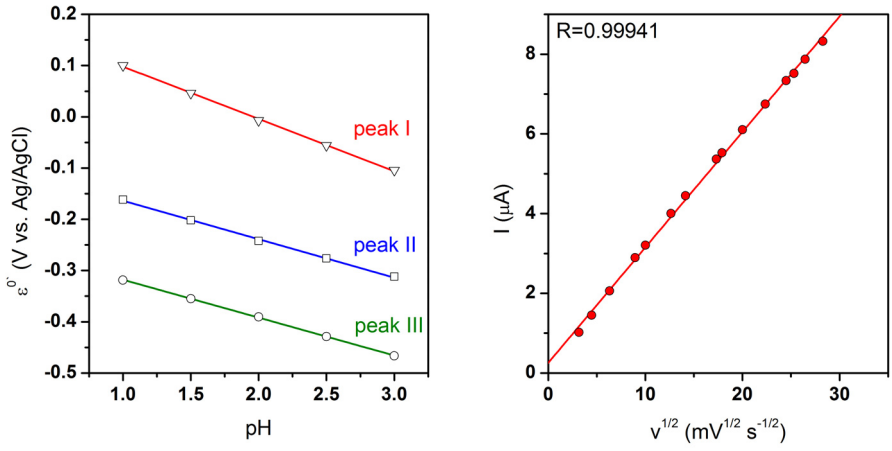

Figure 8. Dependence of the formal standard potentials on the pH for **α_2-$CrP_2Mo_2W_{15}$** (a); dependence of cathodic peak II current on the scan rate (b).

The linear relationship between peak currents and the square root of scan rates for cathodic peak II (Figure 8b) provides evidence for a diffusion controlled process [39].

CONCLUSIONS

The spectroscopic and electrochemical investigations of **α_2-$CrP_2Mo_2W_{15}$** provide evidence for the coordination of Cr(III) by the $[\alpha_2\text{-}P_2Mo_2W_{15}O_{61}]^{10-}$ Dawson monolacunary polyoxometalate. Both chromium and molybdenum atoms are located to the same cap of the anion. Cr(III) ion binds to five oxygen atoms, surrounding the vacancy of the ligand **α_2-$P_2Mo_2W_{15}$**, and to one water molecule. The electrochemical behavior of **α_2-$CrP_2Mo_2W_{15}$** illustrates the influence exerted by chromium upon the redox character of **α_2-$P_2Mo_2W_{15}$**. The redox behavior of the new chromium (III) derivative **α_2-$P_2Mo_2W_{15}$** recommends it as a promising mediator (electrocatalyst) in indirect electrochemical reactions.

EXPERIMENTAL SECTION

1. Materials

The monolacunary polyoxometalate $[P_2Mo_2W_{15}O_{61}]^{10-}$ was prepared according to the published method [19], starting from the Dawson polyoxometalate $[P_2W_{18}O_{62}]^{6-}$ (see Figure 1). The identity of precursors was established by ^{31}P-NMR and FT-IR spectra.

1.1. Preparation of $K_4Li_3[Cr(H_2O)P_2Mo_2W_{15}O_{61}]\cdot 17H_2O$

A sample of 1.33 g (5 mmol) of $CrCl_3\cdot 6H_2O$ was dissolved in 110 mL of molar acetic acid - lithium acetate buffer (pH=3.5), and 25.00 g (5.25 mmol) of $K_{10}[P_2Mo_2W_{15}O_{61}]\cdot 21H_2O$ was added with stirring. The mixture was heated at 40°C for 1 hour while the colour changed from green to brown, and then the clear solution was treated with 150 mL saturated KCl. The white precipitate was removed by filtration over a synthered glass frit and the brown filtrate was kept at 5°C. After three days, brown needle-like crystals appeared which were collected by filtration over a synthered glass frit, washed with ethanol and ether, and dried in air. Yield: 15 g (64.7%). Calcd. for $K_4Li_3[Cr(H_2O)P_2Mo_2W_{15}O_{61}]\cdot 17H_2O$: K 3.43, Li 0.46, Cr 1.14, P 1.36, Mo 4.30, W 60.70. Found: K 3.05, Li 0.40, Cr 1.12, P 1.44, Mo 4.05, W 62.08. FT-IR (cm^{-1}, KBr pellets, polyoxometalate region): 1093, 1014, 953, 912, 779, 686, 598, 565, 525, 476. ^{31}P NMR (D_2O, δ): -11.58 (s).

2. Methods

Elemental analysis was performed by inductively coupled plasma atomic emission spectroscopy on an ICP-OES Perkin Elmer Optima 3500 DV spectrometer. The water content was determined thermogravimetrically, with a METTLER-TOLEDO TG/SDTA 851 thermogravimeter (Pt crucible, 20 mL/min nitrogen flow, 5ºC/min heating rate).

A JASCO 610 FTIR spectrophotometer was used to record the FT-IR spectra (KBr pellets).

UV-Vis spectra were recorded on a Shimadzu UV-3101PC instrument using Teflon-stoppered quartz cells with a path length of 1 cm. A 10 μM aqueous solution of **α_2-$CrP_2Mo_2W_{15}$** was used to record the UV spectrum, while for the Vis spectrum was used a 1mM aqueous solution of **α_2-$CrP_2Mo_2W_{15}$**.

^{31}P-NMR spectra were recorded at 101.2561380 MHz using an ARX 250 spectrometer. Chemical shifts are reported in ppm using D_3PO_4 as external reference.

A Bruker EMX Micro spectrometer with a liquid nitrogen cooling system was employed for EPR spectra. Instrument conditions were: microwave frequency 9.43 GHz, microwave power 15.89 mW, modulation frequency 100 kHz, modulation amplitude 5 G, sweep rate 22.6 G/s; time constant 81.92 ms, average of three sweeps for each spectrum, temperature 100 K. To find the magnetic parameters, the experimental spectrum was simulated using the program POWFIT (http://epr.niehs.nih.gov/).

Electrochemical measurements were performed using a computer controlled AUTOLAB PGSTAT302N potentiostat. A conventional (single-compartment) three electrode electrochemical cell was used, with a Metrohm planar platinum counter electrode and a Metrohm Ag/AgCl reference electrode. Glassy carbon (Metrohm, Φ~ 3mm) was used as a working electrode (WE). This was polished with 0.3 μm alumina, followed by sonication for 3 min. in purified water before each run. The WE was polarized in a 10^{-3} M solution of the complex in 0.5 M HSO_4^- buffer (pH = 1.0 - 3.0) with a scan rate between 10 and 900 mV s^{-1}. Solutions were deoxygenated using purified N_2 gas (99.9%). While recording the voltammograms, N_2 was passed over the solution surface. All measurements were performed at room temperature.

ACKNOWLEDGMENTS

The authors gratefully acknowledge the financial support from the Romanian National Council for Scientific Research (PNCDI II - IDEI, Project No. 329/2007). We also thank Dr. Laura Elena Mureşan for TG-DSC measurements and Ioana Mihaela Perhăiță for elemental analysis.

REFERENCES

1. M.T. Pope, A. Müller (Eds.), “Polyoxometalates: From Platonic Solid to Antiretroviral Activity”, Kluwer Academic Publishers, Dordrecht, **1994**.
2. M.T. Pope, A. Müller (Eds.), “Polyoxometalate Chemistry: From Topology via Self-Assembly to Applications”, Kluwer Academic Publishers, Dordrecht, **2001**.
3. T. Yamase, M.T. Pope (Eds.), “Polyoxometalate Chemistry for Nano-Composite Design”, Kluwer Academic Publishers, Dordrecht, **2002**.

4. J.J. Borrás-Almenar, E. Coronado, A. Müller, M.T. Pope (Eds.), "Polyoxometalate Molecular Science", Kluwer Academic Publishers, Dordrecht, **2004**.
5. M. Misono, *Chemical Communications*, **2001**, 1141.
6. N. Mizuno, M. Misono, *Chemical Reviews*, **1998**, *98*, 199.
7. M. Sadakane, E. Steckhan, *Chemical Reviews,* **1998**, *98*, 219.
8. J.T. Rhule, C.L. Hill, D.A. Judd, *Chemical Reviews*, **1998**, *98*, 327.
9. T. Yamase, *Journal of Materials Chemistry*, **2005**, *15*, 4773.
10. E. Coronado, C. Giménez-Saiz, C.J. Gómez-García, S.C. Capelli, *Angewandte Chemie, International Edition,* **2004**, *43*, 3022.
11. E. Coronado, P. Day, *Chemical Reviews*, **2004**, *104*, 5419.
12. E. Coronado, C. Giménez-Saiz, C.J. Gómez-García, *Coordination Chemistry Reviews*, **2005**, *249*, 1776.
13. E. Coronado, J.R. Galán-Mascarós, C. Giménez-Saiz, C.J. Gómez-García, S. Triki, *Journal of American Chemical Society*, **1998,** *120,* 4671.
14. E. Papaconstantinou, *Chemical Society Reviews*, **1989**, *16*, 1.
15. A. Hiskia, A. Mylonas,E. Papaconstantinou, *Chemical Society Reviews*, **2001**, *30*, 62.
16. T. Yamase, *Chemical Reviews*, **1998**, *98*, 307.
17. D.P. Smith, M.T. Pope, *Analytical Chemistry*, **1968**, *40*, 1906.
18. D.E. Katsoulis, *Chemical Reviews*, **1998**, *98*, 359.
19. B.J. Hornstein, R.G. Finke, *Inorganic Chemistry*, **2002**, *41*, 2720.
20. M. Abbessi, R. Contant, R. Thouvenot, G. Hervé, *Inorganic Chemistry*, **1991**, *30*, 1695.
21. B. Keita, L. Nadjo, R. Contant, *Journal of Electroanalytical Chemistry,* **1998**, *443*, 168.
22. B. Keita, Y. Jean, B. Levy, L. Nadjo, R. Contant, *New Journal of Chemistry* **2002**, *26*, 1314.
23. B. Keita, Y.W. Lu, L. Nadjo, R. Contant, M. Abbessi, J. Canny, M. Richet, *Journal of Electroanalytical Chemistry*, **1999**, *477*, 146.
24. K. Wassermann, R. Palm, H.J. Lunk, J. Fuchs, N. Steinfeldt, R. Stösser, R., *Inorganic Chemistry*, **1995**, *34*, 5029.
25. K. Wassermann, H.J. Lunk, R. Palm, J. Fuchs, N. Steinfeldt, R. Stösser, R., M.T. Pope, *Inorganic Chemistry*, **1996**, *35*, 3273.
26. C. Rocchiccioli-Deltcheff, R. Thouvenot, *Spectrochimica Acta*, **1976**, *32A*, 587.
27. H. So, M.T. Pope, *Inorganic Chemistry*, **1972**, *11*, 1441.
28. A.R. Tomşa, D. Cioloboc, A.M. Todea, L. Mureşan, V. Paşcalău, M. Rusu, *Studia Universitatis Babeş-Bolyai, Seria Chemia*, **2009**, *LIV*, 33.
29. A.B.P. Lever, "Inorganic Electronic Spectroscopy", Elsevier, New York, 2nd edn., **1984.**
30. A.B.P. Lever, *Journal of Chemical Education*, **1968**, *45*, 711.
31. D.K. Lyon, W.K. Miller, T. Novet, P.J. Domaille, E. Evitt, D.C. Johnson, R.G. Finke, *Journal of American Chemical Society*, **1991**, *113*, 7209.
32. C. Rong, F.C. Anson, *Inorganic Chemistry*, **1994**, *33*, 1064.

33. R.P.S. Chakradhar, J.L. Rao, G. Sivaramaiah, N.O. Gopal, *Physica Status Solidi (b)* **2005**, *242*, 2919.
34. M. Sadakane, E. Steckhan, *Chemical Review*, **1998**, *98*, 219.
35. S. Dong, X. Xi, M. Tian, *Journal of Electroanalytical Chemistry*, **1994**, *385*, 227.
36. X. Xi, G. Wang, B. Liu, S. Dong, *Electrochimica Acta*, **1995**, *40*, 105.
37. L. David, C. Crăciun, M. Rusu, O. Cozar, P. Ilea, D. Rusu, *Polyhedron*, **2000**, *19*, 1917.
38. A.R. Tomşa, L. Mureşan, A. Koutsodimou, P. Falaras, M. Rusu, *Polyhedron*, **2003**, *22*, 2901.
39. A.J. Bard, L.R. Faulkner, "Electrochemical Methods Fundamentals and Applications", Wiley, New York, **2001**.

STUDIA UNIVERSITATIS BABEŞ-BOLYAI, CHEMIA, LIV, 4, 2009

PREDICTIVE ROLE OF ANALYTICAL INVESTIGATIONS ON THE BIOCHEMICAL HOMEOSTASIS IN YOUTH NOTE I. LIPID METABOLITES RELATED TO SOMATOMETRY

GARBAN GABRIELA[a], AUMÜLLER CORINA[b], GARBAN ZENO[b]

ABSTRACT: Research concerning the homeostasis of lipid metabolites elicits interest due to its predictive value of the pathobiochemical risk.

In this context the investigations were performed on a number of 423 subjects aged between 10-18 years (174 boys and 248 girls), pursuing the status of lipid metabolites in blood serum, i.e. triacylglycerols and total cholesterol. Also, the analytical data were correlated with the body mass index (BMI) – a somatometric index. Thus, it was possible to identify the overweight subjects (BMI over 95 percentile) as well as the overweight subjects with homeostatic disturbances (dyshomeostasis). As these adolescents might develop cardiovascular and/or other related diseases in adulthood, they were included in a preventive monitoring system.

Keywords: chemical investigations on lipid metabolites in human blood serum – dyshomeostasis, pathobiochemistry

INTRODUCTION

Biochemical homeostasis in human organism is fundamental for the maintenance of its morphophysiological status [1], [2]. Analytical and bio-analytical chemistry offer means for the investigation of various metabolites, e.g.: carbohydrates, lipids, proteins and electrolytes.

In metabollomics theoretical concepts and applicative chemical investigations are more and more developed in relation with biomarkers. In biochemistry and clinical chemistry such markers define the normal functioning of tissues and organs.

Dyshomeostasis is defined as a decrease or increase in the concentration of various metabolites. These changes can occur, among others, as a consequence to malnutrition (lack or excess of nutrients), the presence of different chemical xenobiotics from the environment. [3], [4].

[a] *Laboratory of Environment and Nutrition, Institute of Public Health Timisoara, Bd. Dr. V. Babes Nr.16, RO-300 242 Timisoara, Romania, garban_g@yahoo.com;*

[b] *Department Biochemistry and Molecular Biology, Faculty of Food Products Technol., University Agricultural Sciences and Veterinary Medicine of Banat Timisoara, Calea Aradului Nr. 119, RO-300 645 Timişoara, Romania, zeno_garban@yahoo.com*

The problem of lipid metabolites presents interest from different point of view: e.g.: nutritional (hypercaloric foods), medical (pathobio-chemistry of cardiovascular system), social (stress in human activity) and others.

Investigations were performed successively on the concentration of the main serum lipid metabolites: triacylglycerols, total cholesterol and correlated with the body mass index - BMI (Note I); on HDL-cholesterol, LDL-cholesterol and extended to blood metallograms - regarding Ca and Mg (Note II). On the whole, peculiarities of the biochemical homeostasis in young people were monitored.

MATERIALS AND METHODS

Investigations included a group of 423 healthy young people from a school collectivity and is the first study in this domain in Romania. Youth were divided in two groups: group n_1 – including 174 boys and group n_2 – including 249 girls. The age limits of subjects were between 10-18 years which, according to WHO, covers the period of adolescence.

In the first step the weight and height of young people were measured, thus obtaining the somatometric data. Then blood samples were collected for biochemical analysis (lipids, lipoproteins and some metals).

This paper presents the results obtained on serum lipid fractions: triacylglycerols (TAG) and total cholesterol (T-Chol). The analytical results were correlated with the somatometric data expressed in body mass index (BMI) in order to evidence the subjects with risk to develop cardiovascular or other diseases [5], [6].

Analytical determinations were made by using a LABSYSTEM-901 analyzer and specific Clinilab reagents. The method of Fossatti and Prencipe [7] was used for triacylglycerols and the method of Allain et al. [8] for total cholesterol determination.

Serum triacylglycerols determined by the enzymatic spectrophoto-metric method has the following principle: serum triacylglycerols are transformed, in the presence of lipoproteinlipase, into glycerine-3-phosphate. Finally, the measurements were performed at the wavelength 540 nm.

Total cholesterolemia determined by the enzymatic spectrophotometric method was based on the following principle: the transformation of cholesterol ester in cholesterol and fatty acids in the presence of cholester-esterase. Final determinations were made at the wavelength 500 nm.

The analytical data were statistically processed; for each age group the mean value (X) and the standard deviation (SD) were calculated.

RESULTS AND DISCUSSIONS

Blood triacylglycerols result mainly from the catabolism of dietary glycerides and in a more reduced amount from the conversion of carbohydrates and of some aminated acids (in the frame of specific biochemical pathways of the tricarboxylic acid cycle).

The obtained data on triacylglycerolemia are presented in Table 1. These are mentioned for gender groups (noted n_1 the boys and n_2 the girls) and within gender groups for age categories – see Table 1. Comparative data regarding triacylglycerolemia (in mg / dL) in the studied boy and girl groups.

Table 1. Comparative data regarding triacylglycerolemia (in mg/dL) in the studied boy and girl groups

Age groups (years)	Group (boys)		Group (girls)		ΔX (X_1-X_2)
	n_1	$X_1 \pm DS$	n_2	$X_2 \pm DS$	
10	15	66.07 ± 33.92	14	69.50 ± 35.65	+ 3.43
11	23	86.09 ± 37.25	33	78.21 ± 42.28	- 7.88
12	29	76.72 ± 44.14	45	78.82 ± 48.77	+ 2.10
13	35	59.06 ± 25.14	26	87.73 ± 59.48	+ 28.77
14	30	52.83 ± 23.88	36	78.86 ± 45.03	+ 26.03
15	13	62.46 ± 26.41	36	73.77 ± 31.27	+ 11.31
16	18	67.56 ± 23.33	25	72.48 ± 34.32	+ 4.92
17	8	76.75 ± 20.44	16	91.56 ± 35.92	+ 14.81
18	3	80.33 ± 46.48	18	76.22 ± 32.52	- 4.11

According to the method for triacylglycerolemia determination the normal values range between 50-160 mg/dL in boys and between 45-140 mg/dL for girls. In this context the resulted mean values were in normal limits.

As seen in Table 1 the highest values of triacylglycerolemia in boys were found at 11 years age and the lowest at 14 years age. In girls the values were higher than in boys excepting age groups of 11 and 18 yrs.

A similar study was performed in Greece by Schulpis and Karikas [9] on a number of 7767 subjects (3980 boys and 3785 girls) aged between 6-14 years. Their results showed a maximum level for triacylglyceridemia in boys aged 11 yrs and a diminishing to age13 yrs. The same results were revealed in girls with the observation that in the group of 10 yrs and 14 yrs old girls the values were over the normal limit.

Another study performed by Khalil et al. [10] on the serum lipid profile in a number of 410 healthy Indian subjects aged 3-12 years revealed no significant difference between genders. The mean value for triglycerides was 91.1 mg/dL and for total cholesterolemia 134.5 mg/dL. It is to mention that the mean value of triacylglycerols was higher than in our study but total cholesterolemia was much lower.

Bistrizer et al. [11] evaluated the serum lipids profile in 107 children and their parents (40 families) in which the father had a myocardial infarction or coronary heart disease (CHD) before age 40 years. Regarding the results for children, significant hyperlipidaemia were found in 42%.

Studies performed by Tamir et al. [12] and Williams et al. [6], evidenced the complex influence of morphophysiologic factors in adolescents.

The American Heart Association set guidelines for serum triacylglycerol levels (values were expressed in mg/dL), thus: normal < 150 (no risk); borderline high 150-199; high 250-499; very high > 500 (high risk)

In the human organism augmented levels of triacylglycerols in the bloodstream have been linked to atherosclerosis, even in the absence of hypercholesterolemia, and, by extension the risk of heart disease and stroke.

Between the causes of hypertriacylglycerolemia one can mention obesity, high intakes of fat and concentrated sweets, genetic predisposition and others. The values found by us indicate changes related to age and maturation which could reflect the influence of sex hormones on serum lipoprotein metabolism [13], [14].

Homeostasis changes in cholesterolemia originate in the metabolic disturbances of sterides – macronutrients present in diet [15], [16]. In table 2 there are presented the values of the T-Chol in the studied groups.

Normal values according to the used method for cholesterolemia range between 160-199 mg/dL. Thus, in our subjects the mean values did not exceed normal limits, but in girls the values are higher, except for girls aged 14 and 15 years.

The 1987 report of National Cholesterol Education Program, suggest the total serum cholesterol level should be: < 200 mg/dL normal serum cholesterol, 200–239 mg/dL borderline-high, > 240 mg/dL high cholesterol [17]. Nowadays, the link between cholesterol and atherosclerosis is accepted by the majority of medical scientists [18].

Table 2. Comparative data regarding cholesterolemia (in mg/dL) in the studied boy and girl groups

Age groups (years)	Group n_1 (boys)		Group n_2 (girls)		ΔX (X_1-X_2)
	n_i	$X_1 \pm DS$	n_i	$X_2 \pm DS$	
10	15	150.50 ± 24.79	14	159.14 ± 34.87	+ 8.64
11	23	143.60 ± 29.54	33	155.82 ± 30.10	+ 12.22
12	29	147.70 ± 32.35	45	155.27 ± 32.57	+ 7.57
13	35	131.70 ± 20.29	26	141.42 ± 24.08	+ 9.72
14	30	140.50 ± 29.25	36	138.11 ± 20.25	- 2.39
15	13	147.80 ± 27.66	36	143.81 ± 29.18	- 3.99
16	18	136.10 ± 24.36	25	157.40 ± 22.61	+ 21.30
17	8	122.40 ± 26.12	16	146.56 ± 32.25	+ 24.16
18	3	137.70 ± 16.29	18	146.06 ± 35.42	+ 8.36

Investigations concerning cholesterolemia is of great importance because this steroid compound is present in blood, bile and brain tissue. In metabolic processes cholesterol is a precursor in the synthesis of bile acids, steroid hormones and vitamine D [19], [20]. The level of T-Chol in blood serum is associated with metabolic processes and their disturbances in some cardiovascular disease and infections [21]. There are also experimental studies on young subjects [22], [23].

Genetics play an important role in determining adolescents`s cholesterol level. Also, the family lifestyle and diet will have an important effect on an adolescent's cholesterol.

Cholesterol and other cardiovascular risk factors often persist from childhood to adulthood. Autopsy studies demonstrated that aortic and coronary atherosclerosis are commonly seen before age 20 years. High total cholesterolemia, LDL-Chol, VLDL-Chol and low HDL-Chol are correlated with extent of early atherosclerotic lesions in adolescent and young adult [12], [24].

Usually, dyshomeostasis of TAG and T-Chol in youth give evidence of „metabolic syndrome" which develops in time to atherosclerotic processes [25].

Based on somatometric data (weight and height) the body mass index (BMI) - an anthropometric index, defined as the individual`s body weight in kilograms divided by the square of his or her height, were calculated. BMI is widely used to define overweight and obesity, because it correlates well with accurate measures of body fatness.

Using the BMI-for-age gender specific charts recommended by Center for Disease Control and Prevention – Atlanta, USA, the adolescents were classified as: under-weighted - BMI < 5th percentile; normal weighted - BMI between 5 < 85 percentile; at risk of overweight - BMI between 85 < 95 percentile or overweighted - BMI > 95 percentile [26]. The obtained results are presented in Table 3.

Having in view the somatometric criteria, exactly the BMI and assessing the distribution of subjects in the percentile limits, there were revealed 14 boys and 16 girls between 85-95 percentile, and 6 boys and 12 girls over 95 percentile.

Recent studies indicate an increasing prevalence of overweight and obesity in childhood in developed and developing countries, e.g. the prevalence among children and adolescents in USA has doubled in the past two decades [27], [28].

It is known that obesity is associated with significant health problems in childhood and adolescence and is an important early risk factor for much of adult morbidity and mortality [29], [30]. In obese children and adolescents the cardiovascular system is affected (e.g. hypercholes-terolemia, dyslipidemia, hypertension) – see [31], [32]. At the same time, perturbations were found in endocrine system (hyperinsulinism, insulin resistance, impaired glucose tolerance, type 2 diabetes mellitus, menstrual irregularity) and mental health (depression).

Table 3. Distribution of the studied subjects according to percentile (BMI-for-age) evaluation

Age group	Scale of BMI in boys					Scale of BMI in girls				
	< 5	5-85	85-95	> 95	Total	< 5	5-85	85-95	> 95	Total
10	0	12	1	2	**15**	0	13	1	0	**14**
11	2	15	3	3	**23**	1	30	0	2	**33**
12	3	23	3	0	**29**	3	35	6	1	**45**
13	4	28	3	0	**35**	0	24	1	1	**26**
14	4	24	1	1	**30**	1	26	5	4	**36**
15	2	9	2	0	**13**	3	29	2	2	**36**
16	1	16	1	0	**18**	1	22	1	1	**25**
17	1	7	0	0	**8**	1	15	0	0	**16**
18	0	3	0	0	**3**	2	15	0	1	**18**
Total	**17**	**137**	**14**	**6**	**174**	**12**	**209**	**16**	**12**	**249**

Detailed results on TAG and T-Chol determination for overweighted subjects (18 cases) with high risk for “metabolic syndrome” – i.e. category of subjects over 95 percentile of BMI, are presented in Table 4.

Table 4. Serum TAG and T-Chol (mg/dL) in boys and girls with BMI over 95

Gender	Age (years)	Identified subjects		TAG	T-Chol
		No.	Cases		
Boys (6)	10	1.	CS	**164**	167
		2.	TD	89	171
	11	3.	BA	**193**	176
		4.	CA	50	137
		5.	MA	83	116
	14	6.	SM	49	136
Girls (12)	11	1.	NI	**191**	117
		2.	CA	**194**	195
	12	3.	TA	56	**211**
	13	4.	CV	**259**	158
	14	5.	BS	**251**	173
		6.	PR	84	153
		7.	PM	68	147
		8.	KA	84	127
	15	9.	RB	101	146
		10.	MI	72	174
	16	11.	TM	48	162
	18	12.	FC	61	**201**

Regarding the obtained analytical results of TAG and T-Chol in overweighted subjects, high values (over the normal limits) were observed in 8 cases (2 boys and 6 girls). In boys 2 cases of hypertriacyl-glycerolemia were evidenced. In girls 4 cases of hypertriacyglicerolemia and 2 cases of hypercholesterolemia were found. The values over the normal limits are evidenced in table 4 by using bold.

Vanhala et al. [33] found that obese children who went on to be obese adults had a threefold increased risk of developing the metabolic syndrome compared with those who became obese as adults.

The probability of childhood obesity persisting into adulthood is estimated to increase from approximately 20% at 4 years of age to approximately 80% by adolescence [34]. In addition, it is probable that comorbidities will persist into adulthood [35].

In light of the literature data, in order to prevent the development of cardiovascular and other related diseases all the young subjects found with BMI over 95 and high values of TAG and T-Chol will be monitored.

CONCLUSIONS

Investigations on some serum lipid fraction by using methods based on bioanalytical chemistry, the values of TAG and T-Chol were determined in 423 adolescents (174 boys and 248 girls) aged 10-18 years. Also, the somatometric index, i.e. body mass index (BMI), for each subject was calculated. Thus, a number of 18 adolescents (6 boys and 12 girls) was detected with BMI over 95 (considered as overweight). This category of young people is exposed to pathobiochemical risk in time.

When correlated the BMI of the 18 overweight adolescents with their analytical findings only a number of 8 subjects were find with hyper-lipidemia: 2 boys and 4 girls with hypertriacylglycerolemia and 2 girls with hypercholesterolemia. The subjects with hyperlipidemia will be included in a monitoring system with a strict treatment (diet and medication) in order to reduce body weight and to decrease TAG and T-Chol values, thus preventing the development of cardiovascular and/or other related diseases.

The identified 10 subjects (4 boys and 6 girls) only with BMI over 95 percentile will be included also in a preventive monitoring program in order to reduce their body weight, e.g. with energy-restricted diet (lowered lipid and carbohydrate nutrients in ratio), increase of physical activity, and others.

Using methods which are specific for analytical chemistry in lipidology and calculations to obtain the somatometric index, permitted the identification of subjects with “metabolic syndrome”. These subjects have a major risk to develop biochemical injuries characteristic to atherosclerosis. In order to prevent adulthood diseases in these subjects they must be monitored.

REFERENCES

1. T. Brody T., „Nutritional biochemistry", Academic Press, San Diego, **1994**.
2. J. W. Marshall, K. S. Bangert, „Clinical Biochemistry. Metabolic and clinical aspects", Churchill Livingstone, New York-Edinburgh-London-Madrid, **1995**.
3. A. G. Gornall (Ed.), „Applied Biochemistry of Clinical Disorders", J. B. Lippincott Company Philadelphia, **1986**.
4. G.A. Kaplan, A. J. Pesce, S.C. Kazmierczak (Eds.), "Clinical chemistry: theory, analysis and correlation", 4th ed., C.V. Mosby Comp., St. Louis-Toronto-Princeton, **2002**.
5. R. Monge-Rojas, *Arch. Latinoam. Nutr*., **2001**, *51*, 236.
6. C. L. Williams, L. L. Hayman, S. R. Daniels, T. N. Robinson, J. Steinberger, S. Paridon, T. Bazzarre, *Circulation*, **2002**, *106*, 143.
7. P. Fossati, L. Prencipe, *Clin. Chem*., **1982**, *28*, 2077.
8. C.C. Allain, L. S. Poon, C. S. Chan, W. Richmond, P. C. Fu, *Clin. Chem*., **1974**, *20*, 470.
9. Kleopatra Schulpis, A.G. Karikas, *Pediatrics*, **1998**, *101*(5), 861.
10. A. Khalil, R. Gupta, A. Madan, M. Venkatesan, *Indian Pediatr.*, **1995**, *32*, 1177.
11. T. Bistritzer, L. Rosenzweig, J. Barr, S. Mayer, E. Lahat, H. Faibel, Z. Schlesinger, M Aladjem - *Arch Dis Child*., **1995**, *73,* 62.
12. I. Tamir, G. Heiss, C. J. Glueck, B. Christensen, P. Kwiterovich, B. M. Rifkind, *J. Chron. Dis*., **1981**, *34*, 27-39.
13. T.B. Newman, A.M. Garber, N.A. Holtzman, S.B. Hulley, *Arch. Pediatr. Adolesc. Med*., **1995**, *149*, 241-247.
14. Gabriela Garban, Corina Aumüller, Z. Garban, *Physiology*, Supplement, **2006** (16), 39.
15. W.W. Christie, „Lipid Analysis", 3rd edition, Oily Press, Bridgwater, **2003**.
16. Corina Aumüller, Gabriela Garban, Z. Garban, *Journal of Agroalimentary Processes and Technologies*, **2006**, *12*(2), 557.
17. S.S. Gidding, W. Bao, S.R. Srinivasan, G.W. Berenson, *J Pediatr.***1995**, *127*, 868.
18. *** *Arch. Intern. Med.,* **1987**, *148* (1), 36.
19. J. A. Morrison, I. de Groot, B.K. Edwards, *Pediatrics*, **1978**, *62*, 990.
20. M. T. Pugliese, F. Lifshitz, G. Grad, P. Fort, M. Marks-Katz, *N. Engl. J. Med*., **1983**, *309*, 513.
21. M.H. Steiner, L.S. Neinstein, J. Pennbridge, *Pediatrics*, **1991**, *88*, 269-278.
22. L. Gallo, C. Bennett, S. Myers, G. Vanouny, *J. Lipid Res*., **1984**, *25*, 604.
23. Y.B. Park, S.M. Jeon, S.J. Byun, H.S. Kim, M.S. Choi, *Life Sci.*, **2002**, *70*, 1849.
24. G.S. Berenson, S.R. Srinivasan, J.L. Cresanta, T.A. Foster, L.S. Webber, *Am. J. Epidemiol*., **1981**, *113*, 157.
25. Ana Carolina R. Vieira, Marlene M. Alvarez, S. Kanaan, Rosely Sichieri, Gloria V. Veiga, *Rev. Saúde Pública*, **2008**, *42(6),* 1.

26. *** Centers for Disease Control and Prevention, BMI for children and teens, 2003. http://www.cdc.gov/nccdphp/dnpa/bmi/bmi-for-age.htm.
27. J.H. Himes, W.H. Dietz, *Am J Clin Nutr.*, **1994**, *59*, 307.
28. *** US Dept Health and Human Services. *The Surgeon General's Call to Action to Prevent and Decrease Overweight and Obesity.* Rockville, MD: US Department of Health and Human Services, Public Health Service, Office of the Surgeon General; **2001**.
29. D.S. Freedman, W.H. Dietz WH, S.R. Srinivasan, G.S. Berenson, *Pediatrics,* **1999**, *103*, 1175.
30. A. Must, P.F. Jacques, G.E. Dallal, C.J. Bajema, W.H. Dietz, *N. Engl. J. Med.,* **1992**, *327*, 1350.
31. J.A. Morrison, P.M. Laskerzewski, J.L. Rauh, *Metabolism,* **1979**, *28*, 641.
32. D. Steinberg, *The Cholesterol Wars: The Cholesterol Skeptics vs the Preponderance of Evidence*, 2007, Boston, Academic Press.
33. M. Vanhala, P. Vanhala, E. Kumpusalo, P. Halonen, J. Takala, *BMJ,* **1998**, *317*, 319.
34. S.S. Guo, W.C. Chumlea, *Am J Clin Nutr.,* **1999**, *70(suppl)*, 145S.
35. W. Wisemandle, L.M. Maynard, S.S. Guo, R.M. Siervogel, *Pediatrics,* **2000**, *106(1)* Available at: http://www.pediatrics.org/cgi/content/full/106/1/e14

STUDIA UNIVERSITATIS BABEŞ-BOLYAI, CHEMIA, LIV, 4, 2009

SYNTHESIS, CHARACTERIZATION AND OPTIMUM REACTION CONDITIONS FOR NANOSTRUCTURED ZINC OXIDE

OANA CADAR[a], CECILIA ROMAN[a], LUCIA GAGEA[b], ILEANA CERNICA[c], ALINA MATEI[c]

ABSTRACT. In the present paper were established the optimum conditions for the synthesis of Ag-doped ZnO nanopowders. The 0.05% Ag-doped ZnO nanopowders were successfully synthesized by coprecipitation, followed by a washing-drying-calcination treatment. It was found that the optimum conditions for the preparation with high yield and high surface area were as follows: pH value 6.9-7.1, calcination temperature 400 - 500 °C and calcination time 2 h, respectively. The obtained nanopowders were investigated by X-ray diffraction (XRD), Fourier transform infrared spectroscopy (FTIR) and specific surface. The silver doping improves the antibacterial activity of ZnO nanopowders. Therefore the materials based on the obtained nanopowders represent an attractive opportunity for the construction industry.

Keywords: zinc oxide, silver, synthesis, coprecipitation, characterization.

INTRODUCTION

In the past decades, the synthesis and characterization of “so-called” nanoparticles have attracted much attention, not only for the fundamental scientific interest, but also for many technological applications [1–4]. These particles have distinctly different electrical, optical, mechanical and chemical properties in comparison with their corresponding bulk material.

The interior mould attack has become a problem of increasing importance. The medical researchers and phisicians have been observing more and more respiratory and allergic complaints arising from exposure to moulds. Also, paint on outside attack must be taken into account [5, 6].

In recent years, ZnO and ZnO-based powders have been extensively studied due to their properties and technological applications [7]. As well known, zinc oxide has a long history of usage for pigments and protective coatings on metals [8]. Zinc oxide is a very important material due to the interesting

[a] *INCDO-INOE 2000 Institutul de Cercetări pentru Instrumentație Analitică, Str. Donath, Nr. 67, RO-400293 Cluj-Napoca, România, icia@icia.ro*

[b] *Universitatea Babeş-Bolyai, Facultatea de Chimie şi Inginerie Chimică, Str. Kogălniceanu, Nr. 1, RO-400084 Cluj-Napoca, România, gagea@chem.ubbcluj.ro*

[c] *Institutul Național de Cercetare – Dezvoltare pentru Microtehnologie, Str. Erou Iancu Nicolae Nr. 126A, RO-077190 Bucureşti, România, ileanac@imt.ro*

characteristics (fluffy white, density 5.61 g/cm^3, melting point 1975^{o}C) [9]. ZnO is cheaper than other white oxides and insoluble in water, a very important property of the quality of a pigment.

As well known, silver and silver ions exhibit an excellent antibacterial activity against many types of bacteria, even at lower concentrations, and do not cause adverse health effects [10, 11]. Recently, several inorganic antibacterial materials containing silver and silver ions have been successfully prepared and some of them are already commercialized products. These materials are more chemically durable, discharge slowly the silver ion and more slowly affected by light. Therefore, it is rational that introduction of silver ions into ZnO may improve antibacterial capacity of ZnO.

Until now, several methods, such as the mechanical mixing method [12], sol-gel process [13, 14], thermal hydrolysis [15] and coprecipitation [16] have been used to prepare metal-doped ZnO nanopowders.

The coprecipitation method seems to be the most attractive due to its easy control, without requiring expensive and complex equipments. Coprecipitation is the process whereby the fractional precipitation of a specified ion in a solution results in the precipitation not only of the target ion but also of other ions existing in the solution. The additional precipitation of unwanted ions represent an impediment to the analytical process [17]. Some of the most commonly substances used in coprecipitation operations are hydroxides, carbonates, sulfates and oxalates. pH is evidently an important factor in this type of process.

During last years our interests were focused on the preparation and characterization of new ZnO-based nanopowders [18]

The objective of the present study is to continue our research related to determining the optimum parameters for the synthesis of Ag-doped ZnO nanopowders *via* coprecipitation and the properties of the obtained nanoparticles. The obtained nanopowders have a low doping metal content (0.05 wt.%) in order to avoid cytotoxicity and not to affect the white color of the powders. The materials that incorporate these nanopowders may be used in construction industry, increasing the security of living, durability and comfort.

RESULTS AND DISCUSSION

Preparation

Establishing the adequate conditions for complete precipitation from zinc solution is not a simple process due to the amphoter character of Zn. In order to obtain the desired material, the zinc hydroxide is dissolved in a small excess of sodium or potassium hydroxide resulting in the corresponding alkali metal zincate. Because the zinc hydroxide is soluble in the presence of ammonium ions, different complex ions resulted too. Therefore, the solution pH is an important factor for the process.

The zinc hydroxide in the presence of alkaline carbonates form some basic zinc carbonates as $(CO)_3Zn_4(OH)_2$. Thus, it was appeal to the simultaneous precipitation of Zn^{2+} and Ag^{+} using an alkaline carbonate. The obtained carbonates were calcinated at an appropriate temperature resulting in a homogenous mixture of oxides containing particles of small dimensions.

The degree of precipitation control was realized by titration of the unprecipitated cation from the solution resulted after filtration, at controlled pH values. Thus, the quantity of precipitated Zn^{2+} could be calculated as the difference between initial and final content from the filtrate filled up to constant volume. The experiments were realized at different pH values, *i.e*. 6.0-8.0. In Figure 1 are presented the values for the zinc remained unprecipitated in solution. The optimum precipitation pH value is 6.9-7.1.

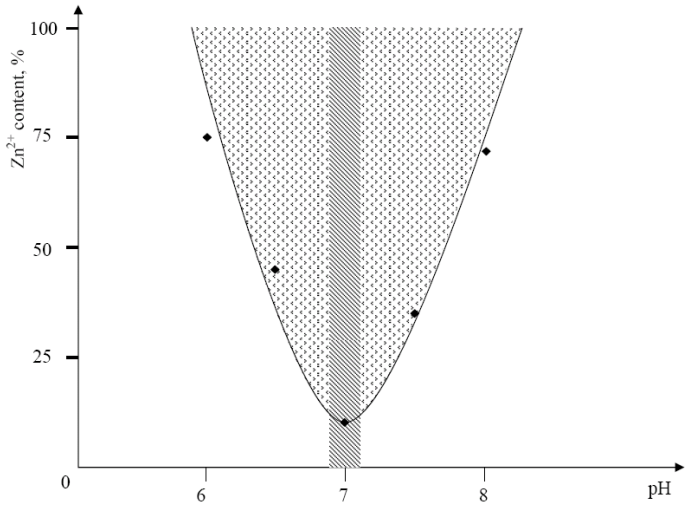

Figure 1. Relationship between the pH of solution and Zn^{2+} content.

It was found experimentally that the optimal synthesis method can be divided into two parts: one is the preparation of the precursor by the coprecipitation method and the other one is the formation of silver doped ZnO nanopowders by calcination (Figure 2) [18].

The zinc oxide diffraction peaks start to appear after the powder was calcinated at 380^{o}C. With the increase of thermal treatment temperature, the microcrystallites are formed more obviously and also the diffraction peaks become more intense.

The commercial ZnO has a wurtzite crystal structure. Literature data demonstrate that ZnO crystals begin to nucleate at about 380^{o}C, and then ZnO crystal growth is completed at about 800^{o}C [19].

At 600ºC X-ray diffraction analysis of the prepared Ag-doped ZnO nanopowder show sharp diffraction peaks corresponding to the hexagonal wurtzite structure: 31.8º (1 0 0), 34.5º (0 0 2), 36.4º (1 0 1), 47.7º (1 0 2), 56.7º (1 1 0), 62.9º (1 0 3), 66.4º (2 0 0), 68.2º (1 1 2) and 69.3º (2 0 1).

The typical silver diffraction peaks were not observed, mainly because the low dosage of silver ions.

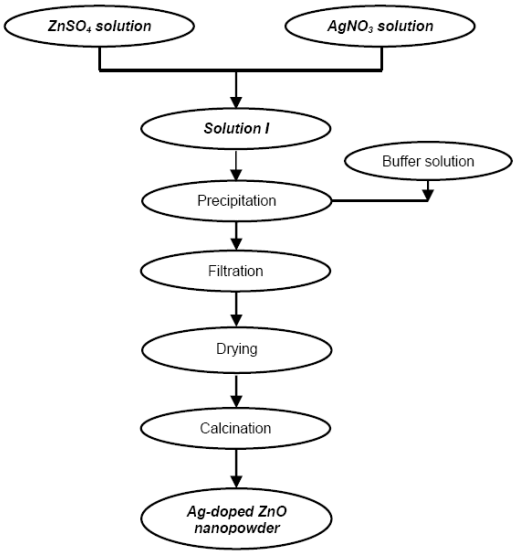

Figure 2. Flow diagram for the synthesis of Ag-ZnO nanopowders.

Structural characterization

X-ray diffraction spectra

Figure 3 shows the XRD patterns of the samples calcinated at different temperatures.

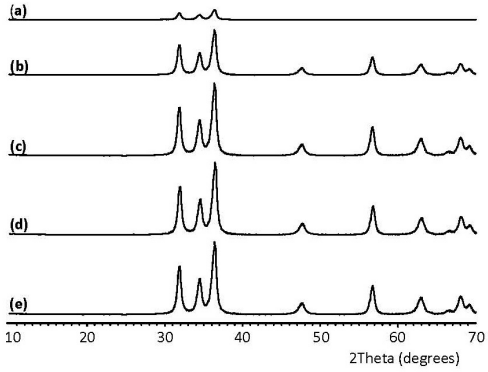

Figure 3. XRD patterns of the ZnO nanopowders calcinated at different temperatures: (a-e) 300, 380, 400, 450 and 600ºC, respectively.

Specific surface

The temperature heat treatment is the factor that mostly influences the formation and growth of crystalline particles obtained from precipitates after calcination. The diffusion in solids, the mobility of constituent particles and their possibility of migration to interfaces increase as temperature increases. The control of particle size increasing is realized indirectly by determining specific surface of the calcinated product at the temperatures of interest.

The studies were realized on precipitates calcinated at 300, 400 and 600°C. The results of the specific surface area analyses are reported in Table 1.

Table 1. Specific surface area of the powders calcinated at different calcination temperatures.

Temperature (°C)	Specific surface area (m^2/g)	Average diameter (nm)
300	70.8-74.3	14.39-15.10
400	49.8-51.5	20.90-21.39
600	20.46-28.6	52.27-62.40

Fourier transform infrared spectroscopy

In FTIR spectra of the samples undoped and doped ZnO (calcinated at 400°C) were observed bands with maximum well defined, centred at 593, 555, 547, 522, 517, 503, 500, 490 cm^{-1} (Figure 4).

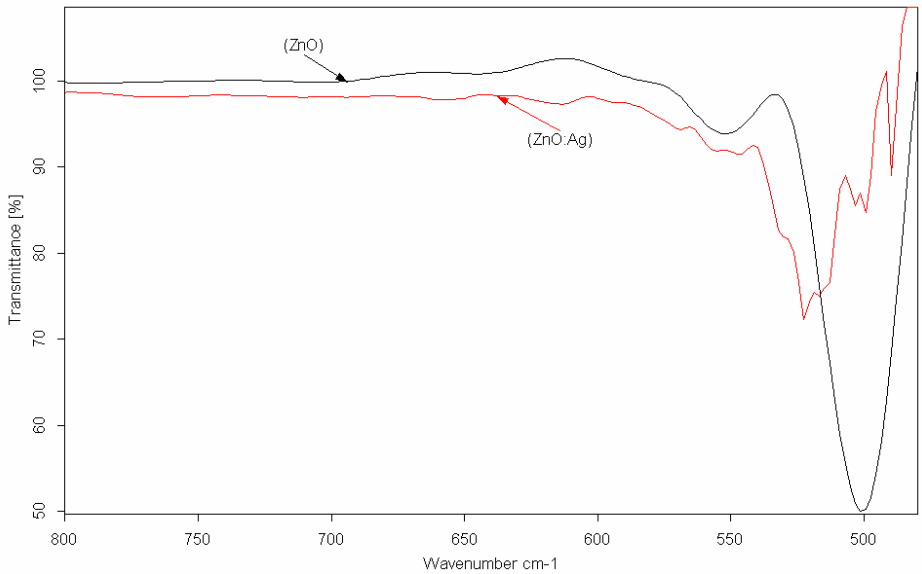

Figure 4. FT-IR spectra of undoped ZnO and Ag - doped ZnO nanopowder, calcinated at 400ºC.

The FTIR spectra of undoped ZnO powders show a high intensity broad band around 490 cm^{-1} due to the stretching mode of Zn–O bond. A similar band was also observed in doped ZnO powder.

The absorption bands observed in the low energy region is formed by the stretching vibration modes of Zn–O and Ag–O bonds (593 and 490 cm^{-1}) [20].

In the FTIR spectra for doped ZnO sample, in comparison with undoped ZnO spectra, we can see a slight displacement of characteristic Zn-O band, concurrent with modification of the peaks and appearance of the new bands which can be attributed to the Zn-O-Ag bonds.

The broad absorption band from 490-600 cm^{-1} indicates the presence of Ag in the ZnO powder and this could be due to a small concentration of silver.

The materials based on these nanopowders could be used in public spaces which necessitate high quality standards and special technical requirements (hospitals, surgeries, bathrooms, food processing facilities, storage rooms, laboratories, nurseries, schools, sport rooms, etc.). General advantages and benefits in the use of materials based on these nanopowders are: environmentally friendly, significant reduction of moos and algae, improvement of the air quality, housing comfort and healthy dwelling, inexpensive, long-term prevention, convenient and easily synthesizable.

CONCLUSIONS

The synthesis of Ag-doped ZnO samples by coprecipitation is simple, stable, repeatable and inexpensive. Several parameters that may influence the synthesis have been discussed. It has been concluded that the optimum reaction conditions are: pH: 6.9-7.1, calcination temperature: 400-500 °C and calcination time: 2 h. The silver concentration must be enough small not to influence the pigment color. The characterization of the obtained samples by specific techniques clearly indicates nano-sized particles.

These nanopowders may be incorporated into a coating in order to obtain materials with superior characteristics for the construction industry.

EXPERIMENTAL SECTION

The Ag-doped ZnO nanopowders were prepared by the coprecipitation method similar to that one previously reported [18].

All reagents were purchased from commercial suppliers and used without further purification. There were used precipitant solution of different pH values, *i.e*. 6.0-8.0) and the calcination temperatures were: 300, 380, 400, 450 and 600ºC, respectively).

The obtained powders were investigated using powder X-ray diffraction (XRD), Fourier transform infrared spectroscopy (FTIR) and specific surface studies. X-ray diffraction (XRD) patterns of these powders were measured on

the SHIMADZU 6000 diffractometer using a CuKα radiation source (40.0 KV, 30.0 mA) and a graphite monochromator. The samples were characterized by FTIR measurements using a model Tensor 27 Bruker spectrometer, in the wavelength range 4000-400 cm^{-1}, after 64 scans, with resolution of 4 cm^{-1}. The specific surface was determined using a modified BET installation.

The detailed preparation process can be described as follows: firstly, under vigorous stirring, the aqueous solution of zinc sulfate was added into silver nitrate aqueous solution. Subsequently, a buffer solution was used to adjust the pH of the reaction system to about 6.9-7.1. The resulted precursor of Ag-doped, $Zn_5(CO_3)_2(OH)_6$ precipitate, was thoroughly washed with distilled water and dried at room temperature (for more than 24 h) and then thermally decomposed under static air atmosphere to give silver doped zinc oxide. The calcination temperature was relatively low, in the range of 400-500 ^oC and the calcination time was 2 h, after which the material was cooled in the furnace and a white powder was obtained. A similar procedure was used for other pH and calcination conditions.

REFERENCES

1. G. Schmid, "Nanoparticles: From Theory to Application", Wiley-VCH, Weinheim, **2004**.
2. K.J. Klabunde, "Nanoscale Materials in Chemistry", Wiley-Interscience, New York, **2001**.
3. A.P. Alivisatos, *Science*, **1996**, *271*, 933.
4. Zhong Lin Wang, *J. Phys.: Condens. Matter*, **2004**, *16*, 829.
5. S. E. Henshon, "Mildew on the Wall", Royal Fireworks Publishing Company, New York, **2004**.
6. F.H. Kayser, K.A. Bienz, J. Eckert, R.M. Zinkernagel, "Medical Microbiology", Ed. Georg Thieme Verlag, Stuttgart, **2005**.
7. S.R. Dhagea, R. Pasrichab, V. Ravia, *Materials Letters*, **2005**, *59*, 779.
8. G.E. Weismantel, "Paint Handbook", Ed. McGraw-Hill, New York, **1981**.
9. C.G. Macarovici, D. Macarovici, "Chimia oxizilor dubli si utilizarile lor", Ed. Academiei Republicii Socialiste Romania, Bucuresti, **1975**.
10. A. Panacek, L. Kvitek, R. Prucek, M. Kolar, R. Vecerova, N. Pizurova, V.K. Sharma, T. Nevecna, R. Zboril, *J. Phys. Chem. B*, **2006**, *110*, 16248.
11. H.J. Lee, S.Y. Yeo, S.H. Jeong, *J. Mater. Sci.*, **2003**, *38*, 2199.
12. P.B. Joshi, N.S. S. Murti, V.L. Gadgeel, V.K. Kaushik, P. Ramakrishnan, *Journal of Materials Science Letters*, **1995**, *14*, 1099.
13. B. Houng and C.-J. Huang, *Surf. Coat. Technol.*, **2006**, *201*, 3188.
14. M.J. Alam, D.C. Cameron, *J. Vac. Sci. Technol.*, A, *Vac. Surf. Films*, **2001**, *19*, 1642.

15. Y. Liu, C. Liu, Q. Rong, Z. Zhang, *Appl. Surf. Sci.,* **2003**, *220*, 7.
16. O.D. Jayakumar, H.G. Salunke, R.M. Kadam, M. Mohapatra, G. Yaswant, S.K. Kulshreshthaa, *Nanotechnology*, **2006**, *17*, 1278.
17. P. Patnaik, "Dean's Analytical Chemistry Handbook", 2nd ed. McGraw-Hill, **2004**.
18. O. Cadar, C. Roman, L. Gagea, I. Cernica, A. Matei, *Revista Romana de Materiale*, **2007**, *37 (4)*, 316.
19. T. Masaki, S.J. Kim, H. Watanabe, K. Mizamoto, M. Ohno, K.H. Kim, *J. Cer. Proces. Res.*, **2003**, *4 (3)*, 135.
20. A.S. Tas, P. J. Majewski, F. Aldinger, *J. Am. Ceram. Soc.*, **2000**, *83*, 2954.

STUDIA UNIVERSITATIS BABEŞ-BOLYAI, CHEMIA, LIV, 4, 2009

CHLORINATED SOLVENTS DETECTION IN SOIL AND RIVER WATER IN THE AREA ALONG THE PAPER FACTORY FROM DEJ TOWN, ROMANIA

VANCEA SIDONIA[a], KOVACS MELINDA HAYDEE[b], DUMITRU RISTOIU[b], SILAGHI-DUMITRESCU LUMINITA[c]

ABSTRACT. Considerable amounts of chlorinated solvents compounds were identified and measured in raw water and soil samples collected during several month studies, along the Somes River near Dej city region of Romania. The most common organochlorine solvents detected were trichloroethylene (C_2HCl_3), tetrachloroethylene (C_2Cl_4), carbon tetrachloride (CCl_4) and chloroform ($CHCl_3$) with the range between 3.05 – 68.92 μg L^{-1}, 5.62 – 55.48 μg L^{-1}, 2.11 – 29.45 μg L^{-1} and 0.37 – 80.29 μg L^{-1}. They were detected using a mass spectrometer coupled at a gas chromatograph with electron capture detector and quantified using chlorinated solvent standards. Organochlorine compounds have different chemical properties that lead into a broad range to uses. Many of them have significant biological activities and some of them can be very toxic for plant, animals and humans. Because of that they present seriously environmental concern. This study presents the source of the pollution and also the levels of these pollutants in river water and the soil.

Keywords: chlorinated solvents, environmental pollution, GC-MS, GC-ECD.

INTRODUCTION

Starting with October 2006 it was observed in several water sample collected from Somes River Basins a high level of some chlorinated solvents. The aim of this study was to identify the chlorinated solvent species presence in river water and established the amount of them. Starting with results obtained from river water analysis was supposed also the possibility of soil contamination, so in the same time were analyzed even the soil sampled near the Somes River. Another goal of this study was to identify the possible pollution source. As shown previous medical and environmental researches, these compounds can induce serious adverse effects to humans and environment [1]. Chlorinated solvents are associated with a series of adverse human health effects such

[a] *Garda de Mediu, Comisariatul Judetean Cluj, str. G-ral T. Mosoiu, nr. 49, Cluj-Napoca, Romania*
[b] *Babes Bolyai University of Cluj-Napoca, Faculty of Environmental Science, Str. P-ta Stefan cel Mare, no.4, 400084, Cluj-Napoca, email: dristoiu@enviro.ubbcluj.ro*
[c] [c]*Universitatea Babeş-Bolyai, Facultatea de Chimie, str. Arany Janos, nr.11, 400068, Cluj-Napoca, Cluj-Napoca*

as toxicity of central nervous system, reproductive, liver and kidney and also carcinogenicity [2 - 5]. Several chlorinated solvents are used in large volume amount in industry because they own a batch proper chemical and physical property [6 - 9]. They are widely used as solvents for fats, oils, waxes and resins or adhesives solvent, in dry cleaning operations, cleaning printed circuit boards, vapour degreasing, parts cleaning, engine cleaner or degreasing agent and paint remover. Many times they are used primarily to produce other chemicals or as chemical intermediate, also are used in organic synthesis, fluorocarbon and polymer manufacture, aerosol propellant and foam plastic blowing agents.

Dej is a small city located at 60 km from Cluj-Napoca town where Somesul Mic River meet Somesul Mare River. At the outlying of Dej city is water making factory. It is known as the pulp and paper industry has been consuming much water. The simple process of paper making is almost the same as the method of Cailun who is the invitatory of paper in ancient China. In Dej paper making factory, the Kraft process is the main process applied in the paper production. The main chemicals are sodium hydroxide (NaOH) for pulping and chlorine for bleaching. The production of paper can be divided in seven steps: a. raw material selection and preparation; b. digestion; c. washing; d. bleaching; e. washing; f. refining or beating and g. paper making – as shown in scheme 1. This paper making unit (g) consists of many unit operations such as: sheet forming, transferring, pressing, and drying. Finally is obtained the paper.

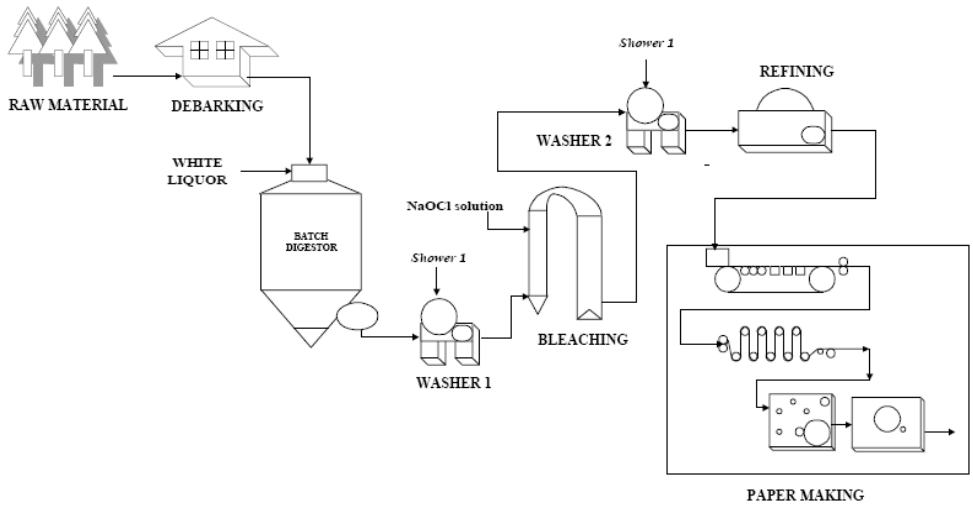

Scheme 1

RESULTS AND DISCUSSION

Organochlorine are organic compounds and from it class make part chlorinated solvents. Some of chlorinated solvents are volatile organic compounds. The most common organochlorine and chlorinated solvents founded in Somes river water were: carbon tetrachloride, 1,2-dichloroethane, 1,1-dichloroethylene, cis-1,2-dichloroethylene, trans-1,2-dichloroethylene, methylene chloride, tetrachloroethylene, 1,1,1-trichloroethane, trichloroethylene, vinyl chloride and chloroform, dichlorobromomethane, dibromochloromethane.

Chlorinated solvents are widely used in industry such as in the paper making factory and also in common household products. These chemicals are used as degreasing fluids for many different purposes such as dry-cleaning clothes, de-caffeinate coffee, cleaning metal machinery, dissolving grease build up in septic tanks and in making paper industry.

Because some of the organochlorine compounds are volatile organic compounds (VOCs) they can move easily through the environment. If improperly discarded onto the ground, these chemicals can travel downward through the soil and eventually end up in the groundwater. Organochlorine compounds such as chloroform, trichloroethylene or tetrachloroethene are not usually found in river water because they tend to evaporate from the water into the air but they can appear in river just if exist a source of man made pollution. Even that in all sample collected from Somes River was found such of kind's organochlorine compounds and in the high concentration level. That could de explain by the fact that near the Somes River outlying Dej district is located the paper factory where in the paper making process is used high amount of chlorine based solvents. Actually in the bleaching steps from the paper making process – where the purposes of this process are to whiten the pulps is used high amount of organochlorine solvents. In that process unbleached pulps are loaded to the bleaching tanks (see scheme 1), the common bleaching chemicals used normally are sodium hypochlorite or calcium hypochlorite. Also in the washing steps the bleacher bark is transferred to the concrete tanks for washing. This washing steps in performed 2 - 5 times or until the smell of chlorine disappears. The factory evacuates that water in Somes River. It was observed that after the closing of factory for two weeks the concentration level of these compounds started to decreased – table1.

When the factory was closed organochlorine compounds concentration was followed every day in the water sample during October. In the middle of the month the factory was closed (in 15 October the factory was closed to 28 October when the factory was opened again). Our measurement show that the concentration for the followed compounds started to decreased after the factory was closed. Before the concentration for chloroform was between 65 – 85 μg/l and after that the factory was closed the concentration was between 35 – 55 μg/l – see figure 1. The same situation was observed for trichloroethylene and tetrachloroethene, their concentration decreasing with 30 -50 %, after that the factory was closed.

Table 1. Chloroform and trichloroethylene concentration variation when factory are working on and after that the factory was closed

Observation	Data of sampling	$CHCl_3$ μg L^{-1}	C_2HCl_3 μg L^{-1}
Factory on working	1	77.42	66.79
	2	78.65	48.59
	3	68.88	56.73
	4	61.26	50.12
	5	65.94	55.08
	6	66.05	57.49
	7	71.19	49.37
	8	79.05	69.28
	9	78.01	66.35
	10	79.53	68.11
	11	80.42	52.94
	12	86.79	48.97
	13	88.29	54.26
	14	87.41	54.92
	15	85.23	51.05
Factory are closed	16	76.48	44.11
	17	68.99	42.68
	18	60.27	35.16
	19	54.29	29
	20	59	11.59
	21	53.84	24.61
	22	54.59	30.94
	23	58.93	22
	24	49.02	21.54
	25	52.61	13.98
	26	43.27	10
	27	38.75	14.29

It is known that are several natural sources that may contribute significantly to the chlorocarbons in the environment [8]. For example chloroform is a major contributor to natural gaseous chlorine. It was found to be emitted by several anthropogenic and natural sources including the terrestrial areas. The origin of chloroform in the terrestrial environment can be anthropogenic point sources, atmospheric deposition, released by vegetation and production directly in the soil. Among terrestrial sources, forest has recently been identified as contributing to the release of chloroform into the environment [9]. But in our case it was found that the major chlorinated compounds detected in the Somes river are industrial origin alone, once due the factory that evacuate the dirty used water directly in the river and on the other hand due to atmospheric pollution that is an important source of contamination of surface water and soil by rain [9].

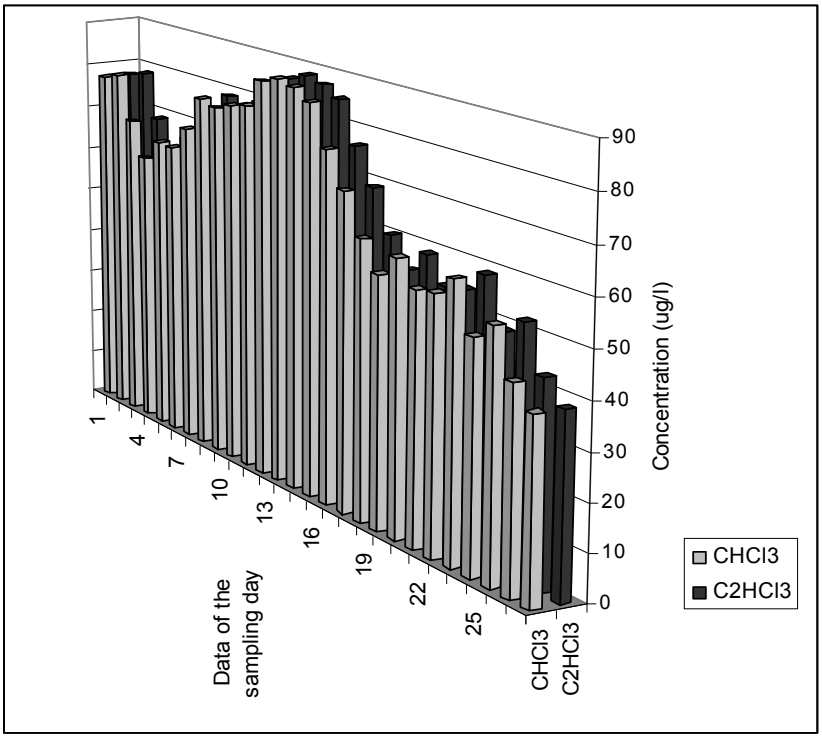

Figure 1. Trichloroethylene (C_2HCl_3) concentration (µg L^{-1}) and $CHCl_3$ concentration (µg L^{-1}) measured in Somes river water sample in October when the paper factory was working and after that the factory was closed.

In analysis of the water sample and soil sample the main found organochlorine were chloroform, TCE and PCE (see table 2 and 3). The presence of chloroform in terrestrial natural sources is still poorly investigated.

Table 2. Chloroform, trichloroethene and tetrachloroethene concentration value (µg/l) during May – October 2007 from soil sample from Dej sampling point.

Month	Chloroform (µg/l)	Trichloroethylene (µg/l)	Tetrachloroethylene (µg/l)
May	57.92	36.09	27.66
June	66.29	33.26	54.37
July	79.5	52.1	76.28
August	86.22	44.68	69.45
September	74.92	43.95	35.82
October	43.95	29.41	39

Table 3. Chloroform, trichloroethylene and tetrachloroethene concentration value (μg/l) during May – October 2007 from raw water sample.

Month	Chloroform (μg/l)	Trichloroethylene (μg/l)	Tetrachloroethylene (μg/l)
May	22.14	25.09	18.26
June	15.92	28.71	34.08
July	28.34	18.44	42.08
August	19.05	37.09	44.51
September	11.53	28.69	27.63
October	14.02	19.48	20.49

The formation and emission of chloroform by forest soil and observed large variation seen between sampling areas to the question of whether a seasonal variation exist (see figure 2 and 3). This may be expected if the production is biologically catalyzed.

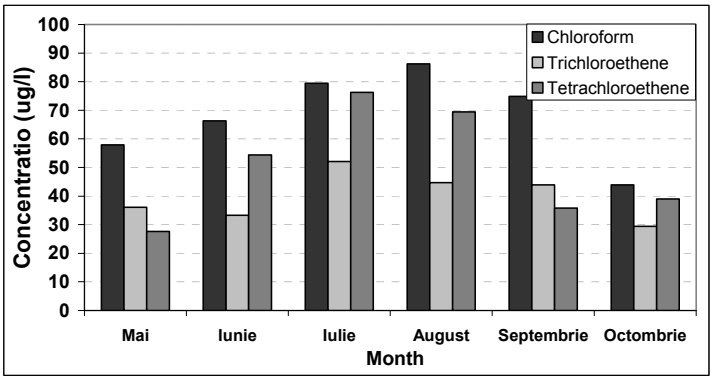

Figure 2. Chloroform, trichloroethene and tetrachloroethene variation during May – October 2007 from soil sample.

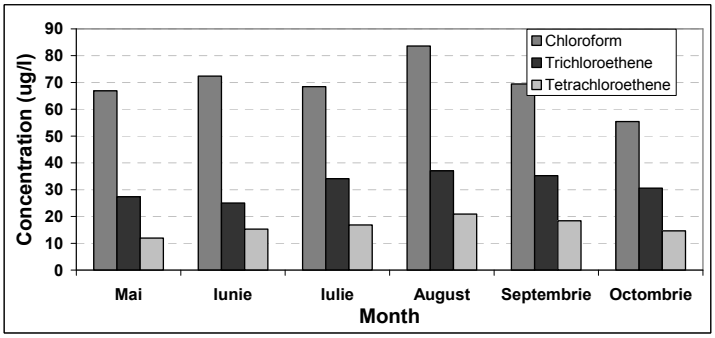

Figure 3. Chloroform, trichloroethene and tetrachloroethene variation during May – October 2007 from surface water sample.

CONCLUSIONS

The measurements of the Somes river water samples have shown that the industrial pollution is the most important sources of the chloroform, trichloroethylene and tetrachloroethene in the environment.

The major identified organocglorine compounds in the water and soil sample was chloroform, trichloroethen and tetrachloroethene. The presence of TCE and PCE can be explained by human hand made pollution of the environmental especially in Dej city where in the sample were measured higher concentration of this compounds. That could be caused from the factory that leased the used water in the Somes River. Also they used in their work process substances like TCE and $CHCl_3$. But also the natural source for chloroform exists and makes a contribution to the global sources. While chloroform alone may play a minor role in the global chlorine cycle, it may play be worth considering more seriously when taken together with other naturally – produced chlorocarbons. During the different month it was observed a highly seasonally variability for that compounds. That can be explaining by the fact that when the temperature increases, reaction is faster. In the winter months it is wait to be less concentration of these compounds because in some case ice cover protects surface of raw water and soil, and in that case the concentration of TCE, PCE and $CHCl_3$ found in nature due to their anthropogenic source are lower due to lower temperature and natural organic matter.

Also the results have shown that the concentration measured for the chloroform, trichloroethylene and tetrachloroethene was high in the period when the factory was on working. After that the factory was shot down the concentration for the followed compounds start to decrease. The difference between the concentration measured in the period of function of factory and in the period when the factory was close is high (almost 50%) – see figure 1. The major pollution of the soil and waste water is due to the paper factory.

EXPERIMENTAL SECTION

Water samples: were collected in 40 mL screw cap glass vials equipped with PTFE-faced single use septa. Prior to use the vials were washed with hot soapy water then rinse thoroughly with ultrapure water. After that, all cleaned vials were dry at 200 °C for 6 – 10 hours in an oven. All water samples were collected in duplicate and preserved. Phosphate buffer were used to inhibit base catalyzed degradation of some chlorinated solvents and to standardize the pH of all samples. The buffer were prepared as a dry homogenous mixture of 1 % Na_2HPO_4/99 % KH_2PO_4, from that mixture 0.8 g were add to all 40 mL vials before sampling. Water sample or extract were store at 4 °C in a freezer until the analysis. All extracts of the samples were analyzed within 14 days after sampling. The primary dilution standard

was prepared in 50 mL buffered reagent water, from it 500 μL with acetone were add in a 50 mL volumetric flask. This yields a final concentration in water of 10 μg/L and this solution were fortified into the aqueous sample prior to extraction. The chlorinated solvents were extracted from water samples with MTBE (high purity) after addition of surrogate analyte fortification solution. 10 g NaCl were add to the water sample before extraction. The NaCl/MTBE/water sample mixture was shaking vigorously and consistently by hand. After that the separator funnel was invert for 3-5 minutes to allow the water and MTBE phases to separate. 1 mL from the solvent phase was transferred to analysis vial and it analysis was done on gas chromatography equipped with an electron capture detector (GC-ECD) and splitless injector. The column used for analysis was Trace TR-V1 cyanopropylphenyl based phase, 30 mm x 0.53 mm ID x 3.0 μm film and with temperature program 40 °C (hold time 7 minutes), 2 °C/minutes to 80 °C (hold time 3 minutes), 7 °C/minutes to 120 °C (hold time 2 minutes), 15 °C/minutes to 180 °C (hold time 10 minutes).

The *soil samples* (25 g) were centrufugated for 5 minutes at 3000 rpm to remove the excess water. The samples were wetted with 30 mL MeOH/Acetone. The extraction was done with hexane (50 mL) with 20 mL MeOH/Acetone and was shaken manual for 30 minutes at room temperature. The extractions were repeated tree times with hexane.

Identification of the compounds was confirmed by a quadrupole mass spectrometer (DSQ II MS - Termo Electron Corporation) coupled to gas chromatograph (GC) with a split/splitless injector, using the Selective Ion Monitoring (SIM) modality. Cromatographyc separation on GC-MS was achieved using TR-5MS, 5% Phenyl (equiv) Polysilphenylene-siloxane column (Thermo Finnegan, USA). The operation condition is shown in table 4. All injection was done with TriPlus HS autosampler. It working condition are presented in table 4. Quantification was performed using the standard stock solution for organochlorine compounds and based on peak area.

Table 4. GC – ECD, MS-GC and TriPlus HS operation conditions.

MS - GC
Carrier gas flow: helium (He_2) 10 mL min^{-1}
Split ratio: splitless
Injector temperature: 200^0C
Detector temperature: 300^0C
Oven temperature: 40^0C (hold time 7 minutes), 2^0C/minutes to 80^0C (hold time 3 minutes), 7^0C/minutes to 120^0C (hold time 2 minutes), 15^0C/minutes to 180^0C (hold time 10 minutes)
Solvent delay: 1.5 minutes
MS scan program: 40 – 750 m/z
Ionization: 70 eV electron impact

GC - ECD
Carrier gas flow: nitrogen (N_2) 30 mL min^{-1} Make up: nitrogen (N_2) 30 mL min^{-1} Split ratio: 1:5 Injector temperature: 200^0C Detector temperature: 300^0C Oven temperature: 35^0C (hold time 3 minutes), 15^0C/minutes to 200^0C (hold time 3 minutes)
TriPlus HS
Incubation time: 45 min Incubation mode: constant Agitator temperature: 60^0C Agitator on – 20 sec/ Agitator off – 20 sec Syringe temperature: 80^0C Injection depth: 35 mm Injection speed: 40 mL/min Filling volume: 1.2 mL Filling counts: 1 /Filling delay: 0 sec Post injection syringe flush: 30 sec

The organochlorine compounds after analysis were shown in chromatograms obtain after the water sample analysis on GC-MS – see figure 4.

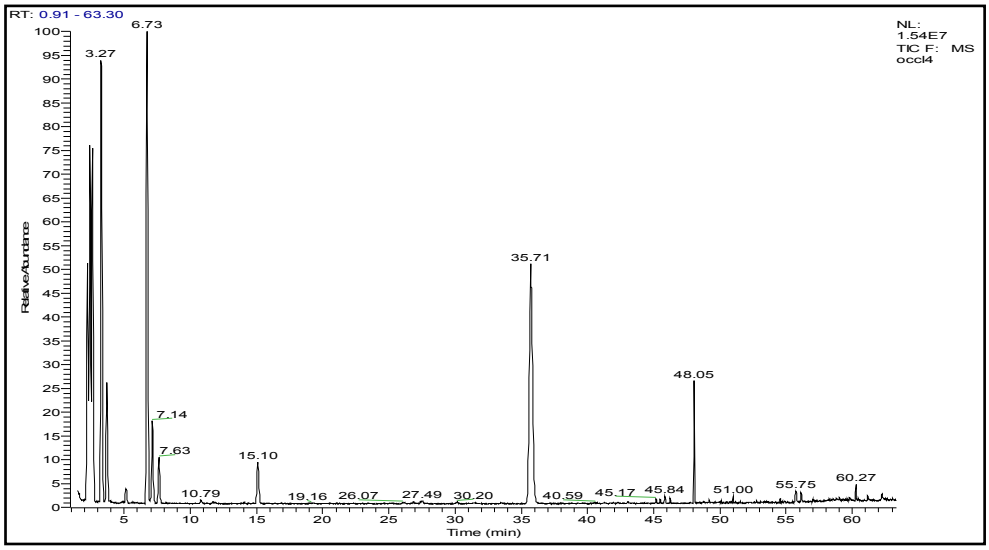

Figure 4. Chromatogram obtained after analysis of water sample on GC-MS with SIM method.

REFERENCES

1. A. Blair, P. Hartage, P.A. Stewart, M. McAdams, J. Lubin, *J. of Occupational Environmental Medicine*, **1998**, *55*, 161.
2. G.C. Windham, D. Shusterman, S.H. Swan L. Fenster, B. Eskenazi, *American Journal of Industrial Medicine,* **1991**, *20*, 241.
3. M. Sallmwn, M-L. Lindbohm, P, Kyyronen, *American Journal of Industrial Medicine*, **1995**, *27*, 699-713.
4. D. H. Garabrant, J.V. Lacey, T.J. Laing, B.W. Gillespie, M.D. Mayes, B.C. Cooper, D. Schottenfeld, *American Journal of Epidemiology*, **1999**, *157* (6), 493.
5. M. Dosemeci, P. Cocco, W.H. Chow, *American Journal of Industrial Medicine,* **1999**, *36*, 54.
6. E.F. Heihneman, P. Cocco, R.M. GOMEZ, M. DOSEMECI, P.A. STEWART, R.B. Hayes, S.H. Zahm, T.L. Thomas, A. Blair, *American Journal of Industrial Medicine*, **1994**, *26*, 155.
7. A. Anttila, E. Pukkala, M. Sallmen, S. Hernberg, K. Henminki, *J. of Occupational Environmental Medicine*, **1995**, *37* (7), 797.
8. G.W. Gibbs, J. Amsel, K. Soden, *J. of Occupational Environmental Medicine*, **1996**, *38*, 693.
9. S. F. Lanes, K. J. Rothman, N. A. Dreyer K. J. Soden, *Scandinavian Journal of Work, Environment and Health*, **1993**, *19*, 426.

STUDIA UNIVERSITATIS BABEŞ-BOLYAI, CHEMIA, LIV, 4, 2009

KINETIC MODEL FOR CHLORINE DECAY AND DISINFECTION BY-PRODUCTS FORMATION USING ABTS METHOD AND DPD METHOD

KOVACS MELINDA HAYDEE[a], DUMITRU RISTOIU[a], SIDONIA VANCEA[b], LUMINIȚA SILAGHI-DUMITRESCU[c]

ABSTRACT. The kinetics of chlorine decay of the pre-treated water collected once a month from the Gilau Water Treatment Plant after one of the sand filters was investigated. The chlorine species reacts with ABTS (2,2-azino-bis(3-ethylbenzothiazoline)-6-sulfonicacid-diamonium salt) to yield a green colour product that is measured at 405 nm wavelength with a spectrophotometer. The second method used for the investigation of chlorine consumption was by means of DPD (N,N-diethyl-p-phenylenediamine), where chlorine oxidizes DPD which takes on a red colour. The absorption is measured with a spectrophotometer at a wavelength of 515 nm. Both methods are useful for the determination of chlorine consumption in the treated water from distribution systems.

Keywords: Disinfection by-products, ABTS method, Chlorine consumption, THM formation.

INTRODUCTION

Chlorine is mostly used in water treatment plants from Romania for water disinfection. The regulation and monitoring of disinfection by-products has become a current issue after Romania's entry to the UE and after many previous studies have shown the possible adverse health effects on humans of this compounds [1, 2]. Their formation in treated water depends by the type of disinfection process and the type of disinfectant agent that is used.

Chlorine's popularity is not only due to lower cost, but also to its higher oxidizing potential which provides a minimum level of residual chlorine throughout the distribution systems and protects against microbial recontamination [2, 3]. For that, over of many years, chlorine became the most popular disinfecting agent due to its ability to kill most pathogens. In 1974 was finding that after adding of chlorine to water in order to disinfect it, this resulted the formation of compounds such as chloroform (one of the component of trihalomethanes class) due to

[a] *Babes Bolyai University of Cluj-Napoca, Faculty of Environmental Science, Str. P-ta Stefan cel Mare, no.4, 400084, Cluj-Napoca*
[b] *Garda de Mediu, Comisariatul Judetean Cluj, str. G-ral T. Mosoiu, nr. 49, Cluj-Napoca, Romania*
[c] *Universitatea Babeş-Bolyai, Facultatea de Chimie, str. Arany Janos, nr.11, 400068, Cluj-Napoca, Cluj-Napoca*

reaction of chlorine with the organics present in the water. After then hundreds of additional disinfection by-products have been identified including haloacetic acids and haloacetonitriles [4, 5]

Trihalomethanes (THMs) is the class of disinfection by-products that are most identified in treated water. Usually chloroform is the most commonly THMs compound in drinking water and it is present in the highest concentration.

Many parameters have an important influence on the formation of THMs. Previous research studies have shown that the major variables that affect THM formation are chlorine dose, concentration and nature of natural organic matter, contact time, pH, temperature of water and the presence of inorganic ions like bromide [3, 4].

The major factor that influence the THMs formation is the organic matter present in water supplies, they reacts with chlorine and leads to the formation of THMs. The type and characteristics of organic precursors directly affect the formation of THMs. Naturally occurring humic and fulvic substances which constitute a large fraction of the organic matter in water are the major THMs precursors [6]. Increase of chlorine dose has been reported to have positive influence of disinfection by-products yield. The same is true for increased concentrations of natural organic matter and increased temperature. The presence of bromine ions shifts the speciation of disinfection by-products to more brominated analogues, while increased pH can enhance the formation of some categories of disinfection by-products, ex. THMs and inhibits the formation of some others, ex. haloacetonitriles and haloketones [3]. Higher THM concentrations are expected at higher levels of the above mentioned parameters [7,8].

RESULTS AND DISCUSSION

Total chlorine (including all species: $HOCl$, NH_2Cl, ClO_2 and ClO_2^- react rapidlly with ABTS or DPD and it is impossible to have a distinction between the different species (relations 1, 2):

$$ClO_2 + ABTS + 2\,H^+ \rightarrow ClO^- + ABTS^+ \quad (1)$$

$$ClO_2^- + 4\,ABTS + 4\,H^+ \rightarrow Cl^- + 4\,ABTS^+ + 2\,H_2O \quad (2)$$

To determine NH_2Cl both HOCl and ClO_2 are destroyed by the addition of nitrite prior to ABTS addition. Nitrite rapidly reacts with ClO_2 and HOCl but only slowly with NH_2Cl. Nitrite does not react with ABTS and does not interfere in the determination of NH_2Cl fraction [6, 7, 8]. Four minutes are sufficient for a complete destruction of ClO_2 and HOCl. The concentration of free chlorine is calculated by subtracting monochloramine from total available chlorine fraction. Table 1. shows the concentration ($mg \cdot L^{-1}$) obtained for total chlorine, free chlorine and NH_2Cl in laboratory kinetic experiments with both methods: ABTS and DPD.

It is observed a slightly small difference between the results.

Table 1. Comparison between results obtained with ABTS and DPD method for determination of total chlorine, free chlorine and NH_2Cl.

Time (minutes)	ABTS method			DPD method		
	Total chlorine (mg/l)	Free chlorine (mg/l)	NH_2Cl (mg/l)	Total chlorine (mg/l)	Free chlorine (mg/l)	NH_2Cl (mg/l)
0.333	1.62	1.6	0.03	1.73	1.68	0.04
0.666	1.32	1.2	0.06	1.35	1.26	0.08
1	1.26	1.2	0.07	1.29	1.24	0.10
3	1.1	1	0.07	1.14	1. 7	0.11
6	0.92	0.8	0.12	0.98	0.84	0.15
15	0.81	0.5	0.21	0.85	0.67	0.28
40	0.7	0.4	0.21	0.74	0.55	0.23
60	0.62	0.36	0.17	0.68	0.39	0.19
90	0.56	0.3	0.17	0.60	0.37	0.17
120	0.52	0.3	0.17	0.54	0.34	0.16
240	0.46	0.28	0.14	0.48	0.29	0.13
600	0.26	0.2	0.08	0.29	0.22	0.06
690	0.19	0.14	0.06	0.23	0.18	0.05
780	0.12	0.1	0.04	0.15	0.13	0.04

The advantages of these methods are:

- they are easy to use and can determine with a high precision the total chlorine, free chlorine and NH_2Cl concentration.
- can help us to try to predict the potential formation of chlorination by-products, such as trihalomethanes – see figure 1.
- help in the prediction of chloroform formation in the distribution system if we respect the water condition (Chlorine dose, pH, temperature).

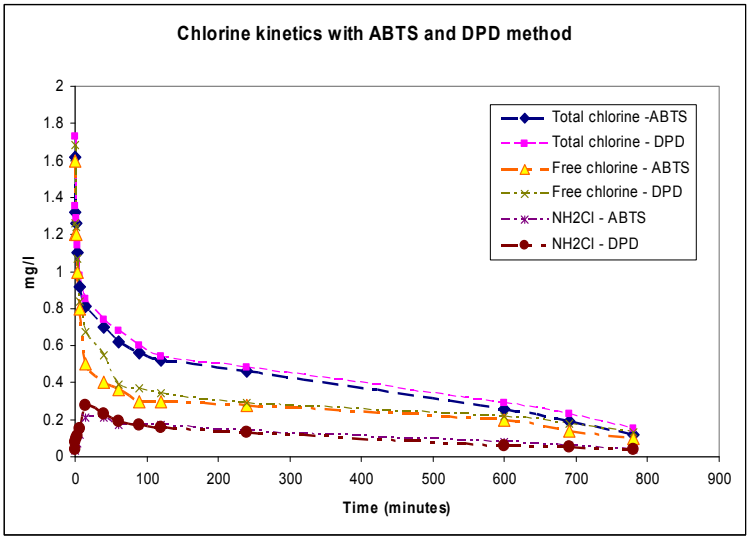

Figure 1. Total Cl_2 and NH_2Cl concentration vs. reaction time for both methods (ABTS and DPD).

In figure 2.a., is shown the result of chlorine kinetics experiment in laboratory and in figure 1.b., is shown the chloroform kinetics formation obtained from chlorine kinetics experiment. At each desired reaction time, in the water sample was injected thiosulfate solution to quench chlorine and stop the THM formation.

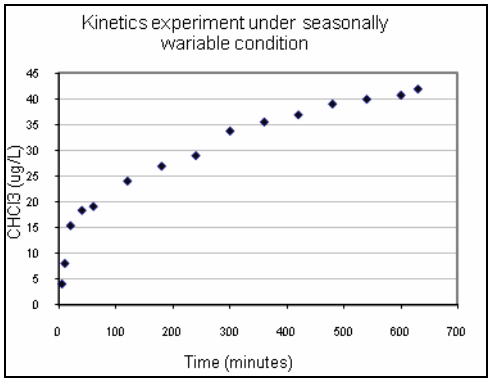

Figure 2.a.: represent the chlorine kinetics experiment (total chlorine kinetics, free chlorine and NH_2Cl kinetics.

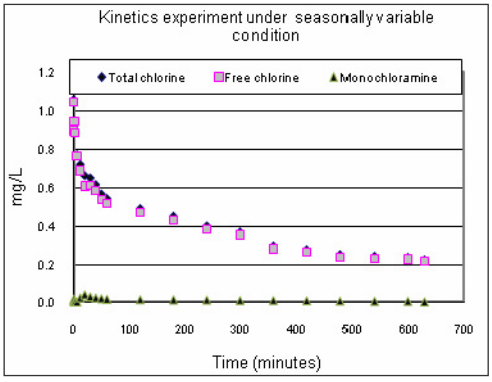

Figure 2.b.: Show the chloroform formation kinetics from experiments.

To assess the possibility to simulate the THM formation in the distribution system, $CHCl_3$ formed in laboratory experiments was compared with $CHCl_3$ concentration measured in the distribution system on the sampling day – see table 2.

Table 2. Chloroform formation in laboratory experiment and the chloroform value measured in the sampling point.

Sampling point	Chloroform concentration ($\mu g \cdot L^{-1}$) in water sample taken from Gilau Water Treatment Plant – Cluj (a) and chloroform ($\mu g \cdot L^{-1}$) concentration obtained in laboratory experiment (b) for different month									
	1a	**1b**	**2a**	**2b**	**3a**	**3b**	**4a**	**4b**	**5a**	**5b**
A	0.6		0		0		0		0	
B	4.9	2.1	0	0	0	0	0	0	0	0
C	12.4	13.2	8.4	7.8	2.22	3.8	8.09	7.9	8.22	7.9
D	18.7	19.1	47.7	50.1	9.34	11.0	16.71	15.98	20.81	21.14
E	28.4	29.6	47.0	49.3	6.36	7.8	18.70	19.03	29.26	30.06
F	35.2	36.6	66.9	70.4	27.77	26.8	18.99	19.8	27.12	28.24
G	37.1	38.3	66.6	69.3	21.08	20.9	20.90	21.14	32.41	33.56
H	23.2	24.8	71.1	72.8	28.17	29.3	21.60	22.05	33.86	34.09

The sampling was started from Gilau water treatment plant to distribution system in Cluj Napoca (A – raw water, B – filtrated water, C – exit reservoir, D – Sapca Verde, E – Beer factory, F – Chemistry faculty, G – Environmental

science faculty, H – Institute of public health) in different month (1a –$CHCl_3$ concentration in July in the water take from sampling point, 1b – $CHCl_3$ concentration in July in laboratory kinetics experiment which correspond in time with the water that arrived to the sampling point; the same is for 2a and 2b but for September water sample; 3a, 3b – December; 4a, 4b – March; 5a, 5b - May).

CONCLUSIONS

Both colorimetric methods are easy to use and give precise results. The difference between the two different methods was very small (3 %). The difference between ABTS and DPD method is, ABTS method is easier to apply in comparison with DPD for a long experiment like a kinetics experiment.

The two methods give really information between the chlorine consumption and the $CHCl_3$ formation. That helps us in the future to make the prediction of total THMs formation. The results of measured THMs show that $CHCl_3$ is the main THMs formed in distribution system and its amount is in the range 0.6 – 73 $\mu g \cdot L^{-1}$, value that is under the maximum permissible level according to the EU drinking water safety regulation.

EXPERIMENTAL SECTION

Sampling: Pre-treated water was collected at the treatment plant after one of the sand filters once a month and stored in 5 L plastic bottles at 4 ^0C until the chlorination experiments. pH and water temperature were measured at the sampling site when the sample were taken.

Reagents: $NaNO_2$, NaB_7O_5 and $Na_2S_2O_3$ were purchased from Reactivul Bucuresti (Bucharest, Romania). KI (purissim p.a.) was purchased from Merk (Darmstadt, Germany). NaH_2PO_4 used was from BPH Chemicals (Poole, England). ABTS (2,2-azino-bis(3-ethylbenzothiazoline)-6-sulfonicacid-diamonium salt) was purchased from Fluka (Buchs, Switzerland). DPD (N,N-diethyl-p-phenylenediamine) was taking from Merk (Darmstadt, Germany). Aqueous chlorine dilution was prepared from a chlorine solution for cleaning purposes (2-5 %, Sun Industries, Ilfov, Romania). NaOH, H_2SO_4 and KIO_3 were purchased from Fluka (Buchs, Switzerland).

Chlorine experiments: The chlorine dose in the water treatment plant from Gilau (where was collected the filtrated water) is regulated manually to achieve a free chlorine concentration at the exit reservoir (where the water arrives approximately 15 minutes after chlorination) of 0.5 – 0.7 $mg \cdot L^{-1}$ Cl_2 in winter and 0.7 – 0.9 $mg \cdot L^{-1}$ Cl_2 in summer. Chlorination experiments were carried out monthly with raw water collected at the treatment plant after one of the sand filters. To assess the influence of the seasonal variances in the water matrix, kinetic experiments with filtrated water will be performed monthly under the two conditions.

The experiments were conducted under two conditions:

- *Base line conditions* (pH 7, 21^{0}C, 2.5 mg/l Cl_2) to gain information about the change of the organic matter in the raw water, and seasonally variable conditions to simulate the actual process at the treatment plant.
- Experiments under *seasonally variable conditions* were carried out with pH and temperature as measured in the pretreated water on the sampling day and an initial chlorine dose according to a free chlorine concentration after 15 minutes as prescribed in the guidelines of the water treatment plant.

The chlorine concentration was determined by the ABTS method at a wavelength of 405 nm and ε has a value of 28 500 M^{-1} cm^{-1} (see figure 3.a.), and also with DPD method at a wavelength of 515 nm (see figure 3.b.). In laboratory experiment the chlorine dose added to filtrate water was the same that in the sampling day, also the temperature and the pH. The kinetics experiment time was 13 hour (is the time for the water to arrive from Gilau water treatment plant to the centre of city). The THM samples taken from kinetics experiment were preserved with sodium thiosulfate. The experiment results in the first one will give information about the seasonal variance of NOM and its influence on the THM formation potential, while the second one is an attempt to simulate the conditions at the WTP which will give information about the actual process.

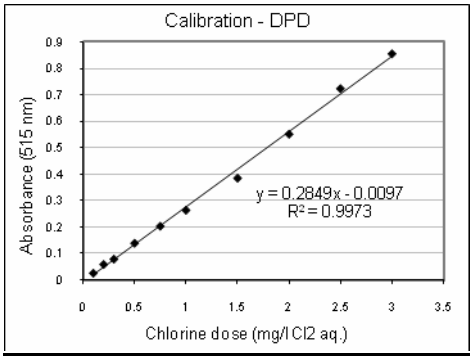

Figure 3.a.: Present the calibration curve of Cl_2 with DPD method.

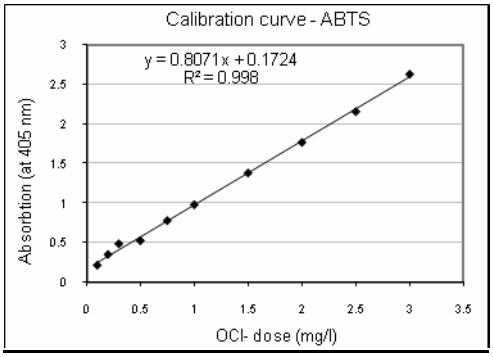

Figure 3.b.: Represent the calibration curve of OCl^- with ABTS method.

Monochloramine, total and free chlorine are measured with the ABTS method. Monochloramine and HOCl react with ABTS to a green coloured product, which can be measured at a wavelength of 405 nm.

Instrumental measurements: For the *kinetic studies* chlorine was measured colorimetrically according to standard method 8021 DPD method (powder pillow) for free chlorine determination and standard method 8167 DPD method (powder pillows) for total chlorine determination using a Hach Dr 2800 analyzer. A 25-ml cell was filled with samples and added DPD free chlorine reagent (powder pillow). After mixing, chlorine was read at a wavelength of 530 nm wavelength. Also, the chlorine concentration was determined by the ABTS method at a wavelength of 405 nm with a molar absorption coefficient ε of 28 500 M^{-1} cm^{-1}. Monochloramine, total and free chlorine are measured with the ABTS method. Monochloramine and HOCl react with ABTS to a green coloured product, which can be measured at a wavelength of 405 nm.

Trihalomethanes analysis: THMs were measured by a Thermo Finningan U.S. Trace GC Ultra gas chromatography system with an electron capture detector (GC-ECD) equipped with a TriPlus HS auto sampler. The analysis was made using headspace technique. 10 ml of sample was filled into 20 ml headspace vials and closed with Teflon lined screw caps. After that, the samples were equilibrated in an oven at 60^0C for 45 minutes. 1 ml of the headspace was then injected into the GC (Cyanopropylphenyl Polysiloxane column, 30 m x 53 mm, 3 μm film thickness, Thermo Finnigan, USA). The column program was 35^0C (hold time 3 minutes), 15^0C/minutes to 200^0C (hold time 3 minutes).

REFERENCES

1. USEPA, Toxicological review of Chloroform, **2001**, EPA /635/R-01/00.
2. WHO: Background document for development of WHO Guidelines for Drinking-water Quality, **2005**, WHO/SDE/WSH/ 05.08/64.
3. EU, Official Journal of the European Community, **1998**, L 330, Directive 98/83/Ec.
4. USEPA, National Primary drinking water Regulation: Disinfectants and Disinfection Byproducts, **1998**, Federal Register *63* (241): 69390-69476, 115.
5. WHO Guidelines for drinking water quqlity,Third edition, **2006**, 138.
6. U. Gunten, A. Driedjer, H. Gallard, E. Salhi, *Water Resources*, **2001**, *35*, 2095.
7. L. Clesceri, A. Greenberg, D. Eaton, *American Water Works Association*, **1999**,109.
8. U. Pinkernell, B. Nowark, H. Gallard, U. VonGunten, *Water Resources*, **2006**, *34*, 4343.

STUDIA UNIVERSITATIS BABEŞ-BOLYAI, CHEMIA, LIV, 4, 2009

OPTIMIZATION OF METHODS FOR THE DETERMINATION OF DISINFECTION BY-PRODUCTS IN DRINKING WATER

MELINDA HAYDEE KOVACS[a], DUMITRU RISTOIU[a]

ABSTRACT. Chlorination is the most widely disinfection process of drinking water in Romania. The goal of the water disinfection is to protect it in the distribution systems against microbial contamination and to prevent and control re-growth of microorganism in the distribution system. The presence of DBPs in drinking water is a matter of concern for human health and can also produce unpleasant organoleptic taste. Under Stage I of the Disinfectants/Disinfection By-products (D/DBP) Rule, USEPA sets maximum contaminant levels (MCLs) for total trihalomethanes (chloroform, bromodichloromethane, dibromochloromethane and bromoform) at 80 $\mu g \cdot L^{-1}$; for a total of five haloacetic acids (monochloroacetic, dichloroacetic, trichloroacetic, monobromoacetic and dibromoacetic acids) at 60 $\mu g \cdot L^{-1}$; for bromate at 10 $\mu g \cdot L^{-1}$ and for chlorite 1.0 $mg \cdot L^{-1}$. Other DBPs have been added to the US Environmental Protection Agency's Candidate Contamination List (CCL), which is the list from which future regulated drinking water compounds will be selected. In Europe, the 98/83/CEE Directive is less restrictive than that applied in the USA. The only DBPs that must be controlled are the four trihalomethanes, and their proposed maximum level being 100 $\mu g\ l^{-1}$. Due to the fact that their identification and quantization have become extremely important to drinking water companies in order to reduce or remove their presence, other analytical methods different from those proposed by U.S. EPA have been optimized and are now commented in this article.

Keywords: disinfection by-products, gas chromatography-electron capture detector, headspace extraction.

INTRODUCTION

A particularly significant group of water pollutants consists of volatile organic compounds (VOCs). This group includes compounds, which are insoluble or sparingly soluble in water, with boiling points up to 200 °C and molecular masses between 16 and 250 Dalton [1, 2]. The compounds vary greatly in their structures and properties, e.g. hydrocarbon halogen derivatives, aliphatic hydrocarbons, aromatic hydrocarbons, alcohols, ketones, esters, ethers, amines, phenols, etc [3]. Many of them are toxic or considered carcinogenic,

[a] *Babes Bolyai University of Cluj-Napoca, Faculty of Environmental Science, Str. Fantanele, no.30, 400294, Cluj-Napoca, email: haydee_kovacs@yahoo.com*

mutagenic or teratogenic [4]. VOCs group include also some disinfection by products. They appear after the reaction of disinfectant agent with organic matter from water.

In many state, like in Romania, chlorine is the most usually disinfectant agent use for water disinfection due to its ability to kill most pathogens. However, in 1974 it was discovered that the chlorination of drinking waters resulted in the production of trihalomethanes (THMs) due to reaction of chlorine with organics in the water [1]. Since 1980's THMs raised significant concern due to evidence of their adverse human health effects, in particular cancer and reproductive disorders [5, 6]. THMs are the organohalogen compounds that are most monitored by protection agencies from treated water. Usually chloroform is the THM most commonly found in drinking water and in most of case is present in the highest concentration [7].

In choosing an appropriate analytical procedure to analyze the DBPs from water sample, it must be taken into account are not only precision, accuracy, selectivity, detectability, and reproducibility, but also limiting the time, labour and other costs involved in the procedure. The aim is also to determine a number of components of various properties in a single analytical cycle [8]. Automation of analytical procedures and making field determinations possible is also of importance. Reduction in the use of solvents in the analytical procedure and to in the amount of environment-threatening waste produced is becoming essential [9].

RESULTS AND DISCUSSION

The THMs were extracted from water sample by two different procedures, one LLE and the second HSE. In that case of HSE, the head space devices is connected directly to gas chromatography (GC) coupled with ECD.

In the analysis of THMs samples using TriPlus HS auto sampler the four peaks belonging to the four THM compounds were well separated, see figure 1.

Accuracy (%) for the four THMs compounds were in the range of 0.0003 – 0.2634 % in case of HSE and in the range of 0.52 – 4.2 % for LLE. The accuracy was determinate for every THMs compounds on 7 different samples and for the follow concentration 1 $\mu g \cdot L^{-1}$, 10 $\mu g \cdot L^{-1}$ and 100 $\mu g \cdot L^{-1}$.

The detection limit (MDLs) for $CHCl_3$, $CHCl_2Br$, $CHClBr_2$ and $CHBr_3$ were 0.3, 0.2, 0.3 and 0.6 $\mu g \cdot L^{-1}$ respectively (n=7). The RSD of 1 $\mu g \cdot L^{-1}$, 20 $\mu g \cdot L^{-1}$ and 80 $\mu g \cdot L^{-1}$ spiked samples were between 0.05 – 3.7 % after HSE and between 2.1 – 6.4 % after LLE.

The results regarding the methods performance show us good values in case of HSE than in case of LLE. Also it can be observed that the precision increase using the TriPlus HS and the incubation with agitation. That permit a better separation of the THMs compounds by the sample matrix (see table 1). The recovery in the two cases for 1 $\mu g \cdot L^{-1}$, 20 $\mu g \cdot L^{-1}$, and 80 $\mu g \cdot L^{-1}$ are

in the range 93-120 % and also the limit of detection for THMs compounds were: $CHCl_3$ is 0.3 μg/l, $CHCl_2Br$ is 0.2 $\mu g \cdot L^{-1}$, $CHClBr_2$ is 0.3 $\mu g \cdot L^{-1}$ and $CHBr_3$ is 0.6 $\mu g \cdot L^{-1}$.

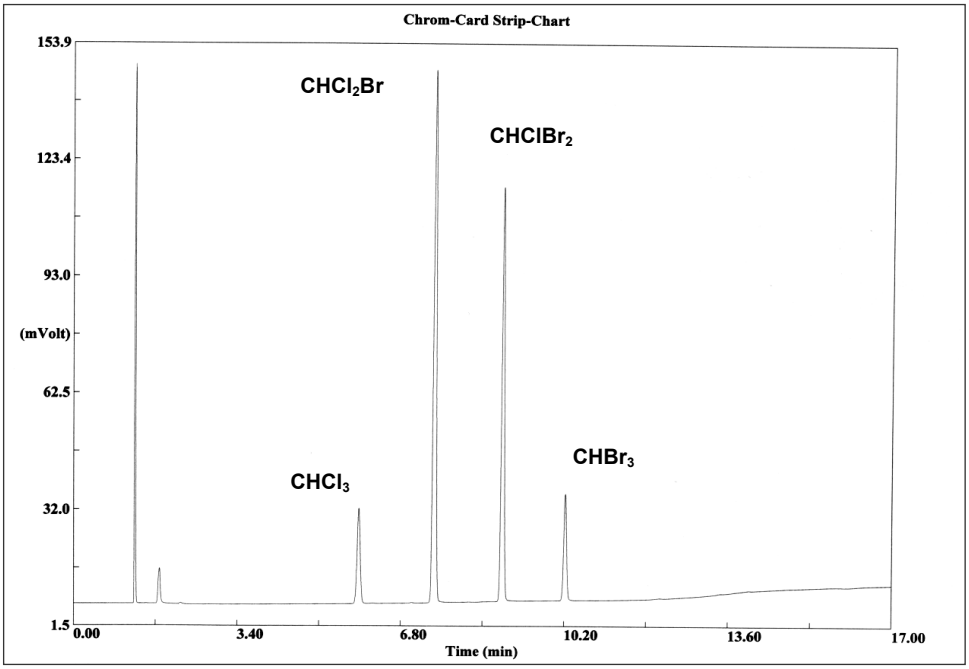

Figure 1. Chromatogram obtained after analysis of water sample – the four trihalomethanes compounds

Table 1. Relative standard deviation using the two procedures for the four THMs compounds analysis.

Compounds	TriPlus HS Autosampler		LLE Manually Injection	
	Relative standard deviation %		Relative standard deviation %	
	20 μg/l	***80 μg/l***	***20 μg/l***	***80 μg/l***
$CHCl_3$	1.43	1.17	2.05	1.91
$CHCl_2Br$	2.28	1.51	2.77	2.35
$CHClBr_2$	1.86	1.06	2.53	1.89
$CHBr_3$	2.40	1.92	3.21	2.97

CONCLUSIONS

The method of headspace extraction compared with liquid-liquid extraction has been presented in case of THMs analysis from water. HSE allows direct, trace analysis of components without disrupting the natural equilibrium established between the gas phase and the liquid phase of sample.

This method provides a better statistical accuracy. Collecting just the headspace eliminates the need to dispose of the liquid or solid sample. Present the best possible statistical accuracy. Using this method in analysis of disinfection by products on chromatography we obtain better sensitivity for THMs compounds and better statistical accuracy.

HSE sample preparation and analysis with GC-ECD can be used well for quantitative analysis of disinfection by products in environmental samples. Using it, for THMs were found good results for relative standard deviation, recovery and detection limit for each THMs compounds. Also the time necessary to perform the THMs analysis from water samples is less than in case of LLE.

EXPERIMENTAL SECTION

Sampling: Several treated and untreated water were collected in the period of January – December 2008 from Gilau and Dej Water Treatment Plant in every month. The collection and the preparation of water samples make up the most important element of every analytical procedure, which directly affects the quality and accuracy of final results. The basic problem is preserving the representative character (original composition) of the collected water sample to be analyzed in the laboratory avoiding positive deviations such as contamination under operation or negative deviation like losses of the target compounds. In order to avoid any possible contamination the sample were collected in duplicate in 40 mL vials that were previously cleaned with Millipore water and dried in oven at 150 °C for 10 hour. Also in order to keep out the possibility to miss of these compounds from our water sample all vials were full filed with sample and closed with Teflon lined screw cap. Because the THMs are formed after the reaction of chlorine with the natural organic matter present in water, every sample was preserved with sodium thiosulfate ($Na_2S_2O_3$) to quench residual chlorine. Samples were stored at 4 °C for a maximum 7 days until analysis.

Methods: Tree methods of extraction were used to determine the THMs presence in the water sample. These extraction methods were performed in order to compare these methods and to establish the most exactly and easily practicable method for analysis of these compounds. After extraction THMs were carried out by Thermo Finningan U.S.S. Trace GC Ultra gas chromatography with electron capture detector (GC-ECD). In case of head space analysis was used a TriPlus HS auto sampler.

Liquid-liquid extraction: The most commune extraction method for disinfection by-products is liquid-liquid extraction (LLE). After sampling, in laboratory 2 mL of hexane (extraction solvent) was added to ten mL of water sample in a separator funnel. The partitioning is then brought to equilibrium

by shaking the separator funnel for 5 minutes vigorously and allows it to stand. Then 1 µL of aliquot of the organic layer was removed with a microsyringe for gas chromatographic analysis.

Head-space extraction: One of the most common techniques used for the isolation of THMs from water samples is extraction into the gaseous phase. Headspace analysis techniques are based on the phenomenon of partition of analytes between the liquid and the gaseous phase. The gaseous phase (headspace) is analyzed together with the volatile compounds freed from the liquid sample (see Figure 2). In this figure is presented with G the gas phase (headspace) and with S the sample phase. The gas phase is commonly referred to as the headspace and lies above the condensed sample phase. The sample phase contains the compound(s) of interest. It is usually in the form of a liquid or solid in combination with a dilution solvent or a matrix modifier.

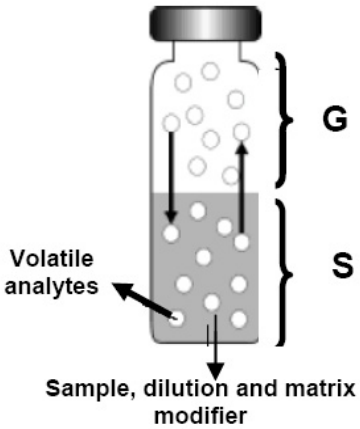

Figure 2. Schematic presentation of headspace process.

The equipment necessary for this type of analysis is very simple. The determination limit of the headspace analysis technique in a static system depends, besides the sensitivity of the detector employed, on the value of its coefficient of partition between the liquid and gaseous phase. For some compounds, the value of partition coefficient can be increased even by two orders of magnitude by varying temperature, pH, and salt effect (usually NaCl).

The analysis was made using headspace technique. 10 ml of sample was filled into 20 ml headspace vials and closed with Teflon lined screw cap. The agitator temperature was set at 60^0C, and the agitator on and the agitator off were set at 20 seconds and respectively 20 seconds. The incubation time was 30 minutes. Also the syringe was set at 80^0C. On GC the column

temperature program was 35^0C (hold time 3 minutes), 15^0C/minutes to 200^0C (hold time 3 minutes). The inlet was set at 200^0C. After this process 1 ml of the headspace was then injected into the GC (Cyanopropylphenyl Polysiloxane column, 30 m x 53 mm, 3 μm film thickness, Thermo Finnigan, USA). The column program was 35^0C (hold time 3 minutes), 15^0C/minutes to 200^0C (hold time 3 minutes). The inlet was set at 200^0C. In case of LLE extraction the same column and column program was used.

REFERENCES

1. H. A. Duong, M. Berg, M. H. Hoang, H.V. Pham, H. Gallard, W. Giger, U. Gunten, *Water Research*, **2003**, *37*, 3242.
2. J. Huang, C.G. Smith, *Journal of American Water Works Association*, **1984**, *76*(4) 168.
3. T.F. Marhaba, M.B. Washington, *Advances in Environmental Research*, **1998**, *2*, 103.
4. A.D. Nikolau, M.N. Kostopolou, T.D. Lekkas, *Global Nest: The International Journal,* **1999**, 1(3), 143.
5. USEPA, *Alternative Disinfectants and Oxidants Guidance Manual,* USEPA, **1999**, EPA 815-R-99-014.
6. USEPA, *National primary drinking water standards*, USEPA; **2001**, 816-F-01-007.
7. J.J. Rook, *Water Works Association*, **1976**, *68*(3), 168.
8. Standard Methods for the Examination of Water and Wastewater, 20th Edition, APHA, AWWA, WEF, **1998**, Washington DC, USA.
9. C. Vogt, S. Regli, *Journal of American Water Works Association*, **1981**, *73*(1), 33.

STUDIA UNIVERSITATIS BABEŞ-BOLYAI, CHEMIA, LIV, 4, 2009

SYNTHESIS AND STRUCTURAL ANALYSIS OF SOME NEW STERICALLY HINDERED DIENES

FLAVIA PIRON[a], ELENA BOGDAN[a], CRINA CISMAŞ[a], ANAMARIA TEREC[a], ION GROSU[a]

ABSTRACT. The good yields synthesis of some new tetrabromo and tetraiodo dienes obtained via the Hay homo coupling reaction of two polyethyleneoxy terminal alkynes and the structural investigations on these sterically hindered compounds are reported.

Keywords: dienes, axial chirality, atropenantiomers, coupling reactions, diynes

INTRODUCTION

Compounds with axial chirality are of high interest in the field of chiral catalysts and chiral discriminators. Many biphenyl and binaphtyl derivatives [1] are commercially available as single enantiomers.

Besides the very well known atropenantiomeric compounds with biaryl units many other unexpected compounds (e.g. styrenes I [2], 2-aryl,2-methyl-1,3-dioxanes II [3], *EE*-tetrahalogeno-1,3-butadienes III [4,5]; Scheme 1) exhibit axial chirality and atropenantiomers.

The atropisomers of *EE*-1,3-butadienes are due to the hindrance of the rotation around the formal simple bond C^2-C^3. These compounds prefer the conformation with perpendicular arrangement of the double bonds, which insures the highest distance between the large substituents at positions 2 and 3 (**III**, Scheme 1). The racemization of the atropenantiomers (*aR*⇆*aS*) occurs by the rotation of the molecule around the C^2-C^3 bond, via either the *s-trans* isomer (*transoid*) or the *s-cis* structure (*cisoid*) of the 1,3-butadiene core. The barrier via the *transoid* conformation is considerably lower and the compounds prefer this itinerary for the racemisation reaction.

The values of the barriers of racemization depend of X and R groups (named internal substituents). The reported barriers were measured either by dynamic NMR [6], DHPLC [4] or using polarimetry measurements [7]. The R^1 groups (named external substituents) are not involved directly in the hindrance of the rotation around the C^2-C^3 bonds, but if they are large they increase the barrier of rotation by the *buttressing* effect. [8]

[a] *Universitatea Babeş-Bolyai, Facultatea de Chimie şi Inginerie Chimică, Str. Kogălniceanu, Nr. 1, RO-400084 Cluj-Napoca,Romania, igrosu@chem.ubbcluj.ro*

We considered of interest to develop the investigations in the field of chiral dienes and to obtain new compounds exhibiting a tetrahalogeno-1,3-butadiene core, to determine their structure and to estimate the hindrance of the rotation around the formal simple bond of the 1,3-butadiene unit.

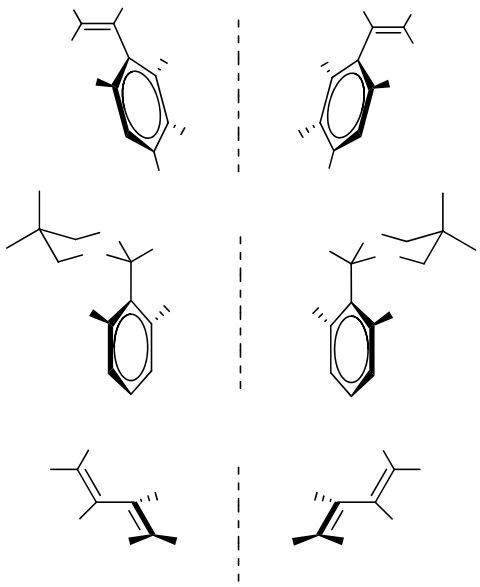

Scheme 1

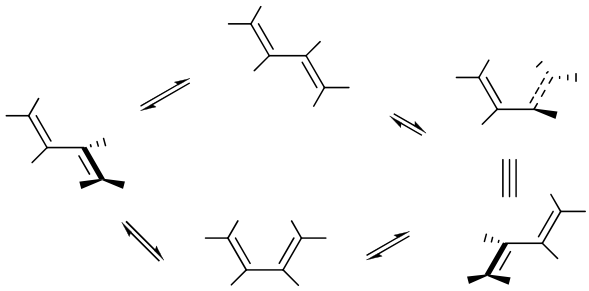

Scheme 2

RESULTS AND DISCUSSION

New tetrahalogeno dienes (**3**-**6**) were synthesized by halogen addition reactions to the corresponding diynes (**1** and **2;** Scheme 3). The reactions underwent stereoselectively with the formation of the *EE* isomers.

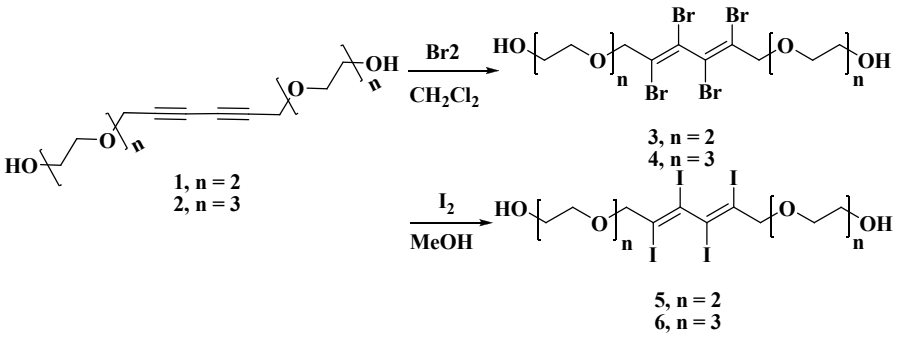

Scheme 3

Diynes **1** and **2** were synthesized by the coupling reaction of the monoalkyne alcohols **7** and **8** (Scheme 4) which were obtained by the reaction of the corresponding polyethyleneglycols (**9** and **10**) with propargyl bromide (Scheme 5). Even if compounds **7** and **8** are known [9] and their synthesis has been reported, they could be obtained in good yields only by adapting a procedure described in the literature for similar compounds [10].

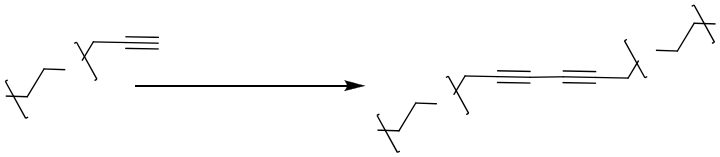

Scheme 4

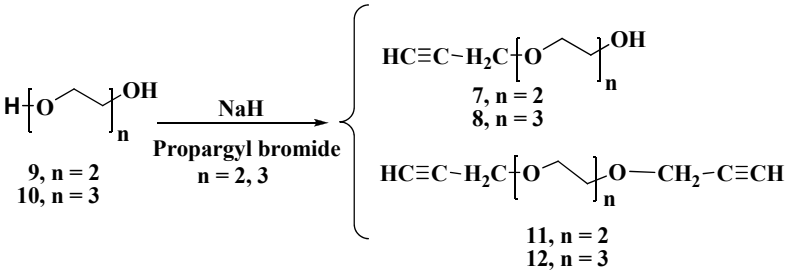

Scheme 5

The main product in the reaction of polyethyleneglycols with propargyl bromide is the monoalkyne, but the formation of dipropargyl derivatives **11** and **12** cannot be avoided. Diterminal diynes **11** and **12** were isolated but the yields in this case are poor. These diynes are interesting compounds and their good yields synthesis and structural investigations were reported in the literature [11].

Diyne **1** was reported by Wegner [12], but diyne 2 is a new compound.

The structural investigations on **3**-**6** were performed using NMR and LR ESI MS experiments.

The key signals in ^{1}H NMR spectra are those corresponding to the protons belonging to the CH_2 groups connected directly to the diene system (allylic positions). If the rotation of the 1,3-diene around the central simple bond is free the chirality of the system has no influence (an achiral average structure has to be considered) on the NMR signals and the ^{1}H NMR spectrum should show for the designed protons a singlet. If the rotation of the diene unit is hindered, the axial chirality of the molecule determines the diastereotopicity of the protons of the prochiral centers (CH_2 groups). In this situation the spectrum should exhibit two doublets (AB system) for the protons of the allyl CH_2 groups. The spectra for the investigated dienes (**3**-**6**) exhibit two doublets for the protons of the considered CH_2 groups (Figure 1, Table 1) proving the hindrance of the rotation in the diene unit.

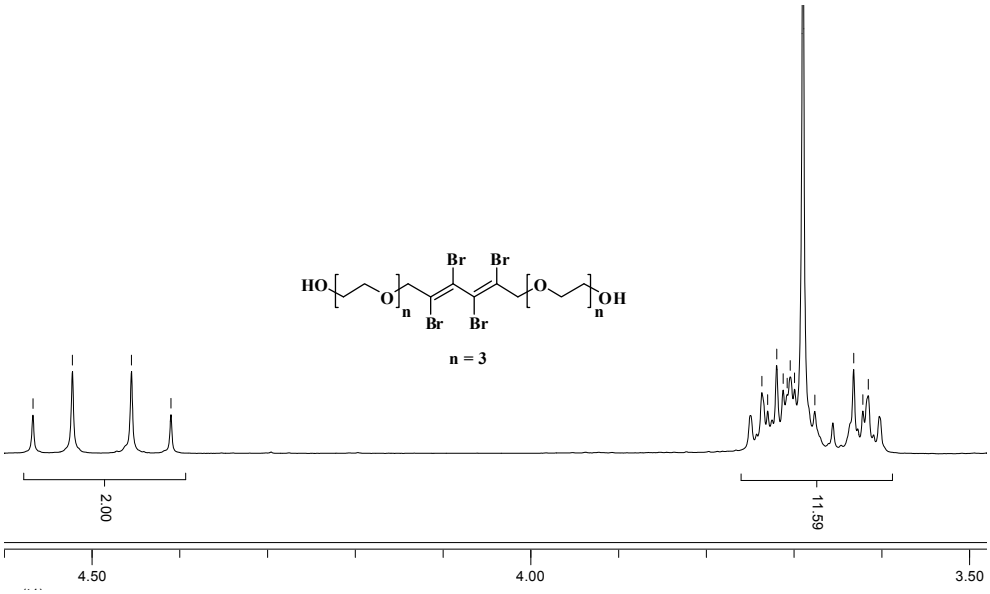

Figure 1. ^{1}H NMR spectrum ($CDCl_3$ rt,, fragment) of compound **4**

Table 1. Relevant NMR data for **3**-**6**

Compd.	δ (ppm)		Δδ (ppm)	*J* (Hz)
	-CX=CX-C*H*(H)-	-CX=CX-CH(*H*)-		
3	4.44	4.55	0.10	13.5
4	4.43	4.54	0.09	13.5
5	4.30	4.40	0.10	13.5
6	4.28	4.38	0.10	13.5

The spectrum of **4** run at *rt* (Figure 1) shows the two reference doublets at δ = 4.43; 4.53 ppm (J = 13.5 Hz), while the signals for the other protons of the CH_2 groups could not be assigned and they are all overlapped in the range 3.6-3.75 ppm. In the spectrum run at 60 °C no modification could be observed. This result is in agreement with the reported barriers for the racemization of other chiral tetrabromo $\Delta G^{\#}$ = 69.57±0.627 kJ/mol [5a] and tetraiodo $\Delta G^{\#}$ = 143 ± 1 kJ/mol [4] chiral dienes and reveals the high stability of the atropenantiomers of these compounds (the rotation in the diene unit is hindered at high temperatures, too).

CONCLUSIONS

Four new tetrahalogeno dienes with axial chirality were obtained in good yields and were investigated by NMR and ESI MS. The hindrance of the rotation in the diene unit and the high stability of the atropenantiomers of the compounds were also revealed. The high stability of the chiral unit located between two polyethylene glycol substituents recommend these compounds as useful building blocks for the obtaining of chiral host molecules.

EXPERIMENTAL SECTION

^{1}H NMR (300 MHz) and ^{13}C NMR (75 MHz) spectra were recorded in $CDCl_3$. LR ESI MS were recorded on ion trap spectrometer in positive mode. Melting points are uncorrected. Thin layer chromatography (TLC) was carried out on aluminium sheets coated with silica gel 60 F_{254} using UV and $KMnO_4$ visualization.

General procedure for the acetylenic coupling:

CuI (60 mmol) was added to a solution of alkynes **7** or **8** (3 mmol) in dry dichloromethane (200 mL) containing dry TMEDA (120 mmol). The reaction mixture was stirred for 1 hour under a stream of dry air. The mixture was then diluted with dichloromethane (100 ml) transferred into a separating funnel and washed with a solution of HCl 2M (2 x 30 ml) and then several times with water till the aqueous layer remains colourless. The organic layer was then separated, dried over Na_2SO_4 and evaporated. The final product was then purified by column chromatography (silica gel, diisopropylether/acetone 1/1).

3,6,13,16-tetraoxaoctadeca-8,10-diyne-1,18-diol (**1**) Colorless liquid, yield: 35% (300 mg); Calculated for $C_{14}H_{22}O_6$; C, 58.73; H, 7.74. Found: C, 58.89; H, 7.51. ^{1}H-NMR (300 MHz, $CDCl_3$) δ = 2.03 (2H, OH), 3.55-3.75 (m, 16H, 1-H, 2-H, 4-H, 5-H, 14-H, 15-H, 17-H, 18-H), 4.27 ppm (s, 4H, 7-H, 12-H); ^{13}C-NMR (75 MHz, $CDCl_3$) δ = 58.91 (7-C, 12-C), 61.70 (1-C, 18-C), 69.37, 70.13 (2-C, 4-C, 15-C, 17-C), 70.53 (9-C, 10-C), 72.47 (5-C, 14-C), 75.22 ppm (8-C, 11-C).

ESI-MS; m/z = 287.1 $[M+H]^+$, 309.1 $[M+Na]^+$.

3,6,9,16,19,22-hexaoxatetracosa-11,13-diyne-1,24-diol (**2**) Colorless liquid, yield: 33% (400 mg); Calculated for $C_{18}H_{30}O_8$; C, 57.74; H, 8.08. Found: C, 57.63; H, 8.28.^{1}H-NMR (300 MHz, $CDCl_3$) δ = 2.13 (2H, OH), 3.59-3.74 (m, 24H, 1-H, 2-H, 4-H, 5-H, 7-H, 8-H, 17-H, 18-H, 20-H, 21-H, 23-H, 24-H), 4.27 ppm (s, 4H, 10-H, 15-H); ^{13}C-NMR (75 MHz, $CDCl_3$) δ = 58.89 (10-C, 15-C), 61.69 (1-C, 24-C), 69.28, 70.24, 70.27, 70.60 (2-C, 4-C, 5-C, 7-C, 18-C, 20-C, 21-C, 23-C), 70.50 (12-C, 13-C), 72.51 (8-C, 17-C), 75.25 ppm (11-C, 14-C).
ESI-MS; m/z = 375.2 $[M+H]^+$, 397.2 $[M+Na]^+$.

General bromination procedure

To a solution of compounds **1** or **2** (0.26 mmol) in dichloromethane (20 ml), bromine (0.82 mmol, 130 mg solved in 1 ml dichloromethane) was added dropwise. The mixture was stirred at room temperature overnight, and at the end the organic phase was washed with a solution of sodium sulfite and then with water. After drying over sodium sulfate, the solvent was removed and the crude product was purified by column chromatography (silica gel, diisopropylether/acetone 1/1).

(8E,10E)-8,9,10,11-tetrabromo-3,6,13,16-tetraoxaoctadeca-8,10-diene-1,18-diol (**3**) Yellow liquid, yield: 47% (74 mg); Calculated for $C_{14}H_{22}Br_4O_6$; C, 27.75; H, 3.66; Br, 52.75. Found: C, 27.49; H, 3.78; Br, 52.91. ^{1}H-NMR (300 MHz, $CDCl_3$) δ = 1.88 (2H, OH), 3.61-3.76 (m, 16H, 1-H, 2-H, 4-H, 5-H, 14-H, 15-H, 17-H, 18-H), 4.44, (d, 2H, *J* = 13.5, 7-H, 12-H), 4.55 ppm (2d 2H, *J* = 13.5, 7'-H, 12'-H); ^{13}C-NMR (75 MHz, $CDCl_3$) δ = 61.79 (1-C, 18-C), 69.35, 70.18 (2-C, 4-C, 15-C, 17-C), 72.42 (5-C, 14-C), 73.06 (7-C, 12-C), 117.53 (8-C, 11-C), 124.79 ppm (9-C, 10-C).
ESI-MS; m/z (%) = 602.8 (21), 604.8 (79), 606.7 (100), 608.8 (66), 610.7 (16) $[M+H]^+$.

(11E,13E)-11,12,13,14-tetrabromo-3,6,9,16,19,22-hexaoxatetracosa-11,13-diene-1,24-diol (**4**) Yellow liquid, yield: 46% (85 mg); Calculated for $C_{18}H_{30}Br_4O_8$; C, 31.15; H, 4.36; Br, 46.05. Found: C, 31.44; H, 4.09; Br, 46.33. ^{1}H-NMR (300 MHz, $CDCl_3$) δ = 2.07 (2H, OH), 3.61-3.73 (m, 24H, 1-H, 2-H, 4-H, 5-H, 7-H, 8-H, 17-H, 18-H, 20-H, 21-H, 23-H, 24-H), 4.43, (d, 2H, *J* = 13.5, 10-H, 15-H), 4.54 ppm (d, 2H, *J* = 13.5, 10'-H, 15'-H); ^{13}C-NMR (75 MHz, $CDCl_3$) δ =61.75 (1-C, 24-C), 69.35, 70.29, 70.33, 70.67 (2-C, 4-C, 5-C, 7-C, 18-C, 20-C, 21-C, 23-C), 72.50 (8-C, 17-C), 73.09 (10-C, 15-C), 117.44 (11-C, 14-C), 124.85 (12-C, 13-C).
ESI-MS; m/z (%) = 690.9 (15), 692.9 (67), 694.9 (100), 696.8 (67), 698.8 (15) $[M+H]^+$.

General iodination procedure:

To a solution of compounds **1** or **2** (0.26 mmol) in methanol (10 ml), iodine (0.82 mmol) was added. The mixture was stirred at room temperature overnight, and at the end solvent was removed by low pressure evaporation.

Extraction was made with dichloromethane and was washed with water. After drying over sodium sulfate, the solvent was removed and the crude product was purified by column chromatography (silica gel, diisopropylether/ acetone 1/1).

(8E,10E)-8,9,10,11-tetraiodo-3,6,13,16-tetraoxaoctadeca-8,10-diene-1,18-diol (**5**) Red-brown liquid, yield: 40% (83 mg); Calculated for $C_{14}H_{22}I_4O_6$; C, 21.18; H, 2.79; I, 63.94. Found: C, 20.95; H, 2.93; I, 64.07. ^{1}H-NMR (300 MHz, $CDCl_3$) δ = 2.09 (2H, OH), 3.63-3.78 (m, 16H, 1-H, 2-H, 4-H, 5-H, 14-H, 15-H, 17-H, 18-H), 4.30, (d, 2H, *J* = 13.5, 7-H, 12-H), 4.40 ppm (d, 2H, *J* = 13.5, 7'-H, 12'-H); ^{13}C-NMR (75 MHz, $CDCl_3$) δ = 61.81 (1-C, 18-C), 69.27, 70.25 (2-C, 4-C, 15-C, 17-C), 72.40 (5-C, 14-C), 80.84 (7-C, 12-C), 97.08 (8-C, 11-C), 105.90 ppm (9-C, 10-C).

ESI-MS; m/z = 794.7 $[M+H]^+$, 816.7 $[M+Na]^+$.

(11E,13E)-11,12,13,14-tetraiodo-3,6,9,16,19,22-hexaoxatetracosa-11,13-diene-1,24-diol (**6**) Red-brown liquid, yield: 51% (120 mg); Calculated for $C_{18}H_{30}I_4O_8$; C, 24.51; H, 3.43; I, 57.55. Found: C, 24.44; H, 3.56; I, 57.74. ^{1}H-NMR (300 MHz, $CDCl_3$) δ = 1.86 (2H, OH), 3.61-3.74 (m, 24H, 1-H, 2-H, 4-H, 5-H, 7-H, 8-H, 17-H, 18-H, 20-H, 21-H, 23-H, 24-H), 4.28, (d, 2H, *J* = 13.5, 10-H, 15-H), 4.38 ppm (d, 2H, *J* = 13.5, 10'-H, 15'-H); ^{13}C-NMR (75 MHz, $CDCl_3$) δ =61.79 (1-C, 24-C), 69.30, 70.38, 70.73 (2-C, 4-C, 5-C, 7-C, 18-C, 20-C, 21-C, 23-C), 72.50 (8-C, 17-C), 80.87 (10-C, 15-C), 104.27 (11-C, 14-C), 106.02 (12-C, 13-C).

ESI-MS; m/z = 882.7 $[M+H]^+$, 903.7 $[M+Na]^+$.

ACKNOWLEDGMENTS

We acknowledge the financial support of this work by PNCDI II program (UEFISCSU; projects IDEAS 515, 570, 2358).

REFERENCES

1. a. Y. J. Zhang, H. Wei, W. B. Zhang, *Tetrahedron*, **2009**, *65*, 1281.; b. Y. Alpagut, B. Goldfuss, J. M. Neudoerfl, *Beilstein J. Org. Chem.*, **2008**, *4*, 25.; c. M. Kitamura, S. Shirakawa, Y. Arimura, X. Wang, K. Maruoka, *Chem. Asian. J.*, **2008**, *3*, 1702; d. Y. Sudo, D. Shirasaki, S. Harada, A. Nishida, *J. Am. Chem. Soc.*, **2008**, *130*, 12588.
2. Y.Q. Fang, M. Lautens, *Org. Lett.,* **2005**, *7*, 3549.
3. I. Grosu, G. Plé, S. Mager, E. Mesaros, A. Dulau, C. Gego, *Tetrahedron*, **1998**, *54*, 2905.
4. F. Piron, N. Vanthuyne, B. Joulin, J.-V. Naubron, C. Cismaş, A. Terec, R. A. Varga, C. Roussel, J. Roncali, I. Grosu, *J. Org. Chem*., 2009, Doi: 10.1021/jo901762j

5. a. G. Köbrich, A. Mannschreck, R. A. Misra, G. Rissmann, M. Rösner, W. Zündorf, *Chem. Ber.,* **1972**, *105*, 3794; b. G. Köbrich, B. Kolb, A. Mannschreck, R. A. Misra, *Chem. Ber.*, **1973**, *106*, 1601; c. H. L. Elbe, G. Köbrich, *Chem. Ber.*, **1974**, *107*, 1654; d. M. Rösner, G. Köbrich, *Angew. Chem. Int. Ed.,* **1974**, *13*, 741; e. H. O. Bödecker, V. Jonas, B. Kolb, A. Mannschreck, G. Köbrich, *Chem. Ber.,* **1975**, *108*, 3497; f. M. Rösner, G. Köbrich, *Angew. Chem.* **1975**, *87*, 715.
6. a. A. J. P. Devaquet, R. E. Townshend, W. J. Hehre, *J. Am. Chem. Soc.*, **1976**, *98*, 4068; b. S. M. Bachrach, M. Liu, *J. Am. Chem. Soc*., **1991**, *113*, 7929; c. M. E. Squillacote, F. Liang, *J. Org. Chem*., **2005**, *70*, 6564; d. A. E. Hansen, K. L. Bak, *J. Phys. Chem. A*, **2000**, *104*, 11362.
7. a. A. Mannschreck, M. Mintas, G. Becher, G. Stühler, *Angew. Chem*., **1980**, *92*, 490; b. G. Becher, A. Mannschreck, *Chem. Ber*., **1981**, *114*, 2365.
8. a. U. Berg, T. Liljefors, C. Roussel, J. Sandström, *Acc. Chem. Res*., **1985**, *18*, 80; b. R. Gallo, C. Roussel, U. Berg, *Adv. Heterocycl. Chem*., **1988**, *43*, 173.
9. a. b. G. Lu, S. Lam, K. Burgess, *Chem. Commun.*, **2006**, *15*, 1652.
10. S. Auricchio, S. Bruchner, L. Malpezzi, O. Vrajna de Pava, *J. Chem. Research (Miniprint)*, **1983**, 1201.
11. a. Z. J. Yao, H. P. Wu, Y. L. Yu, *J. Med. Chem.*, **2000**, *43*, 2484; b. M. M. McPhee, S. M. Kerwin, *Bioorg. Med. Chem.*, **2001**, *9*, 2809.
12. G.Wegner, *Makromolekulare Chemie* **1970**, *134*, 219.

STUDIA UNIVERSITATIS BABEŞ-BOLYAI, CHEMIA, LIV, 4, 2009

ELECTROCHEMICAL TREATMENT OF ACID WASTEWATERS CONTAINING METHYLORANGE

ADRIANA SAMIDE[1], MĂDĂLINA DUMITRU[a], ADINA CIUCIU[a], BOGDAN TUTUNARU[a], MIRCEA PREDA[a]

ABSTRACT. The degradation process of solutions containing Methylorange using electrochemical measurements, on Ti electrode was studied. In order to estimate the contribution of pure adsorption, behavior of Methylorange in open circuit was investigated. The color removal (CR) due to adsorption was estimated at 8.86%. From the anodic polarization, Ti electrode in the blank solution of 0.1 M HCl containing 0.035 M NaCl (ASB) or dye solution of 0.1 M HCl containing 0.035 M NaCl and Methylorange (ASC) a different behaviour was observed. In cathodic polarisation case, the ASC behavior being completely different towards ASB. It can be concluded that the polarisation curve for ASC in the potential range of-426mV to -900mV can be attributed to the dye reduction; thus the color removal was estimated at value of 23.6%. Galvanostatic method to evaluate the effect of current density on solution discoloration process was applied. The color removal at 250min increases of the value of 68.4% calculated at current density of 5mA/cm^2 until the value of 73.4% at current density equal to 15 mA/cm^2. Degradation process of Methylorange follows a first order kinetics reaction. Rate constants increase with the increase of current densities and their values are: 0.0047min^{-1}, in the case of degradation at a current density of 5 mA/cm^2, and 0.006min^{-1}, in the case of degradation at a current density of 15mA/cm^2.

Keywords: Methylorange, electrochemical degradation, titanium electrode, kinetics process

INTRODUCTION

Wastewaters contain a range of organic pollutants (about 10.000 different dyes) such as acids, alkalies, solid particles, toxic compounds and dyes which even in low concentrations must be removed. Synthetic dyes are used in textile industry (60%), paper industry (10%), plastic manufacture (10%) and it is estimated that 10-15% of the dyes is lost during fabrication processes. It is reported that approximately 5 tonnes of dyes discharge from coloration industries every year. Furthermore, some azo dyes, their precursors and a number of their reaction products are carcinogenic.

Due to environmental requirements in recent years, different techniques have been used for removal of such waste as adsorption, oxidation, reduction and electrochemical reactions. To eliminate dyes from aqueous coloured

[1] *Universitatea din Craiova, Facultatea de Chimie, Str. Calea Bucureşti, Nr. 107I, RO-200285, Craiova, Romania, samide_adriana@yahoo.com*

effluents and reduce their ecological impact, several biological, physical and chemical methods have been proposed: biological treatment [1-4], physical or chemical flocculation, electrofilteration, membrane filtration, electrokinetic coagulation [5-8], adsorption and precipitation [9-11] and other oxidative/ reductive chemical and photochemical processes [12-17].These methods have individual advantages, but also have some constrains when they are applied individually. Development of the appropriate techniques for treatment of dye wastewater is important for the natural waters protection. Other techniques including radiation and discoloration with ozone in combination with H_2O_2 are also employed [18].

Electrochemical treatments have certain advantages by comparison with other methods, namely: wide application, simple equipment, easy operation, lower temperature requirements and no sludge formation. It is important to select the proper electrode material, because the reaction products strongly depend on those materials as well as the experimental conditions. Selection of a proper electrode material is vital for an efficient and enduring operation of an electrode. Several researchers have tested the feasibility of electrochemical degradation using various electrode materials:glassy carbon, Pt, Pt+Ir, Ti, Al, Co+Pd, Fe, IrO_2, PbO_2, SnO_2, diamond paste doped with boron [19-33].

The objective of this research was to evaluate the electrochemical discoloration process of solutions with Methylorange content by direct electrochemical degradation, with an electrode made of Ti using a synthetic solution with Methylorange disolved in 0.1 M HCl aditivate with 0.035 M NaCl.

RESULTS AND DISCUSSION

The Methylorange was the organic compound studied, whose structure and spectrum are shown in Figure 1. This azo dye was purchased from Fluka and used as received. All others chemical compounds used were of analytical type. As it can be seen from Figure 1, the maximum absorption for dye in the visible region was at 502 nm. Beside the main peak, other two characteristic absorption peaks at the wavelength of 273 and 321 nm in the ultraviolet region, were identified.

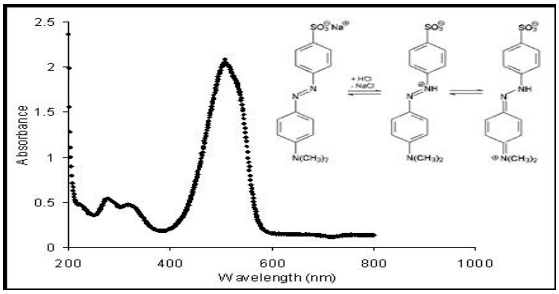

Figure 1. UV-Vis spectrum of initial Methylorange solution and molecular structure of Methylorange in acid medium aditivate with NaCl.

Study of Methylorange adsorption process

In order to estimate the contribution of pure adsorption, behaviour of Methylorange in open circuit was studied. In the open circuit, in ASB solution, the potential is stabilized after approximately 10 min, being of -306 mV at the end of the experiment (Figure 2 as an example). In the dye presence (ASC), within the first 25 minutes, the potential changes are major and can be attributed to a tendency of adsorption-desorbtion of dye on the titanium surface with the formation of a non-adherent and ruggedness film, which is interposed at the metal / solution interface. After 40 min the potential is stabilized, reaching the value of -266mV, at the end of the experiment. The potential shift to less negative values can be associated with the formation of a relative, uniform film, which is due to Methylorange adsorption on the titanium surface. This adsorption has a weak effect on the discoloration and it results from the fact that the titanium surface texture shows affinity for Methylorange, which can be adsorbed on the substrate through free electrons from azot atoms.

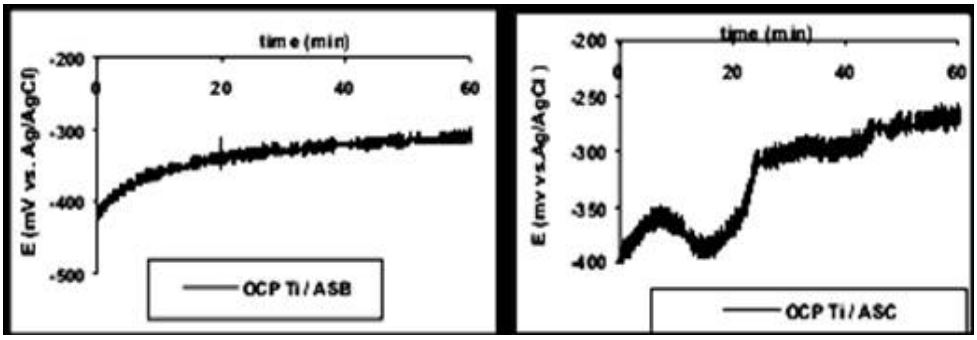

Figure 2. The potential dependence of time registered in open circuit in the absence and in the presence of Methylorange in 0.1 M HCl / 0.035 M NaCl solution.

UV-Vis spectra registered in open circuit, at the initial time and after 60 minutes are shown in Figure 3. A decrease of absorbance value from 2.03 to 1.85 which is attributed of Methylorange adsorption on the titanium surface was observed. Color removal (CR) due to the pure adsorption was determined using the following equation:

$$CR = (1 - A / A_0) \cdot 100 \quad (1)$$

where: A_0 and A represents the initial absorbance and absorbance at a moment “t”, 60 min in this case, respectively.

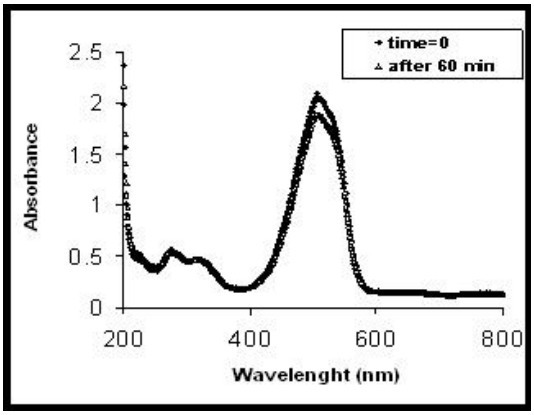

Figure 3. UV-Vis spectrum of Methylorange solution registered in open circuit.

The colour removal was 8.86% at an initial Methylorange concentration of 0.15 M.

Study of anodic and cathodic processes

The polarization curves of ASB and ASC on Ti electrode are shown in Figures 4 and 5. From the anodic polarization (Figure 4), it can be observed that Ti has a different behaviour in the blank solution and dye solution, respectively.

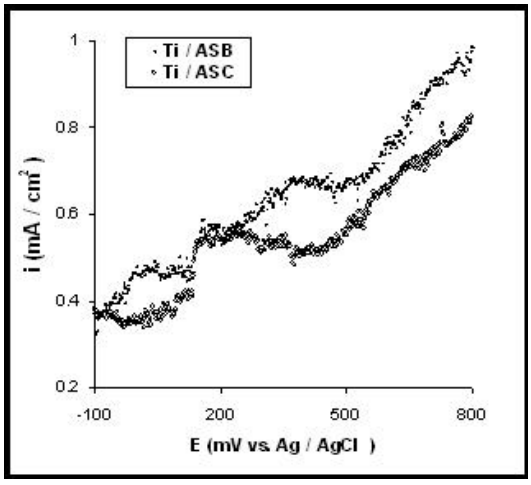

Figure 4. Anodic polarization curves of ASB and ASC on Ti electrode.

For the titanium electrode ASC has a major effect on the reaction in the range of positive potential; thus the potentials were shifted to less negative values, and current densities decreased. These changes may be associated with the formation of a film on the titanium surface, which modified the electronic change at metal / electrolyte interface. The anodic peak which appears at 200 mV is not attributed to an electro-oxidation, but to a tendency of titanium passivation. In spectrum UV-Vis the absorbance level was maintained on the initial value of 2.03. From cathodic polarization curve, a different behaviour of titanium electrode in ASC solution, by comparison with the ASB solution was observed. In the presence of Methylorange the current densities increased from a value of potential equal to -430 mV to -556 mV. This evolution could be attributed to the fact that the cathodic process is too slow to be controlled, therefore no characteristic peaks are obtained. Literature data [33] mentioned on glassy electrode the existence of two reduction peaks of azo group, first bielectronic at ε = - 425 mV / Ag, AgCl, with the formation of hydrazoderivate (according to Scheme 1), and the second tetraelectronic, at more negative potentials, up to -875 mV / Ag, AgCl leading to adequate amines according to Scheme 2:

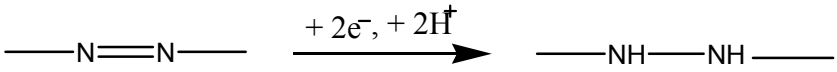

Scheme 1

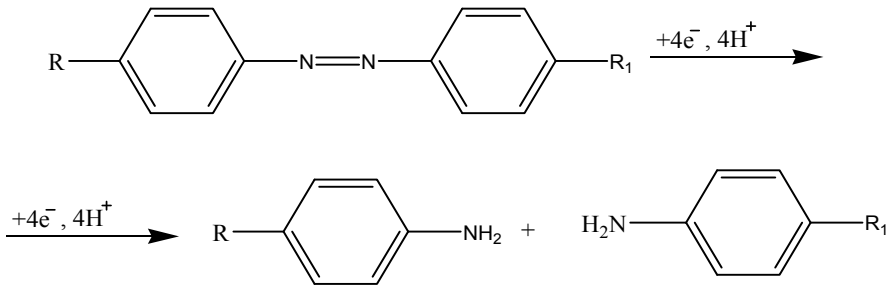

Scheme 2

Therefore, the ASC behaviour being completely different towards ASB, it can be concluded that the polarisation curve carriage for ASC in the potential range of -426 mV to -900 mV can be attributed to dye reduction.

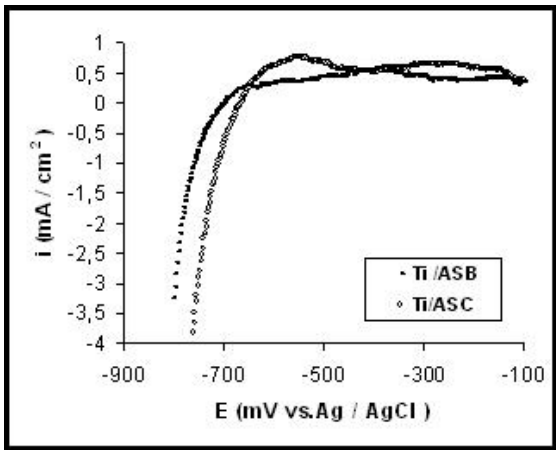

Figure 5. Cathodic polarization curves of ASB and ASC on Ti electrode.

UV-Vis spectrum of Methylorange solution registered at the end of the cathodic process is shown in Figure 6. A decrease of the absorbance from the 2.03 to 1.55 was observed, therefore the color removal calculated using the equation (1) has been calculated 23.6%.

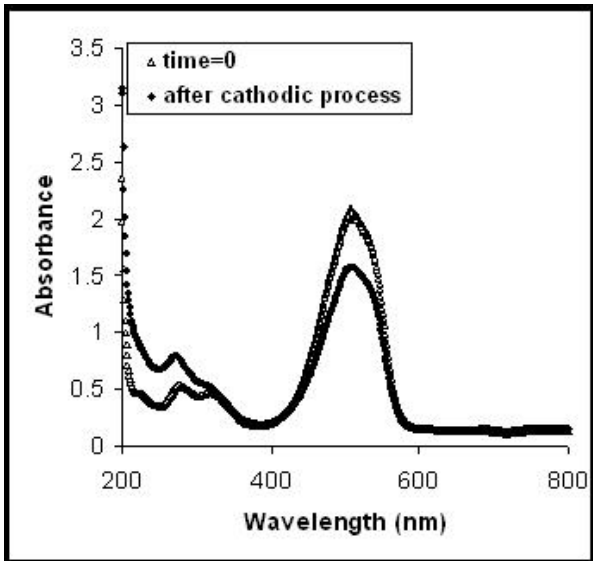

Figure 6. UV-Vis spectrum of Methylorange solution registered after cathodic process.

Study of discoloration process at different current densities

Galvanostatic technique was applied to evaluate the current density effect on discoloration process of dye solution. Electrochemical measurements, for two different current densities 5 mA/cm^2 and 15 mA/cm^2, respectively, were carried out. Each experiment ran for a time of 250 min, samples being analysed at certain time intervals, namely: 20 min, 40 min, 60 min, 80 min, 100 min, 150 min, 200 min, 250min. At specified time intervals absorbances values were evaluated. The degradation process of dye was followed by means of color removal (CR) values, which were calculated using equation (1). UV-Vis spectra of discolorated Methylorange at different current densities, 5 mA/cm^2 and 15 mA/cm^2 respectively, applied for 250 min, at room temperature are shown in Figures 7 and 8.

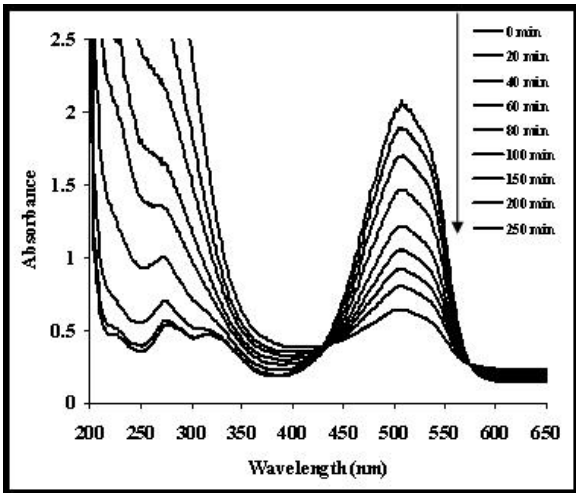

Figure 7. UV-Vis spectrum of Methylorange solution registered for current density of 5 mA/cm^2, for 250 min.

Figures 7 and 8 show that absorbance decreases in time, on the same current density, which demonstrates Methylorange degradation and discoloration. Absorbance values, at the same reaction time, present a significant decrease, hence a greater rate of degradation, with the current density increase. This may be shown by determining the colour removal (CR) using the equation 1, at time values when the spectral recordings were performed. Dependence of colour removal of time, at different current densities, is shown in Figure 9. Thus, the color removal at 250 min increases from 68.4% calculated at current density of 5 mA/cm^2 to the value of 73.4% at a current density equal to 15 mA/cm^2.

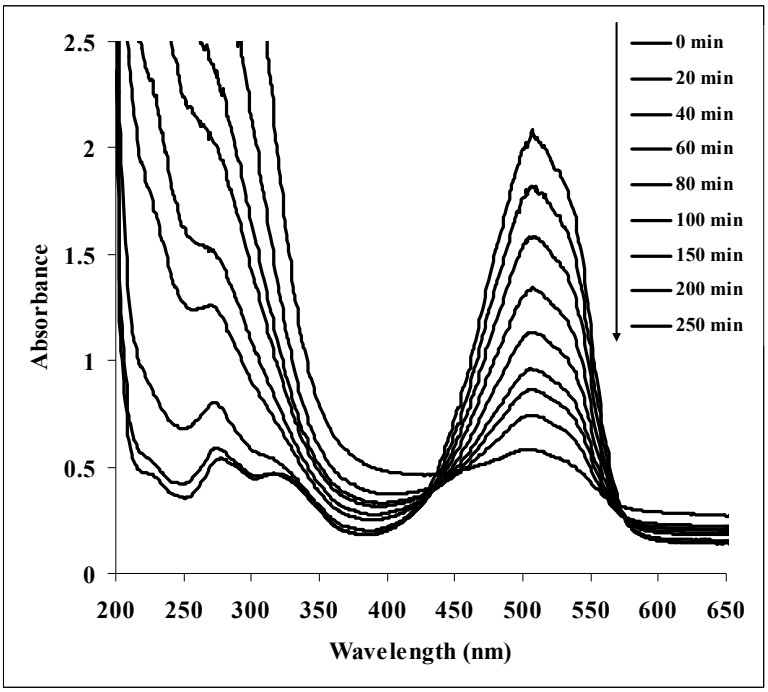

Figure 8. UV-Vis spectrum of Methylorange solution registered for current density of 15 mA/cm^2, for 250 min.

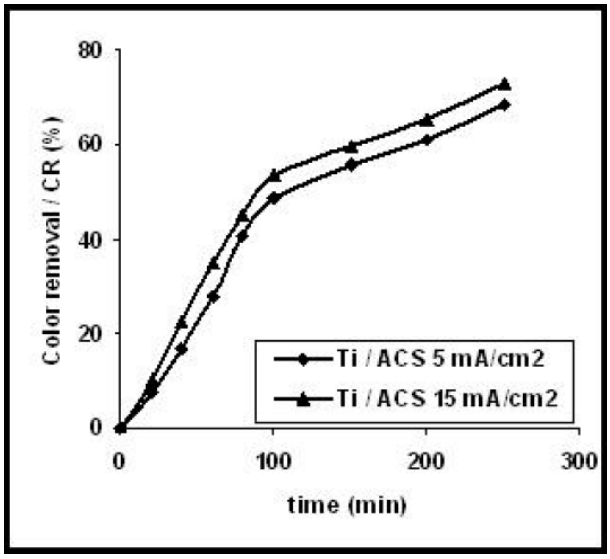

Figure 9. Dependence of color removal on time at different current densities.

Kinetics of Methylorange degradation

1). Determination of apparent rate constant

In general, degradation curves of dyes follow a first order kinetics reaction. The first order kinetic can written as follows:

$$-d[dye] / dt = k_{ap}[dye] \quad (2)$$

where: k_{ap} is apparent rate constant.

Integrating the equation (2), a first order kinetics equation was obtained:

$$\ln [dye]_0 / [dye]_t = k_{ap} \times t \quad (3)$$

Straight line plots $\ln [dye]_0 / [dye]_t = f(t)$ allow us to obtain the apparent rate constants for Methylorange, at both current densities. The absorbance is directly proportional with the concentration of Methylorange degraded; equation (3) can be written as:

$$\ln A_0 / A_t = k_{ap} \times t \quad (4)$$

where: A_0 and A represent the initial absorbance and absorbance at a given "t" time, respectively.

2) Verification of first order kinetics

a) Absorbance variation in time

The variation of absorbances resulted in the given experimental conditions were be evaluated, in time and as a function of the current densities whereat the degradation process of Methylorange had been studied. Absorbance versus time evolutions are shown in Figure 10.

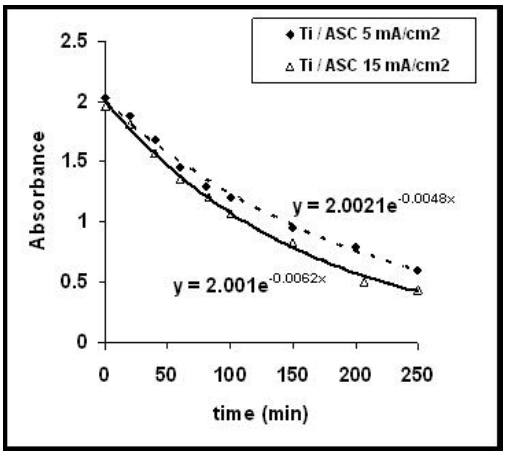

Figure 10. Absorbances variation during Methylorange degradation at different current densities applied.

It was noticed that, for the same current density, absorbance decreases exponentially with time, according to a relation $A = A_0 \exp(-kt)$, which corresponds to a first order kinetics, related to Methylorange degradation. From Figure 10, it can be seen that apparent rate constants values are: 0.0048 min^{-1}, in the case of degradation at a current density of 5 mA/cm^2, and 0.0062 min^{-1}, in the case of degradation at a current density of 15 mA/cm^2.

b) Integrated equation constant rate verification.
Rate constants determination

The curves $\ln A_0 / A = f$ (time) obtained from experimental data during the degradation process of Methylorange are shown in Figure 11. From Figure 11, it can be noticed that straight lines were obtained, passing through the origin and whose slope is $dy / dx = k_{ap}$;it can be observed that the value of R^2 is approximately equal 1;this proves that the degradation of ASC respects the first order kinetic. Rate constants (k_{ap}) increase with the increasing of current densities and have values ranging of 0.0047min^{-1}, in case of degradation at a current density of 5 mA/cm^2 and 0.006 min^{-1}, in case of degradation at a current density of 15 mA/cm^2, respectively.

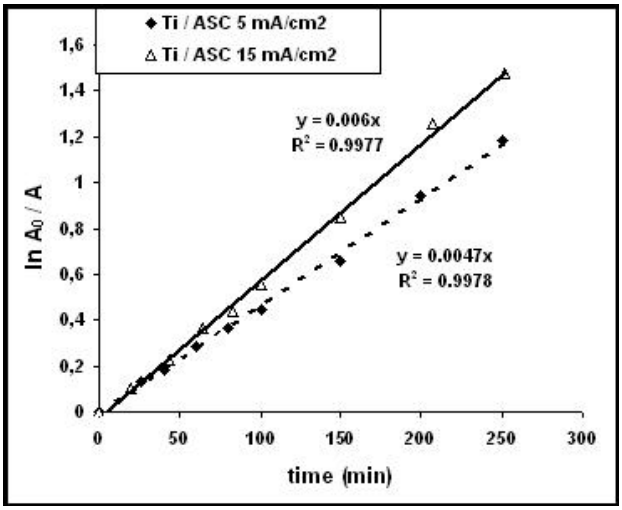

Figure 11. Diagrame corresponding with the first order kinetics in case of Methylorange degradation at different current densities.

From Figures 10 and 11, it can be observed that are obtained values of apparent rate constants approximately equal, for the same values of current densities; so it can be concluded that in the case of ASC degradation on Ti, it is respected the first order kinetics.

CONCLUSIONS

Electrochemical degradation process of a synthetic solution with Methylorange disolved in 0.1 M HCl solution aditivate with 0.035 M NaCl was studied.

In order to estimate the contribution of pure adsorption, behaviour of Methylorange in open circuit was studied. UV-Vis spectra registered in open circuit, at the initial moment and after 60 min had shown a decrease of the absorbance from t2.03 to 1.55, which was atributed to Methylorange adsorption on the titanium surface. The color removal (CR) due to adsorption was calculated to be 8.86% for a concentration of 0.08 mM Methylorange in ASB.

For the anodic polarization, observed that Ti in the blank and dye solution has a different behaviour. The anodic peak that appeared at 200 mV was not attributed to an electro-oxidation, but to a tendency passivation of titanium. In spectrum UV-Vis the absorbance level was maintained at the initial value of 2.03.

In cathodic polarisation case, the ASC behavior being totaly different towards ASB, it can be concluded that the polarisation curve carriage for ASC in the potential range of -426mV to -900mV can be atributted to the dye reduction. UV-Vis spectrum of Methylorange solution registered at the end of cathodic process had shown a decrease of the absorbance from 2.03 to 1.85; thus, the color removal was calculated to be 23.6%.

Galvanostatic technique was applied to evaluate the current density effect on discoloration process of dye solution. Thus, the color removal at 250 min increases from 68.4% calculated at current density of 5 mA/cm^2 to the value of 73.4% at a current density equal to 15 mA/cm^2.

The degradation process of Methylorange in ASB at studied current densities, 5 mA/cm^2 and 15 mA/cm^2, respectively, follows the first order kinetic reaction. Rate constants (k_{ap}) increase with the increase of current densities and their values are: 0.0047 min^{-1}, in the case of degradation at a current density of 5 mA/cm^2, and 0.006 min^{-1}, in the case of degradation at a current density of 15 mA/cm^2.

EXPERIMENTAL SECTION

Electrochemical measurements were carried out using a standard cell, with a working electrode made of Ti (the surface area of 2 cm^2), an auxiliary electrode in the form of glossy platinum plate (the surface area of 1 cm^2) and an Ag/AgCl electrode was used as a reference electrode. The electrode made of titanium was polished with very fine metallographic paper, washed with distilled water, degreased with acetone and dried. By electrochemical measurements azo dye Methylorange was degraded using a titanium electrode. The electrochemical behaviour of Methylorange was

evaluated by potentiostatic method using computerized electrochemical equipment VoltaLab 40 with software. The electrochemical degradation process was examined at positive and negative polarization, respectively, including open circuit condition, in a range of potential between -200mV and 800mV for the anodic process, and between -200 mV and -1000mV for the cathodic process, applying a scan rate of 10 mV/s. Galvanostatic technique was applied to evaluate the effect of current density on dyeing solution discoloration process. A SourceMeter 2420 3A potentiostat / galvanostat was used to controll the current density. The experiments were performed for two different current densities, 5 mA/cm^2 and 15 mA/cm^2, respectively. Each experiment ran for 250 min, samples being collected at certain time intervals. At specified time intervals absorbance values were assessed using an UV-Vis spectrophotometer, Varian Cary 50 with software.Temperature was maintained at 20ºC. Electrochemical solutions tested contained: acid blank solution composed of 0.035M NaCl, 0.1M HCl (ASB) and dye solution, which had the following components: 0.08mM Methylorange, 0.035M NaCl, 0.1M HCl (ASC).

REFERENCES

1. C.B. Shaw, C.M. Carliell, A. D. Wheately, *Water Research*, **2002**, *36*, 1193.
2. A.A. Oxpring, G. McMullan, W. F. Smyth and R. Merchant, *Biotechnology Letters*, **1996**, *18,* 527.
3. C.T. Matos, S. Velizarov, J.G. Crespo and M. A. M. Reis, *Water Research,* **2006**, *40*, 231.
4. H. Zilouei, B. Guieysse and B. Mattiasson, *Process Biochemistry*, **2006**, *41*, 1083.
5. J.I. Garrote, M. Bao, P. Castro, M.J. Bao, *Water Research*, **1995**, *29*, 26.
6. S.J. Judd and P. Hillis, *Water Research*, **2001**, *35*, 2895.
7. A.A. Chan, *Environmental Progress.*, **2006**, *25*, 152.
8. J. Bandara, J.A. Mielczarski and J. Kiwi, *Applied Catalysis B: Environmental*, **2001**, *34*, 321.
9. K.R. Ramakrishna and T. Viraraghavan, *American Dyestuff Reporter*, **1996**, *81*, 15.
10. S. Rio, L. Le Coq, C. Faur and P. Le Cloirec, *Water Science Technology*, **2006**, *53*, 237.
11. G. Crini, *Bioresource Technology*, **2006**, *97*, 1061.
12. J. Tokuda, R. Ohura, T. Iwasaki, Y. Takeuchi, A. Kawashida *Textiles Research J*ournal, **1999**, *69*, 956.
13. M. Dumitru, A. Samide, M. Preda, A. Moanta, *Revista de Chimie*, **2009**, *60*, 957.
14. H.Kusic, N.Koprivanac, L.Srsan, *Journal of Photochemistry and Photobiology A: Chemistry*, **2006**, *181*, 195.
15. B. Nasr and G. Abdellatif, *Journal of Electrochemical Society*, **2005**, *152*, D113.

16. M. Panizza, P.A. Michaud, G. Cerisola and Ch. Comninellis, *Electrochemistry Communications*, **2001**, *3*, 336.
17. N.H. Ince, *Water Research*, **1999**, *33*, 1080.
18. H.Y. Shu, *Journal of Hazardous Materials*, **2006**, *133*, 92.
19. J. Feng and D.C. Johnson, *Journal of Electrochemical Society*, **1991**, *138*, 3329.
20. R. Kotz, S. Stucki and B. Carcer, *Journal of Applied Electrochemistry*, **1991**, *21*, 1420.
21. J.M. Kesselman, O. Weres, N. SLewis and M.R. Hoffmann, *Journal of Physical Chemistry*, 1997, *101*, 2637.
22. C. Comninellis, C. Pulgarin, *Journal of Applied Electrochemistry*, **1993**, *23***,** 108.
23. S. Stucki, R. Kotz, B. Carcer, W. Suter, *Journal of Applied Electrochemistry*, **1991**, *21***,** 99.
24. A.M. Polcaro, S. Palmas, F. Renoldi, M. Mascia, *Journal of Applied Electrochemistry*, **1999**, *29*, 147.
25. J. Feng, L. Houk, D.C.Johnson, S. Lowery, J. Carey, *Journal of Electrochemical Society*, **1995**, *142*, 3626.
26. N.B. Tahar, A. Savall, *Journal of Applied Electrochemistry*, **1999**, *29*, 277.
27. X.M. Chen, G.H. Chen and P.L. Yue, *Journal of Physical Chemistry B*, **2001**, *105*, 4623.
28. B. Correa-Lozano, C. Comninellis, A.D. Battisti, *Journal of Applied Electrochemistry*, **1997**, *27*, 970.
29. R. Kotz, S. Stucki and B. Carcer, *Journal of Applied Electrochemistry*, **1991**, *21*, 14.
30. C. A.Martínez-Huitle, E.Brillas*, Applied Catalysis B: Environmental*, **2009**, *86*, 105.
31. N. Daneshvar, S. Aber, V. Vatanpour, M. Hossein Rasoulifard*, Journal of Electroanalytical Chemistry*, **2008**, *615*, 165.
32. Kai-sung Wang, Hsueh-Yu Chen, Long-Chiu Huang, Yu-Chun Su, Shih-Hsien Chang, *Chemosphere*, **2008**, *72*, 299.
33. M. Jitaru, A. Scorțeanu, C. Moldovan, *Revista de Chimie*, **2002**, 53, 35.

STUDIA UNIVERSITATIS
BABEŞ-BOLYAI

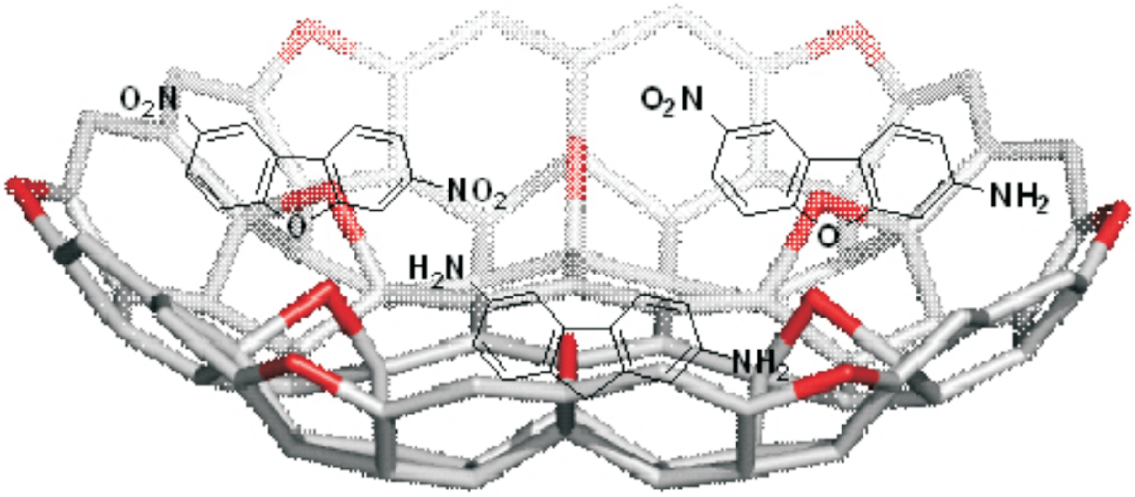

CHEMIA

4/2009
tom II

ANUL LIV **2009**

S T U D I A

UNIVERSITATIS BABEŞ-BOLYAI

CHEMIA

4

tom II

Desktop Editing Office: 51ST B.P. Hasdeu Street, Cluj-Napoca, Romania, Phone + 40 264-405352

CUPRINS – CONTENT – SOMMAIRE – INHALT

Studia Universitatis Babes-Bolyai Chemia has been selected for coverage in Thomson Reuters products and custom information services. Beginning with V. 53 (1) 2008, this publication is indexed and abstracted in the following:

- Science Citation Index Expanded (also known as SciSearch®)
- Chemistry Citation Index®
- Journal Citation Reports/Science Edition

STUDIA UNIVERSITATIS BABEŞ-BOLYAI, CHEMIA, LIV, 4, 2009

CORSU NETWORK - A NEW GRAPHENE DESIGN

MIRCEA V. DIUDEA[a] AND ALEKSANDAR ILIĆ[b]

ABSTRACT. A new graphene pattern, called CorSu, was designed and the energy of some small fragments of the lattice, functionalized by groups containing oxygen, carbon, nitrogen and phosphorus, was evaluated at the level of semiempirical method PM3. The topology of the network is described in terms of Omega counting polynomial. Close formulas for calculating the polynomial and the Cluj-Ilmenau index derived from this polynomial are given.

Keywords: Counting polynomial, lattice, CI index.

INTRODUCTION

Nano-era can be the name of the last twenty years, period when several new carbon allotropes have been discovered and studied for applications in nano-technology, in view of reducing the dimensions of devices and increasing their performance, al a lower cost of energy and money. Among the carbons structures, fullerenes (zero-dimensional), nanotubes (one dimensional), graphene (two dimensional) and spongy carbon (three dimensional) represent the novelty [1,2]. The attention of scientists was also focused to inorganic compounds, a realm where almost any metal atom can form clusters, tubules or crystal networks, very ordered structures at the nano-level. Recent articles in crystallography promoted the idea of topological description and classification of crystal structures [3-8]. They present data on real, but also hypothetical lattices, designed by computer.

The present study deals with a hypothetical graphene patterned by coronene- and sumanene-like units, described in terms of Omega counting polynomial and evaluated as energy by the PM3 method.

OMEGA POLYNOMIAL

Let $G(V,E)$ be a connected graph, with the vertex set $V(G)$ and edge set $E(G)$. Two edges $e = uv$ and $f = xy$ of G are called *codistant e co f* if they obey the following relation [9]:

[a] *Faculty of Chemistry and Chemical Engineering, "Babes-Bolyai" University, 400028 Cluj, Romania, diudea@gmail.com*

[b] *Faculty of Sciences and Mathematics, University of Niš, Višegradska 33, 18000 Niš, Serbia, aleksandari@gmail.com*

$$d(v,x) = d(v,y) + 1 = d(u,x) + 1 = d(u,y) \quad (1)$$

Relation *co* is reflexive, that is, *e co e* holds for any edge *e* of *G*; it is also symmetric, if *e co f* then *f co e*. In general, relation *co* is not transitive; an example showing this fact is the complete bipartite graph $K_{2,n}$. If "*co*" is also transitive, thus an equivalence relation, then *G* is called a *co-graph* and the set of edges $C(e) := \{f \in E(G);\ f\ co\ e\}$ is called an *orthogonal cut oc* of *G*, *E*(*G*) being the union of disjoint orthogonal cuts:

$$E(G) = C_1 \cup C_2 \cup ... \cup C_k,\ C_i \cap C_j = \varnothing, i \neq j\ .$$

Klavžar [10] has shown that relation *co* is a theta Djoković-Winkler relation [11,12].

We say that edges *e* and *f* of a plane graph *G* are in relation *opposite, e op f,* if they are opposite edges of an inner face of *G*. Note that the relation *co* is defined in the whole graph while *op* is defined only in faces. Using the relation *op* we can partition the edge set of *G* into *opposite* edge *strips, ops.* An *ops* is a quasi-orthogonal cut *qoc*, since *ops* is not transitive.

Let *G* be a connected graph and S_1, S_2, ..., S_k be the *ops* strips of *G*. Then the *ops* strips form a partition of *E(G)*. The length of *ops* is taken as maximum. It depends on the size of the maximum fold face/ring F_{max}/R_{max} considered, so that any result on Omega polynomial will have this specification.

Denote by *m*(*G*,*s*) the number of *ops* of length *s* and define the Omega polynomial as [13-15]:

$$\Omega(G,x) = \sum_s m(G,s) \cdot x^s \quad (2)$$

Its first derivative (in *x*=1) equals the number of edges in the graph:

$$\Omega'(G,1) = \sum_s m(G,s) \cdot s = e = |E(G)| \quad (3)$$

On Omega polynomial, the Cluj-Ilmenau [9] index, *CI*=*CI*(*G*), was defined:

$$CI(G) = \{[\Omega'(G,1)]^2 - [\Omega'(G,1) + \Omega''(G,1)]\} \quad (4)$$

Within this paper, the main results refer to $F_{max}(6)$. If rings instead of faces are considered, the polynomial is different. The inclusion of hexagons lying "under" the bridge brings complications in the number and length of *ops*, particularly at the maximum length.

Data were calculated by an original program called Nano Studio [16], developed at the TOPO Group Cluj.

LATTICE BUILDING

The lattice was built on the graphene sheet, of (6,3) tessellation, by decorating it with coronene-like flowers, having sumanene units as petals. The pattern, called CorSu, can be described as: [6:(6:(5,6)3)6], with vertices/atoms of degree 3 (sp^2) and 4 (sp^3), as shown in Figure 1.

This idea came out from the TOPO Group Cluj older studies on aromaticity, in which circulene/flower units were proposed as extensions of the Clar theory of aromaticity. Notice, the coronene and sumanene are molecules synthesized in the labs. It was also supported by the synthesis of several bowl-shaped molecules, inspired from the architecture of fullerenes and, more recently, by the direct synthesis of fullerenes starting from open precursors. The design of various domains on the graphene sheet is nowadays a challenge study and practice.

The pentagonal rings, possibly entering as local bridges over the graphite sheet by reactions like oxidation, amination, or carbene action, will force the geometry of graphene to a bowl-shaped one (Figure 1, the right hand column). The overall positive curvature depends on the bond length of the atoms involved in the bridges, it being as bowl-shaped as the atom covalent radius is smaller (see Table 1). The lattice appears as alternating positive (sumanene) and negative (coronene) curved domains.

MAIN RESULTS

The graphene lattice patterned by CorSu repeat units was designed in the idea of coronene [17] circulene [6:6_6] whose petals were replaced by sumanene [18,19] units, two molecules appearing as domains in fullerenes. Data in Table 1, computed at the PM3 level of theory, show the fragments of the lattice, functionalized by groups containing oxygen, carbon, nitrogen and phosphorus, as relatively stable ones, both as the total energy per atom and HOMO-LUMO geap. The bond lengths are quite reasonable, slightly elongated than the normal values. In comparison, the total energy per atom (in kcal/mol) for C_{60} is -2722.45, while the gap is around 6.59 eV. The bridges defining the pentagonal rings of the sumanene units, will force the planar graphene to adopt a bowl-shaped form and the sp^2 carbon atom is supposed to shift to the sp^3 hybridization. In the whole, the lattices appears as a waved surface, with margins eventually positively curved (Figure 1) or in sent to hyperbolic geometry.

Table 1. Energy and structural data for two fragments of the hypothetical lattice CorSu

	Structure	C_X (A)	TE/HeavyN (Kcal/mol)	HOMO-LUMO Gap (eV)
	CorSu_96 _X			
1	O	1.52	-3271.32	5.950
2	C (CH2)	1.64	-2925.55	6.655
3	N (NH)	1.61	-3007.54	6.740
4	P (PH)	2.06	-2889.53	6.057
	CorSu_198 _X			
5	O	1.52	-3289.57	8.776
6	C (CH2)	1.62	-2889.05	8.603
7	N (NH)	1.58	-2967.23	8.143
8	P (PH)	2.05	-2853.45	6.590

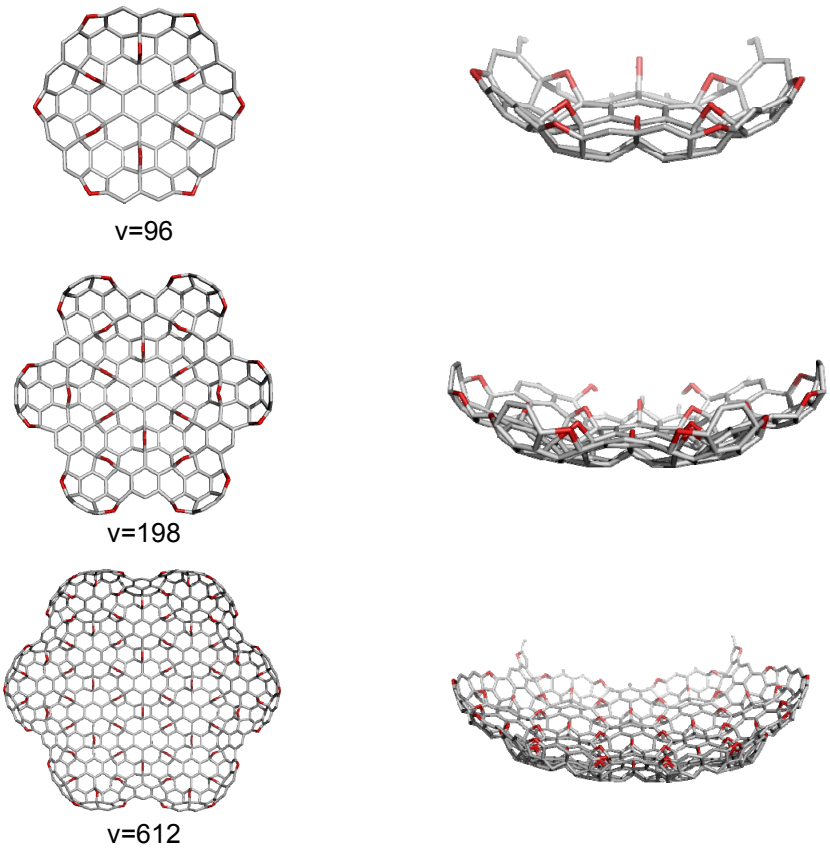

Figure 1. Hexagonal domains in the CorSu graphene sheet: top view (left hand column) and side view (right hand column).

This is the first description of a completely new (hypothetically, yet) lattice, of which functionalization we believe to be soon performed. Of course, the route to such structures is not suggested, remaining as a challenge.

The topology of the lattice is described here in terms of Omega polynomial. Table 2 gives examples for hexagonal (complete) domains.

Table 2. Omega polynomials of hexagonal domains $CorSu_{h,k}$

k	Omega	CI	Atoms	Bonds
0	$24x + 12x^2 + 24x^3 + 3x^6$	18648	96	138
1	$144x + 36x^2 + 156x^3 + 39x^6$	839628	612	918
2	$372x + 60x^2 + 396x^3 + 129x^6$	6013296	1614	2454
3	$708x + 84x^2 + 744x^3 + 273x^6$	22506948	3102	4746
4	$1152x + 108x^2 + 1200x^3 + 471x^6$	60717096	5076	7794

The Omega polynomial for the CorSu lattice of hexagonal domains of $CorSu_{h,k}$ type is:

$$\Omega(CorSu_{h,k}, x) = a_k x + b_k x^2 + c_k x^3 + d_k x^6 .$$

For the starting values, we have $a_0 = 24, b_0 = 12, c_0 = 24, d_0 = 3$. Based on the composition rule, we can deduce the following recurrent formulas:

$$a_{k+1} = a_k + 120 + 108k$$
$$b_{k+1} = b_k + 24$$
$$c_{k+1} = c_k + 132 + 108k$$
$$d_{k+1} = d_k + 36 + 54k$$

After solving these recurrent relations, we get:

$$\Omega(CorSu_{h,k}, x) = (24 + 66k + 54k^2)x + (12 + 24k)x^2 + (24 + 78k + 54k^2)x^3 + (3 + 9k + 27k^2)x^6$$

The number of atoms in the lattice is:

$$v = 96 + 273k + 243k^2 ,$$

while the number of bonds, following (3):

$$e = 138 + 402k + 378k^2 .$$

CI index follows from (4), and is given by the following formula:

$$CI(CorSu_{h,k}) = 18648 + 109764k + 264420\,k^2 + 303912k^3 + 142884k^4$$

Parallelogram domains were also considered; data are given in Table 3.

Table 3. Omega polynomials of parallelogram domains p(a,b)

a	b	Omega	CI	Atoms	Bonds
1	1	$24x + 12x^2 + 24x^3 + 3x^6$	18648	96	138
1	2	$46x + 20x^2 + 50x^3 + 6x^6$	73192	187	272
1	3	$68x + 28x^2 + 76x^3 + 9x^6$	163648	278	406
1	4	$90x + 36x^2 + 102x^3 + 12x^6$	290016	369	540
1	5	$112x + 44x^2 + 128x^3 + 15x^6$	452296	460	674
2	2	$86x + 28x^2 + 94x^3 + 18x^6$	281332	359	532
2	3	$126x + 36x^2 + 138x^3 + 30x^6$	624672	531	792
2	4	$166x + 44x^2 + 182x^3 + 42x^6$	1103212	703	1052
2	5	$206x + 52x^2 + 226x^3 + 54x^6$	1716952	875	1312
3	3	$184x + 44x^2 + 200x^3 + 51x^6$	1383688	784	1178
3	4	$242x + 52x^2 + 262x^3 + 72x^6$	2440696	1037	1564
3	5	$300x + 60x^2 + 324x^3 + 93x^6$	3795696	1290	1950
4	4	$318x + 60x^2 + 342x^3 + 102x^6$	4302468	1371	2076
4	5	$394x + 68x^2 + 422x^3 + 132x^6$	6688528	1705	2588
5	5	$488x + 76x^2 + 520x^3 + 171x^6$	10395448	2120	3226

Let $v(a,b)$ be the number of atoms in the parallelogram domain. We have the following symmetric recurrent formulas

$$v(a,b) = v(a,b-1) + (10+81a)$$
$$v(a,b) = v(a-1,b) + (10+81b)$$

After solving this second degree recurrent relation, using the starting value $v(1,1) = 96$, it follows:

$$v(a,b) = 81ab + 10a + 10b - 5.$$

Similarly, we can calculate the number of bonds and CI index

$$e(a,b) = 126ab + 8a + 8b - 4$$
$$CI(a,b) = (126ab + 8a + 8b - 4)^2 - 108 + 108(a+b) - 504ab.$$

In case of parallelogram p(a,b) domains, the Omega polynomial equals:

$$\Omega(CorSu_{p(a,b)}, x) = (-2 + 4a + 4b + 18ab)x + (-4 + 8a + 8b)x^2 + (-10 + 8a + 8b + 18ab)x^3 + (6 - 6a - 6b + 9ab)x^6$$

CONCLUSIONS

A new graphene lattice, patterned by CorSu units, was functionalized by groups containing oxygen, carbon, nitrogen and phosphorus, and its stability evaluated at the level of semiempirical method PM3. The small fragments, taken into consideration, showed relatively good stability, as compared with the data for the well-known C_{60}. The topology of the network is described in terms of Omega counting polynomial. Close formulas for calculating the polynomial and the Cluj-Ilmenau index derived from this polynomial were given.

ACKNOWLEDGMENTS

The work was supported in part by the ID_506 Romanian GRANT 2009, and the Research grant 144007 of the Serbian Ministry of Science.

REFERENCES

1. M.V. Diudea, Ed., “Nanostructures, novel architecture”, NOVA, **2005**.
2. M.V. Diudea and Cs. L. Nagy, “Periodic Nanostructures”, Springer, **2007**.
3. L. Carlucci, G. Ciani and D. Proserpio, *Coord. Chem. Rev.*, **2003**, *246*, 247.
4. L. Carlucci, G. Ciani and D. Proserpio, *Cryst. Eng. Comm.*, **2003**, *5*, 269.

5. V.A. Blatov, L. Carlucci, G. Ciani and D. Proserpio, *Cryst. Eng. Comm*., **2004**, *6*, 377.
6. I.A. Baburin, V.A. Blatov, L. Carlucci, G. Ciani and D. Proserpio, *J. Solid State Chem.*, **2005**, *178*, 2452.
7. O. Delgado-Friedrichs and M. O'Keeffe, *J. Solid State Chem*., **2005**, *178*, 2480.
8. V.A. Blatov, O. Delgado-Friedrichs, M. O'Keeffe, and D. Proserpio, *Acta Cryst.,* **2007**, *A63*, 418.
9. P.E. John, A.E. Vizitiu, S. Cigher, M.V. Diudea, *MATCH Commun. Math. Comput. Chem.*, **2007**, *57*, 479.
10. S. Klavžar, *MATCH Commun. Math. Comput. Chem.,* **2008**, *59*, 217.
11. D.Ž. Djoković, *J. Combin. Theory Ser. B*, **1973**, *14*, 263.
12. P.M. Winkler*, Discrete Appl. Math.,* **1984**, *8*, 209.
13. M.V. Diudea, *Carpath. J. Math.,* **2006**, *22*, 43.
14. M.V. Diudea, S. Cigher, P.E. John, *MATCH Commun. Math. Comput. Chem.*, **2008**, *60*, 237.
15. M.V. Diudea, S. Cigher, A.E. Vizitiu, M.S. Florescu, P.E. John, *J. Math. Chem.*, **2009**, *45*, 316.
16. Cs. L. Nagy, M.V. Diudea, *Nano Studio software*, Babes-Bolyai Univ., **2009**.
17. K. Yamamoto, *Pure Appl. Chem.,* **1993**, *65*, 157.
18. H. Sakurai, T. Daiko, T. Hirao, *Science,* **2003**, *301*,1878.
19. H. Sakurai, T. Daiko, H. Sakane, T. Amaya, T. Hirao, *J. Am. Chem. Soc.*, **2005**, *127*, 11580.

STUDIA UNIVERSITATIS BABEŞ-BOLYAI, CHEMIA, LIV, 4, 2009

DETERMINATION OF STEROID HORMONES IN SOMES RIVER WATER BY SOLID PHASE MICROEXTRACTION AND GAS CHROMATOGRAPHY - MASS SPECTROMETRY

LACRIMIOARA SENILA[a], MIRELA MICLEAN[a], CECILIA ROMAN[a], CORNELIA MAJDIK[b], GYULA ZÁRAY[c]

ABSTRACT. In this study, the occurrence of steroid hormones in Somes River was evaluated. The water samples were collected downstream of municipal sewage treatment plant of Cluj-Napoca, Romania. The used method was based on solid-phase microextraction (SPME), on-fiber silylation and, final, analysis by gas chromatography–mass spectrometry (GC-MS). The target compounds were estrone and beta-estradiol and were detected in wastewater effluent and river water. The values of target compounds in water samples were in the range of 0.010–0.080 µg/l.

Keywords: steroid hormones, SPME, MSTFA, GC-MS

INTRODUCTION

Humans and animals produce hormones, constantly excreted into the environment. The steroids of major concern are estrone and β-estradiol, since they exert their physiological effects at lower concentrations than other steroids [1, 2]. Estrone and β-estradiol cause reproductive disorders and abnormal development in wildlife and reduced fertility in human males, problems that may be caused by so-called endocrine disrupting chemicals (EDCs) released anthropogenically into the environment [3, 4].

Natural steroids, like estrone and β-estradiol are released into the aquatic environment through discharges from sewage treatment [5, 6, 7].

The purpose of this paper is to determine two natural steroid hormones in Somes River water samples using a sensitive and rapid technique. The method employs the solid-phase microextraction (SPME) by direct immersion in aqueous samples, with on-fiber silylation to separate the target compounds from the samples, followed by simultaneous determinations of the silylated

[a] *INCDO-INOE 2000, Research Institute for Analytical Instrumentation, Donath 67, 400293, Cluj-Napoca, Romania; E-mail: icia@icia.ro*

[b] *"Babes-Bolyai" University, Faculty of Chemistry and Chemical Engineering, Arany Ianos 11, 400028, Cluj-Napoca, Romania*

[c] *Institute of Chemistry, Department of Analytical Chemistry, L. Eötvös University, Budapest, Hungary*

derivatives by GC–MS. N-Methyl-N-(trimethylsilyl) trifluoroacetamide (MSTFA) was used as derivatization reagent to enhance selectivity and sensitivity [8, 9]. The chemical structures of estrone and β-estradiol are shown in Figure 1.

Due to the very low concentration (ng/l) of estrogenic compounds in the aqueous environment, sensitive and reliable methods are required for their determination [10, 11].

The most used analytical technique for estrogen detection and quantification is gas chromatography coupled to mass spectrometry (GC–MS), tandem mass spectrometry (GC–MS–MS), liquid chromatography coupled to mass spectrometry (LC–MS) and tandem mass spectrometry (LC–MS–MS). The drawback of GC-MS technique is the use of derivatization step prior to chromatographic analysis. The target compounds need to be derivatised to produce less polar compounds [12, 13].

Until this study, we did not find any information about hormones levels in Somes River water obtained using SPME-GC/MS method.

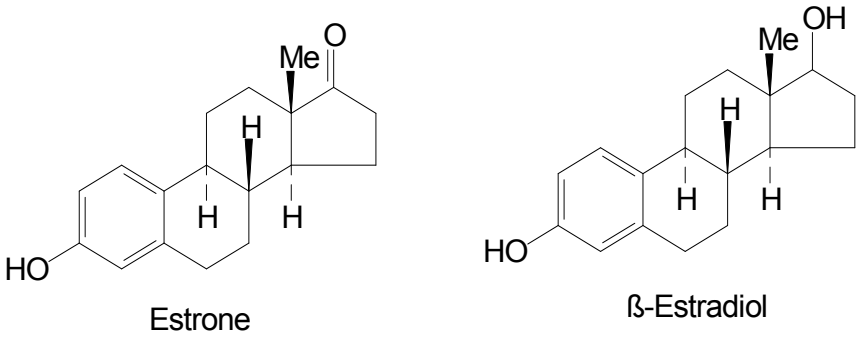

Figure 1. Structures of the steroid hormones

EXPERIMENTAL SECTION

Study area and sampling

The water samples were collected downstream of municipal sewage treatment plant, which collect and filter the urban residues of Cluj-Napoca, a city with approximate 400000 inhabitants. The geographic coordinates of sampling points are shown in Table 1.

Table 1. Geographic coordinates of sampling points

Sampling point	Latitude, N	Longitude, E
1	46°47'29,03"	23°41'7,53"
2	46°47'37,03"	23°43'10,60"
3	46°48'54,65"	23°44'56,61"

The study area comprising the three sampling points along the Somes River, downstream of sewage water treatment plant of Cluj-Napoca city is shown in Figure 2.

The samples collected in sampling point 1 point contained effluent sewage water after filtration, and the samples collected in sampling points 2 and 3 contained river water, downstream the treatment plant, approximately 3.5 km and 10 km, respectively.

Water samples were collected in triplicate, in August 2009 and were collected in pre-cleaned amber-glass bottles. Samples were stored at 4°C until filtration and extraction.

Filtered sewage water was filtered again in the laboratory through a 1µm glass fibre filter (Whatman, Mainstone, UK) prior to extraction.

Figure 2. Study area (source Google Earth)

Chemicals

Methanol HPLC-grade was purchased from Merck (Darmstadt, Germany). Steroid hormones: estrone (99 %) and ß-estradiol (98 %) were supplied by Sigma–Aldrich. Sodium chloride (NaCl, 99%) and hydrochloric acid (HCl, 37%) were obtained from Merck (Darmstadt, Germany). The derivatization agents N-Methyl-N-(trimethylsilyl) trifluoro acetamide (MSTFA) were purchased from Sigma–Aldrich.

Sodium chloride was used to decrease the solubility of organic compounds in water. A concentration level of 100 g/l NaCl was selected, according to other studies [8].

Hydrochloric acid was used to adjust the pH of the sample at value 5, in order to increase the extraction efficiency of the analytes [8].

Stock standard solutions of estrone and β-estradiol (1 mg/ml) were prepared in methanol and stored at −18 °C in dark. Working solutions were prepared by appropriate dilution of the stock standard solutions with ultrapure water and were stored at 4 °C in dark. Ultrapure water was obtained from a Milli-Q system (Millipore, Bedford, MA, USA).

Instrumentation

A gas chromatograph 6890N (Agilent Technologies) coupled with a mass spectrometer 5973N MSD (Agilent Technologies) and a capillary column HP-5 MS (30 m×0.25 mm×0.25 μm) were used to analyze the steroid hormones.

For the SPME extraction a manual fiber holder Supelco Inc. (Bellefonte, PA, USA) with an 85 μm polyacrylate (PA) fiber Supelco Inc. (Bellefonte, PA, USA) were used. After every analysis the fiber was conditioned in the GC inlet for 2 h at 300 °C [8].

Direct SPME extraction and headspace derivatization

Solid phase microextraction (SPME) is a unique sample preparation technique that requires no solvents or complicated apparatus. It can concentrate volatile and nonvolatile compounds (in liquids or gaseous samples), for subsequent analysis by GC or HPLC. Because analytes are concentrated on the fiber, and are rapidly delivered to the column, minimum detection limits are improved and resolution is maintained [11].

A volume of 18 ml sample, 1.8 g NaCl and a magnetic stirring bar for sample homogenization were put in a 20 ml sampler vial sealed with septa. The needle of the manual fiber holder pierced the septa, the PA fiber was released into the water sample and the extraction was performed at 120 min, and the temperature at 45 °C [8, 9].

After SPME, the analytes were derivatized using the headspace derivatization technique, by exposing the fiber to the vapor of 100 μl MSTFA, in a sampler vial sealed with a septum, for 60 min at 25 °C [8, 9].

GC-MS analysis

For quantitative determination, the MS system was operated in SIM mode. The injector was equipped with a 4 mm-I.D. glass liner. The carrier gas was helium at constant flow rate of 1.0 $mLmin^{-1}$. The GC column temperature program is shown in Table 2.

Table 2. GC column temperature program

Step	Ramp, °C/min	Temperature, °C	Holding time, min
1		90	2
2	30	180	0
3	10	240	0
4	3	270	0
5	15	300	2

The identification of steroid hormones was based on the standard mass spectra of the MS spectral library.

RESULTS AND DISCUSSION

The SIM chromatograms of the steroid hormones after silylated derivatization are shown in Figures 3-4. The ions monitored for each compound are listed in Table 3. Both target compounds in this work contained hydroxyl-group (Figure 1).

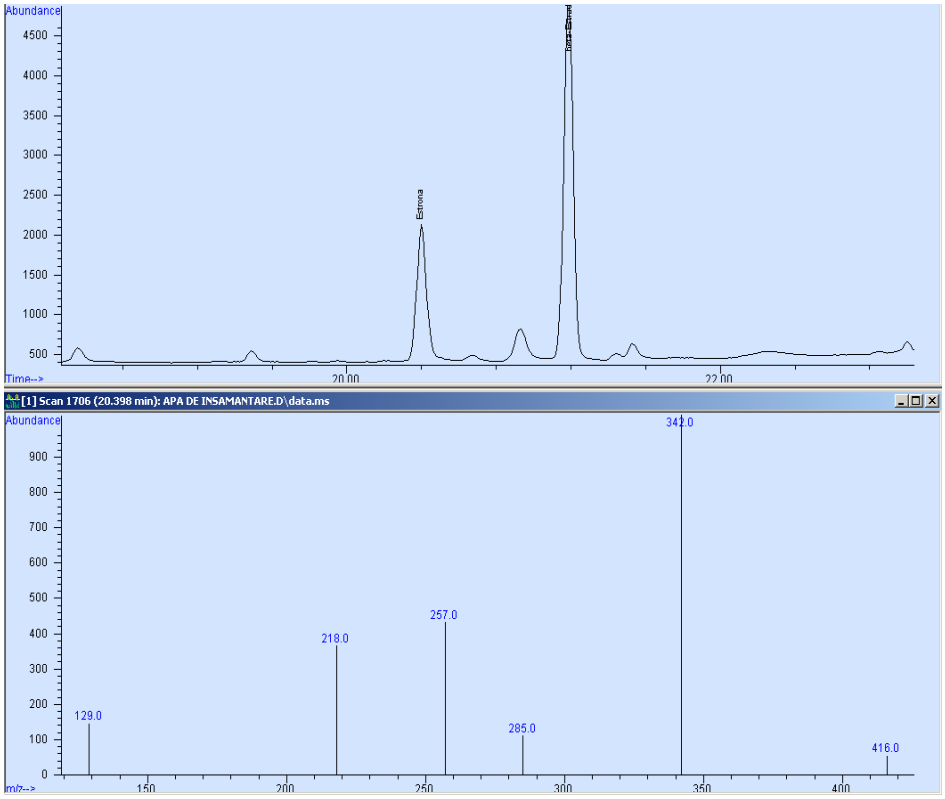

Figure 3. The SIM chromatogram of target compounds from waste water effluent (and the ions for the quantitative and qualitative analysis of silylation derivatives of estrone)

Estrone contained one hydroxyl group, the mono-TMSi derivatives were formed, and ß-estradiol contained two hydroxyl groups, the bis- TMSi derivatives were formed. The mono derivates for estrone were evidenced by the presence of *m/z* 342, 218 and 257, respectively. For ß-estradiol containing bis-hydroxi groups, the molecular ion at *m/z* 416 was show in the mass of derivative for ß-estradiol, indicating silylation of both hydroxyl groups. The ions monitored for estrone and ß-estradiol are listed in Table 3.

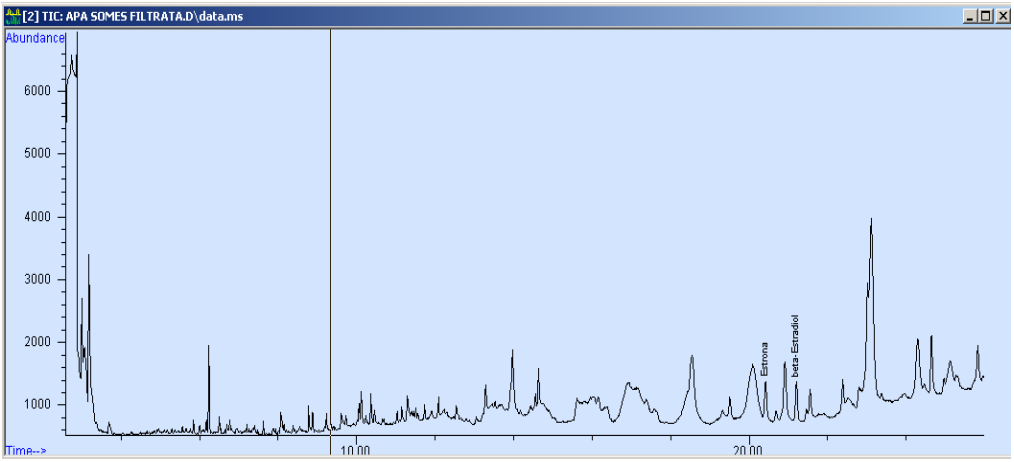

Figure 4. The SIM chromatogram of target compounds from river water (sampling point 2)

Table 3. Ions for the quantitative and qualitative analysis of silylation derivatives of target compounds

Compounds	Molecular mass	Ret. time (min)	Quantitative ions	Qualitative ions
Estrone	270	20.550	342	218, 257
ß-estradiol	272	21.368	416	129, 285

The relative standard deviations (RSD) for the target compounds were 10.2 and 11.5% for estrone and ß-estradiol, respectively, showing good reproducibility for the analytes. The RDSs were calculated for 6 replicates of a water sample. The limit of detection (DL), defined as the concentration that corresponds to three times the standard deviation of blanks, was measured by integrating blank peak area for each compound in 10 independent analyses with ultrapure water as blank [8]. The obtained DL for estrone and ß-estradiol were 0.013 and 0.008, respectively.

Highest concentrations of both estrogens were found in sampling point 1, the concentrations decreased after waste water treatment plant, along the Somes River. The obtained concentrations are shown in Table 4.

Table 4 The concentrations of estrogenic compounds in river water obtained by SPME GC-MS

Sampling point	Concentration estrone, μg/l	Concentration ß-estradiol, μg/l
1	0.056	0.080
2	0.032	0.040
3	0.020	< DL

The optimizations of reactions conditions (temperature, pH, derivatization time, extraction time) were selected according to other studies [8, 9].

Beta-estradiol was not detected in sampling point 3, suggesting that the concentration of this estrogen compound decreased due to the dilution effect.

The concentrations of this hormones obtained in the present study were higher than those obtained by Yang et al. (2006) in water samples collected from a pond in Sanjiao district (China), where the concentrations for estrone and ß-estradiol were 0.18 and 0.10 μg/l, respectively [8].

Extraction of estrogens from Somes River by SPME with on-fiber silylation with MSTFA is a simple and fast analytical method, environmental friendly and capable to analyze small sample volume.

CONCLUSIONS

Exposure of aquatic organisms to steroid hormones is an important concern due to the possible harmful effect. Discharges of municipal sewage in Somes River at Cluj-Napoca are the primary sources of estrogenic steroids. In this study, the analysis of estrogenic steroids in treated sewage, after dilution in Somes River was investigated. The results indicated the presence of natural estrogens, estrone and β-estradiol in water samples. The concentrations of both estrogens decreased along the Somes River, downstream from waste water treatment plant.

ACKNOWLEDGEMENTS

This work was supported by the Bilateral Project Romanian-Hungarian No. 19/2009, CONTALIM (ANCS Program).

REFERENCES

1. L.S. Shore, M. Shemesh, *Pure Applied Chemistry,* **2003**, *75 (11–12),* 1859–1871.
2. J.Q. Jiang, Q. Yin, J.L. Zhou, P. Pearce, *Chemosphere*, **2005**, *61(4*), 544-550.
3. M.S. Colucci, H. Bork, E. Topp, *Journal of Environmental Quality*, **2001**, *30*, 2070-2076.
4. A.N. Neale, B.I. Escher, A.I. Schäfer, *Science of the Total Environment*, **2009**, *407,* 1167-1173.
5. Z. Zhang, H. Duan, L. Zhang, X.Chen, Wei Liu, G. Chen, *Talanta*, **2009**, *78*, 1083-1089.
6. S. Zorita, P. Hallgren, L. Mathiasson, *Journal of Chromatography A*, **2008**, *1192*, 1-8.

7. C. Chia-Yang, W. Tzu-Yao, W. Gen-Shuh, C. Hui-Wen, L. Ying-Hsuan, L. Guang-Wen, *Science of the Total Environment,* **2007***, 378,* 352-365.
8. L. Yang, T. Luan, C. Lan, *Journal of Chromatography A*, **2006**, *1104*, 23–32.
9. L. Yang, C. Lan, H. Liu, J. Dong, T. Luan, *Analytical and Bioanalytical Chemistry,* **2006**, *386*, 391-397.
10. H. Noppe, B.L. Bizec, K. Verheyden, H.F. Brabander, *Analytica Chimica Acta*, **2008**, *611*, 1-16.
11. H.S.N. Lee, M.T. Sng, C. Basheer, H.K. Lee, *Journal of Chromatography A,* **2007***, 1148,* 8-15.
12. R. Liu, J.L. Zhou, A. Wilding, *Journal of Chromatography A,* **2004***, 1022,* 179-189.
13. http://www.sigmaaldrich.com/analytical-chromatography/.html

STUDIA UNIVERSITATIS BABEŞ-BOLYAI, CHEMIA, LIV, 4, 2009

CHANGES IN FATTY ACIDS COMPOSITION OF ANIMAL FATS DURING STORAGE

FLAVIA POP[a]

ABSTRACT. In this article the fatty acids composition for 2 types of animal fats (pork fat and beef tallow), following the variation of saturated and unsaturated fatty acids proportion during freezing storage was studied. Determination of chemical composition of animal fats is important in establishing organoleptic and physico-chemical parameters, the variation of them in time, nature and proportion of fatty acids conferring specific characteristics to them. For pork fat was determined the following chemical composition: saturated fatty acids (SFA) 48.32%, monounsaturated fatty acids (MUFA) 36.78% and polyunsaturated fatty acids (PUFA) 14.89%. After 4 months of storage under freezing there was a change in fatty acids proportion, saturated fatty acid content increased slightly to 48.83%, due to installation of hydrolysis leading to release of fatty acids from triglycerides, monounsaturated fatty acids content decreased to 35.99%, and polyunsaturated fatty acids content increased to 15.18%. In the case of beef tallow there was an increasing in saturated and monounsaturated fatty acids content and a decreasing in polyunsaturated fatty acids content.

Keywords: fatty acids, animal fats, storage

INTRODUCTION

In chemical terms fats are glycerol esters with fatty acids. Theoretically there is the possibility that one group of alcoholic glycerine is esterificated with a fatty acid molecule (monoglyceride), or two alcoholic groups are esterificated with two fatty acids molecules (diglyceride). In nature we meet only triglycerides. There are opinions that fats are made from simple triglycerides such as tripalmitin, tristearin, triolein, etc. But it turned out that in most of cases, fats are glycerin esters with 2 or 3 different fatty acids [1, 5]:

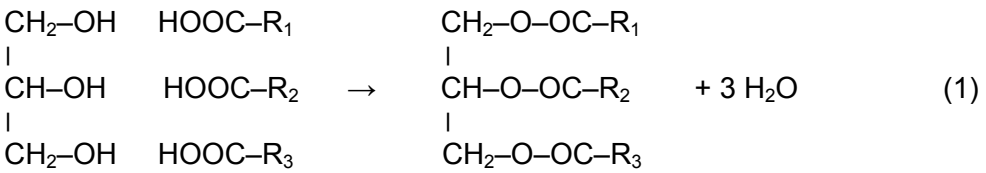

[a] *North University, Department of Chemistry-Biology, 76 Victoriei str., 430122, Baia Mare, Romania, flavia_maries@yahooo.com*

Fatty acids represent the variable structure of lipids, the characteristics of the fats being conferred by the nature and proportion of fatty acids that enters into their composition [11].

Major fatty acids from animal fats composition are those who have a number of 4 to 18 carbon atoms in the molecule, namely [5, 7]:

Butyric acid	$CH_3–(CH_2)_2–COOH$
Caproic acid	$CH_3–(CH_2)_4–COOH$
Caprylic acid	$CH_3–(CH_2)_6–COOH$
Caprynic acid	$CH_3–(CH_2)_8–COOH$
Lauric acid	$CH_3–(CH_2)_{10}–COOH$
Miristic acid	$CH_3–(CH_2)_{12}–COOH$
Palmitic acid	$CH_3–(CH_2)_{14}–COOH$
Stearic acid	$CH_3–(CH_2)_{16}–COOH$

The main unsaturated fatty acids in animal fats are oleic and linoleic acid. Oleic acid has 18 carbon atoms and one double link located between C9 and C10: $CH_3–(CH_2)_7–CH=CH–(CH_2)_7–COOH$. Linoleic acid has 18 carbon atoms, but two double links located between C9 and C10, C12 and C13: $CH_3–(CH_2)_4–CH=CH–CH_2–CH=CH–(CH_2)_7–COOH$ [28].

Animal fats has nutritional-biological and sensory value through: the provision of essential fatty acids for human body (linoleic, linolenic and arachidonic acids); concentrated sources of energy (cca.9 kcal/g, proteins and carbohydrates providing approx. 4 kcal/g); medium for transport/storage of liposoluble vitamins (A, D, E, K); formation of phospholipids with essential role in proper functionation of membranes; precursors of prostaglandins, essential hormones for the body; texture formers; structure formers in certain products (fillings for bakery products and confectionery); lipids confer softness (a slight bite and mastication), smaller the dry and granular feeling of food consumption (due to the lubrication effect and the liquid part of the fat); flavor providers (with positive or negative effect on the overall flavor of the product) and medium for hydrophobic flavour compounds [2, 3].

RESULTS AND DISCUSSION

The content of SFA in pork fat was higher (48.32%) than MUFA (36.78%) and PUFA (14.89%), the major fatty acids present in pork fat were palmitic, stearic, oleic and linoleic acids. Oleic acid was determined in the largest proportion (33.51%), these results are in agreement with previous studies on this type of fat [4, 6].

Figure 1 illustrates sample chromatogram for pork fat in witch fatty acids are registered in the form of peaks separated from each other by increasing the length chain, and at the same length chain by increasing of unsaturated degree.

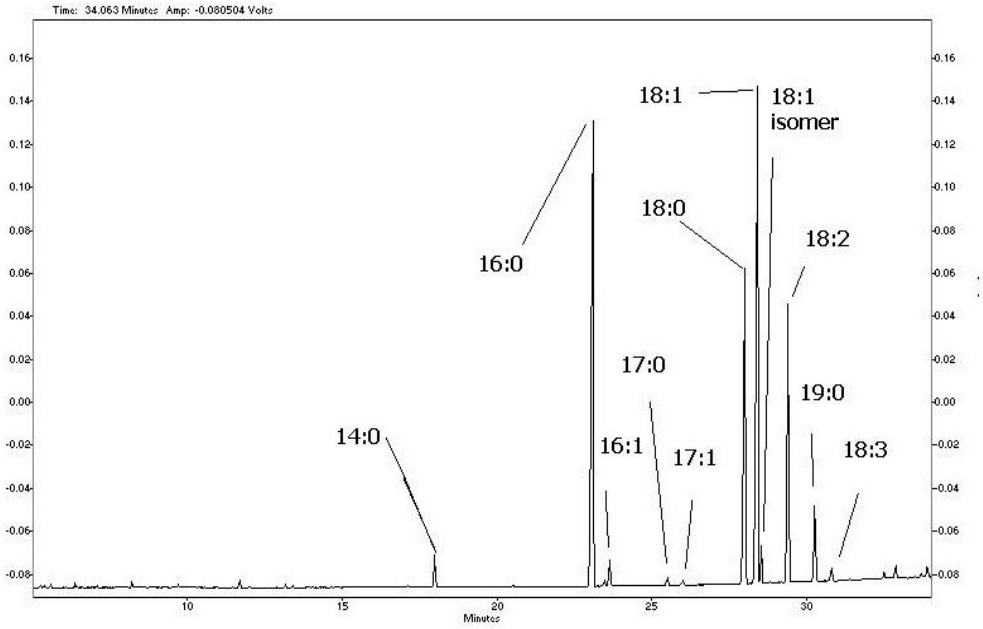

Figure 1. Chromatogram for fresh pork fat

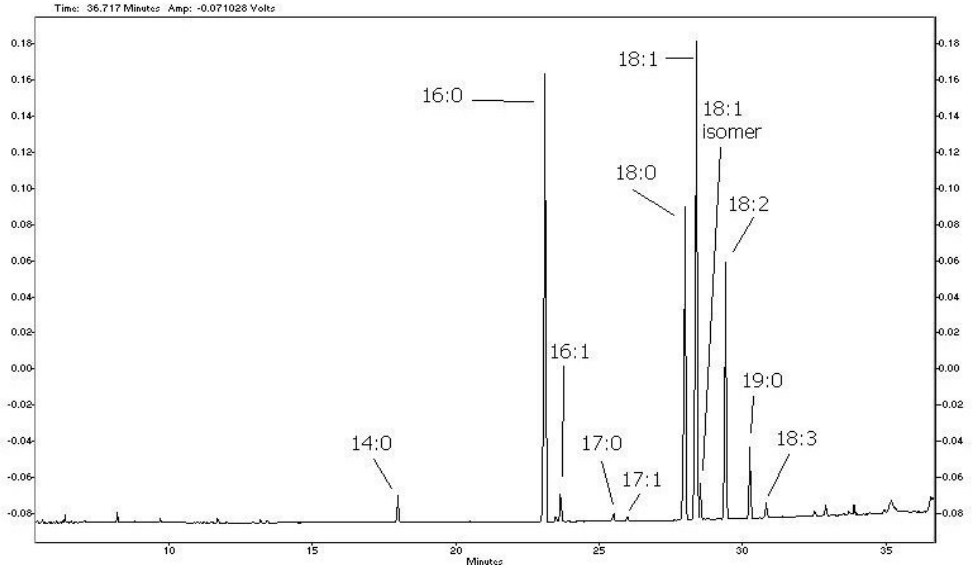

Figure 2. Chromatogram for pork fat at 4 months freezing

In pork fat sample to 4 months freezing there were some differences from the fresh sample: miristic acid content decreased to 1.29%, palmitic acid increased to 27.15%, palmitoleic acid increased to 1.35%, margaric acid decreased to 0.35%, *cis*-10-heptadecanoic acid remained constant, stearic acid increased to 20.03%, oleic acid decreased to 32.66%, vaccenic acid remained constant, linoleic acid increased to 14.41% and alfalinoleic acid increased to 0.76%. In general, the SFA content increased to 48.83%, the MUFA content decreased to 35.99% and the PUFA content increased to 15.18% (fig.2). The increas of saturated and polyunsaturated fatty acids content is due to the installation of hydrolysis leading to the release of acids from glycerides structure, which translates through the increas of titrable acidity.

The content of SFA in beef tallow was higher (57.13%) than MUFA (34.47%) and PUFA (8.4%), the major fatty acids present were palmitic, stearic and oleic acids [8, 10, 12]. Oleic acid was determined in the largest proportion (30.14%).

Figure 3 illustrates sample chromatogram for beef tallow in witch fatty acids are registered in the form of peaks separated from each other by increasing the length chain, and at the same length chain by increasing of unsaturated degree.

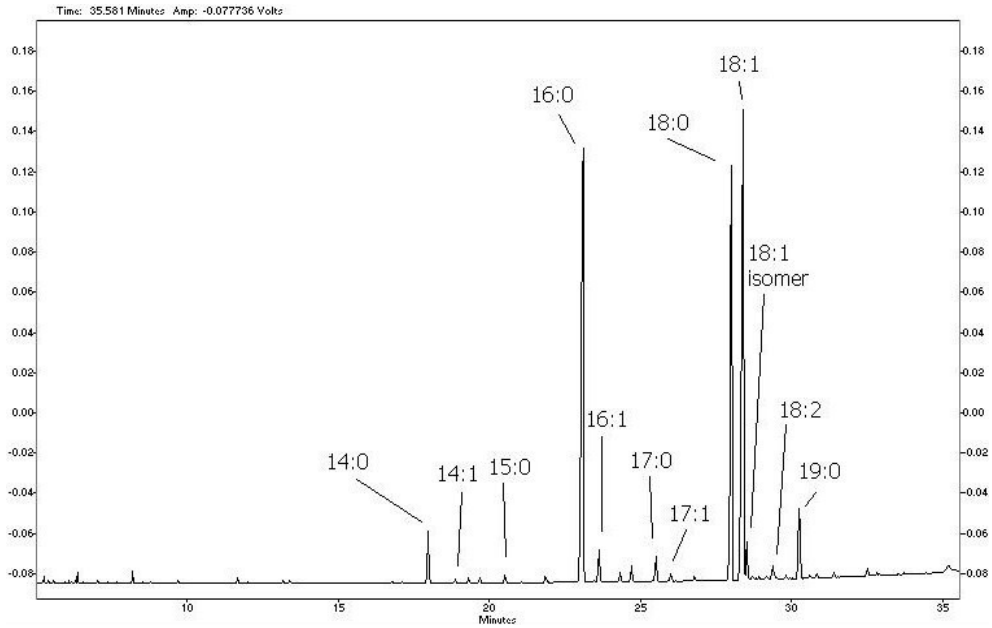

Figure 3. Chromatogram for fresh beef tallow

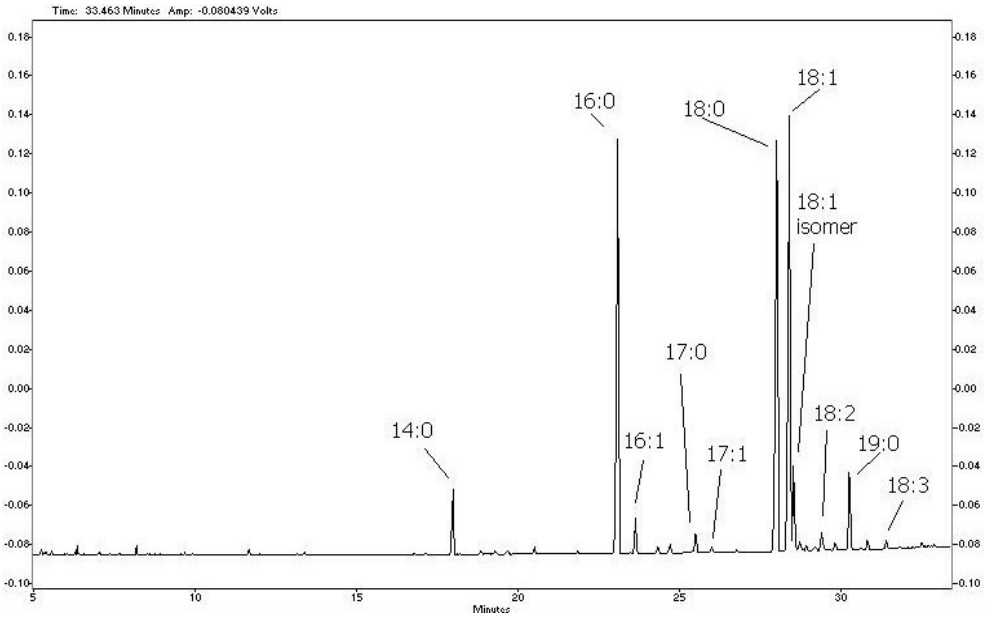

Figure 4. Chromatogram for beef tallow at 4 months freezing

In beef tallow sample at 4 months freezing there were some differences from the fresh sample: miristic acid content increased to 3%, pentaedecanoic and miristoleic acid were not detected, palmitic acid increased to 27.03%, palmitoleic acid increased to 1.77%, margaric acid decreased to 1.19%, *cis*-10-heptadecanoic acid decreased to 0.35%, stearic acid increased to 30.09%, oleic acid decreased to 30.09%, vaccenic acid increased to 4.64% and linoleic acid decreased to 1.32%. In general, the content of SFA increased to 61.3%, the MUFA content to 36.86% and the content of PUFA decreased to 1.84% (fig.4). In the case of beef tallow at 4 months congelation, monounsaturated fatty acids recorded an increase and polyunsaturated fatty acids a decrease, for pork fat at 4 months freezing we found the opposite.

Pork fat presents a highest proportion of mono and polyunsaturated fatty acids, than beef tallow, having aspect of alifios and homogeneous mass, beef tallow is presented as a compact and dense mass, fine granulated, with hard consistence, brittle to break or jam due to the higher content of saturated fatty acids [9, 11, 13].

CONCLUSIONS

Determination of chemical composition of animal fats is important in establishing organoleptic and physico-chemical parameters, the variation of them in time, being an indicator of their stability compared to alterative processes.

Beef tallow presented the lowest content of PUFA (8.4%), which are the most susceptible to autooxidation, it can be kept for a long period of time under refrigeration and freezing. Of studied fats, the most susceptible to altering is pork fat because its high content of PUFA (14.89%).

Chemical composition of fats influence their consistency, pork fat having aspect of alifios and homogeneous mass, beef tallow is presented as a compact and dense mass, fine granulated, with hard consistence, brittle to break or jam, with a higher value for melting point and a lower value for refractive and iodine index.

EXPERIMENTAL SECTION

Samples

Pork fat was obtained by melting of fresh bacon and lard pork and beef tallow was obtained by raw tallow melting, collected from "Baltata Romaneasca" race, female, age of 8 years, which were determined the chemical composition in fresh state and after 4 months of storage under freezing (-15 ...- 18^{o}C).

Physicochemical examination

Fatty acid composition was determined using gas chromatography (GC) Shimadzu GC-17 A coupled with flame ionisation detector FID. Gas chromatography column is Alltech AT-Wax, 0.25 mm I.D., 0.25 μm thick stationary phase (polyethylene), used helium as carrier gas at a pressure of 147 kPa, temperature of the injector and detector was set to 260^{o}C, the oven programm was the following: 70^{o}C for 2 min., then the temperature was raised up to 150^{o}C with a gradient of 10^{o}C/min., a level of 3 min. and the temperature was raised up to 235^{o}C with a gradient of 4^{o}C/min.

The method consists in transforming of fatty acids in methyl esters in the sample under analysis, followed by separation of components on a chromatography column, their identification by comparison with standard chromatograms and quantitative determination of fatty acids. Esterificated analyzed sample is introduced in column chromatography. By chromatography separation the sample chromatogram is obtained in which fatty acids are recorded in the form of peaks separated from each other by increasing the length chain, and at the same length chain by increasing of unsaturated degree. By comparing the distances of each peak from analyzed sample chromatogram with peaks distances from standard chromatograms, we identify each fatty acid present in the analyzed sample [14, 15, 16].

REFERENCES

1. C. Banu et al., *Tratat de chimia alimentelor*, Ed. Agir, Bucureşti, **2002**
2. C. Banu et al., *Alimentația şi sănătatea*, Editura Macarie, Târgovişte*,* **2001**
3. C. Banu, N. Preda, S. Vasu, *Produsele alimentare şi inocuitatea lor*, Editura Tehnică, Bucureşti, **1982**
4. J. Cháves, A. Castellote, M. Martin, R. Chifré, C. López-Sabater, *Food Chem.,* **2008**, *113*, 484
5. D. Ciobanu, R. Ciobanu, *Chimia produselor alimentare*, Ed. Tehnică-INFO, Chişinău, **2001**
6. A. Flåtten, A. Bryhni, A. Kohler, B. Egelandsdal, T. Isaksson, *Meat Sci.,* **2005**, *69,* no.3, 433
7. M. Leonte, T. Florea, *Tratat de chimia alimentelor*, I, Ed. Pax-Aura Mundi, Galaţi, **1998**
8. P. Manglano, M.J. Lagarda, M.D. Silvestre, C. Vidal, G. Clemente, R. Farre, *Eur. J. of Lipid Sci. and Tech*., **2005**, *107*, no.11, 815
9. S. Naz, R. Siddiqi, H. Sheikh, S. Asad Sayeed, *Food Res. Int*., **2005**, *38*, 127
10. E. Olsen, E.O. Rukke, A. Flátten, T. Isaksson, *Meat Sci*., **2007**, *76*, no.4, 628
11. N. Popescu, S. Meica, *Bazele controlului sanitar veterinar al produselor de origine animală*, Ed. Diacon Coresi, Bucureşti, **1995**
12. O. Samet-Bali, M.A. Ayadi, H. Attia, *Food Sci. and Tech*., **2008**, *30*, 7
13. V. Vito, F. Ferioli, Y. Riciputi, G. Iafelice, E. Marconi, M.F. Caboni, *Food Chem.*, **2008**, *78*, 384
14. ***Standard român SR ISO 661, **1998**
15. ***Standard român SR EN 14082, **2003**
16. ***International Standard ISO 3976, **2006**

STUDIA UNIVERSITATIS BABEŞ-BOLYAI, CHEMIA, LIV, 4, 2009

THE EFFECT OF ELECTROMAGNETIC FIELDS ON BAKER'S YEAST POPULATION DYNAMICS, BIOCATALYTIC ACTIVITY AND SELECTIVITY

DALIA SANDU[a], IOSIF LINGVAY[b], SZABOLCS LÁNYI[c], DAN DORU MICU[d], CLAUDIA LAURENTA POPESCU[e], JÜRGEN BREM[a], LÁSZLÓ CSABA BENCZE[a], CSABA PAIZS[*a]

ABSTRACT. The influence of ultralow frequency in the range of 23.8 -35.7 mT electromagnetic field on growth dynamics of *Saccharomyces cerevisiae* cells and the activity and selectivity for the cellular bioreduction of the prochiral 1-(benzofuran-2-yl)ethanone has been evaluated. The interaction of cell populations with the electromagnetic field reduced their growth rate, their activity and selectivity. The effects directly depends on the intensity of the applied field.

Keywords: Saccharomyces cerevisiae, electromagnetic field, cell growth dynamics, activity, selectivity, bioreduction, biocatalysis

INTRODUCTION

Electromagnetic fields with low frequencies (50-60 Hz) and low intensity are associated with the production, transmission and use of electricity. They interfere with the frequency of many biological processes involving changes in the electrical charges movements of the biomolecules. Furthermore, nowadays, due to the antropic activities, a large spectrum of electromagnetic fields, differing in their frequency are present in the biosphere as presented in Table 1 [1]. Communication, remote controls are the most common such applications.

Being a part of our environment, these fields were considered among potential interference factors that can modify the behavior of organism. That explains the great number of studies on this topic, dedicated to cells [2], tissues,

[a] *Babeş-Bolyai University, Faculty of Chemistry and Chemical Engineering, Str. Kogălniceanu, Nr. 1, RO-400084 Cluj-Napoca,Romania, paizs@chem.ubbcluj.ro*
[b] *National Institute of Research and Development in Electrical Engineering, Bucharest, Sector 3, Splaiul Unirii Nr. 313.*
[c] *Sapientia University, Faculty of Technical and Social Siences Piața Libertății, Nr. 1, Miercurea Ciuc, RO-530104,*
[d] *Technical University of Cluj Napoca, Faculty of Electrical Engineering, Constantin Daicoviciu Nr 15, Cluj-Napoca, RO-400020*
[e] *Politehinca University of Bucharest, Faculty of Electrical Engineering, Splaiul Independentei Nr. 313, Sector 6, RO- 060042*

whole living organisms [3]. Also the cell dynamics, the ion transport or gene transcription and expression [4] were consistent study objects. The effects of magnetic fields are numerous and apparently contradictory, depending on their static or alternative nature, intensity and frequency, by influencing the production of certain metabolites [5] they can stimulate or inhibit the cell growth [6- 7].

Electromagnetic fields influence DNA structure even at extremely low frequency. Based on the reported effects, the International Agency for Research on Cancer (IARC) has classified the extremely low-frequency (ELF) electromagnetic fields (EMF) as "possible carcinogenic" [8].

Saccharomyces cerevisiae is a validated experimental model, being one of the most intensively studied eukaryotic organisms in molecular and cell biology [9]. Our interest was focused on the investigation of possible action of the electromagnetic field on the catalytic parameters (activity and selectivity) and growth dynamic of *Saccharomyces cerevisiae*.

Table 1. Clasification of electromagnetic fields according to the frequency and use [1]

Frequency zone	**Frequency**	**Wavelength in the air**	**Use**
Extremely low	0-300 Hz	>1000 km	Many biological processes, electricity transport
Low, middle, high	30 kHz-30 MHz	10 km -10 m	Amateur radio, remote controls
Very, ultrahigh	30-300 MHz	10-1 m	Radio/TV
Superhigh	300 Mhz- 30 GHz	1 m-10 cm	Satellite communication
Extremely high	30-300 GHz	10-1 cm	RADAR
Infrared	300 GHz- 300 THz	1 cm-100 mm	
Visible light	429-750 THz	700-400 nm	Light

RESULTS AND DISCUSSION

Literature data showed that in the range of extremely low frequencies associated to commercial electric power at low values of amplitude (0.2-12 mT), a slight stimulation of cell growth [10] and also dehydrogenase activity [11] may occur. We investigated the influence of a 50 Hz magnetic field, generated in a toroidal coil, on *Saccharomyces cerevisiae* cellular proliferation. The activity and selectivity of yeast dehydrogenases in the reduction reaction of a substrate was tested in both the presence and the absence of the electromagnetic field.

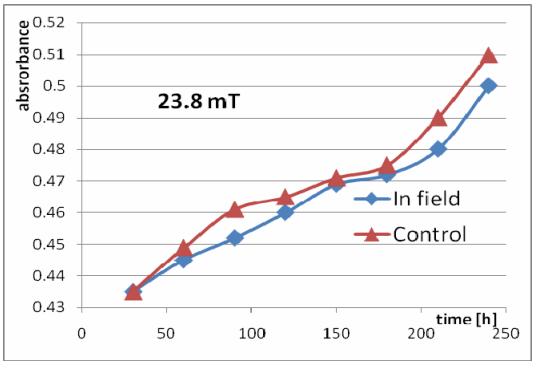

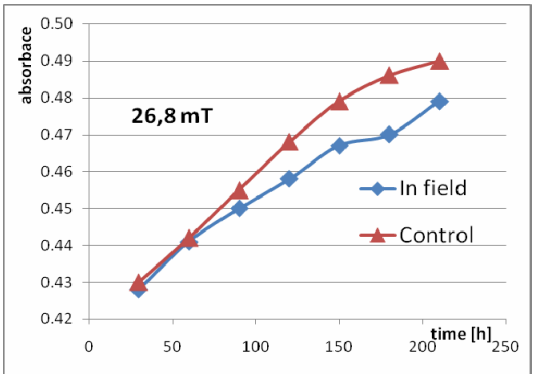

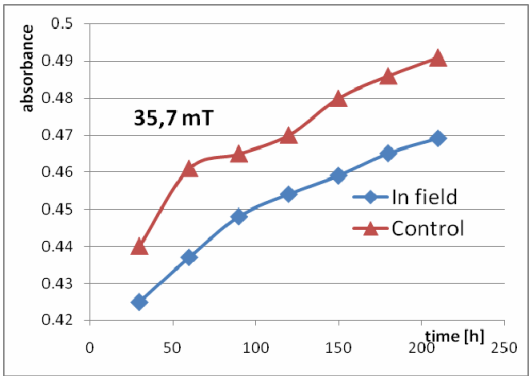

Figure 1. Comparative cell population dynamics in a magnetic field

a) The effect of the electromagnetic field on Saccharomyces cerevisiae growth dynamics

The cellular growth rate was slowed at all tested intensities of the electromagnetic field with the frequency of 50 Hz. As shown in Figure 1, the growth curves of the exposed yeast populations had lower values than the curves of the control populations.

In all cases the growth was positive, but the electromagnetic field showed a slight inhibitory effect.

The slowing of the cell growth was proportional with the intensity of the field.

b) The effect of the electromagnetic field on enzyme activity and selectivity

Biocatalyst-assisted conversion of the substrate is an estimate of the biocatalytic activity of the cells.

Parallel determinations in presence of the electromagnetic field at 26.8 and 35.7 mT and in unexposed cultures showed that in the range of these intensities the field reduced the catalytic activity (Figure 2) and selectivity of yeast dehydrogenases (Table 2).

The selectivity of the biocatalytic reaction was estimated by measuring the enantiomeric excess of the bioreduction product using as substrate 2-acetyl-benzofuran (Figure 3).

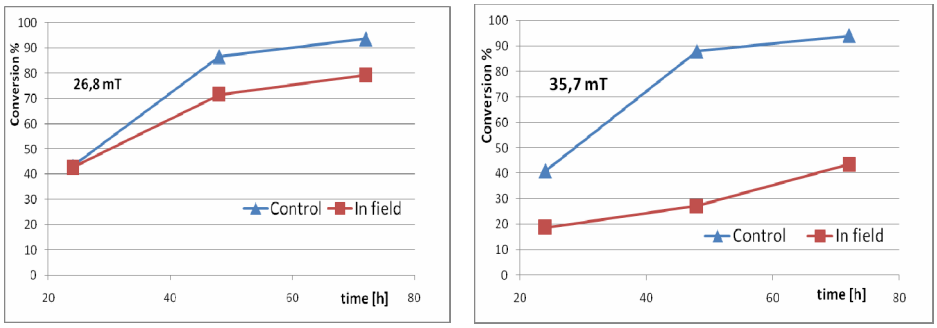

Figure 2. Influence of electromagnetic field on the conversion of the bioreduction of 2-acetylbenzofuran

As for enzymatic activity, determinations showed that samples exposed to the electromagnetic field, in the range of 26.8 and 35.7 mT intensity, lead to enantiomeric excesses of the product under the values found for the unexposed samples.

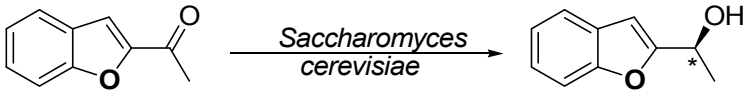

1-(benzofuran-2-yl)ethanone (*S*)-1-(benzofuran-2-yl)ethanol

Figure 3. Cellular reduction of 2-acetyl-benzofuran

Table 2. Enantiomeric excesses of the reaction product obtained with exposed and unexposed cells

Enantiomeric excesses (ee%)	**1.8 A**			**2.4 A**		
	24h	48h	72h	24h	48h	72h
Control sample	72%	73%	75.4%	66%	71%	77%
Exposed sample	67%	72%	74%	38%	44%	45%

CONCLUSIONS

The electromagnetic field generated by an alternative current of 50 Hz, applied at intensities in the range of 23.8-35.7 mT on *Saccharomyces cerevisiae* suspensions produced significant alterations in the growth dynamics of the cell populations. The catalytic activity and the selectivity in the reduction of the investigated prochiral 1-(benzofuran-2-yl)ethanone were impaired.

The results obtained in parallel experiments, with samples unexposed and exposed to the electromagnetic field, are in aggreement with the literature data and demonstrate the lowering of the growth dynamics.

Our original experiments on the biocatalytic activity and selectivity showed that the interference of the electromagnetic field with the biochemical process resulted the decrease of the substrate transformation rate and also reduced the discrimination capability of the enzymatic equipment for the two enantiotope faces of the substrate.

EXPERIMENTAL SECTION

The electromagnetic field was generated in a toroidal coil powered by an autotransformer at three values of the AC power: 1.6 A, 1.8 A and 2.4 A, which produced in the coil axis magnetic inductions of 23.8, 26.8 and 35.7 mT, respectively.

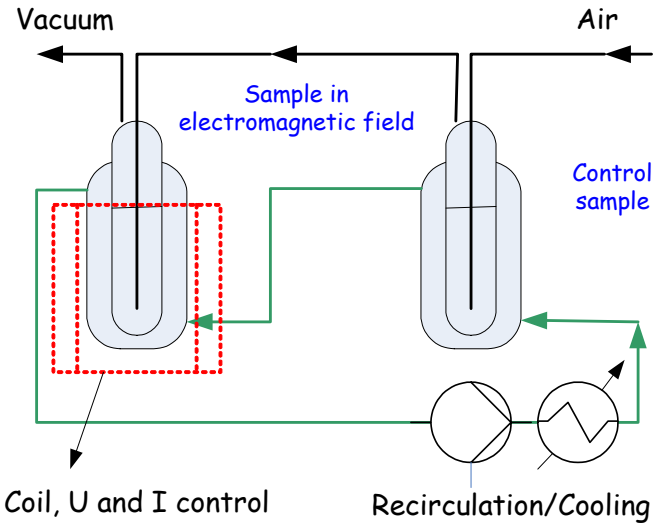

Figure 4. Experimental design for studying the effect of the electromagnetic field on certain functional parameters in *Saccharomyces cerevisiae*

A glass vial (bioreactor) provided with a cooling jacket and an air bubbler was introduced in the axis of the coil. An identical inexposed vial was used as control reactor. Both vials were termostated at 25 ^{o}C. The yeast suspensions were agitated with the same rate by air bubbling using an arrayed assembly as shown in Figure 4. Two experiments were performed, one at three different intensity values of the field and the second at two values of field intensity. In the first experiment it was investigated the influence of the intensity of the field upon the cell population growth and in the second one the effect of the field upon the stereoselectivity and the reaction rate for the cellular bioreduction of 2-acetyl-benzofuran was monitored. In all experiments commercially available baker's yeast was used.

For the growth experiment first a calibration curve was draw on, using the correlation between absorbance at 600 nm, and cellular concentration (gl^{-1}). The absorbance was measured using an UV-VIS Perkin-Elmer, type Lambda 1 spectrophotometer.

A suspension with the initial concentration of 0.500 gl^{-1} yeast and 2.5 gl^{-1} sugar was introduced in the two bioreactors. Samples were taken every 30 min. from both bioreactors, for a period of 240 min.

In the selectivity experiment, the investigated reaction was the enantiotope selective reduction of 2-acetyl-benzofuran (1-(benzofuran-2-yl)ethanone). The synthesis and the reduction of acetyl-benzofuran was synthesized according to literature data in the literature and was performed as earlier described by us [12].

The non-fermentative system was used in these experiments which provide a superior selectivity, but a prolonged reaction time in comparison with the fermenting system.

The solution of 2-acetyl-benzofuran (50 mg) in absolute ethanol (5 ml) was added into each bioreactor containing a suspension of 20 g yeast in 100 ml distilled water. Samples (1 ml) taken perodically (24h) from both exposed and unexposed bioreactor to appreciate the difference in biocatalyst selectivity due to the action of the electromagnetic field were extracted with ethyl acetate (3ml). The organic layer was dried over anhydrous sodium sulphate and the solvent was eliminated by rotary evaporation. The crude solide was redissolved in hexane (0.5 ml) and the solution was subjected for chromatographic analysis using an Agilent 1200 HPLC. Using a Chiracel OJ-H analytical column and a mixture of hexane:isopropanol 90:10 (v/v) as eluent previously tested succesfully for the enantiomeric separation of the racemic 1-(benzofuran-2-yl) ethanol, the enantiomeric excess of (*S*)-1-(benzofuran-2-yl) ethanol produced in both bioreactors were measured.

The conversion of the substrate was calculated from using the area of the alcohol and prochiral ketone chromatograpic signals corrected with the *ratio* of the specific molar absorbance of the compounds.

ACKNOWLEDGMENTS

The financial support from the Romanian Ministry of Education and Research (No. **X2C37/2006**, within the PN2 Program) is gratefully acknowledged.

REFERENCES

1. R. Funk, T. Monsees, N. Özkucur. *Progress in Histochemistry and Cytochemistry,* **2009**, *43*: 87.
2. S. Kwee, P. Raskmark. *Bioelectrochemistry and Bioenergetics,* **1995**, *36*: 109.
3. R. Beraldi, I. Sciamanna, R. Mangiacasale, R. Lorenzini, C. Spadafora. *Mutation Research/Genetic Toxicology and Environmental Mutagenesis,* **2003**, *538*: 163.

4. J.L. Phillips, N.P. Singh, H. Lai. *Pathophysiology,* **2009**, *16*: 79.
5. D.C. Alvarez, V.H. Pérez, O.R. Justo, R.M. Alegre. *Process Biochemistry,* **2006**, *41*: 1967.
6. L. Potenza, L. Ubaldi, R. De Sanctis, R. De Bellis, L. Cucchiarini, M. Dachŕ. *Mutation Research/Genetic Toxicology and Environmental Mutagenesis,* **2004**, *561*: 53.
7. W. Triampo, G. Doungchawee, D. Triampo, J. Wong-Ekkabut, I.M. Tang. *Journal of Bioscience and Bioengineering,* **2004**, *98*: 182.
8. M. Ruiz-Gómez, M.-M. M. *Electromagn Biol Med,* **2009**, *28*: 201.
9. J. Novák, L. Strasák, L. Fojt, I. Slaninová, V. Vetterl. *Bioelectrochemistry,* **2007**, *70*: 115.
10. M. Mehedintu, H. Berg. *Bioelectrochemistry and Bioenergetics,* **1997**, *43*: 67.
11. L. Zhang, H. Berg. *Journal of Electroanalytical Chemistry,* **1992**, *343*: 341.
12. C. Paizs, M. Tosa, C. Majdik, P. Moldovan, L. Novák, P. Kolonits, A. Marcovici, F.-D. Irimie, L. Poppe. *Tetrahedron: Asymmetry,* **2003**, *14*: 1495.

STUDIA UNIVERSITATIS BABEŞ-BOLYAI, CHEMIA, LIV, 4, 2009

SYNTHESIS OF ESTER DERIVATIVES OF CALIX[N]ARENE

ALINA SAPONAR[a], ELISABETH-JEANNE POPOVICI[a], RODICA GRECU[a], IOAN SILAGHI-DUMITRESCU[b], NICOLAE POPOVICI[a]

ABSTRACT. The synthesis of *p-tert*-butyl calix[n]arene derivatives with two and four, as well as, four and six (ethoxycarbonyl)methoxy groups at the lower rim is reported. The selective alkylation of the parent calix[n]arenes is performed in organic solvents, with ethyl bromoacetate in the presence of potassium carbonate or sodium hydride as a base. UV-Vis, FTIR, ^{1}H-NMR investigations confirmed the formation of the ester derivatives of calix[n]arene with variable number of ester groups at the narrow rim.

Keywords: Calix[n]arene, selective O-alkylation, ethyl bromoacetate

INTRODUCTION

A dedicated class of [1n] metacyclophanes generally designed as calixarene are nowadays receiving an increasing attention in the field of supramolecular chemistry because of their simple synthesis, easy modification (functionalisation) and unique properties [1, 2]. It is well known that calixarene derivatives containing oxygen donor groups, acid, ester or keto, linked at the phenolic oxygen at the narrow rim, exhibit excellent properties as neutral receptors for metallic ions [3-16]. Many recent works have been focussed on the utilisation of calixarene derivatives as prospective ionophores for ion selective electrodes, optical sensors or colorimetric reagents for use in the determination of clinically important species [17].

Our earlier findings on the synthesis of calix[n]arene for sequestration of rare earth and precious ions revealed that derivatives having three 2-butenyl (crotyl) groups at the narrow rim show good extraction ability for europium and palladium ions [18]. Good results we also obtained with organo-phosphorus and/or crotyl functionalised calix[6]arene [19,20].

Aiming to develop new ionophores or cation extraction reagents based on calixarene derivatives, a variable number of oxygen donor groups e.g. ester groups was grafted on the parent *p-tert*-butyl calix[6,8]arenes.

[a] *Raluca Ripan Institute for Research in Chemistry, Babes Bolyai University, 400294, Cluj-Napoca, Romania, salina@chem.ubbcluj.ro*

[b] *Faculty of Chemistry and Chemical Engineering, Babes-Bolyai University, 40084, Cluj-Napoca, Romania.*

Due to the presence of the *p*-electrons of the ester groups, these derivatives are of practical interest for rare earth and precious metal sequestration.

Herein we present our study referring to the synthesis and characterization of new derivatives of *p-tert*-butyl calix[6]arene and *p-tert*-butyl calix[8]arene with two and four, as well as, four and six (ethoxycarbonyl)methoxy groups. We previously reported the synthesis of some other ester derivatives [25-27] in this class of compounds.

RESULTS AND DISCUSSION

The chemistry we followed is shown in scheme 1 (depicted).

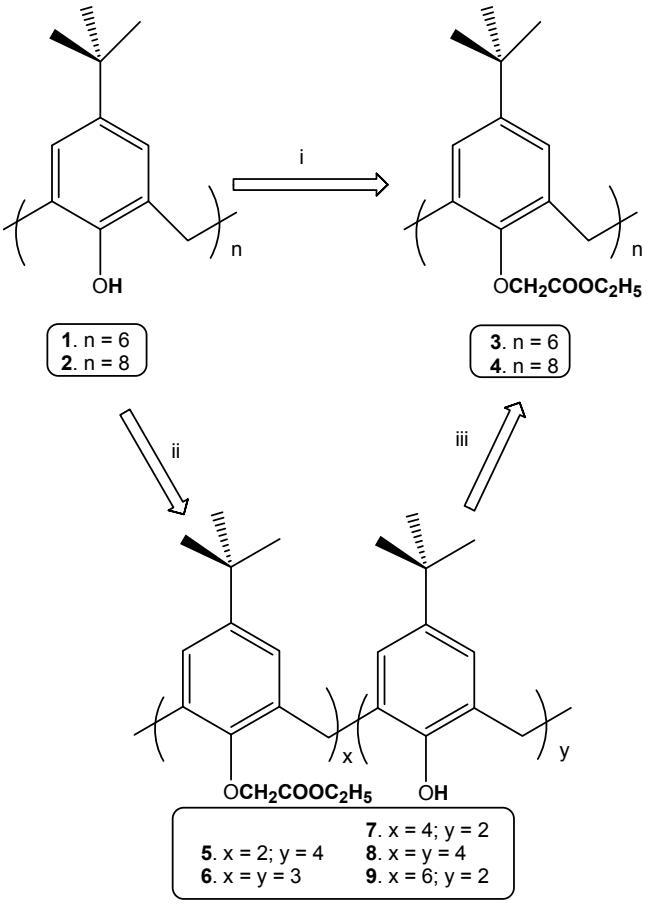

Scheme 1

Thus, the parent calix[n]arenes were O-alkylated with ethyl bromoacetate in alkaline conditions in order to prepare derivatives with two-to-eight [(ethoxycarbonyl)methoxy] groups grafted at the narrow rim.

Reaction of *p-tert*-butyl calix[n]arene (**1-2**) in the presence of K_2CO_3 or NaH as a base, with the required amount of ethyl bromoacetate in organic solvents or mixture of them, yielded calix[n]arene ester derivatives with two (**5**), three (**6**), tetra (**7,8**), hexa (**3,9**) and octa (**4**) ester groups respectively.

UV-Vis, FTIR and ^{1}H-NMR investigations confirmed the formation of the desired O-functionalised calix[n]arene.

^{1}H-NMR spectra

The ^{1}H-NMR spectra of calixarene contain several broad bands which are characteristic for the conformational flexibility of calix[6]- and calix[8]arene derivatives. Indeed, the ^{1}H-NMR spectra showed the expected differences between the chemical shifts of the parent calixarene and their derivatives. The position of the singlet belonging to the phenolic OH groups varies with the ring size of the calixarene. Thus the chemical shifts of OH groups appeared at 10.55 ppm for compound **1**, and 9.86 ppm for compound **2**, whereas calixarene derivatives **5** and **7-9** showed the chemical shifts at: 7.11 (**5**), 7.11 (**7**), 7.10 (**8**) and 7.06 (**9**) ppm.

Table 1 collects the relevant ^{1}H-NMR data of calixarene derivatives.

Table 1. Selected ^{1}H-NMR data of compounds **5,7-9** in comparison with the parent calixarenes **1, 2**

	$C(CH_3)_3$	$O\text{-}CH_2\text{-}CH_3$	$O\text{-}CH_2\text{-}CH_3$	$ArCH_2Ar$	$O\text{-}CH_2\text{-}CO$	ArH	ArOH
1	1.27,s	-	-	3.78,bs	-	7.16,s	10.55,s
2	1.26,s	-	-	3.53,d; 4.39,d	-	7.17,s	9.86,s
5	0.87,s; 1.19,s	1.24,t	4.06-4.20,m	3.48,bs	4.49,s	6.99,s; 7.04,s	7.11,s
7	1.15,s; 1.20,s	1.17,t	4.06 – 4.12,m		4.47,s	6.84,s; 6.90,s	7.11,s
8	0.93s; 1.04,s	1.02,t	3.64 – 4.07,m			6.83,s; 6.87,s	7.10,s
9	1.02,s; 1.18,s	0.94,t	3.93 – 4.37,m		4.61,s	6.83,s; 6.86,s	7.06, s

FTIR spectra

FTIR spectra of the parent calixarene showed the stretching vibration of the phenol group at 3149 (**1**) and 3244 (**2**) cm^{-1}, respectively, in agreement with literature data [2]. By functionalisation at the narrow rim, the strong circular hydrogen bonding was supressed and derivatives **5-9** show the OH vibrations to be shifted at 3423 (**5**), 3448 (**7**), 3448 (**8**) 3438 (**9**) cm^{-1}, close to the OH stretching in isolated phenolic OH.

The stretching vibration arising from carbonyl group were observed as two strong bands at 1762, 1740 (**5**), 1759, 1735 (**7**), 1759, 1730 (**8**), and 1760, 1738 (**9**) cm^{-1}, respectively. The presence of two $\nu_{C=O}$ bands in the IR spectra suggests that two different carbonyl groups exist in these calixarene under different environments [28].

A relevant example is shown in Figure 1.

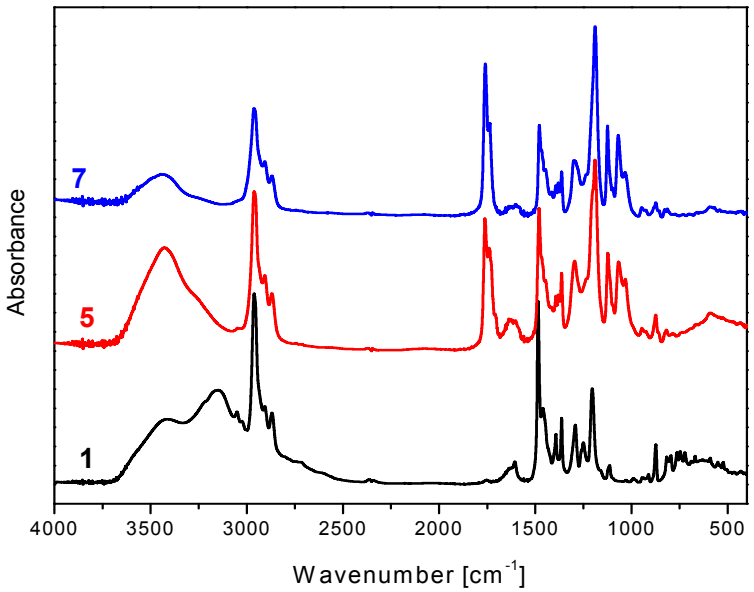

Figure 1. FTIR spectra of compounds **1** (parent calix[6]arene), **5** (diester derivative) and **7** (tetraester derivative)

UV-VIS spectra

The functionalisation of parent calixarene **1, 2** induced significant changes in the UV-Vis absorption spectra allowing pertinent analysis of the resulting ester derivatives (Figure 2). absorption maxima at about 280 and 288 nm in the UV region. The

According to literature [2], such cyclic oligomers have a pair of absorption ratio of these two maxima is a function of the ring size.

The starting calixarene revealed the specific absorption bands at 280, 288 (**1**), and 283, 291 (**2**) nm, respectively. In parallel with the increase of the number of phenolic rings, the shift of the maxima toward longer wavelengths as well as the rise of the band ratios were noticed.

The specific UV absorptions of our O-functionalised calixarene appeared at 278, 286 (sh) (**5**), 273, 279 (**7**), 273, 278, 289 (sh) (**8**) and 270, 278 (**9**). For comparison, the complete O-alkylation of calix[8]arenes (**4**) is also presented, showing the specific absorption bands at 271 and 279 nm, respectively.

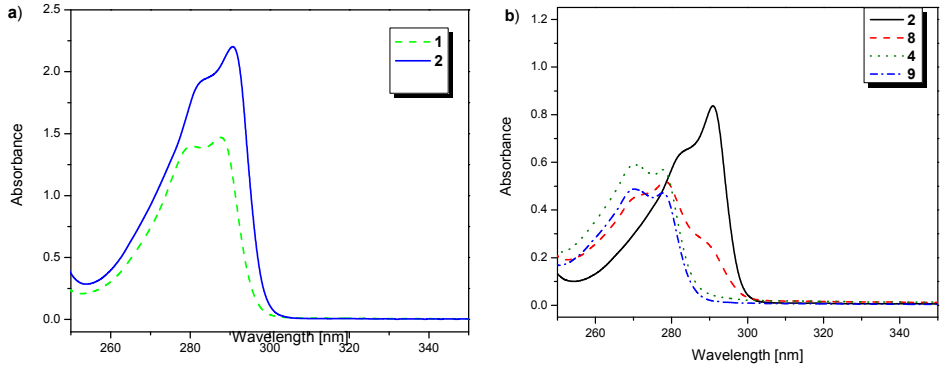

Figure 2. UV-vis absorption spectra of *p-tert*-butyl calix[n]arene and their derivatives ($CHCl_3$ solution;$1x10^{-4}$M): a) **1** (calix[6]arenes), **2** (calix[8]arenes); b) **4** (octaester derivative), **8**(tetraester derivative), **9** (hexaester derivative) and **2**(calix[8]arenes; $0.322x10^{-4}$M).

One note that the ester functionalisation brings about a new absorption band at shorter wavelength that increases in intensity with the number of grafted ester groups. The decrease of the absorption energy with the increasing of number of phenolic rings is also evident.

The ester calix[n]arene derivatives were tested as extracting reagent for precious metal and rare earth ions. Extraction was performed at pH= 2-3, from $1x10^{-3}$ M aqueous solution of $PdCl_2/Eu(NO_3)_3$, using $1x10^{-3}$ M solution of calixarene in $CHCl_3$. Relative high ability for the sequestration of divalent palladium was found, especially, for half substituted calix[6]arene or calix[8]arene. For instance, the extraction yield was ~53% for compound **6** and ~35% for compound **3**. The extraction capability for trivalent europium ions was low for all the ester calix[n]arene derivatives.

CONCLUSIONS

Calix[n]arene [n=6,8] derivatives comprising bi-, tetra-, hexa- and octa (ethoxycarbonyl)methoxy groups were obtained by O-alkylation of calix[n]arene with variable amounts of ethyl bromoacetate. Their structure was confirmed by spectroscopic investigations (UV-Vis, FTIR, ^{1}H-NMR).

Ester calix[n]arene derivatives with variable number of oxygen donor groups e.g. ester linked at the narrow rim, showed ability for the extraction of precious metal ions e.g. palladium from aqueous medium.

EXPERIMENTAL SECTION

All reactions were performed under nitrogen atmosphere using oven-dried glassware. Reagents were purchased from commercial suppliers and were used without further purification. All solvents were dried over standard

drying agents and distilled prior to use. Reactions were monitored by TLC on Kiselgell 60 F_{254} plates with detection by UV or Iodine.

Melting points were determined with POINT METER KSP II apparatus in a sealed capillary and are uncorrected values. ^{1}H-NMR spectra were recorded on VARIAN GEMINI 300 S (300 MHz) spectrometer. Deuterated chloroform was used as solvent and TMS as references. IR spectra were recorded on FTIR (JASCO) 610 and UV-Vis spectra on UNICAM UV 4 spectrometers. Elemental analysis (E.A.) was performed with a Vario EL analyser.

The starting calixarenes **1** and **2** were synthesised according to literature [21-23].

Reaction of *p-tert*-butyl calix[n]arene **1** or **2** with the required amount of ethyl bromoacetate was performed in the presence of K_2CO_3 or NaH as a base, using THF/DMF or acetone as solvent (Scheme 1). *p-tert-* butyl calix[n]arene derivatives containing two (**5**), three (**6**), tetra (**7, 8**), hexa (**3, 9**) and octa (**4**) ester groups were isolated and recrystallised from dichloromethane-ethanol mixture. The synthesis of compounds **3** and **4** [24] and **6** [25] was carried out according to literature.

The preparation yield was 81%(**3**), 61%(**4**), 62%(**5**), 38%(**6**), 72%(**7**), 71%(**8**) and 49%(**9**).

The main characteristics of the new synthesised calixarenes derivatives are presented bellow. For the 1H chemical shifts, see Table 1.

5,11,17,23,29,35-hexa-*tert*-butyl-bis[(ethoxycarbonyl)methoxy]-tetrahydroxy-calix[6]arene (5)
M.p.=221°C
M.W. calcd. for $C_{74}H_{96}O_{10}$=1144
E.A: Calcd: C=77.59; H=8.45 ; *Found:* C=77.90; H=8.21
UV-Vis: [$CHCl_3$; λ_{max} (nm)/ε($M^{-1}cm^{-1}$)]=278/6373; 286/5000
FTIR: ($\nu_{max.}$, KBr, cm^{-1}): $\nu_{C=O}$=1740, 1762; ν_{OH}=3423

5,11,17,23,29,35-hexa-*tert*-butyl-tetrakis[(ethoxycarbonyl)methoxy]-dihydroxy-calix[6]arene (7)
M.p.=261°C
M.W. calcd. for $C_{82}H_{108}O_{14}$=1316
E.A.: Calcd: C=74.74; H=8.26 ; *Found:* C=74.90; H=8.21
UV-Vis: [$CHCl_3$; λ_{max} (nm)/ε($M^{-1}cm^{-1}$)]=273/5880; 279/5697
FTIR: ($\nu_{max.}$, KBr, cm^{-1}): $\nu_{C=O}$=1759, 1735; ν_{OH}=3448

5,11,17,23,29,35,41,47-octa-*tert*-butyl -tetrakis-((ethoxycarbonyl)methoxy)- tetrahydroxy-calix[8]arene (8)
M.p.=195°C
M.W. calcd. for: $C_{104}H_{136}O_{16}$=1640
E.A.: Calcd: C=76.06; H=8.35; *Found:* C=74.90; H=8.21
UV-Vis: [$CHCl_3$; λ_{max} (nm)/ε($M^{-1}cm^{-1}$)]=273/4680; 278/5210;289(sh)/2670
FTIR: ($\nu_{max.}$, KBr, cm^{-1}): $\nu_{C=O}$=1759, 1730; ν_{OH}=3448

5,11,17,23,29,35,41,47-octa- *tert*-**butyl -hexakis-((ethoxycarbonyl)methoxy)- dihydroxy-calix[8]arene (9)**
M.p.=216°C
M.W. calcd for: $C_{112}H_{148}O_{20}$=1812
E.A. Calcd: C=74.14; H=8,22; *Found:* C=74.60; H=8.45
UV-Vis: [$CHCl_3$; λ_{max} (nm)/ε($M^{-1}cm^{-1}$)]=270/4900; 278/4760
FTIR: ($\nu_{max.}$, KBr, cm^{-1}): $\nu_{C=O}$=1760, 1738; ν_{OH}=3438

ACKNOWLEDGEMENTS

The financial support of the Romanian Ministry of Education and Innovation under the project PNII-71-062 is gratefully appreciated.

REFERENCES

1. Z. Asfari, V. Bohmer, J. Harrowfield, J. Vicens, “Calixarenes 2001”, Kluwer, Dordrecht, **2001**.
2. C.D. Gutsche, “Calixarene revisited”, J.F. Stoddart Ed., J.F. Royal Society of Chemistry, London, **1998**.
3. A. Arduini, G. Giorgi, A. Pochini, A. Secchi, F. Ugozzoli, *Tetrahedron*, **2001**, *57*, 2411.
4. N.J. Wolf, E.M. Georgiev, A.T. Yordanov, B.R. Whittlesey, H.F. Koch, D.M. Roundhill, *Polyhedron*, **2002**, *21*, 763.
5. M. Bochenska, R. Banach, A. Zielinska, V.C. Kravtsov, *J. Incl. Phenom. Makromol. Chem*, **2001**, *39*, 219.
6. H. Halouani, I. Dumazet-Bonnamour, C. Duchamp, C. Bavoux, N. Ehlinger, M. Perrin, R. Lamartine, *Eur.J. Org. Chem.*, **2002**, 4202.
7. A. Casnati, L. Baldini, N. Pelizzi, K. Rissanen, F. Ugozzoli, R. Ungaro, *J. Chem. Soc. Dalton Tr.*, **2000**, 3411.
8. A. Casnati, S. Barboso, H. Rouqueette, M. J. Schwing-Weill, F. Arnaud-Neu, J.F. Dozol, R. Ungaro, *J. Am. Chem. Soc.*, **2001**, *123*, 12182.
9. A. Moser, G.P.A. Yap, C. Detllier, *J. Chem. Soc. Dalton Tr.*, **2002**, 428.
10. P.D. Beer, M.G.B. Drew, M.I. Ogden, *J. Chem. Soc. Dalton Tr.*,**1997**, *11*, 1489.
11. P.D. Beer, M.G.B. Drew, P.B. Leeson, M.I. Ogden, *Inorg. Chim. Acta*, **1996**, *246*, 133.
12. P.D. Beer, M.G.B. Drew, M.Kan, P.B. Leeson, M.I. Ogden, G. Williams, *Inorg. Chim. Acta*, **1996**, *35*, 2202.
13. P.D. Beer, M.G.B. Drew, A. Grieve, M.I. Ogden, *J. Chem. Soc. Dalton Tr.*, **1995**, 3455.

14. P.D. Beer, M.G.B. Drew, P.B. Leeson, M.I.Ogden, *J. Chem. Soc. Dalton Tr.*, **1995**, 1273.
15. F. Arnaud-Neu, G. Barrett, D. Corry, S. Cremin, G. Ferguson, J.F. Gallagher, S.J. Harris, M.A. McKervey, M.J. Schwing-Weil, *J. Chem. Soc. Perkin Tr. 2*, **1997**, 575.
16. M.I. Ogden, B.W. Skelton, A.H. White, *J. Chem. Soc. Dalton Tr.*, **2001**, 3073.
17. B.T.T. Lan, K. Toth, *Analytical Sciences*, **1998**, *14*, 191.
18. T. Ursales, I. Silaghi-Dumitrescu, R. Ciocan, N. Palibroda, N. Popovici, E.J. Popovici, *Rev. Roum. Chim.*, **2004**, *49*, 741.
19. T. Ursales, I. Silaghi-Dumitrescu, E.J. Popovici, A. Ursales, N. Popovici, *J. Optoelectron. Adv. Mater.*, **2004**, *6(1)*, 307.
20. T. Ursales, I. Silaghi-Dumitrescu, E.J. Popovici, A. Ursales, N. Popovici, *Studia Universitatis Babes-Bolyai, Physica*, **2003**, XLVII(*2)*, 370.
21. C.D. Gutsche, M. Iqbal, *Org. Synthesis*, **1989**, *68*, 234.
22. C.D. Gutsche, B. Dhawan, M. Leonis, D. Stewart, *Org. Synthesis*, **1989**, *68,* 238.
23. J.H. Munch, C.D. Gutsche, *Org. Synthesis*, **1989**, *68*, 243.
24. G. McMahon, R. Wall, K. Nolan, D. Diamond, *Talanta*, **2002**, *57*, 1119.
25. N. Popovici, E.J. Popovici, M. Ladar, R. Grecu, *Studia Universitatis Babes-Bolyai, Physica*, **2005**, *L(4b)*, 650.
26. A. Saponar, I. Silaghi-Dumitrescu, E.J. Popovici, N. Popovici, *Studia Universitatis Babes-Bolyai, Chimia*, **2007**, *LII(4)*, 67.
27. A. Saponar, I. Silaghi-Dumitrescu, E.J. Popovici, N. Popovici, *Rev. Chim.*, **2007**, *58(5)*, 481.
28. P. Leyton, C. Domingo, S. Sanchez-Cortes, M. Campos-Valette, J.V. Garcia-Ramos, *Langmuir,* **2005**, *21(25)*, 11814.

MORE DETAILS CONCERNING THE USE OF THE THOMSON RADIAL FREQUENCIES $\omega_{Th,s}$, $\omega_{Th,p}$ (OF THE SERIES, RESPECTIVE PARALLEL, CIRCUITS, CONSIDERED INSTEAD OF THE WARBURG PSEUDO CAPACITANCE C_W), AS CRITERIA OF CLASSIFYING THE DRUGS

NICOLAE BONCIOCAT[a] AND ADINA COTARTA[a]

ABSTRACT. In a very recent communication we have shown that the EIS method may be used for classifying the drugs. More precisely it has been shown that to explain the phase difference between the current and the tension it is necessary to use instead of the Warburg pseudo-capacitance $C_W(\omega_1)$, two physically quantities, namely: a pseudo-inductance $L_W(\omega_1)$ and a pseudo-capacitance $C_W(\omega_1)$, which may be arranged in series or in parallel. Consequently, two criteria of classifying the drugs have resulted: for the series arrangement the Thomson radial frequency $\omega_{Th,s} = [L_s(\omega_1)C_s(\omega_1)]^{-1/2}$, respective for the parallel arrangement, the Thomson radial frequency $\omega_{Th,p} = [L_p(\omega_1)C_p(\omega_1)]^{-1/2}$. As for ω_1 it represents the lowest radial frequency used in getting the Nyquist plots(e.g., 1.256 s^{-1}) and has a very important physical meaning: it represents the resonance Thomson radial frequency of both series or parallel circuits, and expresses the highest efficiency that a drug may have, irrespective of the fact that it belongs to the class characterized by the criterion $\omega_{Th,s}(\omega_1)$ or by the criterion $\omega_{Th,p}(\omega_1)$. At the resonance Thomson radial frequency, ω_1 the electric energy of the drug, transforms in its magnetic energy and back in its electric energy and this oscillation between electric and magnetic energies occur permanently with a maximum amplitude. This explains why at the resonance radial Thomson frequency $\omega_{Th,s} = \omega_{Th,p} = \omega_1$ the efficiency of drug is maximum.

Keywords: multielectrode, Thomson radial frequencies, drugs classification

INTRODUCTION

In a series of papers, Bonciocat et al., have shown that the faradaic current density of an electrode redox reaction occuring with combined limitations of charge transfer and nonstationary, linear, semiinfinite diffusion is the solution

[a] *University Politehnica of Bucharest, Department of Applied Physical Chemistry and Electrochemistry, Computer Aided Electrochemistry Laboratory UPB-LEAC, Bucharest, Romania, PO BOX 12-112, e-mail: adina@cael.pub.ro*

of an integral equation of Volterra type[1-6]. By solving this integral equation, new methods of direct and cyclic voltammetry have been developed [7-15]. The above mentioned equation has led to a new approach to the Electrochemical Impedance Spectroscopy (EIS) when only the charge transfer and diffusion limitations are present. Very recently has been shown that the E I S method may have important applications in drug research[16-19].

In this paper, one analysis more deeply the physical meaning of this *resonance* Thomson radial frequency, and how it is related to the *normal* Thomson radial frequencies $\omega_{Th,s}$, respective $\omega_{Th,p}$. Two formulae have resulted, expressing the quantities $\omega_1^2 / \omega_{Th,s}^2$, respective $\omega_{Th,p}^2 / \left(\omega_{Th,p}^2 - \omega_1^2\right)$, in terms of the contributions that a drug may have upon the processes occurring at the electrode/ solution interface. Thus, it may introduce new electrode reactions, or it may change the *Warburg diffusion resistance*, if the drug adsorbs at the electrode/ solution interface, and, in this way, the surface of the electrode changes from A to ${}_iA^*$, or ${}_iA^{**}$. Of course, the drug may introduce new ionic species in the RRD solution, but, because the concentrations of these species are very small in comparison with those of $[Fe(CN_6)]^{3-}$, $[Fe(CN_6)]^{4-}$ the effect of these new ionic species may be neglected. Consequently, taking into account only the two effects that a drug may have, i.e., the change of both, charge transfer and Warburg diffusion resistances, Bonciocat and Adina Cotarta have proposed the following expressions for the two quotients $\omega_1^2 / [\omega_{Th,s}^2]_0$, respective : $[\omega_{Th,p}^2]_0 / [\omega_{Th,p}^2]_0 - \omega_1^2$:

$$J^* = \frac{\omega_1^2}{\left[\omega_{Th,s}\right]_0^2} = \frac{\left(A_{ct}\right)_{RRD} - \left({}_iA_{ct}^*\right)_{(ME)_{Di}^*}}{\left[R_W(\omega_1)\right]_{RRD} \cdot \left(\frac{A}{{}_iA^*}\right)} \qquad (1*)$$

respective:

$$J^{**} = \frac{\left[\omega_{Th,p}\right]_0^2}{\left[\omega_{Th,p}\right]_0^2 - \omega_1^2} = \frac{\left(A_{ct}\right)_{RRD} - \left({}_iA_{ct}^{**}\right)_{(ME)_{Di}^{**}}}{\left[R_W(\omega_1)\right]_{RRD} \cdot \left(\frac{A}{{}_iA^{**}}\right)} \qquad (1**)$$

where the Thomson radial frequencies $[\omega_{Th,s}]_0$ and $[\omega_{Th,p}]_0$ have the meanings:

$$\left[\omega_{Th,s}\right]_0 = \left\{\omega_{Th,s}\left[\alpha_D^*(\omega_1)\right]\right\}_{\eta(0)=0} = \frac{\omega_1}{\sqrt{1-\alpha_D^*(\omega_1)}}$$

$$\left[\omega_{Th,p}\right]_0 = \left\{\omega_{Th,p}\left[\alpha_D^{**}(\omega_1)\right]\right\}_{\eta(0)=0} = \omega_1\sqrt{1-\alpha_D^{**}(\omega_1)} \qquad (2*)$$

and:

$$0 \le \alpha_D^{*}(\omega_1) \le 1; \qquad 0 \le \alpha_D^{**}(\omega_1) \le 1 \qquad (3*)$$

In this paper one shows that J^* and J^{**} represent two criteria very useful for a better and more correct classification of the drugs which belong to the classes (I^*), respective (I^{**}).

THEORETICAL SECTION

Introduction

The quotients (1^*) and (1^{**}) permit to consider the following situations:

A) $D_i \in$ (I), i.e., has no effect. Then:

$$\frac{\omega_1^2}{\left[\omega_{Th,s}\right]_0^2} = \frac{\left[\omega_{Th,p}\right]_0^2}{\left[\omega_{Th,p}\right]_0^2 - \omega_1^2} = 0 \qquad (4*)=(4**)$$

which means:

either $\left[\omega_{Th,s}\right]_0 = \left\{\omega_{Th,s}[\alpha_{D_i}^{*}(\omega_1)=1]\right\}_{\eta(0)=0} = \infty$

or $\left[\omega_{Th,p}\right]_0 = \left\{\omega_{Th,p}[\alpha_D^{**}(\omega_1)=1]\right\}_0 = 0 \qquad (5*)=(5**)$

B) $D_i \in$ (I^*) and has effect if:

$$J^* = \frac{\omega_1}{\left[\omega_{Th,s}\right]_0} = \frac{\omega_1}{\left\{\omega_{Th,s}\left[1 \rangle \alpha_D^{*}(\omega_1) \rangle 0\right]\right\}_0}$$ = finite and positive value less than 1, and:

$D_i \in$ (I*) has a maximum effect if:

$$J^* = \frac{\omega_1}{[\omega_{Th,s}]} = \frac{\omega_1}{\left\{\omega_{Th,s}\left[\alpha_D^{*}(\omega_1)=0\right]\right\}_0} = 1 \qquad (6*)$$

C) $D_i \in$ (I^{**}) and has effect if:

$$J^{**} = \frac{\left[\omega_{Th,p}\right]_0^2}{\left[\omega_{Th,p}\right]_0^2 - \omega_1^2} = \frac{\left\{\omega_{Th,p}[1 \rangle \alpha_D^{**}(\omega_1) \rangle 0]\right\}_0^2}{\left\{\omega_{Th,p}[1 \rangle \alpha_D^{**}(\omega_1) \rangle 0\right\}_0^2 - \omega_1^2}$$ =finite and negative value $(7*)$

and

$D_i \in (I^{**})$ has a maximum effect, if :

$$J^{**} = \frac{\left[\omega_{Th,p}\right]_0^2}{\left[\omega_{Th,p}\right]_0^2 - \omega_1^2} = \frac{\left\{\omega_{Th,p}\left[\alpha_D^{**}(\omega_1) = 0\right]\right\}_0^2}{\left\{\omega_{Th,p}\left[\alpha_D^{**}(\omega_1) = 0\right]\right\}_0^2 - \omega_1^2} \rightarrow - \infty \qquad (8^{**})$$

Therefore, from (5*) and (6*), respective (7*) and (8**), it follows:

$$0 \leq J^{*} \leq 1 \qquad (9*)$$

respective:

$$-\infty \leq J^{**} \leq 0 \qquad (9**)$$

Anti -oxidizer and Pro -oxidizer drugs

The inequalities (9∗) and (9∗∗) show that the pair (J^* , J^{**}) satisfies the necessary conditions for being a pair of criteria of classifying the drugs, because the values of J^* are greater than zero, while those of J^{**} are less than *zero.* The class of drugs characterized by the criterion J^{**} will be a sub-class of the class (I^{**}), while the class of drugs characterized by the criterion J^*, will be a sub-class of the class (I^*).

We shall write these two subclasses by $\left(J_{A.O}^{**}\right)$, respective $\left(J_{P.O}^{*}\right)$, because, as we shall see further, in these sub-classes enter the *anti-oxidant* drugs (i.e., A.O-drugs), respective the *pro-oxidant* drugs (i.e., P.O-drugs). Thus, $(J_{A.O}^{**}) \subset (I^{**})$, while $(J_{P.O}^{**}) \subset (I^{*})$.

The most important conclusion concerning the Theoretical Section:

- A drug $D_i \in (I^*)$ is characterized by the radial Thomson frequency $\omega_{Th,s}[\alpha_{D_i}^{*}(\omega_1) = 0]$ and has a maximum effect if his radial Thomson frequency is equal to the *resonance* Thomson frequency

$$res\ \omega_{Th,s}\ [\alpha_{D_i}^{*}(\omega_1) = 0] = \omega_1\ ;$$

- A drug $D_i \in (I^{**})$ is characterized by the radial Thomson frequency $\omega_{Th,p}\,[\alpha_{D_i}^{*}(\omega_1) = 0]$ and has a maximum effect if his radial Thomson frequency ω is equal to *the resonance* Thomson frequency

$$\text{res}\ \omega_{Th,p}\ [\alpha_{D_i}^{**}(\omega_1) = 0] = \omega_1.$$

- An A.O- drug is characterized by the criterion $J_{A.O}^{**}$, and has a maximum effect, if his $J_{A.O}^{**}$ criterion has the value - ∞.

- An P.O –drug is characterized by the criterion $J_{P.O}^{*}$, and has a maximum effect, if his $J_{P.O}^{*}$ criterion has the value 1.

EXPERIMENTAL

In the paper hold at Journees d'Electrochimie 2009, Sinaia (6-10 Jouillet), Roumanie, we have investigated 6 drugs and 2 mixtures of drugs, namely:

B (Sweedish Bitter), Am (Achillea Millefolium), Cf_1 and Cf_2 (Calendula floss), Uh_1 and Uh_2 (Urticae herba), M_1 = Uh + Am, M_2 = B + Am + Cf + Uh[1].

By using eqs.(37') and (37'') [1], where $Re^{**}(\omega_1)$, $Re^{**}(\omega_2)$ represent the abscissa of the first two points of the Nyquist plots(i.e., corresponding to ω_1=1.256s^{-1} and ω_2=1.582s^{-1}) recorded for the drugs and mixtures of drugs investigated, while $Re(\omega_1)$, $Re(\omega_2)$ represent the abscissa of the first two points of the Nyquist plots, recorded for the RRD-dielectrode, it was possible to get the values of the quantities a^{**} and b^{**}[1]. Because the values thus obtained have proved to obey all the inequality $a^{**} \langle b^{**}$, it results that all drugs and mixtures of drugs investigated belong to the class (I^{**}), i.e., in their electrical schemes, the Warburg pseudo-capacitance $C_W(\omega)$ must be replaced by a parallel circuit of a pseudo-inductance $L_W(\omega)$, in parallel with a pseudo-capacitance $C_W(\omega)$. Once the values a^{**} and b^{**} known, the radial Thomson frequency $\left\{\omega_{Th,p}[\alpha_D^{**}(\omega_1)=0]\right\}_0 = [\omega_{Th,p}]_0$, have resulted by means of eq.(37) [1].

In Table 1 is shown, in *details,* the procedure by which have been obtained the values of a^{**} , b^{**} and $[\omega_{Th,p}]_0$ in the case of the drug B.

$$a^{**} = 1.122\,[\mathrm{Re}(\omega_2) - \mathrm{Re}^{**}(\omega_2)]; \qquad b^{**} = \mathrm{Re}(\omega_1) - \mathrm{Re}^{**}(\omega_1)$$

(37') and (37'')[1]

$$\left[\omega_{Th,p}\right]_0 = \left\{\frac{-a^{**}+b^{**}}{1.121\left[\mathrm{Re}^{**}(\omega_1) - \mathrm{Re}^{**}(\omega_2)\right] - a^{**}+b^{**}}\right\}^{1/2} \cdot \omega_1$$

(37)[1]

Further, the procedure exemplified in Table 1, has been used for obtaining the values $[\omega_{Th,p}]_0$, corresponding to all drugs and mixtures of drugs investigated. The results are given in Table 2, where for sake of simplicity, are given the multielectrods containing the respective drugs or mixtures of drugs, and the mean values of $[\omega_{Th,p}]_0$ obtained from 4 experimental values.

Table 1. Example of obtaining the values a^{**} and b^{**} (by means of eqs.(37') and (37")) and of the values of $[\omega_{Th,p}]_0$ (by means of eq.(37))[1]

We mention that $[\omega_{Th,p}]_0$ is the mean value of the 4 values $\left\{\omega_{Th,p}[\alpha_D^{**}(\omega_1)=0]\right\}_0$ obtained by applying eq.(37)[1].

Dielectrode RRD V= 300mL	Re(ω_1) (Ω)	Re(ω_2) (Ω)	
	319 329 318 320	291 291 289 290	

Multi electrode	$\mathrm{Re}^{**}(\omega_1)$ (Ω)	$\mathrm{Re}^{**}(\omega_2)$ (Ω)	a^{**} (Ω)	b^{**} (Ω)	$\left\{\omega_{Th,p}[\alpha_D^{**}(\omega_1)=0]\right\}_0$ (s^{-1})
$(ME)_B$ V=300mL V=20mL	10447 10936 11688 12721	9944 10409 11125 12266	-10830 -10761 -12158 -13370	-10128 -10614 -11370 -12401	0.935 0.561 0.936 0.994

Table 2. The Thomson radial frequencies $[\omega_{Th,p}]_0 = \left\{\omega_{Th,p}[\alpha_D^{**}(\omega_1)=0]\right\}_0$ estimated by using eq.(37)[1]

Multielectrode	$[\omega_{Th,p}]_0$ Mean values	Multielectrode	$[\omega_{Th,p}]_0$ Mean values
$(ME)_B$ V= 300mL v= 20mL	0.857	$(ME)_{Uh}$ V= 300mL v= 20mL	0.949
$(ME)_{Am}$ V= 300mL v= 30mL	0.823	$(ME)_{Uh2}$ V= 300mL v= 30mL	1.002

Multielectrode	$[\omega_{Th,p}]_0$ Mean values	Multielectrode	$[\omega_{Th,p}]_0$ Mean values
$(ME)_{Cf_1}$ V= 300mL v= 20mL	1.067	$(ME)_{Uh+Am}$ V= 300mL v=20mL+20mL	0.898
$(ME)_{Cf_2}$ V= 300mL v= 30mL	0.874	$(ME)_{B+Am+Cf+Uh}$ V= 300mL v=(10+10+10+10)mL	0.954

Because all drugs and mixtures of drugs investigated have proved to belong to the class (I^{**}), it is important to decide if they are AO-drugs, i.e., if they belong to the sub-class $J^{**}_{A.O} \subset \left(I^{**}\right)$.

Therefore it is necessary to estimate the values of the criterion:

$$J^{**} = \frac{[\omega_{Th,p}]_0^2}{[\omega_{Th,p}]_0^2 - \omega_1^2}$$

for these 6 drugs and 2 mixtures of drugs.

The corresponding values are given in Table 3.

As one sees in Table 3, all the values of the criterion J^{**} are negative, and belong to the interval (9^{**}). Consequently, *the most important conclusions of the Experimental Section are:*

- All the drugs and mixtures of drugs investigated, belong to the sub-class ($J^{**}_{A.O} \subset \left(I^{**}\right)$), i.e., are A.O-drugs.
- The drug Cf_1 has the maximum effect, because $J^{**}_{Cf_1}$ = -2.586, i.e., has the most negative value. This means that this drug acts by changing both, the charge transfer resistance and the Warburg diffusion resistance, i.e., this drug *adsorbs significantly* at the electrode/solution interface. This adsorption process explains also why, by increasing the concentration of the drug, i.e., by passing from Cf_1 to Cf_2 the value of $\left|J^{**}_{Cf}\right|$ decreases from +2.586 to +0.939 because the quotient $A/{}_iA^{**}$ increases (see eq.(1^{**})).
- In the case of the drug Uh, by increasing its concentration, the value of $\left|J^{**}_{Uh}\right|$ increases too, from 1.331 to 1.749. This may be explained by the fact that the drug Uh acts *firstly by changing the charge transfer resistance*, which, of course, *increases* if the concentration of drug *increases.*

Table 3. The values of the criterion $J^{**} = [\omega_{Th,p}]_0^2 / \left\{[\omega_{Th,p}]_0^2 - \omega_1^2\right\}$ for the investigated drugs and mixtures of drugs

Drugs and mixtures of drugs	$[\omega_{Th,p}]_0^2$ (s^{-2})	ω_1^2 (s^{-2})	J^{**}
B	0.901	1.578	-1.331
Am	0.677	1.578	-0.751
Cf_1	1.138	1.578	-2.586
Cf_2	0.764	1.578	-0.939
Uh_1	0.901	1.578	-1.331
Uh_2	1.004	1.578	-1.749
Uh+Am	0.806	1.578	-1.044
B+Am+Cf+Uh	0.910	1.578	-0.247

This two effects (i.e., changing of the charge transfer resistance and of the Warburg diffusion resistance may compensate each other, and this may explain why the values $\left|J^{**}\right|$ corresponding to the two mixtures of drugs investigated are not far away from the values $\left|J^{**}\right|$ corresponding to their individual components.

It remains to explain how an A.O-drug acts. Let's start by remembering the reactions of the RRD-dielectrode. They are:

$$\frac{1}{4}O_2 + H^+ + e \rightarrow \frac{1}{2}H_2O \text{ cathodic reaction}$$

$$[Fe(CN)_6]^{4-} \rightarrow [Fe(CN)_6]^{3-} + e \text{ anodic reaction}$$

The electrons resulted by the oxydation of $[Fe(CN)_6]^{4-}$ are consumed by the reduction of the physically dissolved oxygen and H^+-ions (i.e., $\frac{1}{4}O_2 + H^+$) to $\frac{1}{2}H_2O$.

Therefore, $\frac{1}{4}O_2 + H^+$ acts as an *oxidizer* of $[Fe(CN)_6]^{4-}$. It thus results that an A.O- drug **reduces** the oxidating effect of $\frac{1}{4}O_2 + H^+$, *by consuming a part, or all electrons resulted by the oxidation* of $[Fe(CN)_6]^{4-}$ to $[Fe(CN)_6]^{3-}$.

This consuming of electrons may take place, either by a *chemical* reaction in solution, e.g.,

$$(A.O-D)_{\mathrm{Re}d}+\frac{1}{4}O_2+H^+\rightarrow(A.O-D)_{Ox}+\frac{1}{2}H_2o$$

when the A.O-drug (see A.O-D) passes from its reduce form, to its oxidize form, when at the electrode / solution interface, occur three electrode reactions, e.g.,

$$\frac{1}{4}O_2+H^+ + e\rightarrow\frac{1}{2}H_2O$$
$$[Fe(CN)_6]^{4-}\rightarrow[Fe(CN)_6]^{3-}+e$$
$$[A.O-D]_{\mathrm{Re}d}\rightarrow[A.O-D]_{Ox}+e$$

In both ways of action, the important effect of the A.O - D is the reduction of the intensity of the *important oxydation reaction.*

If this important *oxidation* is a biological reaction, responsible for a very dangerous illness, the A.O-drugs may have *very important therapeutic applications*, in fighting against this dangerous illness.

As for the P.O-drugs, there are two ways in which they may act.

A first possibility is to act chemically, i.e., by a reaction in solution, e.g.,

$$(A.O-D)_{Ox}+\frac{1}{2}H_2O\rightarrow(A.O-D)_{\mathrm{Re}d}+\frac{1}{4}O_2+H^+$$

increasing the concentration of the $\frac{1}{4}O_2+H^+$ and in this way *increasing* the intensity of the oxidation reaction:

$$[Fe(CN)_6]^{4-}\rightarrow[Fe(CN)_6]^{3-}+e$$

or electro-chemically when at the electrode / solution interface, occur the reactions:

$$\frac{1}{4}O_2+H^+ + e\rightarrow\frac{1}{2}H_2O$$
$$[Fe(CN)_6]^{4-}\rightarrow[Fe(CN)_6]^{3-}+e$$
$$[P.O-D]_{\mathrm{Re}d}\rightarrow[P.O-D]_{Ox}+e$$

when, a part of the electrons necessary to the first cathodic reaction come from the de-electronation (i.e., oxydation) of the P.O-D- drug.

In both ways of action, the important effect of a P.O.-drug is the *increase* of the intensity of the important oxydation reaction.

CONCLUSIONS

Because the efficiency of an A.O-drug increases if the value of $\left| J^{**} \right|$ increases, it results the following sequence concerning the efficiencies of the 6 drugs and 2 mixtures of drugs (all A.O-drugs) investigated:

$$\left| J^{**}_{Am} \right| \langle \left| J^{**}_{B} \right| \langle \left| J^{*\cdot *}_{C\, f_2} \right| \langle \left| J^{**}_{Uh+Am} \right| \langle \left| J^{**}_{Uh_1} \right| \langle \left| J^{**}_{B+Am+Cf+Uh} \right| \langle \left| J^{**}_{Uh_2} \right| \langle \left| J^{**}_{Cf_1} \right|$$

Finally, it is very important to underline that, presently, are known many oxidation reactions, occurring in biological systems, about which one supposes that are at the origin of many illnesses, and for this reason, the development of experimental methods for estimating the therapeutic efficiencies of the A.O.-drugs represents the most important aim of the future researchers in the domain of biological and pharmaceutical sciences.

From this point of view, one may conclude that the two EIS methods presented at Journees d'Electrochimie 2009 and RICCCE 2009, have the necessary conditions for playing a very important role for a *scientific classification of drugs*, produced by the *chemical industry*, or taken from the **God pharmacy** [i.e., by an *adequate transforming of the medicinal plants*].

Unfortunately, such an action necessitates about 4-5 years, and a team of researchers in which must enter: electrochemists, biochemists, physicist and specialists in medicinal plants. Although such an action implies so many difficulties, it must be done, because the results that will be obtained, will justify the efforts, and what it is much more important, will decide the directions in which the future developments of the medical sciences in Romania must be made. This also explains the importance of the criteria $[\omega_{Th,s}]$, $[\omega_{Th,p}]_0$, respective $J^{*}_{P.O}$, $J^{**}_{A.O}$, for the future development of drug-sciences not only in Romania, but also in the world.

REFERENCES

1. N. Bonciocat, A. Cotarta, *Journees d'Electrochimie 6-10 Jouillet 2009, Sinaia, Romania,* Communication Orale 3-O-13, *Studia Universitatis Babes-Bolyai*, *Seria Chemia*, **2009**, in press
2. Adina Cotarta, Ph.D Thesis, Chemical Research Institute, Bucharest, **1992**
3. N. Bonciocat, *Electrokhimiya*, **1993**, *29*, 97.
4. N. Bonciocat, *Electrochimie si Aplicatii*, Dacia Europa - Nova, Timisoara, **1996**, chapter 5, 262.
5. N. Bonciocat and A. Cotarta, *Revue Roumaine de Chimie*, **1998**, *43*, 925.

6. N. Bonciocat, "*Alternativa Fredholm in Electrochimie*", Editura Mediamira, Cluj-Napoca, **2005**, chapter 2.
7. N. Bonciocat, *Electrochimie si Aplicatii*, Dacia Europa-Nova, Timisoara, **1996**, chapter 6, 268-277; 283.
8. I.O. Marian, E. Papadopol, S. Borca and N. Bonciocat*, Studia Universitatis Babes-Bolyai, Cluj Napoca, Ser. Chemia*, **1998**, *43*, 91.
9. N. Bonciocat, Scientific Bulletin Chemistry, Series Politechnica University Timisoara, **1998**, *43 (57*), 5.
10. N. Bonciocat, "*Alternativa Fredholm in Electrochimie*", Editura Mediamira, Cluj-Napoca, vol.I, **2005**, chapter 5.
11. N. Bonciocat, E. Papadopol, S. Borca and I.O. Marian, *Revue Roumaine de Chimie*, **2000**, *45*, 981.
12. I.O. Marian, R. Sandulescu and N. Bonciocat, *Journal of Pharmaceutical and Biomedical Anal*ysis, **2000**, *23*, 227.
13. I.O. Marian, N. Bonciocat, R. Sandulescu and C. Filip, *Journal of Pharmaceutical and Biomedical Anal*ysis, **2001**, *24*, 1175.
14. N. Bonciocat, A. Cotarta, J. Bouteillon and J.C. Poignet, *Journal of High Temperature Material Processes*, **2002**, *6*, 283.
15. N. Bonciocat, I.O. Marian, R. Sandulescu, C. Filip and S. Lotrean, *Journal of Pharmaceutical and Biomedical Analysis*, **2003**, *32*, 1093.
16. N. Bonciocat and A. Cotarta, Annals of West University of Timisoara, Series Chemistry, **2006**, *15*(2), 137.
17. N. Bonciocat and A. Cotarta, *Scientific Bulletin Chemistry Series Politehnica University Timisoara*, **2007***, 52*(66), 1-2, 90.
18. N. Bonciocat, *Studia Universitatis Babes-Bolyai, Cluj Napoca, Seria Chemia, LIII*, 1, **2008**, 31.
19. N. Bonciocat, A. Cotarta, *Scientific Bulletin Chemistry Series Politehnica University Timisoara,* **2009**, in press.

HYPERVALENT TETRA- AND TRIORGANOLEAD(IV) COMPOUNDS CONTAINING 2-(R_2NCH_2)C_6H_4 GROUPS (R = Me, Et)

ADINA CRISTEA[a], ANCA SILVESTRU[a], CRISTIAN SILVESTRU[a]

ABSTRACT. Reaction of [2-(R_2NCH_2)C_6H_4]Li with R'_3PbCl or Ph_2PbCl_2, in 1:1 molar ratio, gave the new organolead(IV) compounds [2-(R_2NCH_2)C_6H_4]R'_3Pb [R = Me, R' = Me (**1**), Ph (**2**); R = Et, R' = Ph (**3**)] and [2-(Me_2NCH_2)C_6H_4]Ph_2PbCl (**4**). Treatment of [2-(R_2NCH_2)C_6H_4]Ph_3Pb with iodine resulted in isolation of [2-(R_2NCH_2)C_6H_4]Ph_2PbI [R = Me (**5**), Et (**6**)]. The iodide **5** was also obtained by halogen exchange reaction between **4** and KI. The compounds were characterized in solution by ^1H and ^{13}C NMR. The molecular structure of **2** and **4** was established by single-crystal X-ray diffraction. In both cases the nitrogen atom from the pendant Me_2NCH_2 arm is coordinated intramolecularly to the lead atom [Pb-N 3.051(9) Å in **2** and 2.635(8) Å in **4**, respectively] leading to distorted trigonal bipyramidal geometry around the metal atom and thus to hypervalent 10-*Pb*-5 species. Compounds **2** and **4** crystallize as 1:1 mixtures of *R*- and *S*-isomers (planar chirality induced by the non-planar PbC_3N chelate ring).

Keywords: organoleadIV) compounds, hypervalent, solution NMR studies, single-crystal X-ray diffraction

INTRODUCTION

Aromatic ligands with pendant arm containing nitrogen as donor atom, such as 2-(Me_2NCH_2)C_6H_4 or related organic compounds have been largely used in organotin chemistry in last years [1-17]. By contrast, such ligands were only sparingly used in organolead chemistry. Only one lead(II) compound, [2-(Me_2NCH_2)C_6H_4]$_2$Pb [18], and few organoled(IV) derivatives, *i.e.* [2-(Me_2NCH_2)C_6H_4]$_4$Pb [18], [2-(Me_2NCH_2)C_6H_4](4-MeC_6H_4)$_2$PbI [19] and [2-(Me_2NCH_2)C_6H_4](4-MeC_6H_4)(4-$MeOC_6H_4$)PbI [19,20], were described in early works and the structure of the latter chiral compound was established by single-crystal X-ray diffraction. Some related derivatives, *i.e.* [CpFe{C_5H_3(CH_2NMe_2)-2}]$_2$Pb [21] and [CpFe{C_5H_3(CH_2NMe_2)-2}]$_2$PbM(CO)$_5$ (M = Cr, Mo, W) [22], were also recently described.

We report here on the synthesis and solution behavior of new tetraorganolead(IV) compounds, [2-(R_2NCH_2)C_6H_4]R'_3Pb [R = Me, R' = Me (**1**), Ph (**2**); R = Et, R' = Ph (**3**)], and triorganolead(IV) halides, [2-(Me_2NCH_2)C_6H_4]Ph_2PbCl (**4**), [2-(R_2NCH_2)C_6H_4]Ph_2PbI [R = Me (**5**), Et (**6**)], as well as the molecular structure of **2** and **4**.

[a] *Babeş-Bolyai University, Faculty of Chemistry and Chemical Engineering, Arany Janos 11, 400028 Cluj-Napoca, Romania; E-mail: cristi@chem.ubbcluj.ro*

RESULTS AND DISCUSSION

The new tetraorganolead(IV) compounds **1**-**3** were obtained by reacting R'_3PbCl with $[2\text{-}(R_2NCH_2)C_6H_4]Li$ in 1:1 molar ratio, in hexane, at at –78 °C, while reaction of Ph_2PbCl_2 with $[2\text{-}(Me_2NCH_2)C_6H_4]Li$ in 1:1 molar ratio, in same conditions, resulted in isolation of the chloride **4** (Scheme 1).

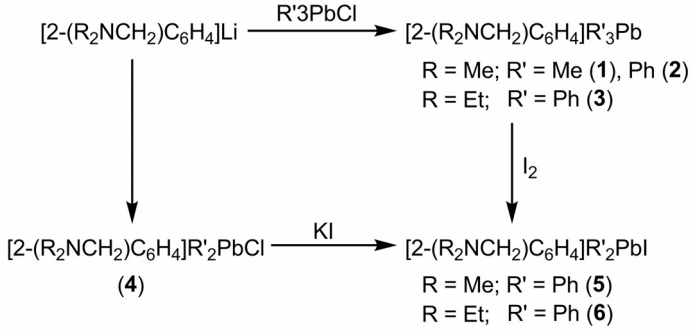

Scheme 1

Treatment of $[2\text{-}(R_2NCH_2)C_6H_4]Ph_3Pb$ with iodine, in CH_2Cl_2, at room temperature, resulted in selective cleavage of one phenyl group and isolation of the iodides $[2\text{-}(R_2NCH_2)C_6H_4]Ph_2PbI$ [R = Me (**5**), Et (**6**)]. This suggests that the presence of the CH_2NR_2 pendant arm on the aromatic ring stabilizes the Pb-C bond established by the $[2\text{-}(Me_2NCH_2)C_6H_4]$ group with respect to that which involves the phenyl moiety, probably through the intramolecular N→Pb interaction. The same iodide **5** was obtained by halogen exchange when the chloride **4** was treated with excess of KI, in CH_2Cl_2/water.

The new organolead(IV) compounds were isolated in rather good yields (50-90%) as colorless (**1**-**4**) or yellowish (**5**, **6**) crystalline solids. They are air-stable compounds, soluble in common organic solvents. The compounds were investigated by NMR spectroscopy (^1H, ^{13}C, 2D) in solution and for compounds **2** and **4** the molecular structures were established by single-crystal X-ray diffraction.

The NMR spectra for the compounds **1**-**6** were recorded in $CDCl_3$, at room temperature. The assignment of the ^1H and ^{13}C chemical shifts was made according to the numbering schemes shown in Scheme 2, based on 2D experiments and the lead-carbon coupling constants.

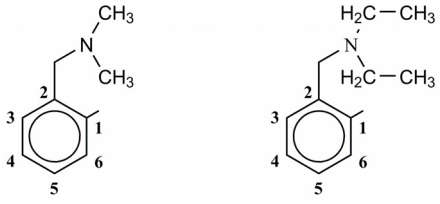

Scheme 2

The NMR (^{1}H, ^{13}C) spectra of compounds **1**, **2**, **4** and **5** are very similar with respect to the [2-(Me_2NCH_2)C_6H_4] group attached to the lead atom, showing the expected resonances in the alkyl and the aryl regions. All four compounds show in the alkyl region singlet resonances for NMe_2 and CH_2 protons of the pendant arm, respectively, with the latter surrounded by lead satellites. The ^{1}H NMR spectrum of the mixed alkyl-aryllead(IV) derivative **1** exhibits in the alkyl region an additional singlet resonance for the protons of the methyl groups bonded to lead. The aromatic region is much better resolved for compound **1**, with four multiplet resonances (that for the H_3 proton is partially overlapped by the resonance of residual $CHCl_3$). For the mixed tetraaryllead(IV) compound **3** the aromatic region is more complicated due to overlapping of the resonances for the protons of the C_6H_4 group and those corresponding to the phenyl groups, respectively. The main influence of the halogen atom attached to lead in the chloride **4** and the iodide **5** is the downfield shift of the resonance for the proton H_6 with respect to the other *ortho* protons from the phenyl groups bonded to lead. For compounds **3** and **6**, containing the [2-(Et_2NCH_2)C_6H_4] group attached to lead, in addition to a broad signal for the benzylic CH_2 protons, one triplet and one quartet resonance were observed for the ethyl groups in the aliphatic region of the ^{1}H NMR spectra. The aromatic region exhibits a rather complex pattern due to partial overlapping of the resonance signals.

According to the ^{1}H NMR data, the ^{13}C NMR spectra of compounds **2**-**5** contain, in addition of six resonances for the different aromatic carbons of the [2-(R_2NCH_2)C_6H_4] group, a single set of four resonances for the phenyl groups, indicating their equivalence in solution. Most of these singlet resonances are surrounded by lead satellites due to lead-carbon coupling. The unambiguous assignment of the ^{13}C resonance signals for these organolead(IV) compounds was based on the 2D correlation spectra and carbon-lead coupling constants, respectively.

The NMR data suggest that in solution these compounds might have similar structures as found in solid state for **2** and the chloride **4**, *i.e.* a trigonal bipyramidal coordination geometry around the lead atom due to the intramolecular N→Pb coordination (assuming a fast conformational change in solution for the nonplanar, five-membered PbC_3N chelate ring, which gives averaged ^{1}H NMR signals). Alternatively, a tetrahedral geometry around the lead atom can also be considered, a behavior which will assume the lack of intramolecular coordination in solution. Unfortunately, the ^{207}Pb NMR spectra, which might provide further information on the coordination degree of the lead atom, could not be yet recorded.

Single-crystals suitable for X-ray diffraction studies were obtained by slow diffusion from a mixture of CH_2Cl_2 and hexane (1/4, v/v) for compounds [2-(Me_2NCH_2)C_6H_4]Ph_3Pb (**2**) and [2-(Me_2NCH_2)C_6H_4]Ph_2PbCl (**4**).

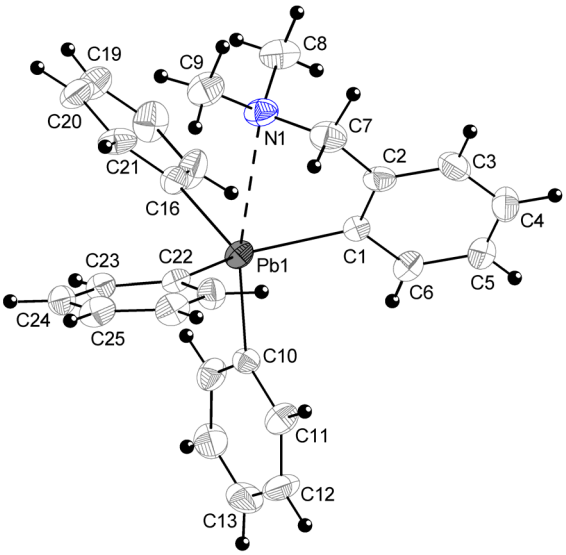

Figure 1. ORTEP representation at 30% probability and atom numbering scheme for R_N-**2** isomer.

The crystal of **2** consists of discrete monomers separated by normal van der Waals distances, while compound **4** has two independent, very similar, molecules (**4a** and **4b**) in the unit cell and therefore the subsequent discussion will refer only to molecule **4a**. The ORTEP diagrams of the molecular structures of **2** and **4a**, with the atom numbering scheme, are shown in Figures 1 and 2. Selected interatomic distances and angles are listed in Tables 1 and 2.

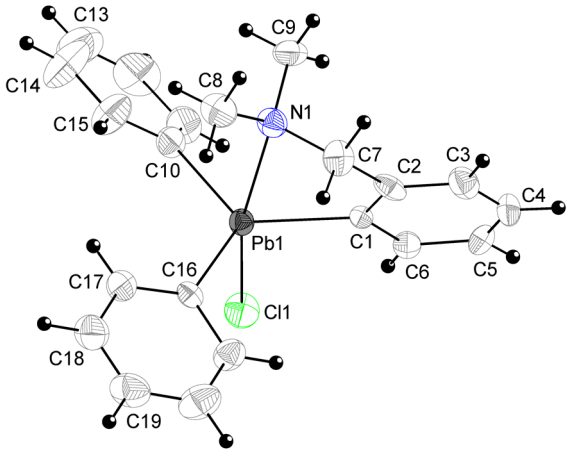

Figure 2. ORTEP representation at 30% probability and atom numbering scheme for R_N-**4a** isomer.

Table 1. Interatomic bond distances (Å) and angles (°) for compound **2**.

Pb(1)-C(1)	2.223(8)	Pb(1)-C(16)	2.222(8)
Pb(1)-C(10)	2.253(8)	Pb(1)-C(22)	2.207(8)
Pb(1)-N(1)	3.051(9)		
N(1)-C(7)	1.475(12)	N(1)-C(9)	1.453(11)
N(1)-C(8)	1.440(12)		
C(1)-Pb(1)-C(10)	102.2(3)	C(10)-Pb(1)-C(16)	105.7(3)
C(1)-Pb(1)-C(16)	118.6(3)	C(10)-Pb(1)-C(22)	104.9(3)
C(1)-Pb(1)-C(22)	114.2(3)	C(16)-Pb(1)-C(22)	109.6(3)
N(1)-Pb(1)-C(10)	169.1(3)		
N(1)-Pb(1)-C(1)	66.8(3)	N(1)-Pb(1)-C(22)	80.8(3)
N(1)-Pb(1)-C(16)	80.6(3)		
C(7)-N(1)-C(8)	109.0(8)	Pb(1)-N(1)-C(7)	94.8(6)
C(7)-N(1)-C(9)	111.0(8)	Pb(1)-N(1)-C(8)	110.3(6)
C(8)-N(1)-C(9)	111.3(8)	Pb(1)-N(1)-C(9)	119.2(7)

Table 2. Interatomic bond distances (Å) and angles (°) for compound **4**.

4a		**4b**	
Pb(1)-C(1)	2.202(8)	Pb(2)-C(22)	2.205(9)
Pb(1)-C(10)	2.191(10)	Pb(2)-C(31)	2.197(9)
Pb(1)-C(16)	2.190(9)	Pb(2)-C(37)	2.198(9)
Pb(1)-Cl(1)	2.597(3)	Pb(2)-Cl(2)	2.616(2)
Pb(1)-N(1)	2.636(8)	Pb(2)-N(2)	2.646(9)
N(1)-C(7)	1.489(13)	N(2)-C(28)	1.478(15)
N(1)-C(8)	1.481(13)	N(2)-C(29)	1.458(14)
N(1)-C(9)	1.462(13)	N(2)-C(30)	1.452(14)
Cl(1)-Pb(1)-N(1)	166.11(19)	Cl(2)-Pb(2)-N(2)	167.2(2)
Cl(1)-Pb(1)-C(1)	94.9(2)	Cl(2)-Pb(1)-C(22)	93.3(3)
Cl(1)-Pb(1)-C(10)	93.4(3)	Cl(2)-Pb(1)-C(31)	99.1(2)
Cl(1)-Pb(1)-C(16)	98.5(2)	Cl(2)-Pb(1)-C(37)	93.9(3)
N(1)-Pb(1)-C(1)	72.9(3)	N(2)-Pb(1)-C(22)	74.2(3)
N(1)-Pb(1)-C(10)	89.0(3)	N(2)-Pb(1)-C(31)	89.0(3)
N(1)-Pb(1)-C(16)	92.6(3)	N(2)-Pb(1)-C(37)	91.3(3)
C(1)-Pb(1)-C(10)	126.7(4)	C(22)-Pb(1)-C(31)	117.0(3)
C(1)-Pb(1)-C(16)	113.7(3)	C(22)-Pb(1)-C(37)	124.3(3)
C(10)-Pb(1)-C(16)	116.8(4)	C(31)-Pb(1)-C(37)	116.1(4)
C(7)-N(1)-C(8)	108.8(9)	C(28)-N(1)-C(29)	109.6(10)
C(7)-N(1)-C(9)	111.2(9)	C(28)-N(1)-C(30)	108.3(10)
C(8)-N(1)-C(9)	110.0(9)	C(29)-N(1)-C(30)	111.0(10)
Pb(1)-N(1)-C(7)	98.0(6)	Pb(2)-N(1)-C(28)	97.7(6)
Pb(1)-N(1)-C(8)	118.4(6)	Pb(2)-N(1)-C(29)	111.8(7)
Pb(1)-N(1)-C(9)	109.8(7)	Pb(2)-N(1)-C(30)	117.4(8)

The molecule of **2** contains an intramolecular N→Pb interaction [Pb(1)-N(1) 3.051(9) Å] placed *trans* to the carbon atom of a phenyl group attached to lead. The strength of this interaction is enough strong to be taken into account [c.f. the sum of the van der Waals radii, Σr_{vdW}(Pb,N) 3.54 Å] [23]. The overall geometry at the lead atom is distorted trigonal bipyramidal, with the axial positions occupied by the nitrogen and the carbon atom [N(1)-Pb(1)-C(10) 169.1(3)°], while the carbon atoms of the other two phenyl groups and that of the pendant arm aryl ligand are in the equatorial positions. The distortion of the coordination geometry is due to the small bite of the *C,N*-ligand [N(1)-Pb(1)-C(1) 66.8(3)°]. The C_3PbN chelate ring is not planar, the nitrogen atom being out of the plane defined by the remaining C_3Pb unit. This results in coordination isomers, *i.e.* planar chirality, with C(1)-C(6) aromatic ring and the N(1) atom as chiral plane and pilot atom, respectively [24]. As result compound **2** crystallizes as a 1:1 mixture of R_N and S_N isomers.

In the molecule of the chloride **4a** a much stronger intramolecular N→Pb interaction is established in the *trans* to the chlorine atom and the overall molecular structure is very similar to that reported for the related tin compound, [2-$(Me_2NCH_2)C_6H_4$]Ph_2SnCl [4]. The lead-nitrogen interatomic distance [Pb(1)-N(1) 2.636(8) Å] is of similar magnitude as observed in the related chiral iodide, [2-$(Me_2NCH_2)C_6H_4$](4-MeC_6H_4)(4-$MeOC_6H_4$)PbI [2.686(8) Å] [20], pointing out the lack of significant influence of the electronegativity of the atom placed in the *trans* position relative to nitrogen in the N→Pb-X fragment.

The axial positions in the resulted distorted trigonal bipyramidal geometry achieved around the metal centre are occupied by nitrogen and chlorine atoms [Cl(1)-Pb(1)-N(1) 166.11(19)°], while the aromatic carbon atoms are in the equatorial positions.

The *trans* effect is reflected in the length of the Pb-Cl bond, considerably shorter in **4a** [Pb(1)-Cl(1) 2.597(3) Å] than in the polymeric Ph_3PbCl [2.7059(7) Å] [25]. This is consistent with the stronger *trans* influence of the more electronegative chlorine atom in the Cl→Pb-Cl bridge in Ph_3PbCl than in the N→Pb-Cl system.

As in the case of **2**, the C_3PbN chelate ring in the molecule of **4** is not planar, resulting in planar chirality. The crystal of the chloride **4** consists of a 1:1 mixture of R_N-**4a** / S_N-**4a** and R_N-**4b** / S_N-**4b** isomers, separated by normal van der Waals distances between heavy atoms. However, a closer check of the crystal structure revealed that weak intermolecular Cl···H interactions are established between neighboring molecules. This results in helicoidal chain polymers formed by alternating R_N-**4a** / R_N-**4b** and S_N-**4a** / S_N-**4b** isomers (Figure 3), respectively, supported by $Cl(1)\cdots H(30A)_{methyl}$ (2.95 Å) and $Cl(2)\cdots H(13b)_{phenyl}$ (2.87 Å) interactions [c.f. Σr_{vdW}(Cl,H) ca. 3.01 Å] [23]. No inter-chain contacts are present between parallel polymeric chains developed along the *b* axis.

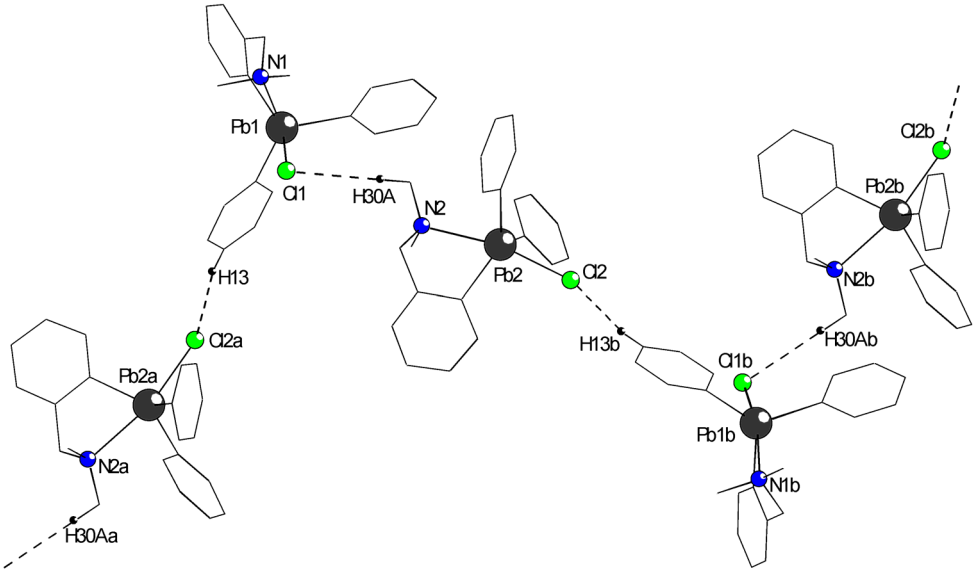

Figure 3. View of a chain polymer based on Cl···H contacts between S_N-**4a** and S_N-**4b** isomers in the crystal of **4** (only hydrogens involved in intermolecular interactions are shown) [symmetry equivalent atoms: Pb2a (1.5 – *x*, 0.5 + *y*, 0.5 – *z*); Pb1 (–0.5 + *x*, 0.5 – *y*, –0.5 + *z*); Pb1b (2 – *x*, –*y*, 1 – *z*) and Pb2b (1.5 – *x*, –0.5 + *y*, 0.5 – *z*)].

CONCLUSIONS

Six new hypervalent organolead(IV) compounds of the type $[2\text{-}(R_2NCH_2)C_6H_4]R'_3Pb$ (R = Me, R' = Me, Ph; R = Et, R' = Ph) and $[2\text{-}(R_2NCH_2)C_6H_4]Ph_2PbX$ (R = Me, X = Cl, I; R = Et, X = I) were obtained. All compounds were characterized in solution using multinuclear and 2D NMR spectroscopy. For both type of compounds single-crystal X-ray diffraction studies provide evidence for an intramolecular N→Pb interaction, resulting in distorted trigonal bipyramidal geometry around the lead atom (hypervalent 10-*Pb*-5 species). It was also found that cleavage of a phenyl group under treatment with iodine is preferred *versus* cleavage of the pendant arm aryl ligand, probably due to the intramolecular N→Pb interaction. All compounds crystallize as 1:1 mixtures of R_N- and S_N isomers (planar chirality induced by the non-planar PbC_3N chelate ring).

EXPERIMENTAL SECTION

All compounds were prepared under an inert atmosphere of argon (Linde, 99.999%) using Schlenk techniques. Solvents were dried and freshly distilled under argon prior to use. Ph_3PbCl, Me_3PbCl and Ph_2PbCl_2 were

commercially available. The other starting materials were prepared accordingly to literature methods: [2-(Me_2NCH_2)C_6H_4]Li [26] and [2-(Et_2NCH_2)C_6H_4]Li [27]. The ^{1}H, ^{13}C and 2D NMR spectra were recorded at room temperature, in dried $CDCl_3$, on Bruker Avance 300 instrument. The chemical shifts are reported in ppm relative to the residual peak of the solvent (ref. $CHCl_3$: ^{1}H 7.26, ^{13}C 77.0 ppm). The NMR spectra were processed using the *MestReC* and *MestReNova* software [28].

*Preparation of [2-(Me_2NCH_2)C_6H_4]Me_3Pb (**1**)*

A suspension of [2-(Me_2NCH_2)C_6H_4]Li (0.72 g, 5.1 mmol) in hexane (30 ml) was added dropwise, under stirring, to a solution of Me_3PbCl (1.49 g, 5.1 mmol) in hexane (50 ml), cooled (–78 °C). After the organolithium suspension was added, the reaction mixture was stirred for 1 h at –78 °C, and then left over night to reach the room temperature. The reaction mixture was filtered in open atmosphere and the solvent was removed in vacuum from the clear filtrate. The white solid residue was recrystallized from hexane to give the title compound as colorless crystals. Yield: 1.3 g (65%), m.p. 234 °C. ^{1}H NMR (300 MHz, 20 °C): δ 1.60s (9H, Pb-CH_3, $^2J_{PbH}$ 82.6 Hz), 2.33s (6H, N-CH_3), 3.64s (2H, -CH_2-N, $^4J_{PbH}$ 16.1 Hz), 7.25m (1H, H_3, partially overlapped by $CDCl_3$ resonance), 7.32ddd (1H, H_4, $^3J_{HH}$ 7.3, $^4J_{HH}$ 1.3 Hz), 7.42ddd (1H, H_5, $^3J_{HH}$ 7.3, $^4J_{HH}$ 1.4 Hz), 8.31dd (1H, H_6, $^3J_{HH}$ 7.4, $^4J_{HH}$ 0.9, $^3J_{PbH}$ 115.5 Hz). ^{13}C NMR (75.4 MHz, 20 °C): δ 16.28s (Pb-CH$_3$), 45.39s (N-CH$_3$), 65.78s (-CH$_2$-N), 128.16s (C_3), 129.00s (C_4), 129.24s (C_5), 137.78s (C_6), 142.28s (C_2), 156.67s (C_1).

*Preparation of [2-(Me_2NCH_2)C_6H_4]Ph_3Pb (**2**)*

A suspension of [2-(Me_2NCH_2)C_6H_4]Li (0.69 g, 4.9 mmol) in hexane (30 ml) was added dropwise, under stirring, to a cooled (–78 °C) solution of Ph_3PbCl (1.9 g, 4.9 mmol) in hexane (50 ml). After the organolithium suspension was added, the reaction mixture was stirred for 1 h at –78 °C, and then left over night to reach the room temperature. The reaction mixture was filtered and the solvent was removed in vacuum from the clear filtrate. The white solid residue was recrystallized from hexane to give the title compound as colorless crystals. Yield: 1.1 g (47%), m.p. 245 °C. ^{1}H NMR (300 MHz, 20 °C): δ 1.76s (6H, N-CH_3), 3.35s (2H, -CH_2-N, $^4J_{PbH}$ 9.0 Hz), 7.39m (12H, $H_{3\text{-}5}$ + C_6H_5-*meta+para*), 7.69m (7H, H_6 + C_6H_5-*ortho*, $^3J_{PbH}$ 78.7 Hz). ^{13}C NMR (75.4 MHz, 20 °C): δ 44.96s (N-CH$_3$), 66.07s (-CH$_2$-N, $^3J_{PbC}$ 31.5 Hz), 127.78s (C_5, $^3J_{PbC}$ 92.9 Hz), 127.88s (C_6H_5-*para*, $^4J_{PbC}$ 18.2 Hz), 128.35s (C_4, $^4J_{PbC}$ 19.7 Hz), 129.05s (C_6H_5-*meta*, $^3J_{PbC}$ 78.1 Hz), 130.22s (C_3, $^3J_{PbC}$ 75.6 Hz), 137.38s (C_6H_5-*ortho*, $^2J_{PbC}$ 65.3 Hz), 138.51s (C_6, $^2J_{PbC}$ 78.1 Hz), 145.98s (C_2, $^2J_{PbC}$ 51.6 Hz), 151.59s (C_1, $^1J_{PbC}$ 579.8 Hz), 153.40s (C_6H_5-*ipso*, $^1J_{PbC}$ 484.8 Hz).

*Preparation of [2-(Et_2NCH_2)C_6H_4]Ph_3Pb (**3**)*

A solution of Ph_3PbCl (2.52 g, 6.5 mmol) in hexane (20 ml) was added during 1 h to a stirred suspension of [2-(Et_2NCH_2)C_6H_4]Li (1.1 g, 6.65 mmol) in hexane (50 ml), kept at –78 °C. The reaction mixture was stirred at this temperature for 1 h and then over night to reach the room temperature. The reaction mixture was filtered under argon and the solvent was removed in vacuum from the clear filtrate. The white solid residue was recrystallized from hexane to give the title compound as colorless crystals. Yield: 2.0 g (58%), m.p. 223 °C. ^{1}H NMR (300 MHz, 20 °C): δ 0.68t (6H, N-CH_2-C*H*$_3$, $^3J_{HH}$ 7.1 Hz), 2.20q (4H, N-C*H*$_2$-CH_3, $^3J_{HH}$ 7.1 Hz), 3.50s (2H, -C*H*$_2$-N, $^4J_{PbH}$ 10.6 Hz), 7.33m (12H, *H*$_{3\text{-}5}$ + C_6*H*$_5$-*meta+para*), 7.63m (7H, *H*$_6$ + C_6*H*$_5$-*ortho*, $^3J_{PbH}$ 79.4 Hz). ^{13}C NMR (75.4 MHz, 20 °C): δ 9.84s (N-CH_2-*C*H_3), 44.80s (N-*C*H_2-CH_3), 60.85s (-*C*H_2-N, $^3J_{PbC}$ 41.1 Hz), 127.53s (*C*$_5$, $^3J_{PbC}$ 90.2 Hz), 128.11s (*C*$_6$H$_5$-*para*, $^4J_{PbC}$ 18.4 Hz), 128.53s (*C*$_4$, $^4J_{PbC}$ 19.4 Hz), 129.19s (*C*$_6$H$_5$-*meta*, $^3J_{PbC}$ 78.4 Hz), 129.89s (*C*$_3$, $^3J_{PbC}$ 72.0 Hz), 137.49s (*C*$_6$H$_5$-*ortho*, $^2J_{PbC}$ 65.9 Hz), 138.19s (*C*$_6$, $^2J_{PbC}$ 77.5 Hz), 146.90s (*C*$_2$, $^2J_{PbC}$ 54.0 Hz), 151.02s (*C*$_1$, $^1J_{PbC}$ 542.0 Hz), 152.32s (*C*$_6$H$_5$-*ipso*, $^1J_{PbC}$ 472.2 Hz).

*Preparation of [2-(Me_2NCH_2)C_6H_4]Ph_2PbCl (**4**)*

A suspension of [2-(Me_2NCH_2)C_6H_4]Li (0.69 g, 3.8 mmol) in hexane (30 ml) was added dropwise, under stirring, to a cooled (–78 °C) solution of Ph_2PbCl_2 (1.62 g, 3.77 mmol) in hexane (50 ml). After the organolithium suspension was added, the reaction mixture was stirred for 1 h at –78 °C, and then left over night to reach the room temperature. The reaction mixture was filtered and the solvent was removed in vacuum from the clear filtrate. The white solid residue was recrystallized from hexane to give the title compound as colorless crystals. Yield: 1.33 g (66%), m.p. 225 °C. ^{1}H NMR (300 MHz, 20 °C): δ 2.02s (6H, N-C*H*$_3$), 3.57s (2H, -C*H*$_2$-N, $^4J_{PbH}$ 16.4 Hz), 7.44m (9H, *H*$_{3\text{-}5}$ + C_6*H*$_5$-*meta+para*), 7.77 d (4H, C_6*H*$_5$-*ortho*, $^3J_{HH}$ 7.8, $^3J_{PbH}$ 111.6 Hz), 8.60d (1H, *H*$_6$, $^3J_{HH}$ 7.4, $^3J_{PbH}$ 130.7 Hz). ^{13}C NMR (75.4 MHz, 20 °C): δ 45.72s (N-*C*H_3), 65.32s (-*C*H_2-N, $^3J_{PbC}$ 38.5 Hz), 128.96s (*C*$_3$, $^3J_{PbC}$ 44.5 Hz), 129.47s (*C*$_6$H$_5$-*para*, $^4J_{PbC}$ 24.1 Hz), 129.57s (*C*$_4$, $^4J_{PbC}$ 24.8 Hz), 130.06s (*C*$_6$H$_5$-*meta*, $^3J_{PbC}$ 110.6 Hz), 136.01s (*C*$_6$H$_5$-*ortho*, $^2J_{PbC}$ 87.3 Hz), 138.51s (*C*$_6$, $^2J_{PbC}$ 70.7 Hz), 142.66s (*C*$_2$, $^2J_{PbC}$ 68.4 Hz), 154.45s (*C*$_1$, $^1J_{PbC}$ 826.6 Hz), 157.92s (*C*$_6$H$_5$-*ipso*, $^1J_{PbC}$ 726.3 Hz) (the resonance for *C*$_5$ carbon is overlapped by the resonance for the *C*$_6$H$_5$-*para* carbon).

*Preparation of [2-(Me_2NCH_2)C_6H_4]Ph_2PbI (**5**)*

Method A. The chloride **4** (0.2 g, 0.45 mmol) was suspended in CH_2Cl_2 (20 ml) and solvent was added until the solid compound was completely solved. An aqueous solution of KI (0.375 g, 2.26 mmol, 500% excess) was then added and the obtained mixture was stirred for 3 h at room temperature. The organic

layer was separated from the water layer and the latter was washed with CH_2Cl_2 (2 x 5 ml). The organic solution was dried over anhydrous Na_2SO_4. The solvent was removed in vacuum and the remaining yellow material was recrystallized from a CH_2Cl_2/hexane mixture to give the title compound. Yield: 0.22 g (91%).

Method B. Compound **2** (0.2 g, 0.4 mmol) was suspended in CH_2Cl_2 (20 ml) and solvent was added until the solid compound was completely solved. A solution of iodine (0.1 g, 0.4 mmol) in CH_2Cl_2 was added and the mixture was stirred for 2 h at room temperature. The solvent was removed under vacuum and the remaining yellow solid was recrystallized from a CH_2Cl_2/hexane mixture to give the title compound. Yield: 0.15 g (68%), m.p. 236 °C. ^{1}H NMR (300 MHz, 20 °C): δ 1.95s (6H, N-CH_3), 3.54s (2H, -CH_2-N, $^4J_{PbH}$ 15.0 Hz), 7.42m (9H, $H_{3\text{-}5}$ + C_6H_5-*meta+para*), 7.77dd (4H, C_6H_5-*ortho*, $^3J_{HH}$ 7.9, $^4J_{HH}$ 1.2, $^3J_{PbH}$ 111.6 Hz), 8.66dd (1H, H_6, $^3J_{HH}$ 7.4, $^4J_{HH}$ 1.0, $^3J_{PbH}$ 134.4 Hz). ^{13}C NMR (75.4 MHz, 20 °C): δ 45.72s (N-CH$_3$), 65.18s (-CH$_2$-N, $^3J_{PbC}$ 33.3 Hz), 128.86s (C_3), 129.29s (C_6H_5-*para*), 129.55s (C_4), 129.61s (C_5), 129.96s (C_6H_5-*meta*, $^3J_{PbC}$ 108.7 Hz), 135.88s (C_6H_5-*ortho*, $^2J_{PbC}$ 84.3 Hz), 140.67s (C_6, $^2J_{PbC}$ 74.0 Hz), 142.61s (C_2), 150.51s (C_1), 157.21s (C_6H_5-*ipso*).

*Preparation of [2-(Et_2NCH_2)C_6H_4]Ph_2PbI (**6**)*

Compound **3** (0.25 g, 0.4 mmol) was suspended in CH_2Cl_2 (20 ml) and solvent was added until the solid compound was completely solved. A solution of iodine (0.1 g, 0.4 mmol) in CH_2Cl_2 was added and the mixture was stirred for 2 h at room temperature. The solvent was removed under vacuum and the remaining yellow solid was recrystallized from a CH_2Cl_2/hexane mixture to give the title compound. Yield: 0.18 g (67%), m.p. 223 °C. ^{1}H NMR (300 MHz, 20 °C): δ 0.69t (6H, N-CH$_2$-CH_3, $^3J_{HH}$ 7.1 Hz), 2.30q (4H, N-CH_2-CH$_3$, $^3J_{HH}$ 7.1 Hz), 3.63s (2H, -CH_2-N, $^4J_{PbH}$ 12.8 Hz), 7.44m (9H, $H_{3\text{-}5}$ + C_6H_5-*meta+para*), 7.78d (4H, C_6H_5-*ortho*, $^3J_{HH}$ 7.4, $^3J_{PbH}$ 110.7 Hz), 8.66d (1H, H_6, $^3J_{HH}$ 7.4, $^3J_{PbH}$ 129.9 Hz).

X-ray Crystallographic Study

Data were collected with a SMART APEX diffractometer (*National Center for X-Ray Diffractometry*, "Babes-Boyai" University, Cluj-Napoca, Romania) at 297 K, using a graphite monochromator to produce a wavelength (Mo-$K\alpha$) of 0.71073 Å. The crystal structure measurement and refinement data for compounds **2** and **4** are given in Table 3. Absorption correction was applied for **2** (semi-empirical from equivalents). The structure was solved by direct methods (full-matrix least-squares on F^2). All non hydrogen atoms were refined with anisotropic thermal parameters. For structure solving and refinement a software package SHELX-97 was used [29]. The drawings were created with the Diamond program [30].

Table 3. Crystallographic data for compounds **2** and **4**.

	2	**4**
chemical formula	$C_{27}H_{27}NPb$	$C_{21}H_{22}ClNPb$
crystal habit	colorless block	colorless block
crystal size [mm]	0.30 x 0.20 x 0.15	0.20 x 0.19 x 0.18
crystal system	monoclinic	monoclinic
space group	*P2(1)/c*	*P2(1)/n*
a [Å]	9.5351(12)	9.3153(5)
b [Å]	27.172(3)	24.2365(13)
c [Å]	10.1510(12)	17.8184(10)
α [deg]	90	90
β [deg]	117.036(2)	97.286(1)
γ [deg]	90	90
U [Å^3]	2342.6(5)	3990.4(4)
Z	4	8
D_c [g cm^{-3}]	1.624	1.768
M	572.69	531.04
F(000)	1112	2032
θ range [deg]	1.50 – 25.00	1.43 – 25.00
μ(Mo Kα) [mm^{-1}]	7.214	8.591
no. of reflections collected	16748	28670
no. of independent reflections	4114 (R_{int} = 0.0534)	7016 (R_{int} = 0.0463)
R_1 [$I > 2\sigma(I)$]	0.0490	0.0567
wR_2	0.0955	0.1048
no. of parameters	264	437
no. of restraints	0	0
GOF on F^2	1.133	1.292
largest difference electron density [e Å^{-3}]	0.987, –2.018	1.768, –1.675

CCDC-750465 (**2**) and -750466 (**4**) contains the supplementary crystallographic data for this paper. These data can be obtained free of charge at www.ccdc.cam.ac.uk/conts/retrieving.html [or from the Cambridge Crystallographic Data Centre, 12, Union Road, Cambridge CB2 1EZ, UK; fax: (internat.) +44-1223/336-033; E-mail: deposit@ccdc.cam.ac.uk].

ACKNOWLEDGEMENTS

We thank the Ministry of Education and Research of Romania (CNCSIS, Research Project No. 709/2007 and TD-342/2007) for financial support. We also thank the NATIONAL CENTER FOR X-RAY DIFFRACTION (”Babes-Bolyai” University, Cluj-Napoca, Romania) for the support in the solid state structure determinations.

REFERENCES

1. J. T. B. H. Jastrzebski, G. van Koten, Adv. Organomet. Chem., **1993**, *35*, 241.
2. R. Jambor, L. Dostál, in *The Chemistry of Pincer Compounds* [D. Morales-Morales, C. Jensen (Eds.)], Elsevier, Amsterdam, **2007**, pp. 357.
3. J. T. B. H. Jastrzebski, D. M. Grove, J. Boersma, G. van Koten, J. M. Ernsting, *Magn. Reson. Chem.*, **1991**, *29*, S25.
4. R. Varga, Schürmann, C. Silvestru, *J. Organomet. Chem.*, **2001**, *623*, 161.
5. J P. Novák, Z. Padělková, L. Kolářová, I. Císařová, A. Růžička, J. Holeček, *Appl. Organomet. Chem.*, **2005**, *19*, 1101.
6. P. Novák, J. Brus, I. Císařová, A. Růžička, J. Holeček, *J. Fluorine Chem.*, **2005**, *126*, 1531.
7. R. A. Varga, C. Silvestru, C. Deleanu, *Appl. Organomet. Chem.*, **2005**, *19*, 153.
8. R. A. Varga, A. Rotar, M. Schürmann, K. Jurkschat, C. Silvestru, *Eur. J. Inorg. Chem.*, **2006**, 1475.
9. R. A. Varga, C. Silvestru, *Acta Crystallogr. Sect. E*, **2006**, *62*, m1964.
10. P. Novák, Z. Padělková, I. Císařová, L. Kolářová, A. Růžička, J. Holeček, *Appl. Organomet. Chem.*, **2006**, *20*, 226.
11. R. A. Varga, C. Silvestru, *Acta Crystallogr. Sect. C*, **2007**, *63*, m48.
12. A. Rotar, R. A. Varga, C. Silvestru, *Acta Crystallogr. Sect. C*, **2007**, *63*, m355.
13. R. A. Varga, C. Silvestru, *Acta Crystallogr. Sect. C*, **2007**, *63*, m2789.
14. Z. Padělková, T. Weidlich, L. Kolářová, A. Eisner, I. Císařová, T. A. Zevaco, A. Růžička, *J. Organomet. Chem.*, **2007**, *692*, 5633.
15. R. A. Varga, K. Jurkschat, C. Silvestru, *Eur. J. Inorg. Chem.*, **2008**, 708.
16. A. Rotar, R. A. Varga, C. Silvestru, *Acta Crystallogr. Sect. E*, **2008**, *64*, m45.
17. A. Rotar, R. A. Varga, K. Jurkschat, C. Silvestru, *J. Organomet. Chem.*, **2009**, *694*, 1385.
18. P. P. De Wit, H. O. Van der Kooi, J. Wolters, *J.Organomet.Chem.,* **1981**, *216***,** C9.
19. H. O. van der Kooi, J. Wolters, A. van der Gen, *Rec. Trav. Chim. Pays Bas*, **1979**, *98*, 353.
20. H. O. van der Kooi, W. H. den Brinker, A. J. de Kok, *Acta Crystallogr.*, **1985**, *C41*, 869.
21. N. Seidel, K. Jacob, A. A. H. van der Zeijden, H. Menge, K. Merzweiler, C. Wagner, *Organometallics*, **2000**, *19*, 1438.
22. N. Seidel, K. Jacob, A. K. Fischer, *Organometallics*, **2001**, *20*, 578.
23. J. Emsley, *Die Elemente*, Walter de Gruyter: Berlin, **1994**.
24. J. Rigauy, S. P. Klesney (Eds.), *Nomenclature of Organic Chemistry – The Blue Book*, Pergamon Press, Oxford, **1979**.
25. H. Preut, F. Huber, *Z. Anorg. Allg. Chem.*, **1977**, *435*, 234.

26. A. Meller, H. Hoppe, W. Meringgele, A. Haase, M. Noltemeyer, *Organometallics*, **1998**, *17*, 123.
27. I. C. M. Wehman-Ooyevaar, I. F. Luitwieler, K. Vatter, D. M. Grove, W. J. J. Smeets, E. Horn, L. A. Spek, G. van Koten, *Inorg. Chim. Acta*, **1996**, *252*, 55.
28. MestReC and MestReNova, Mestrelab Research S.L., A Coruña 15706, Santiago de Compostela.
29. G. M. Sheldrick, *Acta Crystallogr., Sect. A* **2008**, *64*, 112.
30. *DIAMOND – Visual Crystal Structure Information System*, Crystal Impact, Postfach 1251, 53002 Bonn, Germany, **2001**.

STUDIA UNIVERSITATIS BABEŞ-BOLYAI, CHEMIA, LIV, 4, 2009

SYNTHESIS OF A DIMERIC G-2 MELAMINE DENDRIMER. FIRST USE OF A MASKED PIPERIDONE MOTIF IN DENDRITIC CHEMISTRY

FLAVIA POPA[a,b], OANA MOLDOVAN[a], MARIA IUSCO[a], PEDRO LAMEIRAS[c], CARMEN BATIU[a], YVAN RAMONDENCB[b] AND MIRCEA DARABANTU*[a]

ABSTRACT. Using iterative aminations of cyanuric chloride, we account the concise synthesis of a dimeric melamine based G-2 dendrimer having 1,4-dioxa-8-azaspiro[4.5]decane (piperidone ethyleneketal) in tandem with 2-amino-2-hydroxymethylbutanol *("ethylserinol"*) as peripheral groups piperazine and 4,4'-bispiperidine as internal and central linker, respectively.

Keywords: amination, dendrimers, iterative synthesis, 4-piperidone, 4,4'-bispiperidine, serinols.

INTRODUCTION

We have recently reported the strong and resourceful nucleophilicity of piperidone or of its ethyleneketal with respect to selective amination of cyanuric chloride [1, 2a]. From our previous contributions in the field of iterative synthesis directed to melamine dendritic structures based on *C*-substituted 2-aminopropane-1,3-diols (*"serinols"*) [2], we also learned that, until now, only *l*-2-amino-1-arylpropane-1,3-diols (enantiomeric *"phenylserinols"*) are suitable starting materials in the above convergent approaches[*]. Indeed, commercial C-2-substituted-2-aminopropane-1,3-diols [*"methylserinol"*, *"ethylserinol"* and 2-amino-2-(hydroxymethyl)propan-1,3-diol, known as TRIS] provided, up to G-0 dendrons, unstable as difficult to purify intermediates [3].

Therefore, we consider, as an alternative challenging attempt, the use of a C-2-substituted serinol, for example 2-amino-2-(hydroxymethyl)-butanol (*"ethylserinol"*) in tandem with 1,4-dioxa-8-azaspiro[4.5]decane (piperidone ethyleneketal) as peripheral groups in a target dimeric G-2 melamine dendrimer synthesis (Scheme 1).

[a] *"Babes-Bolyai" University, Department of Organic Chemistry, 11 Arany Jànos st., 400 028 Cluj-Napoca, ROMANIA, (darab@chem.ubbcluj.ro)*
[b] *Université et INSA de Rouen, IRCOF – LCOFH, UMR 6014 CNRS COBRA, BP 08, 76131 Mont Saint-Aignan Cedex, FRANCE*
[c] *Université de Reims Champagne-Ardenne, ICMR - LIS, UMR 6229, BP 1039, 51687 Reims Cedex 2, FRANCE*

[*] For continuous discussion in this communication, nomenclature, definitions and concepts according to Tomalia (Ref. [3a]) and Vögtle *et al.* (Ref. [3b]) were used throughout.

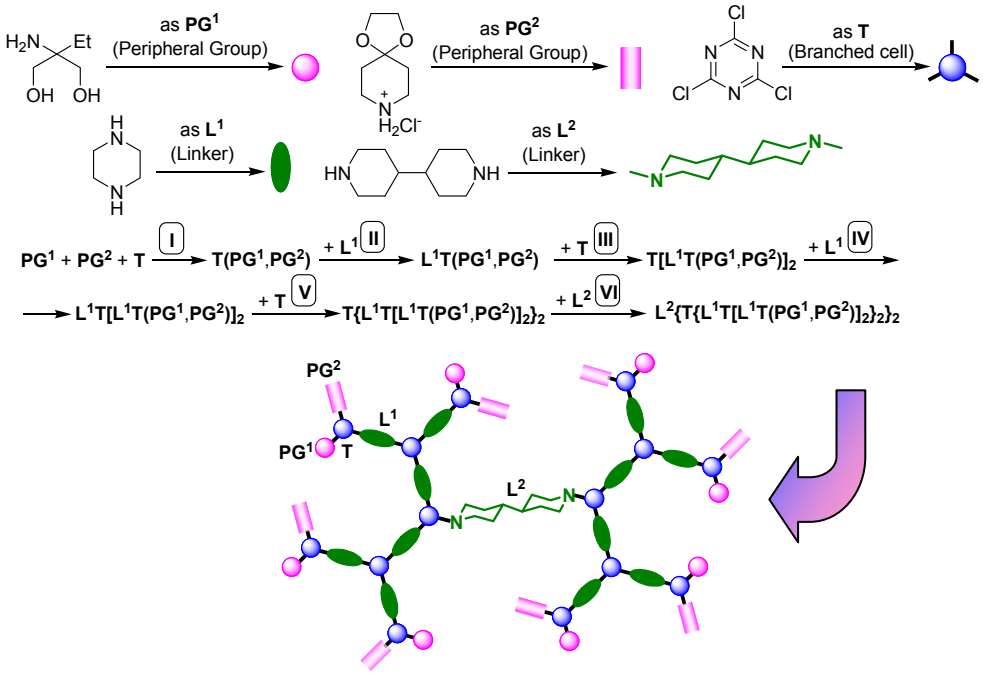

Scheme 1

As shown in Scheme 1, our strategy was convergent, consisting of six linear steps, **I – VI**, as ten selective aminations of cyanuric chloride with the depicted amino nucleophiles. We note the use of 4,4'-bispiperidine (**L^2**), ethylserinol (**PG^1**) and piperidone ethyleneketal (**PG^2**) as central linker and peripheral groups respectively, not reported previously. Along with C-2-substituted serinols, only TRIS (2-amino-2-hydroxymethylpropan-1,3-diol) is known, since 1985 [4a], to be a key element in dendritic chemistry, playing all roles, core, branched cell and peripheral group [4]. Concerning linker **L^1**, piperazine, it is nowadays a widely employed structural motif in dendrimer synthesis connecting cores [5a-d], generations [5e-h] or both [5i-l].

RESULTS AND DISCUSSION

1. Synthesis

We commenced our study (Scheme 2) with the anchorage of peripheral groups on *s*-triazine. Ethylserinol **1**, the less reactive nucleophile, was firstly reacted with cyanuric chloride providing dichloroamino-*s*-triazine **2a** in quantitative yield (TLC monitoring)*. For this reason, **2a** was not isolated but treated with the subsequent nucleophile, piperidone ethylene ketal hydrochloride whose

* We previously discussed the synthesis and structure of **2a**, see Ref. [2a].

free base, generated *in situ*, was, as expected, much more reactive in 10% aq. THF [1]. Indeed, the very mild shown conditions were found step by step, in order to avoid, as much as possible, the complete replacement of chlorine in **2a** by two dioxaazaspiranic units (compound **2c**). We note the optimised yield of **2b**, 58%, to be also mandatory to the purity of commercial **1** (about 80%).

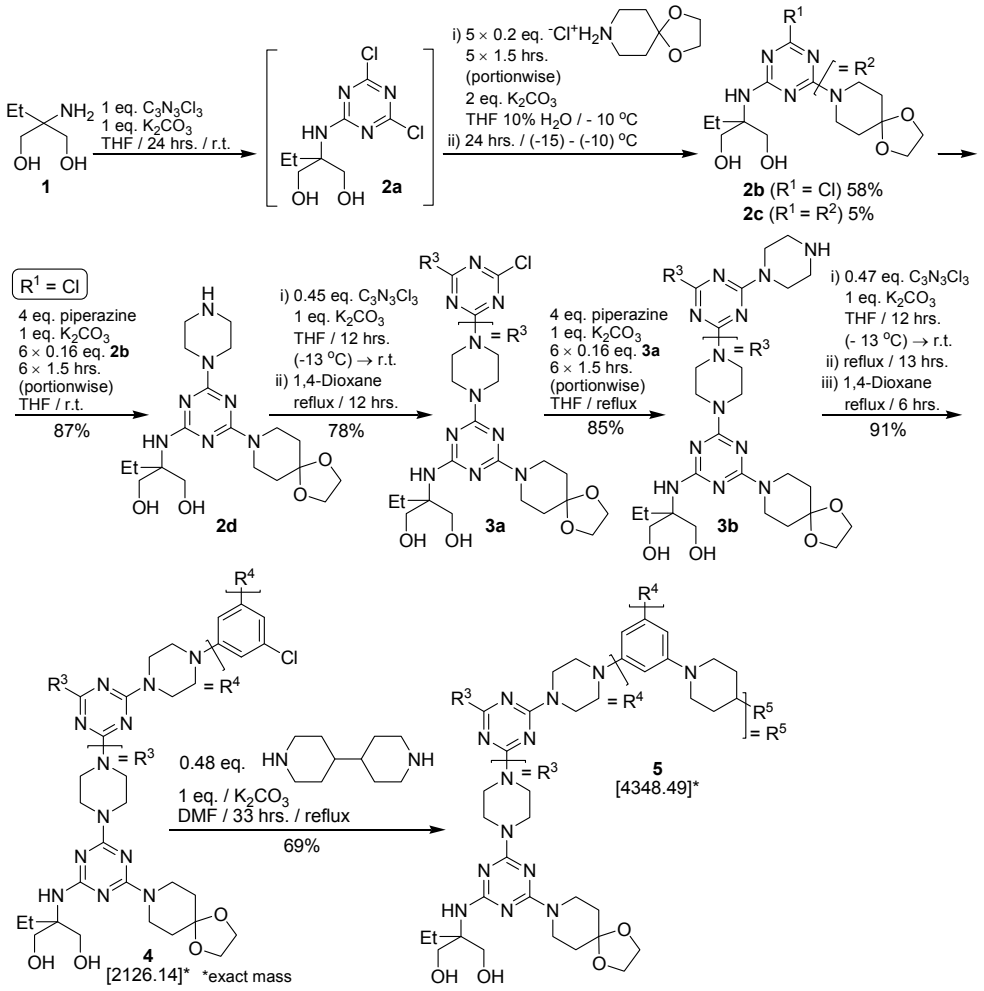

Scheme 2

Reaction of chlorodiamino-*s*-triazine **2b** with excess of piperazine afforded amine **2d** with good yield, following our already established protocol [2a, 2c, 6]. Purification of **2d** by column chromatography on partially deactivated silica gel (eluent *i*-PrOH: aq. NH_3 25% 9:1 v/v) ensured the analytical purity of this intermediate.

With **2d** in our hands, we reiterated the double amination of cyanuric chloride and accessed the G-1 dendron **3a** by operating on a large scale of temperature, from -13 to 102 ^{o}C. That is, only in these conditions we were confident that the contaminating possible side reactions, such as *O*- instead *NH*-anchorage of **2d** on *s*-triazine, were completely eliminated.

Next, selective amination of **3a** by piperazine was realised similarly as for **2b**, the refluxing solvent being however required in agreement with the stronger solvation of **3a** *vs*. **2b** in THF. Although isolated by column chromatography on partially deactivated silica gel, in order to reach analytical purity, the G-1 aminodendron **3b** needed a supplementary routine recrystallisation.

At this stage, the triple anchorage of **3b** on *s*-triazine skeleton upon treatment with 0.3 eq. of cyanuric chloride failed, presumably because of the already manifested starburst effect [7]. Thus, only the chloro-*s*-triazine G-2 dendron **4** could be isolated with small conversion (about 10%) from a complex polymeric reaction mixture (attempt not depicted in Scheme 1).

Therefore, we had to change the final strategy by using 0.47 eq. of cyanuric chloride against **3b**. In a very clean reaction, we were delighted to obtain the G-2 dendron **4** with an excellent yield in very comparable conditions to those in the case of G-1 analogue **3a**. Finally we coupled two G-2 dendrons **4** through a 4,4'-bispiperidine central linker, seen as a larger divalent central spacer than the trivalent *s*-triazine. Both dendritic structures **4** and **5** were isolated and purified by simple crystallisations.

2. Preliminary structural assignments

Besides synthetic and applied interest [5], dendritic melamines have received increased structural attention in the last period [8], [9].

Starting from the pioneering works of Katritzky, Ghiviriga [8a-c] *et al*. [8d-g] focused on restricted rotations about the C(*s*-triazine)-N(exocyclic) partial double bonds, the current concepts with respect to this expected hindered mobility comprise a more concise terminology. Thus, the above connections are seen by us as (pro)diastereomerism axis [2a, 2b] promoting, in some cases, chirality [2a] or, if dendritically exacerbated, an entire "dendrimeric choreography" [9].

For the present communication, we will limit our discussion to the first isolated intermediate, chlorodiamino-*s*-triazine **2b** and the target dendrimer **5**.

At room temperature, NMR spectra of compound **2b** revealed its frozen rotamerism about C(*s*-triazine)-N(exocyclic) partial double bonds, C-4-N-8' (axis of prodiastereomerism[**]) and C-6-N(serinol) (axis of diastereomerism) as two blocked rotational diastereomers, **2b**-*syn* (minor) and **2b**-*anti* (major) (Figure 1). We discriminated the *anti vs. syn* rotamers by taken into account the strong dipole moment induced by the remainder chlorine substituent at C-2 [2a, 2b, 4c, 9]

[**] C-4-N-8' is also an axis of chirality, see ref. [2a] (to be discussed in the full paper).

creating a more deshielding influence of the protons NH in the **2b**-*anti* environment. *Mutatis-mutandis* the resonance of hydroxyl protons in rotamer **2b**-*anti* was located upfield with respect to **2b**-*syn*.

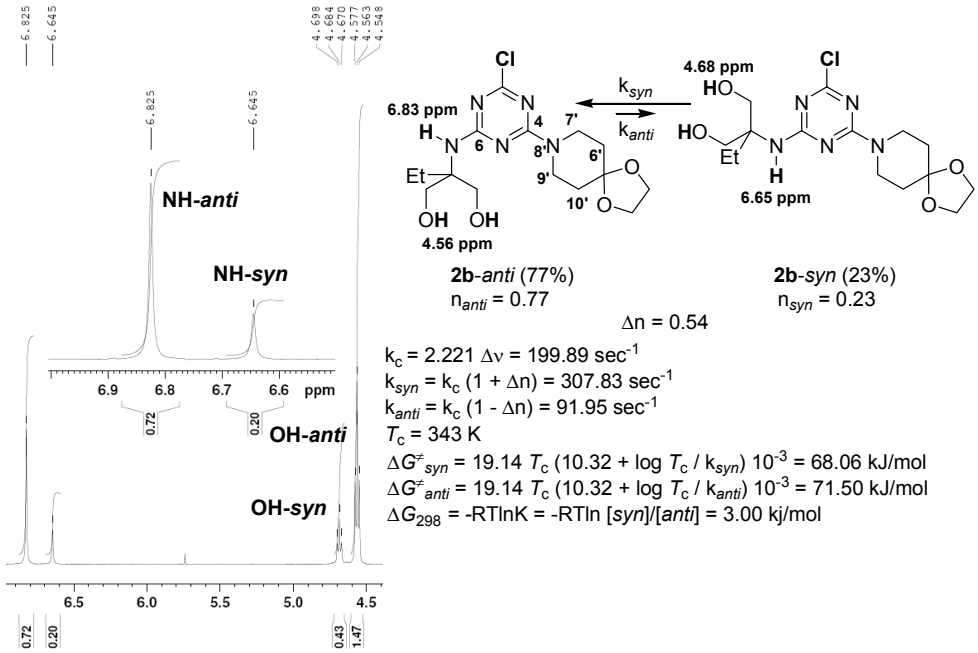

Figure 1. Detailed ^{1}H NMR spectrum (400 MHz, [D_6]DMSO, 293 K) of frozen rotamers of compound **2b**

Evidently, the ^{13}C NMR spectrum exhibited two sets of δ values for almost all positions of the **2b**(*anti* + *syn*) rotameric mixture. For example, although rotamerism about the axis of prodiastereomerism C-4-N-8' was not clearly observed in the ^{1}H NMR spectrum, on 100 MHz time scale, piperidine carbons C-7' *vs.* C-9' and C-6' *vs.* C-10' in the major as detectable **2b**-*anti* rotamer were diastereotopic, Δδ = 0.23 and 0.29 ppm respectively.

By rising the temperature up to 343 K, compound **2b** reached, at 353 K, the fast exchange status between unequally populated sites as freely rotating structure [10a]. Taking into account Eliel's *et al*. recommended precautions [10b], calculation based on Eyring equations [10a] applied for unequally two terms populated systems [10c] provided plausible data of the rotational barriers about the bond C-6-N(serinol) as Enthalpies of Activation $\Delta G^{\neq}$ [2a, 8]. Indeed, the $\Delta G_{298} = \Delta G^{\neq}_{anti} - \Delta G^{\neq}_{syn}$ value was 3.43 kJ/mol *vs.* 3.00 kJ/mol issued from classical two terms equilibrium relationship (Figure 1).

The ΔG *anti vs. syn* at 343 K and up could be not determined since, upon heating, NH protons changed their character, from an “amide” (6.83 - – 6.65 ppm, “rigid” protons) to an “amine” one (6.41 ppm, “mobile” protons).

All these complex rotational phenomena disappeared in the case of the much less π-deficient melamine **2c** which, at room temperature, already displayed a slow exchange status between unequal populated sites.

The mass spectrum of the dendrimer **5** fully confirmed the designed structure (Figure 2).

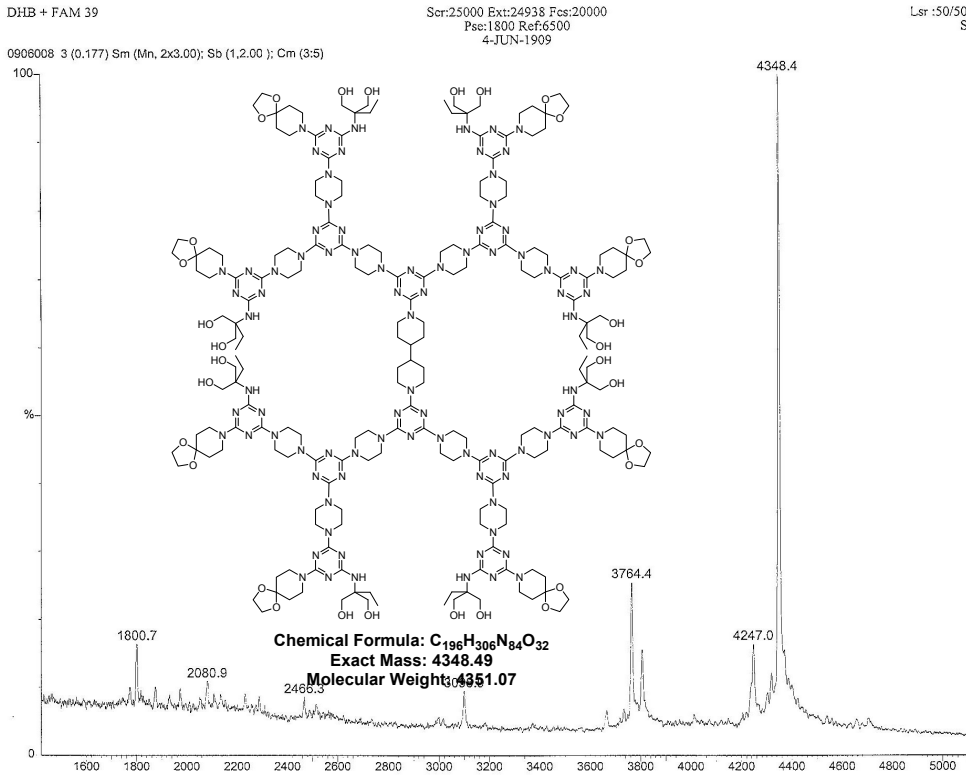

Figure 2. Mass Spectrum of compound **5** (Linear MALDI+ in 2,5-dihydroxybenzoic acid)

The ^{1}H NMR spectrum of **5** (Figure 3) recorded at 353 K indicated for this macromolecule a complex appearance. From rotational point of view, the six membered saturated heterocyclic rings were still in a slow exchange status between unequal populated sites, at least with respect to the ten piperidine peripheral and central units (see the broad signal assigned to the 42 protons at 1.61 ppm). In contrast, the geminal anisochrony of the sixteen peripheral hydroxymethylene groups is clearly visible in the region 3.5 – 3.7 ppm.

In ^{13}QC NMR spectrum, (Figure 4) from 196 carbon atoms, 194 were assignable. Only the two C-4, -4' carbons of the central 4,4'-bispiperidine linker remained obscured.

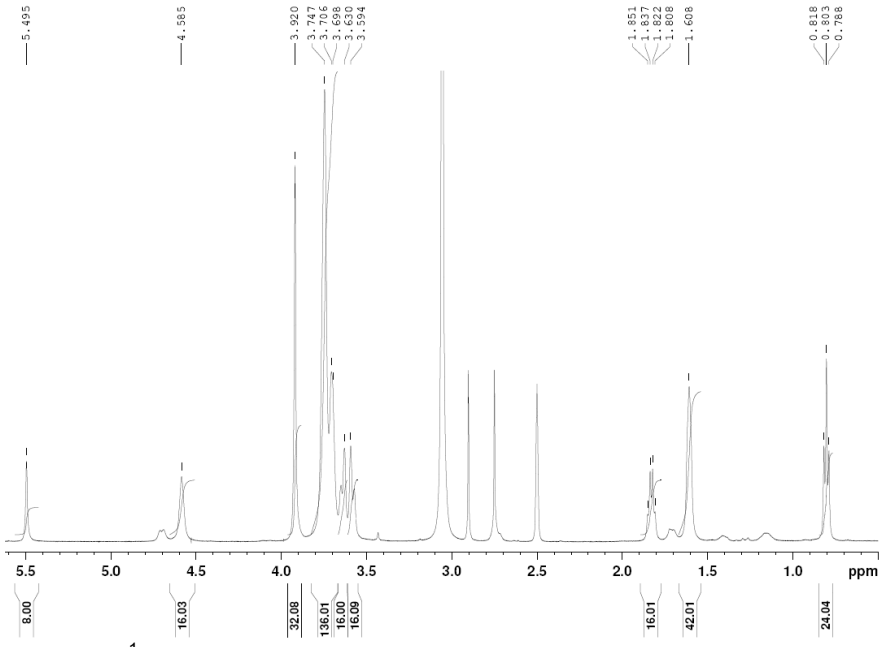

Figure 3. ^{1}H NMR spectrum of compound **5** (500 MHz, [D_6]DMSO, 353 K)

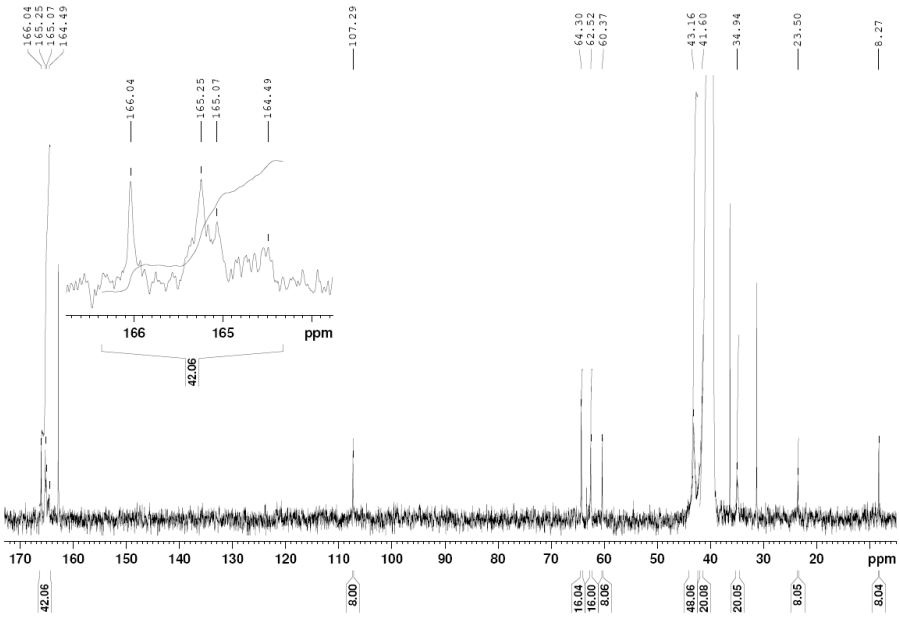

Figure 4. ^{13}QC NMR spectrum of compound **5** (125 MHz, [D_6]DMSO, 298 K)

The signal located at 41.6 ppm (20 carbon atoms) accounts for sixteen piperidine methylenes of the eight spiranic peripheral groups and four piperidine methylenes of the central 4,4'-bispiperidine linker. They are placed at the α-positions with respect to the heterocyclic nitrogens. Accordingly, the signal located at 34.9 ppm discloses the other 20 carbon atoms of the peripheral and central piperidine methylenes located at the β-positions *vs.* azaatom.

Both ^{1}H and ^{13}C NMR spectra also evidenced the presence of DMF, the reaction solvent (Scheme 2), despite of very careful final manipulation of the product. For the moment, we are unable to distinguish between problems of drying the compound or encapsulating phenomena.

CONCLUSIONS

We realised the concise synthesis of the first dimeric G-2 melamine dendrimer comprising, in tandem, eight C-2-substituted serinolic motifs and eight masked piperidone units as peripheral groups. The overall yield was optimised at 19%. More developments *vs.* inherent restrictions of this convergent strategy will be published in due course.

EXPERIMENTAL SECTION

General. Conventional NMR spectra were recorded on a Bruker® AM 300 instrument operating at 300 and 75 MHz for ^{1}H and ^{13}C nuclei respectively. Bruker® AV400 and DMX500 instruments, operating at 400 (500) and 100 (125) MHz for ^{1}H and ^{13}C nuclei respectively, were used for DNMR and QC experiments. All NMR spectra were measured in anhydrous commercially available deuteriated solvents. No $SiMe_4$ was added; chemical shifts were measured against the solvent peak. TLC was performed by using aluminium sheets with silica gel 60 F_{254} (Merck®); flash column chromatography was conducted on Silica gel Si 60 (40–63 μm, Merck®). Microanalyses were performed on a Carlo Erba® CHNOS 1160 apparatus. Mass spectra (MS) were recorded on Bruker® Esquire Instrument.

*Preparation of compound **2b***

2-Amino-2-hydroxymethylbutanol (*"ethylserinol"*) [1.67 g 80%, Aldrich® (Cat. No. 38, 168-3) 1.34 g 100%, 11.2 mmol] and potassium carbonate (> 99%, 1.55 g 100%, 11.2 mmol, S.C.CRISTAL R CHIM SRL) were suspended with stirring in anh. THF (80 mL) then cooled at 0 °C. At this temperature, cyanuric chloride (> 99%, 2.07 g 100%, 11.2 mmol, Merck®, Cat. No. S4249515 526) as anh. THF (20 mL) solution was rapidly injected and the resulted suspension was let to reach room temperature and stirred for additional 24 hrs. At this stage, TLC monitoring (eluent toluene: isopropanol 2: 1 v/v, visualisation in UV 254 nm) indicated the presence of a single compound. Water (10 mL) and potassium

carbonate (3.10 g, 22.4 mmol) were added and the resulted suspension was cooled at (-10) – (-15) ^{o}C. At this temperature, fine powdered 1,4-dioxa-8-azaspiro[4.5]decane (2.01 g, 11.2 mmol) was added portionwise as 5 equal portions each 90 min. The reaction mixture was stirred at -10 ^{o}C for additional 24 hrs. then let to reach room temperature. The suspension was filtered off and minerals were well washed with anh. THF. The organic filtrate was taken and treated under vigorous stirring, with chloroform (150 mL) and water (75 mL). After separation, the organic layer was washed with water to neutrality (× 25 mL) then the combined aqueous layer was extracted with chloroform (2 × 40 mL). The combined organic layer was dried over sodium sulphate, filtered off and evaporated under reduced pressure to provide the crude material (4.10 g). This was separated by column chromatography (eluent toluene: isopropanol 4:1 v/v) to yield 2.41 g compound **2b** and 0.263 g compound **2c** as side product.

2-Chloro-4-(1,4-dioxa-8-azaspiro[4.5]decan-8-ylamino)-4-[1-hydroxy-2- (hydroxymethyl)but-2-ylamino]-s-triazine ***2b***; white crystalline powder; yield 58%; m.p. = 147.4-152.7 ^{o}C; Anal. calcd. for $C_{15}H_{24}ClN_5O_4$: C, 48.19; H, 6.47; N, 18.73%; found: C, 48.44; H, 6.16; N, 18.66%. R_f (80% toluene/isopropanol) = 0.65. ^{1}H NMR (400 MHz, 293 K, [D$_6$]DMSO) 0.73 ppm (3 H, m, CH_2CH_3, *anti* + *syn*), 1.62 ppm (4 H, m, H-6', -10'-ax., -eq., spirane, *anti* + *syn*), 1.71 (2 H, q, ^{3}J = 7.4 Hz, CH_2CH_3, *anti* + *syn*), 3.46 ppm (2 H, dd, ^{2}J = 10.8 Hz, ^{3}J = 6.0 Hz, CH_2OH, *anti* + *syn*), 3.65 ppm (2 H, dd, ^{2}J = 10.8 Hz, ^{3}J = 6.0 Hz, CH_2OH, *anti* + *syn*), 3.72 ppm (4 H, t, ^{3}J = 5.4 Hz, H-7', -9'-ax., -eq., spirane, *anti* + *syn*), 3.91 ppm (4 H, s, H-2', -3', spirane, *anti* + *syn*), 4.56 ppm (1.47 H, dd as t , ^{3}J = 5.8 Hz, CH_2OH, *anti*), 4.68 ppm (0.43 H, dd as t , ^{3}J = 5.6 Hz, CH_2OH, *syn*), 6.65 ppm (0.20 H, bs, NH, *syn*), 6.83 (0.72 H, bs, NH, *anti*). ^{1}H NMR (400 MHz, 353 K, [D$_6$]DMSO) 0.79 ppm (3 H, t, ^{3}J = 7.4 Hz, CH_2CH_3), 1.66 ppm (2 H, dt, ^{3}J = 5.8, 3.8 Hz, H-6', -10'-ax., -eq., spirane), 1.65 ppm (2 H, dt, ^{3}J = 5.6, 4.0 Hz, H-6', - 10'-ax, -eq., spirane), 1.79 (2 H, q, ^{3}J = 7.4 Hz, CH_2CH_3), 3.57 ppm (2 H, dd, ^{2}J = 11.0 Hz, ^{3}J = 5.4 Hz, CH_2OH), 3.68 ppm (2 H, dd, ^{2}J = 10.8 Hz, ^{3}J = 5.6 Hz, CH_2OH), 3.765 ppm (2 H, dt, ^{3}J = 7.0, 5.0 Hz, H-7', -9'-ax., -eq., spirane), 3.760 ppm (2 H, dt, ^{3}J = 5.6, 4.0 Hz, H-7', -9'-ax., -eq., spirane), 3.93 ppm (4 H, s, H-2', -3', spirane), 4.40 ppm (2 H, bs, CH_2OH), 6.41 ppm (1 H, bs, NH). ^{13}C NMR (100 MHz, 293 K, [D$_6$]DMSO, ppm) 7.9 (1 C, CH_2CH_3, *anti*), 8.1 (1 C, CH_2CH_3, *syn*), 22.4 (1 C, CH_2CH_3, *anti*), 23.0 (1 C, CH_2CH_3, *syn*), 34.9, 34.8, 34.6 (4 C, C-6', -10', spirane, *anti* + *syn*), 42.1, 41.9, 41.4 (4 C, C-7', -9', spirane, *anti* + *syn*), 61.5, 60.8 (4 C, CH_2OH, *anti* + *syn*), 61.4 (2 C, Cq, serinol, *anti* + *syn*), 64.4 (4 C, C-2', -3', spirane, *anti* + *syn*), 106.9 (2 C, C-5', spirane, *anti* + *syn*), 163.6 (1 C, C-4, *s*-triazine, *syn*), 164.2 (1 C, C-4, *s*-triazine, *anti*), 165.1 (1 C, C-6, *s*-triazine, *anti*), 165.8 (1 C, C-4, *syn*), 168.4 (1 C, C-2, *s*-triazine, *anti*), 168.6 (1 C, C-2, *s*-triazine, *syn*).

2,4-Bis(1,4-dioxa-8-azaspiro[4.5]decan-8-ylamino)-6-[1-hydroxy-2-(hydroxy methyl)but-2-ylamino]-s-triazine ***2c***; yellowish crystalline powder; yield 5 %; m.p. = 143.1 – 146.8 ^{o}C; Anal. calcd. for $C_{22}H_{36}N_6O_6$: C, 54.99; H, 7.55; N,

17.49%; found: C, 55.22; H, 7.88; N, 17.55%. R_f (80% toluene/isopropanol) = 0.60 ^{1}H NMR (400 MHz, 298 K, [D$_6$]DMSO) 0.73 ppm (3 H, t, ^3J = 7.4 Hz, CH_2CH_3), 1.57 ppm (8 H, t, ^3J = 5.2 Hz, H-6', -6", -10', -10"-ax., -eq., spirane), 1.77 (2 H, q, ^3J = 7.4 Hz, CH_2CH_3), 3.50 ppm (2 H, dd, ^2J = 10.6 Hz, ^3J = 5.4 Hz, CH_2OH), 3.58 ppm (2 H, dd, ^2J = 10.6 Hz, ^3J = 5.8 Hz, CH_2OH), 3.71 ppm (8 H, t, ^3J = 5.6 Hz, H-7', -7", -9', -9"-ax., -eq., spirane), 3.90 ppm (8 H, s, H-2', -2", -3', -3" spirane), 4.73 ppm (2 H, dd as t , ^3J = 5.8 Hz, CH_2OH), 5.60 ppm (1 H, bs, NH). ^{1}H NMR (400 MHz, 353 K, [D$_6$]DMSO) 0.79 ppm (3 H, t, ^3J = 7.6 Hz, CH_2CH_3), 1.60 ppm (8 H, t, ^3J = 5.6 Hz, H-6', -6", -10', -10"-ax., -eq., spirane), 1.81 (2 H, q, ^3J = 7.4 Hz, CH_2CH_3), 3.57 ppm (2 H, d, ^2J = 10.8 Hz, CH_2OH), 3.63 ppm (2 H, dd, ^2J = 10.4 Hz, CH_2OH), 3.73 ppm (8 H, t, ^3J = 5.8 Hz, H-7', -7", -9', -9"-ax., -eq., spirane), 3.92 ppm (8 H, s, H-2', -2", -3', -3" spirane), 4.56 ppm (2 H, bs, CH_2OH), 5.47 ppm (1 H, bs, NH). ^{13}C NMR (100 MHz, 298 K, [D$_6$]DMSO, ppm) 8.2 (1 C, CH_2CH_3), 23.5 (1 C, CH_2CH_3), 34.8 (4 C, C-6', -6", -10', -10"), 41.5, 41.0 (4 C, C-7', -7", -9', -9", spirane), 60.3 (2 C, Cq, serinol), 62.6 (2 C, CH_2OH), 64.2 (4 C, C-2', -2", -3', -3", spirane), 107.3 (2 C, C-5', -5", spirane), 164.7 (1 C, C-2, -4, *s*-triazine), 166.1 (1 C, C-6, *s*-triazine).

Preparation of compound ***5***

Perfectly dried G-2 dendron **4** (analytically weighted 0.515 g, 0.242 mmol), freshly prepared and perfectly dried 4,4'-bispiperidine (analytically weighted 0.0194 g, 0.115 mmol), potassium carbonate (analytically weighted 0.035 g, 0.253 mmol) and freshly distilled dimethylformamide (DMF) (25 mL) were mixed together and the resulting suspension was heated at 100 ^{o}C (CARE! Avoid refluxing DMF to prevent the solvent decomposition!) for 35 hrs. (TLC monitoring, eluent chloroform: ethanol 3:1 v/v, visualisation in UV 254 nm). DMF was distilled under reduced pressure and the solid residue was taken with distilled water (10 mL), stirred at room temperature for 30 min. then filtered off. The crude product was well washed with distilled water (× 5 mL) to neutrality then dried at 70 ^{o}C to constant weight. The crude product was dissolved in distilled DMF (2 mL), then crystallised by adding anh. diethyl ether (6 mL). The resulted suspension was cooled at – 20 ^{o}C for 24 hrs., filtered off and well washed with anh. diethyl ether. After drying at 70 ^{o}C to constant weight, 0.345 g (0.079 mmol) compound **5** were obtained.

4,4'-{4,6-Bis{4-{4,6-bis{4-{4-(1,4-dioxa-8-azaspiro[4.5]decan-8-ylamino)-6-[1-hydroxy-2-(hydroxymethyl)but-2-ylamino]-s-triazin-2-yl}-piperazin-1-yl}-s-triazin-2-yl}-piperazin-1-yl}-s-triazin-2-yl}-bispiperidine **5**; white amorphous powder; yield 69 %; m.p. = 260 - 261 ^{o}C. R_f (75% chloroform/ethanol) = 0.75. ^{1}H NMR (500 MHz, 298 K, [D$_6$]DMSO) 0.75 ppm (24 H, bs, CH_2CH_3), 1.58, 1.79 ppm (58 H, 2 × bs as: 16 H, CH_2CH_3; 32 H, H-6, -10-ax., -eq., spirane; 10 H, H-3, -5, -3', -5'-ax., -eq., H-4, -4', 4,4'-bispiperidine), 3.91 – 3.52 ppm (200 H, bm, as: 96 H, piperazine; 32 H, H-7, -9-ax., -eq., spirane; 32 H, H-2, -3, spirane; 32 H, CH_2OH; 8 H, H-2, -6, -2', -6'-ax., -eq., 4,4'-bispiperidine),

4.76 ppm (16 H, bs, CH_2OH), 5.63 ppm (8 H, bs, NH); ^{1}H NMR (500 MHz, 353 K, [D_6]DMSO) 0.80 ppm (24 H, t, ^3J = 7.5 Hz, CH_2CH_3), 1.61 ppm (42 H, bs, as: 32 H, bs, H-6, -10-ax., -eq., spirane; 10 H, H-3, -5, -3', -5'-ax., eq., H-4, -4', 4,4'-bispiperidine), 1.85 (16 H, q, ^3J = 7.2 Hz, CH_2CH_3), 3.59 ppm (16 H, d, ^2J = 10.5 Hz, CH_2OH), 3.63 ppm (16 H, d, ^2J = 10.0 Hz, CH_2OH), 3.75 – 3.59 ppm (136 H, bm, as: 96 H, piperazine; 32 H, H-7, -9-ax., -eq., spirane; 8 H, H-2, -6, -2', -6'-ax., -eq., 4,4'-bispiperidine), 3.92 (32 H, s, H-2, -3, spirane), 4.59 (16 H, bs, CH_2OH), 5.50 (8 H, bs, NH). ^{13}QC NMR (125 MHz, 298 K, [D_6]DMSO, ppm) 8.3 (8 C, CH_2CH_3), 23.5 (8 C, CH_2CH_3), 34.9 (20 C as 16 C, C-6, -10, spirane; 4 C, C-3, -3', -5, -5', 4,4'-bispiperidine), 41.6 (20 C as 16 C, C-7, -9, spirane; 4 C, C-2, -6, -2', -6', 4,4'-bispiperidine), 60.4 (8 C, Cq, serinol), 62.5 (16 C, CH_2OH), 64.3 (16 C, C-2, -3, spirane), 107.3 (8 C, C-5, spirane), 164.5, 165.1, 165.3, 166.0 (42 C, *s*-triazine). MS (Linear MALDI+ in 2,5-dihydroxybenzoic acid): 4348.4 (100%) [M^+].

ACKNOWLEDGMENTS

Financial support from Grant provided by the *National Council of Scientific Research* C.N.C.S.I.S. (1482) is gratefully acknowledged. F. P. also thanks C.N.C.S.I.S. for the Doctoral Fellowship.

REFERENCES

1. F. Popa, I. Simioanca, M. Pintea, M. Fazekas, L. Gratecap, C. Berghian, C. Batiu, M. Darabantu, *Studia Universitatis Babes-Bolyai, Chemia*, **2008**, LIII, *4*, 5.
2. a) M. Pintea, M. Fazekas, P. Lameiras, I. Cadis, C. Berghian, I. Silaghi-Dumitrescu, F. Popa, C. Bele, N. Plé, M. Darabantu, *Tetrahedron,* **2008**, *64*, 8851; b) M. Fazekas, M. Pintea, P. Lameiras, A. Lesur, C. Berghian, I. Silaghi-Dumitrescu, N. Plé, M. Darabantu, *Eur. J. Org. Chem.*, **2008**, 2473; c) M. Darabantu, M. Pintea, M. Fazekas, P. Lameiras, C. Berghian, I. Delhom, I. Silaghi-Dumitrescu, N. Plé, A. Turck, *Letters in Organic Chemistry*, **2006**, *3*, 905.
3. a) D. A. Tomalia, *Aldrichimica Acta,* **2004***, 37,* 39; b) F. Vögtle, G. Richard, N. Werner, *Dendrimer Chemistry (Concepts, Syntheses, Properties, Applications)*, WILEY-VCH Verlag Gmbh & Co. KGaA, **2009**, pp. 7-22, 25.
4. a) G. R. Newkome, Z. –Q. Yao, G. R. Baker, V. K. Gupta, *J. Org. Chem.*, **1985**, *50*, 2003; b) G. R. Newkome, X. Lin, C. D. Weis, *Tetrahedron Asymmetry*, **1991**, *10*, 957; c) B. A. Hernandez, V. Chang, I. Villanueva, M. D. Heagy, *J. Org. Chem.*, **1999**, *64*, 6905; d) M. Plevoets, F. Vögtle, L. De Cola, V. Balzani, *New. J. Chem.*, **1999**, *23*, 63; e) J. Issberner, F. Vögtle, L. De Cola, V. Balzani, *Chem. Eur. J.*, **1997**, *3*, 706; f) G. R. Newkome, E. He, C. N. Moorefield, *Chem. Rev.*, **1999**, *99*, 1689; g) S. Mattei, P. Seiler, F. Diederich, V. Gramlich, *Helv. Chim. Acta*, **1995**, *78*, 1904; h) S. Mattei, P. Wallimann, B. Kenda, W. Amrein, F. Diederich, *Helv. Chim. Acta*, **1997**, *80*, 2391;

i) P. Wallimann, P. Seiler, F. Diederich, *Helv. Chim. Acta*, **1996**, *79*, 779; j) C.M. Cardona, R. E. Gawley, *J. Org. Chem.*, **2002**, *67*, 1411; k) G. R. Newcome, X. Lin, *Macomolecules*, **1991**, *24*, 1443; k) A. Dupraz, P. Guy, C. Dupuy, *Tetrahedron Lett.*, **1996**, *37*, 1237; l) I. Bury, B. Heinrich, C. Bourgogne, D. Guillon, B. Donnio, *Chem. Eur. J.*, **2006**, *12*, 8396.

5. a) W. Zhang, D. T. Nowlan, L. M. Thomson, M. W. Lackowski, E. E. Simanek, *J. Am. Chem. Soc.*, **2001**, *123*, 8914; b) M. B. Steffensen, E. E. Simanek, *Angew. Chem. Int. Ed.*, **2004**, *43*, 5178; c) J. Lim, E. E. Simanek, *Molecular Pharmaceutics*, **2005**, *2*, 273; d) G. R. Newcome, J. Gross, C. N. Moorefield, B. D. Woosley, *Chem. Commun.*, **1997**, 515; e) A. P. Umali, E. E. Simanek, *Org. Lett.*, **2003**, *5*, 1245; f) H. T. Chen, M. F. Neerman, A. R. Parrish, E. E. Simanek, *J. Am. Chem. Soc.*, **2004**, *126*, 10044; g) L. –L. Lai, L. –Y. Wang, C. -H. Lee, C. Y. Lin, K. –L. Cheng, *Org. Lett.*, **2006**, *8*, 1541; h) E. J. Acosta, S. O. Gonzalez, E. E. Simanek, *J. Polym. Sci. Part A.*, **2005**, *43*, 168; i) W. Zhang, S. O. Gonzalez, E. E. Simanek, *Macromolecules*, **2002**, *35*, 9015; j) E. Hollink, E. E. Simanek, *Org. Lett.*, **2006**, *8*, 2293; k) M. F. Neerman, W. Zhang, A. R. Parrish, E. E. Simanek, *Int. J. Pharm.*, **2004**, *281*, 129; l) L. –L. Lai, C. –H. Lee, L. –Y. Wang, K. L. Cheng, H. –F. Hsu, *J. Org. Chem.,* **2008**, *73*, 485.
6. Z. Antal, C. Batiu, M. Darabantu, *Studia Universitatis Babes-Bolyai, Chemia*, **2008**, LIII, *4*, 51.
7. a) P. –G. de Gennes, H. Hervet, *J. Phys. Lett. Fr.*, **1983**, *44*, L351; b) D. A. Tomalia, A. Naylor, W. A. Goddard III, *Angew. Chem.*, **1990**, *102*, 119; c) D. A. Tomalia, A. Naylor, W. A. Goddard III, *Angew. Chem. Int. Ed.*, **1990**, *29*, 138.
8. a) A. R. Katritzky, I. Ghiviriga, D. C. Oniciu, A. Barkock, *J. Chem. Soc. Perkin Trans. 2*, **1995**, 785; b) A. R. Katritzky, I. Ghiviriga, P. G. Steel, D. C. Oniciu, *J. Chem. Soc. Perkin Trans. 2*, **1996**, 443; c) I. Ghiviriga, D. C. Oniciu, *Chem. Commun.*, **2002**, *22*, 2718; d) M. Amm, N. Platzer, J. Guilhem, J. P. Bouchet, J. P. Volland, *Magn. Reson. Chem.*, **1998**, *36*, 587; e) M. Amm, N. Platzer, J. P. Bouchet, J. P. Volland, *Magn. Reson. Chem.*, **2001**, *39*, 77; f) H. E. Birkett, R. K. Harris, P. Hodgkinson, K. Carr, M. H. Charlton, J. C. Cherryman, A. M. Chippendale, R. P. Glover, *Magn. Reson. Chem.*, **2000**, *38*, 504; g) H. E. Birkett, J. C. Cherryman, A. M. Chippendale, J. O. S. Evans, R. K. Harris, M. James, I. J. King, G. Mc. Pherson, *Magn. Reson. Chem.*, **2003**, *41,* 324.
9. X. K. Moreno, E. E. Simanek, *Macromolecules* **2008**, *41*, 4108.
10. a) H. Friebolin, *Basic One- and Two Dimensional NMR Spectroscopy*; VCH Verlagsgesellschaft /VCH: Weinheim/New York **1991**; p.93, 263; b) E. L. Eliel, H. S. Wilen, *Stereochemistry of the Organic Compounds*; John Wiley & Sons, Inc. **1994**; pp 221–239, 488–507, 678, 788, 1210; c) H. Shanan-Atidi, K. H. Bar-Eli, *J. Phys. Chem.*, **1970**,*74*, 961.

STUDIA UNIVERSITATIS BABEŞ-BOLYAI, CHEMIA, LIV, 4, 2009

STUDY ON THE INHIBITION OF BRIGGS-RAUSCHER OSCILLATING REACTION

LÉNÁRD-ISTVÁN CSEPEI[a,b], CSABA BOLLA[a]

ABSTRACT: We present the results concerning our exploratory study on the effect of four compounds (ascorbic acid, tartaric acid, pyrogallol and salicylic acid) on the Briggs-Rauscher oscillating reaction. In case of ascorbic acid, tartaric acid and pyrogallol, a linear increase of the inhibition time with the concentration of these substances was observed. We also paid attention on the changes of color and redox potential of the reacting mixture in the moment of addition of the above mentioned compounds. The observations showed that ascorbic acid and tartaric acid manifest an inhibitory effect through their strong reducing properties. Pyrogallol acts like other polyphenolic antioxidants studied before. Salicylic acid, unlike all of the phenolic and polyphenolic compounds described before, did not stop instantly the oscillations.

Keywords: Briggs-Rauscher oscillating reaction, inhibitory effect, ascorbic acid, tartaric acid, pyrogallol, salicylic acid

INTRODUCTION

The Briggs-Rauscher (BR) reaction is one of the most spectacular oscillating reactions, which is a hybrid of the well-known Belousov-Zhabotinskii and the Bray-Liebhafsky reactions. The net chemical transformation of the BR reaction is the oxidation and iodination of malonic acid by hydrogen-peroxide and iodate ion, catalyzed by manganous ion in acidic media [1]. The concentration of intermediates (I_2, I^-, HOI, HIO_2, IO_2•, HOO•, etc.) presents more than one extreme point (i.e.: maximum and minimum) in time. The first mechanistic investigations were carried out by Cooke [2], Noyes and Furrow [3-5], De Kepper and Epstein [6], respectively. As a result of these studies, 30 elementary steps have been identified. Two almost identical skeleton mechanisms were proposed, which described qualitatively well the nonlinear behavior of the reacting system in a batch reactor [5] and in a continuous-flow stirred tank reactor (CSTR) [6]. However there was a discrepancy between the experimental

[a] *Universitatea Babeş-Bolyai, Facultatea de Chimie şi Inginerie Chimică, Str. Kogălniceanu, Nr. 1, RO-400084 Cluj-Napoca, Romania, csbolla@chem.ubbcluj.ro*

[b] *Fritz Haber Institute der Max Planck Gesellschaft, Faradayweg 4-6, 14195 Berlin, Deutschland, cslenard@gmail.com*

and the simulated quantitative features (period time, concentration ranges for different intermediates and the cross-shaped phase diagram) of the reaction [5, 6]. Furrow has recognized that the hydroperoxyl radical mediates the autocatalytic HIO_2 production and plays an important role in the reaction [7]. The modification of the skeleton mechanism by inclusion of the elementary steps involving IO_2• and HOO• improved the predicting ability of the model [7, 8].

Cervellati *et al*. reported that the addition of mono- and polyphenolic compounds to the active mixture causes a temporary but instant cessation of oscillations [9, 10]. The time elapsed between the cessation and the subsequent regeneration of the oscillatory regime was denominated as inhibition time. A linear correlation was found between the concentration and the inhibition time for every phenolic substance added in the BR-mixture. The inhibitory effect was accounted for a fast reaction involving the phenolic compound and HOO• radical. Since polyphenols are known to be effective free radical scavengers, they reduce drastically the concentration of HOO• in the BR-mixture. As soon as the antioxidant is totally consumed, the HOO• concentration rises up to the critical range, where the oscillations reappear. The side-reaction between the phenolic compounds and the oxidative species of the BR mixture was also taken into account [10, 11]. For quantitative modeling of the inhibitory effect, the modified skeleton model [8] was complemented with the steps involving the antioxidant [11]. Based on these results it was possible to develop a new analytical method for determination of the antioxidant activity of free radical scavengers.

In contrast with the other antioxidant assays (Trolox Equivalent Antioxidant Capacity /TEAC/, Total Radical Trapping Parameter /TRAP/, Ferric Ion Reducing Antioxidant Parameter /FRAP/, and Oxygen Radical Absorbance Capacity /ORAC/), in the method proposed by Cervellati *et al*. the antioxidants react with HOO• radical [12]. This radical is a reactive oxygen metabolite produced in the human body, to which oxidative stress, cell damage, aging, cancer and other diseases are associated [13, 14]. Therefore the method validated by Cervellati *et al*. gives more reliable data with respect to the reactivity of the antioxidants with reactive oxygen species (ROS).

Furrow *et al*. found that the better known antioxidant, ascorbic acid acts different than the polyphenols. Being a strong reducing agent, the ascorbic acid is oxidized instantly by the reactive oxy-iodide species when is added to the BR-mixture, while iodide ion is produced. An inhibitory effect of iodide ion on the BR-reaction was observed. The qualitative mechanistic interpretation of inhibitory effect of iodide ion was also given [15]. Since the ascorbic acid added to the BR-mixture does not react with HOO• radical, it was concluded that the BR-method is not suitable to determine the antioxidant activity of ascorbic acid.

RESULTS AND DISCUSSION

The effect of ascorbic acid on the BR-reaction

Foremost we tried to reproduce the experiments made by Furrow *et al*. [15]. When we added ascorbic acid solution, the color of the oscillating BR-mixture changed suddenly to brown. At the same time the redox potential rise (ΔE) instantly and then decreased gradually during the inhibition time (Fig.1). When starch was also present in the BR mixture, a sudden deep blue coloration was noticed after addition of the ascorbic acid solution. The blue color faded out gradually during the inhibition period. Nor the appearance of the brown color, neither the redox potential rise was noticed by Furrow *et al.* in the moment of ascorbic acid solution to the BR-mixture.

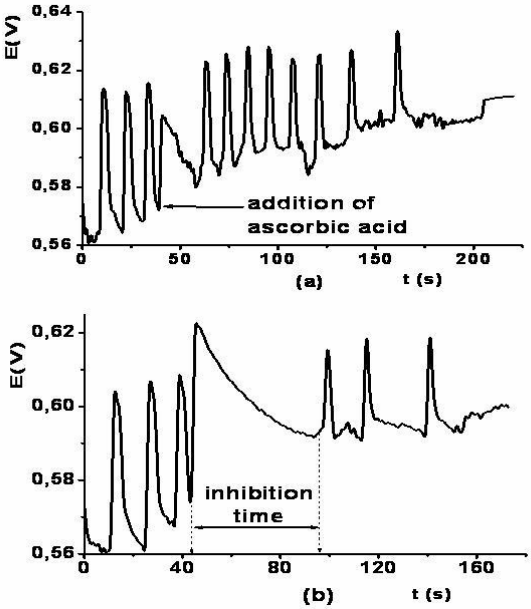

Figure 1. Effect of 3,36 mM (a) and 7,70 mM (b) ascorbic acid on the BR-reaction.

Our observation suggests that there is a rapid and significant I_3^- production when ascorbic acid is added to the BR-mixture. We attribute the sudden change of the redox potential to the fast and coupled redox reaction steps involving ascorbic acid and the oxidizing iodide species (IO_3^-, HOI, HIO_2 and I_2) of the BR-mixture. However the reaction has been monitored using a bright platinum electrode, which is reversible for every redox couple existing in the solution, the measured potential is a mixed potential (i.e. every redox system contributes to the measured potential). Therefore it is not possible to assign directly the potential change to any change of concentration of the species.

The reproducibility of the inhibition time was good. The inhibition time and the magnitude of the redox potential change (∆E) varies linearly with the ascorbic acid concentration within the 3,36−9,97 mM interval (Figure 2.).

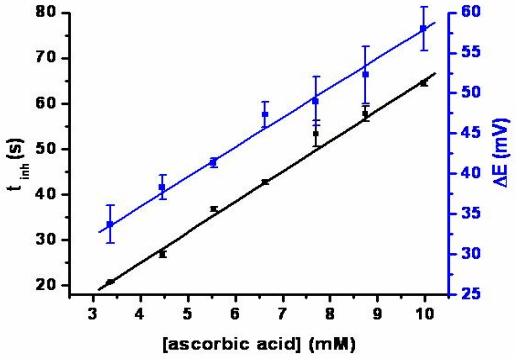

Figure 2. Plot of the inhibition time and the redox potential change against the concentration of ascorbic acid.

$$t_{inh} = (6,7\pm0,1)\cdot[ASC] - (1,8\pm0,5) \quad R^2=0,9985 \quad (1)$$
$$\Delta E = (3,7\pm0,3)\cdot[ASC] - (21,2\pm1,5) \quad R^2=0,9770 \quad (2)$$

If the ascorbic acid concentration was higher than 9,97 mM, the oscillations did not restart after a long time (more than 350 s), however the color of the mixture remained brown or blue (depending on the absence or presence of starch in the initial BR-mixture).

The features of restarted oscillations (amplitude, period) were different of those observed in the non-inhibited reactions. The amplitude of the restarted oscillations were smaller, the period length was longer and steadily increased in the successive periods. These latter observations are in accordance with those reported by Furrow *et al.* [15].

The effect of tartaric acid on the BR-reaction

Since Cervellati *et al*. has shown that the hydroxyl groups are responsible for the antioxidant effect of mono- and polyphenols [9-11], we tried to find out whether a compound containing aliphatic hydroxyl group can inhibit the BR-reaction. Also the ascorbic acid contains two aliphatic hydroxyl groups, which are not affected by the oxidation. However it would be difficult to figure out whether these hydroxyl groups have any inhibitory effect [15]. Thus, we choose tartaric acid, a simple, bi-functional compound to our study. On the other hand this compound can be found in white wines as *trans*-caffeoyl-tartaric acid. Most of the antioxidant activity of the Riesling white wine was accounted for this ester and hydroxy-cinnamic acid derivatives [16]. However in the human stomach the *trans*-caffeoil-tartaric acid is hydrolysed by the gastric juice to caffeic acid and tartaric acid. The antioxidant activity

of caffeic acid is already known from the literature [10], but there is no information about the tartaric acid. Tartaric acid contains, like ascorbic acid, two aliphatic hydroxyl groups, and it is a reducing agent at the same time.

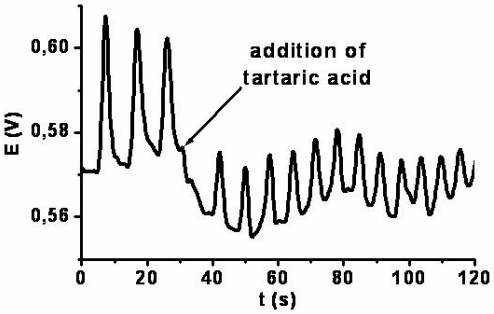

Figure 3. The effect of 10,2 mM tartaric acid on the BR-reaction.

We observed a drop of redox potential (∆E) in the moment of addition of tartaric acid, while the mixture remains colorless. The rapid change of redox potential suggests that a fast redox reaction involving tartaric acid and oxy-iodine species occurred. However compared to the experiments carried out with ascorbic acid, the main difference is that I_3^- was not observed. The more likely is that I^-, HOI or HIO_2 colorless oxy-iodine species were formed. If the concentration of these compounds exceeds a certain limit, they also perturb the oscillatory regime for a while [4, 5, 6, 15].

The inhibition time increased linearly with the concentration of the tartaric acid only within the range of 9,1-17,1 mM (Eq.3). At concentrations larger than 17,1 mM the oscillations did not restart at all.

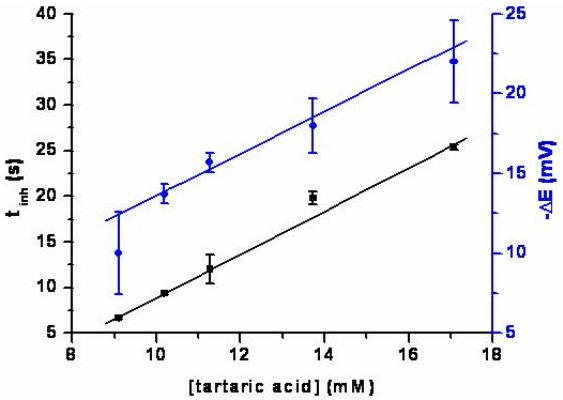

Figure 4. Plot of the inhibition time and the redox potential change against the concentration of tartaric acid.

t_{inh} = (2,4±0,1)·[tartaric acid] − (14,8±0,7) R^2=0,9972 (3)

−∆E = (1,3±0,3)·[tartaric acid] − (0,4±2,5) R^2=0,9180 (4)

The effect of pyrogallol on the BR-reaction

The third compound we studied was pyrogallol. This polyphenol can be prepared by decarboxylation of gallic acid, a naturally occurring organic acid which has an antioxidant activity. Addition of this pyrogallol to the oscillating mixture caused brown coloration and an inhibition time. No significant redox potential change has been noticed in the moment of addition of pyrogallol solution to the mixture, or during the inhibition period. The brown color faded out gradually during the inhibiton period. When starch was also present in the initial BR-mixture, no blue coloration was noted after addition of pyrogallol and/or during the inhibition period. Similarly to other polyphenolic compounds, pyrogallol appeared to be an effective inhibitor of the BR-reaction: it caused an inhibition time of 133,5 s at a concentration of 33 μM. The periods of the oscillations after the inhibition time were the same as those of non-inhibited reaction.

The pyrogallol is also a very strong reducing agent. Therefore the strong oxidants present in the BR reaction oxidized it instantly. However in this case the appearance of the brown color cannot be assigned to I_3^- production because of the following facts: pyrogallol was added to (i) acidic iodate, and (ii) acidic iodate and hydrogen peroxide mixture. In both cases a brown coloration has been observed.

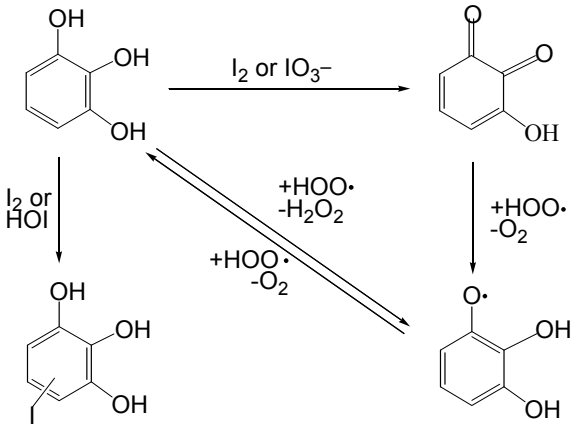

Scheme 1

This coloration did not disappear when tiosulphate solution has been added to the mixture, suggesting that the colored product was not I_3^-, the more likely an oxidized form of pyrogallol. On the other hand based on the stoechiometry, the production of I_3^- in large quantities can be excluded (i.e. the pyrogallol was added to the BR-mixture in the concentration range of several 10 μM which upon oxidation by the oxy-iodine species does not produce such large quantity of I_3^- which would cause a visible and durable coloration).

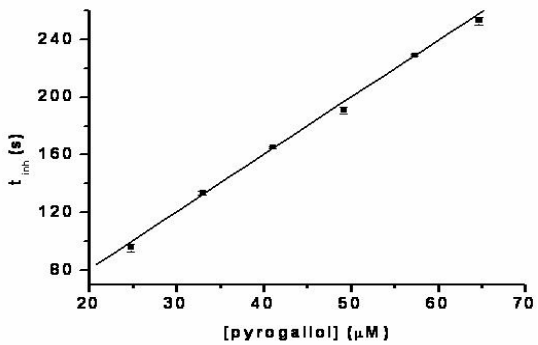

Figure 5. Plot of the inhibition time against the concentration of pyrogallol.

When pyrogallol is oxidized, the aromatic electronic structure is braked up. The product is an unsaturated cyclic di-oxo-compound with a planar structure. The hydroxyl groups in the 1 and 3 positions can not be oxidized, because after the breaking up of the aromatic ring it is not possible to reach a stable electronic structure, hence *meta*-quinones does not exist. Based on the same consideration, the simultaneous oxidation of each hydroxyl group is also impossible [11].

$$t_{inh} = (3{,}96\pm0{,}07)\cdot[\text{pyrogallol}] + (1{,}7\pm3{,}9) \quad R^2=0{,}9986 \quad (5)$$

Cervellati *et al.* pointed out that the quinone derivatives also have antioxidant activity [11]. The inhibitory effect of quinone derivatives is very complicated, and it is not yet fully unraveled. Based on thermodynamic considerations, the HOO· can reduce the quinone derivatives back to polyphenolic compounds. The inhibition time depends on the relative rates of the possible consecutive-parallel steps shown in Scheme 1.

The effect of salicylic acid on the BR-reaction

It was shown that monophenolic compounds (i.e.: 3-(4-hydroxy-3-metoxyphenyl)-prop-2-enoic acid and 4-hydroxy-3-metoxy-benzeneacetic acid) are as efficient inhibitors of the BR reaction as polyphenols [10]. We tried to inhibit the BR reaction with salicylic acid a very simple, naturally occurring monophenolic compound. In the few ten-fold μM concentration range this compound has no effect on the reaction. When we added in the BR mixture in the mM concentration range, we observed that the oscillations were not stopped at all, even at higher concentration they were not stopped immediately. However the amplitudes were progressively reduced in the successive periods. The period length was not affected by the presence of salicylic acid in concentrations lower than 6,18 mM. At 6,18 and 6,94 mM salicylic acid concentration the amplitude reduction and period lengthening was significant. At the last concentration the oscillations were completely stopped for 120 seconds, but only after a damping period of 140 seconds (Figure 6 and Table 1).

The shape of oscillations was modified in the presence of salicylic acid. The uninhibited oscillations have typically four segments [17]: a slightly decreasing segment when the iodine intermediate is consumed relatively slowly by the organic substrate and iodide ion is produced. Then a fast increase in redox potential happens because of the rapid radical steps which consume iodide ions. The slowly decreasing segment corresponds to the slow radical steps that produce iodide ions. During the fast decreasing step, iodine is produced and the color of the mixture changes into brown and then the cycle repeats. However after addition of salicylic acid the oscillations have only two segments: an increasing and a decreasing one. It is also notable that after the addition of salicylic acid the mixture remained transparent until the end of the reaction even in presence of starch, and the potential range of the oscillations decreased slightly from 745-765 to 720-740 mV.

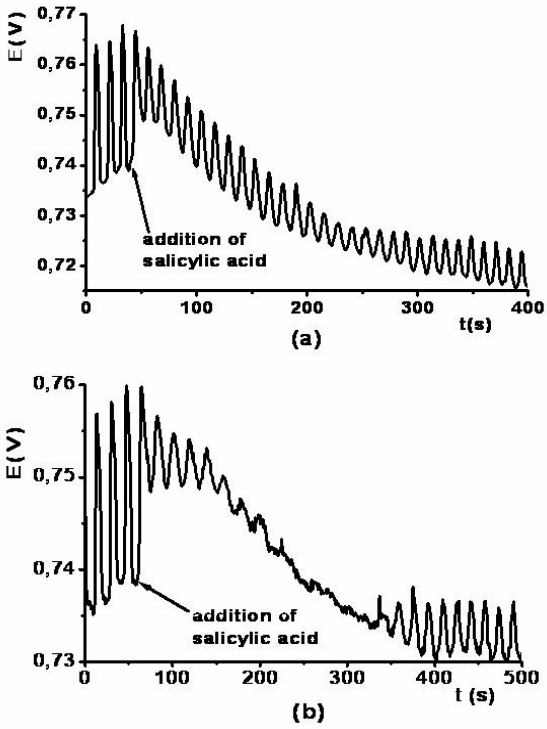

Figure 6. Effect of 5,41 mM (a) and 6,94 mM (b) salicylic acid on the BR reaction.

The unusual effect of salicylic acid constitutes a subject of further studies. By our knowledge, in the literature there is no description of this kind of damping effect of an added substance upon the BR reaction.

We found two descriptions about “spontaneous” oscillation damping phenomena (i.e. without adding a substance in the mixture) in the literature: Wittmann *et al*. used in the Belousov-Zhabotinsky reaction instead of malonic acid an oxalic acid - acetone mixture as organic substrate. They observed that after the first regular periods, the amplitudes of the following oscillations were progressively reduced. In some cases the oscillations were completely damped, and after some time they reappeared. The shape and period length of oscillations observed before and after the oscillation break were different [18].

Table 1. The effect of salicylic acid concentration on the amplitudes and the periods of the oscillations. (a) The salicylic acid solution was added after the minimum of the 3rd oscillation. (b) Completely stopped oscillations for 120 s.

Conc.	4,65 mM		5,41 mM		6,18 mM		6,94 mM	
N	Amp (mV)	p (s)	Amp (mV)	p (s)	Amp (mV)	p (s)	Amp (mV)	p (s)
1	30	13,8	29	12,8	30	13,4	27	14,6
2	31	12,6	28	11,6	31	13,4	26	14,8
3	34	13,2	30	12,2	28	15,4	28	14,8
4 [(a)]	23	13,0	18	11,6	16	17,0	11	17,8
5	17	13,0	14	11,6	11	16,4	8	19,2
6	17	13,8	14	12,0	10	18,4	6	17,6
7	18	14,0	14	12,2	11	19,2	5	20,2
8	19	13,8	14	12,2	9	17,4	5	19,8
9	19	14,0	14	12,0	10	18,4	4	19,4
10	18	13,8	14	12,6	9	17,8	3	20,2
11	20	13,8	13	12,4	11	17,8	3	12,4
12	18	13,8	12	11,6	11	18,4	0 [(b)]	120 [(b)]
13	19	14,0	12	12,6	10	17,8	2	11,8
14	18	14,2	11	12,6	12	17,4	4	15,8
15	18	14,2	9	12,2	10	18,4	7	16,8
16	17	14,6	10	12,4	9	18,4	5	17,6
17	17	13,8	8	12,4	10	17,8	6	16,4
18	14	14,8	7	12,8	7	17,4	6	16,4
19	14	14,2	5	13,8	8	18,4	5	15,6
20	14	14,6	5	11,6	7	18,0	7	15,6

Szabó studied the effect of iodate ion concentration upon the BR reaction. In BR mixtures containing 20 mM, 17,5 mM, and 15 mM iodate ion respectively; he observed a break after the first large amplitude oscillation. At 1,25 mM iodate ion concentration the damping of oscillations occurred only after the 6th period. In this case the duration of oscillation break was 50 seconds [19]. In any cases the amplitudes, the period lengths and the shape of oscillations before and after the break were different.

However it is very important to emphasize that the oscillation breaks observed by Wittmann *et al.* and Szabó should be not considered as inhibition time, because these were not caused by an added substance.

CONCLUSIONS

Among the numerous methods developed to determine the antioxidant activity, the method based on the Briggs-Rauscher oscillating reaction has a unique advantageous feature: the antioxidant reacts with hydroperoxyl radical. This radical is a reactive oxygen species which is also produced by the human body during the metabolism. Therefore the hydroperoxyl radical can be considered to be a biologically more relevant substrate, than the various organic substrates of the other methods. However the BR-method has also its own limitations due to the fact that there are strong oxidizing agents which can oxidize the antioxidant added to the mixture. Furrow *et al.* has shown that ascorbic acid is readily oxidized by these oxidizing agents, while iodide ion is produced which causes a break in the oscillations.

Our aim was to reproduce the effect of ascorbic acid on the BR-reaction and to explore the applicability of this method in case of three other compounds: tartaric acid, pyrogallol and salicylic acid. We have shown that in case of the first three compounds there is a linear relationship between the concentration and the inhibition time. One would be tempted to calculate the relative antioxidant activities based on the inhibition times, but we have shown that all these compounds act differently on the reaction; therefore such a comparison is useless. The fourth compound had the most surprising behavior: we observed a damping effect on the oscillations.

EXPERIMENTAL SECTION

Three stock solutions have been prepared with the following composition:

(A). 1,84 M H_2O_2 (Merck, p.a),
(B). 0,27 M KIO_3 (AnalytiCals, p.a), 0,1 M H_2SO_4 (Riedel de Haen, p.a)
(C). 0,2 M $CH_2(COOH)_2$ (Reachim, p.a), 0,026 M $MnSO_4$ (Reactivul, p.a).

These solutions were thermostated to 25±0,1ºC . A volume of 10,0 of A, 5,0 ml of B and 5,0 ml of C stock solution has been mixed in a double-walled glass reactor, which was thermostated to 25±0,1ºC. The composition of a reactive system was: $[CH_2(COOH)_2]_0=5\cdot10^{-2}$ M, $[H_2O_2]_0=0,92$ M, $[H_2SO_4]_0=2,5\cdot10^{-2}$ M, $[MnSO_4]_0=6,5\cdot10^{-3}$ M, $[KIO_3]_0=6,75\cdot10^{-2}$ M. A Falc-type magnetic stirrer ensured the forceful stirring of the reacting mixture. The solutions of studied compounds [ascorbic acid (Reanal, p.a), tartaric acid (2,3-dihydroxy-succinic acid, used as neutral sodium salt, Shering Kahlbaum, p.a), pyrogallol (1,2,3-trihydroxy-benzene, Laboratorium Chemiczne Gallol, p.a), salicylic acid (2-hydroxy-benzoic acid,

used as sodium salt, Reactivul, p.a)] were added with a micropipette (Labsystems Finnpipette) every time after the minimum of the third oscillation. In some cases we added 1,0 ml 1,0 w/w% starch (Reactivul, p.a) solution in the initial BR-mixture in order to visualize the variation of concentration of iodine, one of the intermediates of the reaction. Every measurement was performed at least three times. The reaction was monitored potentiometrically, employing a bright platinum and double-junction saturated calomel electrode. The potential difference between these electrodes was registered by a computer equipped with National Instruments® Data Acquisition Card. The sampling frequency of data acquisition was set to 5 s^{-1}. For data processing Origin® 6.0 program was used. The average and the standard deviation of the inhibition times were calculated. Inhibition times were plotted against the concentration of compounds, the equation of the straight lines was determined using a weighted linear regression [20].

ACKNOWLEDGMENTS

The author acknowledges the scholarship awarded by the PROFIL Group for the Cluj-Szeged Student Exchange Program to the University of Szeged, Hungary, Faculty of Natural Sciences.

REFERENCES

1. T. S. Briggs, W. C. Rauscher, *J. Chem. Ed*., **1973**, *50*, 469.
2. D. O. Cooke, *Inorg. Chim. Acta*, **1979**, *37*, 259.
3. S. D. Furrow, R. M. Noyes, *J. Am. Chem. Soc*, **1982**, *104*, 38.
4. S. D. Furrow, R. M. Noyes, *J. Am. Chem. Soc*, **1982**, *104*, 43.
5. S. D. Furrow, R. M. Noyes, *J. Am. Chem. Soc*, **1982**, *104*, 45.
6. P. De Kepper, I. R. Epstein, *J. Am. Chem. Soc*, **1982**, *104*, 49.
7. S.D.Furrow, *J. Phys. Chem.*, **1995**, *99*, 11131.
8. S. D. Furrow, R. Cervellati, G. Amadori, *J. Phys. Chem. A,* **2002**, *106*, 5841.
9. R. Cervellati, N. Crespi-Perrelino, S.D. Furrow, A. Minghetti, *Helv. Chim. Acta*, **2000**, *83*, 3179.
10. R. Cervellati, K. Höner, S. D. Furrow, C. Neddens, S. Costa, *Helv. Chim. Acta*, **2001**, *84*, 3533.
11. R. Cervellati, K. Höner, S. D. Furrow, F. Mazzanati, S. Costa, *Helv. Chim. Acta*, **2004**, *87*, 133.
12. D. Huang, B. Ou, R. L. Prior, *J. Agric. Food Chem.*, **2005**, **53**, 1841.
13. B. Halliwell, Chapter I in E. Cadenas, L. Packer (eds.), Handbook of Antioxidants, Oxidative Stress and Disease, Vol. 8, 2nd Edition, CRC Press, **2001**.

14. R. Moreau, W-J Zhang, T. M. Hagen, Chapter VII in E. Cadenas, L. Packer (eds.), Handbook of Antioxidants, Oxidative Stress and Disease, Vol. 8, 2nd Edition, CRC Press, **2001**.
15. S.D. Furrow, K. Höner, R. Cervellati, *Helv. Chim. Acta*, **2004**, *87*, 735.
16. B. Baderschneider, D. Luthria, L. Waterhouse, P. Winterhalter, *Vitis,* **1999**, *38*, 127
17. I. A. Pontos, Diploma Thesis, Babeş-Bolyai University, Faculty of Chemistry and Chemical Engineering, **1999**.
18. M. Wittmann, P. Stirling, J. Bódiss, *J. Chem. Phys. Lett.*, **1987**, *141*, 241.
19. E. Szabó, Diploma Thesis, Babeş-Bolyai University, Faculty of Chemistry and Chemical Engineering, **2000**.
20. Harvey, D., Modern Analytical Chemistry, Mc Graw Hill, **2000**, 104.

STUDIA UNIVERSITATIS BABEŞ-BOLYAI, CHEMIA, LIV, 4, 2009

PHYSICO-CHEMICAL CHARACTERIZATION OF 8YSZ NANOPARTICLES BY MODIFIED SOL-GEL METHOD

C. SUCIU[a,b], A. VIK[a], F. GOGA[b], E. DOROLTI[c], R. TETEAN[c], A.C. HOFFMANN[d]

ABSTRACT. 8 mol% Yttria Stabilized Zirconia (8YSZ) powders have been obtained by the modified sol-gel method using sucrose and pectin as organic precursors. The influence of the amounts of both sucrose and pectin were studied experimentally over a range of calcination temperatures. The obtained gels were investigated by Thermogravimetric/Differential Thermal Analysis (TG/DTA) to identify physico-chemical processes that take place during the process and to establish an optimal calcination temperature diagram. The final powders were investigated by X-ray diffraction (XRD) and Transmission Electron Microscopy (TEM) to evaluate the phase composition, the microstructure and morphology. Crystallite size and particle size of the final powders were determined using Scherrer formula and nitrogen adsorption with the Brunauer–Emmett–Teller (BET) isotherm. The results confirm that the particle properties, size and crystallite size, are strongly dependent on the calcination temperature. On the other hand, the particle properties are rather—but not completely—insensitive to (and therefore the process rather "forgiving" for) variations in the amounts of sucrose or pectin used.

Keywords: YSZ, yttria stabilized zirconia, nanoparticles, sol-gel processing, calcination temperature, organic precursors, sucrose, pectin

INTRODUCTION

The sol-gel method is emerging as a low-cost, flexible method for creating nanoparticles, and is also a promising method for creating thin layers of a controlled porosity [1], although much still remains to be known about the influence of the processing parameters on the final product. The method has been used to synthesize nano-sized particles of various materials, such as NiO, TiO_2, ZrO_2, YSZ (yttria-doped zirconia), La_2O_3, CeO_2, $BaFe_{12}O_{19}$ etc., useful for their mechanical, magnetic, ion conducting or optical properties.

[a] *CMR-PROTOTECH AS, NO-5892 Bergen, Norway, crina@prototech.no*
[b] *Universitatea Babeş-Bolyai, Facultatea de Chimie şi Inginerie Chimică, Str. Arany Janos, Nr. 11, RO-400028 Cluj-Napoca, Romania*
[c] *Universitatea Babeş-Bolyai, Faculatea de Fizică, Str. Kogălniceanu, Nr. 1, RO-400084 Cluj-Napoca, Romania*
[d] *University of Bergen, Institute of Physics and Technology, Allegaten 55, 5007 Bergen, Norway*

In what follows we mention some recent studies aimed at determining the effect of processing parameters on the properties of particles synthesized by sol-gel methods utilizing organic precursors, which are subsequently burnt off in a calcination step.

Most authors found a significant influence of the temperature used in the calcination step on the particles size. Increasing the calcination temperature leads to the formation of larger particles as measured by nitrogen adsorption and by TEM, for instance for YSZ particles [2,3]. Wang et al. [4] looked particularly closely at this issue, and found by TEM analysis that the size of La_2O_3 particles increased not only with temperature, but also with the duration of calcination.

A higher calcination temperature also leads to a higher quality of crystallization. In general, higher calcination temperatures give rise to higher and sharper peaks in XRD profiles. Zhang et al. [2] found this for YSZ, as did Laberty-Robert et al. [3]. The latter workers found diffraction peaks characteristic of a tetragonal crystal structure for calcination temperatures below 600^0C, and only a cubic structure above that temperature; they used 8% of Y_2O_3 dopant. Wang et al. [4] found some chemical transformations at lower calcination temperatures, and did not obtain the pattern characteristic for La_2O_3 until 750^0C, with the XRD diffraction pattern becoming much clearer with sharper peaks at 850^0C. Lian et al. [5] prepared a mixture of NiO and doped CeO_2 particles for use in anodes in SOFCs. They also found that the particles are sintering further after their autocombustion manufacturing process. Related to the higher and sharper XRD peaks is the fact that the Scherrer formula indicates larger crystallites for higher calcination temperatures for various types of particles and manufacturing processes [2,5,6]. Jung et al. [7] found that the photoluminescence intensity of their titania particles was enhanced and that the peak position in the photoluminescence spectrum moved to smaller wavelengths, as the calcination temperature was raised. This was all attributed to a progressively more ordered crystalline structure.

Widoniak et al. [8] carried out a special study in this respect. They produced larger TiO_2 and ZrO_2 particles by aggregation of nanoparticles. These particles were sometimes made porous by the judicious addition of different types of salts and polymers to the reaction mixtures. They found crystallite sizes much smaller than their particle sizes, and also much higher specific areas (up to 300 m^3/g) than the particle size would indicate.

Laberty-Robert et al. [9] studied the influence of the precursor ratios for Pechini synthesis of YSZ particles. They did not find a strong variation in the particle properties when varying the ratios citric acid/ethylene glycol or citric acid/transition metal, although they did find large differences in the viscosity of the gels. They attempted to control the particle size by adding surfactant to the reaction mixture to obtain a colloidal suspension, and found decreasing particle size with increasing surfactant concentration. For their strongly agglomerated particles, the BET surface was less than expected from the particle size, as determined by electron microscopy.

Many investigations [2,4,5,6,8] also include thermal analyses of the polymeric gel as it is being heated in a controlled temperature calcination process. In general, it is possible to recognize endothermic processes corresponding to dewatering and exothermic processes corresponding to combustion of organic material. Also exothermic processes corresponding to solid solutions or crystallographic changes can also be observed.

The objective of this work was to use the new modified sol-gel method, with sucrose and pectin as organic precursors, in order to obtain 8YSZ nanoparticles. The effect of the mass ratio between sucrose and pectin on the obtained powders was investigated at a larger domain compared with our previously work [10]. The obtained powders were calcinated at different temperatures and different thermal treatments (see below) to study the influence of the calcination process.

RESULTS AND DISCUSSION

The TA analysis for the A set (Figure 1) revealed an endothermic process at 200^{0}C (for A1) and 180^{0}C (for A4), visible on the DTA curve with a slight mass loss due to water elimination, followed by a large exothermic process visible extended up to 940^{0}C. Oxidation of the organic compound and formation of cubic zirconia stabilized with yttria take place in this large temperature interval and they may overlap.

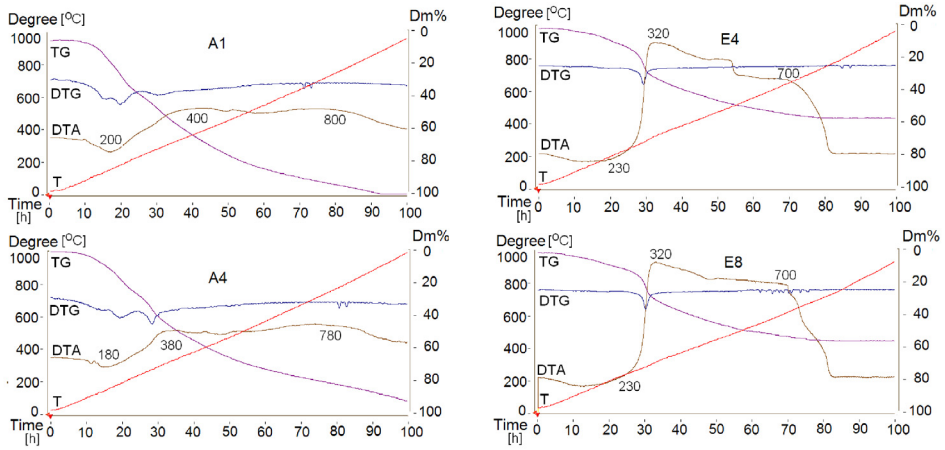

Figure 1. The thermal analysis of the dried gels.

These processes are distinguishable on the DTA curve through the two maxima at 400^{0}C and 780^{0}C (for A1) and at 380^{0}C and 800^{0}C (for A4), respectively. Loss of mass takes place along the whole temperature range from 100 to 940^{0}C, due to the elimination of water vapor and gaseous reaction products, and goes up to 98%.

Turning now to the E set shown in Figure 1, an exothermic peak of high intensity can be observed on the DTA curve. This starts at 230^{0}C and continues up to 840^{0}C. The curves present a maximum at 320^{0}C which corresponds to the oxidation of the organic components followed by a second maximum at around 700^{0}C due to the formation of cubic zirconia. A slight mass loss can be noticed under 200^{0}C on the TG curve due to water elimination. The rate of this process was very low so that no endothermic peak can be distinguished on the DTA curve. The mass loss increased between 230 and 700^{0}C. Overall, a 58% mass loss was determined.

Comparing the two sample sets the following remarks can be made:

– the exothermic effect corresponding to the oxidation of the organic compound was much more intense for the E set, due to the larger amount of organic compound present;

– the total mass variation was higher for the A set (98%) compared to the E set (58%), likely due to the higher water retention in the A set. Also, the gas elimination was slower along the whole temperature interval;

– the strong endothermic process in the A samples under 200^{0}C shows that more residual water was present in these samples. Thus the procedure of obtaining the A set yielded gels which retained water and gasses more strongly, and their elimination was more difficult and required higher temperatures;

– the exothermic effect corresponding to the formation of cubic zirconia was much more intense for the E set and ended at 840^{0}C. In the A set this process was much less intense, and persisted up to higher temperatures (940^{0}C). This shows that the crystallization process into cubic zirconia had a lower rate for the A set.

The obtained BET values of the specific surface area (S), the pore volumes (V_P) and the BJH pore diameter (r_p) for all the samples, at different sintered temperatures, are shown in the Figure 2.

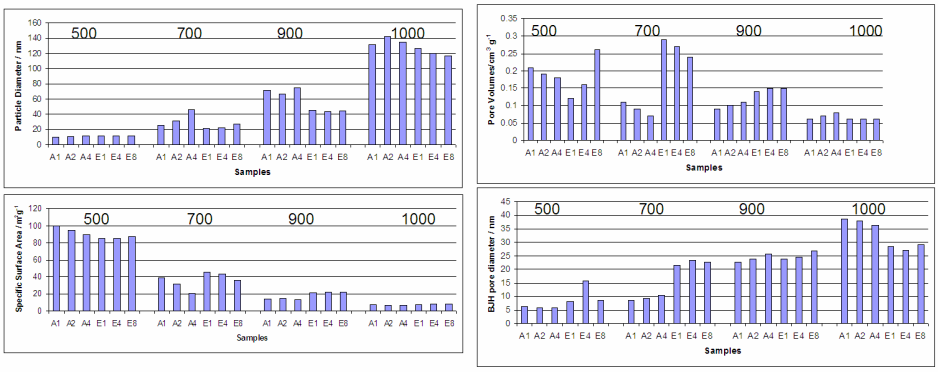

Figure 2. Specific surface area, pore volumes, BJH pore diameter and nanoparticles diameter at different temperatures.

Assuming that the particles are round and the theoretical density (ρ) of 8mol% YSZ is 6100 kg/m^3 [12], the equivalent grain size (D) corresponding to the obtained specific surface areas (S) were calculated following equation: $D=6/(\rho \cdot S)$.

Specific surface area decreased with the increasing of the calcination temperature. For example, the samples calcined at 500^{0}C have the highest specific surface area. However, upon calcination at 1000^{0}C, the specific surface area of the samples is reduced. This seems to be mostly due to the reduction in bulk porosity of the compound. On the other hand it is somewhat insensitive to the amount - and the proportions - of the organic precursors used. The highest specific area of 99.9 m^2/g was obtained at 500^{0}C and the values decreased with increasing temperature down to 6.9 m^2/g at 1000^{0}C.

The mean particle diameter decreased by increasing the temperature and by decreasing specific surface area. The values of the mean particle sizes vary from ~10 nm (500^{0}C) to ~150 nm (1000^{0}C). In the same way, the BJH pore diameters increased by increasing the temperature showing the presence of mesopores (smaller that 40 nm) even for the samples calcined at high temperatures.

Specific pore volume is calculated as the sum of volumes of all pores in one gram of adsorbent. We have to emphasise that for our samples, only internal volume inside the adsorbent particles was counted. At low calcination temperatures (500-700^{0}C), the obtained powders exhibit an increased pore volume, while, as the calcination temperatures increase (900-1000^{0}C), the pore volume decreased. This is mainly due to the longer thermal process, which allows the particles to grow in dimension and the pores to close.

The XRD data from all the samples show the presence of only one single phase, solid solution of ZrO_2 with Y_2O_3. The pattern no. 49-1468 corresponds to Yttrium Zirconium Oxide - $Y_{0.15}Zr_{0.85}O_{1.93}$–$92ZrO_28Y_2O_3$. The presences of other phases were not observed. Based on the phases identified in the XRD patterns, it can be concluded that a homogeneous solid solution of ZrO_2 with Y_2O_3, necessary to form cubic zirconia, was formed (Figure 3). The XRD of the mixtures treated at low temperature (500^{0}C) show a significant difference between the E and the A sets due to the mass ratio of sucrose:pectin used in the experiments. The spectra of the E set, obtained with a smaller amount of pectin, are sharper with relatively less noise, due to a better crystallization. At higher temperatures (700-1000^{0}C) the differences between the shapes of the peaks are less noticeable.

The FWHM and the 2θ values of the first four peaks were used to calculate the crystallite sizes of the obtained powders at different temperatures using the Scherrer formula [13]. In Figure 4 the mean crystallite size for all samples at each temperature in the studied interval are shown. The mean crystallite sizes varied between ~6 and 37 nm showing that the method is effective to synthesize nanosized powders.

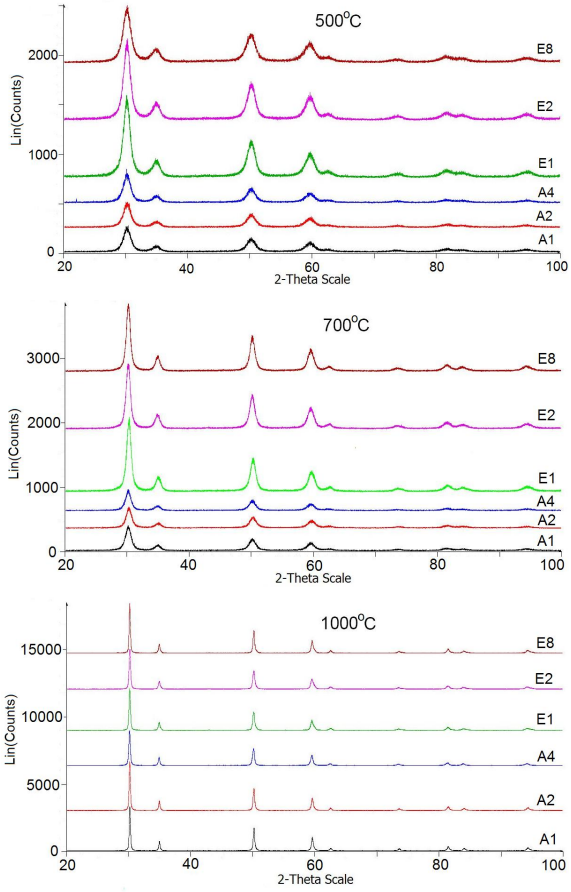

Figure 3. The X-ray diffraction spectra size of the samples calcined at 500, 700, and 1000^{0}C.

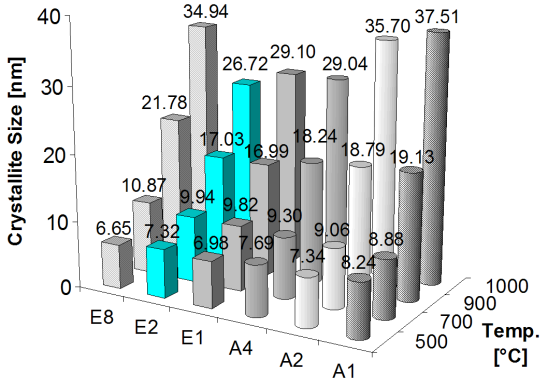

Figure 4. The mean crystallite size of the samples determined by XRD.

A comparison of particle size evaluated from XRD analysis and specific surface area measurements shows that the particles are less agglomerated at low temperatures. The mean particles and agglomerates sizes increase by increasing the calcination temperature. In addition, it can be seen that the specific surface area of the calcined powders regularly decreases when the calcination temperature goes up and the crystallite size of the powders increases. This strengthens the tendency of the particles to form a dense structure in the agglomerate and hence the specific surface area decreases. The calcination temperature and the duration of calcination affect both crystallite size and specific surface area of the powders. The results are comparable with the results obtained by other researchers [2,3,4,9]. Also, the calculated mean crystallites size is smaller than the calculated mean particles size, which is similar to the results obtained by Widoniak et al. [8].

The TEM images confirm the presence in powders of the agglomerates at high temperatures. At 500^{0}C the nanoparticles are relatively regular, rounded shapes, less agglomerated with a narrow size distribution (Figure 6).

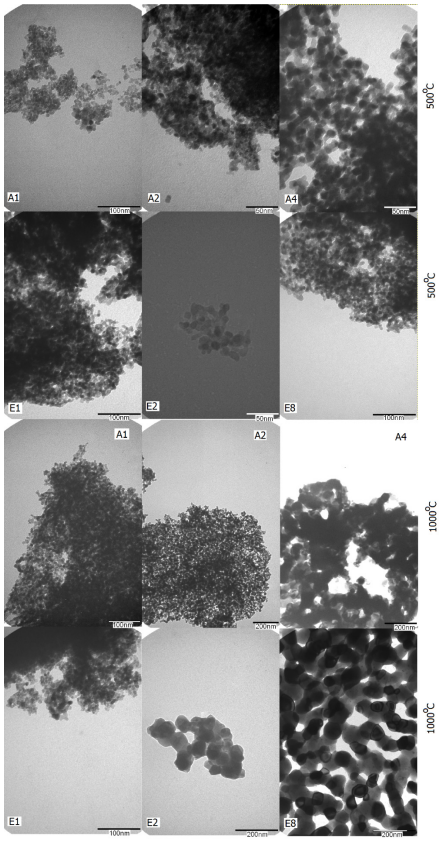

Figure 5. TEM images for the samples calcined at 500 and 1000^{0}C.

The mean particle size of the samples calcined at 500^0C is between 9 and 14 nm. The powder calcined at 1000^0C showed a partial sintering of the primary crystallites. This result is also observed during the synthesis of YSZ by a combustion process [14] or by a modified Pechini method [15], while the particle size measured for the samples calcined at 1000^0C is between 10 and 60 nm.

As it can be observed from the XRD measurements, the obtained crystallite sizes (6 nm at 500^0C and 37nm at 1000^0C, respectively) are smaller than the mean particle size obtained from the specific surface area measurements (10 nm at 500^0C and 150 nm at 1000^0C). The obtained mean particle sizes from the TEM micrographs (10 nm at 500^0C and 60 nm at 1000^0C, respectively) are more close to the crystallite sizes determined from the XRD. Similar results were found in [8], where the crystallites sizes are much smaller than the particles size and also much higher specific areas than the particle sizes due to the nanoparticles aggregation.

CONCLUSIONS

The influence of the process parameters on the properties of nanoparticles produced with a new sol-gel process using sucrose and pectin in place of conventional organic precursors has been investigated. Compared with the conventional sol-gel method, this method also allows the production of 8mol% YSZ powders at a relatively low temperature with good stoichiometric control, high quality of the produced nanoparticles and high degree of crystallization. The obtained powders using different mass ratio of sucrose and pectin and different calcination temperatures are comparable with the powders obtained through other sol-gel methods using different organic precursors. Comparisons can be made from different points of view, e.g. behavior under calcination; crystallite and particle size; specific surface areas and total pore volume.

High specific surface areas, up to ~100 m^2/g, were obtained by the modified sol-gel method and the calculated particle sizes correspond to 10 nm. The specific surface area is inversely proportional to particle diameter. Pore volumes, specific surface area, mean pore diameter and BJH pore diameter are correlated to each other.

The E set, was found to yield cubic yttria stabilized zirconia with a larger crystallite size as indicated by less noise and smaller peak width at low temperatures (500^0C). The calcination temperature was responsible for the higher crystallization quality observable from the XRD measurement (higher and sharper peaks). C. Laberty-Robert et al. [3] obtained tetragonal 8YSZ at temperatures below 600^0C and they also concluded that the calcination temperature influence the crystallization degree of the powders.

The estimated particle size showed a slightly decreasing trend with the decrease in the sucrose/pectin mass ratio concentration though the preparation condition was identical for all the samples. C. Laberty-Robert et al. [9] found

also that the organic precursor ratio (citric acid and ethylene glycol) and the ratio between the citric acid and metal ions does not influence much the particle sizes of the final powders. Additional studies to investigate the viscosity of the gels are required. The possibility of controlling the particle sizes by adding different surfactants to the initial solutions to obtain a colloidal suspension might also be worth of investigating.

EXPERIMENTAL SECTION

Preparation techniques

$ZrCl_4$ (Sigma-Aldrich, technical purity) and $Y(NO_3)_3 \cdot 6H_2O$ (Sigma-Aldrich, 99.9% purity) were used as raw materials at the molar ratios required to obtain 8YSZ (ZrO_2 doped with 8 mol% Y_2O_3). Two sets of samples labeled A and E, containing the sucrose/pectin mass ratios shown in Table 1 were used in order to study the effect of the amounts and proportions of the organic precursors on the process and the product particles.

Table 1. Sucrose/Pectin mass ratio used in experiments.

	A1	A2	A4	E1	E2	E8
Sucrose	100	100	100	100	100	100
Pectin	2	4	8	0.25	0.5	0.75

The flow chart for the synthesis of the 8YSZ compound powders is shown in Scheme 1. Aqueous solutions of the two salts were stirred on a warming plate at 90–100^{0}C in order to mix the solution uniformly. The sucrose/pectin solution was added gradually into the aqueous solutions under stirring until transparent colloidal suspensions were obtained. The transparent sol continuously transformed into wet gel and then into dried gel under heating. Finally, the obtained gels were calcined at different temperatures: 500, 700 and 1000^{0}C to form white 8 mol% YSZ compound nanoparticles. Each gel sample was calcined, in air, at a heating rate of 100^{0}C/h. The calcination temperature diagram, was designed in accordance with the results of the TG/TDA experiments discussed above The plateaus were as follows:

– 500◦C: 1 hr at 200^{0}C, 2 hrs at 400^{0}C and 6 hrs at 500^{0}C
– 700◦C: 1 hr at 200^{0}C, 2 hrs at 400^{0}C and 4 hrs at 700^{0}C
– 900◦C: 1 hr at 200^{0}C, 2 hrs at 400^{0}C, 3 hrs at 600^{0}C and 3 hrs at 900^{0}C
– 1000◦C: 1 hr at 200^{0}C, 2 hrs at 400^{0}C, 3 hrs at 600^{0}C and 2 hrs at 1000^{0}C.

This mechanism, and the role played by sucrose and pectin in the formation of YSZ powders, is discussed in more detail in reference [10]. The addition of sucrose and pectin to the solution of the metal cations forms a polymer matrix in which the Zr^{4+} and Y^{3+} cations are distributed through the polymeric network structure. Sucrose, which is always in excess, acts as a strong chelating

agent and as a pattern material. The sucrose solution contains NO^{3-} ions, which helps to hydrolyze the sucrose molecule into glucose and fructose, and afterwards oxidized to gluconic acid (GA) or polyhydroxyl acid. GA contains carboxilyc acid groups and hydroxyl groups which can participate in the complexation of metal ions and may form branched polymer with pectin. Pectin chains form long layers and sucrose molecules may bind between this layers. In the present process, metallic ions are bound by the sucrose molecule and the resulting complex molecule is trapped between pectin layers. During calcination this polymeric metal ion complex is decomposed into CO_2 and H_2O and a large amount of heat is generated preventing agglomeration by ensuring that the mixture remains porous.

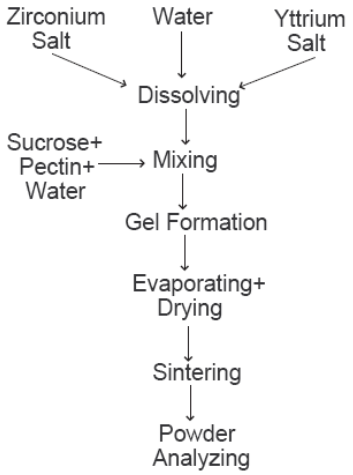

Scheme 1. Flow chart for 8YSZ preparation technique.

Analysis techniques

Thermo-gravimetry and differential thermal analysis (TG/DTA) curves were recoreded with a thermal analyzer Derivatograph Q 1500 (MOM Hungary) up to 1000^0C, in air, at a heating rate of 10^0C/min, using Al_2O_3 as reference. Apart from giving information about the physical and chemical processes taking place during calcination, the TA analyses were used for determining the optimal calcination temperature scheme (the levels and durations of the temperature plateaus described above) to allow the processes, such as dewatering, zirconia formation and solid solution formation to go to completion before proceeding with raising the temperature.

The BET specific surface area SBET and pore volume (V_P) distribution were measured by nitrogen physisorbtion using an Gemini 2380 analyzer from Micromeritics Co.Ltd. The pore size distribution was calculated from the

adsorbtion branch of the isotherms, based on the BJH method. The BJH pore diameter (r_p) was calculated as $4V_p/S_{BJH}$ [11]. All the final powders were degassed at 200^0C for 3h under vacuum before analysis.

X-ray diffraction patterns were generated using a Brucker D-8 Advance X-ray diffractometer with CuKα1 radiation in the 2θ range of 20-100 Å. The crystallite sizes were calculated from the XRD spectra using the Scherrer formula $D = \lambda/(\beta \cos\theta)$, where D is the crystallite size, λ is the wavelength (0.15406 nm), β is the Full Width at Half Maximum (FWHM) and θ is the diffraction angle.

The morphologies of the powders were examined by TEM (transmission electron microscopy) using a JEOL-JEM-1011 transmission microscope. From the samples dispersed in water under stirring, one drop was taken and deposited on a copper grid (Agar G2400C, 400 Square Mesh, copper 3.05mm). The grids were previously covered with an organic layer of Formvar powder (Agar Scientific LTD, Essex) dissolved in chloroform followed by carbon deposition process under vacuum (Agar Turbo carbon coater, Model 208C) and a glow discharge.

ACKNOWLEDGMENTS

This work was funded by the NFR (Norwegian Research Council) and Prototech A.S., Bergen, Norway made laboratory facilities available. Also, the authors are acknowledging the Laboratory for Electron Microscopy, University of Bergen, Norway for helping with all the micrographs.

REFERENCES

1. C.J. Brinker, G.W. Scherer, Sol-gel science: the physics and chemistry of sol-gel processing, Academic Press, New York, **1990**.
2. Y. Zhang, A. Li, Z. Yan, G.Xy, C. Liao, C. Yan, *Journal of Solid State Chemistry*, **2003**, *171*, 434.
3. C. Laberty-Robert, F. Ansart, C. Deloget, M. Gaudon, A. Rousset, *Materials Research Bulletin,* **2001**, *36*, 2083.
4. X. Wang, M. Wang, H. Song, B. Ding, *Materials Letters*, **2006**, *60*, *2261.*
5. J.S. Lian, X.Y. Zhang, H.P. Zhang, Z.H. Zhang, J. Zhang, *Materials Letters* **2004**, *58*, 1183.
6. A. Mali, A. Ataie, *Ceramics International,* **2004**, *30,* 1979.
7. K.Y. Jung, S. B. Park, M. Anpo, *Journal of Photochemistry and Photobiology A: Chemistry,* **2005**, *170,* 247.
8. J. Widoniak, S. Eiden-Assmann, G. Maret, C*olloids and Surfaces A: Physicochem. Eng. Aspects,* **2005**, *270–271,* 329.

9. C. Laberty-Robert, F. Ansart, S. Castillo, G. Richard, *Solid State Sciences,* **2002**, *4*, 1053.
10. C. Suciu, A.C. Hoffmann, A. Vik, F. Goga, *Chemical Engineering Journal,* **2008***,138*, 608.
11. E.P. Barrett, L.G. Joyner, P.H. Halenda, *Journal of the American Chemical Society,* **1951**, *73*, 373.
12. M. El-sayed Ali, Omar A. Abdelal, Ahmed A. Hassan, *Solid State Ionics*, **2007**, *178*, 1463.
13. H.M. Rietveld, *Journal of Applied Crystallography*, **1969**, *2*, 65.
14. K.R. Venkatachari, D. Huang, S.P. Ostrander, W.A. Sculze, G.C. Stangle, *Journal of Materials Research*, **1995**, *10*, 748.
15. C.L. Robert, F. Ansart, C. Deloget, M. Gaudon, A. Rousset, *Ceramics International,* **2003**, *29*, 151.

STUDIA UNIVERSITATIS BABEŞ-BOLYAI, CHEMIA, LIV, 4, 2009

USE AQUEOUS PEG-INORGANIC SALT TWO-PHASE SYSTEMS FOR Bi(III) EXTRACTION IN THE PRESENCE OF INORGANIC EXTRACTANTS

LAURA BULGARIU[a] AND DUMITRU BULGARIU[b, c]

ABSTRACT. The Bi(III) extraction behaviour was studied in aqueous polyethylene glycol (PEG) – $(NH_4)_2SO_4$ two-phase system, using inorganic anions (I^-, Br^-, Cl^- and SCN^-), as extractants. The aqueous two-phase systems were prepared using aqueous solutions of phase-forming components (PEG and $(NH_4)_2SO_4$) in water or in 1N H_2SO_4. The experimental results show that more adequate for Bi(III) extraction is the aqueous two-phase systems, where the aqueous solutions of phase-forming components are prepared in 1N H_2SO_4. Under these conditions, the addition of inorganic extractants determined the partitioning of Bi(III) into PEG-rich phase, easy observable at extractants concentration higher than 0.06 mol/dm^3. The efficiency of extractants follows the order: $I^- >> Br^- > Cl^- >> SCN^-$. Using the Bi(III) distribution coefficients calculated as a function of inorganic extractants concentration, the extracted species were assumed.

Keywords: aqueous PEG-based two-phase system, Bi(III) extraction, inorganic extractants

INTRODUCTION

Various conventional liquid-liquid extraction methods have been proposed for the recovery of bismuth ions, through years [1]. Its utilization at the manufacture of semiconductors, alloys and metallurgical additives, etc., are few cases where the solvent extraction can be used in order to solve environmental problems [2]. Several solvent extractions systems are mentioned for the extraction of bismuth as neutral complexes or ion-pairs, using different organic extractants [3-5]. But, the utilization of conventional extraction methods requires large volumes of organic solvents, which may cause environmental pollution, and thus are not appreciated.

[a] *Universitatea Tehnică "Gheorghe Asachi" din Iaşi, Facultatea de Inginerie Chimică şi Protecția Mediului, Bd-ul D. Mangeron, Nr. 71A, RO-700050 Iaşi, România, lbulg@ch.tuiasi.ro*

[b] *Universitatea "Al. I. Cuza" din Iaşi, Facultatea de Geografie şi Geologie, Bd-ul Carol I, Nr. 20 A, RO-700506 Iaşi, România, dbulgariu@yahoo.com*

[c] *Academia Română, Filiala din Iaşi, Colectivul de Geografie, Bd-ul Carol I, Nr. 18, RO-700506, Iaşi, România*

In recent years, the aqueous PEG-based two-phase systems have been suggested for several applications in metal ion recovery, particularly those formed by polyethylene glycol (PEG) and inorganic salts, as an alternative to the conventional extraction systems. These systems are formed by mixing an aqueous solution of PEG with an aqueous solution of certain inorganic salt (for example: $(NH_4)_2SO_4$, Na_2SO_4, K_2HPO_4, etc.) [6-8] and are composed by two immiscible phases, a superior one – rich in PEG, which has the role of organic phases from conventional extraction systems, and an inferior one – rich in inorganic salt. One of the main advantages of these systems is that the metal species partitioning occurs between two aqueous phases, which is an evident environmental benefit. In addition, the aqueous PEG- inorganic salt two-phase systems permit the utilization of cheaper inorganic anions (such as halide and pseudo-halide ions) as extractants, for the efficient extraction of several soft metal ions. For example, Cu(II), Co(II), Zn(II) and Fe(III) are extracted in presence of SCN^- ions at high acidity of salt stock solution [9-11]. Also, iodide ions can be successfully used for the quantitative extraction of Cd(II) and Hg(II) [12-15].

All these metal ions forms in presence of halide and pseudo-halide ions, anionic complexes and their extraction efficiency is mainly determined both by the properties of chemical species formed in extraction system (stability, hydration degree, electric charge), and by the characteristics of aqueous two-phase systems (nature and concentration of inorganic salt, molecular mass and concentration of PEG, acidity of phase-forming component solutions) [16, 17].

Starting from these observations, we believe that such aqueous PEG-inorganic salt two-phase systems can be used for efficient extraction of Bi(III) in presence of inorganic anions, as extractants. In the case of Bi(III), the stability of its chemical species with inorganic anions, such as I^-, Br^-, Cl^- and SCN^-, increases from SCN^- to I^-, and increase with the increasing of the inorganic anions number from molecule, following the order: $BiX^{2+} < BiX_2^+ < BiX_3 < BiX_4^- < BiX_5^{2-} < BiX_6^{3-}$ [18]. Under these conditions, at high acidity of phase-forming components solutions, a quantitative extraction of Bi(III) is expected to be obtained, and the extraction species should have a maximum number of inorganic anions (most probable 6) associated to metal ion.

In this study we have investigated the extraction behaviour of Bi(III) in aqueous PEG(1500) – $(NH_4)_2SO_4$, in order to establish the optimum experimental conditions for its efficient extraction. The experimental parameters considered in this study have been: initial concentration of metal ions, the type and concentration of inorganic extractants (I^-, Br^-, Cl^- and SCN^-) and the acidity of phase-forming components solutions. The aqueous two-phase systems were prepared using aqueous solutions of PEG and $(NH_4)_2SO_4$ in water and in 1 N H_2SO_4. The differences between these two ways of aqueous two-phase systems preparation have been evidenced using IR spectra of solidified PEG-rich phases. The extracted species were assumed on the basis of experimental distribution coefficients calculated in function of inorganic extractants concentration.

RESULTS AND DISCUSSION

The optimum conditions for Bi(III) extraction were established by varying several experimental parameters, such as: the pH of phase-forming components stock solutions, Bi(III) initial concentration, type and concentration of inorganic extractants.

In the study of Bi(III) extraction in aqueous PEG(1500) – $(NH_4)_2SO_4$ two-phase system, a first experimental parameter which should considered is the acidity of phase-forming components stock solutions. According with the distribution diagram of bismuth species [19], in aqueous solutions the free Bi^{3+} ions are present only in 0 – 0.8 pH range. Over this value the predominant species are BiO^+, which are more stable [18], but have a lower reactivity towards halide and pseudo-halide extractants, in comparison with Bi^{3+} ions.

On the basis of these observations, the influence of salt stock solution acidity on bismuth extraction in presence of 0.10 mol/dm^3 iodide extractants, have been studied in 0.20 – 3.50 pH range. The experimental results (Figure 1) indicate that the extraction efficiency increase with the increasing of salt stock solution acidity, but the maximum value of extraction percent is not higher than 50 %, even the salt stock solution pH is close to 0.

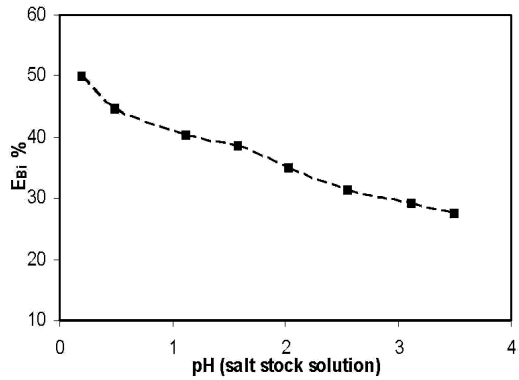

Figure 1. E_{Bi}% vs. salt stock solution pH. (Bi_i = 62.75 μg/cm^3, $[I^-]_{add}$ = 0.10 mol/dm^3; temperature = 24 °C).

This is due to the fact that the 40% (w/w) PEG aqueous stock solution has a higher pH value (6.2), and from this reason at interface, the apparition of a yellow precipitate can be observed, and the extraction process is stopped.

For to eliminated this inconvenient, both PEG and $(NH_4)_2SO_4$ stock solutions have been prepared using 1N H_2SO_4, instead of water. Under these conditions, in extraction systems bismuth is predominant as Bi^{3+} in both phases, and in presence of 0.10 mol I^-/dm^3, the obtained value of extraction percent is 99.65%. Thus, the extraction process could be considered a quantitative one, and this system was used for further Bi(III) extraction experiments.

But, the utilization of phase-forming components prepared in 1N H_2SO_4 instead of water, will change the characteristics of obtained aqueous two-phase system. For to underline the differences between the aqueous two-phase systems prepared using water and 1N H_2SO_4, the IR spectra of polymer-rich phases have been recorded.

In Figures 2 and 3 are presented the IR spectra obtained for solidified 40% (w/w) PEG(1500) solution (PEG) and blank PEG-rich phases (M), in water and 1N H_2SO_4.

It can be observed that the most significant changes are in the spectral region where appears the O–H stretching for water molecules hydrogen bonded by polymer chains [20, 21].

Thus, in the case of PEG solution in water, the large and splitter band from 3550-3238 cm^{-1} from PEG 1 spectra (Figure 2) is more attenuated in the spectra of blank PEG-rich phase (M 1) and moved to low wave number (3296 cm^{-1}). This is due to the fact that at the contact of PEG solution in water and salt stock solution with high acidity (in this case $(NH_4)_2SO_4$ solution with pH= 0.5), the dehydration of polymer chains occurs and the obtained PEG-rich phases are more hydrophobic [21]. This characteristic, plays an important role in extraction process of metal ions with inorganic extractants, and can be directly correlated with the number of extractants from extracted species molecules [10, 12, 14].

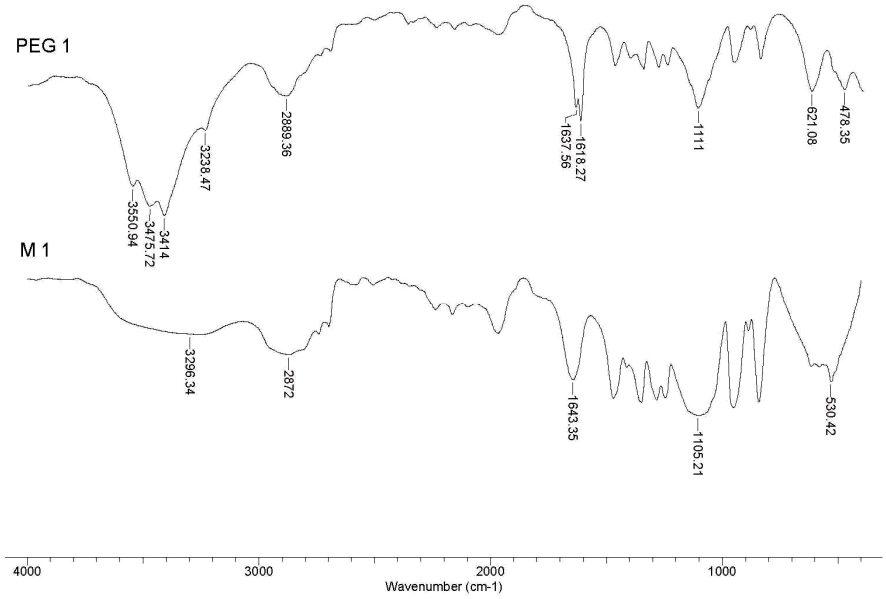

Figure 2. The IR spectra of solidified 40% (w/w) polyethylene glycol solution (PEG 1) and blank phase (M 1), in water.

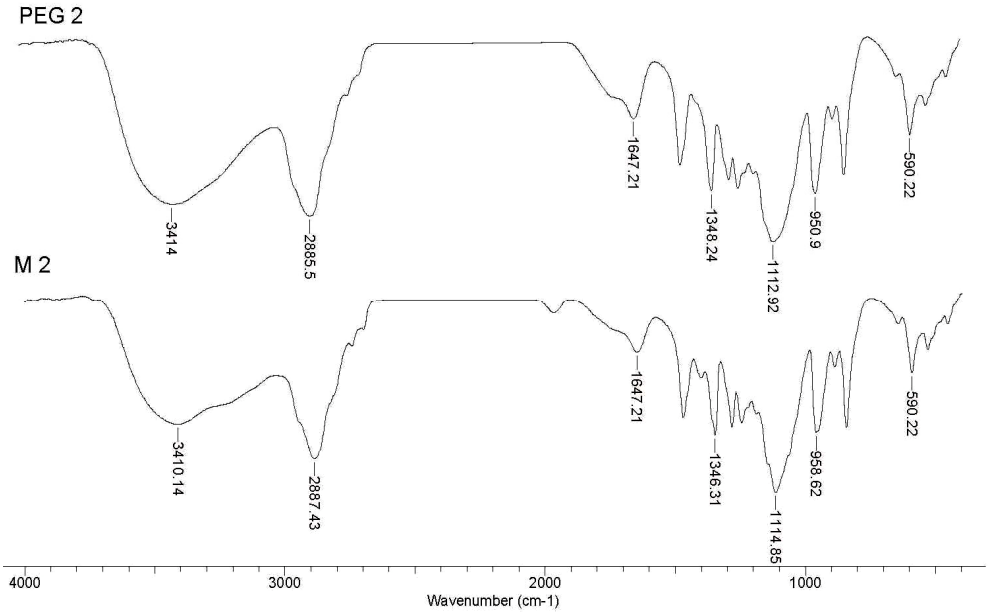

Figure 3. The IR spectra of solidified 40% (w/w) polyethylene glycol solution (PEG 2) and blank phase (M 2), in 1N H_2SO_4.

In case of PEG solution prepared in 1N H_2SO_4 (Figure 3), the maximum absorption band of water molecules is situated at 3414 cm^{-1} in solidified PEG solution (PEG 2) and remains almost unchanged after the formation of aqueous two-phase system (M 2). Thus, by using PEG solution prepared in 1N H_2SO_4, the dehydration degree of polymer chains is not significant changed after aqueous two-phase system formation, and the obtained PEG-rich phases have a lower hydrophobicity. In these conditions, is expected that in the extracted species molecules, the number of extractants associated to metal ion to be lower than maximum (6 in case of Bi(III)).

The influence of Bi(III) initial concentration was studied in the metal concentration range between 21 and 74 $\mu g/cm^3$. At it can seen from Figure 4, the Bi(III) concentration extracted into PEG-rich phase at constant concentration of iodide extractant (0.10 mol/dm^3) in considered aqueous two-phase system, increase with the increasing of initial concentration of metal ion.

On the basis of this observation and considering the limits of spectrophotometrically method used for Bi(III) analysis, in further distribution studies, an initial concentration of 62.75 $\mu g/dm^3$ was selected.

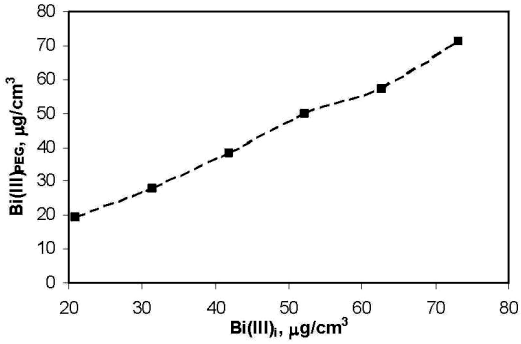

Figure 4. The influence of initial metal ion concentration on bismuth extraction in presence of iodide extractants, in considered aqueous two-phase system. ($[I^-]_{add}$ = 0.10 mol/dm^3; temperature = 24 °C).

The Bi(III) extraction behaviour was also investigated in function of type and concentration of inorganic extractants (I^-, Br^-, Cl^- and SCN^-) added in aqueous two-phase system. Comparatively, the variation of extraction parameters (D_{Bi} and E_{Bi} %) in function of NH_4X concentration added in extraction system are given in Figures 5a and 5b. An increasing of Bi(III) extraction into PEG-rich phase with increasing of inorganic extractants concentration was observed, for all cases. The values of extraction parameters follow the order: I^- >> Br^- > Cl^- >> SCN^-, which is in agreement with the results presented in other studies from literature [22, 23]. As it can seen from Figures 5a and 5b, the Bi(III) extraction parameters have higher values for I^- than Br^-, those for Br^- increase at lower concentrations that for Cl^-, and all of them are higher than the values of extraction parameters obtained in the case of SCN^-. This order could be explained by the increasing of bismuth extracted species stability from SCN^- to I^- [18]. The softness and most polarizable iodide ions have the smallest hydration Gibbs energy (ΔGhydr. = - 220 kJ mol^{-1}) [24] and form stronger complexes with bismuth, which are easy extracted into PEG-rich phase.

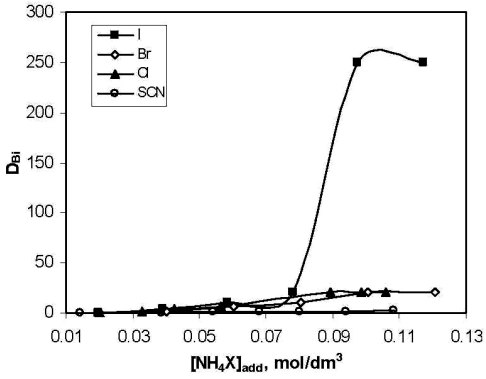

Figure 5a. The variation of Bi(III) distribution coefficient in function of extractants concentration. (Bi_i = 62.75 μg/cm^3, temperature = 24 °C).

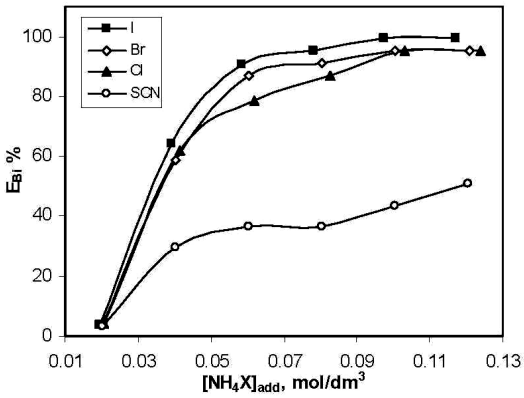

Figure 5b. The variation of Bi(III) extraction percent in function of extractants concentration. (Bi_i = 62.75 μg/cm^3, temperature = 24 °C).

The nature of the extracted species was deduced from log-log plots of distribution coefficients (D_{Bi}) versus the inorganic extractants concentrations in PEG-rich phases (in mentioned experimental conditions). The obtained dependences gave a straight line (Figure 6) with slopes 4 for halide extractants and 2 for SCN^- system, respectively. This indicate that in considered aqueous two-phase system in presence of halide extractants, Bi(III) is extracted predominant as anionic complexes (BiX_4^-), while in case of SCN^- extractant, the main extracted species have a molar ratio Bi : SCN^- = 1 : 2.

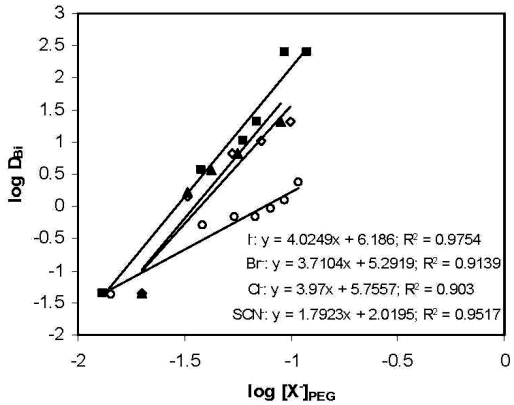

Figure 6. The log D_{Bi} against log $[X^-]_{PEG}$ dependences (Bi_i = 62.75 μg/cm^3, temperature = 24 °C).

The extraction of BiX_4^- species in case of halide extractants (instead of BiX_6^{3-}, which are more stable [18]), is mainly determined by the relative high water content of PEG-rich phases of this aqueous two-phase system (see

Figure 3). Because the hydrophobicity of these phases is lower, the formation of BiX_6^{3-} species (with a too lower hydration degree), is not necessary. In case of SCN^- extractant, the probable extraction of a mixed $Bi(SCN)_2NO_3$ species is a consequence of the appropriate stability of thiocyanate and nitrate bismuth species. This leads to the situation that during the extraction process, the exchange of NO_3^- ions with SCN^- ions, to be mainly determined by kinetics factors.

On the basis of obtained experimental results, the bismuth extraction process in presence of inorganic extractants (I^-, Br^-, Cl^- and SCN^-), in considered aqueous two-phase system can be schematic represented as in Figure 7.

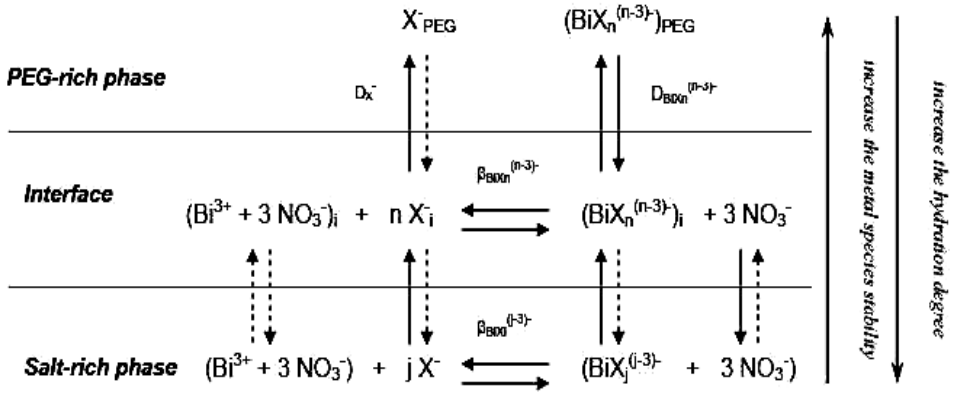

Figure 7. The schematic representation of the main elementary processes involved in Bi(III) extraction in presence of inorganic extractants, in the considered aqueous two-phase system.

According with this representation, the extraction process occurs step by step, until the hydration degree of metal ion become lowered enough (due to its complexation with extractants), and when this state is reached the metal species are immediately transferred into PEG-rich phase. After extractants addition, even in salt-rich phase, intermediary species $BiX_j(NO_3)_{3-j}$ (j = 1, 2 or 3) are probable formed, which are more stable than $Bi(NO_3)_3$, but have a hydration degree large enough for to maintain these species at the interface of this phase. At interface, these species will interact with other extractants, and in consequence the hydration degree of metal species will decrease. When, the metal species have a hydration degree compatible with those of PEG-rich phase, the partition of these occurs immediately.

The compatibility between metal species and PEG-rich phase hydration degree is a necessary condition, but not a sufficient one. According with the experimental results, an efficient extraction is obtained only when the metal ion react with inorganic extractants and form species with high stability. Thus, when in extraction system are formed a stable metallic species, these will

cross the interface with salt-rich phase, and will be efficient partitioned into PEG-rich phase (case of Bi(III) extraction in presence of halide extractants: I^-, Br^-, Cl^-). When, the formed metallic species formed in extraction system have a lower stability, the extraction process to occur until an "equilibrium state" is attained, depends on the hydrophobicity of the two aqueous phases (case of Bi(III) extraction in presence of SCN^- extractants).

CONCLUSIONS

The Bi(III) extraction behaviour in aqueous PEG(1500)–$(NH_4)_2SO_4$ two-phase system was investigated as a function of several experimental parameters: acidity of stock solutions of phase-forming components, initial concentration of Bi(III) in extraction system, type and concentration of inorganic extractants (I^-, Br^-, Cl^- and SCN^-).

The aqueous two-phase systems were prepared using aqueous solutions of phase-forming components in water and in 1N H_2SO_4. The experimental results have indicate that a quantitative extraction of Bi(III) is obtained only when both PEG and $(NH_4)_2SO_4$ stock solutions are prepared in 1N H_2SO_4, and such systems were chosen for the extraction experiments.

The addition of inorganic extractants determined an increasing of Bi(III) partition into PEG-rich phase, due to the formation of bismuth halide complexes, stable and with lower hydration degree. Under these conditions, for a given initial concentration of Bi(III) in extraction system (62.75 $\mu g/dm^3$), the extraction efficiency increase with the increasing of inorganic extractants concentration, and follow the order: $I^- >> Br^- > Cl^- >> SCN^-$. The nature of extracted species was assumed using the experimental distribution coefficients. The obtained results have indicate that in considered aqueous two-phase system in presence of halide extractants, Bi(III) is extracted predominant as BiX_4^-, while in case of SCN^- extractant, the main extracted species have a molar ratio Bi : SCN^- = 1 : 2.

On the basis of experimental results it can say that the Bi(III) extraction in presence of inorganic extractants (I^-, Br^-, Cl^- and SCN^-) occurs step by step, until the hydration degree of metal ion decrease enough (due to his complexation with extractants), and when this state is reach, the metal species are transferred into PEG-rich phase. Even the compatibility between metal species and PEG-rich phase hydration degree is a necessary condition this is not a sufficient one. An efficient extraction is obtained only when the metal species formed between Bi(III) and extractants, have a high stability.

EXPERIMENTAL SECTION

$(NH_4)_2SO_4$ (from Reactivul Bucharest) and NH_4X (X^- = I^-, Br^-, Cl^- and SCN^-) purchased from Aldrich, were analytical reagent degree and used without further purifications. Polyethylene glycol (PEG) with molecular mass

1500 (from Aldrich) was used as received. All aqueous solutions were prepared using double distilled water, obtained from a commercial distillation system.

Stock solutions of 40% (w/w) PEG(1500) were prepared by dissolving of an appropriate mass of solid polyethylene glycol in double distilled water or H_2SO_4 (Reactivul Bucharest) of known concentration. The 40% (w/w) of $(NH_4)_2SO_4$ stock solution was obtained similarly. The solution of ~ 2000 μg Bi(III)/cm^3 (10^{-2} mol/dm^3) was prepared by bismuth nitrate (from Fluka) dissolving in 20 cm^3 of HNO_3 concentrated solution (Reactivul Bucharest) and dilution to volume with double distilled water. After preparation, the exact concentration of Bi(III) was determined by standardization [25]. The solutions of inorganic extractants, containing 1 mol/dm^3 NH_4X (X^- = I^-, Br^-, Cl^- and SCN^-) were obtained by dilution of a known mass of inorganic salt to the volume with appropriate $(NH_4)_2SO_4$ stock solution. This approach provide a sever decreasing of salt forming-phase concentration after the addition of extractants.

For each experiment an aqueous two-phase system was prepared by mixing equal volumes (5 cm^3) of PEG(1500) and $(NH_4)_2SO_4$ stock solutions with different pH (measured with a Radelkis pH/ion-meter OK-281 equipped with a combined glass electrode), in a glass centrifuge tube. The systems were pre-equilibrated by centrifugation for 2 min at 2000 rpm. A 0.1 ÷ 0.5 cm^3 of Bi(III) stock solution and (0.1 ÷ 0.12) cm^3 of 1 mol/dm^3 NH_4X (X^- = I^-, Br^-, Cl^- and SCN^-) were added. The systems were again centrifuged 10 min at 2000 rpm. The centrifugation time was experimentally determined to be sufficient for these systems to reach equilibrium. Before analysis, the phases were separated using Pasteur pipettes and placed in separated tubes. 1.0 cm^3 from each phase were measured for spectrophotometrically Bi(III) analysis with KI (Digital S 104 D Spectrophotometer, 1 cm glass cell, λ= 460 nm, against a blank solution) [26]. Each Bi(III) concentration was determined in duplicate using a prepared calibration graph, and the extraction parameters (distribution coefficient (D_{Bi}) and the extraction percent (E_{Bi} %)) were calculated according to their definitions. The inorganic extractants concentration in PEG-rich phase was determined by conductometric titration with $AgNO_3$, using a Radelkis OK-109 conductometer.

For the IR experiments 1.0 ÷ 1.5 cm^3 from PEG stock solutions and blank PEG-rich phases separated from extraction systems (before the addition of metal ion and extractants), were measured and placed on the glass slides (chemical inert). The samples were solidified at room temperature (24 ± 0.5 °C). The IR spectra have been recorded using a FTIR Bio-Rad Spectrometer, in a 400 – 4000 cm^{-1} spectral domain with a resolution of 4 cm^{-1}, by KBr pellet technique.

ACKNOWLEDGMENTS

The authors would like to acknowledge the financial support from Romanian Ministry of Education and Research (Project PN II no. 51045/07).

REFERENCES

1. H. Reinhardt, *Proceedings of International Conference on Hazardous Waste*, **1998**, Cairo, Egypt, 12-16 December.
2. A.Y. Ku, J. M. Schoenung, *Toxicity, Availability and Extraction of the Metals*, **2002**, UC SMART Workshop UCLA, U.S.A, September 5.
3. S.H. Gaikwad, S.V. Mahamuri, M.A. Anuse, *Indian Journal of Chemistry and Technology,* **2005**, *12(3)*, 365.
4. T.S. Hannel, E.O. Out, M.P. Jensen, *Solvent Extraction and Ion Exchange*, **2007**, *25(2)*, 241.
5. Y. Moriya, M. Sugai, S. Nakata, N. Ogawa, *Analytical Science*, **2001**, *17(2)*, 297.
6. L. Li, C.Y. He, S.H. Li, F. Liu, S. Su, X.X. Kong, N. Li, K.A. Li, *Chinese Journal of Chemistry*, **2004**, *22*, 1313.
7. K.P. Ananthapadmanabhan, E.D. Goddar, *Langmuir*, **1987**, *3*, 25.
8. M. Shibukawa, K. Matsuura, Y. Shinozuka, S. Mizuni, K. Oguma, *Analytical Science*, **2000**, *16*, 1039.
9. M. Shibukawa, N. Nakayama, T. Ayashi, D. Shibuya, Y. Endo, S. Kawamura, *Analytica Chimica Acta*, **2001**, *427*, 293.
10. L. Bulgariu, D. Bulgariu, *Buletinul Institutului Politehnic Iaşi*, **2007**, *tom LIII (LVII)*, 21.
11. L. Bulgariu, D. Bulgariu, *Buletinul Institutului Politehnic Iaşi*, **2008**, *tom LIV (LVIII)*, 7.
12. L. Bulgariu, I. Sârghie, *Analele Stiințifice ale Universității "Al. I. Cuza" Iaşi*, s. Chemistry, **2005**, *tom XIII*, 27.
13. L. Bulgariu, D. Bulgariu, *Journal of the Serbian Chemical Society*, **2008**, *73(3)*, 341.
14. L. Bulgariu, D. Bulgariu, *Central European Journal of Chemistry*, **2006**, *4(2)*, 256.
15. R.D. Rogers, S.T. Griffin, *Journal of Chromatography B*, **1998**, *711*, 277.
16. R.D. Rogers, A.H. Bond, C.B. Bauer, *Separation Science and Technology*, **1993**, *28(5)*, 1091.
17. R.D. Rogers, A.H. Bond, C.B. Bauer, J. Zhang, S.T. Griffin, *Journal of Chromatography B*, **1996**, *680*, 221.
18. J. Lurie, "Handbook of Analytical Chemistry", Mir Publishers, Moscow, **1975**, chapter 4.
19. Bismuth distribution diagram calculated using EpH-web, accessed at 15 February 2008: http://www.crct.pdymtl.ca/ephweb.php.
20. H. Kitako, K. Ichikawa, M. Ide, M. Fukuda, W. Mizuno, *Langmuir*, **2001**, *17(6)*, 1889.
21. L. Bulgariu, D. Bulgariu, I. Sarghie, Th. Malutan, *Central European Journal of Chemistry*, **2007**, *5(1)*, 291.
22. T.A. Graber, B.A. Andrews, J.A. Asenjo, *Journal of Chromatography B*, **2000**, *743*, 57.
23. R.D. Rogers, A.H. Bond, C.B. Bauer, *Solvent Extraction in Process Industry*, **1993**, *3*, 1641.
24. Y. Marcus, *Journal of Chemical Society Faraday Trans*, **1991**, *87(18)*, 2995.
25. J. A. Dean, "Analytical Chemistry Handbook", McGrow-Hill Inc., New York, **1995**, chapter 3.
26. D.Bilba, L. Bulgariu, "Spectrometric methods of analysis" (in Romanian), Performantica, Iaşi, **2005**, chapter 5.

STUDIA UNIVERSITATIS BABEŞ-BOLYAI, CHEMIA, LIV, 4, 2009

DESFERAL EFFECT ON HUMAN ERYTHROCYTE MEMBRANE. AN ATOMIC FORCE MICROSCOPY ANALYSIS

MARIA TOMOAIA-COTISEL[a], DANIELA-VASILICA POP-TOADER[a], ULPIU VLAD ZDRENGHEA[b], GHEORGHE TOMOAIA[c], OSSI HOROVITZ[a] AND AURORA MOCANU[a]

ABSTRACT. The surface topography of erythrocyte membrane was imaged with the atomic force microscope (AFM), operating in tapping mode, and the effect of desferal (deferoxamine mesylate: DFO) at various concentrations on the cell membrane was investigated. The normal (control) human erythrocytes, without DFO, showed a clear concave form. After the incubation of fresh blood with increasing DFO concentrations, from 5 $x10^{-7}$ M to 5 x 10^{-3} M, a progressive increase in both concave depth and surface roughness of erythrocytes were observed. Further, the AFM images indicated that the particles (granules) of the cell surface nanostructure increased with the increasing DFO concentrations. This increase of surface granules is due to the aggregation of lipid nanoparticles and lipid domain formation, induced by DFO. The data are in substantial agreement with our previously published results obtained on lipid membrane models in the presence of DFO. Besides domain formation, the pore formation within human erythrocyte membrane was observed in the presence of desferal.

The DFO effect on lipid membranes might be also associated with the modification of both the conformation and the aggregation of membrane proteins, probably leading to an increased permeability of cell membrane.

Keywords: desferal, domain formation; porous membrane structure; erythrocyte membrane; AFM

INTRODUCTION

The molecular mechanism of the drug interaction with cells and the involvement of interfacial phenomena at the cell membrane are still not well understood, in spite of numerous investigations [1-12]. As a first step, the drugs action presumes that the drug molecules modify the lipid membrane structure [6-12] and thus, they may change the biological membrane properties [5, 9-12].

[a] *Babes-Bolyai University, Faculty of Chemistry and Chemical Engineering, Physical Chemistry Department, 11 Arany J. Str., 400028 Cluj-Napoca, Romania*

[b] *Iuliu Hatieganu University of Medicine and Pharmacy, Psychiatry Department, 43 Babes V. Str., 400012 Cluj-Napoca, Romania*

[c] *Iuliu Hatieganu University of Medicine and Pharmacy, Orthopaedics and Traumatology Department, 47 Mosoiu T. Str., 400132 Cluj-Napoca, Romania. E-mail: mcotisel@chem.ubbcluj.ro*

The objective of the present work is to analyze the effect of a drug, such as desferal, on the structural and topographical characteristics of erythrocyte membrane using atomic force microscopy (AFM). Recently, AFM was used to image the surface of membrane models [13-16] and of cell membranes [17-19]. AFM observations of erythrocyte membranes were used to characterize the membrane structure [20-24] and the AFM images revealed the effect of different organic and inorganic compounds on cellular membrane [25, 26].

Desferal (DFO) or desferrioxamine mesylate is *N*-[5-[3-[(5-aminopentyl)-hydroxycarbamoyl] propionamido] pentyl] -3- [[5-(*N*-hydroxyacetamido)-pentyl] carbamoyl] propionohydroxamic acid monomethanesulfonate (scheme 1). It is a transition metal chelator derived from ferrioxamine B, a sideramine isolated in 1960 from *Streptomyces pilosus*. Since it forms a very stable complex with iron(III), DFO is used for clinically removal of excess iron from blood and tissue [27] and consequently, for the treatment of acute iron poisoning and iron-overload anemia, such as thalassaemia major [28], as well as aluminium poisoning associated with chronic renal dialysis [29].

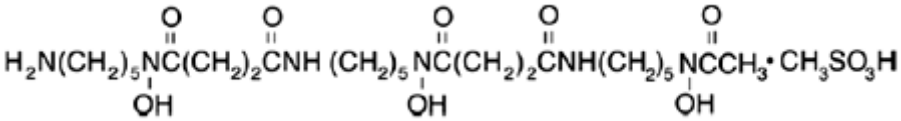

Scheme 1

We have previously investigated the acid and basic properties of desferal [30], and have made a spectroscopic study of this compound and its Fe(III) complex [31, 32]. Since desferal is supposed to act on erythrocyte membrane, we have previously investigated its effects on lipid membrane models, such as lipid monolayers, and determined the domain formation within lipid membrane layers as a function of drug concentration [12].

RESULTS AND DISCUSSION

For this work, we have chosen fresh human blood which offers stable erythrocytes. Erythrocytes samples without or treated with desferal (DFO) are investigated by AFM at room temperature in air.

The erythrocyte cell morphology

AFM images obtained for the whole cell surface morphology of control samples is presented in Figures 1, at two scanned areas of 10 μm x 10 μm and 0.5 μm x 0.5 μm. The AFM images of control samples show that erythrocytes present a concave donut shape with average lateral size.

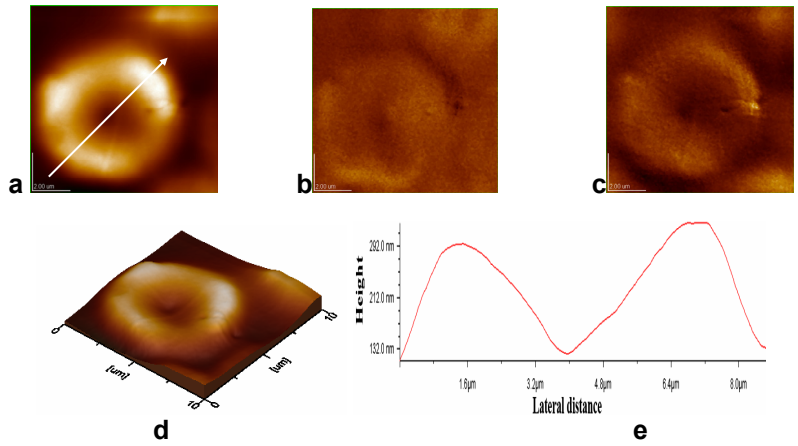

Figure 1A. AFM images of erythrocyte membrane surface, control sample: a) 2D – topography; b) phase image; c) amplitude image; d) 3D-topography; e) profile of the cross section along the arrow in image (a). Scanned area: 10 μm x 10 μm.

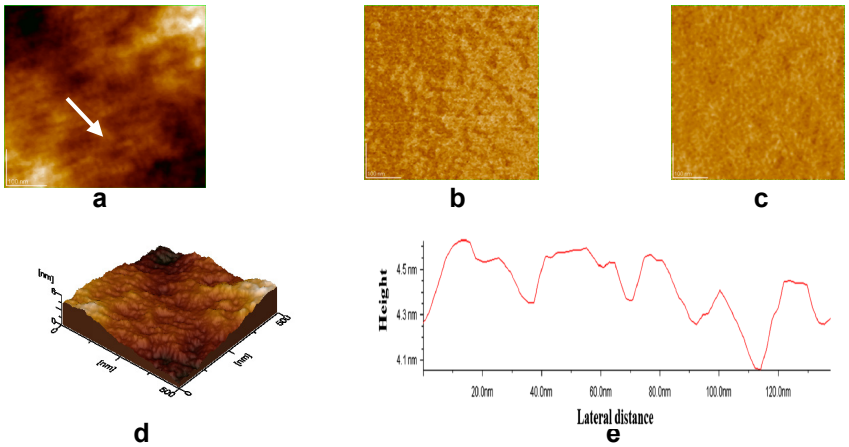

Figure 1B. AFM images of erythrocyte membrane surface, control sample: a) 2D – topography; b) phase image; c) amplitude image; d) 3D-topography; e) profile of the cross section along the arrow in image (a). Scanned area: 0.5 μm x 0.5 μm.

About 8 μm in diameter and nearly 0.14 μm in depth of concave shape (Figure 1A, Table 1). The nanostructure of normal human erythrocytes is featured by closely packed granules or particles with diameter of about 22 nm and almost uniformly distributed (Figure 1B, Table 1).

The granules probably correspond to membrane lipids well packed into the lipid part of the membrane surface in substantial agreement with lipid nanostructure found in monolayer membrane model [16]. These particles might also correspond to membrane protein protruding from the cell surface, mentioned as a probability [20].

The erythrocyte cell morphology in presence of low desferal concentration

Figures 2 and 3 show AFM images of erythrocytes treated with low desferal concentration for two different scanned areas. After mixing of fresh blood with desferal solution the desferal concentration became 5 x 10^{-7} M. The whole surface of erythrocytes is mainly characterized by the same cell shape (Figure 2) as for control sample without DFO (Figure 1A).

The membrane nanostructure in the presence of a low desferal concentration (Figure 3) is only a little different than for control (Figure 1B). The surface roughness, given by root mean square (RMS), is also very similar for these situations at the same scanned area (Table 1).

The erythrocyte cell morphology in presence of medium desferal concentration

The erythrocyte surface morphology is illustrated in Figs 4 and 5, for two different scanned areas, at medium desferal concentration of 5 x 10^{-5} M. AFM images indicate both the cell shape (Figure 4) and membrane surface nanostructures (Figure 5) are perturbed by the presence of desferal at medium concentration.

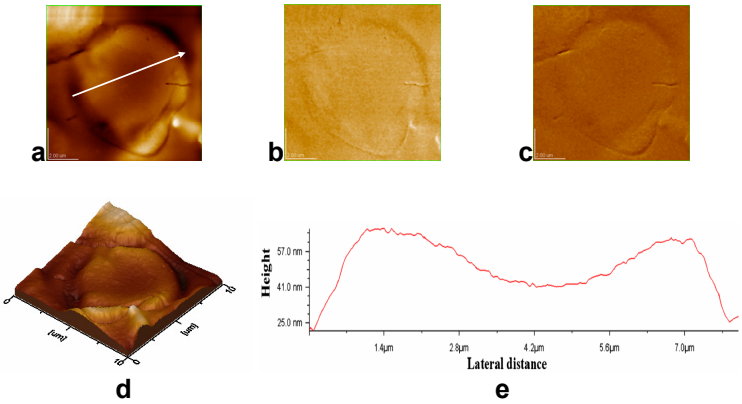

Figure 2. AFM images of erythrocyte membrane surface in the presence of DFO 5 x 10^{-7} M. a) 2D – topography; b) phase image; c) amplitude image; d) 3D-topography; e) profile of the cross section along the arrow in image (a). Scanned area: 10 µm x 10 µm.

Figure 4 presents the AFM images of an erythrocyte at a scanned area of 10 µm x 10 µm. It is clear that the concave form is again preserved as for control sample (Fig 1A), but the concave depth is much higher, to about 340 nm (Figs 4, e). The lateral size of the cell is about 8 or 8.5 µm in diameter.

It is to be noted that in Figure 4, around the cell some NaCl fragments are evidenced, probably formed during the drying process of samples. These small NaCl deposits will not affect the AFM analysis.

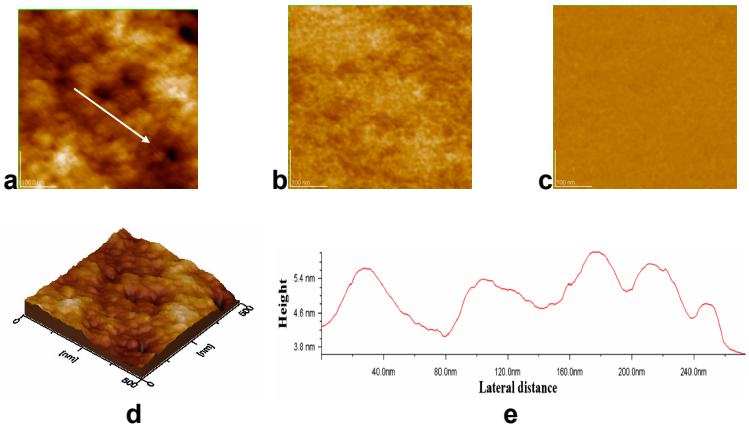

Figure 3. AFM images of erythrocyte membrane surface in the presence of DFO 5 x 10^{-7} M as shown in Figure 2. a) 2D – topography; b) phase image; c) amplitude image; d) 3D-topography; e) profile of the cross section along the arrow in image (a). Scanned area: 0.5 µm x 0.5 µm.

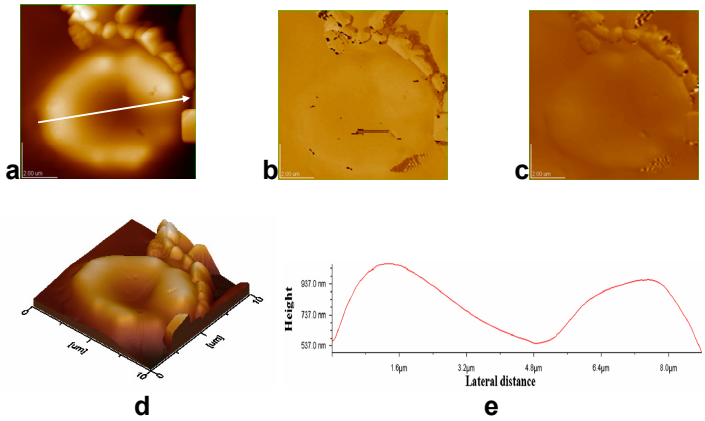

Figure 4. AFM images of erythrocyte membrane surface in the presence of DFO 5 x 10^{-5} M. a) 2D – topography; b) phase image; c) amplitude image; d) 3D-topography; e) profile of the cross section along the arrow in image (a). Scanned area: 10 µm x 10 µm. NaCl crystals were formed during the drying period of the erythrocyte cells on glass surface.

The membrane nanostructure in the presence a medium desferal concentration (Figure 5) is rather different than for control (Figure 1B) or for erythrocytes in presence of low desferal concentration (Figure 3).

The domain formation induced by desferal is well illustrated in Figure 5, particularly in panels b and c. In addition, in Figure 5b it is to be observed a clear tendency to pore formation for this desferal concentration.

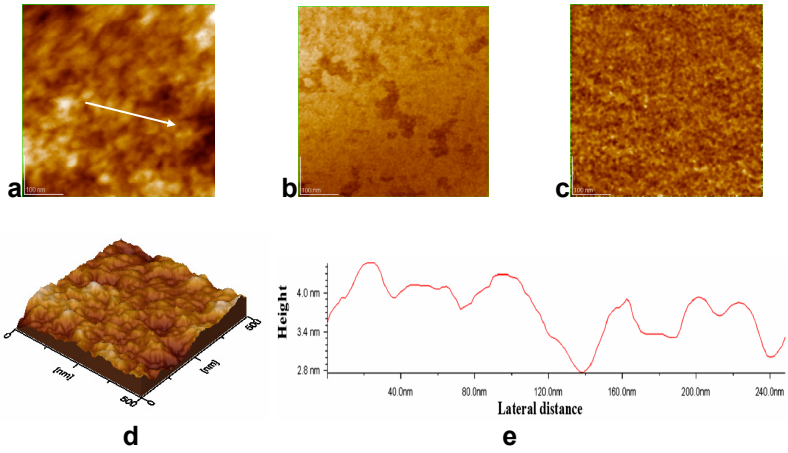

Figure 5. AFM images of erythrocyte membrane surface in the presence of DFO 5 x 10^{-5} M, as shown in Figure 4. a) 2D – topography; b) phase image; c) amplitude image; d) 3D-topography; e) profile of the cross section along the arrow in image (a). Scanned area: 0.5 μm x 0.5 μm.

However, it is to be observed that the membrane nanostructure is relatively uniformed (Figure 5, c and e) and the surface roughness is rather small (Table 1). The granules or surface particles are from about 30 nm to 50 nm (Figure 5 e, and Table 1). From these data, we can suggest a stabilizing effect of desferal on erythrocytes membrane which can be related with the desferal action on sickle cells deformability [33].

The erythrocyte cell morphology in presence of high desferal concentration

The erythrocyte surface morphology is illustrated in Figs 6-10, for four different scanned areas, at high desferal concentration of 5 x 10^{-3} M. AFM images indicate a remarkable change in both cell shape (Figs 6 and 7) and in membrane surface nanostructures (Figs 8-10).

Figure 6 presents the AFM images of several erythrocytes at a scanned area of 15 μm x 15 μm. It is clear that the three cells are somewhat separated from each other, but the cell concave form disappears.

In Figure 7, the AFM images are shown on a single cell (scanned area: 10 μm x 10 μm). Again they show that an erythrocyte is not of concave form, and it is completely different than the control sample (Figure 1A) or than erythrocytes at low (Figure 2) or medium desferal concentration (Figure 4). In other words the concave donut form can no more be identified. This situation can be correlated with a strong interaction of desferal with the cell membrane, leading to the deterioration of the membrane (Figure 6a and Figure 7a).

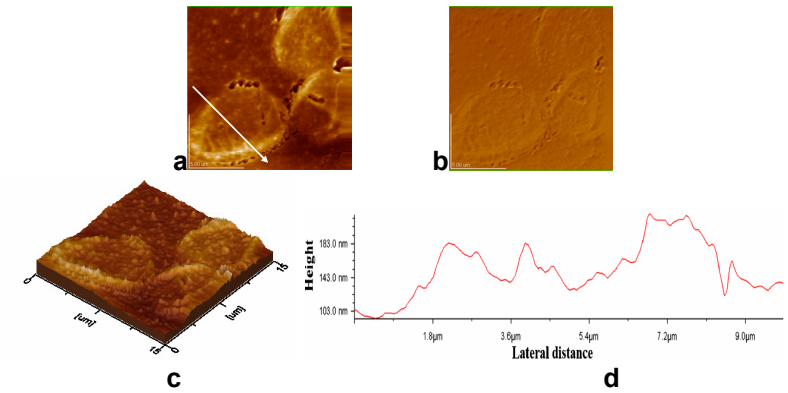

Figure 6. AFM images of erythrocyte membrane surface in the presence of DFO 5 x 10^{-3} M, zone 1. a) 2D – topography; b) amplitude image; c) 3D-topography; d) profile of the cross section along the arrow in image (a). Scanned area: 15 µm x 15 µm.

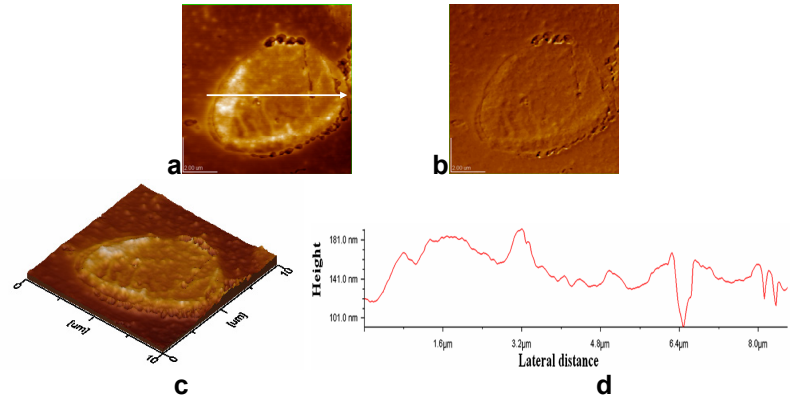

Figure 7. AFM images of erythrocyte membrane surface in the presence of 5 x 10^{-3} M desferal as described in Figure 6. a) 2D – topography; b) amplitude image; c) 3D-topography; d) profile of the cross section along the arrow in image (a). Scanned area: 10 µm x 10 µm.

The membrane nanostructure in the presence of high desferal concentration (Figs. 8 -10) is also much different as that for control sample (Figure 1B) or for erythrocytes in presence of low (Figure 3) or medium desferal concentration (Figure 5).

At this high desferal concentration (5 x 10^{-3} M) the further surface aggregation developed into a long array of aggregated particles and big elongated shaped pores (Figs. 9 and 10). The surface roughness is higher and the granules aggregates are very large (Table 1).

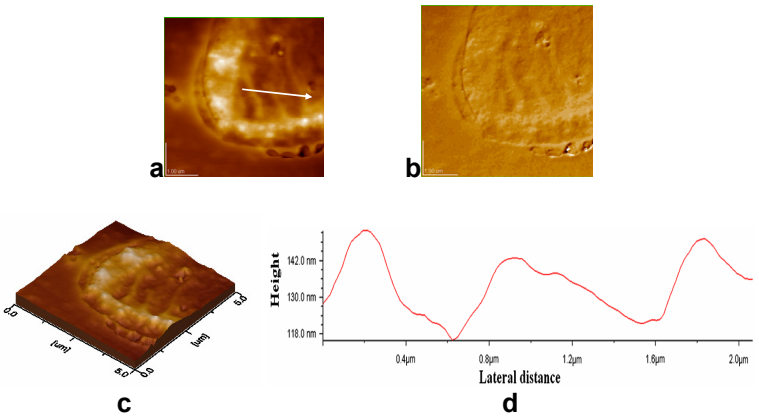

Figure 8. AFM images of erythrocyte membrane surface in the presence of DFO 5 x 10^{-3} M. a) 2D – topography; b) amplitude image; c) 3D-topography; d) profile of the cross section along the arrow in image (a). Scanned area: 5 μm x 5 μm.

Thus, desferal binds to human erythrocyte membranes and induces domain and pore formation on erythrocyte membranes. The domain and pore structures mediated by high desferal concentrations might be responsible for both enhanced surface aggregation of erythrocyte membrane and even perforation.

At low concentration, desferal can only induce the domain structure formation. With a higher DFO concentration, such as 5×10^{-3} M, the further aggregation developed into large pores.

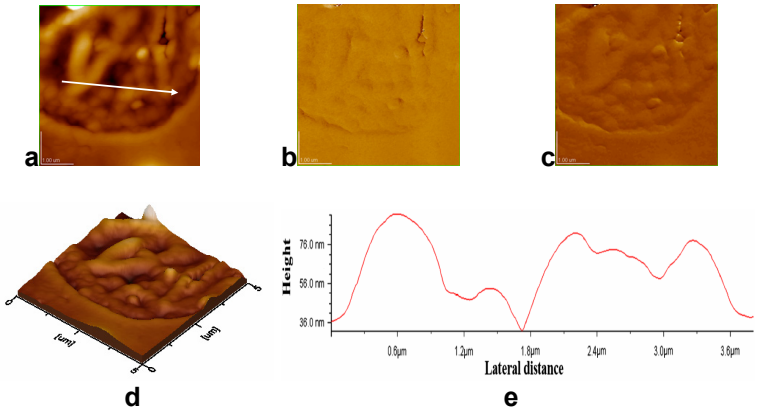

Figure 9. AFM images of erythrocyte surface in the presence of DFO 5 x 10^{-3} M, zone 2. a) 2D – topography; b) phase image; c) amplitude image; d) 3D-topography; e) profile along the arrow in image (a). Scanned area: 5 μm x 5 μm.

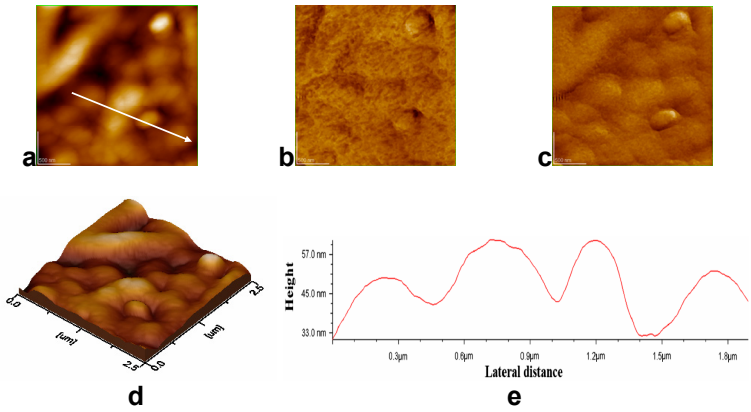

Figure 10. AFM images of erythrocyte membrane surface in the presence of DFO 5 x 10^{-3} M, zone 2. a) 2D – topography; b) phase image; c) amplitude image; d) 3D-topography; e) profile of the cross section along the arrow in image (a). Scanned area: 2.5 µm x 2.5 µm.

The erythrocyte membrane is a mosaic formed from a lipid bilayer with intrinsic and extrinsic proteins. DFO and other drugs may influence the interaction among lipids and proteins and bring changes in the membrane surface structure.

Table 1. Erythrocytes size, concave depth, granules diameter, RMS on scanned areas and on cross profile through the erythrocyte membrane, for fresh blood diluted with 0.15 M NaCl aqueous solution in the 1:1, (v:v), volume ratio, for various desferal (DFO) concentrations.

DFO conc., (M)	Fig.	Scanned areas, (µm x µm)	Cell size (µm)	Concave depth (nm)	Granules (nm)	RMS on scanned areas (nm)	RMS on cross profile (nm)
0	-	10 x 10	8.0	135	-	147	99
	-	0.5 x 0.5	-	-	24	1	0.2
	1A	10 x 10	8.4	140	-	150	101
	1B	0.5 x 0.5	-	-	22	1	0.2
5 x 10^{-7}	2	10 x 10	7.7	180	-	170	102
	3	0.5 x 0.5	-	-	30	2	0.6
5 x 10^{-5}	-	10 x 10	8	300	-	265	161
	-	0.5 x 0.5	-	-	55	3	2
	4	10 x 10	8.5	340	-	274	147
	5	0.5 x 0.5	-	-	50	1	1
5 x 10^{-3}	6	15 x 15	-	-	680	32	32
	7	10 x 10	-	-	600	33	20
	8	5 x 5	-	-	400	25	10
	9	5 x 5	-	-	400	18	16
	10	2.5 x 2.5	-	-	230	14	8

The mechanism of domain and pore formation leading to membrane perforation, provoked by high DFO concentration, could be discussed on the basis of specific interactions among DFO and lipids.

We suggest that the lipid and DFO interactions can lead to the aggregation of membrane lipids and to the coexistence of different lipid and protein phases in the erythrocyte membrane resulting from desferal membrane binding. Of course, the possibility of direct interaction of membrane proteins and desferal can not be eliminated.

The DFO might also alter the interaction of extrinsic proteins with lipid bilayer membrane, again as an effect of the drug binding to the human erythrocytes membranes.

At the same time, desferal molecules penetrated into the lipid membrane can influence the intrinsic membrane proteins and the membrane skeleton.

There might also be a drug distribution into the lipid layers, leading to an increased stability at low DFO concentrations or to a slightly decreased stability of the membrane for medium DFO concentration or even the damage of the erythrocyte membrane at very high DFO concentrations. Domain and pore formation are probably connected to an enhanced permeability of cells in presence of DFO at high concentrations.

Therefore we intend to extend our investigation on erythrocytes in the presence of higher desferal concentrations for a better understanding of desferal effects and potential implications in medical treatment.

CONCLUSIONS

The examination of AFM images on human erythrocytes in the absence and the presence of desferal at different DFO concentrations throw some light on the effect of desferal on cell membranes.

At low DFO concentrations, both the morphology of erythrocyte cells and their membrane nanostructures reveal no a significant difference in comparison with the situation of control sample, erythrocytes without DFO.

At intermediate DFO concentrations, the analysis of AFM images showed that the binding of desferal to erythrocyte membranes led to nanostructured domain formation but at the higher DFO concentration even the pore formation was evidenced.

The domain and pore structures mediated by desferal increased high concentrations might be responsible for both enhanced surface aggregation and the perforation of erythrocyte membrane.

The mechanism of domain and pore formation or the perforation process induced by desferal at its highest concentration used can be discussed on the basis of specific interactions among desferal and the membrane lipids.

These molecular interactions can lead to the aggregation of membrane lipids and to the coexistence of different lipids and proteins phases in erythrocyte membrane resulted from desferal membrane binding.

The possibility of direct interaction of membrane proteins and desferal can also contribute to the erythrocyte membrane changes in the presence of desferal.

EXPERIMENTAL SECTION

Desferal (DFO) of high purity was purchased from Ciba-Geigy, Basle, Switzerland. The DFO concentrations range in aqueous solutions, containing 0.15 M NaCl, was from 5×10^{-7} M to 5×10^{-3} M.

Fresh human blood was used in all experiments. To avoid osmotic pressure modifications, and consequently the swelling of human blood cells, all used aqueous solutions with or without drugs contained 0.15 M NaCl.

Human blood was diluted with 0.15 M NaCl aqueous solution in the 1:1 volume ratio, resulting in the control dispersion. The human blood was also treated with DFO solutions, containing 0.15 M NaCl, in the same 1:1 volume ratio as the control dispersion. The fresh blood was incubated with or without DFO, at room temperature, about 22 ^{o}C, for 30 min.

Then, 10 µL of control and DFO treated blood dispersions were each deposited on optically polished glass plate surface. The residual dispersion was removed with a piece of filter paper placed at the edge of deposited area and the samples were dried in the environmental air conditions.

During the drying process, the control and DFO treated blood samples were covered with a bicker to avoid durst. The dried control samples and DFO treated blood samples were imaged by atomic force microscope, AFM, JEOL 4210.

Atomic force microscopy is a surface imaging technique with a nanometer-scale resolution [13-18]. The cantilevers with a resonance frequency of 250 – 350 kHz were used. Triplicate samples were prepared from each blood sample and at least four separate areas were imaged for every independent sample.

Through this investigation, AFM images were obtained at several drug concentrations in order to examine the effect of desferal on the surface morphology of erythrocytes membrane.

ACKNOWLEDGMENTS

We are grateful for financial support from PN 2, grant no. 41-050.

REFERENCES

1. H. Tsuchiya, M. Mizogami, T. Ueno, K. Takakura, *Inflammopharmacol*., **2007**, *15*, 164.
2. T. Hata, H. Matsuki, S. Kaneshina, *Colloids and Surfaces B*, **2000**, *18*, 41.
3. Z. Leonenko, E. Finot, D. Cramb, *Biochimica et Biophysica Acta,* **2006**, *1758*, 487.

4. H. Matsuki, S. Kaneshina, H. Kamaya, I. Ueda, *Journal of Physical Chemistry B,* **1998**, *102*, 3295.
5. Z. V. Leonenko, D. T. Cramb, *Canadian Journal of Chemistry,* **2004**, *82*, 1128.
6. M. Tomoaia-Cotisel, E. Chifu, A. Mocanu, J. Zsakó, M. Salajan, P.T. Frangopol, *Revue Roumaine de Biochimie,* **1988**, *25* (3), 227.
7. M. Tomoaia-Cotisel, I.W. Levin, *Journal of Physical Chemistry B,* **1997**, *101,* 8477.
8. P. T. Frangopol, D. Mihailescu, *Colloids and Surfaces B,* **2001**, *22*, 3.
9. M. Tomoaia-Cotisel, *Progress in Colloid and Polymer Science*, **1990**, *83,* 155.
10. M. Tomoaia-Cotisel, D. A. Cadenhead, *Langmuir,* **1991**, *7,* 964.
11. B. Asgharian, D. A. Cadenhead, M. Tomoaia-Cotisel, *Langmuir,* **1993**, *9,* 228.
12. M. Tomoaia-Cotisel, A. Mocanu, Gh. Tomoaia, I. Zsako, T. Yupsanis, *Journal of Colloid and Surface Chemistry,* **2001**, *4* (1), 5.
13. M. Tomoaia-Cotisel, "Convergence of Micro-Nano-Biotechnologies, Series in Micro and Nanoengineering", Vol. *9,* Edts. M. Zaharescu, E. Burzo, L. Dumitru, I. Kleps, D. Dascalu, Rom. Academy Press, Bucharest, **2006**, pp. 147-161.
14. K. Hoda, Y. Ikeda, H. Kawasaki, K. Yamada, R. Higuchi, O. Shibata, *Colloids and Surfaces B*, **2006**, *52,* 57.
15. Gh. Tomoaia, M.Tomoaia-Cotisel, A. Mocanu, O. Horovitz, L.-D. Bobos, M. Crisan, I. Petean, *Journal of Optolectronics and Advanced Materials*, **2008**, *10* (4), 961.
16. P. T. Frangopol, D. A. Cadenhead, M. Tomoaia-Cotisel, A. Mocanu, *Studia Universitatis Babes-Bolyai, Chemia*, **2009**, *54* (1), 23.
17. P. C. Zhang, C. Bai, Y. M. Huang, *Scanning Microscopy*, **1995**, *9,* 981.
18. H. J. Butt, E. K. Wolff, S. A. C. Gould, *Journal of Structural Biology,* **1990**, *105*, 54.
19. Y. Cheng, M. Z. Liu, C. I. Bai, *Biochimica et Biophysica Acta,* **1999**, *1421*, 249.
20. X. Y. Zhang, F. H. Chen, P. H. Wei, J. Z. Ni, *Chinese Chem. Letters,* **2006**, *17*, 1105.
21. M. Takeuchi, H. Miyamoto, Y. Sako, H. Komizu, A. Kusumi, *Biophysical Journal*, **1998**, *74*, 2171.
22. S. Yamashina, O. Katsumata. *Journal of Electron Microscopy*, **2000**, *49*, 445.
23. A.H. Swihart, J.M. Mikrut. J.B. Ketterson, R.C. Macdonald, *Journal of Microscopy*, **2001**, *204*, 212.
24. M.S. Ho, F.J. Kuo, Y.S. Lee, *Applied Physics Letters*, **2007**, *91*, 023901.
25. Y. Cheng, M. Liu, R. Li, C. Wang, C. Bai, K. Wang, *Biochimica et Biophysica Acta – Biomembranes,* **1999**, *1421* (2), 249.
26. Y. Cheng, M. Liu, Y. Li, R. Li, C. Bai, K. Wang, *Chinese Science Bulletin*, **2000**, *45*, 426.
27. H. Keberle, *Annals of the New York Academy of Sciences*, **1964**, *119*, 758.
28. W. Banner Jr., T.G. Tong, *Pediatric Clinics of North America*, **1986**, *33,* 393.
29. J.P. Day, P. Ackrill, *Therapeutic Drug Monitoring*, **1993**, *15,* 598.
30. J. Zsako, M. Tomoaia-Cotisel, I. Albu, A. Mocanu, A. Aldea, *Revue Roumaine de Chimie*, **2002**, *47*, 869.
31. O. Cozar, N. Leopold, C. Jelic, L. David, V. Chis, M. Tomoaia-Cotisel, A. Mocanu, R. Grecu, *Studia Universitatis Babes-Bolyai, Physica,* **2004**, *49* (3), 115.
32. O. Cozar, N. Leopold, C. Jelic, V. Chis, L. David, A. Mocanu, and M. Tomoaia-Cotisel, *Journal of Molecular Structure*, **2006**, *788*, 1.
33. M. R. Clark, N. Mohandas, S. B. Shohet, *Journal of Clinical Investigation*, **1980**, *65*, 189.

STUDIA UNIVERSITATIS BABEŞ-BOLYAI, CHEMIA, LIV, 4, 2009

OMEGA POLYNOMIAL IN CUBE MED_MED_AII CRYSTAL-LIKE NETWORK

MIRCEA V. DIUDEA[a*], ALI IRANMANESH[b]

ABSTRACT. Omega polynomial $\Omega(G,x)$ is defined on opposite edge strips *ops* which are quasi orthogonal cuts *qoc* in a graph *G*=*G*(*V*,*E*), with the meaning the transitivity relation is not necessarily obeyed. The first and second derivatives, in *x*=1, of Omega polynomial provide the Cluj-Ilmenau *CI* index. The polynomial provides an appropriate topological description of infinite crystal-like networks. Close formulas for the number of atoms, Omega polynomial and *CI* index are derived for a lattice designed by using operations on maps/networks.

Keywords: graphene, CorSu network, Omega polynomial.

INTRODUCTION

The rigorous architecture of crystal networks attracted the interest of scientists in a broad area, from crystallographers, to chemists and mathematicians [1-9]. The studies on classification were followed by studies on the usefulness, in chemical reactions or in physical devices, and more recently by applied mathematical studies, in an effort to give new, more appropriate characterization of the world of crystals. Thus, recent articles in crystallography promoted the idea of topological description and classification of crystal structures [1-6]. They present data on real but also hypothetical lattices designed by computer.

Counting polynomials have been introduced, in the Mathematical Chemistry literature, by Hosoya [10,11]: *Z*(*G*,*X*) counts independent edge sets while *H*(*G*,*X*) (initially called Wiener and later Hosoya [12,13]) refers to distances in the graph. Hosoya also proposed the sextet polynomial [14-17] for counting the resonant rings in a benzenoid molecule. More about polynomials the reader can find in ref [18].

Some distance-related properties can be expressed in polynomial form, with coefficients calculable from the layer and shell matrices [19-22].

[a] *Faculty of Chemistry and Chemical Engineering, "Babes-Bolyai" University, 400028 Cluj, Romania; diudea@gmail.com*
[b] *Tarbiat Modares University, Tehran, I.R. Iran*
* This paper is dedicated to Professor Padmakar Khadikar, University of Indore, India, for his bright contributions in the field of Chemical Graph Theory.

These matrices are built up according to the vertex distance partitions of a graph, as provided by the TOPOCLUJ software package [23]. The most important, in this respect, is the evaluation of the coefficients of Hosoya $H(G,X)$ polynomial from the layer of counting LC matrix.

The present work describes the design and topology (in terms of Omega polynomial) of a crystal-like lattice, derived from the cube by applying map/net operations. The article is organized as follows: The second section illustrates the construction of the lattice while the third section provides definitions of Omega polynomial and *CI* derived index, and derives close formulas for their calculation in this network. Conclusions and references will close the article.

DESIGN OF NETWORK

A map *M* is a combinatorial representation of a (closed) surface. Some geometrical-topological transformations, called operations on maps, are used to relate parents and transformed associate graphs of fullerenes (in general, nanostructures). In this respect, operations such as: dualization *Du*, medial *Me*, truncation *Tr*, polygonal P_r capping or Snub Sn, are well known [24-28]. Our original software CageVersatile (CVNET), enables such operations and proved to be a useful tool [29].

Medial *Med* is an operation which can be achieved by putting a new vertex in the middle of each original edge and next by joining two such vertices if the parent edges spanned an angle. The *Med* transform is always a 4-valent graph, as can be seen in Figure 1. The medial operation rotates parent *s*-gonal faces by π/s. Points in the medial map represent original edges.

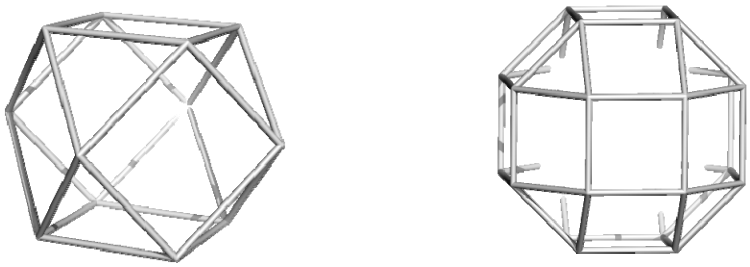

Figure 1. Transforms of the cube by Med (left) and Med(Med) (right) operations.

The objects in the above figure can be used as repeat units in building infinite networks. Figure 2 illustrates the crystal-like network built up by identifying the square faces of the *Med*(*Med*(*C*)) unit, in the three directions of coordinates. The same lattice can be obtained by performing the double medial *Med_Med_all* operation on all the hard rings which form the square 3D network [30].

Any lattice has its co-lattice, thus we focused on the *Med_Med_all* transform and assign it to be the main lattice (Figure 2, left column). Consequently, its co-lattice is that which includes the interstices and borders of the main net (Figure 2, right column).

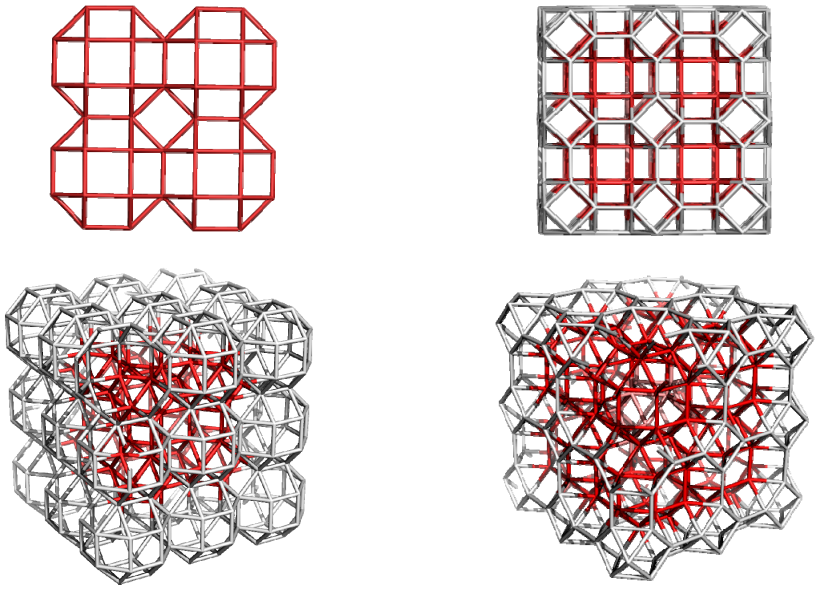

Figure 2. Lattice (333; *v*=432; left) and co-lattice (222; v=324; right) designed by Med(Med(C))_all operation, in plane projection (top) and 3D (bottom)

OMEGA POLYNOMIAL IN MED_MED_All CRYSTAL NETWORK

Let *G*(*V*,*E*) be a connected bipartite graph, with the vertex set *V*(*G*) and edge set *E*(*G*). Two edges *e* = (*x*,*y*) and *f* = (*u*,*v*) of *G* are called *codistant* (briefly: *e co f*) if

$$d(x,v) = d(x,u) + 1 = d(y,v) + 1 = d(y,u) \tag{1}$$

Let $C(e) := \{f \in E(G);\ f\ co\ e\}$ denote the set of edges in *G*, codistant to the edge $e \in E(G)$. If relation *co* is an equivalence relation, then *G* is called a *co-graph*. The set *C*(*e*) is called an *orthogonal cut (oc* for short*)* of *G*, with respect to edge *e*. If *G* is a *co-graph* then its orthogonal cuts $C_1, C_2, ..., C_k$ form a partition of *E*(*G*): $E(G) = C_1 \cup C_2 \cup ... \cup C_k,\ C_i \cap C_j = \varnothing, i \neq j$. Observe *co* is a Θ relation, (*Djoković-Winkler* [31-33]).

We say that edges *e* and *f* of a plane graph *G* are in relation *opposite, e op f,* if they are opposite edges of an inner face of *G*. Note that the relation *co* is defined in the whole graph while *op* is defined only in faces. Using the

relation *op* we can partition the edge set of *G* into *opposite* edge *strips, ops.* An *ops* is a quasi-orthogonal cut *qoc*, since *ops* is not transitive.

Let *G* be a connected graph and $s_1, s_2, ..., s_k$ be the *ops* strips of *G*. Then the *ops* strips form a partition of *E(G)*. The length of ops is taken as maximum. It depends on the size of the maximum fold face/ring F_{max}/R_{max} considered, so that any result on Omega polynomial will have this specification.

Denote by *m*(*G*,*s*) the number of *ops* of length *s* and define the Omega polynomial as [34-36]:

$$\Omega(G,x) = \sum_s m(G,s) \cdot x^s \tag{2}$$

Its first derivative (in *x*=1) equals the number of edges in the graph:

$$\Omega'(G,1) = \sum_s m(G,s) \cdot s = e = \left|E(G)\right| \tag{3}$$

On Omega polynomial, the Cluj-Ilmenau index [37], *CI*=*CI*(*G*), was defined:

$$CI(G) = \left\{ [\Omega'(G,1)]^2 - [\Omega'(G,1) + \Omega''(G,1)] \right\} \tag{4}$$

Within this paper, the main results (see Table) refer to $R_{max}(4)$. If faces instead rings are considered, the polynomial complicates both in much more terms and their structural interpretation. Other rings tested were $R_{max}(6)$ and $R_{max}(8)$. In the first case, the inclusion of hexagons consisting the cubeoctahedral units of the co-lattice brings complications in that the number of structural units, clearly envisaged in case of $R_{max}(4)$ (see below), will be lowered in the expense of longer, but more obscure *ops*. In the last case, there is a single strip and the polynomial is written as: $\Omega(G,x) = 1 \times x^s$. Consequently, the index $CI(G) = s^2 - (s + s(s-1)) = s^2 - s^2 = 0$. In this case, the strip is a "Hamiltonian strip" and its length gives just the total number of edges in *G*.

Resuming to our case $R_{max}(4)$, the Omega polynomial has only three terms (see Table). The term at *s*=2 refers to the squares visited from directions where odd rings are limiting the strip length. The term at *s*=4 counts the cubes filling the space (i.e., the interstices) left free from lattice (cube double medial) and co-lattice (cube single medial) main objects, visited from two isolated directions. Finally, the term at maximum exponent counts the main domains of the 3D structure, visited from the coordinate axe directions. We consider that this description is the most informative with respect to the infinite triple periodic crystal-like network herein studied.

The data on the co-lattice are similar to those for the main lattice (in fact is the same structure), the differences reflecting the different borders (as topology and number of atoms) of the cube domain taken into account. Formulas for counting the *CI* values (examples are given) and the number of atoms lying in the two delimitations of the structure are also included in the table.

Table. Formulas for Omega polynomial in *MedMed_all* transform of the Cube (*k*,*k*,*k*) net.

	Formulas
1	$\Omega(x) = a_2 x^2 + a_4 x^4 + a_{\max} x^{e_{\max}}$
2	$\Omega(MedMed\_all(C), x) = 12k(2k-1)x^2 + 6k(k-1)^2 x^4 + 3kx^{4k(k+1)}$
	$\Omega'(MedMed\_all(C), 1) = 12k^2(3k+1)$
	$\Omega''(MedMed\_all(C), 1) = 12k(4k^4 + 8k^3 + 9k^2 - 9k + 4)$
	$CI(MedMed\_all(C)) = 48k(27k^5 + 17k^4 + k^3 - 3k^2 + 2k - 1)$
3	Examples: (2,2,2): $72x^2+12x^4+6x^{24}$; *CI* = 108960 (4,4,4): $336x^2+216x^4+12x^{80}$; *CI* = 6148416 (7,7,7): $1092x^2+1512x^4+21x^{224}$: *CI* = 166257840
4	$\Omega(co-net, x) = 12(k+1)^2 x^2 + 6k(k+1)^2 x^4 + 3kx^{4(k+1)^2}$
	$\Omega'(co-net, 1) = 12(3k+2)(k+1)^2$
	$\Omega''(co-net, 1) = 12(k+1)^2(4k^3 + 8k^2 + 9k + 2)$
	$CI(co-net) = 48(k+1)^2(27k^4 + 89k^3 + 109k^2 + 57k + 11)$
5	Examples: (2,2,2): $108x^2+108x^4+6x^{36}$; *CI* = 736560 (3,3,3): $192x^2+288x^4+9x^{64}$; *CI* = 4418304 (4,4,4): $300x^2+600x^4+12x^{100}$; *CI* = 17509200
6	$v(MedMed\_all(C)) = 12k^2(k+1)$
	$v(co-net) = 12(k+1)^3$

Data were calculated by the original software Nano-Studio [38], developed at TOPO Group Cluj, Romania.

CONCLUSIONS

Omega polynomial $\Omega(G,x)$, defined on opposite edge strips *ops* which are quasi orthogonal cuts *qoc* in a graph, was aimed to be a simple tool in description of the topology of polyhedral molecules and crystal networks. Indeed, the first and second derivatives, in *x*=1, of Omega polynomial provide the Cluj-Ilmenau *CI* index but also an appropriate topological description of the mentioned structures. Close formulas for the Omega polynomial, *CI* index and the number of atoms, are derived for a lattice designed by using operations on maps/networks.

ACKNOWLEDGEMENTS

The article is supported by the Romanian Grant ID_506/2009.

REFERENCES

1. L. Carlucci, G. Ciani and D. Proserpio, *Coord. Chem. Rev*., **2003**, *246*, 247-289.
2. L. Carlucci, G. Ciani and D. Proserpio, *Cryst. Eng. Comm*., **2003**, *5*, 269-279.
3. V.A. Blatov, L. Carlucci, G. Ciani and D. Proserpio, *Cryst. Eng. Comm*., **2004**, *6*, 377-395.
4. I.A. Baburin, V. A. Blatov, L. Carlucci, G. Ciani and D. Proserpio, *J. Solid State Chem*., **2005**, *178*, 2452-2474.
5. O. Delgado-Friedrichs and M. O'Keeffe, *J. Solid State Chem*., **2005**, *178*, 2480-2485.
6. V.A. Blatov, O. Delgado-Friedrichs, M. O'Keeffe, and D. Proserpio, *Acta Cryst.,* **2007**, *A63*, 418-425.
7. M.V. Diudea and A. Ilić, *MATCH Commun. Math. Chem. Comput*., **2009** (submitted).
8. M.V. Diudea and A. Ilić, *MATCH Carpath. J. Math*., **2009** (submitted).
9. M.V. Diudea, A. E. Vizitiu and S. Chiger, *MATCH, Commun. Math. Chem. Comput*., **2009** (submitted).
10. H. Hosoya, *Bull. Chem. Soc. Japan*, **1971**, *44*, 2332-2339.
11. H. Hosoya, *Discrete Appl. Math*., **1988**, *19*, 239-257.
12. E. V. Konstantinova and M. V. Diudea, *Croat. Chem. Acta,* **2000**, *73*, 383-403.
13. I. Gutman, S. Klavžar, M. Petkovšek, and P. Žigert, *MATCH Commun. Math. Chem.*, **2001**, *43*, 49-66.
14. H. Hosoya and T. Yamaguchi, *Tetrahedron Lett*., **1975**, 4659-4662.
15. N. Ohkami and H. Hosoya, *Theoret. Chim. Acta*, **1983**, *64*, 153-170.
16. N. Ohkami, A. Motoyama, T. Yamaguchi, and H. Hosoya, *Tetrahedron*, **1981**, *37*, 1113-1122.
17. H. Hosoya, *Topics Curr. Chem*., **1990**, *153*, 255-272.
18. M.V. Diudea, I. Gutman, and L. Jäntschi, *Molecular Topology*, Nova, N. Y., **2002**.
19. M.V. Diudea, *J. Chem. Inf. Comput. Sci.*, **1994**, *34*, 1064-1071.
20. M.V. Diudea, *MATCH Commun. Math. Comput. Chem*., **2002**, *45*, 109-122.
21. M.V. Diudea and O. Ursu, *Indian J. Chem*., 42*A*, **2003**, 1283-1294.
22. M.V. Diudea, M. S. Florescu and P. V. Khadikar, *Molecular Topology and Its Applications*, EFICON, Bucharest, **2006**.
23. O. Ursu and M.V. Diudea, *TOPOCLUJ*, Babes-Bolyai University, Cluj, **2005**.
24. M.V. Diudea, P.E. John, A. Graovac, M. Primorac, and T. Pisanski, *Croat. Chem. Acta*, **2003**, *76*, 153-159.
25. M.V. Diudea, *Forma (Tokyo)*, **2004**, *19*, 131-163.

26. M.V. Diudea, M. Ştefu, P.E. John, and A. Graovac, *Croat. Chem. Acta*, **2006**, *79*, 355-362.
27. M. Ştefu, M.V. Diudea, and P. E. John, *Studia Univ. Babes-Bolyai*, **2005**, *50*, 165-174.
28. M.V. Diudea, *J. Chem. Inf. Model.,* **2005**, *45,* 1002-1009.
29. M. Stefu, M.V. Diudea, CageVersatile CVNET, Babes-Bolyai University, Cluj, **2007**.
30. M.V. Diudea and Cs. L. Nagy, *MATCH Commun. Math. Comput. Chem.*, **2008**, *60*, 835-844.
31. D.Ž. Djoković, *J. Combin. Theory Ser. B*, **1973**, *14*, 263-267.
32. P.M. Winkler, *Discrete Appl. Math*., **1984**, *8*, 209-212.
33. S. Klavžar, *MATCH Commun. Math. Comput. Chem.*, **2008**, *59*, 217-222.
34. M.V. Diudea, *Carpath. J. Math*., **2006**, *22*, 43-47.
35. M.V. Diudea, S. Cigher and P.E. John, Omega and Related Counting Polynomials, *MATCH Commun. Math. Comput. Chem.*, **2008**, *60*, 237-250.
36. M.V. Diudea, S. Cigher, A.E. Vizitiu, M.S. Florescu, and P.E. John, *J. Math. Chem.*, **2009**, *45*, 316-329.
37. P.E. John, A.E. Vizitiu, S. Cigher and M.V. Diudea, CI Index in Tubular Nanostructures, *MATCH Commun. Math. Comput. Chem.*, **2007**, *57* (2), 479-484.
38. Cs.L. Nagy and M.V. Diudea, *Nano-Studio software*, "Babes-Bolyai" Univ., **2009**.

STUDIA UNIVERSITATIS BABEŞ-BOLYAI, CHEMIA, LIV, 4, 2009

COMPETING ELECTROCHEMICAL AND CHEMICAL DISSOLUTION OF ALUMINUM IN PHOTOPOLYMERIZED ACRYLIC HYDROGELS

JEREMY P. WILBURN[a], CHARLIE DURHAM[b], MADALINA CIOBANU[a], ADRIAN PATRUT[c], DANIEL A. LOWY[d]*

ABSTRACT. Dissolution of aluminum in acrylic hydrogels was studied in printed ultra-thin galvanic cells, in open circuit potential, when only chemical corrosion occurred, and in the presence of external current flow, when the aluminium anode was electrochemically dissolved. By the appropriate design of the Al/hydrogel interface we were able to control the rate of electrochemical dissolution, a process driven by the applied voltage (upon short-circuiting the galvanic cell), and to avoid spontaneous chemical dissolution (and thus, maximizing the shelf life of devices in the absence of current flow). Aluminum anodes (thickness of 30-90 nm) were used in conjunction with a graphite or MnO_2 cathode. Photopolymerized acrylic gels with incorporated inorganic or quaternary ammonium salts served as the supporting electrolyte. The appearance of the first localized chemical damage of the surface defined the shelf life of the cell, and typically was on the order of days. The choice of anion and cation incorporated in the hydrogel affected both the electrochemical and chemical dissolution of aluminum.

Keywords: aluminum dissolution, aluminum anode, acrylic hydrogel, ultra thin galvanic cell, electrochemistry of aluminum.

INTRODUCTION

Over the past decade the organic electrochemistry of aluminum, an intermediately reactive metal, has developed dynamically [1-15]. Studies on the anodic behavior of Al in organic solutions with different electrolytic salts [1-9] and in ionic liquids [10, 11], respectively, were triggered by the use of Al as current collector in Li^+-ion batteries and the need for attenuating the corrosion of Al in such galvanic cells. By contrast, Yu et al. [2] and Licht et al. [12-14] studied galvanic cells equipped with Al anodes, attempting to increase the electrochemical activity of Al in organic media. Given that Al is electrochemically

[a] *Vanderbilt University, Department of Chemistry, Nashville, TN 37235, U.S.A.*
[b] *The University of Memphis, Tennessee, Department of Chemistry, Memphis, TN 38111, U.S.A.*
[c] *Babes-Bolyai University, Faculty of Chemistry and Chemical Engineering, 11 Arany Janos, RO-400028 Cluj-Napoca, Romania*
[d] *Davia, Inc., Woodbridge, VA 22191, U.S.A.; daniellowy@davia.biz*

passive in most organic electrolytes, specific solution phase activators (e.g., dissolved Hg, In, Ga, Sn, or Bi salts) are required [12]. Other research addressed Al corrosion in non-aqueous and mixed aqueous-organic media [15].

In this paper we investigate the behavior of Al in hydrogel media. We report data on the chemical and electrochemical dissolution of Al in ultrathin galvanic cells, in which the supporting electrolyte is either an inorganic or a quaternary ammonium salt, incorporated in a gel type polymer. Gels are obtained by photopolymerizing mixtures with one or two acrylic-type monomers, with water present in the system (hydrogels). We examine the dissolution rate of Al, when an external short is applied to the galvanic cell, and we are able to prevent (or minimize) the dissolution of Al in the open circuit mode. To the best of the authors' knowledge this is the first account on the electrochemical behavior of aluminum in a hydrogel system.

Presence of the thin, highly adherent native aluminum oxide layer prevents Al dissolution in many environments [16]. Chemical dissolution of Al is noticed when microscopic perforations of the natural protective oxide layer allow for the localized damage of the metal surface. For our purposes, the first localized dissolution of Al defines the *shelf life* of the cell; in the examined systems it typically is on the order of days. Electrochemical dissolution, as opposed to chemical dissolution, occurs only upon short-circuiting the galvanic cell; this causes the perforation of the protective oxide layer, and, hence, the flow of an external current.

Ellipsometry performed on 30-90 nm Al films revealed a variable thickness of the natural oxide layer over the surface, in the range of 1.8-24.8 nm, values in agreement with the average thickness of the oxide film reported in the literature [17].

Several components of the gel electrolyte in contact with the Al surface affect the rate of its electrochemical and chemical dissolution: the identity of the anion and cation present in the gel, the degree of cross-linking, the polymerization time, and the storage conditions. Therefore, we discuss these effects in detail.

RESULTS AND DISCUSSION

Choice of the supporting electrolyte

For the proper selection of the supporting electrolyte we considered: (i) the solubility of the salt in one particular photopolymerizable mixture (inorganic salts were incorporated in the hydrogels), (ii) total ionic strength in the hydrogel (the higher the ionic strength, the better the electrochemical activity); and (iii) reactivity of the anion (Cl^- ions attacked Al, while phosphates and tetraborate protected the metal) [18]. As revealed by gravimetric data (Table 1), the identity of the anion in the hydrogel affected significantly the rate of both the electrochemical and chemical dissolution of aluminum.

In the halide series (each at the same concentration) we found that: I^- inhibited the polymerization (as irradiation likely generated free iodine atoms) [19]; with F^- both chemical and electrochemical dissolutions proceeded very slowly (i.e., galvanic cells with F^- had extended shelf life, and the electrochemical dissolution rate was approximately the same as the chemical dissolution rate); with Cl^- present in the gel, the lifetime of galvanic cell decreased five fold as compared to Br^-; surprisingly, the electrochemical dissolution with Br^- was just slightly slower than with Cl^- (less by only 20%). Chloride ion is the main environmental factor, which accelerates pit initiation [20], which accounts for the much greater chemical dissolution rate in the presence of Cl^-.

Table 1: Effect of anions and cations present in the hydrogel on the dissolution rate of Al (data recorded in the two-electrode ultrathin system)

Salt Concentration	Investigated Ion	Electrochemical Dissolution Rate [$\mu g\ cm^{-2}\ s^{-1}$]	Chemical Dissolution Rate [$\mu g\ cm^{-2}\ s^{-1}$]
Potassium halides (0.88 *M*)	F^-	3.10×10^{-2}	3.10×10^{-2}
	Cl^-	27.9	1.57×10^{-2}
	Br^-	23.2	3.36×10^{-3}
	I^-	Interfered with the polymerization	
Other potassium salts (0.44 *M*)	NO_3^-, ClO_3^-, SO_4^{2-}, $H_2PO_4^-$, HPO_4^{-2}, PO_4^{3-}, $B_4O_7^{2-}$	$5 \times 10^{-5} - 2 \times 10^{-3}$	$< 10^{-5}$
Chlorides (0.48 *M*	Li^+, Na^+, K^+, Rb^+, Cs^+	17.6 ± 2.4	$(1.42 \pm 0.04) \times 10^{-2}$

Polyatomic anions, such as NO_3^-, ClO_4^-, HPO_4^{2-}, $H_2PO_4^-$, PO_4^{3-}, and $B_4O_7^{2-}$ were virtually inert; they did not sustain either chemical or electrochemical dissolution (in each experiment the cation was K^+). Current density, recorded upon short-circuiting the ultrathin galvanic cells, corresponds to the electrochemical dissolution rate of Al. Current delivered by the system over time, with various anions in the hydrogel, is displayed in Figure 1a. Nitrate was the least active, yielding maximum current values of less than 10 μA, which lasted just for a few seconds, the current decaying fast after ca. 10 s. While HPO_4^{2-} and PO_4^{3-} showed 7-9 fold greater initial currents than NO_3^-, they were still unable to sustain a constant current, which would correspond to a uniform dissolution rate of Al. Hence, polyatomic anions are not useful in the supporting electrolyte (despite the corrosion inhibiting properties of several of them, which would defer chemical dissolution of Al). When fast electrochemical dissolution is desired, Br^- exhibits the most favorable properties (Table 1): its electrochemical activity is close to that of Cl^- (only 17% less), and in the meanwhile it allows for an extended shelf life of the device (4.7 times longer than in the presence of Cl^-).

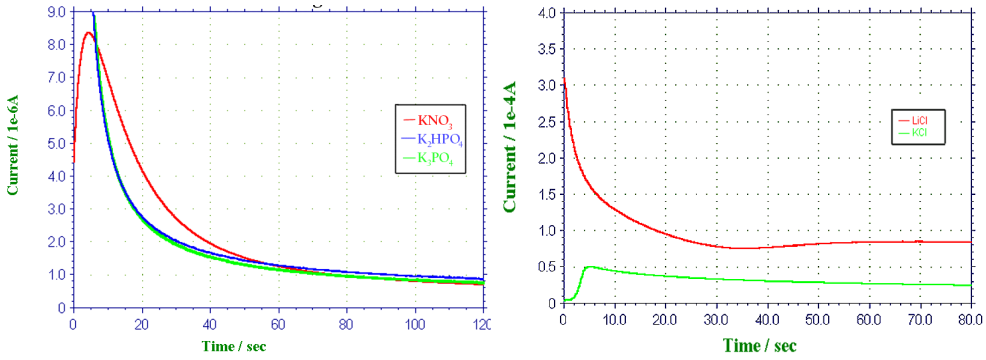

Figure 1. (**a**) Effect of anions on the electrochemical dissolution of Al in acrylic acid/ acrylonitrile copolymers: comparison of NO_3^-, HPO_4^{2-}, and PO_4^{3-}; (**b**) Cation effect on the electrochemical dissolution of Al: comparison of Li^+ (top curve) and K^+ (bottom curve). All experiments were performed with ultra thin galvanic cells (displayed schematically in Figure 3).

When comparing cations immediately after short-circuiting the device, Li^+ showed greater electrochemical dissolution rate than K^+ (Figure 1b), while Na^+ was approximately 40% less active (not shown). Over the long term (200 h) the average dissolution rate became identical for Li^+ and K^+: 102 ng h^{-1}. With CsCl incorporated in the hydrogel, an initial current of 60 μA was recorded over 300 s (a value intermediate between Li^+ and K^+), and then it dropped fast to 10 μA, within 100 s to (graph not shown). Multivalent cations were not useful, as they affected the texture of the hydrogel. Slow chemical dissolution is desirable; therefore, from the cations in Table 1, K^+ is the best choice. However, when fast electrochemical dissolution is attempted, Li^+ salts are the most efficient.

From these studies, best cations were K^+ (for slow electrochemical dissolution) and Li^+ (for fast electrochemical dissolution). When combined with bromide (the most convenient anion), they provided the best salts for being used in hydrogels.

In order to determine the optimal concentration of the supporting electrolyte, we tested the activity of hydrogels, which contained increasing salt concentrations. Electrochemical dissolution rate of Al increased with increasing KCl or KBr content up to 5.5-6.4 wt.%, and then it diminished, probably due to ion pairing. Ion pairs are poor charge carriers, as they do not possess a net charge and stay solvated. Therefore, the conductivity of the hydrogels decreased, and the corrosion current depleted. At high salt concentrations (9.3-11.6 wt.%) charged triplets were formed, and the current increased, again. Unlike ion pairs, triple ions do possess a net charge, and can act as charge carriers. Similar behavior of electrolytes is known in solvents with low dielectric constant [21]. Hence 5.5-6.0 wt.% represents the optimal concentration of the salt in the hydrogel.

These studies on ion effects revealed that while the chemical dissolution rate primarily depends on the adsorption of active anions and the destruction of the natural protective Al_2O_3 layer [22], the electrochemical dissolution is affected by the radius and mobility of the anions. Consequently, the viscosity of the hydrogel and thickness of the hydrogel layer influence to a considerable extent the electrochemical process. In most cases, it has proven an extremely difficult task to identify a system in which electrochemical dissolution can be driven efficiently, while keeping an extended shelf life of the battery via inhibiting spontaneous chemical dissolution.

Selection of monomers and setting the pH of the hydrogel

When keeping the supporting electrolyte concentration constant in the polymer (6.0 wt. %), the corrosion of Al matrices was 10 fold faster in poly(acryloyloxyethyl trimethylammonium chloride), which contains bound charged groups, as compared to acrylic acid/acrylonitrile copolymers, which becomes an ionic conductor via adding a salt to the gel. The looser texture and higher water content of the former hydrogel may allow for an easier migration of the ions, securing by this a better conductivity of the polymer matrix. As a general rule, the recorded current density decreased with decreasing water content of the hydrogel, its lowest value of 5 μA cm^{-2} being observed in the absence of water. We addressed the effect of water content on the polymer matrix in an earlier paper [23].

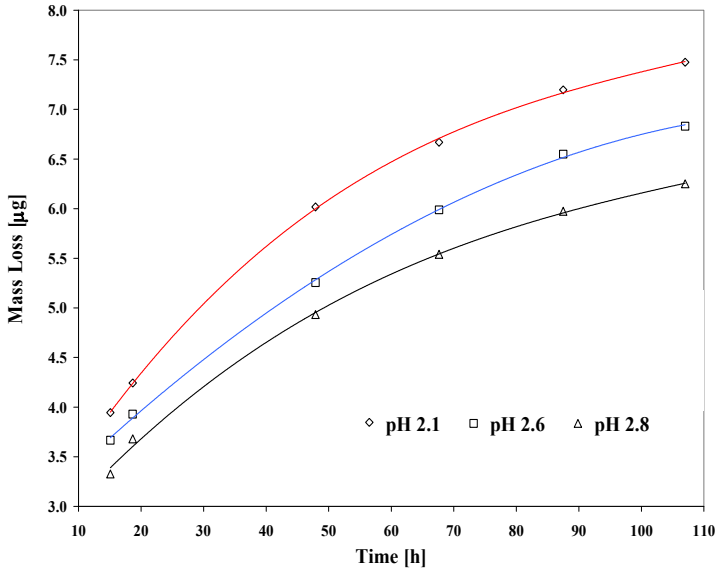

Figure 2. Electrochemical dissolution (mass loss) of Al over time at acidic pH values: bottom line – pH 2.1, middle line – pH 2.6, top line – pH 2.8.

Mass loss of Al over time in contact with hydrogels of decreasing pH value is shown in Figure 2. As the hydrogel becomes more acidic, the system is moved away from the passivity zone of Al (pH 4.0-8.6, according to the Pourbaix diagram [24]). Thus, the electrochemical activity of Al is enhanced and the corrosion rate increases; the average corrosion rate is 38.7 ng h^{-1} at pH 2.8, 40.1 ng h^{-1} at pH 2.6, and 48.6 ng h^{-1} at pH 2.1. Acidic pH values below pH 3.8 are favorable for fast electrochemical dissolution [24]. By setting the pH value we were able to fine-tune the rate of the dissolution process.

CONCLUSIONS

The use of supporting electrolytes incorporated in UV-cured acrylic-type gels allowed for a new approach toward the organic electrochemistry of aluminum. In addition to the chemical identities of the anion and cation, and the selection of the monomer, water content and the pH value of the hydrogel have proven critical to controlling the electrochemical activity of aluminum. Aluminum anodes were active in ultrathin galvanic cells with gel type electrolytes. Driving the electrochemical dissolution, while inhibiting or delaying spontaneous chemical dissolution appears to be an extremely demanding task.

EXPERIMENTAL SECTION

Materials. Gel-type electrolytes were prepared according to previously reported procedures [25, 26]. Typically, hydrogels contained 30-50 wt.% of water and an inorganic salt, such as alkali halides: LiCl, NaCl, RbCl, and CsCl (99+% each, Aldrich), and KCl (Spectro pure, SPEX Industries, Inc.). Several other salts were tested: Na^+ and K^+ chlorates, bromides, nitrates, sulfates, phosphates, hydrogenphosphates, and dihydrogenphosphates (all from Aldrich). For preventing the formation of Al/O_2 batteries, prior to polymerization the curable mixture was degassed with Ar for 15 min [23].

Electrochemical measurements. Electrochemical measurements were conducted with screen-printed ultra thin galvanic cells (Wisconsin Labels Associates, Peachtree City, GA), equipped with Al anode (surface area of 0.20-0.75 cm^2 and thickness of 30-90 nm). Ultrathin galvanic cells operate with Al anode and MnO_2 or graphite cathode; the hydrogel serving as the ionic conductor, is sandwiched between the electrodes (Figure 3). Model 660a Electrochemical Workstation (CH Instruments, Austin, TX) was utilized, measurements being performed under a Faraday cage, at 298.2 ± 0.1 K, thermostated with a Model RTE-210 thermostat (Neslab Instruments, Inc., Newington, NH).

Surface examination. The thickness of the natural protecting Al_2O_3 layer on the surface of Al thin films was determined by ellipsometry with a Model Compel ELC-10 ellipsometer (InomTech Products, Inc., West Hartford, CT), data processing being performed by means of the software supplied

by the manufacturer. Microscopic perforations of the natural protective oxide layer on Al were observed with a stereo magnifier (Bausch & Lomb, magnification 10) and a stereo microscope (Fisher Micromaster®, magnification 400). The thin cell design included a red-colored substrate beneath the thin Al layer to facilitate detection of localized perforations.

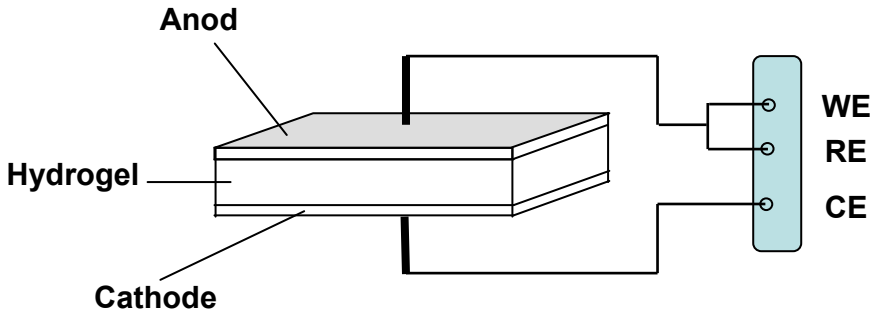

Figure 3. Schematics of the ultra thin galvanic cell setups used for testing of Al in hydrogel electrolytes (Anode: metallic Al; Cathode: graphite or MnO_2; Hydrogel: acrylic polymer; WE – working, RE – reference, and CE – counter electrodes)

Gravimetric method. Dissolution of Al was monitored by gravimetric method, i.e., the weight loss over time of the ultrathin galvanic cell.

ACKNOWLEDGEMENTS

Authors are grateful for support from Wisconsin Labels Associates (Peachtree City, GA), Translucent Technologies, LLC and The University of Memphis (both in Memphis, TN).

REFERENCES

1. J.B. Wang, J.M. Wang, H.B. Shao, X.T. Chang, L. Wang, J.Q. Zhang, C.N. Cao, *Materials and Corrosion – Werkstoffe und Korrosion*, **2009**, *60*, 269.
2. L. Yu, F.C. Liu, Z.W. Fu, *Electrochim. Acta*, **2009**, *54*, 2818.
3. A. Abouimrane, J. Ding, I.J. Davidson, *J. Power Sources*, **2009**, *189*, 693
4. J.B. Wang, J.M. Wang, H.B. Shao, J.Q. Zhang, C.N. Cao, *J. Appl. Electrochem.*, **2007**, *37*, 753.
5. T.C. Hyams, J. Go, T.M. Devine, *J. Electrochem. Soc.*, **2007**, *154*, C390.
6. X.Y. Zhang and T.M. Devine, *Electrochem. Soc.*, **2006**, *153*, B351.

7. X.Y. Zhang and T.M. Devine, *Electrochem. Soc*., **2006**, *153*, B375.
8. X.Y. Zhang, B. Winget, M. Doeff, J.W. Evans, T.M. Devine, *Electrochem. Soc*., **2005**, *152*, B454.
9. T. Kawamura, T. Tanaka, M. Egashira, I. Watanabe, S. Okada, J. Yamaki, *Electrochem. Solid State Lett.*, **2005**, *8*, A459.
10. X.C. Peng, L. Yang, Z.X. Zhang, K. Tachibana, Y. Yang, S.Y. Zhao, *Elchim. Acta*, **2008**, 53, 4764.
11. C.X. Peng, L. Yang, Z.X. Zhang, K.H. Tachibana, Y. Yang, *J. Power Sources*, **2007**, *173*, 510.
12. G. Levitin, C. Yarnitzky and S. Licht, *Electrochem. Solid State Lett.*, **2002**, *5*, A163.
13. S. Licht, G. Levitin, R. Tel-Vered, C. Yarnitzky, *Electrochem. Comm*., **2000**, *2*, 329.
14. S. Licht, R. Tel-Vered, G. Levitin, C. Yarnitzky, *Electrochem. Soc*., **2000**, *147*, 496.
15. L.R.B. Holzle, D.S. Azambuja, C.M.S. Piatnicki, G.E. Englert, *Mater. Chem. Phys*., **2005**, *91*, 375.
16. S.K. Toh, D.G. McCulloch, J. Du Plessis, P.J.K. Paterson, A.E. Hughes, D. Jamieson, B. Rout, J.M. Long, A. Stonham, *Surface Rev. Lett*., **2003**, *10*, 365.
17. E. McCafferty, Surface Hydroxyls: the Outermost Layer of the Passive Film, in: R.G. Kelly, G.S. Frankel, P.M. Natishan, R.C. Newman (Eds.), *Electrochemical Society Proceedings*, Vol. 98-17, 1998, pp. 42-55.
18. D.A. Lowy and J.P. Wilburn, 'Electrochemistry of Aluminum in Organic Hydrogel Systems,' 219th ACS Meeting, San Francisco, CA, March 26-30, 2000, Paper #382231.
19. J.P. Wilburn, M. Ciobanu, N.I. Buss, D.R. Franceschetti, D.A. Lowy, *Anal. Chim. Acta*, **2004**, *511*, 83.
20. J.W. Braithwaite, A. Gonzales, G. Nagasubramanian, S.J. Lucero, D.E. Peebles, J.A. Ohlhausen, W.R. Cieslak, *J. Electrochem. Soc*., **1999**, *146*, 448.
21. J.O'M. Bockris, A.K.N. Reddy, *Modern Electrochemistry*, Plenum Press, New York, 1999.
22. M.Z.A. Munshi, R. Gopalienger, B.B. Owens, *Solid State Ionics*, **1988**, *27*, 259.
23. J.P. Wilburn, M. Ciobanu, D.A. Lowy, *J. Appl. Electrochem.*, **2004**, *34*, 729.
24. R.J. Small, M.L. Peterson, A. Robles, D. Kempa, J. Knittel, *Micro*, **1998**, *16*, 61.
25. M. Ciobanu, J.P. Wilburn, N.I. Buss, P. Ditavong, D.A. Lowy, *Electroanalysis*, **2002**, *14*, 989.
26. M. Ciobanu, J.P. Wilburn, D.A. Lowy, *Electroanalysis*, **2004**, *16*, 1351.

STUDIA UNIVERSITATIS BABEŞ-BOLYAI, CHEMIA, LIV, 4, 2009

GAS CHROMATOGRAPHY-MASS SPECTROMETRY METHOD FOR DETERMINATION OF MONOTERPENE AND SESQUITERPENE EMISSIONS FROM STRESSED PLANTS

LUCIAN COPOLOVICI[a], ASTRID KÄNNASTE, ÜLO NIINEMETS

ABSTRACT. Emissions of biogenic volatile organic compounds (BVOCs) play important roles in plant biology and atmospheric chemistry at a wide range of spatial and temporal scales. This article describes a headspace method coupled with gas chromatography – mass spectrometry (GC-MS) for the detection of volatile terpenes (monoterpenes and sesquiterpenes) and other related compounds emitted from plants, especially under stress conditions. A protocol is developed for simultaneous detection and quantification of isoprene, and mono- and sesquiterpenes from plant emissions.

Keywords: BVOC emission, Mass spectrometry, Monoterpenes, Plant stress, Sesquiterpenes

INTRODUCTION

Plants emit more than 30000 chemically different volatile organic compounds (BVOC). The emissions of some of these compounds result from and serve as markers of activation of certain metabolic pathways in plants, end-products or intermediates of which are volatile [1]. Many of these volatiles also play important roles in plant communication with other plants and animals [2]. There are further constitutive emissions of several specific volatile compounds thought to be involved in plant non-specific defence to various abiotic and biotic stresses [1, 3]. Worldwide, it has been estimated that biogenic production of volatile organic compounds exceeds the anthropogenic production by an order of magnitude. Apart from the significance for plants, these emissions play important role in atmospheric chemistry and physics, in particular in formation of atmospheric pollutant ozone in the troposphere and formation of aerosols [4-7].

The volatile isoprenoids – isoprene (5 carbon atoms, C5) and volatile terpenes consisting of isoprene building blocks, monoterpenes (C10, MT) and sesquiterpenes (C15, SQT) – form a major part of plant-generated BVOC. Several widespread plant species are strong constitutive emitters of volatile isoprenoids, while volatile isoprenoid emissions can be induced by various environmental and biotic stimuli also in species not emitting these compounds constitutively [8, 9].

[a] *Institute of Agricultural and Environmental Sciences, Estonian University of Life Sciences, Kreutzwaldi 1, Tartu 51014, Estonia*

Plant volatile isoprenoid emissions consist of a complex blend of chemically heterogeneous compounds. Often more than 20 different MT [10, 11] are emitted by a single plant species. These compounds have widely differing chemical reactivity and ozone-forming potentials in the atmosphere [12]. A number of SQT and some oxygenated sesquiterpene alcohols, aldehydes, and ketone derivatives ($C_{15}H_{22}O$, $C_{15}H_{24}O$, $C_{15}H_{26}O$) have further been identified in studies on BVOC emissions from both natural [13-17] and agricultural vegetation [18, 19]. All volatile isoprenoids, isoprene, MT and SQT, are anticipated to importantly participate in secondary aerosol-forming processes and in chemical reactions in the lower troposphere [6, 16, 21-23], but SQT are generally more reactive than isoprene and MT. The atmospheric lifetimes of reactive SQT such as β-caryophyllene as determined by their rapid gas-phase reactions with ozone, and OH and NO_3 radicals have been estimated to be on the order of only a few minutes[11, 15], while the life-time of isoprene and most monoterpenes varies between 36 min during daytime in summer and a few hours during nighttime in winter [24].

A vast array of volatile terpenes (MT and SQT) is involved in the communication between plants and between plants and herbivores [9, 25-29]. Under stress, the emissions of volatile isoprenoids may be amplified in constitutive emitters and be induced also in species not emitting these compounds constitutively [8, 9], modifying the plant communication with other organisms. For instance, emission of *de novo* synthesized compounds such as methylsalicylate, farnesenes, (*E*)-*β*-ocimene, linalool, *etc*, which serve as signals of the induced defence reactions in stressed plants, is often observed in plants not emitting isoprenoids in non-stressed conditions [30, 31]. Plant-insect relationships can also be altered by increased emissions of other stress compounds that occur simultaneously with enhanced isoprenoid emissions, e.g. emissions of green leaf volatiles (GLV, volatile aldehydes formed via the lipoxygenase pathway) occur in stressed plants as the result of the destruction of free fatty acids in lipoxygenase pathway [31, 32]. Apart from plant communication, volatile isoprenoid emissions are also thought to increase the plant tolerance to a variety of biotic and abiotic stresses [3 for a review].

Simultaneous measurement of the wide spectrum of plant volatiles with different physico-chemical characteristics constitutes an analytical challenge. Preconcentration of BVOCs on cartridges filled with solid adsorbents followed by thermal desorption and GC analysis has become a well-accepted analysis technique in a wide range of applications [14, 33, 34]. Additionally, other methods based on the sampling of headspace into stainless steel canisters followed by cryo-focusing and analysis by gas chromatography equipped with the flame ionization detector (GC-FID) analysis [35], or the technique for rapid collection of volatiles by solid-phase micro-extraction (SPME) coupled with GC-MS have been used [36-38]. The techniques described in the literature are generally for compounds in the range of volatility of C5–C10. In contrast, the

applicability of adsorbent sampling/thermal desorption for semi-volatile BVOC has received much less attention and application (see [39, 40] for review). The most commonly used adsorbents include diverse carbon adsorbents (active carbon, graphitized carbon, and carbon molecular sieves) and also synthetic polymeric adsorbents (Tenax, Chromosorb, etc.) [39, 41].

The goal of this study was to develop a quantitative method for simultaneous determination of mono- and sesquiterpenes in air samples from plants exposed to different biotic and abiotic stresses. The developed method is based on preconcentration of BVOCs on solid absorbents coupled with GC-MS analysis, and is optimized for quantitative determination of plant volatiles with widely varying physico-chemical properties.

RESULTS AND DISCUSSION

Combinations of adsorbents in a single adsorbent cartridge (volatile trap) have been previously used to trap and analyze compounds over a wider range of volatility than can be achieved with a single adsorbent [42]. In preliminary experiments of our study, the type and the amount of absorbent, and the cleanup method of adsorbent cartridges were optimized. We finally used the combination of Carbotrap C, Carbopack C and Carbotrap X for the multibed cartridges. These chemically neutral carbon-based adsorbents permit trapping of unsaturated compounds (*e.g.* monoterpenes) without intervening chemical reactions in the ambient air that can for instance happen with organic polymer adsorbents such as Tenax TA in oxidative atmosphere [43].

Several GC parameters and oven temperature program were optimized to achieve excellent separation of main mono- and sesquiterpenes emitted from the stressed plants in a single GC column. Different temperature regimes, flow rates of carrier gas and columns with differing polarity were tested. Ions based on the following criteria were selected for compound detection: (i) molecular ions for compound detection (together with the fragment mass spectrum); (ii) fragment ions with high abundance, such as base peaks; (iii) target ions with selectivity minimizing the cross-interferences between different BVOC's. Based on these criteria, scanning tests of the standard solutions trapped in cartridge of each monoterpene and sesquiterpene were carried out to describe the scanning mass spectrum and retention time of various isoprenoids. One target ion and two qualitative ions (qualifiers) for each compound were selected (Table 1). Operative conditions (oven program, time and temperature of desorption etc) were fixed on the basis of optimization results. Overall, the retention times of terpene standards were relatively concentrated in two parts of the chromatogram: one part featuring most of the monoterpene peaks and the other most sesquiterpene peaks. Among the tested columns (DB-1, DB-2, ZB-5) a fused silica ZB-624 column proved to provide the best separation of common monoterpenes and sesquiterpenes present in the emission of stressed plants (Table 1).

Table 1. Chromatographic and mass spectral data obtained by the GC-MS methods for all the tested terpene standards and methylsalicylate

	Molecular mass (g mol^{-1})	Retention time (min.)	Target ion (m/z)	Qualifiers* (m/z)
α-Pinene	136	18.74	93	92, 91
β-Pinene	136	21.44	93	41, 69
α-Phellandrene	136	22.56	93	91, 77
Δ^3-Carene	136	22.88	93	91, 77
α-Terpinene	136	23.33	93	121, 91
(*E*)-β-Ocimene	136	23.72	93	92, 91
Limonene	136	23.94	68	67, 93
β-Phellandrene	136	24.39	93	91, 77
1,8-Cineole (Eucalyptol)	154	24.78	43	81, 71
γ-Terpinene	136	25.60	93	91, 77
α-Terpinolene	136	27.46	93	121, 136
4,8-Dimethyl-1,3,7-nonatriene	150	28.80	69	41, 81
Linalool	154	29.87	71	43, 81
α-Thujone	152	31.74	81	110, 41
β-Thujone	152	32.47	110	81, 41
Methylsalicylate	204	37.73	120	92, 152
Bornyl acetate	204	42.67	95	43, 93
(*Z*)-β-Farnesene	204	49.51	69	41, 93
α-Cedrene	204	50.38	119	93, 105
(*E*)-β-Caryophyllene	204	51.08	41	69, 93
α-Humulene	204	53.25	93	80, 41, 121
(*E*,*E*)-α-Farnesene	204	53.83	93	41, 69
Nerolidol	204	56.33	69	41, 43

* The qualifier ion (or SRM transition) is often an isotope peak or a higher mass product ion as opposed to the second most abundant ion in the spectra.

Terpene quantification was based on the total ion current monitored by the GC-MS system calibrated with terpene standards.

The GC-MS response for all monoterpenes and sesquiterpenes was linear in the concentration range assayed ($3\cdot10^{-9}$-$1\cdot10^{-7}$ mol/L). Relevant data from the calibration plots are summarized in Table 2. It is apparent that the linear calibration ranges and the slopes (analytical sensitivity) of the calibration

graphs are similar for all the mono and sesquiterpenes investigated. The detection limits of the method were estimated as three times of standard deviation of the response (10 determinations) to a blank sample. The values found ranged between 0.1 and 4.7 nmol mL^{-1}, depending on the terpene. The average relative standard deviation was 0.2% for ten samples.

Table 2. Features of calibration plots for the determination of different terpenes

	Slope* (area mol^{-1} L^{-1})	Relative standard deviation of the slope (%)	Correlation coefficient	Detection limit (nmol mL^{-1})
α-Pinene	$6.76 \cdot 10^{16}$	1.0	0.995	1.6
β-Pinene	$5.87 \cdot 10^{16}$	0.9	0.992	1.8
α-Phellandrene	$3.90 \cdot 10^{16}$	5.1	0.994	2.7
Δ^3-Carene	$5.05 \cdot 10^{16}$	5.0	0.995	2.1
α-Terpinene	$4.71 \cdot 10^{16}$	3.1	0.995	2.3
(*E*)-β-Ocimene	$2.28 \cdot 10^{16}$	4.8	0.991	4.7
Limonene	$7.42 \cdot 10^{16}$	5.8	0.993	1.4
β-Phellandrene	$5.19 \cdot 10^{16}$	5.2	0.997	2.1
1,8-Cineole (Eucalyptol)	$7.52 \cdot 10^{16}$	6.1	0.994	1.4
γ-Terpinene	$4.71 \cdot 10^{16}$	6.0	0.995	2.3
α-Terpinolene	$7.72 \cdot 10^{16}$	4.9	0.998	1.4
4,8-Dimethyl-1,3,7-nonatriene	$3.29 \cdot 10^{16}$	4.9	0.992	3.3
Linalool	$7.51 \cdot 10^{16}$	3.5	0.991	1.4
α-Thujone	$3.24 \cdot 10^{16}$	2.2	0.990	3.3
β-Thujone	$2.06 \cdot 10^{16}$	6.1	0.991	5.2
Methylsalicylate	$5.94 \cdot 10^{19}$	1.2	0.993	0.1
Bornyl acetate	$9.93 \cdot 10^{17}$	1.1	0.994	0.1
(*Z*)-β-Farnesene	$2.90 \cdot 10^{16}$	5.2	0.992	2.9
α-Cedrene	$2.03 \cdot 10^{17}$	2.3	0.994	0.4
(*E*)-β-Caryophyllene	$1.39 \cdot 10^{17}$	3.2	0.996	0.6
α-Humulene	$1.23 \cdot 10^{17}$	4.5	0.997	0.7
(*E*,*E*)-α-Farnesene	$2.45 \cdot 10^{16}$	2.4	0.991	3.4
Nerolidol	$2.77 \cdot 10^{17}$	5.6	0.993	0.3

* Based on three calibration curves y = slope x, y: peak-area ratio, x: terpene concentration (mol/L).

In chemistry, the emission rate is defined as the amount of given substance released to the air per unit of time. In plants, the emission rate is normalized with leaf area or leaf dry mass. In the literature, area-based plant emissions are commonly expressed in nmol m^{-2} s^{-1}, while for mass-basis ng g dw^{-1} h^{-1} is often employed [44]. We recommend always to use SI units and express the compound emission in molar units.

Our GC-MS method was applied for quantification of a vast array of mono- and sesquiterpenes released from differently stressed plants. Figure 1 shows chromatograms of sunflower (*Helianthus annuus* L.) leaf emissions under controlled conditions (chamber temperature of 25 °C) (A) and after 5 min. temperature stress at 51 ^{O}C (B) measured 1 min. after application of the heat pulse. This pilot experiment demonstrates that cold stress significantly enhances the emissions of monoterpenes in *Helianthus annuus L.* (Figure 2).

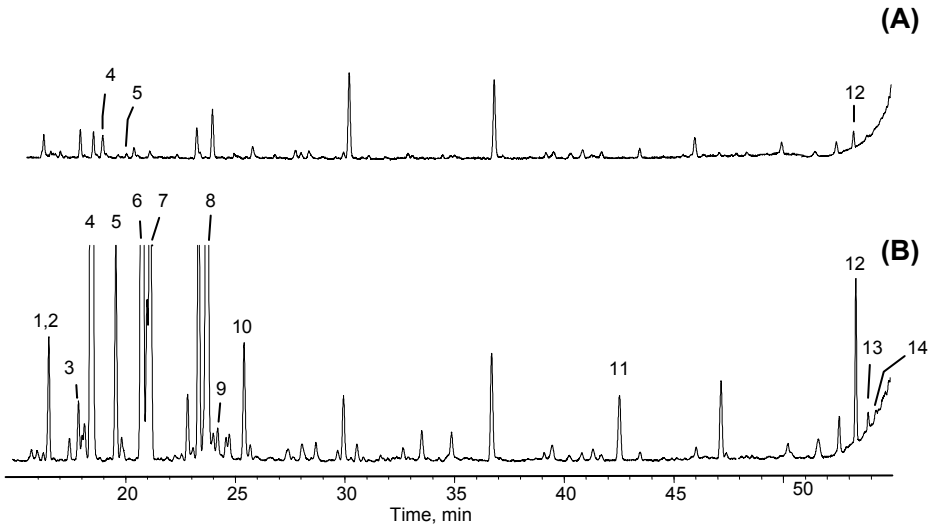

Figure 1. Chromatograms of sunflower (*Helianthus annuus* L.) leaf emissions. A: control plant; B: plant measured 1 min. after application of a 5 min. heat pulse of at 51 ^{O}C. Identified compounds – 1,2: (3*Z*)-hexenol co-eluted with (2*E*)-hexenal; 3: *α*-thujene; 4: *α*-pinene; 5: camphene; 6: sabinene; 7: *β*-pinene; 8: limonene; 9: *β* -phellandrene; 10: γ-terpinene; 11: bornyl acetate; 12: geranyl acetone; 13: (*E*,*E*)-*α*-farnesene; 14: germacrene D.

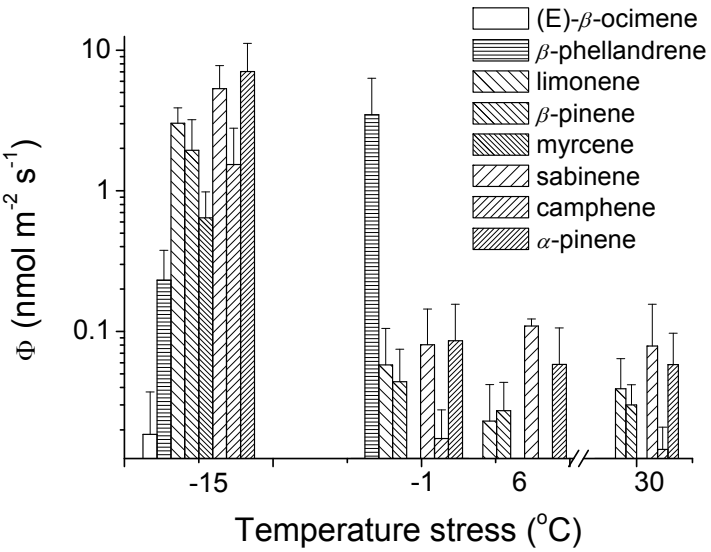

Figure 2. The emission rates (Φ) of monoterpenes from sunflower (*Helianthus annuus* L.) leaves measured after 1 min. exposure to 5 min. pulses of cold stress. *N* = 3 for all treatments.

Analogous results were obtained with tomato (*Lycopersicum esculentum* Mill.) plants under heat and cold stress (Figure 3).

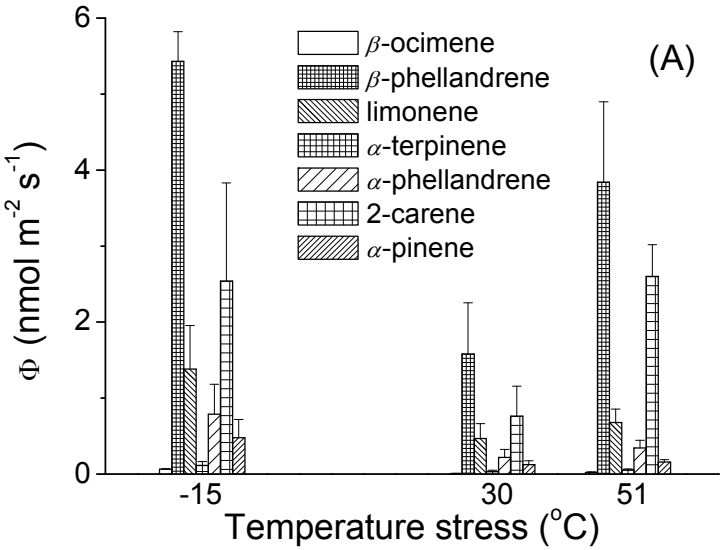

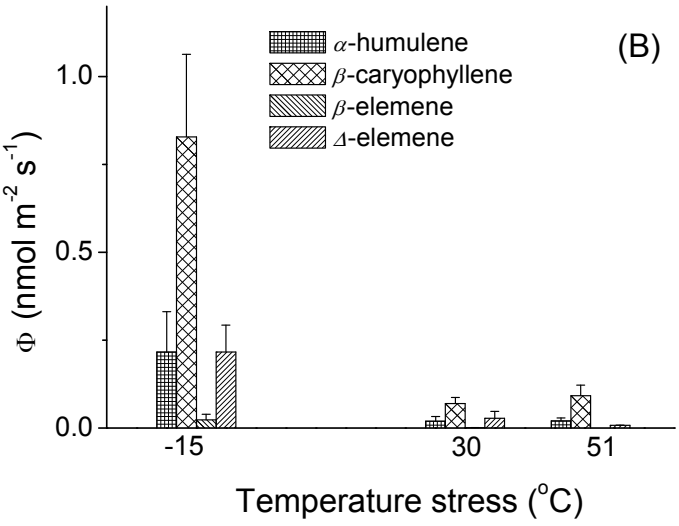

Figure 3. The emission rates (Φ) of monoterpenes (A) and sesquiterpenes (B) from tomato (*Lycopersicum esculentum* Mill.) leaves measured after 1 min. exposure to 5 min. pulses of heat and cold stress. *N* = 3 for all treatments.

CONCLUSIONS

The major drawback with current plant stress studies is that with very few exceptions [8] plant stress responses, including emissions, are not quantitatively assessed. Our method permits to obtain quantitative relationships between signal strength and plant response, and thus, to develop quantitative plant stress models. These models are needed to predict plant responses to environmental stress and simulate plant volatile compound emissions under different environmental conditions.

EXPERIMENTAL SECTION

All chemicals were purchased from Sigma-Aldrich, (St. Louis, MO, USA, GC purity) with exception of 4,8-dimethyl-1,3,7-nonatriene (DMNT) which was synthesized from commercial citral using methyltriphenylphosphonium bromide and butyl lithium at Kuopio University, Kuopio, Finland [45].

All plants used in measurements were grown from seeds. Plants were grown in 1 L clay pots filled with commercially-available potting soil and were watered daily. The gas exchange measurements were performed using a custom-built gas-exchange system described in detail in Rasulov et. al. [46]. Shortly, the flow-through plant chamber of 1.2 L was made of two glass layers. Water with set temperature was circulated between the outer and

inner glass layers to control the chamber temperature. All tubing in the system was made of stainless steel or Teflon. Flow rate through the system was maintained at 1.4 L min^{-1}. Light was provided by four perpendicularly positioned 50 W halogen lamps, and light intensity could be regulated between 0-1000 $\mu mol\ m^{-2}\ s^{-1}$ by changing the lamp voltage. In these experiments the light intensity was kept at 650 $\mu mol\ m^{-2}\ s^{-1}$.

Volatiles from the chamber exhaust air were adsorbed at a flow rate of 200 ml min^{-1} for 20 min. (altogether 4L air) onto multibed stainless steel cartridges (10.5 cm length, 3 cm inner diameter, Supelco, Bellefonte, USA) filled with Carbotrap C 20/40 mesh (0.2 g), Carbopack C 40/60 mesh (0.1 g) and Carbotrap X 20/40 mesh (0.1 g) adsorbents (Supelco, Bellefonte, USA). Before the collection of volatiles, the traps were cleaned by the passage of a stream of ultrapure helium at a flow rate of 200 ml min^{-1} and at temperature of 250 °C for 2 hours. Sampling of plant volatiles was done at room temperature of 25 °C. Background air samples were collected from the empty chamber before and after the measurements. Adsorbent cartridges were analyzed with a combined Shimadzu TD20 automated cartridge desorber and Shimadzu QP2010 plus GC MS instrument (Shimadzu Corporation, Kyoto, Japan). The following TD20-parameters were used: He purge flow 40 ml min^{-1}, primary desorption temperature 250 °C, primary desorption time 6 min, second stage trap temperature during primary desorption: −20°C, second stage trap desorption temperature 280°C, hold time 6 min. Adsorbent cartridges were backflushed with high purity He during thermal desorption. A Zebron ZB-624 fused silica capillary column (0.32 mm i.d.×60 m, 1.8 µm film thickness, Phenomenex, USA) was employed for the volatile separation using the following GC oven program: 40 °C for 1 min, 9 °C min^{-1} to 120 °C, 2 °C min^{-1} to 190 °C, 20 °C min^{-1} to 250 °C, 250 °C for 5 min. The GC carrier gas was He (99.9999%, Elmer Messer Gaas AS, Tallinn, Estonia) with 1.48 ml min^{-1}. Shimadzu QP2010 Plus mass spectrometer was operated in the electron impact mode. The transfer line temperature was set at 240 °C and ion-source temperature at 150 °C. The absolute amounts of terpenes were calculated based on an external standard consisting of known amounts of mono and sesquiterpenes. The compounds were identified by comparing the mass spectrum of an individual compound to the spectra of compounds in external standard and in the NIST Library.

ACKNOWLEDGMENTS

The authors are grateful for the financial support from the Estonian Ministry of Science and Education (grant SF1090065s07) and the Estonian Science Foundation (grant 7645, post-doctoral grants JD101 and MJD8-2/T9094PKPK). Special thanks are due to Prof. Dr. J. Holopainen (Kuopio University, Kuopio, Finland) for their generous supply of 4,8-dimethyl-1,3,7-nonatriene (DMNT).

REFERENCES

1. S.M. Owen, J. Peñuelas, *Trends in Plant Science*, **2005**, *10*, 420.
2. E. Pichersky, J. Gershenzon, *Current Opinion in Plant Biology*, **2002**, *5*, 237.
3. C.E. Vickers, J. Gershenzon, M.T. Lerdau, F. Loreto, *Nature Chemical Biology*, **2009**, *5*, 283.
4. W. Chameides, R. Lindsay, J. Richardson, C. Kiang, *Science*, **1988**, *241*, 1473.
5. K.E. Huff Hartz, T. Rosenørn, S.R. Ferchak, T.M. Raymond, M. Bilde, N.M. Donahue, S.N. Pandis, *Journal of Geophysical Research - Atmospheres*, **2005**, *110*, D14208.
6. T.M. VanReken, N.L. Ng, R.C. Flagan, J.H. Seinfeld, *Journal of Geophysical Research-Atmospheres*, **2005**, *110*.
7. F. Fehsenfeld, J. Calvert, R. Fall, P. Goldan, A.B. Guenther, C.N. Hewitt, B. Lamb, S. Liu, M. Trainer, H. Westberg, P. Zimmerman, *Global Biogeochemical Cycles*, **1992**, *6*, 389.
8. J. Beauchamp, A. Wisthaler, A. Hansel, E. Kleist, M. Miebach, U. Niinemets, U. Schurr, J. Wildt, *Plant Cell and Environment*, **2005**, *28*, 1334.
9. F. Brilli, P. Ciccioli, M. Frattoni, M. Prestininzi, A.F. Spanedda, F. Loreto, *Plant Cell and Environment*, **2009**, *32*, 542.
10. U. Niinemets, M. Reichstein, *Global Biogeochemical Cycles*, **2002**, *16*.
11. N. Theis, M. Lerdau, *International Journal of Plant Sciences*, **2003**, *164*, S93.
12. A. Arneth, R.K. Monson, G. Schurgers, U. Niinemets, P.I. Palmer, *Atmospheric Chemistry and Physics*, **2008**, *8*, 4605.
13. B. Bonn, A. Hirsikko, H. Hakola, T. Kurten, L. Laakso, M. Boy, M. Dal Maso, J. M. Makela, M. Kulmala, *Atmospheric Chemistry and Physics*, **2007**, *7*, 2893.
14. D. Helmig, J. Ortega, T. Duhl, D. Tanner, A. Guenther, P. Harley, C. Wiedinmyer, J. Milford, T. Sakulyanontvittaya, *Environmental Science & Technology*, **2007**, *41*, 1545.
15. N.C. Bouvier-Brown, R. Holzinger, K. Palitzsch, A.H. Goldstein, *Atmospheric Environment*, **2009**, *43*, 389.
16. T. Sakulyanontvittaya, T. Duhl, C. Wiedinmyer, D. Helmig, S. Matsunaga, M. Potosnak, J. Milford, A. Guenther, *Environmental Science & Technology*, **2008**, *42*, 1623.
17. T. R. Duhl, D. Helmig, A. Guenther, *Biogeosciences*, **2008**, *5*, 761.
18. R.J. Bartelt, D. T. Wicklow, *Journal of Agricultural and Food Chemistry*, **1999**, *47*, 2447.
19. P. Ciccioli, E. Brancaleoni, M. Frattoni, V. Di Palo, R. Valentini, G. Tirone, G. Seufert, N. Bertin, U. Hansen, O. Csiky, R. Lenz, M. Sharma, *Journal of Geophysical Research-Atmospheres*, **1999**, *104*, 8077.
20. A. Guenther, C.N. Hewitt, D. Erickson, R. Fall, C. Geron, T. Graedel, P. Harley, L. Klinger, M. Lerdau, W.A. McKay, T. Pierce, B. Scholes, R. Steinbrecher, R. Tallamraju, J. Taylor, P. Zimmerman, *Journal of Geophysical Research*, **1995**, *100*, 8873.

21. M. Claeys, B. Graham, G. Vas, W. Wang, R. Vermeylen, V. Pashynska, J. Cafmeyer, P. Guyon, M. O. Andreae, P. Artaxo, W. Maenhaut, *Science*, **2004**, *303*, 1173.
22. T. Sakulyanontvittaya, A. Guenther, D. Helmig, J. Milford, C. Wiedinmyer, *Environmental Science & Technology*, **2008**, *42*, 8784.
23. W. Vizuete, V. Junquera, D. . Allen, *Aerosol Science and Technology*, **2004**, *38*, 167.
24. E. Liakakou, M. Vrekoussis, B. Bonsang, C. Donousis, M. Kanakidou, N. Mihalopoulos, *Atmospheric Environment*, **2007**, *41*, 1002.
25. J.D. Blande, K. Turunen, J.K. Holopainen, *Environmental Pollution*, **2009**, *157*, 174.
26. R. M. C. Jansen, J. W. Hofstee, J. Wildt, F. W. A. Verstappen, H. J. Bouwmeester, M. A. Posthumus, E. J. van Henten, *Annals of Applied Biology*, **2009**, *154*, 441.
27. R.W. Jost, A.V. Rice, D.W. Langor, Y. Boluk, *Journal of Wood Chemistry and Technology*, **2008**, *28*, 37.
28. U. Niinemets, F. Loreto, M. Reichstein, *Trends in Plant Science*, **2004**, *9*, 180.
29. J. Penuelas, J. Llusia, *Trends in Plant Science*, **2003**, *8*, 105.
30. A.B. Johne, B. Weissbecker, S. Schutz, *Journal of Chemical Ecology*, **2006**, *32*, 2303.
31. L. Chen, H. Y. Fadamiro, *Bulletin of Entomological Research*, **2007**, *97*, 515.
32. J.C. Dickens, R.F. Billings, T.L. Payne, *Experientia*, **1992**, *48*, 523.
33. D. Helmig, F. Bocquet, J. Pollmann, T. Revermann, *Atmospheric Environment*, **2004**, *38*, 557.
34. D. Tholl, W. Boland, A. Hansel, F. Loreto, U. S. R. Rose, J.P. Schnitzler, *Plant Journal*, **2006**, *45*, 540.
35. S. Pressley, B. Lamb, H. Westberg, A. Guenther, J. Chen, E. Allwine, *Atmospheric Environment*, **2004**, *38*, 3089.
36. S. Vichi, J.M. Guadayol, J. Caixach, E. Lopez-Tamames, S. Buxaderas, *Journal of Chromatography A*, **2006**, *1125*, 117.
37. N. Yassaa, J. Williams, *Journal of Chromatography A*, **2007**, *1141*, 138.
38. A. Kannaste, N. Vongvanich, A.K. Borg-Karlson, *Arthropod-Plant Interactions*, **2008**, *2*, 31.
39. J. Ortega, D. Helmig, *Chemosphere*, **2008**, *72*, 343.
40. J. Ortega, D. Helmig, R.W. Daly, D.M. Tanner, A.B. Guenther, J.D. Herrick, *Chemosphere*, **2008**, *72*, 365.
41. W. Kornacki, P. Fastyn, T. Gierczak, I. Gawlowski, J. Niedzielski, *Chromatographia*, **2006**, *63*, 67.
42. P. Ciccioli, A. Cecinato, E. Brancaleoni, M. Frattoni, A. Liberti, *Hrc-Journal of High Resolution Chromatography*, **1992**, *15*, 75.
43. A. Calogirou, B.R. Larsen, C. Brussol, M. Duane, D. Kotzias, *Analytical Chemistry*, **1996**, *68*, 1499.
44. J. Kesselmeier, M. Staudt, *Journal of Atmospheric Chemistry*, **1999**, *33*, 23.
45. M.A. Ibrahim, A. Stewart-Jones, J. Pulkkinen, G.M. Poppy, J.K. Holopainen, *Plant Biology*, **2008**, *10*, 97.
46. B. Rasulov, L. Copolovici, A. Laisk, U. Niinemets, *Plant Physiology*, **2009**, *149*, 1609.

STUDIA UNIVERSITATIS BABEŞ-BOLYAI, CHEMIA, LIV, 4, 2009

USING THE TOPOLOGICAL INDEX ZEP IN QSPR STUDIES OF ALCOHOLS

ZOIȚA MĂRIOARA BERINDE[a]

ABSTRACT The paper is devoted to the modelling of a class of molecular compounds containing heteroatoms (alcohols) by means of the concept of weighted electronic distance and the corresponding connectivity matrix CEP. A topological index derived from this matrix, the ZEP topological index, is then correlated with the boiling point (BP) and the water solubility (log(1/S)) of alcohols, using simple and multiple linear regression analysis. In order to improve the simple models we also calculated a novel parameter, H_d, derived from the usual topological distances between the vertices of the graph. The obtained results indicate the combination of ZEP and H_d indices as a promise in the QSPR analysis of complex compounds.

Keywords: weighted electronic distance; CEP connectivity matrix; ZEP topological index; parameter $H_{d,}$ linear regression analysis.

INTRODUCTION

A chemical compound can be represented by using the concept of molecular graph *G*. A molecular graph can itself be represented by several topological matrices [1-4]. The most used matrices are the adjacency matrix, *A*=*A*(*G*), and the distance matrix, *D*=*D*(*G*). The mathematical modelling of chemical structures by using descriptors derived from the molecular graphs, by means of topological matrices, has grown rapidly in the last decade [5-7]. Among these descriptors, the topological indices have been widely used in QSPR (Quantitative Structure-Property Relationship) and QSAR (Quantitative Structure–Activity Relationship) analysis. Both adjacency and distance matrices, in their original form [2-4], are appropriate for modelling chemical compounds with no multiple bonds or heteroatoms. When structurally different molecules, such as isobutane, isobutene, 2-propanol, 2-cloropropane, 2-aminopropane, are under study, difficulties appear in amending the classical topological matrices to account for there structural differences. The question how to represent the multiple bonds and/or heteroatoms, gained more than one answer.

[a] *Department of Chemistry and Biology, North University of Baia Mare, Romania, e-mail: zoitaberinde@ubm.ro; zoita_berinde@yahoo.com*

A first approach to represent heteroatoms and multiple bonds has been proposed by Kier and Hall [8], and also by Barysz and collaborators [9]. Basak and collaborators [10] have treated the presence of heteroatoms by applying the information theory. The method proposed by Balaban [11], considers the electronegativities, the atomic number and the number of the group in Mendeleev's short form of the periodic chart. The same problem has been also tackled successfully by Randić [12], and Estrada [13].

In the present paper we shall treat the presence of heteroatoms, especially those in the alcohols class, by means of the weighted electronic distance (w.e.d.), a new local invariant considered by the author in [14]. By replacing the usual topological distances from the adjacency matrix, by the values of the weighted electronic distances, we obtain a new connectivity matrix, CEP, used for the construction of some topological indices [14-16]. Such a topological index is the ZEP index, which is correlated in this paper to the boiling point (BP) and the water solubility (log(1/S) for aliphatic alcohols.

The weighted electronic connectivity matrix and topologic ZEP index

For a molecule having N atoms, whose graphs is G = (V(G), E(G)), the weighted electronic connectivity matrix, CEP(G), is a square N x N matrix given by:

$$CEP\,(G)=\left\{[CEP\}_{i,j};\quad i,j\in V(G)\right\} \tag{1}$$

where its entries $[CEP]_{i,j}$ are defined as follows:

$$CEP_{ij}=d.e.p.(i,j),\ if\ i\neq j \text{ and } (i,j)\in E(G) \text{ and } CEP_{ij}=0 \text{ otherwise} \tag{2}$$

and:

- d.e.p. (i, j) denotes the weighted electronic distance between the atoms (vertices) i and j;
- V(G) is the set of all vertices (atoms) of the moleular graph G;
- E(G) is the set of all edges (bonds) of the graph G;

The weighted electronic distance, w.e.d. was recently defined in [14] by the formula:

$$w.e.d.(i,j)=\frac{1}{b_r}\cdot\frac{Z_i^{'}+Z_j^{'}}{v_i\cdot v_j} \tag{3}$$

where

- b_r is the bond weight (or bond order) with values: 1 for single bond, 2 for double bond, 3 for triple bond like in Barysz et al. [9]

- ν_i denotes the degree of vertex i (that is, the number of bonds of the atom i to other atoms),

- $Z_i^{`}$ denotes the formal degree of vertex i, it is defined by:

$$Z_i^{`} = Z_i \cdot \nu_i \tag{4}$$

- Z_i being the order of the atom i (that is, the number of all electrons in the atom i).

Similar formulas which use the atomic number and the multiplicity order of bonds have been considered in an other context by Barysz and collaborators [9], where it is detected only the presence of multiple bonds and heteroatoms, but their model is not able to reproduce the information related to the neighborhood of bonds, as in the case of weighted electronic connectivity.

The formal degree $Z_i^{`}$ of the vertex i is in fact a local invariant on vertex (LOVI), which replaces the classical degree of the vertex, while the weighted electronic distance, w.e.d. (i,j) represents a local invariant on edge (LOEI).

Having in view that for oxigen we have $Z = 8$, it results that its formal degrees will be $Z'_O = 8$ for alcohols. The carbon atom in the structure of an alcohol may have the formal degree Z'_j equal to 6, 12, 18 or 24, respectively. These aspects are illustrated in Figure 1, on the molecular graphs of 1-propanol (G.1), 2-propanol (G.2) and 2-methyl-2-propanol (G.3).

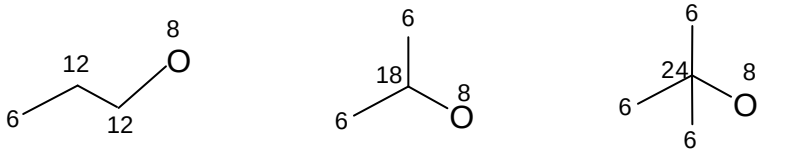

G.1 { Z' } G.2 { Z' } G.3 { Z'}

Figure 1. The graphs G.1, G.2 , G.3 and formal degrees (Z')

By replacing (4) in (3) and taking into account that $b_r = 1$, because the oxigen atom establishes only simple bonds in the class of alcohols, we obtain

$$w.e.d.(i, j) = \frac{Z_i}{\nu_j} + \frac{Z_j}{\nu_i} \cdot \tag{5}$$

The weighted electronic distances computed by means of equation (5) for the covalent bonds carbon–carbon and oxigen–carbon represent local edge invariants (LOEI).

On the edges of each graph in Figure 2 are written the w.e.d., computed by (5).

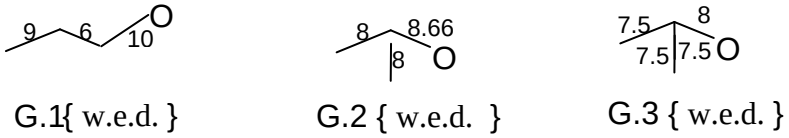

G.1{ w.e.d. } G.2 { w.e.d. } G.3 { w.e.d. }

Figure 2. The graphs G.1, G.2, G.3 and w.e.d.

Figure 3 shows the CEP matrix for 2-propanol whose graph, G.2, is depicted in the same figure, with the values of w.e.d. computed by formula (5).

SEP_i

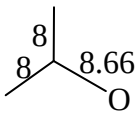

G.2

$$CEP(G.2) = \begin{bmatrix} 0 & 8 & 0 & 0 & 8 \\ 8 & 0 & 8 & 8.66 & 24.66 \\ 0 & 8 & 0 & 0 & 8 \\ 0 & 8.66 & 0 & 0 & 8.66 \end{bmatrix}$$

Figure 3. The CEP matrix for 2-propanol

The sum of all entries on the i-th row in CEP(G.2) is denoted by SEP_i (and is written at the matrix right hand side):

$$SEP_i = \sum_{j=1}^{N} [CEP]_{ij}\,;\; i=1, N \tag{6}$$

The electronic connectivity matrix can function as a basis for the construction of several new topological indices. The simplest index is given by the sum of root square of SEP_i:

$$ZEP = \sum_{i=1}^{N} (SEP_i)^{1/2} \tag{7}$$

The calculation technique of ZEP index is illustrated in Figure 4 for the hydrogen-suppressed graph G.2 of 2-propanol

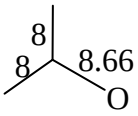

$$ZEP(G.2) = 2 \cdot 8^{\frac{1}{2}} + 24.66^{\frac{1}{2}} + 8.66^{\frac{1}{2}} = 13.565$$

G.2

Figure 4. The calculation technique of ZEP index for the hydrogen-suppressed graph of 2-propanol

A novel parameter H_d

We propose now a novel parameter, denoted by H_d, which is calculated as the arithmetic mean of the distances from the heteroatom to the other atoms, using the usual topological distance between two vertices.

The parameter H_d is hence defined by the formula:

$$H_d = \frac{1}{n}\sum_{i=1}^{n} d_i \qquad (8)$$

where:

- n represents the number of carbon atoms in the molecular graph;
- d_i represents the distance between the heteroatom and the atom *i.*

The calculation technique of parameter H_d is illustrated in Figure 5 for the hydrogen-suppressed graph G.4 of 2-butanol

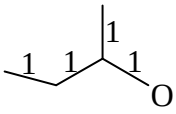

$$H_d = \frac{1}{4}(3+2+2+1) = 2$$

G. 4

Figure 5. The calculation technique of parameter H_d for the hydrogen-suppressed graph of 2-propanol (G.4)

ZEP and H_d could be used together in order to improve the QSPR models for several representative physical properties on several data sets of alcohols by using two-variable linear regression analysis.

RESULTS AND DISCUSSIONS

Correlations to normal boiling points (BP) of 132 alcohols

As a starting point, we consider a data set of 132 alcohols to develop the structure-boiling point model. The observed BP values for the normal boiling points at normal pressure are listed in Table 1 and were taken from [17].

Values of ZEP and H_d index were calculated for the same set of 132 alcohols and are presented in Table 1, too. A boiling point model is then generated using the ZEP index and H_d parameter.

The simple linear regression equation and its statistical parameters for a monovariable correlation with ZEP are shown below:

$$BP = 11.619 + 5.11\ ZEP;\ \ r = 0.960;\ s = 11.126;\ F = 1517;\ N = 132; \quad (9)$$

were: r-represents the correlation coefficient, s- the standard deviation and F is the Fischer ratio.

For the same 132 alcohols the simple linear regression with the ZEP index leads to a poorer correlation (r = 0.960 and s= 11.126 ^{0}C), comparable with the simple model obtained by Lu et al.[17] (r = 0.9665 and s= 9.797^{0}C). Obviously, a single ZEP index cannot give a simple and accurate correlation. It is important to stress that the statistical parameters of the QSPR equations could be improved by using multidimensional correlations involving also other topological descriptors. In this work we propose a combined use of the ZEP index and parameter H_d. The regression equation and its statistical parameters found to describe boiling points of the 132 alcohols considered are depicted below:

$$BP = 17.843 + 3.593\ ZEP + 12.391 H_d;$$
$$r = 0.985;\ s = 6.794;\ F = 2143;\ N = 132 \quad (10)$$

Statistics indicate that equation (10) is a good model for calculating BP. Values of BP predicted by this equation are also shown in Table 1.

The statistical parameters of the model given by Eq. (10) can be compared to several results that have been reported elsewhere. The model found by Yang et al. [18] using the extended adjacency matrix EA∑ and EAmax indices gave r = 0.9837 and s = 6.35 for only 37 alcohols, while our model is applied to 132 alcohols, but the molecular connectivity ^1X and $^1X^v$ indices provided a slightly superior model to those using EA∑ and EAmax indices. Analogously, a multiple linear model constructed by Yao et al. [19] using X_{m1}, X_{m2}, and X_{m3} indices gave r = 0.987 and s = 7.4988 for the same series of 37 alcohols, while our model gave r = 0.985 and s = 6.794 for the richer series of 132 alcohols. Galvez et al. [20] reported that the three-parameter model using N (the number of the vertices) and two charge indices G_1 and J_2 gave r = 0.979 and s = 3.63 for 29 alcohols. Recently, Ren [21] developed a model by using AI and Xu indices and gave r = 0.9957 and s = 3.576 but only for the same restricted data.

Table 1. The index ZEP, parameter H_d and the experimental and calculated boiling points for 132 alcohols using Equation (10)

No.	Compound	ZEP	H_d.	BP (^{0}C)	
				Exp.	Calc.
1	1-propanol	14.035	2	97.1	93.1
2	2-propanol	13.565	1.667	82.4	87.2
3	1-butanol	17.499	2.5	117.6	111.7
4	2-methyl-1-propanol	17.274	2.25	107.9	107.8
5	2-butanol	17.166	2	99.5	104.3
6	2-methyl-2-propanol	16.566	1.75	82.4	99
7	1-pentanol	20.963	3	137.5	130.3
8	3-methyl-1-butanol	20.718	2.8	131	127
9	2-pentanol	20.614	2.4	119.3	121.6
10	2-methyl-1-butanol	20.847	2.6	128	125
11	3-pentanol	20.745	2.2	116.2	119.6
12	3-methyl-2-butanol	20.445	2.2	112.9	118.6
13	2,2-dimethyl-1-propanol	20.382	2.4	113.1	120.8
14	2-methyl-2-butanol	20.223	2	102.3	115.3
15	1-hexanol	24.427	3.5	157	149
16	4-methyl-1-pentanol	24.182	3.333	151.9	146
17	2-hexanol	24.078	2.833	140	139.5
18	3-methyl-1-pentanol	24.291	3.8	153	152.2
19	2-methyl-1-pentanol	24.295	3	148	142.3
20	3-hexanol	24.193	2.5	135	135.7
21	2-ethyl-1-butanol	24.391	2.833	146.5	140.6
22	4-methyl-2-pentanol	23.826	2.667	132	136.5
23	3,3-dimethyl-1-butanol	23.814	2.833	143	138.5
24	2,3-dimethyl-1-butanol	24.115	3	144.5	141.7
25	2-methyl-2-pentanol	23.663	2.333	121.5	131.8
26	3-methyl-2-pentanol	24.009	2.5	134.3	135.1
27	2-methyl-3-pentanol	24.015	2.333	129.5	133
28	2,2-dimethyl-1-butanol	23.979	2.667	136.5	137
29	3-methyl-3-pentanol	23.865	2.167	123	130.4
30	3,3-dimethyl-2-butanol	23.576	2.333	120.4	131.5
31	2,3-dimethyl-2-butanol	23.526	2.167	118.4	129.2
32	1-heptanol	27.891	4	176.4	167.6
33	5-methyl-1-hexanol	27.646	3.85	170	164.9
34	2-heptanol	27.543	3.286	160.4	157.5
35	4-methyl-1-hexanol	27.755	3.714	173.3	163.6
36	2-methyl-1-hexanol	27.760	3.428	164	160.1
37	3-heptanol	27.657	2.857	157	152.6
38	3-methyl-1-hexanol	27.739	3.571	169	161.8
39	4-heptanol	27.641	2.714	156	150.8
40	5-methyl-2-hexanol	27.551	3.143	151	155.8
41	2-methyl-3-hexanol	27.463	2.571	145.5	148.4
42	2-methyl-2-hexanol	27.127	2.714	143	148.9
43	2,4-dimethyl-1-pentanol	27.508	3.285	159	157.4
44	5-methyl-3-hexanol	27.405	2.714	148	149.9
45	3-methyl-3-hexanol	27.304	2.428	143	146

No.	Compound	ZEP	H_d.	BP (^{0}C)	
				Exp.	Calc.
46	2,4-dimethyl-2-pentanol	26.871	2.571	133.1	146.2
47	2,4-dimethyl-3-pentanol	27.282	2.428	140	146
48	3-ethyl-3-pentanol	27.487	2.286	142	144.9
49	2,3-dimethyl-2-pentanol	27.085	2.428	139.7	145.2
50	2,3-dimethyl-3-pentanol	27.161	2.286	139	143.8
51	3-methyl-2-hexanol	27.457	2.857	151	151.9
52	6-methyl-1-heptanol	31.110	4.375	188.6	183.8
53	2-octanol	31.007	3.75	180	175.7
54	3-octanol	31.122	3.25	175	169.9
55	4-methyl-1-heptanol	31.204	4.125	188	181.1
56	4-octanol	31.106	3	176.3	166.8
57	2-ethyl-1-hexanol	31.303	3.5	184.6	173.7
58	2-methyl-2-heptanol	30.591	3.125	156	166.5
59	2,5-dimethyl-1-hexanol	30.979	3.75	179.5	175.6
60	5-methyl-2-heptanol	30.871	3.5	172	172.1
61	6-methyl-3-heptanol	30.877	3.125	174	167.5
62	3.5-dimethyl-1-hexanol	30.952	3.875	182.5	177.1
63	3-methyl-2-heptanol	30.922	3.25	166.1	169.2
64	2-methyl-3-heptanol	31.155	2.875	167.5	165.4
65	2-methyl-4-heptanol	30.854	2.875	164	164.3
66	5-methyl-3-heptanol	30.979	3	172	166.3
67	3-methyl-3-heptanol	30.768	2.75	163	162.5
68	4-methyl-3-heptanol	31.028	2.875	170	165
69	3-methyl-4-heptanol	31.028	2.75	162	163.4
70	3,4-dimethyl-2-hexanol	30.838	3	165.5	165.8
71	4-methyl-4-heptanol	30.743	2.625	161	160.8
72	3-ethyl-3-hexanol	30.927	2.5	160.5	159.9
73	2,3-dimethyl-2-hexanol	30.533	2.75	160	161.6
74	3,5-dimethyl-3-hexanol	30.512	2.625	158	160
75	2,3-dimethyl-3-hexanol	30.600	2.5	158.1	158.8
76	2-methyl-3-ethyl-2-pentanol	30.611	2.625	156	160.4
77	2,4,4-trimethyl-2-pentanol	29.961	2.75	147.5	159.6
78	2,2,4-trimethyl-3-pentanol	30.407	2.5	150.5	158.1
79	2,2-dimethyl-3-hexanol	30.589	2.625	156	160.3
80	2,5-dimethyl-3-hexanol	30.675	2.75	157.5	162.1
81	4,4-dimethyl-3-hexanol	30.774	2.625	160.4	160.9
82	6-methyl-2-heptanol	30.762	3.625	174	173.3
83	3-methyl-1-heptanol	31.204	4	186	179.5
84	2-methyl-3-ethyl-3-pentanol	30.777	2.375	158	157.9
85	2,3,4-trimethyl-3-pentanol	30.456	2.375	156.5	156.7
86	7-methyl-1-octanol	34.574	4.889	206	202.6
87	2-nonanol	34.471	4.222	198.5	194
88	3-nonanol	34.586	3.667	195	187.5
89	4-nonanol	34.569	3.333	192.5	183.3
90	5-nonanol	34.569	3.222	193	182
91	2-methyl-2-octanol	34.055	3.555	178	184.3
92	2,6-dimethyl-2-heptanol	33.810	3.444	173	182

No.	Compound	ZEP	H_d.	BP (^{0}C)	
				Exp.	Calc.
93	2,6-dimethyl-3-heptanol	33.987	2.75	175	174
94	2,6-dimethyl-4-heptanol	34.065	3	174.5	177.4
95	3,6-dimethyl-3-heptanol	30.675	3	173	165.2
96	3,5-dimethyl-4-heptanol	34.410	2.778	171	175.9
97	2,3-dimethyl-3-heptanol	34.065	2.777	173	174.6
98	2,4-dimethyl-4-heptanol	33.952	2.777	171	174.2
99	2,4,4-trimethyl-3-hexanol	34.039	2.667	170	173.2
100	3,4,4-trimethyl-3-hexanol	33.932	2.555	165.5	171.4
101	4-methyl-4-octanol	35.075	2.889	180	179.7
102	4-ethyl-4-heptanol	34.366	2.667	182	174.4
103	2-methyl-2-octanol	34.055	3.555	178	184.3
104	8-methyl-1-nonanol	38.039	5.4	219.9	221.4
105	2-methyl-3-ethyl-3-heptanol	34.006	2.8	177.5	174.7
106	2-methyl-3-ethyl-1-heptanol	38.124	4	193	204.4
107	5-methyl-3-ethyl-3-heptanol	34.709	2.9	172	178.5
108	2-decanol	37.935	4.7	211	212.4
109	4-decanol	38.034	3.7	210.5	200.3
110	3,7-dimethyl-1-octanol	37.887	4.8	212.5	213.4
111	2,7-dimethyl-3-octanol	37.611	3.5	193.5	196.3
112	2,6-dimethyl-4-octanol	34.696	3.2	195	182.2
113	2,3-dimethyl-3-octanol	38.816	3.1	189	195.7
114	5-methyl-5-nonanol	37.672	3.1	202	191.6
115	4-methyl-1-nonanol	38.132	5	216	216.8
116	2-methyl-3-nonanol	37.856	3.6	200	198.5
117	2,2,5,5-tetramethyl-3-hexanol	33.952	2.9	170	175.8
118	4-propyl-4-heptanol	33.932	2.8	191	174.5
119	2,4,6-trimethyl-4-heptanol	37.160	2.9	181	187.3
120	3-ethyl-3-octanol	37.855	3.1	199	192.3
121	3-ethyl-2-methyl-3-heptanol	37.681	2.8	193	187.9
122	1-undecanol	41.748	6	245	242.2
123	2-undecanol	41.399	5.182	228	230.8
124	3-undecanol	41.514	4.545	229	223.3
125	5-undecanol	41.498	3.818	229	214.3
126	6-undecanol	41.498	3.727	228	213.1
127	1-dodecanol	45.212	6.5	261.9	260.8
128	2-dodecanol	42.035	5.667	246	239.1
129	1-tridecanol	48.676	7	276	279.5
130	1-tetradecanol	52.140	7.5	289	298.1
131	1-pentadecanol	55.604	8	304.9	316.8
132	1-hexadecanol	59.068	8.5	312	335.4

Correlations to water solubility (log(1/S)) of 60 alcohols

Aqueous solubility, S, of liquids and solids is defined as the concentration (moles per liter) of solute in the aqueous phase, at equilibrium whih a pure solute phase. This property of organic compounds is very important and widely

applied in many research areas, such as pharmaceutical chemistry, biological chemistry or environmental science.

We consider in our study a data set of 60 alcohols [17] to develop the structure-water solubility model. The experimental water solubility as log (1/S), for these alcohols, are listed in Table 2.

The simple linear correlation found is illustrated by the following equation and statistical parameters:

$$\log 1/S = -3.218 + 0.167\ ZEP;\ r = 0.972;\ s = 0.248;\ F = 992;\ N = 60; \quad (11)$$

A better water solubility point model was generated by using a two variable linear model constructed with the index ZEP and parameter H_d and is expressed by equation (12):

$$\log 1/S = -3.196 + 0.129\ ZEP + 0.337H_d;$$
$$r = 0.988;\ s = 0.164;\ F = 1175;\ N = 60; \quad (12)$$

Values of log (1/S) predicted by equation (12) are also shown in Table 2.

Table 2. Experimental and calculated log (1/S) for 60 alcohols

No	Compound	Log (1/S)		No	Compound	Log (1/S)	
		Exp.	Calc.			Exp.	Calc
1	etanol	-1.10	-1.33	31	3-heptanol	1.44	1.33
2	1-propanol	-0.62	-0.71	32	4-heptanol	1.40	1.28
3	1-butanol	-0.03	-0.10	33	5-methyl-2-hexanol	1.38	1.42
4	2-methyl-1-propanol	-0.10	-0.21	34	2-methyl-3-hexanol	1.32	1.21
5	2-butanol	-0.47	-0.31	35	2-methyl-2-hexanol	1.07	1.22
6	1-pentanol	0.59	0.52	36	2,4-dimethyl-1-pentanol	1.60	1.46
7	3-methyl-1-butanol	0.51	0.42	37	3-methyl-3-hexanol	0.98	1.14
8	2-pentanol	0.28	0.27	38	2,4-dimethyl-2-pentanol	0.93	1.14
9	2-methyl-1-butanol	0.46	0.37	39	2,4-dimethyl-3-pentanol	1.22	1.14
10	3-pentanol	0.21	0.22	40	2,3-dimethyl-2-pentanol	0.87	1.12
11	3-methyl-2-butanol	0.18	0.18	41	2,3-dimethyl-3-pentanol	0.84	1.08
12	2-methyl-2-butanol	-0.15	0.09	42	1-octanol	2.35	2.37
13	1-hexanol	1.21	1.13	43	2-octanol	2.09	2.07
14	4-methyl-1-pentanol	1.14	1.05	44	2-ethyl-1-hexanol	2.11	2.02
15	2-hexanol	0.87	0.86	45	2-methyl-2-heptanol	1.72	1.80
16	2-methyl-1-pentanol	1.11	0.95	46	3-methyl-3-heptanol	1.60	1.70
17	3-hexanol	0.80	0.77	47	1-nonanol	3.01	2.98
18	2-ethyl-1-butanol	1.01	0.91	48	7-methyl-1-octanol	2.49	2.91
19	4-methyl-2-pentanol	0.79	0.78	49	2-nonanol	2.74	2.67
20	3,3-dimethyl-1-butanol	0.50	0.83	50	3-nonanol	2.66	2.50
21	2,3-dimethyl-1-butanol	0.37	0.93	51	4-nonanol	2.59	2.39
22	2-methyl-2-pentanol	0.49	0.64	52	5-nonanol	2.49	2.35
23	3-methyl-2-pentanol	0.71	0.74	53	2,6-dimethyl-4-heptanol	2.16	2.21
24	2-methyl-3-pentanol	0.70	0.69	54	3,5-dimethyl-4-heptanol	2.51	2.18
25	2,2-dimethyl-1-butanol	0.91	0.80	55	1-decanol	3.63	3.60
26	3-methyl-3-pentanol	0.36	0.61	56	1-dodecanol	4.67	4.83
27	3,3-dimethyl-2-butanol	0.61	0.63	57	2,2-dimethyl-3-pentanol	1.15	1.12
28	2,3-dimethyl-2-butanol	0.37	0.57	58	2,2-dimethyl-1-pentanol	1.52	1.36
29	1-heptanol	1.81	1.75	59	4,4-dimethyl-1-pentanol	1.55	1.53
30	2-heptanol	1.55	1.46	60	2,2-diethyl-1-pentanol	2.42	2.36

The two-variable regression model (12) is slightly better than the two-variable regression model based on the combined use of Lu index and DAI (-OH) indices [17], which produces an model with r = 0.984 and s = 0.1807, while our model has r = 0.988 and s = 0.164. Actually, our two-variable regression model (12) is slightly better even than the three-variable regression model based on the combined use of Lu, DAI (-OH) and DAI (CH_3-) [18], which produces a model with r = 0.9876 and s = 0.1604.

CONCLUSIONS

According to the results previously presented, we conclude that the topological index ZEP based on the concept of weighted electronic distance and weighted electronic matrix CEP of the molecular graph can accurately describe the molecular structures involving heteroatoms, in this case the presence of oxigen.

The w.e.d. has the merit that it is able to differentiate not only the covalent bonds carbon-oxigen from the ones of carbon–carbon, but is also able to discriminate the covalent bonds of oxigen to a primary carbon from that to secondary or tertiary carbons. To our best knowledge, no other models have similar discrimination power for the covalent bonds with regard to their structural neighbourhood.

Two variable linear regression using ZEP and $\mathbf{H_d}$ can provide high-quality QSPR models for the two studied properties of alcohols: boiling point and water solubility.

REFERENCES

1. M. Randić, W.L. Woodworth, A. Graovac*, Int. J. Quantum. Chem*., **1983**, *24*, 435-452
2. A.T. Balaban*, Rev. Chim*., **1988**, *39*, Nr. 12, 1026-1031
3. M. Diudea, O. Ivanciuc*, Topologie moleculară*, Comprex, Cluj-Napoca, **1995**
4. M. Randić*, J. Math. Chem*., **1991**, *7*, 155-168
5. Z. Mihalić, S. Nikolić, N. Trinajstić*, Inf. Comput. Sci*., **1992**, *32*, 28-37
6. O. Ivanciuc, *Rev. Roum. Chim*., **2000**, *45*, 1037-1054
7. M. Randić, P.J. Hansen, P.C. Jurs*, J. Chem. Inf. Comput. Sci*., **1988**, *28*, 60-68
8. L.B. Kier, L.H. Hall*, Molecular Connectivity in Structure-Activity Analysis*, John Wiley & Sons, New York, **1986**
9. M. Barysz, G. Jashari, R.S. Lall, V.K. Srivastaya, N. Trinajstić*,* in "*Chemical Applications of Graph Theory and Topology*", King, R.B. (Ed), Elsevier, Amsterdam, **1983**, 222-230

10. S.C. Basak, V.R. Magnuson, G.J. Nieni, R.R. Regal, G.D. Veith**,** *Math. Modelling*, **1987**, *8*, 300-305
11. A.T. Balaban, *J. Chem*. *Inf. Comput. Sci*., **1985**, *25*, 334-343
12. M. Randić, *Chemometrics Intel. Lab. Syst*., **1991**, *10*, 213-227
13. E. Estrada, *J. Chem. Inf. Comput. Sci*., **1995**, *35*, 701-707
14. Z. Berinde, *Applications of molecular topology in the study of physico-chemical properties of organic compounds (in Romanian),* Cub Press 22, Baia Mare, **2001**
15. Z. Berinde, Rev. Chim. (Bucureşti), **2001**, *52*, No. 12, 788-792
16. Z. Berinde, Revue Roumaine de Chimie, **2006**, *51*, No. 11, 1131-1135
17. Lu, C. Guo, W., Wang, Y. and Yin, C., J. Mol. Model, **2006**, *12,* 749-756
18. YQ Yang, L. Xu, CY Hu, *J. Chem. Inf. Comput. Sci*., **1994**, *34*, 1140-1145
19. YY Yao, L. Xu, YQ Yang, YS Yuan, *J. Chem. Inf. Comput. Sci*., **1993**, *33*, 590-594
20. J. Gavez, R. Garcia, MT. Salabert, R. Soler, *J. Chem. Inf. Comput. Sci*., **1994**, *34*, 520-525
21. B. Ren, *J. Chem. Inf. Comput. Sci*., **2002**, *42*, 858-868